Durham E-Theses

Continental crustal growth in collision zones on the Northern Tibetan Plateau

HUANG, HUI

How to cite:

HUANG, HUI (2014) *Continental crustal growth in collision zones on the Northern Tibetan Plateau*, Durham theses, Durham University. Available at Durham E-Theses Online: http://etheses.dur.ac.uk/10539/

Use policy

The full-text may be used and/or reproduced, and given to third parties in any format or medium, without prior permission or charge, for personal research or study, educational, or not-for-profit purposes provided that:

- a full bibliographic reference is made to the original source
- a link is made to the metadata record in Durham E-Theses
- the full-text is not changed in any way

The full-text must not be sold in any format or medium without the formal permission of the copyright holders.

Please consult the full Durham E-Theses policy for further details.

Academic Support Office, Durham University, University Office, Old Elvet, Durham DH1 3HP
e-mail: e-theses.admin@dur.ac.uk Tel: +44 0191 334 6107
http://etheses.dur.ac.uk

Continental crustal growth in collision zones on the Northern Tibetan Plateau

Hui Huang

A THESIS SUBMITTED IN PARTIAL FULFILMENT OF THE

REQUIREMENTS FOR THE DEGREE OF DOCTOR OF PHILOSOPHY

AT DURHAM UNIVERSITY

Department of Earth Sciences

Durham University

March 2014

“If you can’t explain it simply, you don’t understand it well enough.”

Albert Einstein

Abstract

The continental crustal growth has been a great interest to geoscientists and its importance is self-evident. Any models trying to reveal how it works must be able to explain 1) how the continental crust gains its andesitic bulk composition with juvenile isotope signatures; 2) how the volume of the crust increases episodically. Granitoids with the juvenile isotopic signatures in the collision zones provide the special insights into the nature of the continental crust and a unique opportunity to investigate the mechanism of crust growth. This thesis reports results from major and trace element data, whole rock Sr-Nd-Hf-Pb isotopic data, zircon geochronology and *in situ* Hf isotopes of granitoids as well as, if any, the enclosed mafic magmatic enclaves (MMEs) from the three ancient collision zones crossing the Northern Tibetan Plateau.

I-type granitoids and their MMEs from the East Kunlun Orogenic Belt (EK) in the Northern Tibetan Plateau are dated as 250 Ma years old. They are cal-alkaline in nature with compositions resembling the bulk continental crust (BCC). Whole rock Sr-Nd-Pb-Hf isotopes reveal that they are products of partial melting of the 'trapped' subducted oceanic crust at the onset of the collision and the MMEs are the aggregated early cumulates in the parental magma rather than the mafic endmember involved in the magma mixing as previously suggested.

I- and S-type granitoids from the Qilian Block (QB) further north in the Great Plateau are dated as 450 Ma. Their lithological and geochemical heterogeneity and isotopic changes with time are inferred to correspond to the collision. The abundant inherited zircons with ages as old as Archean reveal the presence of the Archean basement underneath the Qilian Block and indicate that the Qilian Block may have been a micro continent during its drift in the ancient ocean.

Granitoids and their enclosed cumulates from Kekeli Batholith further north in the plateau are 500 Ma years old. They have decoupled whole rock Nd and Hf isotopes and discrepancy between whole rock Hf and zircon *in situ* Hf isotopes. These inconsistences are understood to result from different mineral crystallization timings during mixing between endmembers with distinct isotopes. This highlights the need for detailed whole-rock or non-zircon phases Hf isotopic investigation in order to develop a comprehensive understanding of the granitoids of hybrid origin.

Declaration

I, Hui Huang, declare that this thesis, presented for the degree of Doctor of Philosophy at Durham University, is my own original research and has not been previously submitted to Durham University or any other institution except where reference is made to previously published or unpublished work.

Hui Huang

Durham University

March 2014

Copyright © Hui Huang

The copyright to the material within this thesis rests with the author and any information or quotation taken from it, should be acknowledged and pbulished only if prior consent has been given.

Acknowledgements

The past 3 and half years were full of smiles, tears and memories. Here comes the moment to look over the journey past, appreciate and remember all the happiness that life has given. I offer my sincere gratitude to the following people, to only some of whom it is possible to mention here. It would never have been possible to complete this doctoral thesis without your great help and support.

First and foremost I would like to express my heartfelt thanks to my long-suffering supervisor Yaoling Niu, who is not only my adviser but dear friend. You are the source of academic knowledge and life enlightenment which has helped turn me into an independent thinker and a mature human being from a poorly educated naive person. I would not be where I am today without your continuous education and encouragement. I also owe a big thank you to my dear second supervisor Geoff Nowell for being a great guide with patience and inspiration throughout my difficult labbing time, instrumenting time and paper writing. Without the inputs and efforts squeezed out of your busy schedule this work would not have been efficient or possible. My previous supervisor Zhidan Zhao in China University of Geosciences (Beijing), I thank you for the precious advice at each turning point of my life. Thank you to Durham University and China Scholarship Council for providing the funding that has made all of this possible.

Thanks go to the Mark Allen, Pierre Bouilhol, Vali Memeti, Iain Neill, Jeroen van Hunen, Alex B.J., Valentina Magni, Dicheng Zhu, Shuguang Song, Li Su and Shuijiong Wang for your brilliant academic informations and suggestions which helped me overcome those difficulties. Thanks are owed to Chris Dale and Scot Dempsey for their kind help in the clean laboratories; Stuart Jones and Stephan Stricker for the mineral point counting; Shuo Ding, Huixin Hei, Lei Wu, Dong Liu, Li Su and Shuijiong Wang for sample collection, preparation, major and trace elements analyses and zircon *in situ* analyses. I extend further thanks to the editor of *Chemical Geology* Laurie Reisberg for her patient detailed constructive comments which significantly hone my painstaking first paper.

Special thanks go to my fellow grad students and department administrative/technical staff. In particular, thank you to Helen Foster, my dearest friend and best housemate, for always being there throughout my ups and downs. Life in a foreign country cannot be so great without you. Suize, Ute, Alex, Pete, Bansri, Jingxiu, Jing, Yang, Ang, Yuanyuan, Fran, Cui, Li, Salim, Stephan, Vale, Hongliang, Yi, Rachel, Simon, Chris, Lily, Roberto, Yan, Mark, Ian, Amelie and Andy, thank

you for your friendship and support during my time in Durham. And thank you to my friends in China and other corners of the world for the endless love.

Finally, thank you to Mom, Dad and Shuijiong for the warmest careness crossing the Eura-Asia continent and the Atlantic. Thank you for the support, understandings and forgiving my temporary absence.

Contents

Abstract i

Declaration ii

Acknowledgements iii

Contents v

List of Figures ix

Chapter 1: Introduction 1

1.1. Thesis Rationale 2

1.2. Chapter contributions 5

1.2.1. Chapter 2 5

1.2.2. Chapter 3 6

1.2.3. Chapter 4 7

1.2.4. Chapter 5 7

1.2.5. Chapter 6 8

Chapter 2: Methodology 9

2.1. General sample preparation 10

2.2. Major element geochemistry-XRF 10

2.2.1. The loss on ignition (LOI) 10

2.2.2. Glass disc preparation 11

2.3. Trace elements-ICP-MS 11

2.4. Zircon U-Pb geochronology 11

2.5. Zircon *in situ* Hf isotope-LA-ICP-MS 12

2.6. Whole rock Sr-Nd-Pb-Hf isotopes 13

2.6.1. Dissolution procedure 13

2.6.2. Sr-Spec column chemistry for collecting Nd-Hf, Sr and Pb fractions---Sr and Pb is ready in this step 14

2.6.3. Column chemistry for collections of Hf and Nd 15

2.6.3.1. Sample preparation 15

2.6.3.2. Nd and Hf cation column procedure—Nd fraction is ready in this step 15

2.6.3.3. Hf column chemistry—Hf fraction is ready in this step 16

2.6.4. Beak cleaning 17

2.7. References 18

Chapter 3: Granitoids and their enclaves from the East Kunlun Orogenic Belt 19
3.1. Introduction 20
3.2. Geological setting 21
3.2.1. Regional and local geology 21
3.2.1.1. Stratigraphy and metamorphic rocks in the EKOB 21
3.2.1.2. East Kunlun Batholiths (EK batholiths) 22
3.2.2. Petrography 22
3.3. Analytical results 23
3.3.1. Major and trace elements 23
3.3.2. Zircon U-Pb Geochronology 28
3.3.3. Whole rock Sr-Nd-Pb-Hf isotopes 30
3.4. Discussion 33
3.4.1. Isotope constraints on the formation of MMEs 33
3.4.2. Geochemical constraints on the source 37
3.4.3. Mechanism and conditions of Paleo-Tethyan oceanic crust melting 40
3.4.4. Continental crust growth in the collision zone 42
3.5. Conclusions 43
3.6. References 44
Chapter 4: The nature and history of the Qilian Block 49
4.1. Introduction 50
4.2. Tectonic setting and geology background 51
4.2.1. Strata, metamorphic rocks and mafic rocks in the QOB 51
4.2.2. Paleozoic granitoids in the QOB 53
4.3. Methods 54
4.4. Petrology, zircon geochronology and geochemistry 54
4.4.1. Old rocks—924 Ma, 797 Ma and 503 Ma 56
4.4.2. ~450 Ma I-type and S-type 60
4.4.3. Ages of I- and S-type samples 61
4.5. Discussion 63
4.5.1. Origin of 924 Ma and 797 Ma magmatism 63
4.5.2. Origin of 503 Ma granite 63
4.5.3. Origin of ~450 Ma I-type and S-type granites 64
4.5.3.1. ‘Mixing process’ 64

4.5.3.2. Implications of tectonic context 67
4.5.3.3. Melting of subducted oceanic crust 68
4.5.4. Tectonic evolution 69
4.5.5. Nature of the Qilian Block 71
4.6. References 73
Chapter 5: Tectonic implications of zircon in situ Hf isotopes and whole rock Sr-Nd-Pb-Hf isotopes of Gcha and HY granitoids in the Qilian Block 78
5.1. Introduction 79
5.2. Results 79
5.3. Discussion 83
5.3.1. The Archean basement underneath the Qilian Block 83
5.3.2. Implications for sources 86
5.3.3. Re-evaluation of previous metamorphic interpretation 87
5.3.4. Re-evaluation of the previous collision timing 88
5.4. References 91
Chapter 6: Mixing induced discrepancy between whole rock Hf isotopes and zircon in situ Hf isotopes: A case study in Kekeli batholith, the North Qilian Orogenic belt 93
6.1. Introduction 94
6.2. Tectonic setting and geologic background 96
6.3. Samples 97
6.4. Sample preparation and analytical techniques 99
6.5. Results 99
6.5.1. Major and trace elements 99
6.5.2. Zircon geochronology and geochemistry 100
6.5.3. Whole rock Sr-Nd-Pb-Hf isotopes and zircon in situ Hf isotopes 102
6.6. The discrepancy between in situ zircon Hf and whole rock Hf isotopes 104
6.6.1. Ti-rich minerals— important Hf host 105
6.6.2. Can Ti-rich minerals cause the decoupling in initial Nd-Hf isotopes? 107
6.6.3. Mixing—magma endmembers 109
6.6.4. Mixing induced discrepancy between WR-Hf and Zir-Hf isotopes 110
6.7. Magma chamber evolution—mixing associated with crystal fractionation 111
6.8. Magma generation and continental crust growth 113
6.9. Conclusions 115
6.10. References 116

Chapter 7: Conclusions and future work 120
7.1. The East Kunlun Orogenic Belt (Chapter 3) 121
7.2. The Qilian Orogenic Belt 121
7.2.1. The Qilian Block (Chapter 4) 122
7.2.2. The Qilian Block (Chapter 5) 122
7.2.3. The North Qilian Orogenic belt (Chapter 6) 123
7.3. Problems and Future work 124
Appendices: Data 129
Data for Chapter 3 130
Data for Chapter 4 150
Data for Chapter 5 169
Data for Chapter 6 186
Appendix A. Standard Data for trace elements. 205
Appendix B. Standard Data for Sr-Nd-Hf isotopes. 206
Appendix C. Standard Data for Pb isotopes. 207
Appendix D. Repeated analyses of Nd isotopes. 208
Appendix E. Isotope blanks. 209
Appendix F. Zircon trace elements for Chapter 4. 210
Appendix G. Zircon trace elements for Chapter 5. 222
Appendix H. Zircon trace elements for Chapter 6. 230

List of Figures

Fig. 3.1. A, Schematic map showing major tectonic units of West China. B, Schematic map showing three sub-tectonic zones of the East Kun Orogenic Belt (EKOB; after Jiang et al., 1992). C, Simplified geological map of the East Kunlun Orogenic Belt and the adjacent Qaidam Basin region showing the distribution of granitoids and ophiolites (after Pan et al., 2004). 1: Naomuhun Pluton, 261 Ma (Xiong et al., 2011). 2: Yuegelu Pluton, 243 ~ 256 Ma (Liu et al., 2004b); Halagetu Pluton: 255 Ma (Sun et al., 2009). 3-4 data is from Yang et al., (1996). 3: Qingshuiquan Ophiolite, 518 Ma (Zircon U-Pb). 4: Buqingshan Ophiolite: poorly dated, maybe late Permian to early Triassic. 5: Xiadawu Ophiolite, 260 Ma (Rb-Sr), (Jiang et al., 1992). 6-8 data is from Yang et al., (1996). 6: Majixueshan Ophiolite, Volcanic rocks: 260 Ma (Rb-Sr). 7: Maqen Ophiolite: poorly dated, maybe late Permian to early Triassic. 8: Wanbaogou Ophiolite: poorly dated, maybe late Permian to early Triassic. 9: Dur'ngoi Ophiolite, 308 Ma (Zircon U-Pb) (Yang et al., 2009a). 10, Deqia granitic complex, 250 Ma (Zircon U-Pb) (Yang et al., 2005). 11: Golmud East, Granodiorite, 240±6 Ma (Zircon U-Pb) (Harris et al., 1988a). 12, Xiangride Pluton, 242 Ma, compilation after Chen et al., (2007b). 12, Chahannuo Pluton, 242 Ma, compilation after Chen et al., (2007b). 13, data from compilation of Chen et al., (2011). 24

Fig. 3.2. Field photos in the Dulan area (A-B) and photomicrographs under plane polarized light of the representative granitoid host rock (C) and enclaves (MME) (D).....25

Fig. 3.3. Total alkalis (Na_2O+K_2O) versus SiO_2 (TAS) diagram showing the compositional variation of EKOB samples. The MMEs are generally less felsic than the hosts. Three samples in the gabbro field are actually mafic-diorite without pyroxene. All the samples are calc-alkaline. The dashed line represents the division between Alkaline and Cal-alkaline fields (Irvine and Baragar, 1971).....26

Fig. 3.4. SiO_2 variation diagrams of representative elements of the EKOB samples, showing fractional crystallization dominated trends.....27

Fig. 3.5. A, Chondrite-normalized (Sun and McDonough, 1989) rare earth elements (REE) patterns for average compositions of the EKOB granitoid hosts (H) and mafic magmatic enclaves (MME, M). Bulk continental crust (BCC; Rudnick and Gao, 2003) and average of Andean continental arc (yellow line, data from http://georoc.mpch-mainz.gwdg.de/georoc/, basaltic andesitic to andesitic

compositions) are also shown for comparison. B, Primitive mantle-normalized (Sun and McDonough, 1989) multi-element patterns as in panel A. C, One-to-one plot to show the similarity between the granitoid hosts of the EKOB samples and the BCC in terms of the analyzed major and trace elements. D, Comparision between the granitoid hosts and the BCC in terms of key elemental ratios.....28

Fig. 3.6. Cathodoluminescence (CL) images of zircons from representative samples. White circles are the analyzed spots. The values with error are ages in Ma. 29

Fig. 3.7. Zircon U-Pb Concordia diagrams. The majority of zircons give ~ 250 Ma crystallization age for both granitoid hosts and the MMEs. Various amounts of inherited old zircons contained in hosts and enclaves indicate the presence and involvement of old crustal material.....31

Fig. 3.8. A and B, Plots of isotope ratios vs. parent-daughter ratios, giving Rb/Sr pseudo-isochrone age of 295 Ma and Lu/Hf pseudo-icochron age of 294 Ma, which are close to the zircon *in situ* dating age of ~ 250 Ma of the EKOB granitoids. C, no correlation between $^{143}Nd/^{144}Nd$ and $^{147}Sm/^{144}Nd$. The 250 Ma reference line is shown to demonstrate the small ingrowth of radiogenic Nd isotopes. 32

Fig. 3.9. Isotopes versus MgO and SiO_2 plots showing overlapping isotopes between MMEs with higher MgO/lower SiO_2 and the granitoid hosts with lower MgO/higher SiO_2. The negative $\varepsilon_{Nd}(t)$ values are suggestive of the crustal contribution while the dominant positive $\varepsilon_{Hf}(t)$ values are suggestive of mantle input. 34

Fig. 3.10. Small scale age-corrected (250 Ma) isotope variation diagrams showing overlapping isotopes between the granitoid hosts and MMEs and isotopic variations within individual host and MME, which actually reflect magma heterogeneity (with some superimposed mineralogical differences) rather than mixing process. MME(M)-Host(H) pairs: ①:DL09-07(M), DL09-08(H), DL09-09(H) (two host rocks for the same MME); ②: DL09-15(H), DL09-16(M), DL09-17(M) (two enclaves for the same host rock); ③: DL09-30 (H), DL09-31 (M), DL09-32 (H) (two host rocks for the same enclaves). Others, ④: DL09-13(H), DL09-14(M); ⑤: DL09-21(H), DL09-22(M). H: host rock; M: MME. 36

Fig. 3.11. Showing that the mafic enclaves (MME), host rocks in this study and mafic-diorite veins in the literature (Liu et al., 2004b; Xiong et al., 2011.) all have indistinguishable isotope compositions and they plot along an apparent 'mixing' trend between Paleo-Tethyan MORB and terrestrial sediments (the Shaliuhe gneiss). Terrestrial array is from Chauvel et al., (2008). Sr, Nd and Pb isotopes and elemental concentrations for Paleo-Tethyan MORB are from the east part of the northernmost branch of the Paleo-Tethyan realm ($^{87}Sr/^{86}Sr$:0.7055, $^{143}Nd/^{144}Nd$:0.51313, $^{206}Pb/^{204}Pb$: 17.257, $^{207}Pb/^{204}Pb$:15.532, Sr: 69.07ppm, Nd: 6.5ppm, Hf: 1.87ppm, Pb: 1.91ppm) (Xu et al., 2002). Hf isotope for MORB is inferred from Nd isotope following the equation ($\varepsilon_{Hf}=1.59\varepsilon_{Nd}+1.28$) given by (Chauvel et al., 2008) because of the statistically significant Hf-Nd isotope ratio correlation (Zindler and Hart, 1986). Sr isotope ($^{87}Sr/^{86}Sr$: 0.7180, Sr: 300ppm) for the Shaliuhe Gneiss is from Harris et al., (1988a). Nd and Pb isotope data ($^{143}Nd/^{144}Nd$:0.5121, $^{206}Pb/^{204}Pb$: 20.000, $^{207}Pb/^{204}Pb$:15.750, Nd: 33ppm, Pb: 19.50ppm) for the Shaliuhe Gneiss are from Chen et al., (2007b) and Meng et al., (2005a). Hf isotope data ($^{176}Hf/^{177}Hf$: 0.28218, Hf: 4ppm) for the Shaliuhe Gneiss are from Chen et al., (2007c). Grey Square: Host rocks and enclaves from (Xiong et al., 2011). Triangle: host rocks, enclaves and mafic veins from (Liu et al., 2004b).....38

Fig. 3.12. Simplified phase diagram showing hydrous solidi of basalts and granitic rocks quoted from Mo et al. (2008; after Niu, 2005). The solid line with arrow illustrates the concept of the subducted oceanic crust (A'nyemaqen Ocean) evolve along a high T/P path as a result of retarded subducting and enhanced heating upon continental collision at a prior active continental margin setting.....41

Fig. 3.13. Cartoons showing the A'nyemaqen seafloor spreading during the Carbonifeous time (A) (308 Ma: the protolith age of Dur'ngoi ophiolite (Yang et al., 2009a)), subduction of A'nyemaqen oceanic crust and related magmatism (B) and the syncollisional magmatism (C; See Figure 12 for mechanisms). 42

Fig. 4.1. A, Schematic map showing major tectonic units of the Qilian Orogenic Belt, after Song et al. (2013).B, Simplified geological map of the Qilian Block showing the distribution of granitoids and ophiolites (after Pan et al., 2004). Data are from the literature given in Table 4.1. C, Detailed geological map of the sampling locations (after Pan et al., 2004). 51

Fig. 4.2. Photomicrographs under plane polarized light showing partial melting textures of QL09-01, representative S-type granite QL09-10, I-type granite QL10-32 and enclave QL09-19 in QL09-18. 55

Fig. 4.3. Total alkalis (Na_2O+K_2O) versus SiO_2 (TAS) diagram showing the compositional variation of the QB samples. All the samples are calc-alkaline. The dashed line is the division between alkaline and sub-alkaline fields (Irvine and Baragar, 1971). 55

Fig. 4.4. Harker diagrams showing correlated compositional variations among samples. 56

Fig. 4.5. Left column, Chondrite-normalized (Sun and McDonough, 1989) rare earth element (REE) patterns for the Qilian Block (QB) samples with varying compositions. Right column, Primitive mantle-normalized (Sun and McDonough, 1989) multi-element patterns. Majority of the samples show similar patterns resembling bulk continental crust (BCC, dash line). S-type rocks have a few exceptions: QL09-10 has upward HREEs due to the garnet. QL09-02/07 has depleted HREEs due to the garnet in the source. QL10-40F/41F are highly evolved melts. Average of Andean continental arc (yellow line) is also shown for comparison (data from http://georoc.mpch-mainz.gwdg.de/georoc/, basaltic andesitic to andesitic compositions).....58

Fig. 4.6. Cathodoluminescence (CL) images of zircons from representative samples. Black circles with white outlines are analyzed spots. The numerals are ages in Ma.....59

Fig. 4.7. Zircon U-Pb Concordia diagrams. Old rocks 924 Ma QL09-15, 797 Ma QL09-01 and 503 Ma QL09-18 are well dated. 450 Ma I-type and S-type rocks have large age ranges and are not well dated. We choose the youngest peak at ~450 Ma on the histogram as the emplacing time (see text). 60

Fig. 4.8. Isotope plots with all the samples (including 923 Ma, 797 Ma, 503 Ma and 450 Ma) age corrected to ~ 450 Ma, showing significant correlations among these samples. QL09-02 has similar isotopes to 797 Ma QL09-01. The 503 Ma granite has similar isotopes to eclogites in NQ-UHPM based on the current available data for eclogites. The ~ 450 Ma granitoids are plotted on apparent 'mixing' trend (thick line in A) between eclogites (Qilian Ocean) and 2348-2470 Ma Mohe basement. Blue dash line in A is modelling using younger crustal endmember QL09-01 (797Ma, this study). Sr and Nd isotope data for eclogites are from Zhang et al. (2008). Hf isotope data for

eclogitesare simply adopted global MORB composition (Workman and Hart, 2005). Hf isotope data for Mohe basement are from Li et al. (2007). Sr-Nd isotope data for Mohe basement are from Chen et al.(2007b). 62

Fig. 4.9. The histogram of all the zircon ages ($^{206}Pb/^{238}U$ for ages <1.0 Ga and $^{207}Pb/^{206}Pb$ for ages >1.0 Ga). A: emphasis the inherited ages >1.0 Ga. B: emphasis the inherited ages between 700 Ma and 500 Ma. C: comparison between North China Craton (NCC), Yangtze Craton (YC) (modified after Grimmer et al., (2003)) and Qilian Block (QB) (this study).....65

Fig. 4.10. Comparision of two models proposed by this study and Yang et al., (2006), respectively.A, this study: Cartoons showing the Qilian Ocean floor spreading between Qaidam Block and Qilian Block during the Proterozic time (a) (877 Ma: the protolith age of eclogites in NQ-UHPM (Zhang et al., 2011), initiation of subduction and related back-arc extension(b), and the syncollisional magmatism at ~ 450 Ma (c). B, Yang et al., 2006: Cartoons showing the Neoproterozoic Ocean opened and closed. Two independent Qilian oceans opened and closed during Paleozoic time. See details in Yang et al, (2006) 72

Fig. 5.1. A, Schematic map showing major tectonic units of the Qilian Orogenic Belt (after Song et al., 2013). B, Simplified geological map of the Qilian Block (QB) showing the distribution of granitoids and sampling area. 79

Fig. 5.2. Zircon U-Pb Concordia diagrams showing the continuous age spread along the Concordia. 80

Fig. 5.3. Histograms of zircon ages for Gcha and HY rocks showing that Gcha rocks slightly predate HY rocks. The inherited zircons are shown in red with different scales (red scale on the right side). 81

Fig. 5.4. SiO_2 variation diagrams of representative elements of I- and S-type granitoids. 82

Fig. 5.5. Isotope plots show that samples in this study are plotted in the area defined by the previous study (Chapter, 4) and have good correlations (A-D). Fig. 5E shows that HY rocks have big discrepancies between whole rock $\varepsilon_{Hf}(450)$ and averages of zircon $\varepsilon_{Hf}(450)$ whereas, Gcha rocks do not. 83

Fig. 5.6. Histograms of zircon *in situ* $\varepsilon_{Hf}(450)$ values for HY (A) and Gcha rocks (B). 84

Fig. 5.7. A, $\varepsilon_{Hf}(t)$ versus the zircon ages. Ages are corrected to the individual zircon ages to show the isotopic composition of the zircons at the time of crystallization. B, $\varepsilon_{Hf}(450)$ versus the zircon ages. All ages are corrected to 450 Ma to show the source materials involved in the 450 Ma magmatism. C, Two-stage zircon Hf model ages versus zircon crystallization ages. 85

Fig. 5.8. A, Collision between the Qaidam Block and Qilian Block initiated at ~500 Ma and the syn-collisonal magmatism. B. the slab started steepening since collision and caused the enhanced mantle wedge convection producing magmatism. C, slab finally broke off at ~450 Ma. The uprising hot asthenosphere mantle caused the extensive magmatism at ~450 Ma. 89

Fig. 6.1. A, Schematic map showing major tectonic units of the Qilian Orogenic Belt (after Song et al., 2013). B, Simplified geological map of the North Qilian Orogenic Belt (NQOB) showing the distribution of granitoids and ophiolites (after Song et al., 2013). Data compilation for granitoid intrusions is from Huang et al. (2013b), and for ophiolites is from Song et al., (2013). Dongcaohe, 497 Ma (Tseng et al., 2007); Aoyougou, 504 Ma (Xiang et al., 2007); and Yushigou, 529 Ma (Song et al., 2013); Yushigou, 550 Ma (Shi et al., 2004); Jiugequan ophiolite, 448-490 Ma (Song et al., 2013; Xia and Song, 2010); Laohushan ophiolite, 448 Ma (Song et al., 2013).....95

Fig. 6.2. Photomicrographs under plane polarized light and SiO_2-variation diagrams showing the correlations among samples. QL10-22: cumulate texture. QL10-21: heteradcumulate texture. QL10-26: Secondary Amp and Bi rims on the pyroxene. QL10-14: granitic group 1 contains Bi without Amp. QL10-23: group 2 with intermediate composition containing Amp. (Amp: amphibole, Pl: plagioclase, Q: quartze, Ep: epidote, Opx: othorpyroxene, Cpx: clinopyroxene, Bi: biotite, Kfs: K-feldspar, ilm: ilmenite. MME: mafic magmatic enclave). 96

Fig. 6.3. Zircon U-Pb Concordia diagrams to show host rocks and MMEs have the same crystalline age of ~ 500 Ma. 98

Fig. 6.4. Chondrite-normalized rare earth element patterns and primitive mantle-normalized diagrams (Sun and McDonough, 1989). QL10-26 has no Eu anomaly and displays the fairly flat LREE pattern; Group 1 has a largest negative Eu anomaly. Group 2 and other MMEs have the intermediate negative Eu anomalies 99

Fig. 6.5. Zircon cathodoluminescence photos and trace elements. 101

Fig. 6.6. A, Age corrected bulk-rock Nd isotopes vs SiO_2 to show a broad negative correlation. Group 1 samples have lowest $\varepsilon_{Nd}(t)$. Group 2 samples have intermediate isotope composition between two endmembers. B, Age corrected bulk-rock Hf isotopes vs. SiO_2 to show the broad negative correlation. Group 1 samples have lowest $\varepsilon_{Hf}(t)$. Group 2 samples have the intermediate isotope composition between two endmembers. Zircon in situ Hf (Zir-Hf) data (open symbols) are also plotted for comparison. C, negative correlation between Nd and Sr isotopes. D, negative correlation between Hf and Sr isotopes. E, scatter Pb isotope plot showing between-sample heterogeneity. F, comparison between Zir-Hf and WR-Hf to show the discrepancy between the two. G, Zir-Hf (open symbols) and WR-Hf plot against Nd isotope showing the discrepancy between Zir-Hf and WR-Hf and decoupling between WR-Hf and Nd isotope. H, Correlations between age corrected /non-corrected WR-Hf and TiO_2. 103

Fig. 6.7. A, Zircon in situ Hf isotopic composition plot against zircon Ti contents showing no correlation between the two. B, Zircon Hf contents and whole rock Hf contents plot against SiO_2 showing that (1) the whole rock Hf concentration remains more or less the same throughout; (2) Hf concentration in zircon increases from mafic to felsic. C, comparison of whole rock, zircon and non-zircon phases Hf isotopes. 106

Fig. 6.8. Model time-integrated modern isotopic compositions in the residual magma for removal of up to 60% of pure ilmenite. Rayleigh fractionation equations are used. For clarification, we start with andesitic elemental composition (data from Niu and O'Hara (2009)) with chondritic isotopes. Results showing the huge in-growth of ε_{Hf} with negligible changes in ε_{Nd}. However, to achieve the 26 units shift in ε_{Hf} from the mantle array ($\varepsilon_{Hf}=1.33*\varepsilon_{Nd}+3.19$, (Vervoort and Blichert-Toft, 1999)) in QL10-26, up to 60% of pure ilmenite and 500 myrs integration is required. Fractionation of 60% pure ilmenite means original magma should contain at least 30 wt% TiO_2 (ilmenite has 50% TiO_2) and experience 600% (6 times of its own volume) fractionation if there is up to 10% ilmenite in the fractionated assemblages. Importantly, 500 myrs integration is too long to be realistic for any fractionation process within the magma chamber. Therefore, ilmenite fractionation cannot explain the radiogenic Hf in our samples despite its great potential. 107

Fig. 6.9. Carton showing the mixing and crystallization process where mantle-derived lithologyinteracts with the crustal melt. See details in the text. I: Px and Ilm start to crystallize from

the evolved basaltic magma at ~ 950-1100 °C (gabbronorite QL10-26). II: Amp started to crystallize by replacing Px as rims and Bt due to the lower P-T conditions and interaction with granitic melts at stage III. III: granitic melts (Group 1) by hydrous partial melting of mid-lower crust due to the basaltic magma (I) underplating. IV: hybrid andesitic magma (Group 2) of mantle lithology (part of QL10-26) and crustal melt (Group 1). V: Amp and Pl cumulated from the hybrids (Group 2).....112

Chapter 1: Introduction

1.1. Thesis Rationale

This thesis aims to investigate the processes through which continental crust grows in the ancient collisions on the Northern Tibetan Plateau. The significance of continental crust is self-evident, yet our understanding of its origin and evolution remains unsatisfactory and has been a major goal of Earth scientists for decades. Continental crust has andesitic bulk composition. Its arc-like geochemical signature characterized by enrichment in large ion lithophile elements (e.g., Rb, Cs, K, and especially Pb) and depletion in high field strength elements (e.g., Nb, Ta, and Ti) have led to the standard "island arc model" in which continental crust is produced through subduction-zone magmatism (Taylor, 1967, Taylor, 1977, Taylor and McLennan, 1985 and Rudnick and Gao, 2003). In spite of its popularity, this model fails to explain several basic observations (see Niu and O'Hara, 2009 and Niu et al., 2013). For example, bulk island arc rocks are basaltic (Arculus, 1981, Gill, 1981 and Pearcy et al., 1990) while the bulk continental crust is andesitic (Taylor and McLennan, 1985, Hans Wedepohl, 1995 and Rudnick and Gao, 2003; also see Mo et al., 2008); and arc rocks are highly enriched in Sr while bulk continental crust is relatively depleted in Sr (Niu and O'Hara, 2009). Besides, arc crust production and continental destruction (sediment recycling and subduction-zone erosion) have been demonstrated repeatedly to be mass balanced (von Huene and Scholl, 1991, Clift and Vannucchi, 2004, Clift et al., 2009, Niu and O'Hara, 2009 and Scholl and von Huene, 2009), implying that there is no net crustal growth associated with active seafloor subduction and arc magmatism. It has been accepted that the bulk continental crust has grown progressively through episodic magmatism over Earth history (Reymer and Schubert, 1984 and Condie, 2000). This notion requires a tectonic setting where juvenile crust is produced and also preserved in order to maintain the net crustal growth (see Niu and O'Hara, 2009 and Niu et al., 2013).

A hypothesis that continental collision zones are primary sites of net continental crustal growth was recently proposed by Niu et al. (2007), Mo et al. (2008) and Niu and O'Hara (2009) based on

studies of the India-Asia syncollisional (~ 55 Ma) andesitic rocks from southern Tibet (Mo et al., 2007a and Mo et al., 2008) in order to resolve the major problems that the standard 'island arc' model faces (see the above, and reviewed by Niu et al., 2013). These rocks, in particular the syn-collisional andesites, show remarkable compositional similarity to the bulk continental crust (Rudnick and Gao, 2003), yet have strong mantle isotopic signatures (Mo et al., 2007a and Mo et al., 2008). Their petrogenesis is interpreted to represent net mantle-derived materials added to the continents via partial melting of last fragments of underthrusting Tethyan ocean crust under amphibolite-facies conditions in a syn-collisional setting (Niu and O'Hara, 2009). Nevertheless, whether this hypothesis is valid for older syncollisional granitoids on a global scale still needs testing (Niu et al., 2013). The tectonic framework of the Northern Tibetan Plateau is characterized by the assembly of several collisions zones. Each syncollisional batholith belt is in excess of 1000 km long. If our petrologic and geochemical study proves that all these batholiths are dominated by juvenile material at the time of accretion, then we will be able to develop the concept into a quantitative theory on the origin and evolution of the continental crust.

In detail, these syn-tectonic granitoids deserve a comprehensive study using modern technics also because (1) these granitoids are voluminously important and tectonically associated with the regional metamorphisms; (2) they have not been neither precisely dated nor geochemically investigated, therefore, their petrogenesis is not clear nor convinced; (3) understanding of petrogenesis of these granitoids are of particular importance to understand the mechanisms of the continental crust growth; (4) the relationship between the sub-tectonic units are complex and contentious. Understanding of these granitoids can place more constraints on the orogenic evolution.

We conducted two two-week field trips in 2009 and 2010, respectively. We sampled from three batholith belts: the East Kunlun batholiths in the southern which is ~250 Ma years old; the granitoids in the Qilian Block in the middle, and the North Qilian Orogenic Belt which is ~ 500 Ma years old further in the north. We focused on the I-type granitoids containing the mafic magmatic

enclaves (MMEs) as well as some representative S-type granitoids. This thesis reports results from major and trace element data, whole rock Sr-Nd-Hf-Pb isotopic data, zircon geochronology and *in situ* Hf isotopes of granitoids as well as, if any, the enclosed MMEs.

The Giant East Kunlun Batholiths extend east–west for up to 1500 km with a north–south width of 50–200 km. In the light of the lack of knowledge (Chapter 3), the geochemical nature of representative granitoids from these batholiths as well as their enclosed mafic magmatic enclaves (MMEs) in the eastern part of the East Kunlun Orogenic Belt (EKOB), were investigated. These samples were chosen for study as they contain abundant MMEs and for this reason, offer particular insights into evolution of the granitoid magma and the mechanism of crust growth in the EKOB. The multiple geochemical data enable us to evaluate the relationship between these MMEs and their hosts which is essential to understand their petrogenesis as a whole and to quantify the geochemical endmembers in the source in order to further constrain the crust growth processes.

Samples in the Qilian Block (QB), north to the EKOB, provide the opportunity to reveal the nature and history of this region. These samples were chosen because (1) the QB is a unique tectonic unit which is important to understand the debatable tectonic history of the entire Qilian Orogenic Belt; (2) the granitoids cover a large compositional range and were little investigated, which limited the understanding of the QB.

In addition to the samples from the EKOB and the QB, samples from the Kekeli Batholith in the northern part of the Qilian Orogenic Belt are also studied in this Ph.D. project. Kekeli batholith is characterized by the abundant mafic cumulates and considered as the fossil magma chamber. It offers a unique opportunity to look into the early stage geochemical evolution of the granitoid magma.

Chapter 2 briefly introduces the analytical techniques and methods used throughout this study. The methods are also indicated and summarized in each chapter where appropriate.

Chapter 3 focuses on the petrography, geochronology and whole rock geochemistry and isotopes of the EKOB granitoids as well as their MMEs. The *in situ* U-Pb age analyses of zircon separates yield constraints on the age and evolution of the EKOB. Through geochemical compositions of the hosts and MMEs, their congenetic relationship is characterized. Petrogenesis of the granitoids and crust growth in terms of the tectonic evolution of the EKOB is discussed in this chapter.

Chapter 4 focuses on the petrography, geochronology and whole rock geochemistry and isotopes of the Qilian Block granitoids. Through the *in situ* U-Pb age analyses of zircon separates, the nature of the Qilian Block basement is characterized and the emplacement age of these granitoids is evaluated. Petrogenesis of the granitoids, crust growth and tectonic evolution of the Qilian Orogenic Belt is discussed in this chapter.

Chapter 5 presents additional zircon *in situ* Hf isotopes for the samples discussed in Chapter 4. More similar samples are investigated in this chapter. Some interpretations in Chapter 4 are re-evaluated and a new tectonic model is proposed.

Chapter 6 focuses on the petrography, geochronology, whole rock geochemistry and isotopes and zircon *in situ* Hf isotopes of samples from Kekeli Batholith in the North Qilian Orogenic belt. The effect of different mineral crystallizing timings on the Hf isotopic system is investigated.

Chapter 7 summarises the conclusions from each of the previous chapters and future work in order to present a comprehensive, concise and critical account of the nature and evolution of the magmatisms in the old collisions zones on the Northern Tibetan Plateau.

1.2. Chapter contributions

1.2.1. Chapter 2

I wrote this chapter in its entirety in order to provide a concise descriptions of techniques used throughout this study.

1.2.2. Chapter 3

The contents of this chapter have been published in Chemical Geology:

Huang, H., *Niu, Y.L., Nowell, G., Zhao, Z.D., Yu, X.H., Zhu, D.C., Mo, X.X. and Ding, S. 2014. Geochemical constraints on the petrogenesis of granitoids in the East Kunlun Orogenic belt, northern Tibetan Plateau: Implications for continental crust growth through syn-collisional felsic magmatism, Chemical Geology, 370, 1 – 18.*

Hui Huang: I collected the samples and carried out all of the lab work including petrography, cutting and crushing samples, major elements, trace elements, zircon U-Pb dating and whole rock Sr-Nd-Hf-Pb isotopes. I wrote the manuscript then passed it on to the co-authors.

Yaoling Niu: Yaoling is my primary supervisor. He provided the funding to do the entire Ph.D. project. He planned and carried out the sampling program. As the second corresponding author, he provided significant help with the discussion of the results and constructive criticism throughout the preparation and publication of the paper.

Geoff Nowell: As my second supervisor, Geoff provided unwavering assistance and support during the whole-rock Sr-Nd-Hf-Pb isotope analysis in the lab and on the instrument. He assisted data processing, assessed data quality and discussed the initial data interpretations.

Zhidan Zhao: Zhidan was one of major members who carried out the field work. He arranged the zircon U-Pb dating analysis in China University of Geosciences, Wuhan in 2009 and 2010.

Xuhui Yu: Xuehui was one of the major members who carried out the field work.

Dicheng Zhu: Dicheng was one of the major members who carried out the field work.

Xuanxue Mo: Xuanxue was one of the major members who carried out the field work.

Shuo Ding: Shuo provided invaluable assistance throughout the field and lab work except the whole-rock isotope analysis.

1.2.3. Chapter 4

The work presented here has been submitted to *Gondwana research* and is currently in press.

Hui Huang: I did the sampling and carried out all of the lab work including petrography, cutting and crushing samples, major elements, trace elements, zircon U-Pb dating and whole rock Sr-Nd-Hf-Pb isotopes. The interpretations and discussion were benefitted from the discussions with Yaoling. I wrote the manuscript then passed it on to the co-authors.

Yaoling Niu: Yaoling provided the funding to carry out the project in the field and in the lab. He was the one of the major members in the field. He provided constructive feedback throughout the preparation and publication of the paper.

Geoff Nowell: Geoff was available for technical assistance with the instrument, assessing the data quality and data processing.

Zhidan Zhao: Zhidan was one of major members who carried out the field work. He arranged the zircon U-Pb dating analysis in China University of Geosciences, Wuhan in 2009 and 2010.

Xuhui Yu: Xuehui was one of the major members who carried out the field work.

Xuanxue Mo: Xuanxue was one of the major members who carried out the field work.

1.2.4. Chapter 5

The work detailed here will be submitted as a paper to *lithos*.

Hui Huang: I did the sampling and carried out all of the lab work including petrography, cutting and crushing samples, major elements, trace elements, zircon U-Pb dating, zircon *in situ* Hf isotope and whole rock Sr-Nd-Hf-Pb isotopes. I arranged the zircon *in situ* Hf isotope analysis in Northwest city, Xi'an in 2009 and in Chinese Academy of Sciences, Beijing in 2011. The interpretations and discussion were benefitted from the discussions with Yaoling.

Yaoling Niu: Yaoling provided the funding to carry out the project in the field and in the lab. He was the one of the major members in the field. He provided constructive criticism on the original manuscript.

1.2.5. Chapter 6

The work detailed here will be submitted as a paper to *Earth and Planetary Science Letters.*

Hui Huang: I did the sampling and carried out all of the lab work including petrography, cutting and crushing samples, major elements, trace elements, zircon U-Pb dating, zircon *in situ* Hf isotope and whole rock Sr-Nd-Hf-Pb isotopes. I arranged the zircon *in situ* Hf in Chinese Academy of Sciences, Beijing in 2011. The data was modelled and interpreted by me.

Yaoling Niu: Yaoling provided the funding to carry out the project in the field and in the lab. He was the one of the major members in the field. He provided constructive criticisms on the original manuscript.

Geoff Nowell: Geoff was available for technical assistance with the instrument and assessing the data quality. He discussed the initial data interpretations.

Chapter 2: Methodology

2.1. General sample preparation

Samples were collected from the Northern Tibetan Plateau in 2009 and 2010. All the analyzed samples were fresh rock chips by chipping off the weathered surfaces and saw/pen marks. Each sample was split into 2 or 3 parts. One part was for 30 μm and 60 μm thick thin sections. One part was crushed into rock powders (particle size < 50 μm) using agate ball mills. Six samples can be done in one run. Before crushing, all the chips were leached in 5% HCl solution, washed ultrasonically in milli-Q water and dried in a clean environment. The agate ball mills were thoroughly cleaned in water, ethanol and compressed air. The remaining parts (for some dated samples) were crushed to extract zircons. Thin sections are for petrographic observations. Zircon extractions are for zircon U-Pb dating and *in situ* Hf analysis. Whole rock powders are for major and trace element concentrations and Sr-Nd-Pb-Hf isotopic compositions.

2.2. Major element geochemistry-XRF

Major element analysis was done using XRF（PANalytical Axios Advanced PW4400) on fused glass disks in Tianjin Institute of Geology and Mineral Resources, China following the method of Li et al. (2011). The precision on standards (GSR-1, GSR-3, GSR-8, GSR-9) was better than 3% and mostly better than 0.5%. Standard data are given in Appendix A.

2.2.1. The loss on ignition (LOI)

The volatile phases within the sample powders, e.g. chlorine, CO_2, fluorine, H_2O can be lost during the fusion process and lead to the weight change, i.e. LOI, which cannot be detected by XRF analysis. LOI values can also be negative due to the weight gain by iron oxidation, i.e. FeO to Fe_2O_3.

~ 0.5g of rock powder (M1) was weighed out and dried at 120 °C in a Gallenkamp oven overnight to remove the non-structural moisture. The weight of clean Pt-At crucibles was measured as M2, then ~ 0.5g of sample (M1) was weighed into the crucible. After that, crucibles were placed in the

furnace at 1000°C for 2 hours and weighed as M3 after cooling. The LOI values were calculated as 100×(M1+M2-M3)/M1.

2.2.2. Glass disc preparation

~ 5 g mixed flux with lithium tetraborate ($Li_2B_4O_7$): lithium metaborate ($LiBO_2$) ratio of 67:33 was added to each sample in Pt-Au crucibles to aid dissolution. 1 ml 300 g/L ammonium nitrate (NH_4NO_3) was used as oxidant. Two drops of lithium bromide (LiBr) was used as mold-release agent. They were pre-oxidized at 600 °C for 200 s and then fused at 1000 °C for 9 mins. The melt in the crucible was cooled and a disc-shaped sample piece was formed and ready for analysis.

2.3. Trace elements-ICP-MS

Trace element analysis was done using ICP-MS (Thermo Scientific X seriesII) after acid digestion/dissolution in Teflon bombs in Tianjin Institute of Geology and Mineral Resources, China. Standard data are given in Appendix A.

Fifty mg of rock powder was digested with mixture of 1 ml of HF and 0.5 ml of HNO_3 in a Teflon beaker within a screw top stainless steel bomb at 190°C for 24 hours. Teflon beakers were taken out after cooling and left on a hot plate at 200°C to evaporate until the dryness. Then 0.5 ml HNO_3 was added into the beaker and evaporated to dryness. Another 0.5 ml HNO_3 was added and evaporated to dryness. The beaker was put back inside the steel jackets (bomb) after another 5 ml HNO_3 was added. The bomb was tightly sealed and kept on hot plate at 130°C for 3 hours. Then, the sample was transferred into clean beaker and the final dilution was made to 50 ml using 18M Mili-Q water. The instrument is Thermo Scientific X series^{II} ICP-MS. The reproducibility of elemental concentrations assessed by triple runs of the same solution during an analysis period.

2.4. Zircon U-Pb geochronology

About 100-150 zircon grains for each of the studied samples were mounted in an epoxy resin disc and then grinded/polished to expose the zircon interiors for imaging and analysis. All the polished

zircon grains were photographed under transmitted- and reflected-light, and further examined using cathodoluminescence (CL) images prior to the U-Pb analyses. Laser ablation ICP-MS zircon U-Pb analysis was carried on an Agilent 7500 ICP-MS instrument equipped with a GeoLas 2005 at China University of Geosciences, Wuhan. Detailed operating conditions for the laser ablation system and ICP-MS instrument and data reduction are the same as described by Liu et al. (2008). Zircon 91500 was used as the external standard and ran twice every 5 samples. Standard silicate glass NIST610 was used to optimize the instrument. Beam diameter was 30 μm. Common Pb was corrected by ComPbCorr#3_17 (Andersen, 2002). Age calculations and Concordia plots were made using isoplot (Ludwig, 2003).

2.5. Zircon *in situ* Hf isotope-LA-ICP-MS

Zircon *in situ* Hf isotopes were conducted for samples from the Qilian Block and Kekeli batholiths. Some zircons have obvious cores and some of them show complex internal growth domains, it is important to have the ages and Hf isotopes analysed within the same and adjacent spots. We selected zircons with <10% discordancy between $^{207}Pb/^{235}U$ and $^{206}Pb/^{238}U$, the ages and Hf isotopic compositions are thought to record largely or entirely magmatic events, with the zircons with >10% discordancy (not analyzed for Hf isotopes) reflecting either inherited components, Pb loss, or metamorphic overgrowth.

Samples collected in 2009 with "QL09" initials in their names were analysed using a Nu Plasma HR MC-ICP-MS equipped with a GeoLas 2005 laser-ablation system, with a spot size of 44 μm and a repetition rate of 10 Hz, at the State Key Laboratory of Continental Dynamics, Northwest University in Xi'an, China. The detailed analytical technique was described by Yuan et al. (2004). High-purity argon (99.9995%) and high-purity helium (99.9995%) were used as the carrier gas to enhance the efficiency of the aerosol transport. Raw count rates for ^{172}Yb, ^{173}Yb, ^{175}Lu, ^{176}(Hf+Yb+Lu), ^{177}Hf, ^{178}Hf, ^{179}Hf, ^{180}Hf and ^{182}W were collected and isobaric interference corrections was made for ^{176}Hf. $^{179}Hf/^{177}Hf$ ratio was applied to calculate the mass fractionation of Hf (βHf), the

^{175}Lu signal was used to calculate the interference of ^{176}Lu on ^{176}Hf, and ^{173}Yb–^{172}Yb–^{171}Yb was applied to calculate both βYb and the interference of ^{176}Yb on ^{176}Hf. A ^{176}Yb/^{172}Yb of 0.5887 and mean βYb on the same spot were applied for the interference correction of ^{176}Yb on ^{176} Hf. ^{176}Hf/^{177}Hf and ^{176}Lu/^{177}Hf ratios of the standard zircon (91500) were 0.282294±15 (2σ, n =38 and 0.00031(2σ, n =30),. 91500, MON-1 and GJ-1 standard zircons were run during of analyses and gave ^{176}Hf/^{177}Hf ratios of 0.282295 ±0.000007) and 282013 ±0.000009 respectively. Interference of ^{176}Lu on^{177}Hf was corrected by measuring the intensity of an interference-free ^{175}Lu isotope and using a recommended ^{176}Lu/^{175}Lu ratio of 0.02669 to results of the samples.

Samples collected in 2010 with "QL10" initials in their names were analyzed using the Neptune multicollector (MC) ICP-MS, equipped with a 193 nm laser, at the Institute of Geology and Geophysics, Chinese Academy of Sciences in Beijing, China. The analytical technique was described by Wu et al., (2006).

2.6. Whole rock Sr-Nd-Pb-Hf isotopes

Whole rock Sr-Nd-Pb-Hf isotope ratios were determined using a PIMMS (Plasma Ionisation Multicollector Mass Spectrometry) ThermoElectron Neptune instrument at the Arthur Holmes Isotope Geology Laboratory (AHIGL), Durham University. Water used throughout the procedure was Milli-Q water (~18.3 MΩ m^{-1}) for diluting acids and as a reagent. All dissolutions were undertaken in laminar flow fume hoods and in Teflon beakers. The standard data, blanks and repeated Nd isotope analyses throughout this study are given in Appendices B-E.

2.6.1. Dissolution procedure

~100 mg of sample is required for the whole rock Sr-Nd-Pb-Hf analyses. The USGS reference standards were BHVO-1 and BIR-1. Each batch contains 16-18 samples, 1~2 standards and 1~2 chemical blanks.

1. Weigh out ~ 0.1 g of sample and BHVO-1 and ~ 0.5 g of BIR-1 into a clean 7 ml Teflon beakers.

2. Add 3 ml TD 29N HF and 1 ml TD 16N HNO3. Place on hotplate in a hotplate overnight at 100 °C.

3. Dry down solution to a paste at 100 °C.

4. Add 1 ml TD 16N HNO_3 to re-dissolve. Leave on hotplate overnight at 100 °C.

5. Dry down solution to a paste at 100 °C.

6. Add 1 ml TD 16N HNO_3 and dry down completely.

7. Add 0.5ml TD 3N HNO_3 and leave on hotplate at 40 °C to dissolve the samples.

8. Transfer solution to 1.5 ml microcentrifuge tubes pre-rinsed with 3N TD HNO_3. Centrifuge at 13000 rpm for 15 minutes. Any insoluble precipitates will form a solid mass at the base of the tube.

2.6.2. Sr-Spec column chemistry for collecting Nd-Hf, Sr and Pb fractions---Sr and Pb is ready in this step

Column (1000 µl pipette tips**) set up:**

1. Rinse with 1 CV (column volume) of MQ H_2O.

2. Rinse with 1 CV of TD 6N HCl.

3. Rinse with 1 CV (column volume) of MQ H_2O.

4. Load ~60 µl Sr-spec resin as a slurry in MQ H_2O. Ensure column is free of air bubbles in and around the frit.

5. Elute 1 CV TD 6N HCl.

6. Elute 2 CV MQ H_2O.

7. Precondition resin with 200 µl TD 3N HNO_3.

Elution Procedure:

1. sample loading: 100~ 500 µl TD 3N HNO_3 from 500 µl microcentrifuge tube using 2 x200 µl pipette – **do not** disturb the solid precipitates, collect in clean 7 ml Teflon beaker.

2. Hf-Nd collection: Add 2x 250 µl TD 3N HNO_3, collected to Nd-Hf fraction beaker.

3. Sr collection: Add 2x 200 µl MQ H2O and collect Sr fraction to the Sr fraction micro-tubes (rinsed with 6N HCl).

4. waste elution: Elute 2x100 µl TD 2.5N HCl, not collecte.

5. Elute 2×50 µl TD 8N HCl, collected to Pb fraction in micro-tubes.

Finish: Dispose of column by wrapping it carefully in cling film so that the dry resin will not become airborne.

Dry Sr and Pb fractions down on hotplate at 80 °C.

2.6.3. Column chemistry for collections of Hf and Nd

2.6.3.1. Sample preparation

Dry collected Nd-Hf fractions on the hotplate at 100°C.

Dissolve in 1 ml 1N TD HCl on hotplate at 100°C.

2.6.3.2. Nd and Hf cation column procedure—Nd fraction is ready in this step

Note: unless stated, collect to waste beakers.

Pre-procedure cleaning

1. Wash Nd-Hf cation column tips with 6N HCl.

2. Rinse with 5 mls TD 29N HF.

3. Rinse with 10 mls MQ H_2O.

4. Rinse with 10 mls 6N TD HCl.

5. Rinse with 10 mls MQ H_2O.

6. preconditioning with 10 mls TD 1N HF – 1N HCl.

Hf and Nd elution procedure

1. sample loading: 1 ml TD 1N HCl, collect

2. Hf collection: Elute 3 mls TD 1N HF– 1N HCl

3. waste elution: Elute 14 mls TD 2.5N HCl

4. Ba elution: 10mls TD 2N HNO_3.

5. Nd collection: Elute 12mls TD 6N HCl.

Nd-Hf column cleaning

1. Wash column tips with 5mls TD 29N HF.

2. Rinse with 10 mls MQ H_2O

3. Rinse with 10 mls 6N TD HCl.

2.6.3.3. Hf column chemistry—Hf fraction is ready in this step

Hf elution procedure

Sample Loading: 1ml 0.52N H_2SO_4-5%H_2O_2, not collected

Ti elution: 5ml 0.52N H_2SO_4-5%H_2O_2, not collected

Ti elution: 5ml 0.52N H_2SO_4-5%H_2O_2, not collected, elute until the yellow color is gone.

Hf collection: 4 ml TD 1N HF-2N HCl, collected

Hf column cleaning

1, 5ml TD 29N HF

2, 5ml MQ H_2O

3, 4ml 12N H_2SO_4

4, 5ml MQ H_2O

Precondition the column with 5ml H_2SO_4-5%H_2O for next batch.

2.6.4. Beak cleaning

1. Remove any labels with ethanol.

2. Rinse beakers and lids with MQ H_2O.

3. Wipe inside of beaker with micropure wipe to dislodge any remnant material.

4. Fill beaker to a depth of 1 cm with ANALAR HCl. Rotate beaker to dispatch HCl around the beaker and discard.

5. Fill to a depth of 0.5 cm with 29N HF (used HF stock from step 14) and leave on hotplate at 90 °C for 24 hours.

6. Remove from hotplate and leave to cool for 30 minutes -1 hour.

7. Remove HF and rinse beaker with MQ H_2O.

8. Immerse beakers in 900 ml of 90% MQ H_2O – 10% 16N HNO_3 for 24 hours at 100 °C.

9. Remove beakers from acid and rinse twice with MQ H_2O.

10. Immerse beakers in 1 litre of MQ H_2O for 24 hours at 60-100 °C.

11. Remove beakers from MQ H_2O and rinse thoroughly with MQ H_2O.

12. Fill beakers to a depth of 0.5 cm, cap, and place on hotplate overnight at 100 °C.

13. Remove from hotplate and leave to cool for 30 minutes -1 hour.

14. Discard HF and rinse with MQ H_2O.

15. Leave beakers and lids to dry upside down on micropure wipe.

16. Beakers cleaned and ready for use.

2.7. References

Andersen, T., 2002. Correction of common lead in U–Pb analyses that do not report 204Pb. Chemical Geology, 192, 59–79.

Li, X.L., Chen, X., Ge, H. J., Wu, Y.T., Xian, X.L., Han, W., 2011. XRF determination of chlorine etc multi-elements in sea sediments with sample preparation by fusion. Physical Testing and Chemical Analysis Part B: Chemical Analysis 47 (12), 1420-1423 (in Chinese with English abstract).

Liu, Y.S., Hu, Z.C., Gao, S., Gunther, D., Xu, J., Gao, C.G., Chen, H.H., 2008. *In situ* analysis of major and trace elements of anhydrous minerals by LA-ICP-MS without applying an internal standard. Chemical Geology 257 (1-2), 34-43.

Ludwig, K.R., 2003. A geochronological toolkit for microsoft excel. Isoplot, 3, 1-70.

Wu, F.-Y., Yang, Y.-H., Xie, L.-W., Yang, J.-H., Xu, P., 2006, Hf isotopic compositions of the standard zircons and baddeleyites used in U-Pb geochronology: Chemical Geology, 234, 105–126.

Yuan, H.L., Gao, S., Liu, X.M., Li, H.M., Gunther, D., Wu, F.-Y., 2004, Accurate U-Pb age and trace element determinations of zircon by laser ablation–inductively coupled plasma mass spectrometry: Geostandards and Geo-analytical Research, 28, 353–370.

Chapter 3: Granitoids and their enclaves from the East Kunlun Orogenic Belt

3.1. Introduction

The Greater Tibetan Plateau is an ideal test ground as it records several continental collision events since the Early Paleozoic (Dewey et al., 1988, Harris et al., 1988a and Yin and Zhang, 1997), as indicated by a number of suture zones with associated syn-collisional granitoid batholiths increasingly younger from the northeast to southwest (Fig. 1A, Harris et al., 1988a). The East Kunlun Orogenic belt (EKOB) in the northern part of the Plateau, which includes abundant syn-collisional granitoids, is one of the largest continental collision zones. It is much older than the India-Asia collision (~ 250 Ma vs. ~ 55 Ma). The A'nyemaqen suture zone in the southern EKOB records the closure of the Paleo-Tethyan Ocean and a continental collision event (Yang et al., 1996 and Yang et al., 2009). The abundant late Permian to early Triassic granitoids along the EKOB have not been properly studied but only mentioned in regard to subduction/collision related (Harris et al., 1988a, Jiang et al., 1992 and Yin and Harrison, 2000) hybrids between mantle-derived melts and crustal materials (Luo et al., 2002, Deng et al., 2004, Chen et al., 2005 and Mo et al., 2007b). This interpretation is based on the observations that most EKOB intrusions are I-type granitoids containing mafic magmatic enclaves (MMEs, see definition by Barbarin, 2005) with the latter being considered as representing mantle-derived melts. The same age and overlapping radiogenic isotope compositions between the host granitoids and MMEs are considered as evidence for mixing and "homogenizing" processes (Liu et al., 2004a and Mo et al., 2007b) although it is physically not straightforward how the invoked mixing and "homogenizing" processes only 'homogenized' isotopes without affecting major element compositions.

Here we report major elements, trace elements and bulk-rock Sr-Nd-Pb-Hf isotopes and zircon U-Pb age data on granitoids and MMEs from the EKOB to constrain the petrogenesis of these rocks in the context of understanding the evolution of the EKOB, which also helps understand the evolution of the Paleo-Tethyan system and mechanisms of crust growth in response to continental collision.

3.2. Geological setting

3.2.1. Regional and local geology

The EKOB records a complex history of seafloor spreading, subduction and continental collision since the early Paleozoic (Jiang et al., 1992, Yang et al., 1996 and Yin and Harrison, 2000). It lies on the northern Tibetan Plateau with the Songpan-Ganzi Basin to the south and Qaidam Basin to the north (Fig. 1A), and can be subdivided into three tectonic zones according to the major faults (northern, middle and southern zones, see Fig. 1B, Jiang et al., 1992 and Yang et al., 1996).

3.2.1.1. Stratigraphy and metamorphic rocks in the EKOB

The basement is dominated by Precambrian granitic gneisses with minor Proterozoic granitoids and migmatites. It crops out in all the three zones overlain by early Paleozoic sedimentary rocks (Harris et al., 1988a, Jiang et al., 1992 and Yang et al., 1996) and is considered to have been emplaced between 1.8 Ga and 0.9 Ga (Mo et al., 2007b and references therein). The granitic gneiss represented by the Shaliuhe granitic gneiss in the north EKOB has a peak magmatic age of ~ 920 Ma (Chen et al., 2007c) and a metamorphic age of ~ 400–500 Ma (Zhang et al., 2003b and Chen et al., 2007c). Whole rock Sr–Nd–Pb and zircon *in situ* Hf isotope data indicate that its protolith is upper crustal sedimentary rocks of middle Proterozoic age (Harris et al., 1988a, Chen et al., 2007b and Chen et al., 2007c). The late Permian molasses and the angular unconformity between the upper-Permian to lower-Triassic marine strata and lower-Permian terrestrial strata have been recognized in the Paleozoic–Mesozoic sedimentary cover (Jiang et al., 1992, Zhang et al., 2004 and Li et al., 2008), indicating a continental uplift event during that time.

Some ophiolites (Yang et al., 1995 and Yang et al., 1996) are exposed along the central Kunlun fault (CKLF) and Kunlun Fault (Fig. 3.1C), especially in the southern zone, named the A'nyemaqen ophiolite belt. The most precise zircon U–Pb age on these ophiolites within the southern zone is reported for the Dur'ngoi ophiolitic basalt, which is ~ 308 Ma (Yang et al., 2009).

3.2.1.2. East Kunlun Batholiths (EK batholiths)

The EKOB contains one of the two largest granitic batholiths on the Greater Tibetan–Plateau (the other being the Gangdese belt in Southern Tibet). The 'Kunlun Batholiths' (Jiang et al., 1992 and Mo et al., 2007b) cover 48,400 km^2, cropping out mostly in the EKOB middle zone (Fig. 3.1C). The batholiths are mainly monzonite and granodiorite in composition with ages ranging from the Proterozoic to the late Mesozoic (Jiang et al., 1992). The Proterozoic granitoids are part of the Precambrian basement. Early Paleozoic granitoids (400–500 Ma) have been interpreted as resulting from subduction–collision events comparable to that which produced magmatism in the Qilian orogenic belt to the north (Mo et al., 2007b). The granitoids of Late Permian–Early Triassic (P–T) age are dominant in the EKOB with an area of 23,000 km^2 (Liu et al., 2004a), almost half of the entire batholiths (Mo et al., 2007b). Previous studies indicate that the P–T granitoids are calc-alkaline and formed during the major subduction-related orogenic period (240– 260 Ma) (Harris et al., 1988b, Yin and Harrison, 2000 and Mo et al., 2007b). Minor mid-late Mesozoic granitoids are also present which might be related to the post-collisional magmatism (Jiang et al., 1992 and Mo et al., 2007b). The crystallization ages of P–T granitoids have been determined reliably, yet the origin and petrogenesis of the giant batholiths remains poorly understood. For example, what tectonic setting were they emplaced in during a relatively short time period?

We collected 30 representative samples from 14 locations (GPS data are given in Table 3.1) around south Dulan and southwest Qinghai Lake (Fig. 3.1C). The granitoids contain abundant MMEs (Fig. 3.2A), and thus are ideal to test our hypothesis on the origin of these MMEs in the context of the granitoid petrogenesis. Duplicate samples from some host rocks and MMEs were collected on a meter/centimeter scale in order to look into the potential heterogeneity.

3.2.2. Petrography

The granitoids are mainly granodioritic in nature with minor granitic and dioritic compositions. They are medium to coarse-grained with equigranular textures. The mineralogy is relatively simple, and is dominated by quartz (Qz, 45–35%), plagioclase (Pl, 35–45%), K-feldspar (Kfs, 5–10%), biotite (Bt, 5%) and minor amphibole (Amp, 2–5%) (Fig. 3.2C). Accessory minerals include apatite, zircon, and Fe–Ti oxides. The fine grained MMEs are mafic diorite to diorite in composition (Figs. 3.2D and 3.3) with oval shapes and varying sizes (Fig. 3.2A, B). An important observation is that the MMEs have the same mineralogy as the granitoid hosts with higher modes of the mafic minerals such as Amp (30–45%) and Bt (5–10%) (Fig. 3.2D). No crystal resorption textures and reactive overgrowths have been observed (Fig. 3.2D).

3.3. Analytical results

30 samples (17 granitoid hosts and 13 MMEs including 10 host-MME pairs; Table 1) were analysed for major and trace elements. Thirteen samples (including 6 enclaves) were extracted for zircons. Seventeen samples (including 7 enclaves) were analysed for whole rock Sr-Nd-Pb-Hf isotopic compositions.

3.3.1. Major and trace elements

Host granitoids are more silicious than the contained MMEs (Fig. 3.3). All of them are calc-alkaline (Fig. 3.3) and metaluminous (A/CNK < 1.1, Table 3.2). Three MME samples chemically fall into the gabbro field (Fig. 3.3), but they are Amp-rich mafic-diorites with no pyroxene present.

Host rocks and MMEs define good linear trends for most elements on Harker diagrams (Fig. 3.4). TiO_2, Al_2O_3, FeO, MnO, MgO, CaO, Eu and Yb exhibit well defined negative trends, which likely reflect the fractionation of Amp, Bt and Pl.

Both MMEs and granitoid hosts have an enriched LREE and flat HREE profile lacking a garnet signature (no depletion of HREEs) (Fig. 3.5A, B). The average compositions of the granitoid hosts

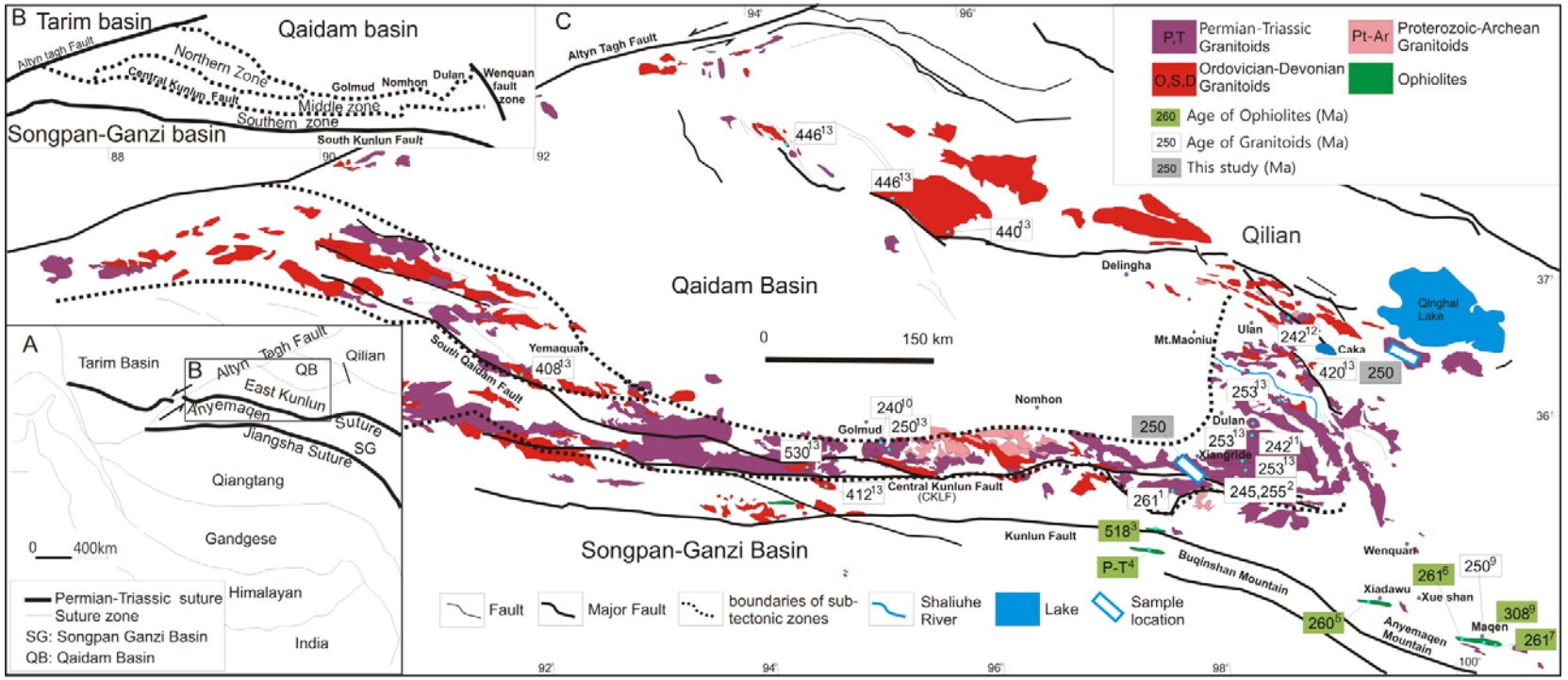

Fig. 3.1. A, Schematic map showing major tectonic units of West China. B, Schematic map showing three sub-tectonic zones of the East Kun Orogenic Belt (EKOB; after Jiang et al., 1992). C, Simplified geological map of the East Kunlun Orogenic Belt and the adjacent Qaidam Basin region showing the distribution of granitoids and ophiolites (after Pan et al., 2004). 1: Naomuhun Pluton, 261 Ma (Xiong et al., 2011). 2: Yuegelu Pluton, 243 ~ 256 Ma (Liu et al., 2004b); Halagetu Pluton: 255 Ma (Sun et al., 2009). 3-4 data is from Yang et al., (1996). 3: Qingshuiquan Ophiolite, 518 Ma (Zircon U-Pb). 4: Buqingshan Ophiolite: poorly dated, maybe late Permian to early Triassic. 5: Xiadawu Ophiolite, 260 Ma (Rb-Sr), (Jiang et al., 1992). 6-8 data is from Yang et al., (1996). 6: Majixueshan Ophiolite, Volcanic rocks: 260 Ma (Rb-Sr). 7: Maqen Ophiolite: poorly dated, maybe late Permian to early Triassic. 8: Wanbaogou Ophiolite: poorly dated, maybe late Permian to early Triassic. 9: Dur'ngoi Ophiolite, 308 Ma (Zircon U-Pb) (Yang et al., 2009a). 10, Deqia granitic complex, 250 Ma (Zircon U-Pb) (Yang et al., 2005). 11: Golmud East, Granodiorite, 240±6 Ma (Zircon U-Pb) (Harris et al., 1988a). 12, Xiangride Pluton, 242 Ma, compilation after Chen et al., (2007b). 12, Chahannuo Pluton, 242 Ma, compilation after Chen et al., (2007b). 13, data from compilation of Chen et al., (2011).

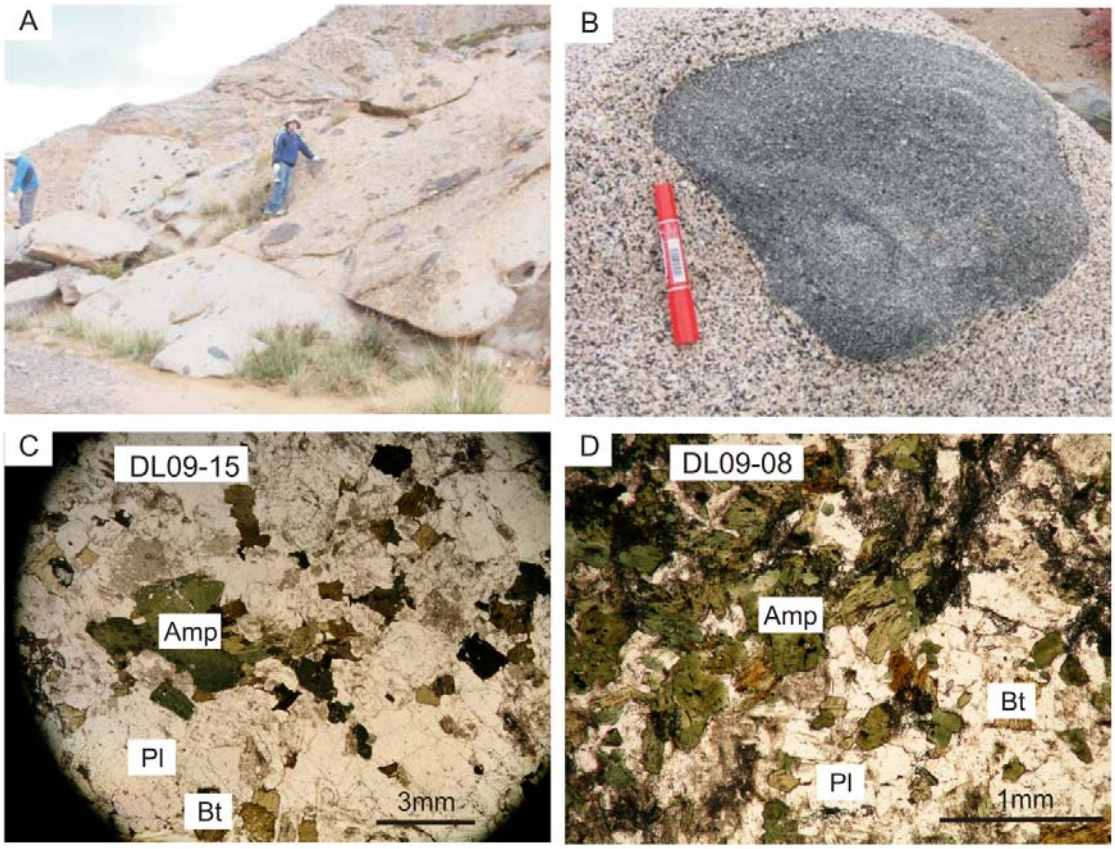

Fig. 3.2. Field photos in the Dulan area (A-B) and photomicrographs under plane polarized light of the representative granitoid host rock (C) and enclaves (MME) (D).

display apparent similarity to the bulk continental crust (BCC) composition in terms of all the analyzed elements and key elemental ratios (Fig. 3.5C, D) except for the lower Cr, Co, Ni, Sc and Mg in granitoids from the EKOB (Fig. 3.5C). The lower concentrations of Ni, Cr and Mg relative to the calculated modal BCC composition are typical for normal andesites (vs. high Mg andesites) and fully discussed by Niu and co-authors (Mo et al., 2008, Niu and O'Hara, 2009 and Niu et al., 2013). The slightly higher Th/U in the hosts compared to BCC (Fig. 3.5D) may be inherited from the Paleo-Tethyan MORB (see below) as it has a distinctly higher $^{208}Pb/^{204}Pb$ at a given $^{206}Pb/^{204}Pb$ compared to other MORB (Xu et al., 2002). MMEs display higher abundances of HREEs (Fig. 3.5A), reflecting their greater

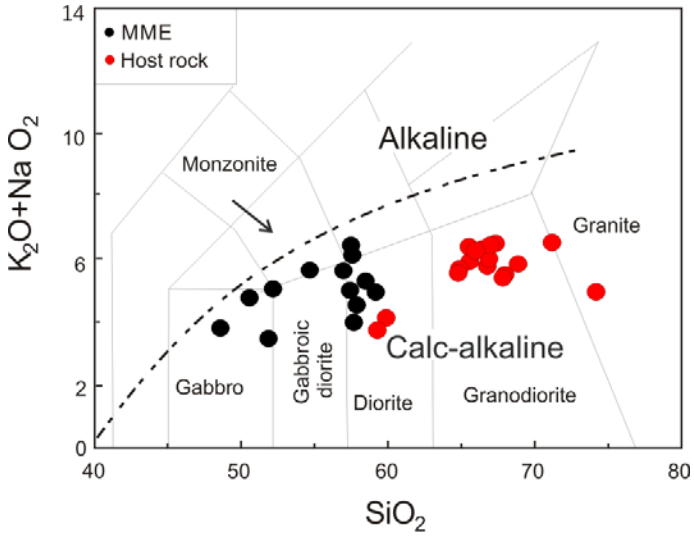

Fig. 3.3. Total alkalis (Na_2O+K_2O) versus SiO_2 (TAS) diagram showing the compositional variation of EKOB samples. The MMEs are generally less felsic than the hosts. Three samples in the gabbro field are actually mafic-diorite without pyroxene. All the samples are calc-alkaline. The dashed line represents the division between Alkaline and Cal-alkaline fields (Irvine and Baragar, 1971).

proportions of mafic minerals (e.g., Amp and Bt). The Nb/Ta ratios are all sub-chondritic (chondritic value of 17.5, Sun and McDonough, 1989), 11.84 for host rocks and 13.07 for enclaves. The slightly higher Nb/Ta ratios for enclaves are consistent with higher modal Amp which has super-chondritic Nb/Ta ratios (Foley et al., 2000) as elaborated by Niu and O'Hara (2009). The Sr/Sr* ($Sr/Sr^* = 2 \times Sr_N / [Pr_N + Nd_N]$) and Eu/Eu* ($Eu/Eu^* = 2 \times Eu_{PM} / [Sm_{PM} + Gd_{PM}]$) for host rocks are 0.78 and 0.84, respectively. The MMEs have slightly lower Sr/Sr* (0.48) and Eu/Eu* (0.67) due to a lesser amount of plagioclase. It is important to note that the sub-chondritic Nb/Ta ratios, Nb–Ta–Ti depletion and slight Sr–Eu depletions of these samples are identical to those of the BCC (Fig. 3.5D) (also see Niu and O'Hara, 2009).

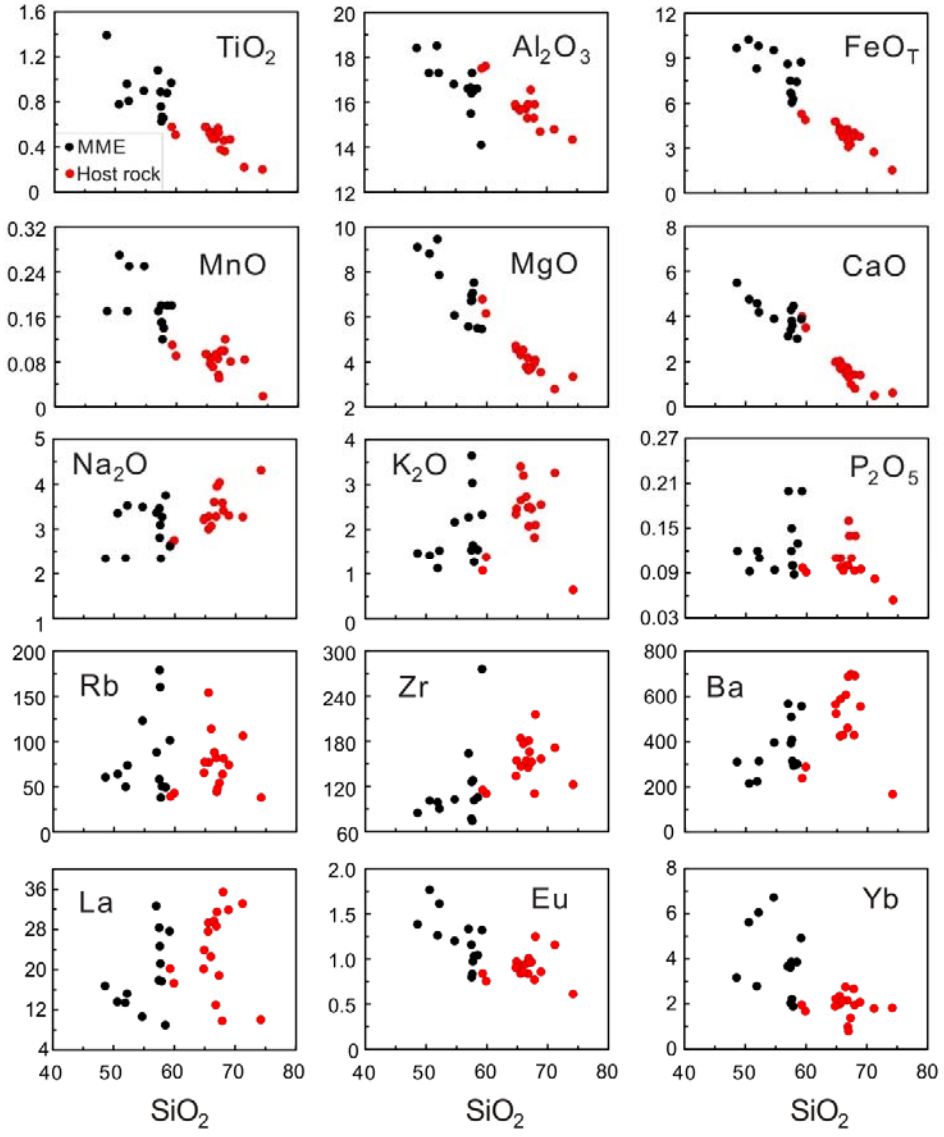

Fig. 3.4. SiO_2 variation diagrams of representative elements of the EKOB samples, showing fractional crystallization dominated trends.

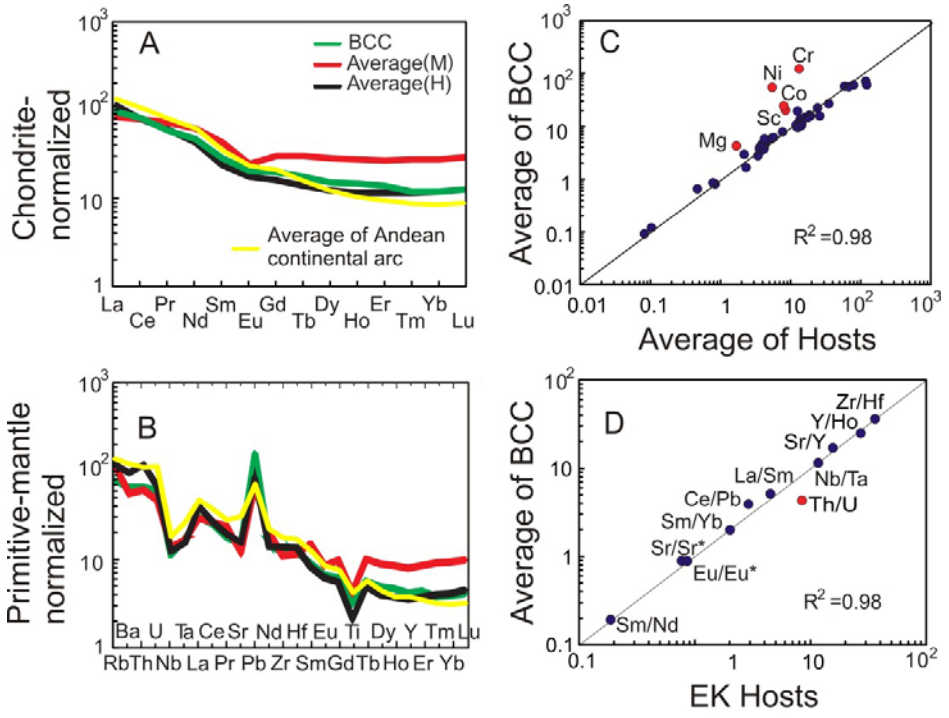

Fig. 3.5. A, Chondrite-normalized (Sun and McDonough, 1989) rare earth elements (REE) patterns for average compositions of the EKOB granitoid hosts (H) and mafic magmatic enclaves (MME, M). Bulk continental crust (BCC; Rudnick and Gao, 2003) and average of Andean continental arc (yellow line, data from http://georoc.mpch-mainz.gwdg.de/georoc/, basaltic andesitic to andesitic compositions) are also shown for comparison. Andean continental arc is remarkably similar to the BCC and our host rocks too. B, Primitive mantle-normalized (Sun and McDonough, 1989) multi-element patterns as in panel A. C, One-to-one plot to show the similarity between the granitoid hosts of the EKOB samples and the BCC in terms of the analyzed major and trace elements. D, Comparision between the granitoid hosts and the BCC in terms of key elemental ratios.

3.3.2. Zircon U-Pb Geochronology

Zircons from host rocks are on average ~ 100–200 μm long, colorless and euhedral with good prisms and pyramid faces, and have small elongation ratio of 1:1 to 3:1. They are either uniform or have oscillatory zoning (Fig. 3.6). Some of them have inherited cores with magmatic overgrowth rims. The Th/U ratios are mostly within the range of 0.4–0.6. A few old inherited zircons with Th/U < 0.1 (Table 3.3) have discordant ages (Fig. 3.7). Zircons from MMEs are brown in color, show cracks under transmitted and reflected light, and are characterized by high length/width ratios

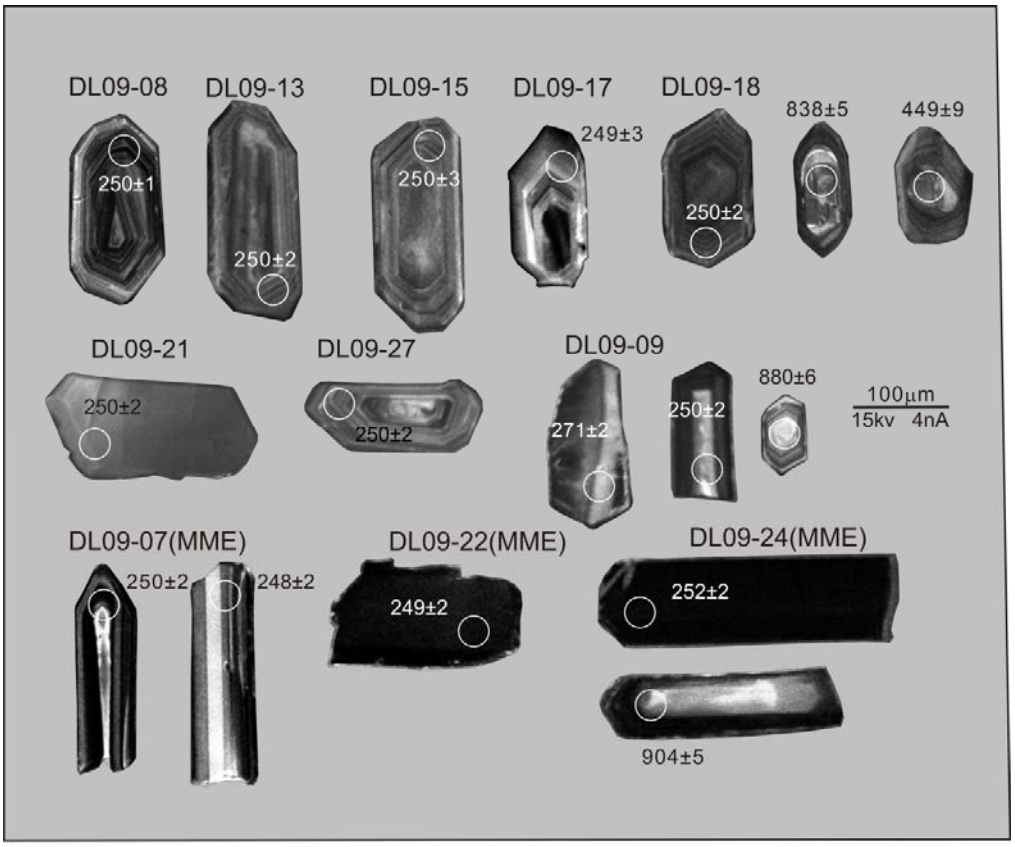

Fig. 3.6. Cathodoluminescence (CL) images of zircons from representative samples. White circles are the analyzed spots. The values with error are ages in Ma.

and straight rhythmic stripes (Fig. 3.6). Most zircons yield concordant or slightly discordant U–Pb ages. Zircon U–Pb ages of 7 granitoid hosts indicate that the intrusions were emplaced principally in the late Permian and early Triassic ~ 250 Ma (Fig. 3.7). All the 6 MMEs have an identical age to host rocks within error, i.e. ~ 250 Ma (Fig. 3.7). Inherited zircon cores which occur in both MMEs and host rocks, plot along or close to the Concordia, yielding age populations around 400–500 Ma and 800–1000 Ma (Fig. 3.6 and Fig. 3.7). These are identical respectively to the metamorphic and magmatic ages recorded in the Shaliuhe gneiss in the region (Zhang et al., 2003a, Meng et al., 2005b and Chen et al., 2007c).

3.3.3. Whole rock Sr-Nd-Pb-Hf isotopes

Whole rock Sr–Nd–Hf–Pb isotope data for 17 samples (including 7 MMEs) are given in Table 3.4, Table 3.5, Table 3.6 and Table 3.7 and plotted in Fig. 3.8, Fig. 3.9, Fig. 3.10 and Fig. 3.11. Contributions from mature continental crust are apparent as I_{Sr} and $Pb_{(i)}$ are radiogenic and all the $\varepsilon_{Nd}(t)$ values are slightly enriched (-5.3 to -2.1 for host rocks and -5.2 to -2.2 for MMEs). I_{Sr}, $Pb_{(i)}$, $\varepsilon_{Nd}(t)$ and $\varepsilon_{Hf}(t)$ refer to the age corrected values and ε_{Nd} and ε_{Hf} refer to the present-day values.

Theoretically, Hf and Nd isotopes are expected to correlate with each other (thus explaining the mantle array, Chauvel et al., 2008) because of the similar behavior of Lu–Hf and Sm–Nd systems during magmatism. However, it has been found that 'Nd' and 'Hf' can isotopically decouple in some circumstances (Bizimis et al., 2004, Schmitz et al., 2004 and Hoffmann et al., 2011). In our study, the majority of $\varepsilon_{Hf}(t)$values are positive (Table 3.6) indicating a significant mantle input, which is apparently inconsistent with the suggestion of negative $\varepsilon_{Nd(t)}$. Note that there are broad Lu/Hf vs. $^{176}Hf/^{177}Hf$ and Rb/Sr vs. $^{87}Sr/^{86}Sr$ correlations, but no Sm/Nd vs. $^{143}Nd/^{144}Nd$ correlation. This observation, combined with the decoupling between ε_{Nd} and ε_{Hf} could put Nd isotopic data quality into question. For this reason, we have randomly reanalyzed 5 samples for Nd isotopes and the reproducibility is good (< 66 ppm; Appendix D). The apparent non-correlation between Sm/Nd and $^{143}Nd/^{144}Nd$ can be explained by the small range in $^{147}Sm/^{144}Nd$ ratios among our samples and the long half-life of ^{147}Sm, which taken together prevent a statistically significant isochron developing in 250 Ma (Fig. 3.8C). On the contrary, the large Lu/Hf variation of up to 500% and the short half-life of ^{176}Lu explain the significant Lu/Hf psedochron.

Nevertheless, it is necessary to consider the potential effect of incomplete digestion of zircons in these samples. For example, our Teflon beaker digestion method for isotope analysis cannot digest zircons completely for the zircon-rich granitoid rocks we study. This can cause problems as > 95% Zr (see partition coefficients of Zr; Fujimaki, 1986) resides in zircons in zircon rich granitoids. If no zircons were dissolved during digestion and assuming all the Hf resides in zircons, the analyzed Hf

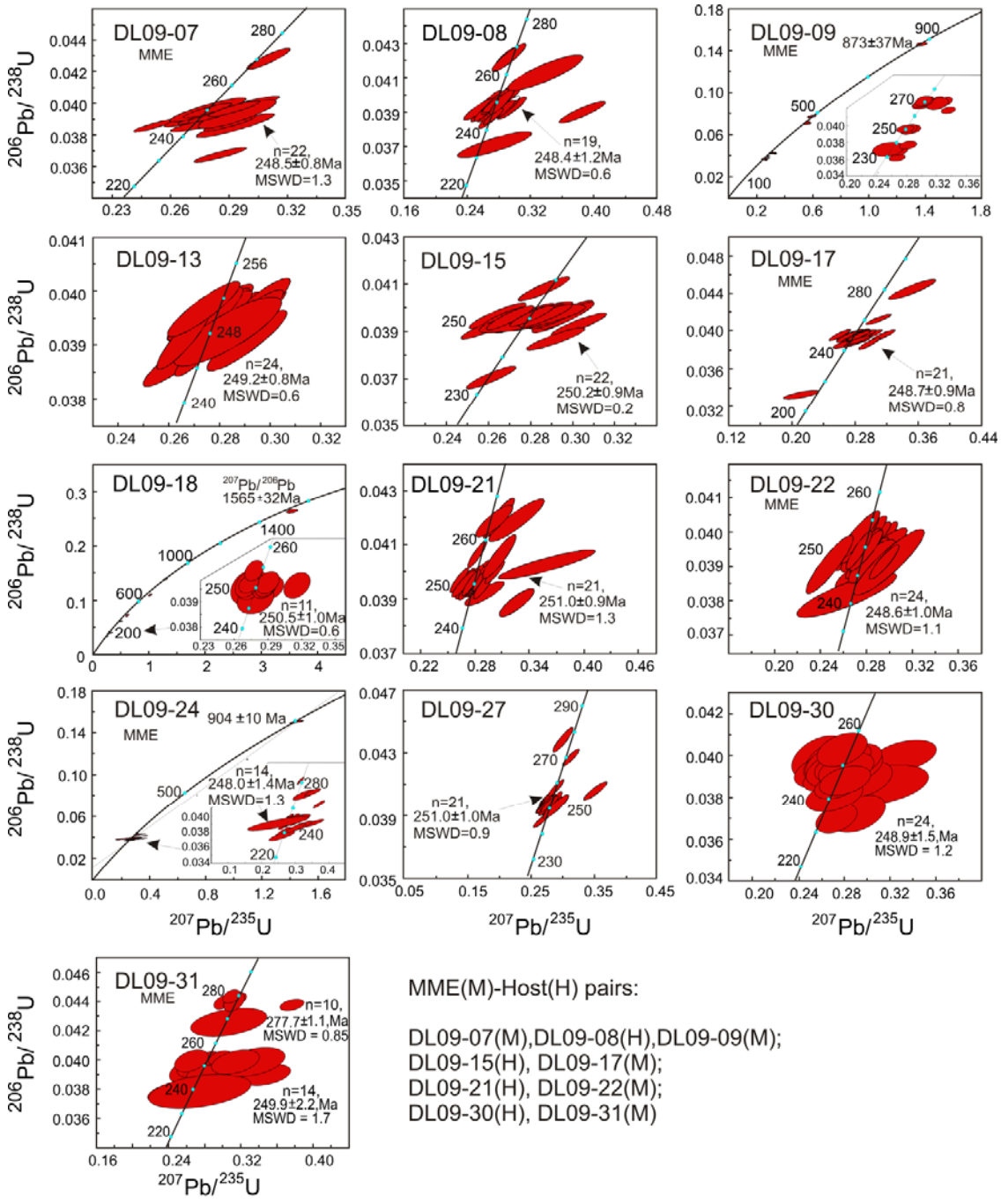

Fig. 3.7. Zircon U-Pb Concordia diagrams. The majority of zircons give ~ 250 Ma crystallization age for both granitoid hosts and the MMEs. Various amounts of inherited old zircons contained in hosts and enclaves indicate the presence and involvement of old crustal material.

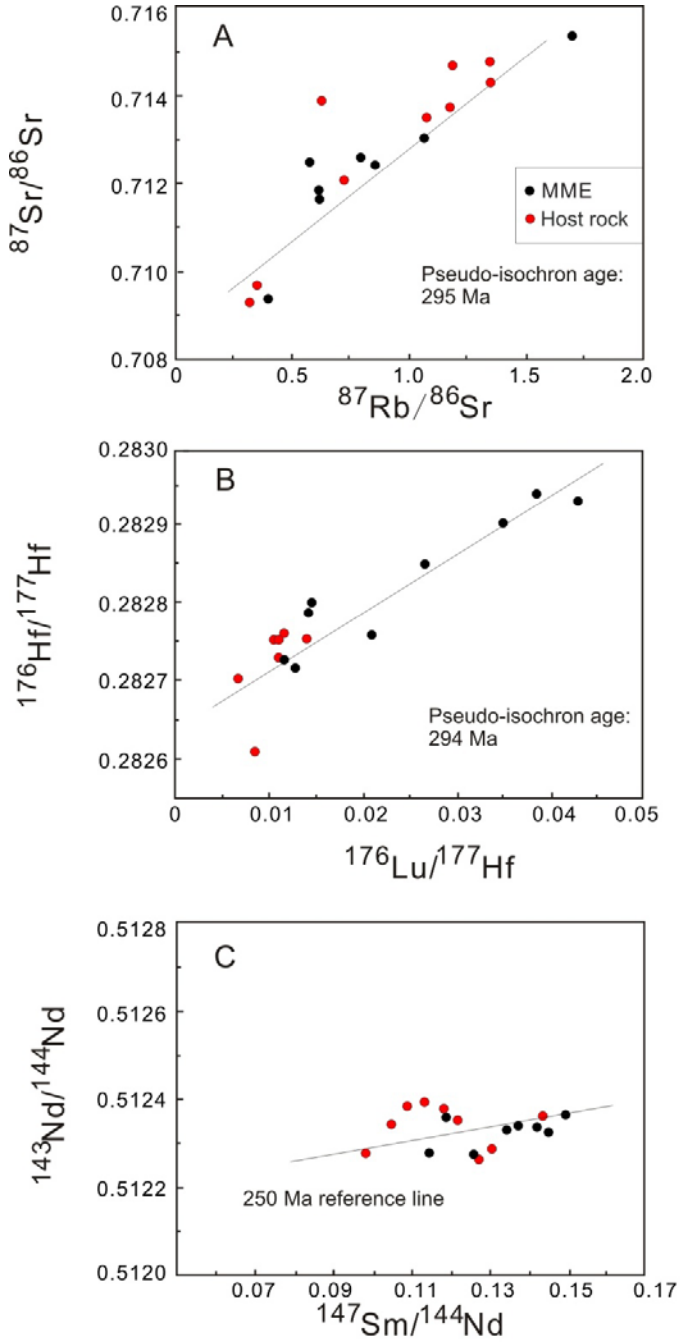

Fig. 3.8. A and B, Plots of isotope ratios vs. parent-daughter ratios, giving Rb/Sr pseudo-isochrone age of 295 Ma and Lu/Hf pseudo-icochron age of 294 Ma, which are close to the zircon *in situ* dating age of ~ 250 Ma of the EKOB granitoids. C, no correlation between $^{143}Nd/^{144}Nd$ and $^{147}Sm/^{144}Nd$. The 250 Ma reference line is shown to demonstrate the small ingrowth of radiogenic Nd isotopes.

must then be Lu decaying product in the non-zircon phases only (Fig. 3.8). However, this is unlikely to be the case for two reasons: firstly, the digestion using Teflon beakers is able to dissolve zircons to some extent, and thus the Hf hosted in the dissolved portions of zircons will enter the solution accordingly; secondly and importantly, the average size of zircons in the studied samples is 100–200 μm (Fig. 3.6), yet the rock powder particle size is ≤ 50 μm (mostly < 5 μm), i.e., the zircon fragments of ≤ 50 μm size in the solution must be well-exposed with enhanced surface areas, facilitating acid dissolution and digestion. This means that even if zircons may not be completely digested using our Hf-isotope procedure, significant portion of zircons must be digested and analyzed, with the obtained $^{176}Hf/^{177}Hf$ ratios likely approaching the bulk-rock ratios. This is demonstrated by the Lu/Hf pseudochron (Fig. 3.8B), where the $^{176}Lu/^{177}Hf$ ratio was obtained through ICP-MS trace element analysis of complete sample digestion (see above).

Therefore, the apparent decoupling of Nd isotope with Hf (and Sr) isotopes is significant, and the age-corrected initial Hf–Nd–Sr isotopic ratios can be reliably used to trace magma sources and processes.

3.4. Discussion

3.4.1. Isotope constraints on the formation of MMEs

I-type granitoids usually contain various amounts of MMEs (Holden et al., 1987 and Winter, 2010). The origin of the MMEs can hold clues to the petrogenesis of the entire granitoid–MME systems, yet the origin remains debated. For example, MMEs have been interpreted as restites (Chappell et al., 1987 and Chappell et al., 1999); as representing mantle derived melts (Barbarin, 2005, Mo et al., 2007b, Yang et al., 2007 and Clemens and Stevens, 2011); or as mafic cumulate (Wall et al., 1987, Dahlquist, 2002 and Niu et al., 2013). In the case of the EKOB, MMEs were interpreted to represent

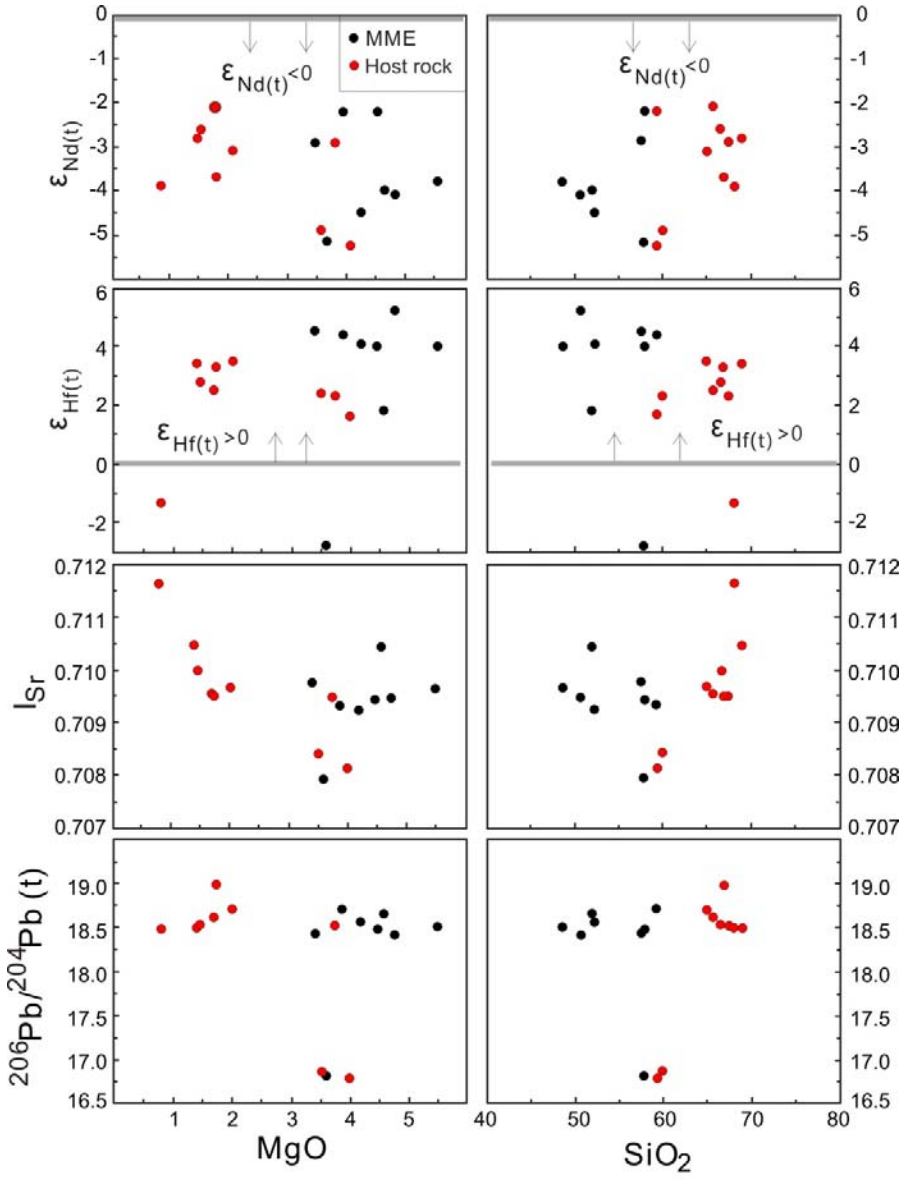

Fig. 3.9. Isotopes versus MgO and SiO_2 plots showing overlapping isotopes between MMEs with higher MgO/lower SiO_2 and the granitoid hosts with lower MgO/higher SiO_2. The negative $\varepsilon_{Nd}(t)$ values are suggestive of the crustal contribution while the dominant positive $\varepsilon_{Hf}(t)$ values are suggestive of mantle input.

mantle melts involved in magma mixing because of their mafic composition. Nevertheless, their negative $\varepsilon_{Nd(t)}$ and relatively radiogenic Sr and Pb isotopes (Liu et al., 2004b, Chen et al., 2011 and Xiong et al., 2011) are indistinguishable from those of the host rocks, arguing that if they

are indeed mantle melts, they must be derived from an unusually enriched mantle source (Liu et al., 2004b and Xiong et al., 2011).

It is not always straight forward to distinguish a cumulate process from a mixing process in terms of major and trace element data because both techniques can produce linear trends on Harker plots (Clemens and Stevens, 2011). In this case, isotopes are robust tools for distinguishing mantle derived magmas (MMEs) (which should be dominated by a mantle isotopic signature) from crustal melts (granitoid hosts) (which should be dominated by a crustal isotopic signature). For example, enclaves from Criffell and Strontian plutons in northern Britain consistently have higher $\varepsilon_{Nd(t)}$ than the adjacent hosts, representing the mixing process (Holden et al., 1987). Fig. 3.9 shows, however, that this is not the case in our study. MMEs do not have consistently higher $\varepsilon_{Nd(t)}$ or $\varepsilon_{Hf(t)}$ than their hosts (Fig. 3.10) but overlapping isotopic compositions and they do not show covariations with SiO_2 or MgO. Furthermore, even samples from the same host or the same enclave can have different initial isotopes, see ①, ②, ③ etc. in (Fig. 3.10). The completely overlapping initial isotopes between the host rocks and MMEs are indicative of their same origin. The initial isotopic ratio variations within individual outcrops or enclaves largely reflect small scale isotopic heterogeneity due to incomplete homogenization of melts affected by crustal assimilation or modal variation or both. This is because granitoid magmas under sub-liquidus conditions are "crystal mashes" and complete homogenization is restricted by the efficient diffusion (Ramos and Reid, 2005 and McLeod et al., 2012).

Some authors have invoked that homogenous mixing may have resulted in the overlapping Sr and Nd isotopes between MMEs and host rocks, by arguing that isotopes and trace elements diffuse faster than major elements (Mo et al., 2007b), however, this is unlikely. Indeed, elements diffuse on microscopic scales (Lesher, 1990, Allen, 1991 and Holden et al., 1991), but cannot explain macroscopic process on whole magma chamber scales with the large isotopic variations within

individual host rocks and MMEs. In contrast, the large variability within the individual host and MME indicates that the diffusion was rather limited. Several observations are indicative of

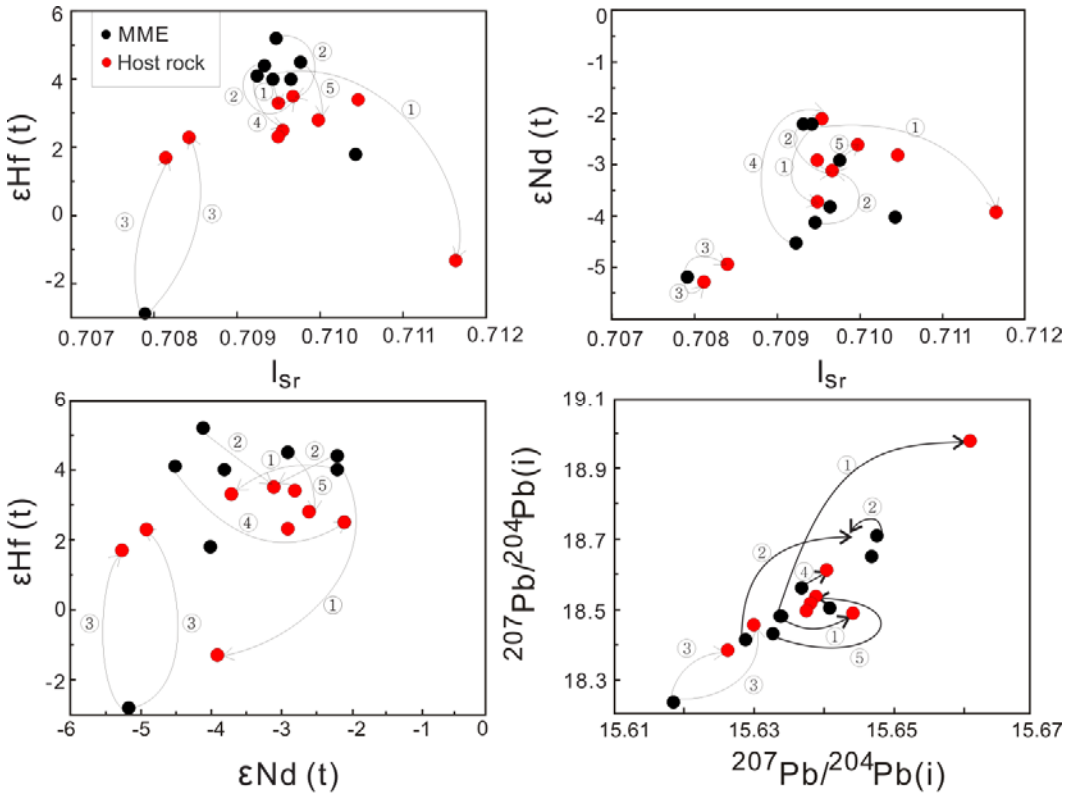

Fig. 3.10. Small scale age-corrected (250 Ma) isotope variation diagrams showing overlapping isotopes between the granitoid hosts and MMEs and isotopic variations within individual host and MME, which actually reflect magma heterogeneity (with some superimposed mineralogical differences) rather than mixing process. MME(M)-Host(H) pairs: ①:DL09-07(M), DL09-08(H), DL09-09(H) (two host rocks for the same MME); ②: DL09-15(H), DL09-16(M), DL09-17(M) (two enclaves for the same host rock); ③: DL09-30 (H), DL09-31 (M), DL09-32 (H) (two host rocks for the same enclaves). Others, ④: DL09-13(H), DL09-14(M); ⑤: DL09-21(H), DL09-22(M). H: host rock; M: MME.

cumulate origin for MMEs: (1) Mineralogically, the MMEs are the same as their hosts but differ in modal abundances (see Fig. 3.2); (2) the oval shapes and shared mineralogy imply that the MMEs were plastic and in thermal equilibrium with their hosts at the time of emplacement; (3) the coherent compositional trend on the Harker diagrams is more like liquid lines of descent (Fig. 3.4); (4) MMEs have higher abundances of HREEs than their respective host (Fig. S1); (5) importantly, the

MMEs and host rocks have overlapping and indistinguishable isotopes (Fig. 3.9 and Fig. 3.10). These all demonstrate that MMEs are disintegrated early liquidus mineral cumulate and then may have been disturbed by subsequent replenishment and induced magma convection in the magma chamber.

In this context, it is worth mentioning that some Sr–Nd–Pb isotope data reported for 'mafic veins' in granitoids from Yuegelu units in the EKOB have been considered as the mafic end-member during magma mixing (Liu et al., 2004b). However, these mafic veins also have the same mineralogy and same isotopes as both enclaves and hosts granitoids (Fig. 3.11). We consider these "mafic veins" to be large bodies of cumulate origin.

Magma mixing is a common process, and we do not intend to invalidate its role in the petrogenesis of the EK granitoids. However, our observations suggest that caution is necessary when invoking 'magma mixing' without a thorough consideration of the data.

3.4.2. **Geochemical constraints on the source**

Our Sr, Pb and Nd isotope data set is in agreement with previous results (Liu et al., 2004b) showing radiogenic Sr and Pb and slightly radiogenic Nd isotopes, which indicate possible contributions of continental crustal materials, whereas the notably positive $\varepsilon_{Hf}(t)$ values are indicative of juvenile crustal materials and argue for significant mantle input. As the crustal contamination during melt emplacement is inevitable, the $\varepsilon_{Hf}(t)$ values in the parental melt would thus have been underestimated and thus should be more positive pointing to even stronger mantle signatures. To produce large volumes of andesitic batholiths with mantle isotope signature, a basaltic source is required (Mo et al., 2008). In this case, oceanic crust is the most probable candidate because it can impart its inherited mantle isotopic signatures to the derivative melt (Niu, 2005, Tatsumi, 2006, Mo et al., 2008 and Niu and O'Hara, 2009). The subducted oceanic crust may be from the A'nyemaqen

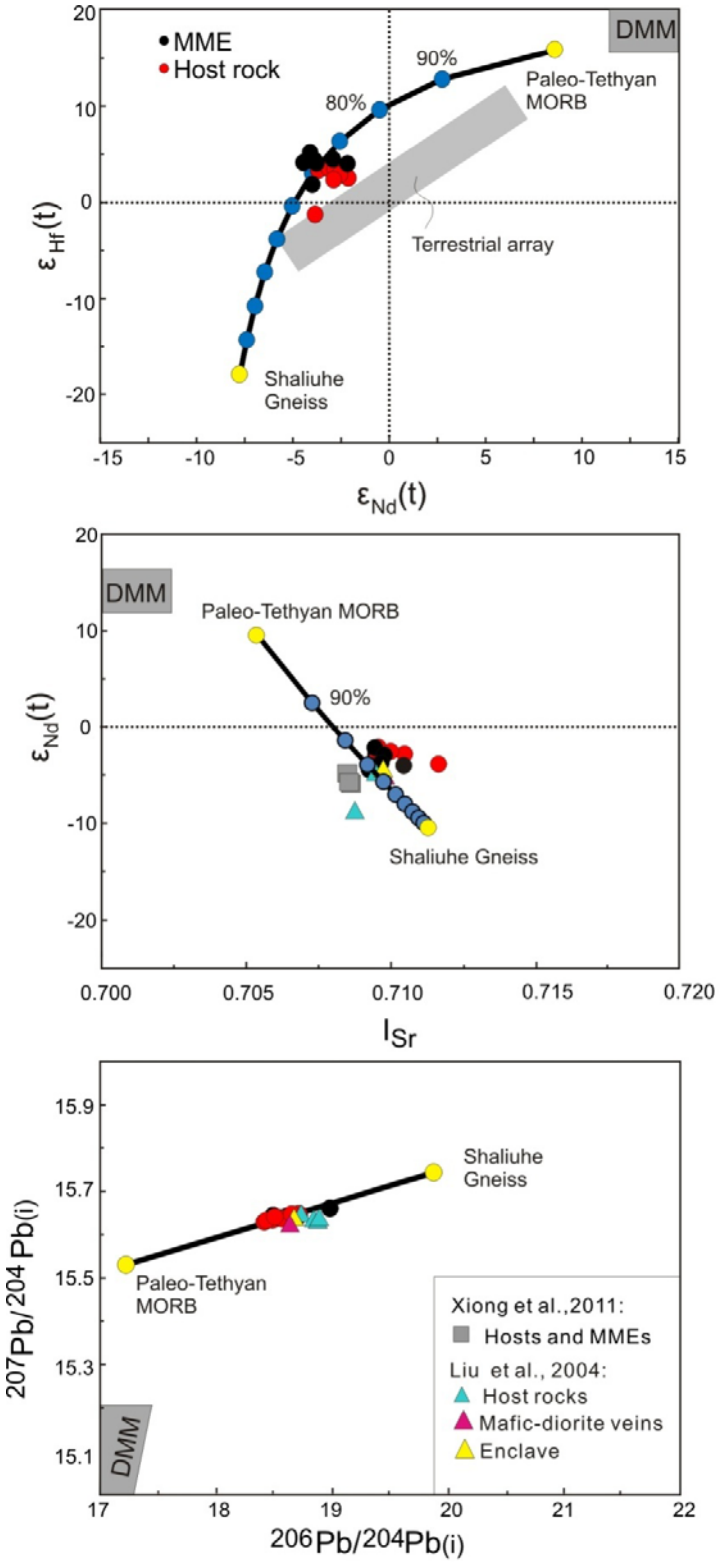

Fig. 3.11. Showing that the mafic enclaves (MME), host rocks in this study and mafic-diorite veins in the literature (Liu et al., 2004b; Xiong et al., 2011.) all have indistinguishable isotope compositions and they plot along an apparent 'mixing' trend between Paleo-Tethyan MORB and terrestrial sediments (the Shaliuhe gneiss). Terrestrial array is from Chauvel et al., (2008). Sr, Nd and Pb isotopes and elemental concentrations for Paleo-Tethyan MORB are from the east part of the northernmost branch of the Paleo-Tethyan realm ($^{87}Sr/^{86}Sr$:0.7055, $^{143}Nd/^{144}Nd$:0.51313, $^{206}Pb/^{204}Pb$: 17.257, $^{207}Pb/^{204}Pb$:15.532, Sr: 69.07ppm, Nd: 6.5ppm, Hf: 1.87ppm, Pb: 1.91ppm) (Xu et al., 2002). Hf isotope for MORB is inferred from Nd isotope following the equation ($\varepsilon_{Hf}=1.59\varepsilon_{Nd}+1.28$) given by (Chauvel et al., 2008) because of the statistically significant Hf-Nd isotope ratio correlation (Zindler and Hart, 1986). Sr isotope ($^{87}Sr/^{86}Sr$: 0.7180, Sr: 300ppm) for the Shaliuhe Gneiss is from Harris et al., (1988a). Nd and Pb isotope data ($^{143}Nd/^{144}Nd$:0.5121, $^{206}Pb/^{204}Pb$: 20.000, $^{207}Pb/^{204}Pb$:15.750, Nd: 33ppm, Pb: 19.50ppm) for the Shaliuhe Gneiss are from Chen et al., (2007b) and Meng et al., (2005a). Hf isotope data ($^{176}Hf/^{177}Hf$: 0.28218, Hf: 4ppm) for the Shaliuhe Gneiss are from Chen et al., (2007c). Grey Square: Host rocks and enclaves from (Xiong et al., 2011). Triangle: host rocks, enclaves and mafic veins from (Liu et al., 2004b)

Ocean, which is a branch of the Paleo-Tethyan that started opening around 308 Ma (Yang et al., 2009). The subducting/subducted materials comprise at least two chemically different components: altered basaltic oceanic crust and more silicic sediments (Tatsumi, 2006). The incompatible elements are depleted in the oceanic crust produced at ocean ridges but can be significantly enhanced through hydrothermal alteration and sea floor weathering especially with the involvement of terrigenous sediments of upper continental crust origin (Niu, 2005 and Niu and O'Hara, 2009).

In Fig. 3.11, the EKOB granitoid isotope data plot along an apparent "mixing" trend between the Paleo-Tethyan oceanic crust (represented by the 350 Ma ophiolitic MORB in Qinling, central China; Xu et al., 2002) and continental crustal compositions (terrigenous sediments represented by the Shaliuhe gneiss; Meng et al., 2005a). The high $\varepsilon_{Hf(t)}$ can be reasonably well modeled by melting of the Paleo-Tethyan MORB along with the subducting/subducted terrigenous sediments of Shaliuhe gneiss composition. The apparent decoupling between Nd and Hf isotopes is caused by the large difference in Nd/Hf ratios between the sediment and the oceanic crust which makes the mixing line highly curved and shift away from the terrestrial array (Fig. 3.11). In terms of Hf-isotopes, mass balance requires ~ 58–77% mantle contribution (i.e., the Paleo-Tethyan MORB), i.e., ~ 23–42% (Table 3.6) terrigenous sediments (i.e., the Shaliuhe gneiss); and requires ~ 60–74% mantle contribution in terms of Nd isotopes (Table 3.5). The Shaliuhe gneiss in the EKOB is dated at 920 Ma and has a metamorphic age of 400–500 Ma (Zhang et al., 2003b, Meng et al., 2005b and Chen et al., 2007a). The ~ 400–500 Ma granitoids are also present in the EKOB. These two time periods are consistent with the ages of inherited zircons, implying that they were both involved in the 250 Ma magmatism. Terrigenous sediments melted alongside oceanic crust also result in the isotope heterogeneity (see above) and radiogenic Sr and Pb isotopes. Despite the substantial proportion of mantle materials indicated by the isotopic compositions, the EKOB parental magmas were likely derived from partial melting of subducting oceanic crust rather than

ascending asthenospheric mantle as proposed by Luo et al. (2002). The latter would produce basaltic rather than granitoids melts.

3.4.3. Mechanism and conditions of Paleo-Tethyan oceanic crust melting

In the pioneering studies, the trace elements for 260–240 Ma intrusions in the EKOB indicate either a post-collisional setting or an active arc (Harris et al., 1988b). But Harris et al. (1988b) emphasized that the large long-lived magmatism required to produce such huge batholiths is more likely to occur in an active arc setting rather than a syn/post-collision setting (Harris et al., 1988b). It has been accepted since then that the period of 260–240 Ma is subduction-related. However, this interpretation did not carefully consider the stratigraphic records. The late Permian molasse (Jiang et al., 1992, Zhang et al., 2004 and Li et al., 2008) indicates that the onset of collision had happened at the late Permian. Also the angular unconformity between the upper-Permian to lower-Triassic marine strata and lower-Permian terrestrial strata in the EKOB (Jiang et al., 1992 and Li et al., 2008) represents a continental uplift event. Considering the strata records, the 260–240 Ma batholiths can be interpreted more precisely as syn-collisional intrusions. Furthermore, Mo et al. (2008) already demonstrated that syn-collisional magmatism is capable of producing volumetrically significant granitoid batholiths. Therefore, we argue that these granitoids were produced in a syn-collisional setting.

More and more geochemical and petrological observations have suggested that partial melting of subducted sediment/basalt is necessary (Kelemen et al., 2003 and references therein). Partial melting of subducted young, hot slab will produce high MgO andesites (Tatsumi, 2006) or ‘adakites’ (Castillo, 2006) rather than the andesitic granitoids with low MgO. Mo et al. (2008) offer a reasonable mechanism to address this issue. In their model, when the collision begins, the subducted slab evolves along a higher T/P geotherm (solid line with arrow in Fig. 3.12) due to the retarded underthrusting rate. This allows the slab to have longer time to approach thermal

equilibrium with the prior hot active continental margin (Fig. 3.13B, see below) and finally melt when the highly altered oceanic crust and sediments intersect the solidus of hydrous basaltic/granitic solidi under amphibolite facies conditions (Fig. 3.13C). The A'nyemaqen ocean started opening in the Carboniferous (Fig. 3.13A, Yang et al., 2009) and closed during the late Permian (Zhang et al., 2004) before the collision between Songpai-Ganzi (SG) and Qaidam (Fig. 3.13B). Abundant magmatism happened during the subduction-collision time (Harris et al., 1988a) establishing a warm active continental margin environment with a geotherm of probably > 20 °C/km (> 900 °C at depths of 45 km beneath an arc; Kelemen et al., 2003) before collision (Fig. 3.13B). Following the simple calculation by Mo et al. (2008), we can expect at least 40,000–55,000 km^3 andesitic rocks produced along the 1,000 km EKOB per Myr under the amphibolite-facies conditions (Fig. 3.12). It is important to note that partial melting must have taken place under the amphibolite-facies conditions because the granitoids have flat HREE

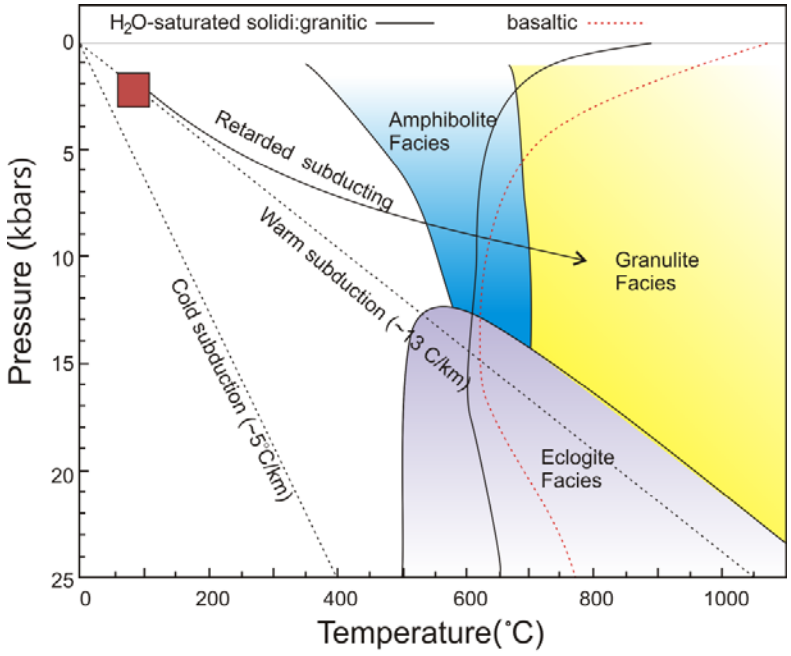

Fig. 3.12. Simplified phase diagram showing hydrous solidi of basalts and granitic rocks quoted from Mo et al. (2008; after Niu, 2005). The solid line with arrow illustrates the concept of the subducted oceanic crust (A'nyemaqen Ocean) evolve along a high T/P path as a result of retarded subducting and enhanced heating upon continental collision at a prior active continental margin setting.

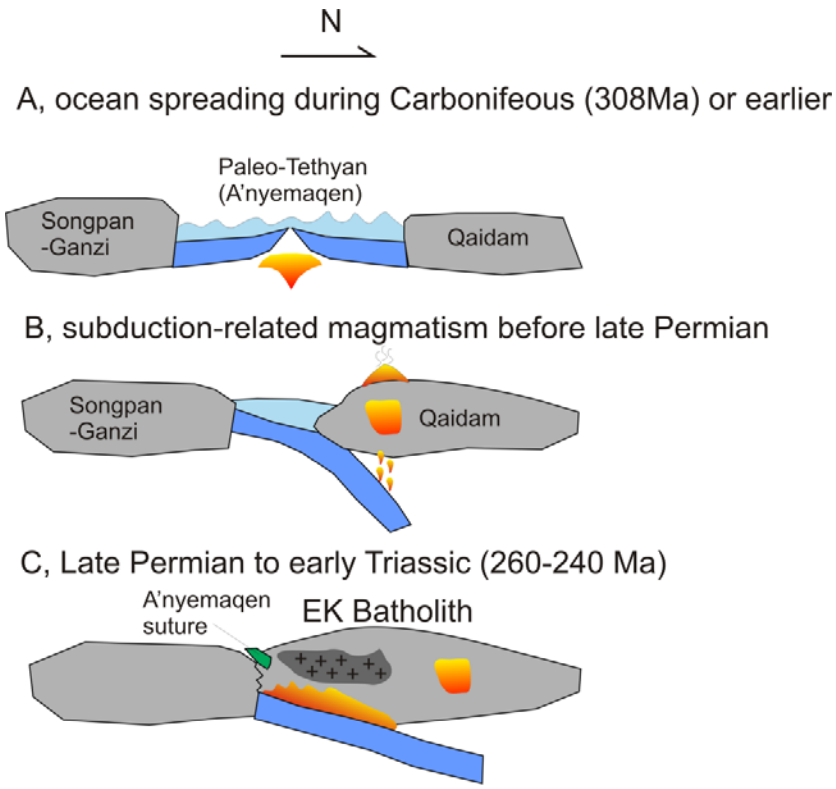

Fig. 3.13. Cartoons showing the A'nyemaqen seafloor spreading during the Carbonifeous time (A) (308 Ma: the protolith age of Dur'ngoi ophiolite (Yang et al., 2009a)), subduction of A'nyemaqen oceanic crust and related magmatism (B) and the syncollisional magmatism (C; See Figure 12 for mechanisms).

patterns (Figs. 3.5, S1) without a 'garnet signature' (Mo et al., 2008 and Wang et al., 2013). More evidence comes from zircon saturation temperature calculated from bulk rock compositions (Watson and Harrison, 1983) giving ~ 734 °C, similar to the Amp-Pl mineral thermometer ~ 737 °C (Xiong et al., 2011). This temperature is well above the wet solidus of basaltic rocks (the wet solidus is relevant because the subducting/subducted oceanic crust must have been hydrothermally altered and weathered on the seafloor) (Mo et al., 2008).

3.4.4. Continental crust growth in the collision zone

Studies of the Linzizong volcanic succession (LVS) in southern Tibet have demonstrated that juvenile continental crust is produced via partial melting of the 'trapped' oceanic crust under the amphibolite facies conditions and preserved as 'net crust growth' in the collision zones (Niu et al., 2007, Mo et al., 2008, Niu and O'Hara, 2009 and Niu et al., 2013). The syn-collisional Kunlun batholiths provide more geochemical and isotopic data to support this hypothesis. First of all, the bulk compositions of granitoids are similar to the bulk continental crust with almost identical sub-chondritic Nb/Ta, and Sr and Eu depletion (Fig. 3.5). Secondly, the whole rock Sr–Nd–Pb–Hf isotopes can be explained by partial melting of subducted Paleo-Tethyan MORB with 20%–40% terrigenous sediments of Shaliuhe gneiss composition in the melting region under the amphibolite-facies conditions (Fig. 3.11). Though the granitoids in the EKOB have relatively unradiogenic Nd isotope ($\varepsilon_{Nd(t)} < 0$) compared to the LVS, they have very positive $\varepsilon_{Hf(t)}$ values (up to 5.2), which is more convincing evidence that they are juvenile crust newly formed from oceanic crust partial melting with inherited mantle isotopic signatures and crustal/sediment contribution.

3.5. Conclusions

The Permian–Triassic batholiths (240–260 Ma) along the East Kunlun Orogenic Belt (EKOB) cover an area of ~ 20,000 km^2, representing about half of all of the intrusions. They are products of syn-collisional magmatism shortly after the Late-Permian closure of the Paleo-Tethyan Ocean (A'nyemaqen branch).

The MMEs and granitoid hosts have the same crystallization age, share the same mineralogy and contain indistinguishable isotope compositions. Therefore, the MMEs are consistent with being cumulate lithologies of more mafic compositions produced at earlier stages of the same magmatic systems derived from partial melting of the subducting/subducted oceanic crust. The isotope variations of similar range for both granitoid hosts and the MMEs are not the evidence of magma

mixing but reflect the magma heterogeneity due to the source heterogeneity and crustal contamination on varying local scales.

The large volumes of these granitoids require partial melting of a basaltic source with mantle isotopic signatures. The radiogenic Sr and Pb isotopes and slightly unradiogenic Nd isotopes indicate the input of crustal materials, while the positive $\varepsilon_{Hf(t)}$values emphasizes the significant mantle contribution. Although $\varepsilon_{Hf(t)}$ is elevated at a given $\varepsilon_{Nd(t)}$, it can be readily explained by partial melting of the subducted Paleo-Tethyan MORB alongside the terrestrial sediments represented by Shaliuhe gneiss under the amphibolite-facies condition. Both Nd and Hf isotopic modelling indicates ~ 60–80% mantle input.

The granitoids have broad compositional similarities to the bulk continental crust and have a large mantle component, thus representing newly formed juvenile crustal contributions in the EKOB. Although the closure time of the Paleo-Tethyan ocean is not well constrained, the stratigraphic records (the late-Permian molasses, the unconformity between upper-Permian to lower-Triassic and lower Permian sequences) indicate that the onset of collision was during the late Permian. Therefore, these granitoids were formed in a syn-collisional setting, and offer new evidence in support of the hypothesis that collision zones are primary sites where net continental crust is produced and preserved.

3.6. References

Allen, C.M., 1991. Local equilibrium of mafic enclaves and granitoids of the turtle pluton, southeast California: Mineral, chemical, and isotopic evidence. American Mineralogist 76, 574-588.

Arculus, R.J., 1981. Island arc magmatism in relation to the evolution of the crust and mantle. Tectonophysics 75 (1-2), 113-133.

Barbarin, B., 2005. Mafic magmatic enclaves and mafic rocks associated with some granitoids of the central Sierra Nevada batholith, California: nature, origin, and relations with the hosts. Lithos, 80, 155-177.

Bizimis, M., Sen, G., Salters, V.J.M., 2004. Hf–Nd isotope decoupling in the oceanic lithosphere: Constraints from spinel peridotites from Oahu, Hawaii. Earth and Planetary Science Letters, 217(1-2), 43-58.

Castillo, P.R., 2006. An overview of adakite petrogenesis. Chinese Science Bulletin 51 (3), 257-268.

Chappell, B.W. White, A.J.R., Williams, I.S., Wyborn, D., Hergt, J.M., Woodhead, J.D., 1999. Evaluation of petrogenetic models for lachlan fold belt granitoids: Implications for crustal architecture and tectonic models - discussion. Australian Journal of Earth Sciences 46 (5), 827-831.

Chappell, B.W., White, A.J.R., Wyborn, D., 1987. The importance of residual source material (restite) in granite petrogenesis. Journal of Petrology 28 (6), 1111-1138.

Chauvel, C., Lewin, E., Carpentier, M., Arndt, N.T., Marini, J.C., 2008. Role of recycled oceanic basalt and sediment in generating the Hf–Nd mantle array. Nature Geoscience 1 (1), 64-67.

Chen, H.W., Luo, Z.H., Mo, X.X., Liu, C., Ke, S., 2005. Underplating mechanism of triassic granite of magma mixing origin in the east Kunlun orogenic belt. Geology in China 32 (3), 386-393 (in Chinese with English abstract).

Chen, N.S., Wang, X.Y., Zhang, H.F., 2007a. Components and metamorphism of the basements of the Qaidam and Oulongbuluke micro-continental blocks, and a tentative interpretation of paleocontinental evolution in NW-Central China. Earth Science Frontiers 14 (1), 43.

Chen, N.S.,Wang, X.Y., Zhang, H.F., Sun,M., Li, X.Y., Chen, Q., 2007b. Geochemistry and Nd-Sr-Pb isotopic compositions of granitoids from Qaidam and Oulongbuluke micro-blocks，NW China constraints on basement nature and tectonic affinity. Journal of Earth Science 32 (1), 7-21 (in Chinese with English Abstract).

Chen, N.S., Xia, X.P., Li, X.Y., Sun, M., 2007c. Timing of magmatism of the gneissic-granite plutons along north Qaidam margin and implications for Precambrian crustal accretions: Zircon U-Pb dating and Hf isotope evidences. Acta Petrologica Sinica 23 (2), 501-512 (in Chinese with English abstract).

Chen, X.H., Yin, A., George, G., Li, L., Jiang, R.B., 2011. Chemical geodynamics of granitic magmatism in the basement of the eastern Qaidam basin, northern Qinghai-Tibet Plateau. Acta Geologica Sinica 85 (2), 157-171 (in Chinese).

Clemens, J.D., Stevens, G., 2011. What controls chemical variation in granitic magmas. Lithos 134-135, 317-329.

Clift, P.D., Vannucchi, P., 2004. Controls on tectonic accretion versus erosion in subduction zones: Implications for the origin and recycling of the continental crust. Reviews of Geophysics 42 (2), 31.

Clift, P.D., Schouten, H., Vannucchi, P., 2009. Arc-continent collisions, sediment recycling and the maintenance of the continental crust. Geological Society, London, Special Publications, 318 (1), 75-103.

Condie, K.C., 2000. Episodic continental growth models: Afterthoughts and extensions. Tectonophysics 322 (1–2), 153-162.

Dahlquist, J., 2002. Mafic microgranular enclaves: Early segregation from metaluminous magma (sierra de chepes), pampean ranges, NW Argentina. Journal of South American Earth Sciences 15 (6), 643-655.

Deng, J., Luo, Z.H., Su, S.G., 2004. Petrogenesis, tectonic setting and mineralization. Beijing: Geol. Pub. House, 1-381. (in Chinese).

Dewey, J.F., Shackleton, R.M., Cheng, C.F., Sun, Y.Y., 1988. The tectonic evolution of the Tibetan Plateau. Philosophical Transactions of the Royal Society of London. Series A, Mathematical and Physical Sciences 327 (1594), 379-413.

Foley, S.F., Barth, M.G., Jenner, G.A., 2000. Rutile/melt partition coefficients for trace elements and an assessment of the influence of rutile on the trace element characteristics of subduction zone magmas. Geochimica et Cosmochimica Acta 64 (5), 933-938.

Fujimaki, H., 1986. Partition-coefficients of Hf, Zr, and REE between zircon, apatite, and liquid. Contributions to Mineralogy and Petrology 94 (1), 42-45.

Gill, J.B., 1981. Orogenic andesites and plate tectonics. Springer-Verlag, New York, 16, pp. 390.

Guo, Z.F., Deng, J.F., 1998. Late Palaeozoic Mesozoic intracontinental orogenic process and intermediate igenous rocks from the eastern Kunlun mountains of Northwestern China. Geoscience-Journal of China University of Geosciences 12 (3), 344-352.

Hans Wedepohl, K., 1995. The composition of the continental crust. Geochimica et Cosmochimica Acta 59 (7), 1217-1232.

Harris, N.B.W., Hua, X.R., Lewis, C.L., Hawkesworth, C.J., Zhang, Y.Q., 1988a. Isotope geochemistry of the 1985 Tibet geotraverse, Lhasa to Golmud, in: The geological evolution of Tibet. Philosophical Transactions of the Royal Society of London, 327, 263-285.

Harris, N.B.W., Xu, R.h., Lewis, C.L., Jin, C., 1988b. Plutonic rocks of the 1985 Tibet geotraverse, Lhasa to Golmud. Philosophical Transactions of the Royal Society of London , 327, 145-168.

Hoffmann, J.E., Münker, C., Polat, A., Rosing, M.T., Schulz, T., 2011. The origin of decoupled Hf–Nd isotope compositions in Eoarchean rocks from southern west Greenland. Geochimica et Cosmochimica Acta, 75 (21), 6610-6628.

Holden, P., Halliday, A.N., Stephens, W., Henney, P.J., 1991. Chemical and isotopic evidence for major mass transfer between mafic enclaves and felsic magma. Chemical Geology 92 (1-3), 135-152.

Holden, P., Halliday, A.N., Stephens, W.E., 1987. Neodymium and strontium isotope content of microdiorite enclaves points to mantle input to granitoid production. Nature 330, 53-55.

Huang, H., Niu, Y.L., 2013. Mixing induced disprepancy between whole rock Hf isotopes and zicon in situ Hf isotopes: A case study in Kekeli Batholith, North Qilian Orogenic Belt. AGU Fall meeting abstract.

Irvine, T.N., Baragar, W.R.A., 1971. A guide to the chemical classification of the common volcanic rocks. Canadian Journal of Earth Sciences 8 (5), 523-548.

Jiang, C.F., Yang, J.S., Feng, B.G., 1992. Opening–closing evolution of the Kunlun mountains. In Jiang C. F., Yang J. S., Feng B. G.. (Eds). Opening closing tectonics of Kunlun mountain. Geological Publishing House, Beijing , 205-271 (in Chinese).

Kelemen, P.B., Rilling, J.L., Parmentier, E., Mehl, L., Hacker, B.R., 2003. Thermal structure due to solid-state flow in the mantle wedge beneath arcs. Geophysical monograph-American Geophysical Union 138, 293-311.

Lesher, C.E., 1990. Decoupling of chemical and isotopic exchange during magma mixing. Nature 344, 235-237.

Li, R.S., Xu, W.H., Yang, Y.C., 2008. Kunlun mountains and geology of adjacent areas. Geological Publishing House, Beijing (in Chinese with English abstract).

Li, X.L., Chen, X., Ge, H. J., Wu, Y.T., Xian, X.L., Han, W., 2011. XRF determination of chlorine etc multi-elements in sea sediments with sample preparation by fusion. Physical Testing and Chemical Analysis Part B: Chemical Analysis 47 (12), 1420-1423 (in Chinese with English abstract).

Liu, C.D., Mo, X.X., Luo, Z.H., Yu, X.H., 2004a. Mixing events between the crust and mantle derived magmas in eastern Kunlun: Evidence from zircon SHRIMP chronology. Chinese Science Bulletin 49, 828-834 (in Chinese).

Liu, C.D., Mo, X.X., Luo, Z.H., Yu, X.H., 2004b. Pb-Sr-Nd-O isotope characteristics of granitoids in east Kunlun orogenic belt. Journal of Earth Science 24 (6), 584-588 (in Chinese with English abstract).

Luo, Z.H., Ke, S., Cao, Y.Q., Deng, J.F., Chen, H.W., 2002. Late Indosinian mantle-derived magmatism in the east Kunlun. Geological Bulletin of China 21 (6), 292-297 (in Chinese with English abstract).

McLeod, C.L., Davidson, J.P., Nowell, G.F., Silva, S.L., 2012. Disequilibrium melting during crustal anatexis and implications for modelling open magmatic systems. Geology, 40 (5), 435-438.

Meng, F.C., Zhang, J.X., Yang, J.S., 2005a. Subducted continental arc: Geochemical and isotope evidence of gneisses in the north Qaidam. Acta Petrologica Sinica 79 (1), 46-55 (in Chinese with English abstract).

Meng, F.C., Zhang, J.X., Yang, J.S., 2005b. Tectono-thermal event of post-HP/UHP metamorphism in the Xitieshan area of the north Qaidam mountain, west China: Isotope and geochemical evidence of granite and gneiss. Acta Petrologica Sinica 21 (1), 45-56 (in Chinese with English abstract).

Miller, C.F., McDowell, S.M., Mapes, R.W., 2003. Hot and cold granites? Implications of zircon saturation temperatures and preservation of inheritance. Geology 31 (6), 529-532.

Mo, X.X., Hou, Z.Q, Niu, Y.L., Dong, G.C., Qu, X.M., Zhao Z.D., Yang, Z.M., 2007a. Mantle contributions to crustal thickening during continental collision: Evidence from Cenozoic igneous rocks in southern Tibet. Lithos 96 (1-2), 225-242.

Mo, X.X., Luo, Z.H., Deng, J.F., Yu, X.H., 2007b. Granitoids and crustal growth in the east-Kunlun orogenic belt. Geological Journal of China Universities 3, 403-414 (in Chinese with English abstract).

Mo, X.X., Niu, Y.L., Dong, G.C., Zhao, Z.D., Hou, Z.Q., Zhou, S., Ke, S., 2008. Contribution of syncollisional felsic magmatism to continental crust growth: A case study of the Paleogene Linzizong volcanic succession in southern Tibet. Chemical Geology 250 (1-4), 49-67.

Niu, Y. L., 2005. Generation and evolution of basaltic magmas: Some basic concepts and a new view on the origin of Mesozoic-Cenozoic basaltic volcanism in eastern China. Geological Journal of China Universities 11 (9), 9-46.

Niu, Y.L., Mo, X.X., Dong, G.C., Zhao, Z.D., Hou, Z.Q., Zhou, S., Ke, S., 2007. Continental collision zones are primary sites of net continental crustal growth: Evidence from the Linzizong volcanic succession in southern Tibet, Eos Trans. AGU, 88 (52), Fall meet., Suppl., Abstract, pp. 01.

Niu, Y.L., O'Hara, M.J., 2009. MORB mantle hosts the missing Eu (Sr, Nb, Ta and Ti) in the continental crust: New perspectives on crustal growth, crust–mantle differentiation and chemical structure of oceanic upper mantle. Lithos 112 (1-2), 1-17.

Niu, Y.L., Zhao, Z.D., Zhu, D.C., Mo, X.X., 2013. Continental collision zones are primary sites for net continental crust growth – A testable hypothesis, Earth Science Reviews (doi: 10.1016/j.earscirev.2013.09.004)

Nowell, G. M., Kempton, P.D., Noble, S.R., Fitton, J.G., Saunders, A.D., Mahoney, J.J., Taylor, R.N., 1998. High precision Hf isotope measurements of MORB and OIB by thermal ionisation mass spectrometry: insights into the depleted mantle. Chemical Geology 149 (3), 211-233.

Nowell, G.M., Parrish, R.R., 2001. Simultaneous acquisition of isotope compositions and parent/daughter ratios by non-isotope dilution solution-mode plasma ionisation multi-collector mass spectrometry (PIMMS). Plasma Source Mass Spectrometry: The New Millennium. Royal Society of Chemistry, Special Publication, 267, pp. 298-310.

Nowell, G.M., Pearson, D.G., Ottley, C.J., Schweiters, J., Dowall, D., 2003. Long-term performance characteristics of a plasma ionisation multi-collector mass spectrometer (PIMMS): The thermofinnigan neptune. Plasma Source Mass Spectrometry: Applications and Emerging Technologies. Cambridge: Royal Society of Chemistry, pp. 307-320.

Pan, G.T., Ding, J., Yao, D.S.W., L. Q., 2004. Geological map of the Qinghai-Xizang (Tibet) plateau and adjacent areas. Chengdu Cartographic Publishing House.

Pearcy, L.G., DeBari, S.M., Sleep, N.H., 1990. Mass balance calculations for two sections of island arc crust and implications for the formation of continents. Earth and Planetary Science Letters 96 (3-4), 427-442.

Ramos, F.C., Reid, M.R., 2005. Distinguishing melting of heterogeneous mantle sources from crustal contamination: insights from Sr isotopes at the Phenocryst Scale, Pisgah Crater, California. Journal of Petrology, 46 (5) 999-1012.

Reymer, A., Schubert, G., 1984. Phanerozoic addition rates to the continental crust and crustal growth. Tectonics 3 (1), 63-77.

Rudnick, R.L., Gao, S., 2003. Composition of the continental crust. Treatise on Geochemistry, pp 1-64.

Rudnick, R.L., Goldstein, S.L., 1990. The Pb isotopic compositions of lower crustal xenoliths and the evolution of lower crustal Pb. Earth and Planetary Science Letters 98 (2), 192-207.

Schmitz, M.D., Vervoort, J.D., Bowring, S.A., Patchett, P.J., 2004. Decoupling of the Lu-Hf and Sm-Nd isotope systems during the evolution of granulitic lower crust beneath southern Africa. Geology 32 (5), 405.

Scholl, D.W., von Huene, R., 2009. Implications of estimated magmatic additions and recycling losses at the subduction zones of accretionary (non-collisional) and collisional (suturing) orogens. Geological Society, London, Special Publications 318 (1), pp. 105-125.

Sun, Y., Pei, X.Z., Ding, S.P., Li, R.B., Feng, J.B., Zhang, Y.F., 2009. Halagatu magma mixing granite in the east kunlun mountains-evidence from zircon U-Pb dating. Acta Petrologica Sinica 83 (7), 1000-1010 (in Chinese with English abstract).

Tatsumi, Y., 2006. High-Mg andesites in the Setouchi volcanic belt, southwestern Japan: Analogy to Archean magmatism and continental crust formation? Ann. Rev. Earth. Planet. Sci. 34, 467-499.

Taylor, S.R., 1967. The origin and growth of continents. Tectonophysics 4 (1), 17-34.

Taylor, S.R., 1977. Island arc models and the composition of the continental crust. Island Arcs, Deep-Sea Trenches and Back-Arc Basins. American Geophysical Union, Washington, DC, 325-335.

Taylor, S.R., McLennan, S.M., 1985. The continental crust: Its composition and evolution. Blackwell Scientific Pub., Palo Alto, CA.

Thirlwall, M.F., 1991. Long-term reproducibility of multicollector Sr and Nd isotope ratio analysis. Chemical Geology: Isotope Geoscience section 94 (2), 85-104.

von Huene, R., Scholl, D.W., 1991. Observations at convergent margins concerning sediment subduction, subduction erosion, and the growth of continental crust. Reviews of Geophysics 29 (3), 279-316.

Wall, V.J., Clemens, J.D., Clarke, D.B., 1987. Models for granitoid evolution and source compositions. The Journal of geology 95 (6), 731-749.

Wang, Z.H., 2004. Tectonic evolution of the western Kunlun orogenic belt, western China. Journal of Asian Earth Sciences 24 (2), 153-161.

Wang, S.J., Li, S.G., Chen, L.J., He, Y.S., An, S.C., Shen, J., 2013. Geochronology and geochemistry of leucosomes in the North Dabie Terrane, East China: implication for post-UHPM crustal melting during exhumation. Contributions to Mineralogy and Petrology. DOI 10.1007/s00410-012-0845-2.

Watson, E.B., Harrison, T.M., 1983. Zircon saturation revisited: temperature and composition effects in a variety of crustal magma types. Earth and Planetary Science Letters 64 (2), 295-304.

Winter, J.D., 2010. An introduction to igneous and metamorphic petrology. London: Prentice Hall. Second edition.

Xiong, F.H., Ma, C.Q., Zhang, J.Y., Liu, B., 2011. The origin of mafic microgranular enclaves and their host granodiorites from east Kunlun, northern Qinghai-Tibet Plateau: Implications for magma mixing during subduction of Paleo-Tethyan lithosphere. Mineralogy and Petrology 104, 1-14.

Xu, J.F., Castillo, P. R., Li, X.H., Zhang, B.R., Han, Y.W., 2002. MORB-type rocks from the Paleo-Tethyan mian-lueyang northern ophiolite in the Qinling mountains, central china: Implications for the source of the low 206Pb/204Pb and high 143Nd/144Nd mantle component in the Indian ocean. Earth and Planetary Science Letters 198 (3–4), 323-337.

Yang, J.S., Qu, J.C., Xu, Z.Q., 1995. Qingshuiquan ophiolite of east Kunlun: A lower Paleozoic suture. Abstract for the symposium of uplift deformation and deep structure of northern Tibet. 1995 September. Montpellier. France, Abstract No.48.

Yang, J.S., Robinson, P.T., Jiang, C.F., Xu, Z.Q., 1996. Ophiolites of the Kunlun mountains, China and their tectonic implications. Tectonophysics 258 (1-4), 215-231.

Yang, J.S., Shi, R.D., Wu, C.L., Wang, X.B., Robinson, P.T., 2009a. Dur'ngoi ophiolite in east Kunlun, northeast Tibetan Plateau: Evidence for Paleo-Tethyan suture in northwest China. Journal of Earth Science 20 (2), 303-331.

Yang, J.S., Wu, F.Y., Wilde, S., Liu, X., 2007. Petrogenesis of late Triassic granitoids and their enclaves with implications for post-collisional lithospheric thinning of the Liaodong Peninsula, North China Craton. Chemical Geology 242 (1-2), 155-175.

Yang, J.S., Xu, Z., Li, Z., Xu, X., Li, T., Ren, Y., Li, H.,Chen, S., Robbison, P.T., 2009b. Discovery of an eclogite belt in the Lhasa block, Tibet: A new border for Paleo-Tethys? Journal of Asian Earth Sciences 34 (1), 76-89.

Yang, J.S., Xu, Z.Q., Li, H.B., Shi, R.D., 2005. The Paleo- Tethyan volcanism and plate tectonic regime in the A'nyemaqen region of east Kunlun, northern Tibet Plateau. Acta Petrologica et Mineralogica 24 (5), 369-380 (in Chinese with English abstract).

Yin, A., Harrison, T.M., 2000. Geologic evolution of the Himalayan-Tibetan orogen. Ann. Rev. Earth Planet. Sci 28 (2), 211-280.

Yin, H.F., Zhang, K.X., 1997. Characteristics of the eastern Kunlun orogenic belt. Earth Science—Journal of China University of Geosciences 22 (4), 339-342.

Zhang, J.X., Meng, F.C., Wan, Y.S., Yang, J.S., Tung, K.A., 2003a. Early Paleozoic Tectono-thermal event of the Jingshuikou group on the south margin of Qaidam: Zircon U–Pb SHRIMP age evidence. Geological Bulletin of China 22, 397-404 (in Chinese with English abstract).

Zhang, J.X., Wan, Y.S., Meng, F.C., Yang, J.S., Xu, Z.Q., 2003b. Geochemistry, Sm-Nd and U-Pb isotope study of gneisses (schists) enclosing eclogites in the north Qaidam mountains---deeply subducted Precambrian metamorphic basement. Acta Petrologica Sinica 19 (3), 443-451 (in Chinese with English abstract).

Zhang, K.X., Zhu, Y.H., Yin, H.F., 2004. Application of tectonic facies in geological mapping in east Kunlun orogenic belt. Earth Science-Journal of China University of Geosciences 29 (6), 661-666 (in Chinese with English abstract).

Zindler, A., Hart, S., 1986. Chemical geodynamics. Earth and Planetary Science Letters 14, 493-571.

Chapter 4: The nature and history of the Qilian Block

4.1. Introduction

The Qilian Orogenic Belt (QOB) (Fig. 4.1A) within the Qilian-Qaidam system at the northernmost margin of the Greater Tibetan Plateau has recorded the histories of continental breakup, seafloor spreading, and the ultimate continental collision from the Neoproterozoic to the Paleozoic (Song et al., 2009, 2013, 2014). The tectonic subdivision of QOB has evolved over the years, and the most recent suggestion is as follows (Song et al., 2006, 2013, 2014) (Fig. 4.1A): (1) the north Qilian orogenic belt (NQOB), (2) the Qilian Block (QB), (3) the North Qaidam ultrahigh-pressure metamorphic (NQ-UHPM) belt, and (4) the Qaidam Block (QDB). The metamorphic history has been well studied and reviewed by Song et al. (2013), while the mechanism of continental growth remains unclear. For example, it is not straightforward why these two huge tectonic units (NQ-UHPM and NQOB) are spatially so close (~ 300–400 km apart; Fig. 4.1A). Several models of Qilian Orogenic Belt have been proposed (Xu et al., 1994; Yin and Harrison, 2000; Yang et al., 2002; Gehrels et al., 2003b; Song et al., 2006; Wu et al., 2006a; Xiao et al., 2009; Wu et al., 2010; Gehrels et al., 2011; Song et al., 2013, 2014). These models are debating on the location of the suture zone and subduction polarity of the Paleo-Qilian Oceanic lithosphere. However, the major hindrance is the lack of adequate knowledge of magmatism during the subduction/collision period and therefore the poor time constraints on the onset of subduction and collision. In contrast to the popular research of metamorphic rocks within the NQOB and the NQ-UHPM and numerous studies of magmatism within the NQOB, little is known about those granitoids which are coeval with metamorphism at the early Paleozoic in the QB. Sandwiched between two important tectonic units, the QB is particularly important for understanding the relationship of these subunits and the tectonic histories of the block itself and the region in the context of the Greater Tibetan Plateau evolution.

In this study, we aim to understand the nature of the Qilian Block by studying the petrology, geochronology and geochemistry of the Paleozoic granitoids with the result also having shed lights

on the evolution histories of its sutures to the north (i.e., the NQOB with seafloor subduction-zone complex) and to the south (i.e., the NQ-UHPM separating the Qaidam Block to the south).

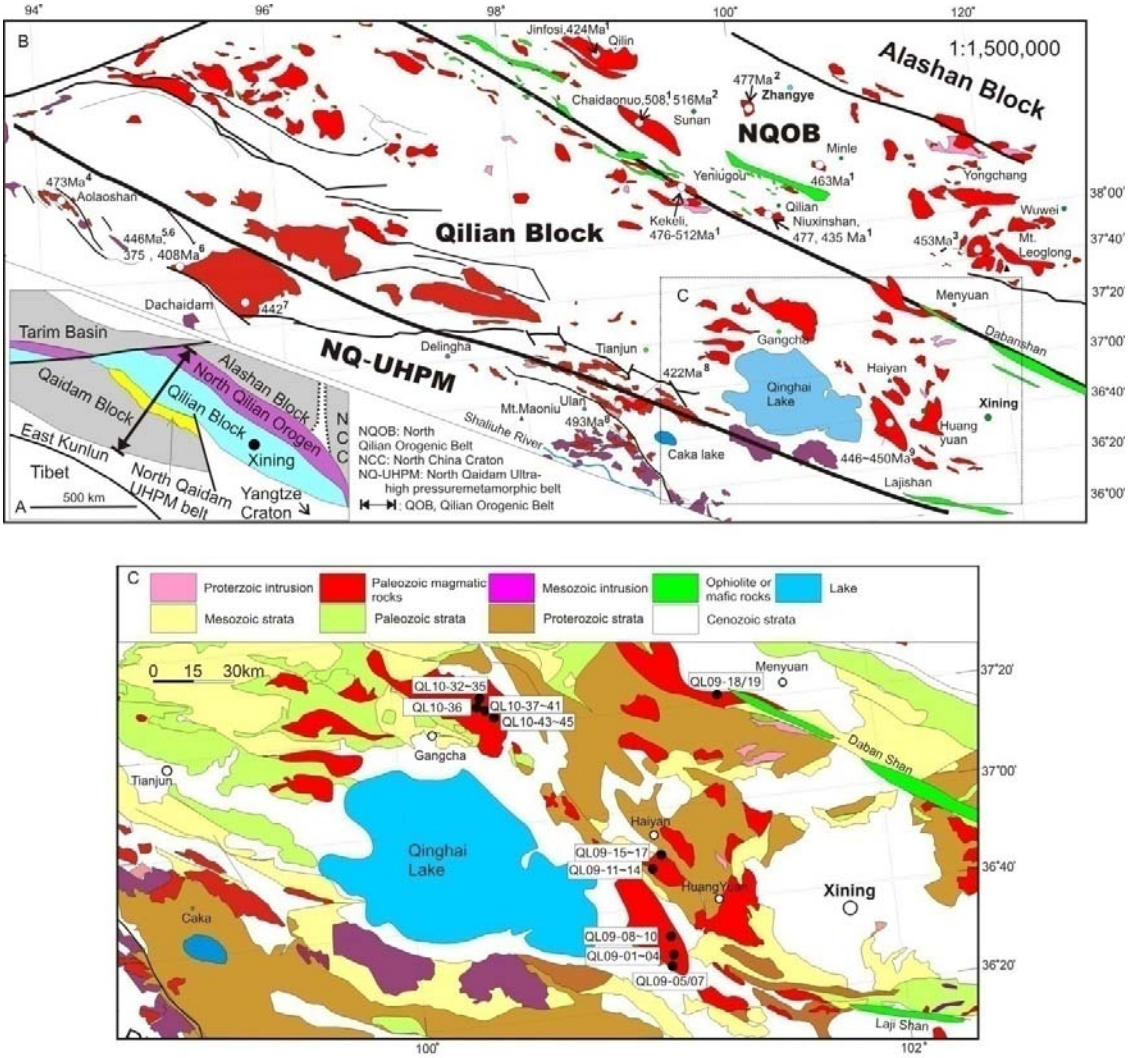

Fig. 4.1. A, Schematic map showing major tectonic units of the Qilian Orogenic Belt, after Song et al. (2013).B, Simplified geological map of the Qilian Block showing the distribution of granitoids and ophiolites (after Pan et al., 2004). Data are from the literature given in Table 4.1. C, Detailed geological map of the sampling locations (after Pan et al., 2004).

4.2. Tectonic setting and geology background

4.2.1. Strata, metamorphic rocks and mafic rocks in the QOB

The QOB is a broad and composite orogenic belt bounded by the Yangtze Craton to the southeast, East Kunlun orogenic belt to the south, Alashan Block to the northeast and Tarim Basin to the northwest (Fig. 4.1A). It has four subunits from North to South: NQOB, QB, NQ-UHPM and QDB (Fig. 4.1A, see above).

The NQOB is covered by Carboniferous to Triassic sedimentary sequences. The magmatic clasts within the Silurian flysch formations are dated at 515–429 Ma (Song et al., 2013). The Devonian molasses are also found in this belt. The NQOB is characterized by the occurrence of low-T/HP blueschist and eclogite-facies rocks (Zheng, et al., 2013). The metamorphic rocks record a cold oceanic subduction zone with a thermal gradient of ~ 6–7°C/km (Song et al., 2007; Zhang et al., 2007). There are two ophiolite belts in the NQOB (Song et al., 2013). Magmatic zircon dating for ophiolites gives ages varying from 496 to 550 Ma (Song et al., 2013) in the south and from 448 to 490 Ma in the north (Xia and Song, 2010; Song et al., 2013).

The QB, bounded by the NQOB to the north and the NQ-UHPM belt to the south is dominantly Precambrian basement (Chen et al., 2007a, 2009a, 2009b) covered with the Paleozoic sedimentary lithologies. Granitic intrusions with ages of 880–940 Ma as well as the coeval metamorphism are documented (Guo et al., 1999; Tung et al., 2007a, 2007b; Xu et al., 2007; Song et al., 2012, 2013). The Dabanshan ophiolite at the NQOB-QB boundary (Fig. 4.1B) mainly outcrops as dismembered lenses, consisting of pillow basalt, gabbro, harzburgite, pyroxenite and hornblendite etc. with minor felsic lithologies. Sm–Nd isochron gives the age of ~ 492 ± 22.6 Ma for basalt (Qinghai Geological Survey Institute, 2006). A few low-K_2O (0.05–0.96 wt%) tholeiitic dikes cut through the Paleoproterozoic basement (Qinghai Geological Survey Institute, 2006). The Lajishan ophiolite associating with tonalite, diorite and plagiogranite in the southern QB near the QB and NQ-UHPM boundary (Fig. 4.1B) is of MORB protolith and dated at 510 Ma (Hou et al., 2005).

The NQ-UHPM belt is characterized by UHPM eclogite-facies blocks and lenses hosted in the UHPM granitic gneisses (Song et al., 2003a, 2003b, 2006; Zhang et al., 2006). The protoliths of the UHPM rocks vary, including granitic gneiss of ~ 1200–900 Ma and ultramafic rocks of 550–500 Ma (Song et al., 2013; and references therein) and ~ 877–750 Ma (Yang et al., 2006; Zhang et al., 2011). Previous studies indicate that the HP-UHP metamorphism and subsequent exhumation happened from 497 Ma to 400 Ma (Yang et al., 2002; Song et al., 2003b, 2005, 2006; Chen et al., 2009a, 2009b). Volcanic arc basalts of 514 Ma are regarded as reflecting seafloor subduction (Shi et al., 2004).

The QDB is dominated by the Precambrian meta-crystalline basement (Chen et al., 2011) covered with Paleozoic-Mesozoic sedimentary rocks. It is located to the northwest of the numerous East Kunlun batholiths of Paleozoic to Mesozoic ages (Chen et al., 2011; Huang et al., 2014).

4.2.2. Paleozoic granitoids in the QOB

The Paleozoic granitoids in the QOB are concisely summarized in Fig. 4.1B and Table 4.1. Generally, I-type rocks (453–512 Ma) predate S-type rocks (424–516 Ma) despite some ages overlap (Table 4.1). They have been interpreted as products in response to varying stages of earlier southward subduction of the Qilian Ocean seafloor underneath the NQOB and later northward subduction underneath the Alashan Block, i.e., the double subduction model (Wu et al., 2006a, 2010) compared to the northward subduction model (Xu et al., 1994; Yin and Harrison, 2000; Song et al., 2013, 2014) and southward subduction model (Gehrels et al., 2003b).

There has been only one study on the Paleozoic batholiths in the QB (Yong et al., 2008). It is a typical S-type batholith of ~ 446–450 Ma in the Huangyuan (HY) area in the eastern part of the QB (Table 4.1, Fig. 4.1B) with $\varepsilon_{Nd}(t)$ of -5.2 and -6.6 (Yong et al., 2008). It is interpreted as derived from metagreywack in a syncollisional setting without giving details (Yong et al., 2008).

Granitoids in the NQ-UHPM are generally I-type before 446 Ma and S-type after 446 Ma (Fig. 4.1B, Table 4.1). The I-type granitoids are interpreted as subduction related and S-type rocks are interpreted as collision related (Wu et al., 2001, 2002; Gehrels et al., 2003b; Wu et al., 2007) based on their geochronology and petrology. Chen et al. (2011) report one I-type sample of 493 Ma and two S-type samples of 422 Ma in the Ulan area (Fig. 4.1B) and propose that they might have a source related to EM II based on the Sr–Nd–Pb–O isotopes, which cannot be justified.

Our samples are collected from 13 locations of several intrusions, generally representative of those in the eastern part of the Qilian Block. GPS data are given in Table 4.2. Two samples QL09-18 and QL09-19 are from an ophiolite in the Dabanshan at the boundary with the NQOB in the north (Fig. 4.1B, C, Table 4.1). Other samples with 'QL09' initials are from Huangyuan (HY) (Table 4.2) where Proterozoic sedimentary rocks dominate with some Mesozoic strata (Fig. 4.1C). Samples with 'QL10' initials are from the Gangcha area (Gcha) (Table 4.2) where Paleozoic and Mesozoic sedimentary strata dominate (Fig. 4.1C).

4.3. Methods

All the 24 samples were analysed for bulk-rock major and trace element compositions. Nine representative samples were selected for zircon U–Pb dating. at China University of Geosciences (Wuhan) following Liu et al. (2008) and China University of Geosciences (Beijing) following Song et al. (2010a). Results from both labs are consistent. The dated samples were analysed for bulk-rock Sr–Nd–Pb–Hf isotopes.

4.4. Petrology, zircon geochronology and geochemistry

Samples can be divided into three groups according to their ages, mineralogy, and geochemical compositions. Age data are given in Table 4.3. Three samples are significantly older than others: 924 Ma, 797 Ma and 503 Ma, respectively. Other samples are ~ 450 Ma I-type granitoids with no Al-rich minerals and S-type granitoids containing Al-rich minerals, e.g. garnet (Grt), muscovite (Ms)

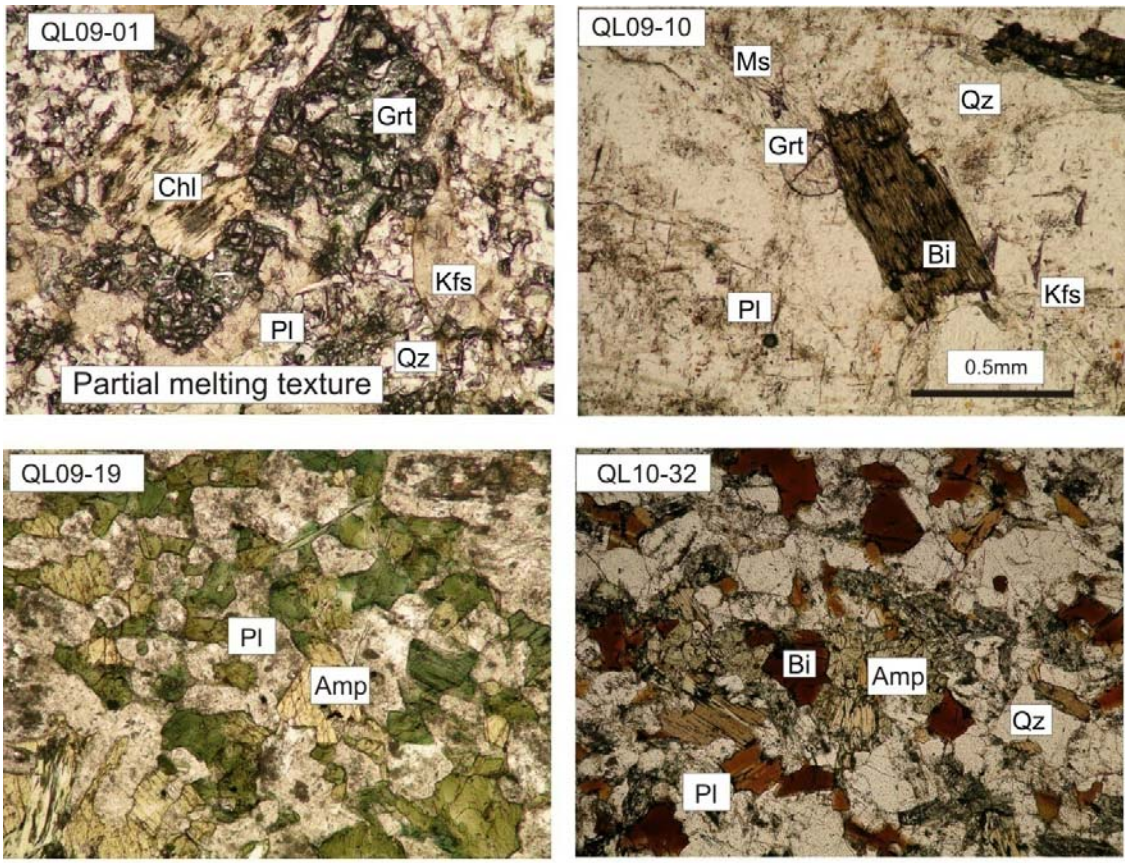

Fig. 4.2. Photomicrographs under plane polarized light showing partial melting textures of QL09-01, representative S-type granite QL09-10, I-type granite QL10-32 and enclave QL09-19 in QL09-18.

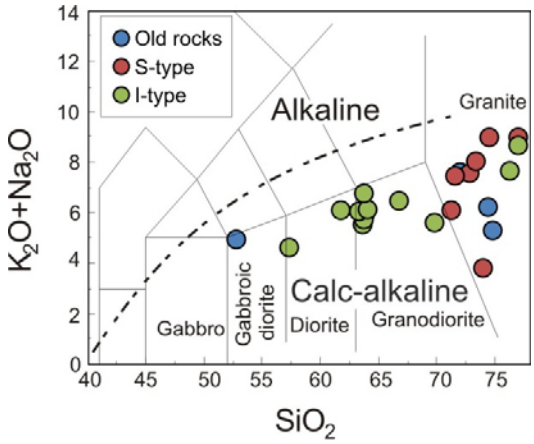

Fig. 4.3. Total alkalis (Na_2O+K_2O) versus SiO_2 (TAS) diagram showing the compositional variation of the QB samples. All the samples are calc-alkaline. The dashed line is the division between alkaline and sub-alkaline fields (Irvine and Baragar, 1971).

and allanite (Aln) (Table 4.2, Fig. 4.2). Bulk-rock major and trace element data are given in Table 4.4, and Sr–Nd–Pb–Hf isotope data are given in Table 4.5. They are all calc-alkaline (Fig. 4.3) and define good correlations on SiO_2-variation diagrams (Fig. 4.4).

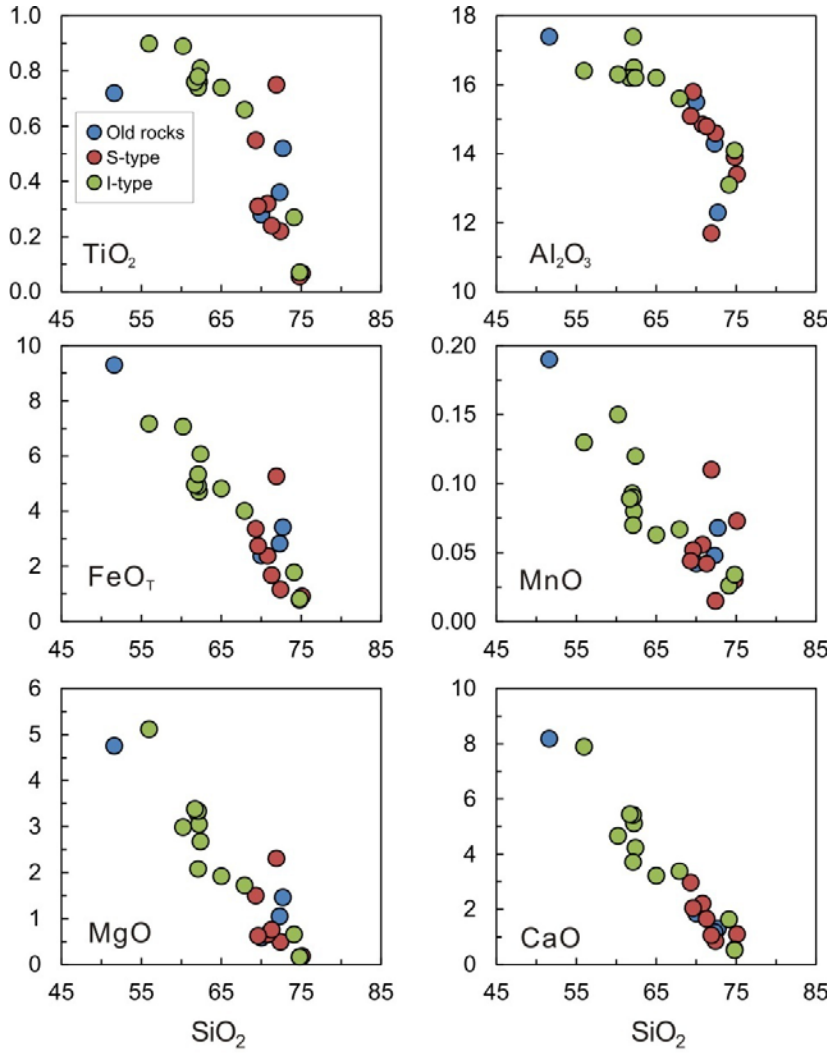

Fig. 4.4. Harker diagrams showing correlated compositional variations among samples.

4.4.1. Old rocks—924 Ma, 797 Ma and 503 Ma

Granite QL09-15 is slightly deformed, containing Qz, Pl, Kfs, and Ms. It has enriched light rare earth element (LREE) patterns with flat heavy REEs (HREEs) (Fig. 4.5). Zircons are weak luminescent and well oscillatory zoned (Fig. 4.6) with high Th/U ratios (0.18 ~ 0.49, Table 4.3).

Twenty one analyses give a coherent concordant $^{206}Pb/^{238}U$ age of 924.1 ± 1.5 Ma (Fig. 4.7), representing the crystallization age. The inherited zircons > 1.0 Ga are discordant and fail to form a Discordia line (Fig. 4.7), but these data indicate the presence of ancient crystalline rocks in the QB. The slightly negative $\varepsilon_{Nd}(924)$ value (-3.8) (Table 4.5) indicates crustal contributions which are demonstrated by inherited old zircons in this sample (Fig. 4.7). The whole-rock $\varepsilon_{Hf}(924)$ value of up to 3.8 (Table 4.5) emphasizes the significant mantle input.

Granite QL09-01consists of Qz, Kfs, Pl, Bt, Grt and Ms with partial melting texture (sieved texture, broken down minerals, vesicles, and small percentage of brown glass along grain boundary) (Fig. 4.2). It has an enriched LREE pattern with flat HREEs (Fig. 4.5). Zircon populations are complex in this sample with Th/U ratios varying from 0.23 to 1.55 (Table 4.3). Some of them display sector zoning, strip zoning, homogeneous in oval shape or clear core-mantle structure (Fig. 4.6). These grains form a Discordia line with an Archean upper intercept of 2769 Ma (Fig. 4.7). Other grains are prismatic with oscillatory zoning (Fig. 4.6) and form two populations (Fig. 4.7): concordant Paleoproterozoic age of ~ 1800 Ma (blue points of QL09-01 in Fig. 4.7) and Neoproterozoic concordant age of 796.7 Ma (Fig. 4.7). Both $\varepsilon_{Nd}(800)$ and $\varepsilon_{Hf}(800)$ are negative (-9.8 and -8.4, respectively, Table 4.5), indicating a crustal origin with less mantle input.

Granite QL09-18 has high SiO_2 (72.3 wt%) and Na_2O (5.11 wt%), low K_2O (0.97 wt%) and moderate CaO (1.18 wt%), and is peraluminous (A/CNK: 1.23) (Table 4.4). Minerals include Qz, Pl and Kfs (Table 4.2). Minor chloride occurs along the mineral boundaries and mineral cracks. It has an enriched REE pattern with a weak negative Eu anomaly and slightly upward HREEs (Fig. 4.5). Zircons are prismatic, oscillatory zoning (Fig. 4.6) and give a concordant weighted mean $^{206}Pb/^{238}U$ age of 502.9 ± 2.0 Ma (Fig. 4.7), representing the crystallization age. No inherited zircons are observed in this sample. The enclosed mafic enclave QL09-19 is composed of amphibole and plagioclase (Fig. 4.2) with 51.6 wt% SiO_2 (Table 4.4). It has similar trace element pattern to its host QL09-18 with higher elemental concentrations (Fig. 4.5A, B). Both QL09-18 and QL09-19 have

the same level of Eu anomaly (Eu/Eu* = 0.86, Table 4.4). QL09-18 carries strong mantle isotopic signature, e.g. highly positive $\varepsilon_{Nd}(503)(3.1)$ and $\varepsilon_{Hf}(503)(16.8)$, is less radiogenic I_{Sr} (0.7062) yet highest Pb isotope ratios ($^{206}Pb/^{204}Pb_i$ = 20.474; $^{207}Pb/^{204}Pb_i$ = 15.731; $^{208}Pb/^{204}Pb_i$ = 39.594) (Fig. 4.8, Table 4.5). Its mineralogy and geochemical composition resemble plagiogranite despite the apparent lack of petrotectonic constraints.

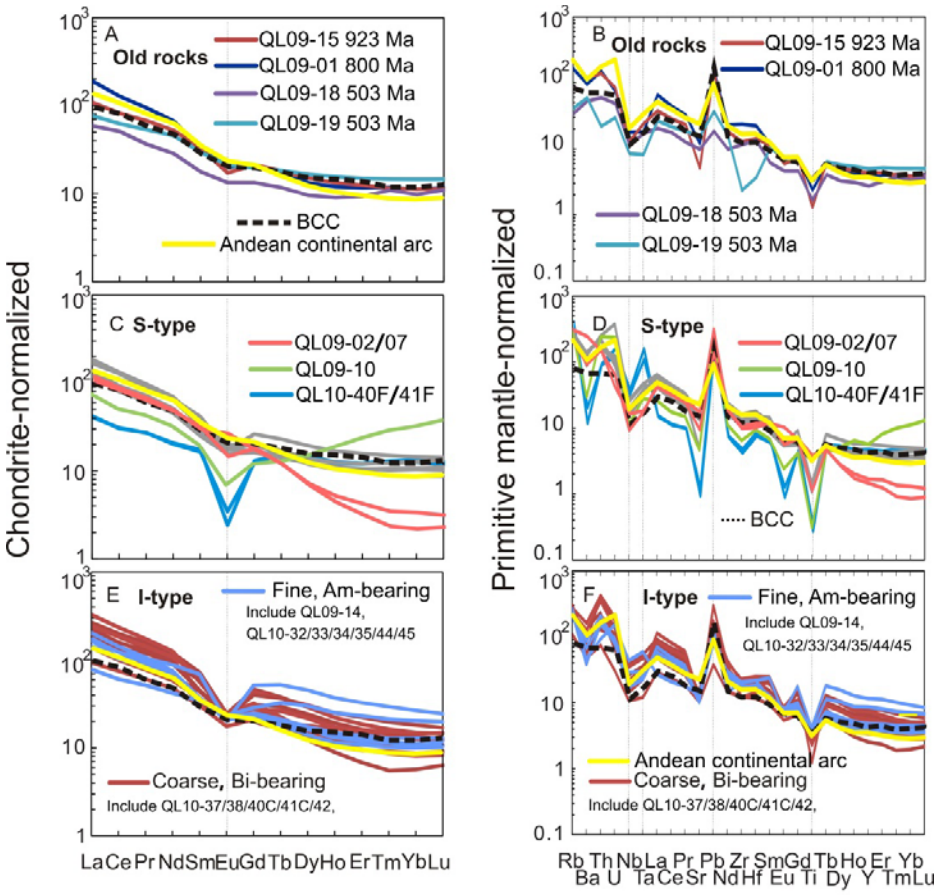

Fig. 4.5. Left column, Chondrite-normalized (Sun and McDonough, 1989) rare earth element (REE) patterns for the Qilian Block (QB) samples with varying compositions. Right column, Primitive mantle-normalized (Sun and McDonough, 1989) multi-element patterns. Majority of the samples show similar patterns resembling bulk continental crust (BCC, dash line). S-type rocks have a few exceptions: QL09-10 has upward HREEs due to the garnet. QL09-02/07 has depleted HREEs due to the garnet in the source. QL10-40F/41F are highly evolved melts. Average of Andean continental arc (yellow line) is also plotted for comparison (data from http://georoc.mpch-mainz.gwdg.de/georoc/, basaltic andesitic to andesitic compositions), which shows a large similarity to the BCC composition.

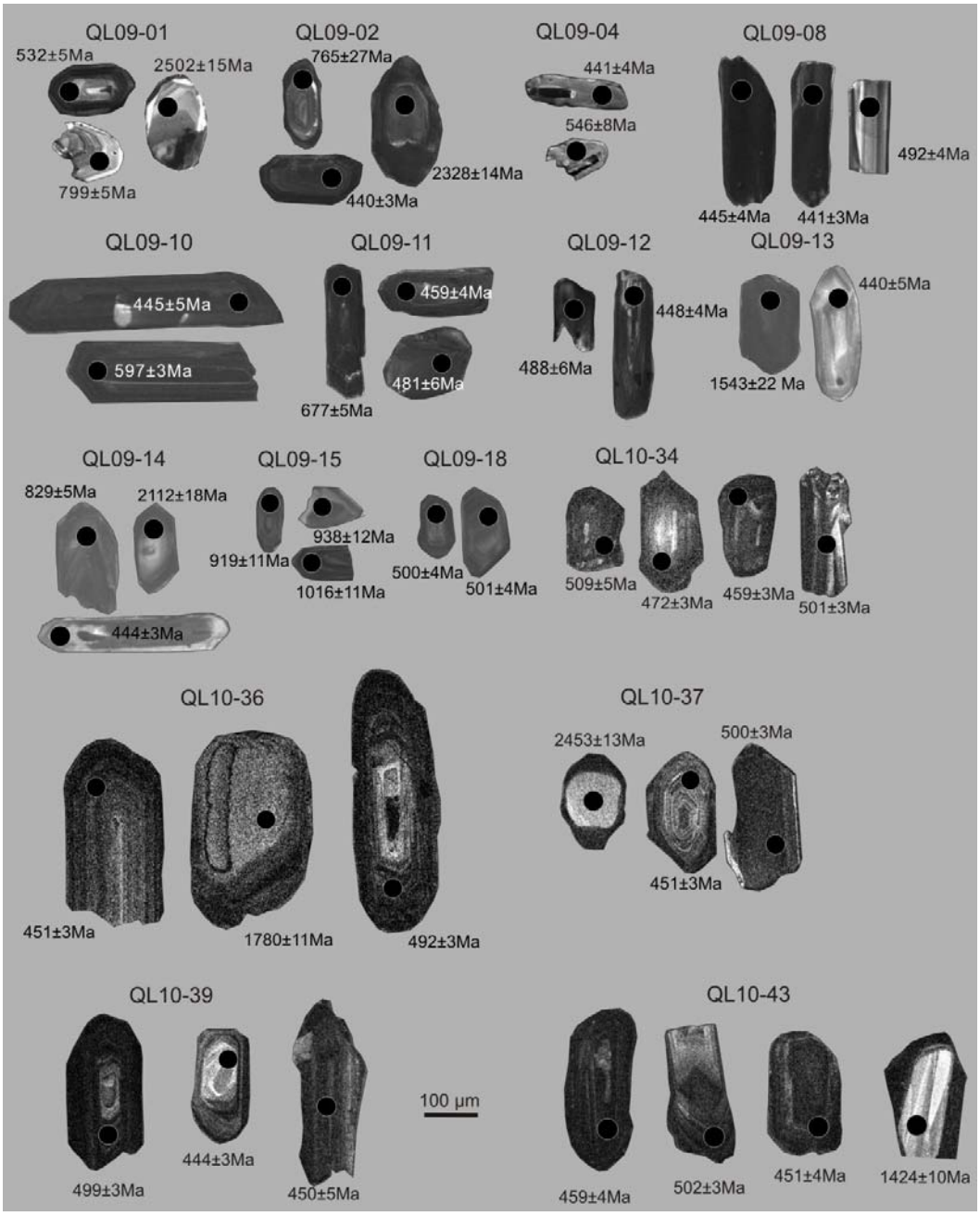

Fig. 4.6. Cathodoluminescence (CL) images of zircons from representative samples. Black circles with white outlines are analyzed spots. The numerals are ages in Ma.

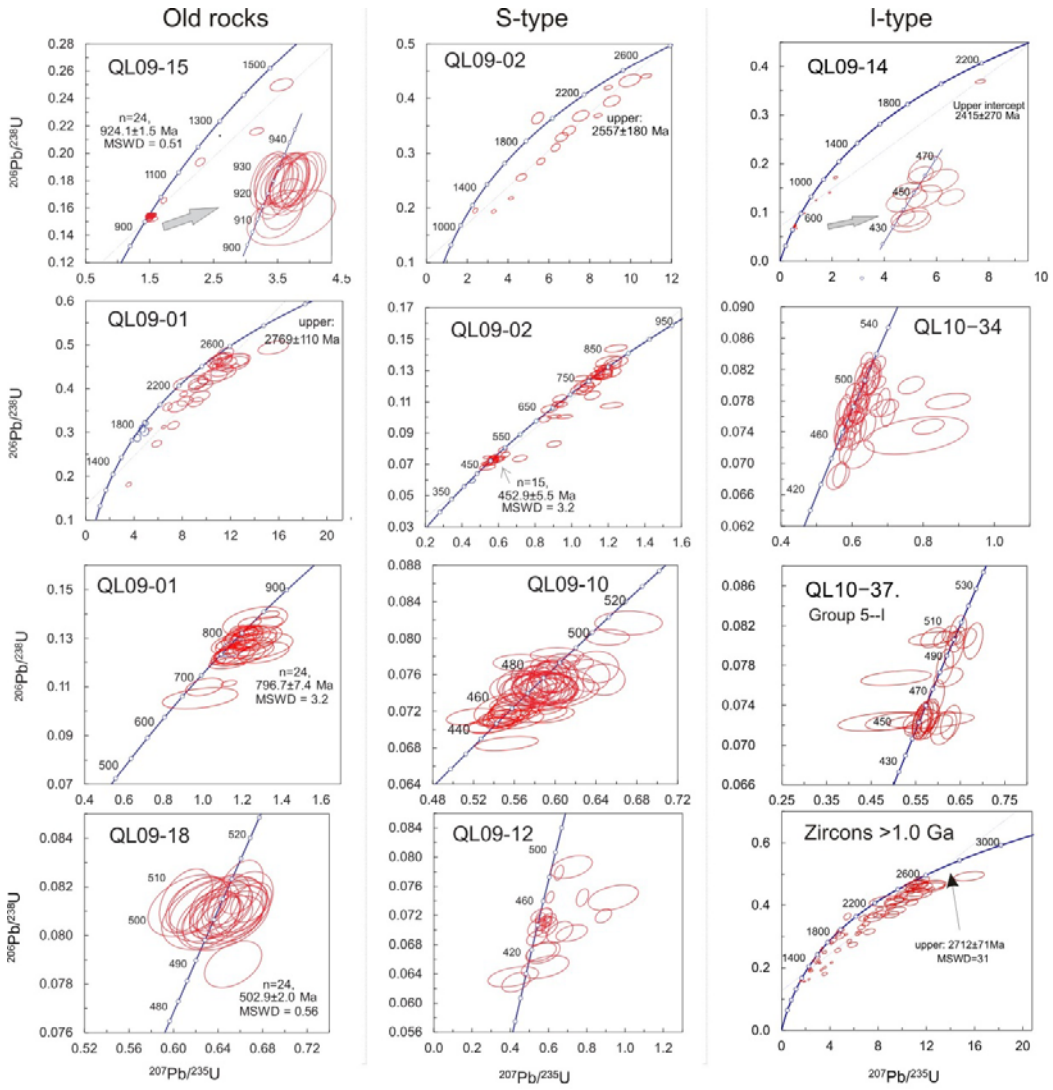

Fig. 4.7. Zircon U-Pb Concordia diagrams. Old rocks 924 Ma QL09-15, 797 Ma QL09-01 and 503 Ma QL09-18 are well dated. 450 Ma I-type and S-type rocks have large age ranges and are not well dated. We choose the youngest peak at ~450 Ma on the histogram as the emplacing time (see text).

4.4.2. ~450 Ma I-type and S-type

S-type samples (Table 4.2, Fig. 4.2) are all highly felsic (SiO_2 > 70.4 wt%) and peraluminous (A/CNK>1.17) (Tables 4.4), consisting of Qz, Kfs, Pl, Bt and Ms. They have LREE enriched patterns with dominant flat HREEs (Fig. 4.5C, D). Two-mica granite sample QL09-02 and QL09-07 are characterized by depleted HREEs (Fig. 4.5C, D), indicating the presence of garnet as a residual phase during melting in the source. Sample QL09-10 has elevated HREEs (Fig. 4.5C, D).

Two fine-grained granites (QL10-40F, QL10-41F, Fig. 4.5C, D; Table 4.2) display a 'V' shape REE pattern with low LREE abundances, a pronounced negative Eu anomaly and high abundance of Ta, resembling highly evolved melts.

I-type rocks (Table 4.2, Fig. 4.2) are fine- and coarse-grained with gradational contact between each other. Fine grained samples consist of Pl, Qz, Amp and Bt. A/CNK values are ≤1. Coarse-grained samples consist of Pl, Qz and Bt without Amp. They all show similar REE patterns (Fig. 4.5E, F), resembling the bulk continental crust signature (BCC) (Fig. 4.5) with negative Eu, Nb-Ta-Ti anomalies, a prominent positive Pb anomaly and a flat HREE pattern.

4.4.3. Ages of I- and S-type samples

Ages of >1.0 Ga are given by the zircons with distinct core-mantle structure. Zircons with ages varying from 420 Ma to 510 Ma (Fig. 4.7) do not have clear differences from each other based on trace elements (Appendix F) and texture. They are all magmatic grains showing similar structures under CL images (Fig. 4.6), i.e., oscillatory zoning, strip zoning or homogenous with Th/U ratios > 0.1 (Table 4.3). Young and old ages can be either on the rims or the centre, which rule out the possibility of cryptic core-mantle structure. The scattering concordant ages along Concordia might be common in the S-type granitoids. But the I-type samples in this study also tend to have the similar age distributions as those S-type samples do, which is neither common nor expected. The key observation is that they have large age variations; therefore, it is difficult to obtain reliable weighted mean ages with small MSWD. Theoretically, the youngest clustering group should be the crystallization age for magmatic rocks. For each sample here, zircons younger than 450 Ma are mostly plotted away from the Concordia (at least not as concordant as 450 Ma points) (Fig. 4.7). Therefore, we interpret 450 Ma as representing the emplacement time, which is consistent with zircon age peaks on the histogram (Fig. 4.9, $^{206}Pb/^{238}U$ ages with > 90 % concordance for zircons <1.0 Ga and $^{207}Pb/^{206}Pb$ ages with > 85 % concordance for zircons >1.0 Ga are plotted). The inherited zircons in these ~ 450 Ma rocks correspond to the ages of aforementioned older rocks and

their inherited zircons. Especially QL09-02 has almost the same inherited zircon distribution as QL09-01(Fig.4.7), e.g. Archean upper intercepts and inherited zircons of ~ 800 Ma in QL09-02 are coherent with the age of QL09-01.

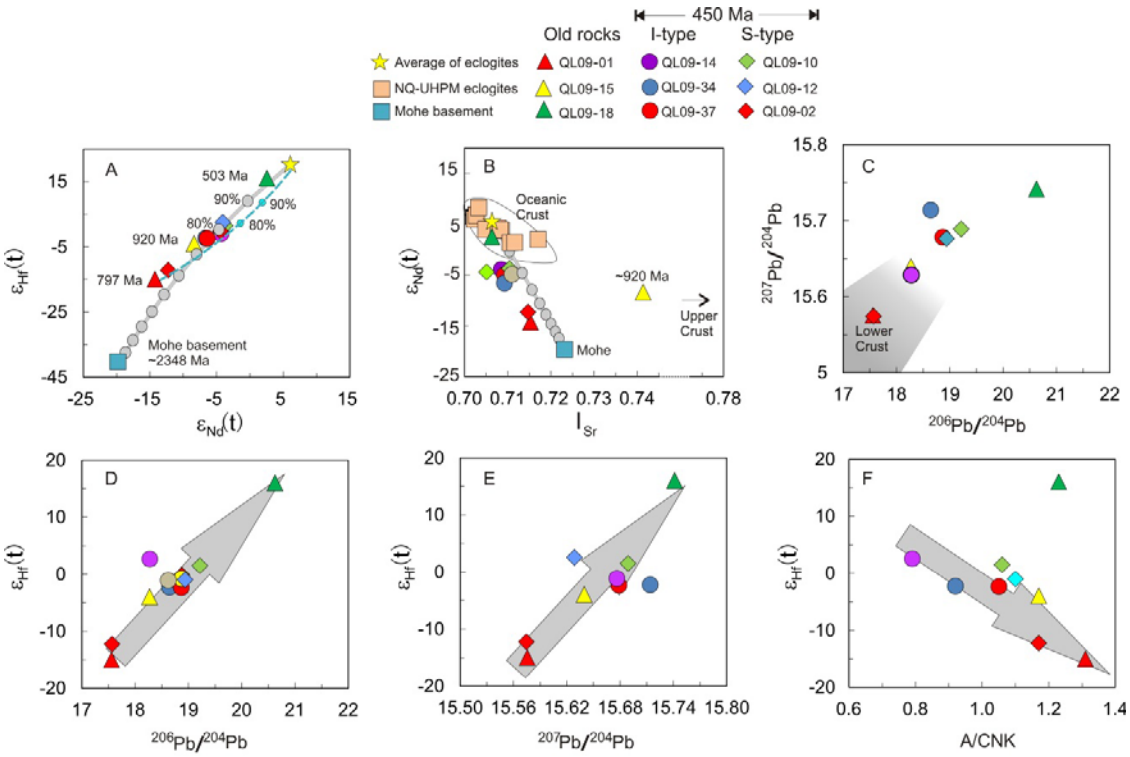

Fig. 4.8. Isotope plots with all the samples (including 923 Ma, 797 Ma, 503 Ma and 450 Ma) age corrected to ~ 450 Ma, showing significant correlations among these samples. QL09-02 has similar isotopes to 797 Ma QL09-01. The 503 Ma granite has similar isotopes to eclogites in NQ-UHPM based on the current available data for eclogites. The ~ 450 Ma granitoids are plotted on apparent 'mixing' trend (thick line in A) between eclogites (Qilian Ocean) and 2348-2470 Ma Mohe basement. Blue dash line in A is modelling using younger crustal endmember QL09-01 (797Ma, this study). Sr and Nd isotope data for eclogites are from Zhang et al. (2008). Hf isotope data for eclogitesare simply adopted global MORB composition (Workman and Hart, 2005). Hf isotope data for Mohe basement are from Li et al. (2007). Sr-Nd isotope data for Mohe basement are from Chen et al.(2007b).

Granitoids of ~ 450 Ma have overlapping isotopic compositions with small negative or positive Nd and Hf isotopes (Table 4.5, Fig. 4.8). The sample depleted in HREEs (QL09-02/07) has distinct large negative $\varepsilon_{Nd}(450)$ and $\varepsilon_{Hf}(450)$ values (-12 and -12, Table 4.5), indicating a crustal origin. Importantly, its isotopes are similar to 797 Ma QL09-01 (Fig. 4.8), most likely genetically related.

The calculated I_{Sr} for QL10-40F is smaller than 0.700, which is likely an artefact in age-correction due to high Rb/Sr (Han et al., 1997).

4.5. Discussion

4.5.1. Origin of 924 Ma and 797 Ma magmatism

Numerous granitoids of ~ 900 Ma have been reported in the NQOB, QB and NQ-UHPM belts (Guo et al., 1999; Guo and Zhao, 2000; Gehrels et al., 2003b; Zhang et al., 2003; Tung et al., 2007a; Song et al., 2012). The 924 Ma QL09-15 is similar to those in the literature (Tung et al., 2008). The small negative zircon $\varepsilon_{Hf}(943)$ (-4.7–0.21) (Chen et al., 2007c) and whole rock $\varepsilon_{Nd(943)}$ (-1.38 – -2.84) (Chen et al., 2007b) have led to the interpretation of reworked crust origin (Chen et al., 2007b, 2007c). Our whole rock $\varepsilon_{Hf}(924)$ is up to 3.8. This value is not completely against the previous interpretations but point to a significant juvenile crust component considering the obvious crustal contribution demonstrated by the inherited zircons older than 1.0 Ga (Fig. 4.7). Therefore, this sample represents a crustal growth event at ~ 920 Ma; however the exact tectonic setting is hard to conclude based only on one sample.

QL09-01 has high SiO_2 (72.7 wt%) and Al_2O_3 (A/CNK: 1.31) (Table 4.4) and negative ε_{Nd} and ε_{Hf} values ($\varepsilon_{Nd}(800)$: -9.8; $\varepsilon_{Hf}(800)$: -8.4, Table 4.5), implying its dominant reworked lower crustal origin which might be induced by the underplating mantle melt. The observation including inherited zircons (Fig. 4.7), Discordia with an upper intercept of Archean age in this study (Fig. 4.7), and the oldest basement of 2348–2470 Ma found in Qilian Block with Archean Hf isotope model ages (Chen et al., 2007b; Li et al., 2007) have particular importance that they offer the evidence of the Archean Basement underneath Qilian Block and that Qilian Block must have been a microcontinent during its journey of drift in the ancient ocean and later-on continental collisions.

4.5.2. Origin of 503 Ma granite

The strong mantle isotopic character of sample QL09-18 (ε_{Nd}(503): 3.1; ε_{Hf}(503): 17, Table 4.5) is similar to the NQ-UHPM eclogites (Zhang et al, 2008) (Fig. 4.8), and indicates that it is either directly or indirectly derived from a depleted mantle source. Though there is no direct evidence for QL09-18 as plagiogranite, we suggest the same origin for it, i.e., it was derived from extensive differentiation (up to 80% ~ 90% fractional crystallization) (Spulber and Rutherford, 1983; Floyd et al., 1998) from a low-K tholeiitic magma under hydrous conditions which is a widely used model for the petrogenesis of plagiogranite (Kay and Senechal, 1976; Flagler and Spray, 1991; Rollinson, 2009). Using the simple batch melting model, the original mantle source can be varying from slightly depleted to slightly enriched in LREEs, depending on the degree of partial melting. The problem is that extensive fractional crystallization could have resulted in the prominent negative Eu anomaly. However, the enclosed mafic diorite enclave QL09-19 representing the earlier cumulate has the identical Eu/Eu* anomaly with QL09-18. This means that fractionation of QL09-19 would have not necessarily resulted in the pronounced negative Eu anomaly in QL09-18.

4.5.3. Origin of ~450 Ma I-type and S-type granites

4.5.3.1. 'Mixing process'

The significant correlations on SiO_2-variation diagrams (Fig. 4.4) and isotope plots (Fig. 4.8) all point to an apparent 'mixing process' which is further demonstrated by positive correlations between initial Pb isotopic ratio and both ε_{Hf} and ε_{Nd} (Fig. 4.8). Importantly, ε_{Hf}(t) is negatively correlated with A/CNK (Fig. 4.8F, except QL09-18), reflecting that the more peraluminous samples have more crustal (vs. mantle) contributions as expected. The old rocks (924 Ma, 797 Ma and 503 Ma) are also plotted on the trend defined by these ~ 450 Ma granitoids (Fig. 4.8) (924 Ma sample has relatively radiogenic Sr isotopes probably due to post-magmatic modification process as it is slightly deformed). However, it is physically unlikely that these granitoids of such a wide spatial and temporal variation are derived from mixing two singular melts. The inherited zircons of aforementioned ages, e.g. 924 Ma, 797 Ma and 503 Ma, repeatedly occur in the 450 Ma rocks (Fig.

4.7). This observation, combined with the linear trends on the isotopes, suggests that these old rocks repeatedly underwent reworking processes with varying proportions of mantle input, in other words, they were essentially derived from the same source at different times.

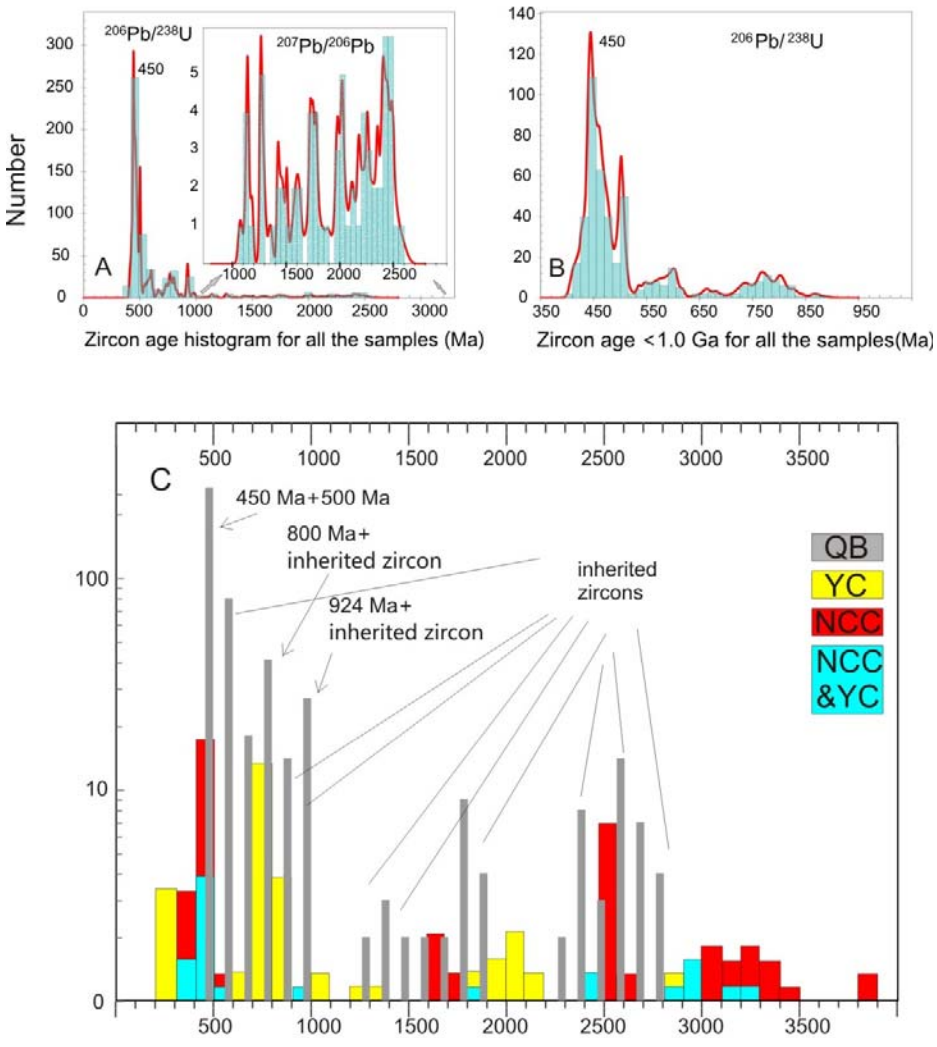

Fig. 4.9. The histogram of all the zircon ages ($^{206}Pb/^{238}U$ for ages <1.0 Ga and $^{207}Pb/^{206}Pb$ for ages >1.0 Ga). A: emphasis the inherited ages >1.0 Ga. B: emphasis the inherited ages between 700 Ma and 500 Ma. C: comparison between North China Craton (NCC), Yangtze Craton (YC) (modified after Grimmer et al., (2003)) and Qilian Block (QB) (this study).

Simple binary isotopic mixing modelling is used to constrain the source materials (Fig. 4.8). The mantle endmember is represented by the eclogites in the NQ-UHPM (yellow star in Fig. 4.8, Zhang et al., 2008) whose protolith is the ocean crust possessing the mantle isotope signatures. Although the Archean basement is involved, we choose to use Mohe basement of 2348–2470 Ma (Chen et al., 2007b; Li et al., 2007) as crustal component because it is the oldest basement with reliable Hf isotopes and inherited zircons of this age are sampled in this study. Therefore the mantle contributions herein are underestimated. The modelling requires 70% ~ 80% mantle contributions for most samples (except for samples QL09-02). This is a strong constraint that the mantle cannot be the appropriate source as 70–80 % mantle derived basalts would make the final magma basaltic rather than peraluminous granitic composition. Hence, the source candidates should be basaltic or andesitic (thus the derived melt can be andestic or granitic) and carry mantle isotopic signatures. They are possibly (1) the subducted oceanic crust, (2) the newly formed island arc crust; (3) the continental arcs. The (2) is unlikely as it is not easy to explain how to melt these topographically high level rocks that are too cold (Niu and O'Hara, 2003, 2009) to produce granitoids at depth. The earlier 'I-type' granitoids in the NQ-UHPM (Wu et al., 2001, 2007; Chen et al., 2011) could be the continental arc and it is very likely that they play a role in the origin of these granitoids evident from the zircons of > 450 Ma (Figs. 4.7 and 4.9). But continental arc alone cannot explain the large compositional variation of the 450 Ma granitoids and also lack of reliable isotope constraints. Importantly, it requires very limited crustal assimilation to maintain the dominant mantle isotope signature. Considering all the petrology and geochemistry, we suggest that the most suitable candidate is the subducted oceanic crust because (1) its derived melt is andesitic, (2) it carries mantle isotopic signatures (see Mo et al., 2008; Niu and O'Hara, 2009; Niu et al., 2013).

Because the inherited zircons in QL09-01 completely covers the range defined by all the samples, it is possible that QL09-01 alone servers as the crustal endmember which can impart its inherited zircons to the derivative melt. We also conducted modelling using 800 Ma QL09-01 as crustal

endmember. It gives similar results (60% ~ 80%) (blue dash line in Fig. 4.8A). This again demonstrates that 797 Ma QL09-01 itself is the hybrid of mantle materials and the ancient basement. Therefore, the continental basement is involved directly or indirectly and the modelling and explanation is independent of which crustal endmembers we choose.

Samples QL09-02 and QL09-07 are distinct from others in terms of less radiogenic Nd and Hf isotopes (Fig. 4.8A) and obvious depleted HREEs (Fig. 4.5) indicative of the presence of garnet as a residual phase in the source region (Defant and Drummond, 1990; Atherton and Petford, 1993; Wolf and Wyllie, 1994; Hou et al., 2012; Wang et al., 2013). Due to the prominent negative $\varepsilon_{Nd}(450)$ and $\varepsilon_{Hf}(450)$ (-12, -12, Table 4.5), the source rocks of these samples must be largely of existing crustal origin. Note that 797 Ma QL09-01 has similar isotopes (Fig. 4.8) to those of QL09-02, contain Grt and present partial melting texture (Fig. 4.2) and that QL09-02 has the same inherited zircon distribution as QL09-01 and some ages matching the age of QL09-01. These indicate that QL09-02/07 is mostly the reworking products of 797 Ma intrusions presented by QL09-01. The more felsic composition of QL09-01 than QL09-02 indicates that QL09-01 may not be the immediate source and the mantle input in QL09-02 is also inevitable as evidenced by its slightly higher $\varepsilon_{Nd}(t)$ and $\varepsilon_{Hf}(t)$ (Fig. 4.8).

To conclude, both I-type and S-type granitoids contain significant mantle derived materials despite the obvious crustal contributions. Therefore, they represent a crustal growth event at ~ 450 Ma. This study is not the only example of 'S-type' granitoids representing crustal growth. Similar samples in South China (Wu et al., 2006b) also represent the crust growth although these rocks were explained as the fast recycling of the sediments of juvenile crust.

4.5.3.2. Implications of tectonic context

The eclogites of MORB protolith in the NQ-UHPM belt (Yang et al., 2002; 2006; Zhang et al., 2008) and the mafic volcanism of MORB affinity in the Lajishan ophiolite (Hou et al., 2005)

suggest the presence of ocean basin located between the QDB and the QB (Yang et al., 2002, 2006). The granitoids in the QB and NQ-UHPM indicate the northward subduction underneath the QB. In the NQ-UHPM, eclogite facies metamorphism happened at 461–497 Ma (Song et al., 2003a; Zhang et al., 2011) which means the collision happened shortly after. The coesite-bearing zircons in the pelitic gneisses indicate that continental material underthrust to depth of 100 ~ 200 km at 420 ~ 430 Ma (Song et al., 2005, 2009). These two time slots constrain that the collision must have happened in between. However, the precise timing remains unclear**.**

As emphasized above, these granitoids are both S-type and I-type intrusions. The inherited zircons of varying age (Figs. 4.7 and 4.9) indicate the very heterogeneous source. Considering the tectonic background, the most likely tectonic setting is the transition time between subduction and collision, e.g. the onset of collision, where the oceanic crust subducting together with the continental masses including the adjacent continental arcs/crust fragments as well as terrigenous sediments (Tatsumi, 2006). These subducted more silicic components and possibly the lower crust material all contribute to the crustal proportions in the 450 Ma granitoids. Varying extents of melting of the crustal rocks which genetically derived from the same source at different times will give the 'apparent mixing' trend and the observed compositional variability of the granitoids**.** The dominant S-type granitoids thereafter (this study; Wu et al., 2002) are the products in response to the collision. The onset of the collision at ~ 450 Ma is also consistent with the exhumation at ~ 420–430 Ma (Song et al., 2005, 2009) which is normally 20–25 Myrs after the onset of continental collision for the old and strong subducting oceanic slab due to the slab break-off (van Hunen and Allen, 2011).

4.5.3.3. Melting of subducted oceanic crust

It has been demonstrated that partial melting of the last fragments of subducted ocean crust in the collision zone is necessary and possible (Mo et al., 2008; Niu and O'Hara, 2009; Huang et al., 2014). The hydrous basaltic (oceanic crust) and granitic (crustal lithologies) solidus is < 650°C at

amphibole-facies (< 40 km) (see Fig. 7 in Mo et al., 2008). This temperature can be easily achieved by the last fragments of oceanic crust because: (1) the arc crust lithosphere is hot; (2) the convergence rate is significantly reduced. Petrological estimates of P–T conditions in the lowermost crust in arcs are generally high (800–1000°C) (Peacock, 2003). Specifically, in the NQ-UHPM belt, the granulite-facies metamorphic rocks record 873–948°C at 2.0 Ga and amphibolite facies metamorphic rocks record 660–695°C at 0.7–0.9 Ga (Song et al., 2003b). Nevertheless, when the collision initiates, the convergence rate would be significantly reduced at least by 50% (Royden and Husson, 2009), which allows the last part of subducted ocean crust to have longer time to be heated up. All these demonstrate that arc crust lithosphere overlying above the mantle wedge during subduction then followed by collision is hot enough to reach ~ 800°C at 40 km depth, therefore sufficient to heat up the subducting slab to its hydrous solidus of 650°C at amphibole-facies (see Fig. 7 in Mo et al., 2008). Partial melting at amphibole-facies is not only supported by thermal permissions but also required by the trace elements as majority of the samples have flat HREE patterns without the garnet signature (Fig. 4.5), indicating garnet is not a stable phase (< 40 km, Mo et al, 2008; Huang et al, 2014).

4.5.4. Tectonic evolution

The NQ-UHPM, located south to the QB, is a better studied continental subduction complex with subducted/exhumed oceanic and continental crustal rocks. It is reasonable to suspect that there was a cold and fast previous subducting oceanic lithosphere to drag down the buoyant continental materials. The basaltic rocks and MORB protolith of eclogites in the NQ-UHPM record two episodes of seafloor spreading: 877–750 Ma (Yang et al., 2006; Zhang et al., 2011) and 550–500 Ma (Hou et al., 2005; Song et al., 2013). If these two periods refer to the same ocean basin spreading (Fig. 4.10A), the ocean must have existed for more than 370 Ma. As no ocean crust > 200 Ma has survived from recycling (Niu et al., 2003), the subduction should have initiated at 677 Ma at the latest. The problem with this model is the lack of the geological record regarded to either the

long lasting subduction-related arc magmatism after 677 Ma prior to 550 Ma or the formation of ocean crust at ocean ridges between 877–750 Ma and 550–550 Ma. Song et al. (2013) suggest that the inherited age of 710 Ma in the eclogite (Zhang et al., 2007) in the NQOB is regarded as the seafloor spreading. We partly agree but consider that it more likely records the earliest back-arc basin opening between QB and Alashan Block. The back-arc spreading at ~ 710 Ma is possible as back-arc basin extension can be shortly after the initiation of cold and fast subduction within 1 Ma (Martinez and Taylor, 2006) due to the extensive mantle wedge convection resulting from steep subduction which is comparable to the modern Mariana subduction zone. Mantle-derived 503 Ma granite might be the product in the back-arc setting. Also the back-back spreading since 710 Ma can explain the quiescence of magmatism after 710 Ma and before 550 Ma. Importantly, the abundant concordant ages younger than 450 Ma (Figs.4.7 and 4.9) could be the xenocrysts and compensate some unexposed or unsampled magmatic events during this quiescence period. These inherited ages could refer to either the oceanic crust formation or subduction-related arc magmatism. In either way, they record the magmatic events. The 450 Ma magmatism is genuinely low temperature hydrous partial melting (< 650 ºC, see above), therefore, has well preserved these xenocrystal zircons. Note that our model is different from the one proposed by Song et al., (2013, 2014). We suggest that the Paleo Qilian Ocean located between the Qaidam Block and the Qilian Block (Fig. 10A) and the whole NQOB area was the back-arc, while they think the Paleo Qilian Ocean located in the NQOB area. In our model, closure of the back-arc basin resulted in the subduction complex in the NQOB and probably has led to the secondary back-arc basin opening further north. The ~ 450 Ma granitoids are the products in response to the closure of the Qilian Ocean and the onset of the Qilian-Qaidam continental collision.

Alternatively, 877–750 Ma (Yang et al., 2006; Zhang et al., 2011) and 550–500 Ma (Song et al., 2013) could record oceanic crust of two different ocean basins, e.g. Neoproterozoic Ocean and Qilian Ocean, respectively (Fig. 4.10B) (Yang et al., 2006). The NQOB and NQ-UHPM are two

independent tectonic units due to the paired subduction at the same time around > 500–400 Ma (Fig. 4.10B) (Yang et al., 2006). This model may explain the lack of direct geological record between 877–750 Ma and 550–500 Ma. But the NQOB is a cold subduction zone (Song et al., 2007; Zhang et al., 2007) which requires the old oceanic lithosphere. In Yang's model (Yang et al., 2006), the 550 – 550 Ma ocean basin lived only for ~50 Ma, which is not old enough to induce the cold subduction. We suggest that our model is more reasonable, but still requires more geological evidence.

4.5.5. Nature of the Qilian Block

Some people consider ~ 920 Ma intrusions/gneisses are the basement of the Qilian Block (Zhang et al., 2003; Tung et al., 2007a, 2008). The Paleoproterozoic and Archean basement has to some extent been overlooked. In our study, all the inherited zircons >1.0 Ga defined a Discordia with an Archean intercept of 2712 Ma (the final panel in Fig. 4.7) which is also seen in the individual sample, e.g. QL09-01, QL09-02 (Fig. 4.7). These clearly confirm the existence of Archean basement. Especially, the isotope modelling (Fig. 4.8) emphasize the important role of Archean basement in the ~ 450 Ma magmatism. The Qilian Block must once be a microcontinent during the assembling and the breaking-up of supercontinent and experienced multiple reworking processes later on. The magmatism of ~ 920 Ma and ~ 800 Ma were previously interpreted to be related to the Rodinia assembly (Guo et al., 1999; Wan et al., 2001a, 2001b; Zhang et al., 2003; Tseng et al., 2006; Song et al., 2010b, 2013) and break-up (Zhang et al., 2003; Li et al., 2008; Song et al., 2010b), respectively. Based on our data, we can only say that 924 Ma and 797 Ma magmatic episodes are respectively crustal growth and crustal reworking processes. It has been debated that the basement of the Qilian Block has a closer link to Yangtze Craton (YC) over North China Craton (NCC) (Tung, 2007a and references therein) because of none magmatism during 0.6 – 1.6 Ga, especially 0.8 – 0.9 Ga in NCC (Fig. 4.9C, modified after Grimmer et al., 2003). Probably the most obvious conclusion from Fig. 4.9C is that the distribution of magmatism in the QB matches neither NCC nor

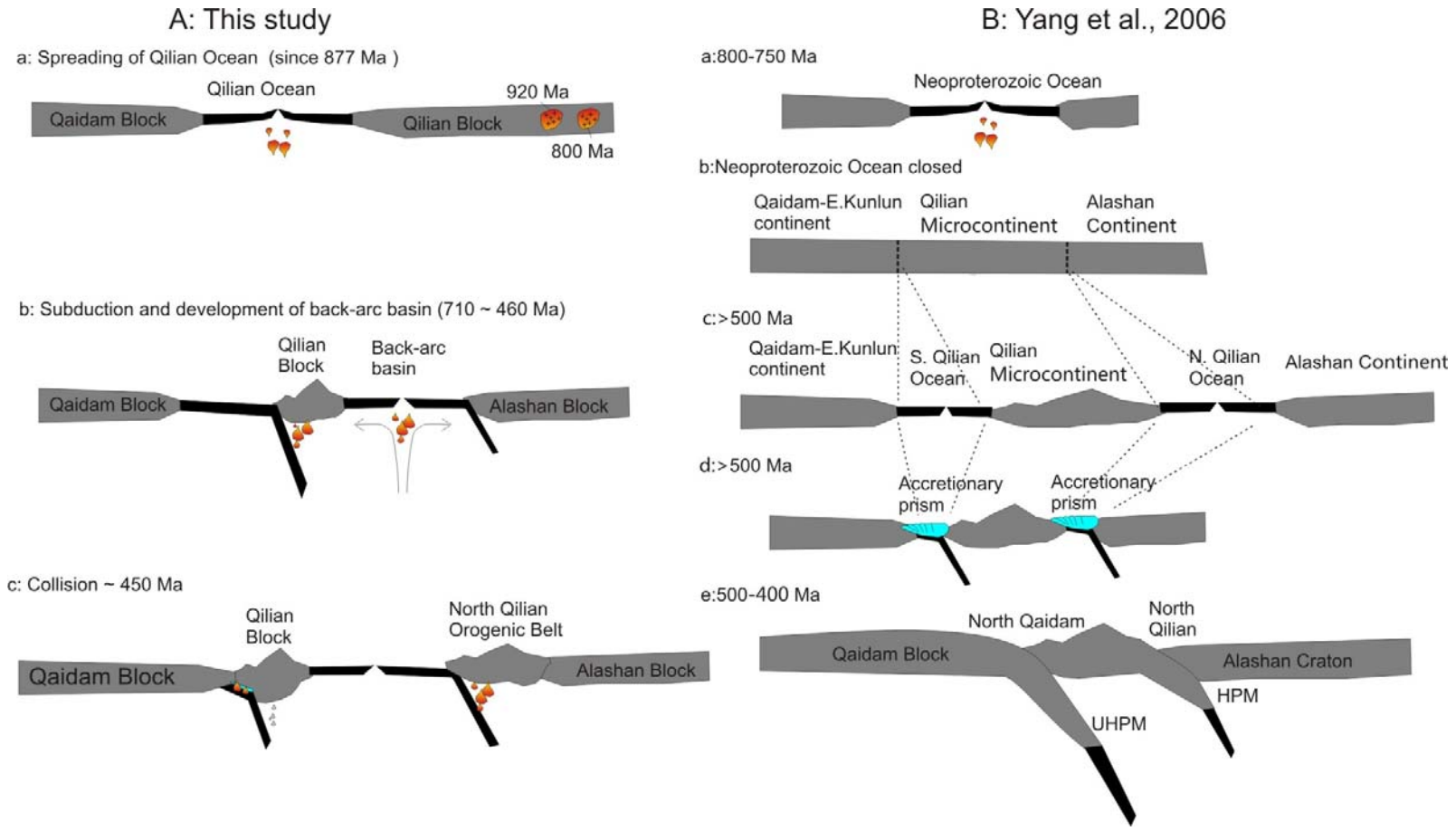

Fig. 4.10. Comparision of two models proposed by this study and Yang et al., (2006), respectively.A, this study: Cartoons showing the Qilian Ocean floor spreading between Qaidam Block and Qilian Block during the Proterozic time (a) (877 Ma: the protolith age of eclogites in NQ-UHPM (Zhang et al., 2011), initiation of subduction and related back-arc extension(b), and the syncollisional magmatism at ~ 450 Ma (c). B, Yang et al., 2006: Cartoons showing the Neoproterozoic Ocean opened and closed. Two independent Qilian oceans opened and closed during Paleozoic time. See details in Yang et al, (2006)

YC. Based on Fig. 4.9, from 1.6 Ga to Archean, the QB is comparable to both NCC and YC or maybe more closer to NCC. During 0.6 ~ 1.6 Ga, the QB and YC experienced coherent history. It might be arbitrary to say that the QB has YC affinity only because of the 0.8 ~ 0.9 Ga magmatism, especially the new finding of the ~ 0.9 Ga continental rifting magmatism in the NCC (Peng et al., 2011a, 2011b) which could be related to the 924 Ma in this study.

4.6. References

Atherton, M.P., Petford, N., 1993. Generation of sodium-rich magmas from newly underplated basaltic crust. Nature 362, 144-146.

Chen, D., Liu, L., Sun, Y., Liou, J., 2009a. Geochemistry and zircon U-Pb dating and its implications of the Yukahe HP/UHP terrane, the North Qaidam, NW China. Journal of Asian Earth Sciences 35, 259-272.

Chen, N., Gong, S., Sun, M., Li, X., Xia, X., Wang, Q., Wu, F., Xu, P., 2009b. Precambrian evolution of the Quanji Block, northeastern margin of Tibet: Insights from zircon U-Pb and Lu-Hf isotope compositions. Journal of Asian Earth Sciences 35, 367-376.

Chen, N.S., Wang, X.Y., Zhang, H.F., 2007a. Components and metamorphism of the basements of the Qaidam and Oulongbuluke micro-continental blocks, and a tentative interpretation of paleocontinental evolution in NW-Central China. Earth Science Frontiers 14, 43-55.

Chen, N.S., Wang, X.Y., Zhang, H.F., Sun, M., Li, X.Y., Chen, Q., 2007b. Geochemistry and Nd-Sr-Pb Isotopic Compositions of Granitoids from Qaidam and Oulongbuluke Micro-Blocks，NW China Constraints on Basement Nature and Tectonic Affinity. Journal of Earth Science 32, 7-21.

Chen, N.S., Xia, X.P., Li, X.Y., Sun, M., 2007c. Timing of magmatism of the gneissic-granite plutons along north Qaidam margin and implications for Precambrian crustal accretions: zircon U-Pb dating and Hf isotope evidences. Acta Petrologica Sinica 23, 501-512 (in Chinese with English abstract).

Chen, X.H., Yin, A., George, G., Li, L., Jiang, R.B., 2011. Chemical geodynamics of granitic magmatism in the basement of the eastern Qaidam basin, Northern Qinghai-Tibet Plateau. Acta Geologica Sinica 85, 157-171 (in Chinese with English abstract).

Defant, M.J., Drummond, M.S., 1990. Derivation of some modern arc magmas by melting of young subducted lithosphere. Nature 347, 662-665.

Flagler, P.A., Spray, J.G., 1991. Generation of plagiogranite by amphibolite anatexis in oceanic shear zones. Geology 19, 70-73.

Floyd, P.A., Yaliniz, M.K., Goncuoglu, M.C., 1998. Geochemistry and petrogenesis of intrusive and extrusive ophiolitic plagiogranites, Central Anatolian Crystalline Complex, Turkey. Lithos 42, 225-241.

Gehrels, G., Kapp, P., DeCelles, P., Pullen, A., Blakey, R., Weislogel, A., Ding, L., Guynn, J., Martin, A., McQuarrie, N., 2011. Detrital zircon geochronology of pre-Tertiary strata in the Tibetan-Himalayan orogen. Tectonics 30, TC5016.

Gehrels, G.E., Yin, A., Wang, X.-F., 2003a. Detrital-zircon geochronology of the northeastern Tibetan plateau. Geological Society of America Bulletin 115, 881-896.

Gehrels, G.E., Yin, A., Wang, X.F., 2003b. Magmatic history of the northeastern Tibetan Plateau. Journal of Geophysical Research 108 (B9), 2423.

Grimmer, J.C., Ratschbacher, L., McWilliams, M., Franz, L., Gaitzsch, I., Tichomirowa, M., Hacker, B.R., Zhang, Y., 2003. When did the ultrahigh-pressure rocks reach the surface? A 207Pb/206Pb zircon, 40Ar/39Ar white mica, Si-in-white mica, single-grain provenance study of Dabie Shan synorogenic foreland sediments. Chemical Geology 197, 87-110.

Guo, J.J., Zhao, F.Q., 2000. New choronoligcal evidence of the age of Huangyuan in teh eastern segment of mid-Qilian massif and its geological significance. Regional Geology of China 19, 26-31(in Chinese with English Agbstract).

Guo, J.J., Zhao, F.Q., Li, H.K., 1999. Jinningian collisional granite belt in the eastern sector of the central Qilian massif and its implication. . Acta geosci Sin 20, 10-15 (in Chinese with English abstract).

Han, B.F., Wang, S.-G., Jahn, B.-M., Hong, D.W., Kagami, H., Sun, Y.L., 1997. Depleted-mantle source for the Ulungur River A-type granites from North Xinjiang, China: geochemistry and Nd-Sr isotopic evidence, and implications for Phanerozoic crustal growth. Chemical Geology 138, 135-159.

Hou, Q.Y., Zhang, H.F., Zhang, B.R., Zhao, Z.D., Zhu, Y.H., 2005. Characteristics and tectonic affinity of Laji Shan Paleo-Mantle in Qilian orogenic belt:a geochemical study of basalts. Journal of China University of Geosciences 30, 61-70 (in Chinese with English abstract).

Hou, Z.-Q., Zheng, Y.-C., Zeng, L.-S., Gao, L.-E., Huang, K.-X., Li, W., Li, Q.-Y., Fu, Q., Liang, W., Sun, Q.-Z., 2012. Eocene–Oligocene granitoids in southern Tibet: Constraints on crustal anatexis and tectonic evolution of the Himalayan orogen. Earth and Planetary Science Letters 349–350, 38-52.

Huang, H., Niu, Y., Nowell, G., Zhao, z., Yu, X., Zhu, D., Mo, X., Ding, S., submitted. Geochemical constraints on the petrogenesis of granitoids in the East Kunlun Orogenic blet, northern Tibetan Plateau: implications fro the continental crust growth through syncollisional felsic magmatism. Chemical Geology.

Irvine, T.N., Baragar, W.R.A., 1971. A guide to the chemical classification of the common volcanic rocks. Canadian Journal of Earth Sciences 8, 523-548.

Kay, R., Senechal, R., 1976. Rare earth geochemistry of the Troodos ophiolite complex. J. Geophys. Res.;(United States) 81.

Li, X.Y., Chen, N.s., Xia, X.P., Sun, M., Xu, P., Wang, Q.Y., Wang, X.Y., 2007. Constraints on the timing of the early-Paleoproterozoic magmatism and crustal evolution of the Oulongbuluke microcontinent: U-Pb and Lu-Hf isotope systematics of zircons from Mohe granite pluton. Acta Petrologica Sinica 23, 513-522. (In Chinese with English abstract).

Li, Z.X., Bogdanova, S.V., Collins, A.S., Davidson, A., De Waele, B., Ernst, R.E., Fitzsimons, I.C.W., Fuck, R.A., Gladkochub, D.P., Jacobs, J., Karlstrom, K.E., Lu, S., Natapov, L.M., Pease, V., Pisarevsky, S.A., Thrane, K., Vernikovsky, V., 2008. Assembly, configuration, and break-up history of Rodinia: A synthesis. Precambrian Research 160, 179-210.

Liu, Y.S., Hu, Z.C., Gao, S., Gunther, D., Xu, J., Gao, C.G., Chen, H.H., 2008. In situ analysis of major and trace elements of anhydrous minerals by LA-ICP-MS without applying an internal standard. Chemical Geology 257 (1-2), 34-43.

Martinez, F., Taylor, B., 2006. Modes of crustal accretion in back-arc basins: Inferences from the Lau Basin. Geophysical Monograph Series 166, 5-30.

Mo, X.X., Niu, Y.L., Dong, G.C., Zhao, Z.D., Hou, Z.Q., Su, Z., Ke, S., 2008. Contribution of syncollisional felsic magmatism to continental crust growth: A case study of the Paleogene Linzizong volcanic Succession in southern Tibet. Chemical Geology 250, 49-67.

Niu, Y. L., Batiza, R., 1997. Extreme mantle source heterogeneities beneath the northern East Pacific Rise-Trace element evidence from near-ridge seamounts, Proc. of 30th IGC, 109-120.

Niu, Y. L.,O'Hara, M. J., 2003. Origin of ocean island basalts: A new perspective from petrology, geochemistry, and mineral physics considerations. Journal of Geophysical Research 108.

Niu, Y. L., O'Hara, M. J., Pearce, J. A., 2003. Initiation of subduction zones as a consequence of lateral compositional buoyance contrast within the lithosphere: a Petrological Perspective. Journal of Petrology 44 (5), 851-866.

Niu, Y. L., O'Hara, M.J., 2009. MORB mantle hosts the missing Eu (Sr, Nb, Ta and Ti) in the continental crust: New perspectives on crustal growth, crust–mantle differentiation and chemical structure of oceanic upper mantle. Lithos 112, 1-17.

Niu, Y.L., Zhao, Z.D., Zhu, D.C. Mo, X.X., 2013. Continental collision zones are primary sites for net continental crust growth – A testable hypothesis. Earth-Science Reviews 127, 96-110.

Nowell, G.M., Pearson, D.G., Ottley, C.J., Schweiters, J., Dowall, D., 2003. Long-term performance characteristics of a plasma ionisation multi-collector mass spectrometer (PIMMS): The thermofinnigan neptune. Plasma Source Mass Spectrometry: Applications and Emerging Technologies. Cambridge: Royal Society of Chemistry, 307-320.

Pan, G.T., Ding, J., Yao, D.S.W., L. Q., 2004. Geological map of the Qinghai-Xizang (Tibet) Plateau and adjacent areas. Chengdu Cartographic Publishing House.

Peacock, S.M., 2003. Thermal structure and metamorphic evolution of subducting slabs. Geophysical Monograph-American Geophysical Union 138, 7-22.

Peng, P., Bleeker, W., Ernst, R.E., Söderlund, U., McNicoll, V., 2011a. U–Pb baddeleyite ages, distribution and geochemistry of 925 Ma mafic dykes and 900 Ma sills in the North China Craton: Evidence for a Neoproterozoic mantle plume. Lithos 127, 210-221.

Peng, P., Zhai, M.-G., Li, Q., Wu, F., Hou, Q., Li, Z., Li, T., Zhang, Y., 2011b. Neoproterozoic (~ 900 Ma) Sariwon sills in North Korea: Geochronology, geochemistry and implications for the evolution of the south-eastern margin of the North China Craton. Gondwana Research 20, 243-254.

Qinghai Geological Survey Institute, 2006. 1：250, 000 regional geological survey digital report of Xining and Menyuan In Chinese.

Rollinson, H., 2009. New models for the genesis of plagiogranites in the Oman ophiolite. Lithos 112, 603-614.

Royden, L.H., Husson, L., 2009. Subduction with variations in slab buoyancy: models and application to the Banda and Apennine systems, Subduction Zone Geodynamics. Springer, 35-45.

Shi, R.D., Yang, J., Wu, C.l., IIzuka, T., Hirata, T., 2004. Island Arc volcanic rocks in North Qaidam UHP metamorphic belt. Acta Geologica Sinica 78, 52-64 (in Chinese with English abstract).

Song, S., Niu, Y., Su, L., Xia, X., 2013. Tectonics of the North Qilian orogen, NW China. Gondwana Research23, 1378-1401.

Song, S., Su, L., Li, X.H., Niu, Y.L., Zhang, L.F., 2012. Grenville-age orogenesis in the Qaidam-Qilian block: The link between South China and Tarim. Precambrian Research 220, 9-22.

Song, S., Niu, Y.L., Wei, C.J., Ji, J.Q., Su, L., 2010a.Metamorphism, anatexis, zircon ages and tectonic evolution of the Gongshan Block in the northern Indochina continent-An eastern extension of Lhasa Block.Lithos 120, 3-4.

Song, S., Su, L., Li, X.-h., Zhang, G., Niu, Y., Zhang, L., 2010b. Tracing the 850-Ma continental flood basalts from a piece of subducted continental crust in the North Qaidam UHPM belt, NW China. Precambrian Research 183, 805-816.

Song, S., Zhang, L., Niu, Y., Su, L., Jian, P., Liu, D., 2005. Geochronology of diamond-bearing zircons from garnet peridotite in the North Qaidam UHPM belt, Northern Tibetan Plateau: A record of complex histories from oceanic lithosphere subduction to continental collision. Earth and Planetary Science Letters 234, 99-118.

Song, S., Zhang, L., Niu, Y., Su, L., Song, B., Liu, D., 2006. Evolution from oceanic subduction to continental collision: a case study from the Northern Tibetan Plateau based on geochemical and geochronological data. Journal of Petrology 47, 435-455.

Song, S.G., Niu, Y.L., Zhang, L.F., Zhang, G.B., 2009. Time constraints on orogenesis from oceanic subduction to continetnal subduction, collision, and exhumation: an example from North Qilian and North Qaidam HP-UHP belts. Acta petrologica Sinica 25, 2067-2077.

Song, S.G., Yang, J.S., Liou, J.G., Wu, C.L., Shi, R.D., Xu, Z.Q., 2003a. Petrology, geochemistry and isotopic ages of eclogites from the Dulan UHPM Terrane, the North Qaidam, NW China. Lithos 70, 195-211.

Song, S.G., Yang, J.S., Xu, Z.Q., Liou, J.G., Shi, R.D., 2003b. Metamorphic evolution of the coesite‐bearing ultrahigh‐pressure terrane in the North Qaidam, Northern Tibet, NW China. Journal of Metamorphic Geology 21, 631-644.

Song, S.G., Zhang, L.F., Niu, Y., Wei, C.J., Liou, J.G., Shu, G.M., 2007. Eclogite and carpholite-bearing metasedimentary rocks in the North Qilian suture zone, NW China: implications for Early Palaeozoic cold oceanic subduction and water transport into mantle. Journal of Metamorphic Geology 25, 547-563.

Spulber, S.D., Rutherford, M.J., 1983. The Origin of Rhyolite and Plagiogranite in Oceanic Crust: An Experimental Study. Journal of Petrology 24, 1-25.

Sun, S.s., McDonough, W.F., 1989. Chemical and isotopic systematics of oceanic basalts: implications for mantle composition and processes. Geological Society, London, Special Publications 42, 313-345.

Tatsumi, Y., 2006. High-Mg andesites in the Setouchi volcanic belt, southwestern Japan: Analogy to Archean magmatism and continental crust formation? Annu. Rev. Earth. Planet. Sci. 34, 467-499.

Tseng, C.-Y., Yang, H.-Y., Yusheng, W., Dunyi, L., Wen, D.-J., Lin, T.-C., Tung, K.-A., 2006. Finding of Neoproterozoic (□775 Ma) magmatism recorded in metamorphic complexes from the North Qilian orogen: Evidence from SHRIMP zircon U-Pb dating. Chinese Science Bulletin 51, 963-970.

Tung, K.A., Yang, H.J., Yang, H.Y., Liu, D.Y., Zhang, J.X., Wan, Y.S., Tseng, C.Y., 2007a. SHRIMP U-Pb geochronology of the zircons from the Precambrian basement of the Qilian Block and its geological significances. Chinese Science Bulletin 52, 2687-2701.

Tung, K.A., Yang, H.R., Yang, H.Y., Liu, D.Y., et al., 2008. Qilian Neoproterozoic granitoids SHRIMP zircon U-Pb geochronology, elemental and Sr - Nd isotope geochemistry. Bulletin of mineralogy , petrology and geochemistry 27, 106-108.

Tung, K.A., Yang, H.Y., Liu, D., Zhang, J.X., Tseng, C.Y., Wan, Y.S., 2007b. SHRIMP U-Pb geochronology of the detrital zircons from the Longshoushan Group and its tectonic significance. Chinese Science Bulletin 52.

van Hunen, J., Allen, M.B., 2011. Continental collision and slab break-off: A comparison of 3-D numerical models with observations. Earth and Planetary Science Letters 302, 27-37.

Wan, Y.S., Xu, Z.Q., Yang, J.S., Zhang, J.X., 2001. Ages and Compositions of the Precambrian High-grade Basement of the Qilian Terrane and Its Adjacent Areas. Acta Geologica Sinica - English Edition 75, 375-384.

Wang, S.-J., Li, S.-G., Chen, L.-J., He, Y.-S., An, S.-C., Shen, J., 2013. Geochronology and geochemistry of leucosomes in the North Dabie Terrane, East China: implication for post-UHPM crustal melting during exhumation. Contributions to Mineralogy and Petrology 165 (5), 1009-1029.

Wolf, M.B., Wyllie, P.J., 1994. Dehydration-melting of amphibolite at 10 kbar: the effects of temperature and time. Contributions to Mineralogy and Petrology 115, 369-383.

Workman, R.K., Hart, S.R., 2005. Major and trace element composition of the depleted MORB mantle (DMM). Earth and Planetary Science Letters 231, 53-72.

Wu, C. L., Yang, J.S., Wooden, J., Liou, J., Li, H., Shi, R., Meng, F., Persing, H., Meibom, A., 2002. Zircon SHRIMP dating of granite from Qaidamshan, NW China. Chinese Science Bulletin 47, 418-422.

Wu, C.L., Yang, J.S., Ireland, T., Wooden, J.L., Li, H.B., Wan, Y.S., Shi, R.D., 2001. Zircon SHRIMP ages of Aolaoshan granite from the south margin of Qilianshan and its geological significance. Acta Petrologica Sinica 17, 215-221.

Wu, C.L., Gao, Y.H., Wu, S., Chen, Q., Wooden, J.L., Mazadab, F.K., Mattinson, C., 2007. Zircon SHRIMP U-Pb dating of granites from the Da Qaidam area in the north margin of Qaidam Basin, NW China. . Acta Petrologica Sinica 23, 1861-1875 (in Chinese with English abstract).

Wu, C.L., Xu, X.Y., Gao, Q.M., Li, X.M., Lei, M., et al., 2010. Early Palaezoic granitoid magmatism and tectonic evolution in North Qilian, NW China. Acta Petrologica Sinica 26, 1027-1044 (in Chinese with English abstract). .

Wu, C.L., Yao, S.Z., Zeng, L.S., al., E., 2006a. Double subduction of the Early Paleozoic North Qilian oceanic plate: evidence from granites in the central segment of North Qilian, NW China. Geology in China 33, 1197-1208 (in Chinse with English abstract).

Wu, R. X., Zheng, Y. F., Wu, Y. B., et al., 2006b. Reworking of juvenile crust: Element and isotope evidence from Neoproterozoic granodiorite in South China. Precambrian Research 146, 179-212.

Xia, X., Song, S., 2010. Forming age and tectono-petrogenises of the Jiugequan ophiolite in the North Qilian Mountain, NW China. Chinese Science Bulletin 55, 1899-1907.

Xiao, W.J., Windley, B.F., Yong, Y., Zhen, Y., Chao, Y., Liu, C.Z., Li, J., 2009. Early Paleozoic to Devonian multiple-accretionary model for the Qilian Shan, NW China. Journal of Asian Earth Sciences 35, 323-333.

Xu, W.C., Zhang, H.F., Liu, X.M., 2007. U-Pb zircon dating constraints on formation time of Qilian high-grade metamorphic rock and its tectonic implications. Chinese Science Bulletin 52, 531-538.

Xu, Z.Q., Xu, H.f., Zhang, J.x., al., e., 1994. The Zoulang Nanshan Caledonian Subduction Complex in the Northern Qilian Mountains and Its Dynamics1. Acta Geologica Sinica - English Edition 7, 225-241.

Yang, J. S., Wu, C.L., Zhang, J., Shi, R., Meng, F., Wooden, J., Yang, H.-Y., 2006. Protolith of eclogites in the north Qaidam and Altun UHP terrane, NW China: Earlier oceanic crust? Journal of Asian Earth Sciences 28, 185-204.

Yang, J.S., Xu, Z.Q., Zhang, J.X., Song, S.G., Wu, C.L., Shi, R.D., Li, H.B., Maurice, B., 2002. Early Palaeozoic North Qaidam UHP metamorphic belt on the north-eastern Tibetan plateau and a paired subduction model. Terra Nova 14, 397-404.

Yin, A., Harrison, T.M., 2000. Geologic evolution of the Himalayan-Tibetan Orogen. Ann. Rev. Earth Planet. Sci 28, 211-280.

Yong, Y., Xiao, W.J., Yuan, C., Yan, Z., Li, J.L., 2008. Geochronology and geochemistry of Paleozoic granitic plutons from the eastern Central Qilian and their tectonic implications. Acta Petrologica Sinica 24, 855-866 (in Chinese with English Abstract).

Zhang, C., Zhang, L., Roermund, H.V., Song, S., Zhang, G., 2011. Petrology and SHRIMP U–Pb dating of Xitieshan eclogite, North Qaidam UHP metamorphic belt, NW China. Journal of Asian Earth Sciences 42, 752-767.

Zhang, G., Song, S., Zhang, L., Niu, Y., 2008. The subducted oceanic crust within continental-type UHP metamorphic belt in the North Qaidam, NW China: Evidence from petrology, geochemistry and geochronology. Lithos 104, 99-118.

Zhang, J.X., Yang, J., Mattinson, C., Xu, Z., Meng, F., Shi, R., 2005. Two contrasting eclogite cooling histories, North Qaidam HP/UHP terrane, western China: Petrological and isotopic constraints. Lithos 84, 51-76.

Zhang, J.X., Meng, F.C., Wan, Y.S., 2007. A cold Early Palaeozoic subduction zone in the North Qilian Mountains, NW China: petrological and U-Pb geochronological constraints. Journal of Metamorphic Geology 25, 285-304.

Zhang, J.X., Wan, Y.S., Meng, F.C., Yang, J.S., Xu, Z.Q., 2003. Geochemistry, Sm-Nd and U-Pb isotope study of gneisses (schists) enclosing eclogites in the North Qaidam Mountains---deeply subducted Precambrian metamorphic basement. Acta Petrologica Sinica 19, 443-451 (in Chinese with English abstract).

Zhang, J.X., Yang, J.S., Meng, F.C., Wan, Y.S., Li, H.M., Wu, C.L., 2006. U-Pb isotopic studies of eclogites and their host gneisses in the Xitieshan area of the North Qaidam Mountains, western China: New evidence for an early Paleozoic HP-UHP metamorphic belt. Journal of Asian Earth Sciences 28, 143-150.

Chapter 5: Tectonic implications of zircon in situ Hf isotopes and whole rock Sr-Nd-Pb-Hf isotopes of Gcha and HY granitoids in the Qilian Block

5.1. Introduction

In this chapter, we discusse 7 more samples from the same sampling area as those samples discussed in Chapter 4 — Huangyuan (HY) and Gangcha (Gcha) in the QB (Fig. 5.1). In addition to the same techniques employed in the previous chapter, 5 samples in this chapter as well as 6 dated samples in the last chapter were further analysed for zircon *in situ* Hf isotopes.

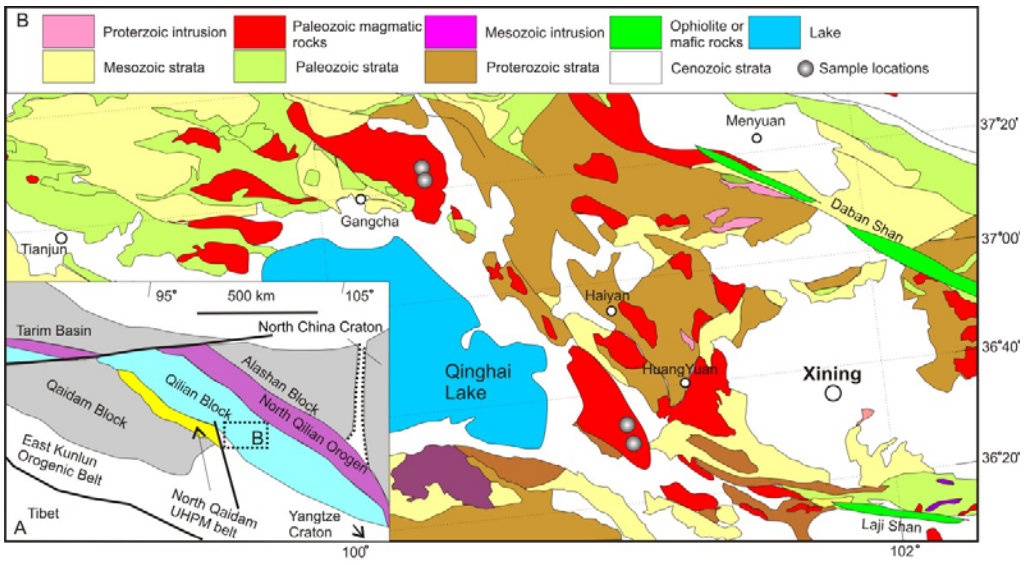

Fig. 5.1. A, Schematic map showing major tectonic units of the Qilian Orogenic Belt (after Song et al., 2013). B, Simplified geological map of the Qilian Block (QB) showing the distribution of granitoids and sampling area.

5.2. Results

Zircon U-Pb dating results for HY and Gcha samples in this chapter show the same character as samples in Chapter 4, e.g. the large age distribution along the Concordia (Fig. 5.2, Table 5.1). The ages between 420 Ma and 510 Ma cannot be subdivided into distinct populations based on textural or chemical criteria (zircon trace elements, Appendix G). The age of ~450 Ma was considered as the emplacing age for both types of rocks according to the youngest clustering concordant ages as well as the age peaks on the histogram in last chapter, However, plotting all the ages together and looking at a large resolution of the histogram, we find that the HY rocks slightly post-date Gcha rocks (~445 Ma vs. ~450 Ma, Fig. 5.3). As ages younger 510 Ma are continuous and not distinguishable from each other, we consider the ages >520 Ma as inherited ages.

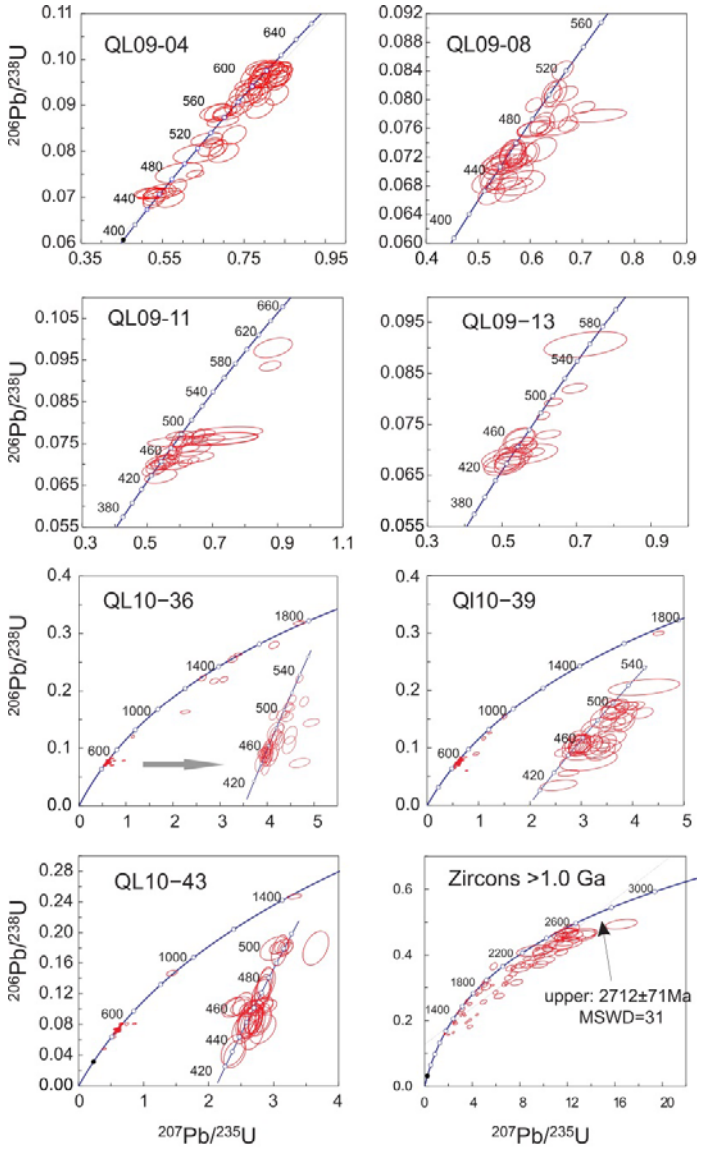

Fig. 5.2. Zircon U-Pb Concordia diagrams showing the continuous age spread along the Concordia.

HY samples in chapter 4 are mostly S-type granitoids. HY samples in this chapter are two-mica granites containing quartz, K-feldspar (>10%), plagioclase, biotite, euhedral muscovite, ±allanite. They are predominantly highly felsic (SiO_2:67.4 – 72.4 wt%) (Table 5.1). High-K and shoshonitic compositions are predominant with two of them in medium-K composition (Fig. 5.4F). Whole rock $\varepsilon_{Nd}(450)$ values range from -4.3 – -3.7 and ~ -11, corresponding to the $\varepsilon_{Hf}(450)$ values of -1.5 – 1.5 and ~ -11(Table 5.2, Fig. 5.5). Initial Pb isotopic signature is relatively radiogenic: 38.423 –38.040

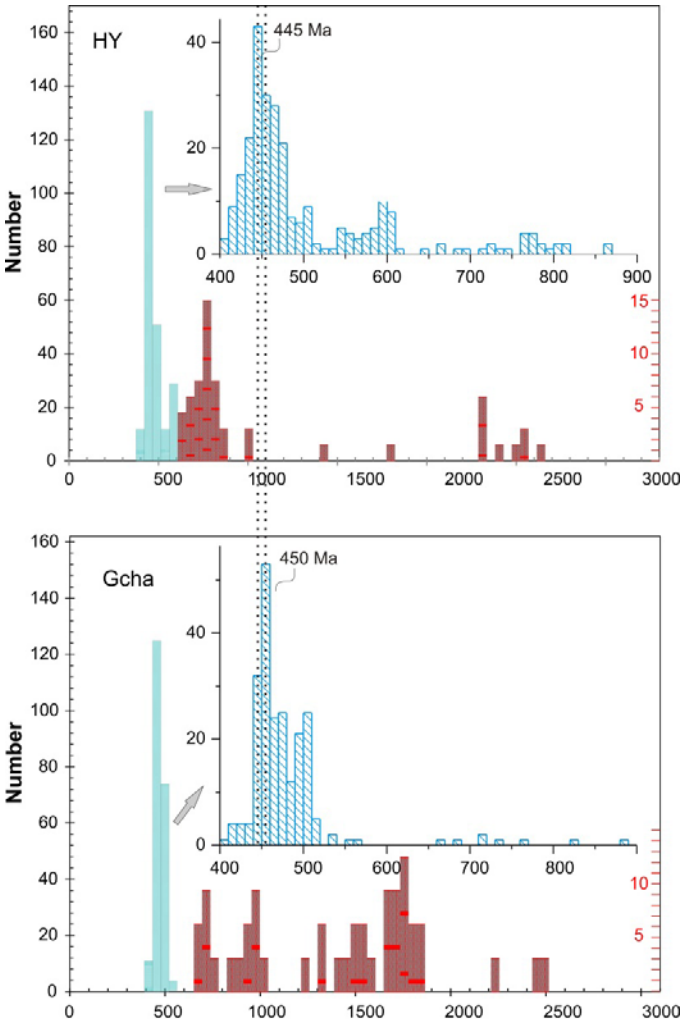

Fig. 5.3. Histograms of zircon ages for Gcha and HY rocks showing that Gcha rocks slightly predate HY rocks. The inherited zircons are shown in red with different scales (red scale on the right side).

($^{208}Pb/^{204}Pb$), 15.601 –15.686 ($^{207}Pb/^{204}Pb$), 17.702 – 19.169 ($^{206}Pb/^{204}Pb$) (Table. 5.2). Initial Sr isotopic ratios range from 0.7090 to 0.7126 (Table 5.2). Zircon *in situ* Hf isotopes at 450 Ma in HY rocks distribute a wide range, dominantly varying from -32 – 0 with a peak at -6 and a few largely negative values at ~ -60 (Fig. 5.6A, Table 5.3). The Hf isotopic variations at the zircon crystallization age are relatively limited, ranging from -30 – 10 (Fig. 5.7A). Two-stage zircon Hf model ages of HY rocks vary from 1000 Ma to 3250 Ma (Fig. 5.7C, Table 5.3).

Compared to the dominant I-type compositions in Chapter 4, Gcha samples in this chapter share the same mineralogy as some of the previous ones but possess more siliceous and peraluminous compositions (Fig. 5.4). They are biotite-granite, mainly consisting of biotite, quartz and plagioclase. K-feldspar is less than 5% and muscovite appears as a minor secondary mineral. They may present the highly evolved unit of the Gcha pluton. The high-K compositions are dominant with two of them in medium-K composition. Whole rock $\varepsilon_{Nd}(450)$ values cluster at -6.4 – -4.8 and $\varepsilon_{Hf}(450)$ values vary from -4.3 – -0.8 (Fig. 5.5, Table 5.2). Initial Pb isotopes vary from 38.335 to 38.725 ($^{208}Pb/^{204}Pb$), 15.659 to 15.676 ($^{207}Pb/^{204}Pb$), and 18.572 to 18.875 ($^{206}Pb/^{204}Pb$) (Fig. 5.5, Table 5.2). Initial Sr isotopic ratios range from 0.7116 to 0.7147, overlapping with the HY rocks.

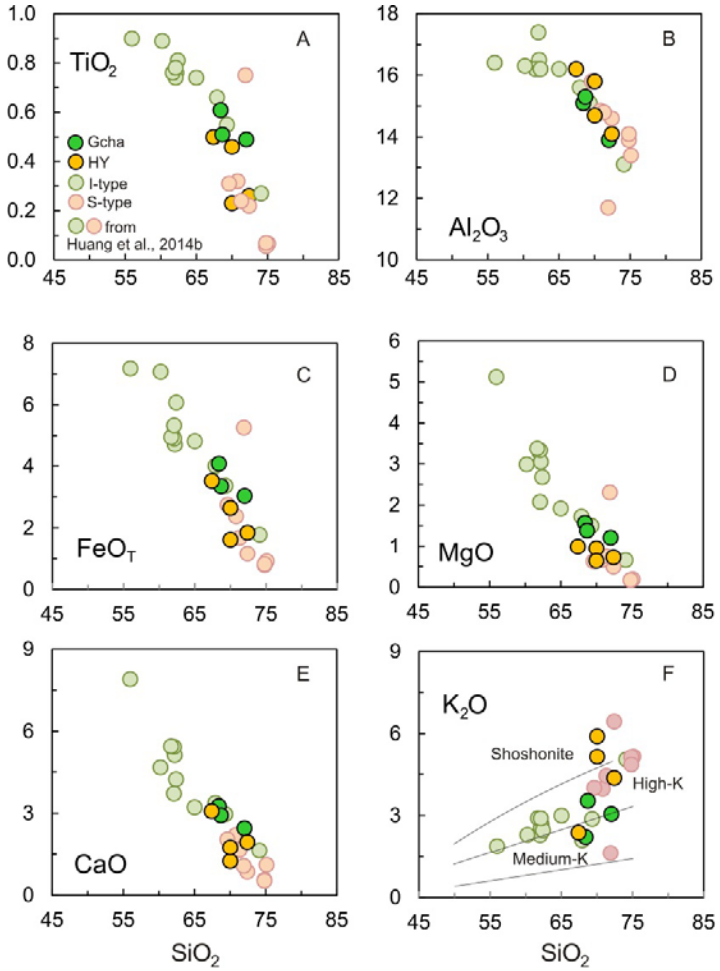

Fig. 5.4. SiO_2 variation diagrams of representative elements of I- and S-type granitoids.

Compared to HY samples, $\varepsilon_{Hf}(450)$ values for Gcha have a limited variation dominantly in the range of -6 – 0 and peak at -2 (Fig. 5.6B). Some largely negative $\varepsilon_{Hf}(450)$ values of ~ -30 and ~ -50 are also present, corresponding to those in HY rocks. If age corrected to the individual zircon crystallization ages, zircon Hf isotopes in Gcha rocks show the similar distribution as HY rocks (Fig. 5.7B), reflecting their similar sources. Two-stage zircon Hf model ages of Gcha samples vary from 1000 Ma to 3000 Ma (Fig. 5.7C, Table 5.3).

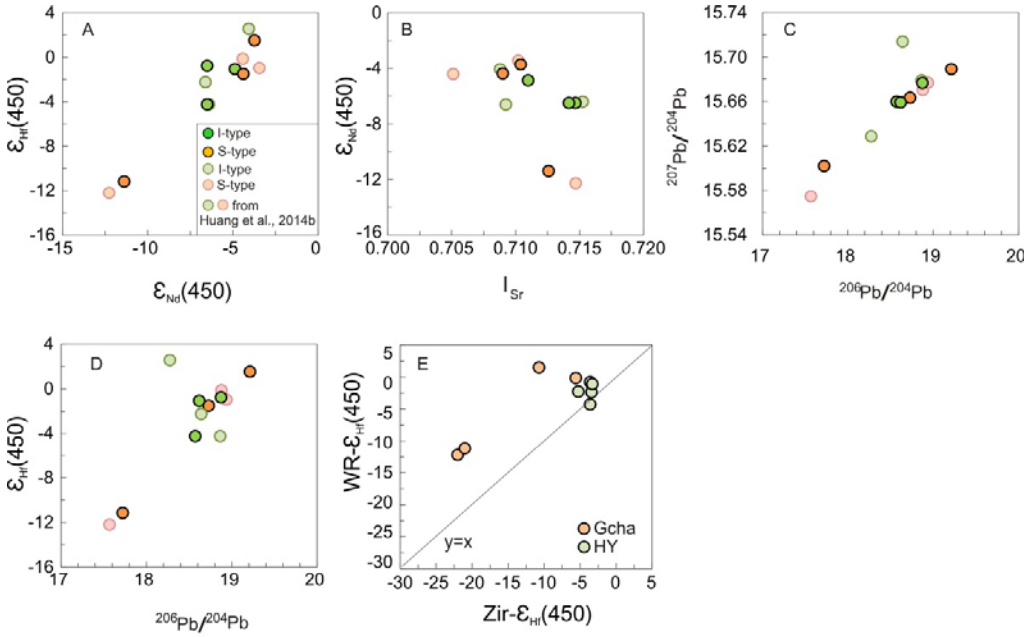

Fig. 5.5. Isotope plots show that samples in this study are plotted in the area defined by the previous study (Chapter, 4) and have good correlations (A-D). Fig. 5E shows that HY rocks have big discrepancies between whole rock $\varepsilon_{Hf}(450)$ and averages of zircon $\varepsilon_{Hf}(450)$ whereas, Gcha rocks do not.

5.3. Discussion

5.3.1. The Archean basement underneath the Qilian Block

For decades, people have considered the basement underneath the Qilian Block is of Proterozoic age on the basis of abundant ~900 Ma intrusions and gneisses. The old Mohe basement age of 2348 – 2470 Ma (Chen et al., 2007b; Li et al., 2007) has been overlooked. Chapter 4 emphasizes the presence of the Archean Basement underneath the QB based on the abundant inherited zircons as

old as 2.7 Ga (the last panel in Fig. 5.2). This notation is further supported by the zircon Hf isotope investigation in this chapter.

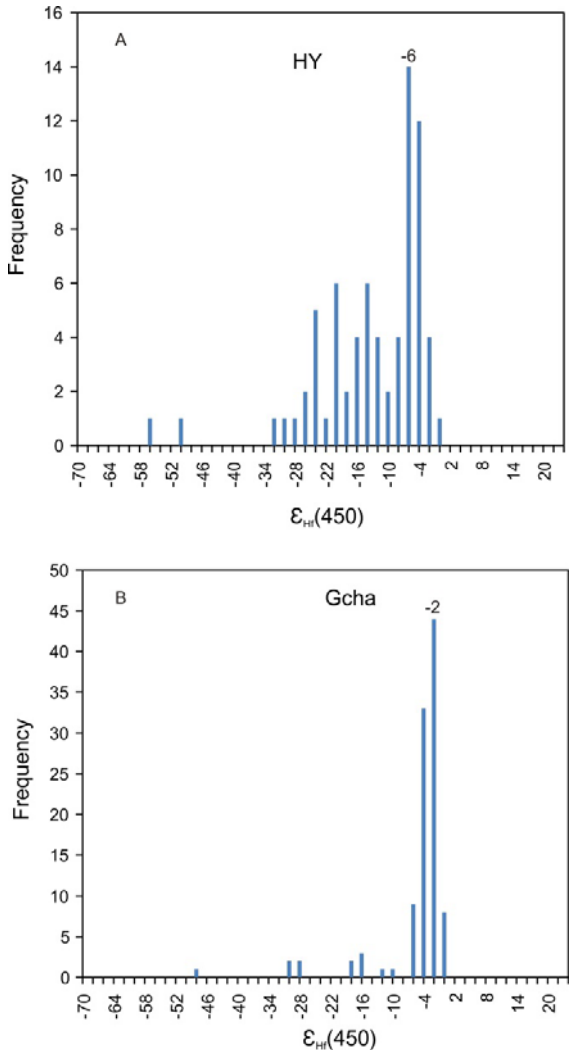

Fig. 5.6. Histograms of zircon *in situ* $\varepsilon_{Hf}(450)$ values for HY (A) and Gcha rocks (B).

Fig. 5.7C shows the zircon Hf model ages versus the zircon ages. The largely negative $\varepsilon_{Hf}(450)$ values (Fig. 5.7B) with 'crustal' model ages significantly older than 2.5Ga (Fig. 5.7C) requires the presence of an Archean basement. In this case, the Qilian Block must have served as a micro-continent during the accretion of the Qilian Orogenic belt. The presence of inherited zircons with

DMM Hf isotopes at ~1.8 Ga and ~2.5 (Fig. 5.7A) strongly indicate the juvenile crust was also formed at that time.

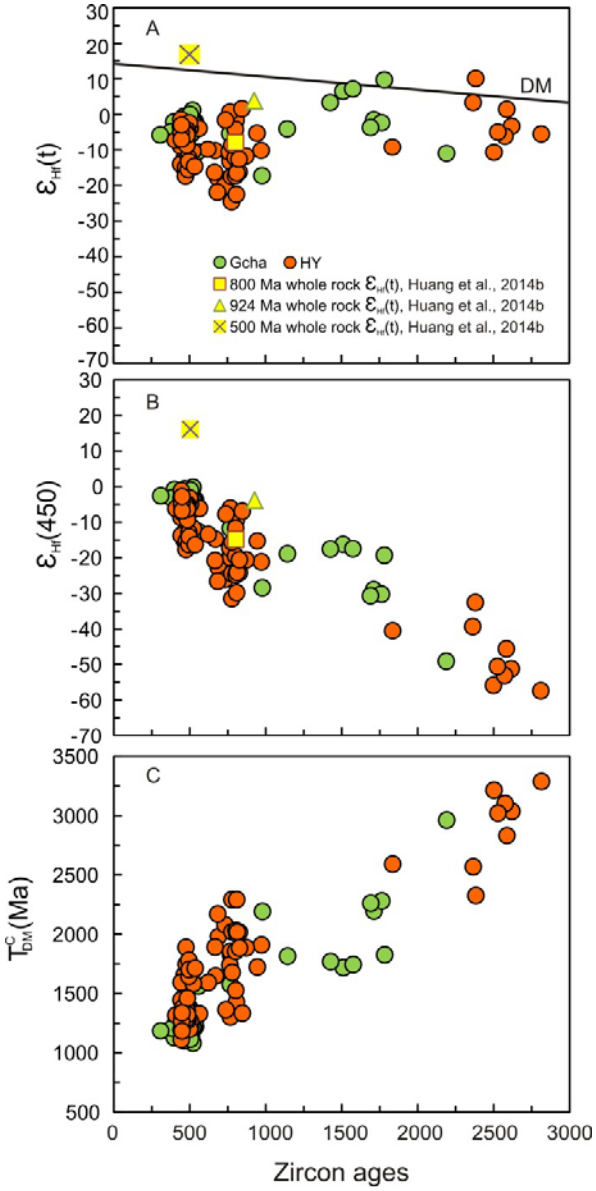

Fig. 5.7. A, $\varepsilon_{Hf}(t)$ versus the zircon ages. Ages are corrected to the individual zircon ages to show the isotopic composition of the zircons at the time of crystallization. B, $\varepsilon_{Hf}(450)$ versus the zircon ages. All ages are corrected to 450 Ma to show the source materials involved in the 450 Ma magmatism. C, Two-stage zircon Hf model ages versus zircon crystallization ages.

5.3.2. Implications for sources

Chapter 4 points out that the old intrusions of ~920 Ma and 800 Ma have been involved in the ~450 Ma magmatism because of the presence of inherited zircons of these ages in the ~450 Ma granitoids and because the whole rock Sr-Nd-Pb-Hf isotopes of old intrusions plot on the trend defined by the ~450 Ma granitoids. This interpretation is further supported by this study. The inherited zircons dated at ~900 and 800 Ma also have zircon Hf isotope composition similar to the whole rock Hf isotopic compositions of 920 Ma and 800 Ma plutons (Fig. 5.7A,B), indicating the reworking of the 800 Ma and 920 Ma crust. Fig. 5.6 shows the histogram of zircon $\varepsilon_{Hf}(450)$ values for Gcha and HY granitoids. Both of them have the same variation range, e.g. the same upper and lower limits, indicating that sources for both are the same or at least have the same isotopes. The difference between the two is that HY rocks display a considerable spread in zircon Hf isotopes (Fig. 5.6A), whereas zircon $\varepsilon_{Hf}(t)$ values for Gcha are relatively uniform (Fig. 5.6B). The limited variation of $\varepsilon_{Hf}(t)$ values (mostly within -6 – 0, Fig. 5.6B) in the Gcha rocks suggest the prominent juvenile components in the source. The relatively homogenous source for Gcha granitoids further comes from the consistence between whole-rock Hf isotopes and zircon in situ Hf isotopes (Fig. 5.5E). Whereas the HY granitoids present a much larger variation in Hf isotope (mostly -22 – 0, Fig. 5.6A) pointing to a rather heterogeneous source. The big discrepancy between whole rock Hf isotopes and zircon in situ Hf isotopes also implies that the limited and likely biased individual zircon Hf analysis cannot completely cover the whole range of the Hf isotope variation especially when the plutons are the hybrids of distinct endmembers (Huang and Niu, 2013).

According to the zircon Hf isotopes, Gcha granitoids compose more juvenile components than HY. However, whole rock Nd-Hf isotopes of HY rocks approach similar or even more radiogenic composition than Gcha rocks (Fig. 5.5A). Considering the discrepancy between whole rock Hf isotopes and zircon Hf isotopes for HY rocks, more proportions of juvenile components are required to compensate the gap, which is inconsistent with the indication by the zircon $\varepsilon_{Hf}(t)$

histogram . This inconsistence might be explained by (1) different degrees of partial melting for the same sources or (2) partial melting of sources with different maficity but with the same isotopes, e.g. oceanic basalts vs the depleted mantle (Mo et al., 2008; Niu, et al., 2013; Huang et al., 2014).

5.3.3. Re-evaluation of previous metamorphic interpretation

Zircons in the eclogites from the NQ-UHPM belt mostly give two age populations, one being interpreted as protolith age for the magmatic cores and the other as metamorphic ages recorded by zircon rims. Interpreting U/Pb ages with respect to the P-T-t of eclogites requires establishing whether the zircon was inherited from the protolith, formed during subduction metamorphism, or formed during exhumation (Baldwin et al., 2004). Zr contents in the bulk compositions of the mafic protolith in the Qilian Orogenic belt range from several ppm to 200 ppm, mostly <100 ppm (Song et al., 2003; Yang, et al., 2006; Zhang et al., 2008). Given the relatively Zr-poor bulk composition in these mafic protoliths, the interpretation of zircon growth from the protolithic magma might be problematic. For example, the Ky-eclogite from the Dulan area, the UHMP assemblage, spatially closest to the granitoids of this study possesses only 4.6 – 12.1 ppm Zr (Zhang et al., 2008). These Ky-eclogites are depleted in LREE and HREE with positive Sr and Eu anomalies, reflecting the troctolitic protolith of cumulative origin. Zircon gives ~516 Ma for the magmatic core and ~445 Ma for the metamorphic rim. These two ages were interpreted respectively as protolith age at a mid ocean ridge and UHP metamorphic age during subduction (Zhang et al., 2008). This interpretation may not be reasonable largely due to the very low Zr content in the bulk rock composition. Zircon saturation for basaltic composition melts is very high, up to thousands of ppm (Dickinson and Hess, 1982; Hanchar and Watson, 2003; Boehnke et al., 2013). According to the latest experiments on the zircon saturation in melts (Boehnke et al., 2013), the basaltic liquids require unrealistically high abundance of >5000 ppm Zr to directly crystallize zircon and the subsequent conclusion is that zircons found in mafic environments must have crystallized from late stage, evolved melts (Boehnke et al., 2013) or crustally contaminated melts (Zheng et al., 2006). 5000 ppm Zr may be

too much; hundreds of ppm might be sufficient to crystallize zircons based on observations in the literature (Visona et al., 2007). The magma parental to troctolite normally have average 60 ppm Zr based on the global data, too low to crystallize any zircon at the early cumulating stage. At this point, the magmatic cores in Ky-eclogites are melt-controlled but may not be crystallized at the mid-ocean ridge but grown during subduction or even collision duration.

5.3.4. Re-evaluation of the previous collision timing

Changes in isotopic compositions of magmatic rocks can be used successfully to trace the impact of the collision on the geochemistry of the igneous rocks (Elburg et al., 2005; Bouilhol et al., 2013). In this study, the Gcha rocks slightly predate the HY rocks (~450 Ma v.s. ~445 Ma, Fig. 5.3) and HY rocks have much more heterogeneous sources than Gcha (Table 5.6). The pronounced changes in the isotopic variations can be explained by the arrival of the leading edge of the Qaidam continental lithosphere beneath the overriding Qilian plate (Fig. 5.8). The large variation of zircon $\varepsilon_{Hf}(450)$ values in the range of the ~ -60 – 0 (Fig. 5.6B) indicate the anatexis of old crustal material and addition of the juvenile components. While their small negative whole rock ε_{Nd} and ε_{Hf} values (Table 5.3, Fig. 5.5A) suggest the prominent juvenile components in the magma sources. We note that the zircon age distributions in the metamorphic rocks (Fig.12 in Zhang et al., 2008, Fig.8 in Zhang et al., 2010) are very similar to those in our granitoids: indistinguishably varying from ~ 440 – 510 Ma (Fig. 5.2). Although zircon ages obtained from the granitoids cannot be grouped based on the zircon structures or the chemical compositions (zircon trace elements, Appendix G), zircon ages collected from the eclogites were subdivided into magmatic population and metamorphic population based on the contrast CL images (Zhang et al., 2008; Zhang et al., 2010). It is discussed above that some zircon core ages may not record the protolith formation age but the underthrusting process. It is possible that the magmatic core in the eclogite has the same origin as those in the granitoids. It is not easy to evaluate that the continuous age spread results from one long lasting event or multiple events due to the continuing replenishment of magmas. It is certain, however, that

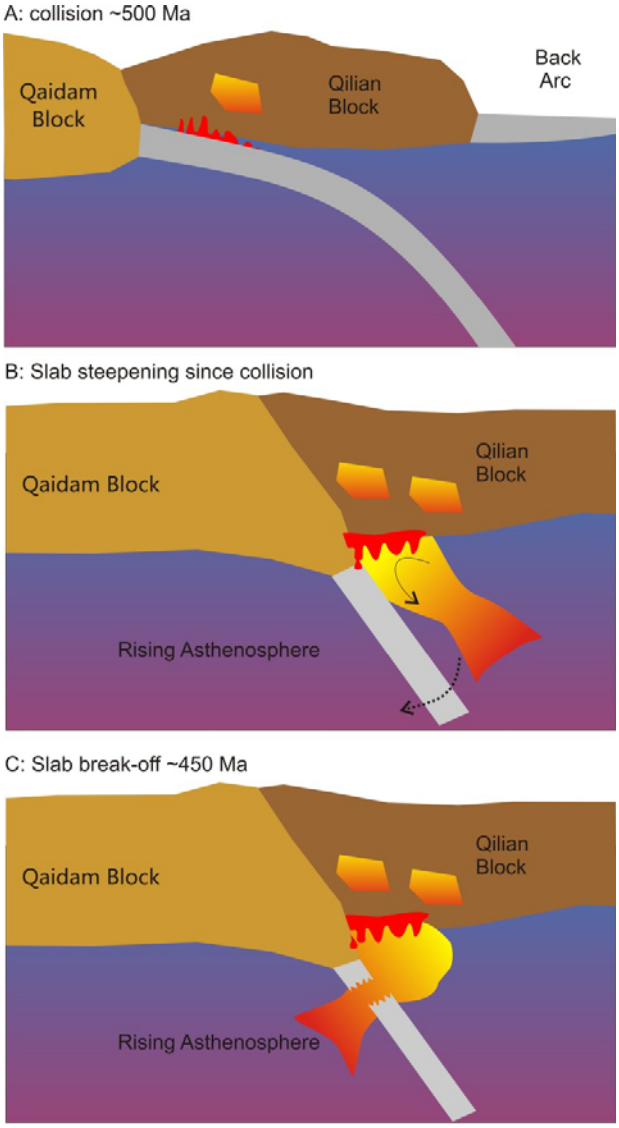

Fig. 5.8. A, Collision between the Qaidam Block and Qilian Block initiated at ~500 Ma and the syn-collisonal magmatism. B. the slab started steepening since collision and caused the enhanced mantle wedge convection producing magmatism. C, slab finally broke off at ~450 Ma. The uprising hot asthenosphere mantle caused the extensive magmatism at ~450 Ma.

the formation of these Gcha and HY granitoids is temporarily overlapping with the eclogite-facies metamorphism at ~450 Ma in the NQ-UHPM belt, suggesting a close relationship between the rapid exhumation of the ultrahigh-pressure metamorphic rocks and the contemporary Gcha and HY rocks. The association of exhumed high-pressure (HP) rocks with igneous rocks may be indicative of the slab break-off (Davies and von Blanckenburg, 1995; von Blanckenburg and Davies, 1995; Sun et al., 2002). The slab break-off would result in the uprising hot asthenosphere which may undergo

decompression melting and also provide sufficient heat to melt the overlying metasomatized mantle lithosphere and produce the basaltic magma to further partial melt the various crust materials. The derivative magma can have varying compositions, ranging from alkaline, ultrapotassic to calc-alkaline melts (Davies and von Blanckenburg, 1995). The calc-alkaline high-K to shoshonitic compositions of our granitoids probably result from partial melting of the hydrous, calc-alkaline to high-K calc-alkaline, mafic to intermediate crustal rocks (Roberts and Clemens, 1993) and possibly mixed with melts derived from the smallest degree melting of enriched layers in the overriding lithosphere (Davies and von Blanckenburg, 1995).

If the age population of ~450 – 460 Ma related to slab break-off, the collision should have happened normally ~ 20 – 25 Ma earlier (van Hunen and Allen, 2011) accompanying abundant magmatic events (Mo et al., 2008; Niu et al., 2013; Huang et al., 2014). The large scale of the magmatism prior to 470 Ma in the NQ-UHPM belt and QB is not yet extensively identified but the abundant magmatic zircon ages since ~510 Ma (Fig. 5.2, and Chapter 4) in the granitoids and metamorphic rocks (Zhang et al., 2008; Zhang, et al., 2010; Song et al., 2013) indicate the existence of magmatism at that time. In this case, the large age spread between 440 – 510 Ma could be explained. The magmatism was initiated since the collision at ~500 Ma. Once the collision started, the subducting oceanic slab started steepening under the gravity and result in the enhanced mantle corner flow which provides the heat to produce magmatism (Fig. 5.8). This is a gradational process until the slab finally detached. Therefore, the magmatism could possibly sustain for ~ 60 Ma until ultimate break-off. This model is also consistent with the metamorphic interpretation by Xu et al. (2006) who concluded according to the high-pressure metamorphic rocks that the exhumation began at 470 – 460 Ma.

The contemporary Gcha and HY granitoids in the Qilian Block were previously in Chapter 4 considered as the syn-collisional products at ~450 Ma and zircons older than 450 Ma had to be interpreted as xenocrysts which record the previous arc magmatism or oceanic crust formation

(Chapter 4). The old model is consistent with the tectonic evolution model built by Song et al. (2006; 2013). The new model is consistent with the tectonic frame suggested by Xu et al., (2006). Based on the current understanding, both of them are technically sound and both need more work to test.

5.4. References

Baldwin, S.L. et al., 2004. Pliocene eclogite exhumation at plate tectonic rates in eastern Papua New Guinea. Nature, 431(7006): 263-267.

Boehnke, P., Watson, E.B., Trail, D., Harrison, T.M., Schmitt, A.K., 2013. Zircon saturation re-revisited. Chemical Geology, 351(0): 324-334.

Bouilhol, P., Jagoutz, O., Hanchar, J.M., Dudas, F.O., 2013. Dating the India–Eurasia collision through arc magmatic records. Earth and Planetary Science Letters, 366(0): 163-175.

Chen, N.S. et al., 2007. Geochemistry and Nd-Sr-Pb Isotopic Compositions of Granitoids from Qaidam and Oulongbuluke Micro-Blocks，NW China Constraints on Basement Nature and Tectonic Affinity. Journal of Earth Science, 32(1): 7-21.

Davies, H.J., von Blanckenburg, F., 1995. Slab breakoff: A model of lithosphere detachment and its test in the magmatism and deformation of collisional orogens. Earth and Planetary Science Letters, 129(1–4): 85-102.

Dickinson Jr, J.E., Hess, P.C., 1982. Zircon saturation in lunar basalts and granites. Earth and Planetary Science Letters, 57(2): 336-344.

Elburg, M.A., Foden, J.D., van Bergen, M.J., Zulkarnain, I., 2005. Australia and Indonesia in collision: geochemical sources of magmatism. Journal of Volcanology and Geothermal Research, 140(1–3): 25-47.

Hanchar, J.M., Watson, E.B., 2003. Zircon saturation thermometry. Reviews in mineralogy and geochemistry: 89-112.

Huang, H. et al., 2014. Geochemical constraints on the petrogenesis of granitoids in the East Kunlun Orogenic blet, northern Tibetan Plateau: implications fro the continental crust growth through syncollisional felsic magmatism. Chemical Geology, 370: 1-18.

Huang, H., Niu, Y.L., 2013. Magma mixing induced discrepancy between whole rock Hf isotopes and zircon in situ Hf isotopes: A case study in Kekeli Batholith, North Qilian Orogenic belt. AGU Fall Meeting.

Li, X.Y. et al., 2007. Constraints on the timing of the early-Paleoproterozoic magmatism and crustal evolution of the Oulongbuluke microcontinent: U-Pb and Lu-Hf isotope systematics of zircons from Mohe granite pluton. . Acta Petrologica Sinica, 23(2): 513-522. (In Chinese with English abstract).

Mo, X.X. et al., 2008. Contribution of syncollisional felsic magmatism to continental crust growth: A case study of the Paleogene Linzizong volcanic Succession in southern Tibet. Chemical Geology, 250(1-4): 49-67.

Niu, Y., Zhao, Z., Zhu, D.-C., Mo, X., 2013. Continental collision zones are primary sites for net continental crust growth — A testable hypothesis. Earth-Science Reviews, 127(0): 96-110.

Pan, G.T., Ding, J., Yao, D.S.W., L. Q., 2004. Geological map of the Qinghai-Xizang (Tibet) Plateau and adjacent areas. Chengdu Cartographic Publishing House.

Song, S.G. et al., 2003a. Petrology, geochemistry and isotopic ages of eclogites from the Dulan UHPM Terrane, the North Qaidam, NW China. Lithos, 70(3–4): 195-211.

Song, S. et al., 2006. Evolution from oceanic subduction to continental collision: a case study from the Northern Tibetan Plateau based on geochemical and geochronological data. Journal of Petrology, 47(3): 435-455.

Song, S., Niu, Y., Su, L., Xia, X., 2013. Tectonics of the North Qilian orogen, NW China. Gondwana Research, 23: 1378-1401.

Sun, W.D., Li, S.G., Chen, Y.D., Li, Y.J., 2002. Timing of Synorogenic Granitoids in the South Qinling, Central China: Constraints on the Evolution of the Qinling‐Dabie Orogenic Belt. The Journal of Geology, 110(4): 457-468.

van Hunen, J., Allen, M.B., 2011. Continental collision and slab break-off: A comparison of 3-D numerical models with observations. Earth and Planetary Science Letters, 302(1-2): 27-37.

Visona, D., Caironi, V., Carraro, A., Dallai, Fioretti, A.M., Fanning, M., 2007. Zircon megacrysts from basalts of the Venetian Volcanic Province (NE Italy): U-Pb ages, Oxygen isotopes and REE data. Lithos 94, 168-180.

von Blanckenburg, F., Davies, J.H., 1995. Slab breakoff: A model for syncollisional magmatism and tectonics in the Alps. Tectonics, 14(1): 120-131.

Xu, Z. et al., 2006. Timing and mechanism of formation and exhumation of the Northern Qaidam ultrahigh-pressure metamorphic belt. Journal of Asian Earth Sciences, 28(2): 160-173.

Zhang, G., Song, S., Zhang, L., Niu, Y., 2008. The subducted oceanic crust within continental-type UHP metamorphic belt in the North Qaidam, NW China: Evidence from petrology, geochemistry and geochronology. Lithos, 104(1-4): 99-118.

Zhang, J., Mattinson, C., Yu, S., Li, J., Meng, F., 2010. U‐Pb zircon geochronology of coesite‐bearing eclogites from the southern Dulan area of the North Qaidam UHP terrane, northwestern China: spatially and temporally extensive UHP metamorphism during continental subduction. Journal of Metamorphic Geology, 28(9): 955-978.

Zheng, Y.-F. et al., 2006. Zircon U–Pb age, Hf and O isotope constraints on protolith origin of ultrahigh-pressure eclogite and gneiss in the Dabie orogen. Chemical Geology, 231(1–2): 135-158.

Chapter 6: Mixing induced discrepancy between whole rock Hf isotopes and zircon in situ Hf isotopes

6.1. Introduction

Many efforts have been made to understand the continental crust growth during the past few decades, in which case, isotopic composition of zircons have been extensively applied. While using zircon Hf isotopes to discuss the magma processes, two important issues need to be carefully considered: (1) Do zircon Hf isotopes faithfully reveal the isotopic compositions of the magma? (2) How does continental crust achieve its characteristic bulk andesitic composition? Zircon can effectively preserve the initial $^{176}Hf/^{177}Hf$ ratios of an igneous host rock (Pettingill and Patchett, 1981; Kinny and Maas, 2003) due to its low Lu/Hf ratio. The Hf isotopic compositions of zircon can be utilized as a geochemical tracer of rocks' origin in the same way whole-rock Nd isotopes are used (Kinny and Maas, 2003) and zircon Hf isotope compositions have been used to trace rock origin and crust-mantle evolution (Kinny et al., 1991; Thirlwall and Walder, 1995; Amelin et al., 1999; Amelin et al., 2000; Griffin et al., 2000; Griffin et al., 2002; Kemp et al., 2007; Pietranik et al., 2013). However, in this paper, we demonstrate the big discrepancy between whole-rock and zircon Hf and we emphasize that zircon Hf isotope data must be used with caution.

Many models have been proposed to explain the continental crust growth including the standard 'island arc' model (Taylor and McLennan, 1985), 'mantle plume' model (Stein and Hofmann, 1994; Condie, 1998, 2000; Niu et al., 2003;) and 'continental collision zone' model (Niu et al., 2007, 2013; Mo et al., 2008; Niu and O'Hara, 2009; Huang et al., 2014; Chapter 4). It has been widely accepted that the continental crust has bulk andesitic composition (Taylor, 1967, 1977; Taylor and McLennan, 1985; Rudnick and Gao, 2003) which cannot be well explained by the standard continental crust growth model—"island-arc" model (Taylor and McLennan, 1985) because products in the island arc setting are basaltic rather than andesitic (Niu and O'Hara, 2009; Niu et al., 2013). To address this problem, the removal of mafic/ultramafic lower arc crust cumulate is strongly recommended (Kay and Mahlburg Kay, 1993; Rudnick, 1995; Plank, 2005). For example, amphibole-bearing mafic enclaves of cumulate origin in the arc have been highlighted to efficiently

drive the mafic magma towards the andestic compositions and provide geological evidence of the crustal differentiation models of arc magma (Hidalgo and Rooney, 2010). The Kekeli batholith in the North Qilian Orogenic belt (NQOB) contains ubiquitous amphibole-rich cumulates. Systematic investigation has never been done there before. In this study, we evaluate the sources and processes of Early Paleozoic Kekeli batholith by analysing major and trace element compositions, zircon in situ Hf and whole rock Sr-Nd-Pb-Hf isotopes of both mafic magmatic enclaves (MMEs) and host rocks in order to look into magma processes as well as the tectonic linkage to the surrounding tectonic units. We provide a consistent picture of magma interaction between isotopically diverse magmas and the induced discrepancy between whole rock Hf (WR-Hf) isotopes and zircon *in situ* Hf (Zir-Hf) isotopes.

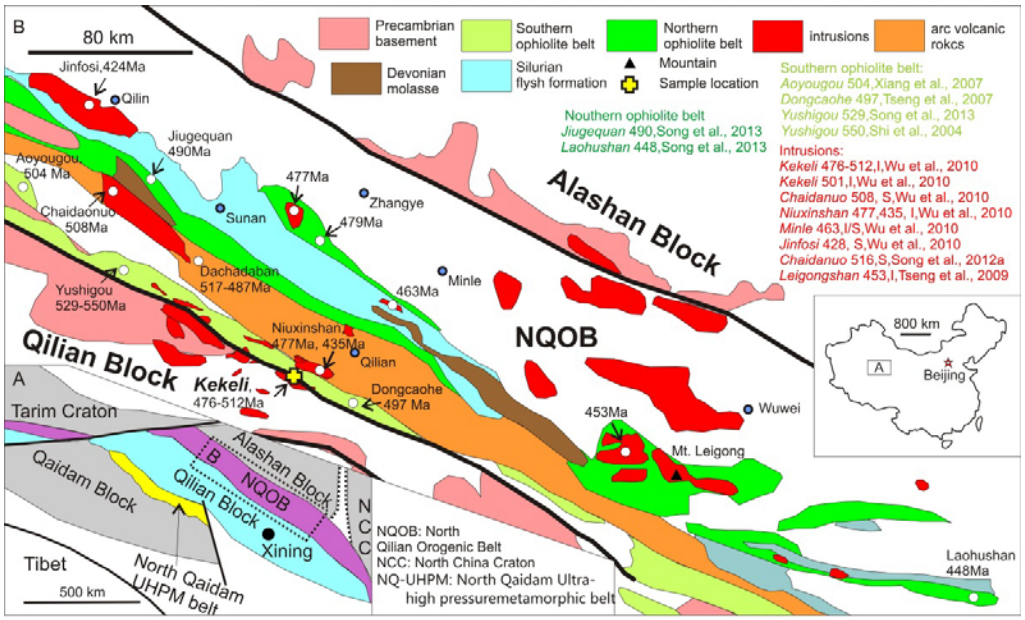

Fig. 6.1. A, Schematic map showing major tectonic units of the Qilian Orogenic Belt (after Song et al., 2013). B, Simplified geological map of the North Qilian Orogenic Belt (NQOB) showing the distribution of granitoids and ophiolites (after Song et al., 2013). Data compilation for granitoid intrusions is from Huang et al. (2013b), and for ophiolites is from Song et al., (2013). Dongcaohe, 497 Ma (Tseng et al., 2007); Aoyougou, 504 Ma (Xiang et al., 2007); and Yushigou, 529 Ma (Song et al., 2013); Yushigou, 550 Ma (Shi et al., 2004); Jiugequan ophiolite, 448-490 Ma (Song et al., 2013; Xia and Song, 2010); Laohushan ophiolite, 448 Ma (Song et al., 2013).

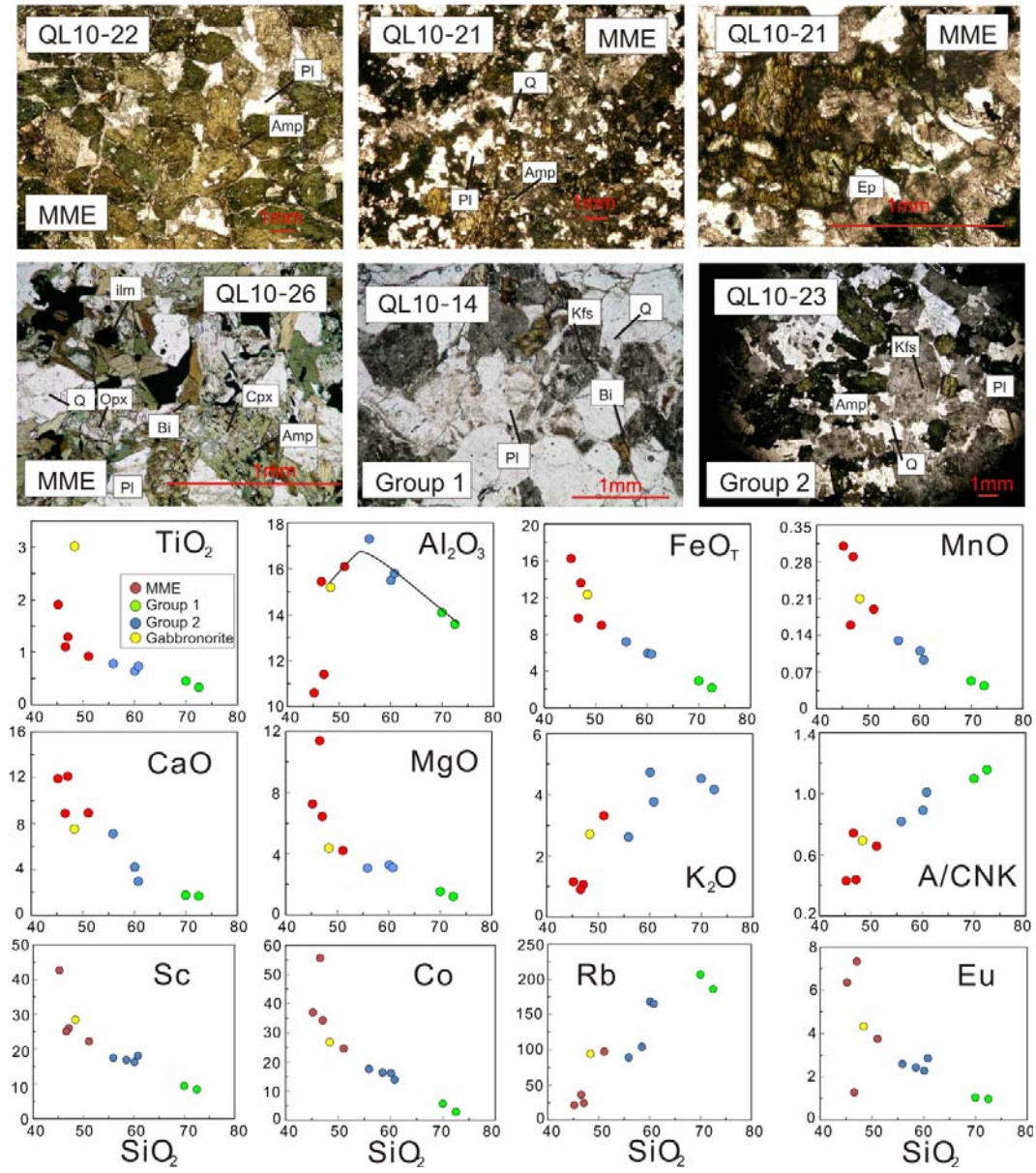

Fig. 6.2. Photomicrographs under plane polarized light and SiO_2-variation diagrams showing the correlations among samples. QL10-22: cumulate texture. QL10-21: heteradcumulate texture. QL10-26: Secondary Amp and Bi rims on the pyroxene. QL10-14: granitic group 1 contains Bi without Amp. QL10-23: group 2 with intermediate composition containing Amp. (Amp: amphibole, Pl: plagioclase, Q: quartze, Ep: epidote, Opx: othorpyroxene, Cpx: clinopyroxene, Bi: biotite, Kfs: K-feldspar, ilm: ilmenite. MME: mafic magmatic enclave).

6.2. Tectonic setting and geologic background

The North Qilian Orogenic belt (NQOB), Qilian Block (QB) and North Qaidam ultrahigh pressure metamorphic belt (NQ-UHPM) are three major tectonic units of the Qilian-Qaidam system on the northernmost margin of the Tibetan Plateau (Fig. 6.1 A, B).

We collected 10 samples including 5 mafic magmatic enclaves (MMEs) from the Kekeli batholith in the NQOB (Table 6.1). The Kekeli batholith is located on the southern margin of the NQOB (Fig. 6.1B) intruding the Precambriam meta-volcanic rocks, pelitic rocks and clastic rocks within the southern ophiolite belt. This batholith is mostly diorite-granodiorite in composition with a few plagiogranites (Wu et al., 2010). It is characterised by the presence of a large amount of MMEs. Wu et al. (2010) report one granodiorite of 501 Ma and one plagiogranite of 512 Ma from Kekeli Batholith. They suggest that the granodiorite was derived from subducted oceanic crust while the plagiogranite was produced by partial melting of gabbro based on age and petrology.

6.3. Samples

The Kekeli batholith contains abundant enclaves with size up to 1.5 m in diameter. The contacts between MMEs and host rocks are gradational, indicating supersolidus condition. Mineralogy for all the samples is listed in Table 6.1 and described below. Mineral modes are determined by point counting.

The gabbronorite enclave QL10-26 contains abundant orthopyroxene (Opx), clinopyroxene (Cpx) and ilmenite (Ilm) (Table 6.1, Fig. 6.2). Opaque Ilm makes up to 5% of the sample which is consistent with its cumulate origin. Hydrous minerals Amphibole (Amp) and biotite (Bt) appear as rims of pyroxene (Px) (Fig. 6.2), suggesting that P-T conditions or compositions had changed with time. Plagioclase (Pl), quartz (Qtz) and K-feldspar (Kfs), plus accessory minerals such as apatite and zircon are also present. The contacts between QL10-26 and host rocks are gradational and Px (both Opx and Cpx) decreases from QL10-26 towards the host.

MMEs are mafic diorite, containing dominantly Amp and Pl (Fig. 6.2). Various Qtz and Kfs are present as interstitial phases. Alteration phases include epidote (Ep) after Amp, chlorite (Chl) after biotite and clay minerals after feldspar. Some epidotes also present as the primary euhedral phase. The advanced hydrothermal alteration of the sample is obvious (actinolite in QL10-25, QL10-27). Some MME display a heteradcumulate texture (QL10-21, Fig. 6.2) where poikilitic amphibole encloses mostly plagioclase which is regarded as imperfect fractional crystallization (Claeson and Meurer, 2004; Larocque and Canil, 2010). The host rocks can be divided into two groups based on their mineralogy and field observations. Group 1 (granite QL10-14/15) is granitic, bearing biotite with no Amp and do not contain MMEs (Fig. 6.2). Group 2 (Diorite QL10-23/24/27) is intermediate in composition, containing Amp and hosting MMEs (Fig. 6.2).

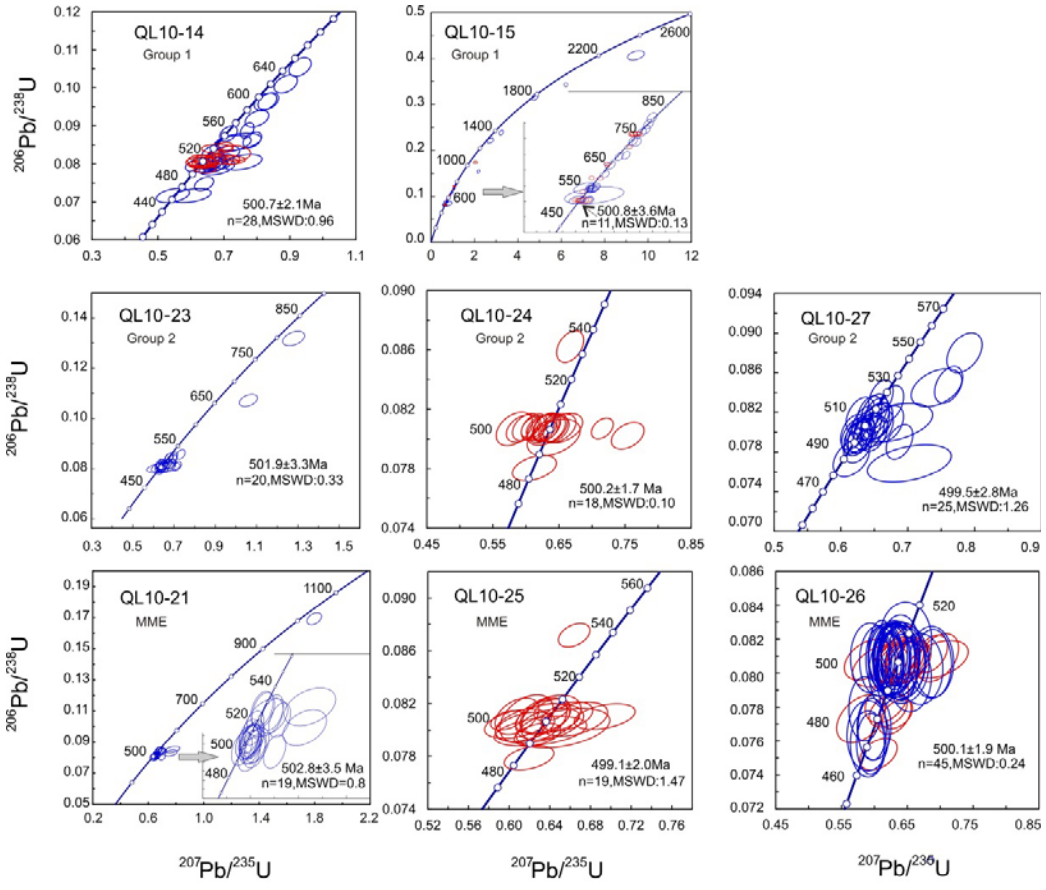

Fig. 6.3. Zircon U-Pb Concordia diagrams to show host rocks and MMEs have the same crystalline age of ~ 500 Ma.

6.4. Sample preparation and analytical techniques

All the samples were analysed for bulk-rock major and trace element. Eight zircon U-Pb dated samples were analysed for bulk-rock Sr-Nd-Pb-Hf isotopes. Zircon in situ U-Pb dating was conducted in both Wuhan (red color, Fig. 6.3) and Beijing (blue color, Fig. 6.3). In situ zircon Hf isotope analysis were determined at the same spot as U-Pb dating.

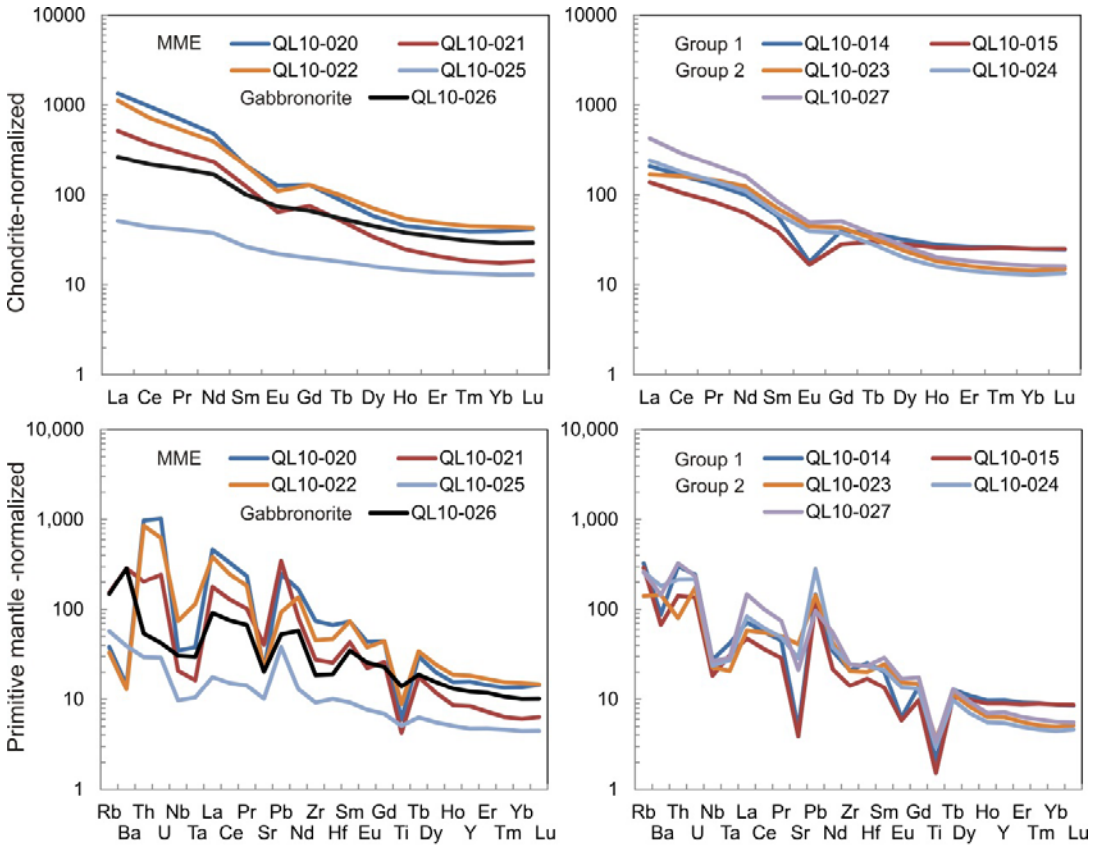

Fig. 6.4. Chondrite-normalized rare earth element patterns and primitive mantle-normalized diagrams (Sun and McDonough, 1989). QL10-26 has no Eu anomaly and displays the fairly flat LREE pattern; Group 1 has a largest negative Eu anomaly. Group 2 and other MMEs have the intermediate negative Eu anomalies

6.5. Results

6.5.1. Major and trace elements

Major and trace elements are given in Table 6.2. All of them define good linear trends on the Harker diagrams (Fig. 6.2). Gabbronorite QL10-26 has less enriched light rare earth elements (LREEs), no Eu anomaly, and small Pb and Ti anomalies (Fig. 6.4). Group1 rocks have biggest Eu, Pb and Ti anomalies. MMEs generally display smaller Eu, Pb and Ti anomalies than host rocks on the rare earth element (REE) patterns and spider diagrams (Fig. 6.4). Group 1 rocks show similar trace element pattern (Fig. 6.4). Group 2 rocks resemble bulk continental crust characters (Fig. 6.4), e.g. negative Nb-Ta-Ti anomalies, positive Pb anomalies and small negative Eu anomaly.

6.5.2. Zircon geochronology and geochemistry

Eight samples were analysed for zircon in situ U-Pb dating and in situ Hf isotopes (Table 6.3, 6.4 respectively). U-Pb Concordia plots are shown in Fig. 6.3. Zircon trace element data are given in Appendix H. Fig. 6.5 reveals multiple zircon populations and complex internal structures. In group 1, QL10-14 and QL10-15 contain abundant zircons displaying chaotic zoning, reflecting the post-magmatic modifications e.g. metamictisation (Fig. 6.5). The magmatic zircons have coherent concordant ages of ~ 500 Ma. The inherited zircons have ages as old as >2.0 Ga, indicating the involvement of old crust. The younger inherited zircons have ages spread out from 550 ~ 800 Ma (Fig. 6.3) on or close to the Concordia. All the other samples have the same coherent crystalline age of ~ 500 Ma. Generally, the QL10-26 has zircon fragmented with strip zoning typical in the mafic rocks and some grains with chaotic zoning; The Group 1 samples have abundant zircons with both chaotic zoning and magmatic zoning; Group 2 and other MMEs contain zircons types both seen in QL10-26 and Group 1. Details are described below.

Group 1

Zircons in granite QL10-14 mostly have core-mantle texture with metamorphic cores and magmatic rims (Fig. 6.5). Magmatic parts were carefully analysed to constrain the crystallization age (Fig. 6.4). Considering the results from both Beijing and Wuhan (red and blue color in Fig. 6.4), apparent $^{206}Pb/^{238}U$ age is 500.7 ± 2.1 Ma.

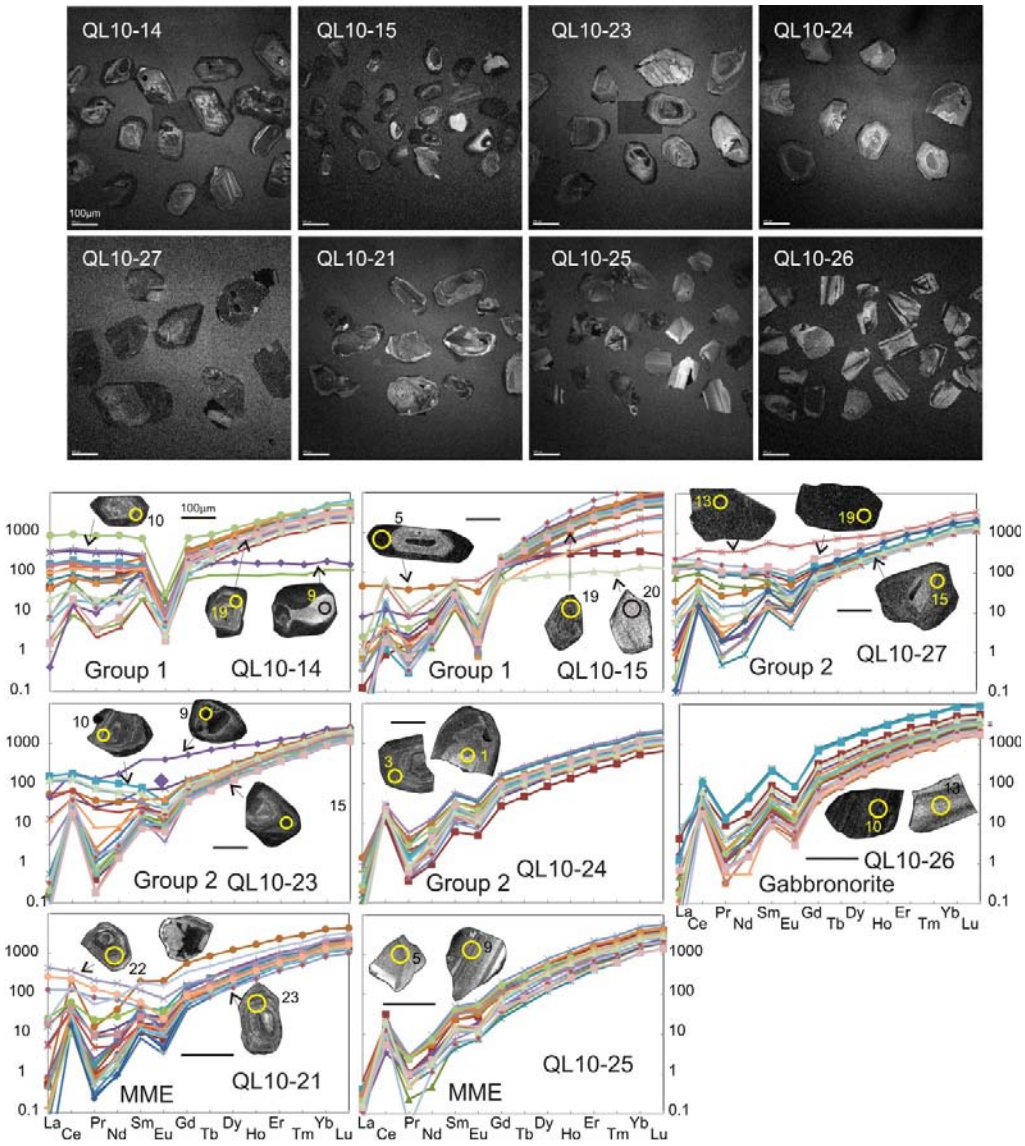

Fig. 6.5. Zircon cathodoluminescence photos and trace elements.

QL10-15 has metamorphic and magmatic grains (Fig. 6.5), showing various internal structure, including oscillatory zoning, homogenous, core-mantle-rim texture, planar banding, patchy, fir-tree or radial sector zoning, reflecting a rather complex history. In situ dating was carried on magmatic grains, and gives apparent $^{206}Pb/^{238}U$ ages of 502.4 ± 4.0 Ma.

Group 2

Diorite QL10-23/24/27 contains more magmatic grains. The zircons with non-magmatic texture are similar to those in QL10-14/15 (Fig. 6.5). Magmatic zircons are mostly homogenous, fir-tree, patchy or sector zoning. Age is constrained as ~ 500 Ma (Fig. 6.3).

MMEs and Gabbronorite

QL10-21 has abundant zircons with chaotic zoning which are common in Group 1 and most of them reveal complex chaotic zoning (Fig. 6.5). We carefully analysed the oscillatory magmatic grains and have $^{206}Pb/^{238}U$ age is 502.8 ± 3.5 Ma, which represents the crystallization age. Zircons in QL10-25/26 are mostly fragments, homogenous or have strip bands (Fig. 6.5). The presence of the zircons with non-magmatic zoning similar to those in QL10-21 indicates their genetic relationship. $^{206}Pb/^{238}U$ ages are ~ 500 Ma.

Majority of zircons display the typical REE pattern (Fig. 6.5), e.g. a steeply-rising slope from LREE to the HREE with a positive Ce-anomaly and negative Eu-anomaly, indicating the original igneous origin. QL10-25 possesses the smallest Eu anomaly, consistent with its small Eu anomaly in the

whole-rock REE pattern (Fig. 6.4). The grains with high LREE abundances probably result from the contamination of apatite inclusions. Some metamorphic grains in Group 1 have flat HREE patterns (Fig. 6.5) probably due to the equilibrium with the minerals rich in HREEs, i.e., garnet (Rubatto, 2002). The dating results indicate that both MME and host rocks crystallized almost simultaneously at ~ 500 Ma.

6.5.3. Whole rock Sr-Nd-Pb-Hf isotopes and zircon in situ Hf isotopes

Whole rock Sr-Nd-Pb-Hf isotopic data for MMEs and host rocks are given in Table 6.5. $I_{Sr,}$ $Pb_{(i),}$ $\varepsilon_{Nd}(t)$ and $\varepsilon_{Hf}(t)$ refer to the age corrected values, whereas ε_{Nd} and ε_{Hf} refer to the present-day values. Group 1 host rocks have lower $\varepsilon_{Nd}(t)$ (-6.05 – -6.70) (Fig. 6.6A) and relatively highly radiogenic I_{Sr} (Fig. 6.6C-D). MMEs have rather limited variation in $\varepsilon_{Nd}(t)$ values (-1.88 – 0.54) (Fig. 6.6A),

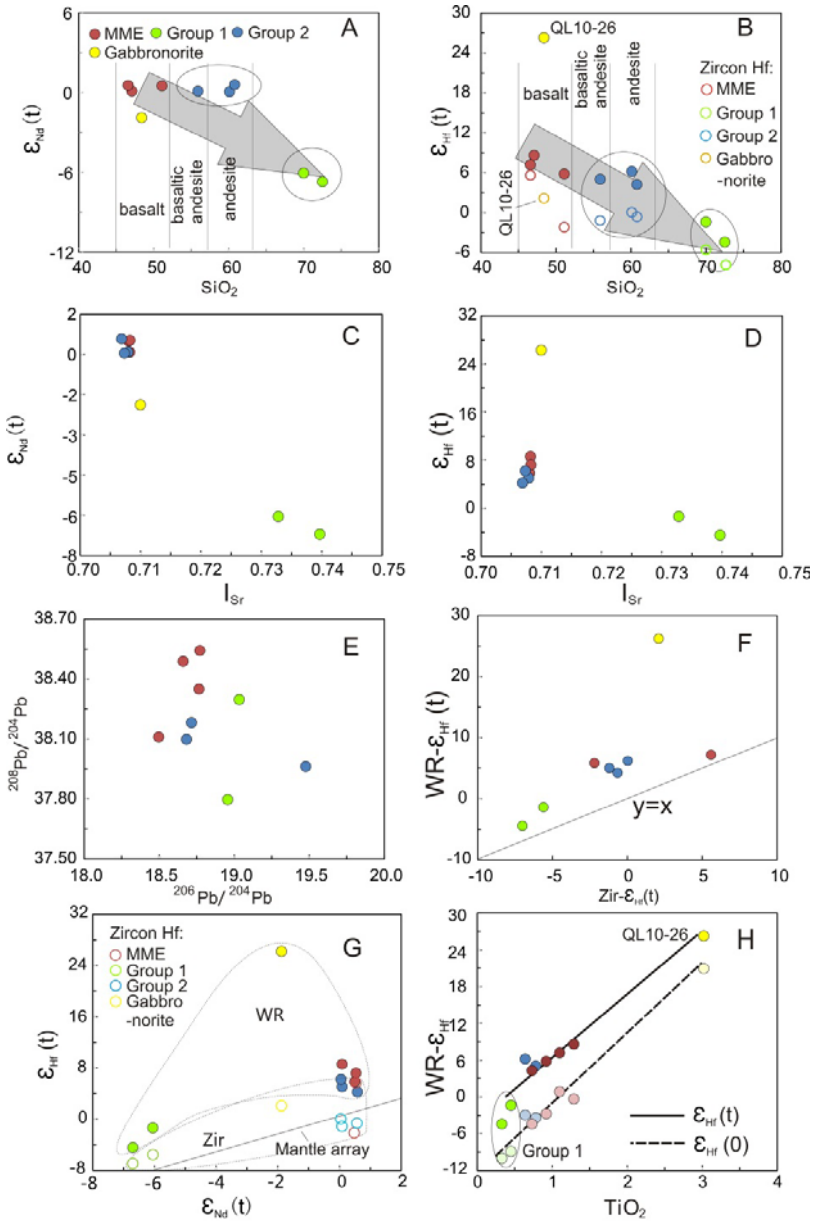

Fig. 6.6. A, Age corrected bulk-rock Nd isotopes vs SiO_2 to show a broad negative correlation. Group 1 samples have lowest $\varepsilon_{Nd}(t)$. Group 2 samples have intermediate isotope composition between two endmembers. B, Age corrected bulk-rock Hf isotopes vs. SiO_2 to show the broad negative correlation. Group 1 samples have lowest $\varepsilon_{Hf}(t)$. Group 2 samples have the intermediate isotope composition between two endmembers. Zircon in situ Hf (Zir-Hf) data (open symbols) are also plotted for comparison. C, negative correlation between Nd and Sr isotopes. D, negative correlation between Hf and Sr isotopes. E, scatter Pb isotope plot showing between-sample heterogeneity. F, comparison between Zir-Hf and WR-Hf to show the discrepancy between the two. G, Zir-Hf (open symbols) and WR-Hf plot against Nd isotope showing the discrepancy between Zir-Hf and WR-Hf and decoupling between WR-Hf and Nd isotope. H, Correlations between age corrected /non-corrected WR-Hf and TiO_2.

overlapping with the range of Group 2 host rocks ($\varepsilon_{Nd}(t)$= 0.05 – 0.59) (Fig. 6.6A) but large variation in $\varepsilon_{Hf}(t)$ (Fig. 6.6B). The scattering on the plot of $^{208}Pb/^{204}Pb_i$ and $^{206}Pb/^{204}Pb_i$ (Fig. 6.6E) indicates the heterogeneity in Pb isotopes.

For samples QL10-14 and QL10-15, we preferentially analysed the magmatic grains along with only a few inherited zircons (QL10-15, Table 6.3). Therefore, these zircon *in situ* Hf isotopes mostly reflect the latest magma composition with a little inheritance. The *in situ* Hf isotopes show very limited variations within each sample (Table. 6.4) indicating the relatively homogenous composition of the magma from which zircons crystallized. A few inherited zircons in granite QL10-15 were also analysed and show the negative ε_{Hf} (500) of -20 (Table. 6.4). Traditionally, zircon *in situ* Hf (Zir-Hf) isotopes is considered to faithfully record the magma isotopes at the time of crystallization (Kinny and Maas, 2003) and whole rock Hf (WR-Hf) isotopes should agree well with Hf composition in constituent zircons (Schmitz et al., 2004). However, in our study, the zircon $\varepsilon_{Hf}(t)$ is dominantly <0 inconsistent with the dominant whole-rock with ε_{Hf} >0 (Fig. 6.6B). The discrepancy between WR- Hf and Zir-Hf isotopes is so significant (Fig. 6.6F-G) that demonstrate the (1) Zir-Hf isotopes do not represent the WR Hf isotopes; (2) zircon is not the only major host of Hf. One may argue that, if not considering the outlier QL10-26 on Fig. 6.6F-G, WR-Hf is not significantly decoupled from Nd isotope. The important observation here is that the WR-Hf isotope is well correlated with TiO_2 (Fig. 6.6H) which suggests that the apparent 'outlier' QL10-26 in Fig. 6.6 is actually a systematic result rather than an accidental outlier. Therefore, the decoupling between WR-Hf and Nd isotopes is real and significant.

6.6. The discrepancy between in situ zircon Hf and whole rock Hf isotopes

There is significant discrepancy between WR-Hf and Zir-Hf isotopes and decoupling between WR-Hf and Nd isotopes (Fig. 6.6G). This discrepancy cannot be explained by 'analytical bias' (i.e., the inherited cores are analysed in the whole rock but not analysed in *in situ* zircons) because the inherited cores have much more negative $\varepsilon_{Hf}(t)$ (see those in QL10-15, Table 6.4), dissolving them

should result in the lower WR $\varepsilon_{Hf}(t)$s rather than the much higher WR $\varepsilon_{Hf}(t)$ than Zircon $\varepsilon_{Hf}(t)$. This demonstrates that non-zircon phases host the abundant radiogenic Hf in the rocks. To understand the decoupling and discrepancy, the correlation between WR-Hf and TiO_2 may offer some clues (Fig. 6.6H).

Previous studies (Heinonen et al., 2010; Pankhurst et al.2013) have reported the positive correlation though broad correlation between initial Hf isotope ratio and Ti contents in zircons and interpret it to result from increasing crustal assimilation-related cooling. In our samples, there is no correlation between zircon Hf isotopes and zircon Ti contents (Fig. 6.7A), which means that crustal assimilation, if any, is not related to Ti contents in zircons nor with magma cooling. The tight (vs. broad) correlation on Fig. 6.6H, therefore can be explained in an alternative way: Ti-rich minerals are the important high $\varepsilon_{Hf}(t)$ host. This could happen in two scenarios: (1) Ti-rich minerals produce the high $\varepsilon_{Hf}(t)$ in the comparable way of 'garnet effect'; (2) high TiO_2 and radiogenic Hf isotope are different products in response to a common process.

6.6.1. Ti-rich minerals— important Hf host

In our samples, average Hf contents in zircons increase as the whole rock SiO_2 increases (Fig. 6.7B). This could be explained by the preference of Zr over Hf in the early-formed zircons (Wooden et al., 2007). At the same time, the WR Hf concentrations remain almost the same throughout cumulates to the host rocks (Fig. 6.7B). Therefore, more proportions of Hf reside in zircons in the felsic lithologies than those in the mafic lithologies because mafic lithologies have (1) lower Hf concentration in zircons (Fig. 6.7B); (2) lower zircon modes (zirconium undersaturation in the mafic magma see below). Simple binary mixing calculation (Table. 6.6) is done to estimate how much Hf resides in the non-zircon phases and how radiogenic they are (Fig. 6.7D). Results show that > 40% Hf in the whole rock Hf hosted by non-zircon phases and they are much more radiogenic than those in the zircons (minimum estimates, see Table. 6.6). Note that, calculation of

Hf isotopes in the non-zircon phases is not involved with Ti contents at any stage, but the results show that the Hf isotopes in the non-zircon phases is positively correlated to whole rock TiO_2 (Fig. 6.7D).

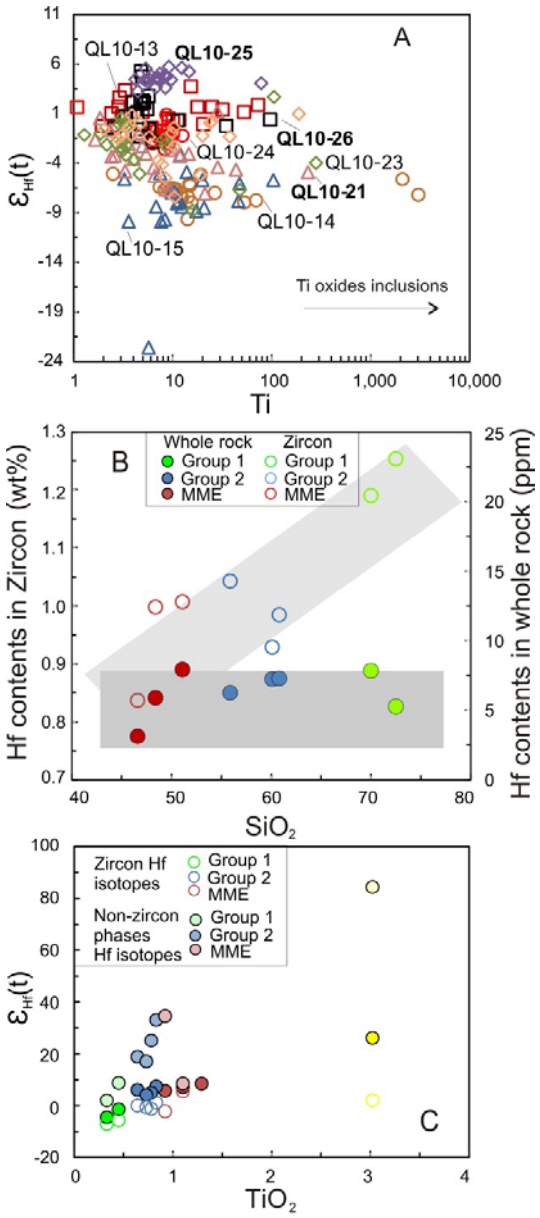

Fig. 6.7. A, Zircon in situ Hf isotopic composition plot against zircon Ti contents showing no correlation between the two. B, Zircon Hf contents and whole rock Hf contents plot against SiO_2 showing that (1) the whole rock Hf concentration remains more or less the same throughout; (2) Hf concentration in zircon increases from mafic to felsic. C, comparison of whole rock, zircon and non-zircon phases Hf isotopes.

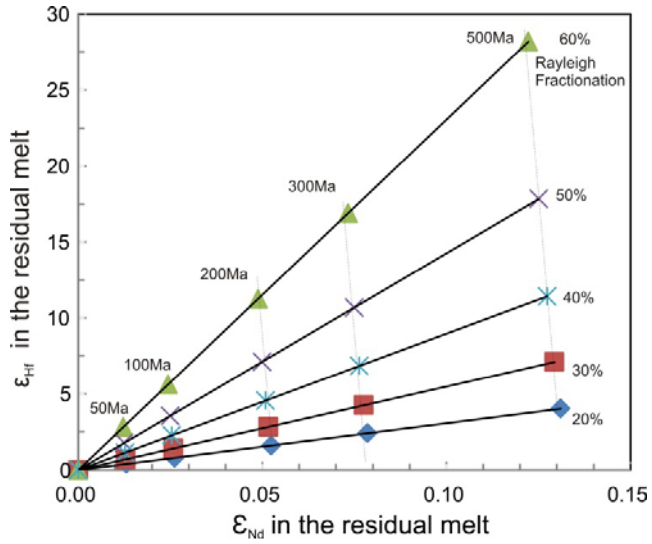

Fig. 6.8. Model time-integrated modern isotopic compositions in the residual magma for removal of up to 60% of pure ilmenite. Rayleigh fractionation equations are used. For clarification, we start with andesitic elemental composition (data from Niu and O'Hara (2009)) with chondritic isotopes. Results showing the huge in-growth of ε_{Hf} with negligible changes in ε_{Nd}. However, to achieve the 26 units shift in ε_{Hf} from the mantle array (ε_{Hf}=1.33* ε_{Nd}+3.19, (Vervoort and Blichert-Toft, 1999)) in QL10-26, up to 60% of pure ilmenite and 500 myrs integration is required. Fractionation of 60% pure ilmenite means original magma should contain at least 30 wt% TiO_2 (ilmenite has 50% TiO_2) and experience 600% (6 times of its own volume) fractionation if there is up to 10% ilmenite in the fractionated assemblages. Importantly, 500 myrs integration is too long to be realistic for any fractionation process within the magma chamber. Therefore, ilmenite fractionation cannot explain the radiogenic Hf in our samples despite its great potential.

6.6.2. Can Ti-rich minerals cause the decoupling in initial Nd-Hf isotopes?

Fe-Ti oxides have been proposed to explain the decoupling of Nd-Hf isotopes in the granulite lower crust (Schmitz et al., 2004) despite the lack of direct data support. The correlation of WR-Hf ~ TiO_2 (Fig. 6.6H) in this study seems to support this hypothesis, especially sample QL10-26 which has the biggest decoupling/discrepancy (Fig. 6.6G, 6.7C), highest TiO_2 (Table 6.2, Fig. 6.6H), and most abundant ilmenite (Table. 6.1, Fig. 6.2). Ilmenite has extremely low $^{176}Lu/^{177}Hf$ (<0.0001, see the mineral separate data in Nowell et al. (2004)) due to different partitioning coefficients of Lu and Hf (Kd_{Hf}=1.39 vs. Kd_{Lu}=0.029, see compilation of Niu and O'Hara, (2009)), thus the crystallization of ilmenite results in extreme fractionation of Lu/Hf between ilmenite and any other co-precipitating phases. Similar to zircon, ilmenite would preserve its initial Hf isotopic ratios at the time of

fractionation while the equilibrating residual magma would evolve to very radiogenic Hf over time. At the same time, Sm and Nd are almost equally incompatible in ilmenite (Kd_{Sm}=0.009, Kd_{Nd}=0.008, Niu and O'Hara, 2009). Therefore, ilmenite may have potential to cause Nd-Hf isotopes decoupling as other minerals do, e.g., perovskite (Salters and Hart, 1991). Because our decoupling resides in the initial Nd and Hf isotopes rather than the present day values, it implies a long time interval between the early ilmenite fractionation and the final remaining magma solidification, in which case the remaining melt can develop decoupled Nd-Hf isotopic compositions from its original un-decoupling point. The simple modelling Fig. 6.8 (see figure caption for calculation) shows that fractionation of ilmenite make the remaining melt have huge in-growth of ε_{Hf} with negligible changes in ε_{Nd} if allowing hundreds of millions of years' integration. However, expecting the Nd-Hf isotopes decoupling in the initial values in our samples, it requires 500 myrs of time interval between early fractionation and solidification of the equilibrating magma in the magma chamber where 10-20 million years is the maximum. Therefore, ilmenite fractionation, although common in the mafic or felsic magma evolution, may cause the present-day Nd-Hf decoupling (Schmitz et al., 2004) but is not the reason of the initial Nd-Hf isotopes decoupling in our samples. Neither do other TiO_2 rich minerals (e.g. Amp, Bt) (similar modelling not shown). Extremely high $^{176}Hf/^{177}Hf$ has been reported in Cpx which is the major Hf host in the mantle (Salters and Zindler, 1995) and might be explained by the metasomatism or the ancient melt depletion and recent enrichment. But this interpretation has nothing to do with the fractionation process in the magma chamber as discussed here. In terms of fractional crystallization, due to the very low Hf and Ti concentrations in pyroxene compared to other Ti-rich minerals, Cpx is less likely the cause.

As demonstrated above, the decoupling is not produced by the fractional crystallization in the magma chamber. However, why $\varepsilon_{Hf}(t)$ is correlated with TiO_2 ? Is this correlation related to the discrepancy between WR-Hf isotopes and Zir-Hf isotopes?

6.6.3. Mixing—magma endmembers

The significant positive correlation between $\varepsilon_{Hf}(t)$ and TiO_2, combined with the broad negative correlations between both $\varepsilon_{Hf}(t)$ and $\varepsilon_{Nd}(t)$ and SiO_2 (Fig. 6.6A-B), is best explained by mixing processes. We consider QL10-26 is not early cumulated from a granitoid magma as other charnockites (Frost et al., 2000) but a hybrid of mafic lithologies and felsic melts. First of all, QL10-26 displays more depleted characters, i.e. 48 wt% silica (Table 6.2, 27 vol% Px (Table 6.1), 5 vol% Fe-Ti oxides (Table 6.1), small Pb and Ti anomalies, and no Eu anomaly (Fig. 6.4). Besides, charnockites are high temperature granitoids (>900 °C) (Kilpatrick and Ellis, 1992), however, Zr-in-whole rock temperature for QL10-26 is only 679 °C and Ti-in-zircon temperature is 715 °C (Table 6.5). Importantly, QL10-26 has the most depleted WR Hf isotopes ($\varepsilon_{Hf}(t)$=26), indicating it crystallized from a depleted source. Most likely, Px and Ilm are products from a basaltic composition, while, Qz, Pl and Kfs are the late-stage minerals from a more felsic composition (see below) and Amp rims on the Px probably record the interaction of these two magmas (see below). QL10-26 has TiO_2 up to 3.02%, significant higher than the normal mafic rocks with similar silica contents. However, Fe-Ti rich melts are natural consequences with relatively low liquidus temperature (1080-1100 °C) (Dick et al., 2000; Niu et al., 2002) during cooling and fractional crystallization of MORB evolution (Clague et al., 1981; Dick et al., 2000; Niu et al., 2002). Probably, QL10-26 crystallized from evolved Fe-Ti rich basalt.

The most felsic rocks QL10-14/15 are peraluminous (A/CNK >1.1), have the highest silica (70 wt %), lowest TiO_2, radiogenic I_{Sr} and negative $\varepsilon_{Hf}(t)$ and $\varepsilon_{Nd}(t)$ (Fig. 6.6C-D), and therefore represent an endmember close to crustal composition. The zircons have flat HREEs (Fig. 6.5) indicating the equilibrium with garnet pointing to mid-lower crust level. Other samples with intermediate composition between these two endmembers also have the intermediate isotopic compositions in between (Fig. 6.6A-B, especially on Fig. 6.6H). All these observations suggest a mixing process.

6.6.4. Mixing induced discrepancy between WR-Hf and Zir-Hf isotopes

The significant positive correlation between $\varepsilon_{Hf}(t)$ and TiO_2 could be the coherent results corresponding to mixing process, i.e., different minerals crystallizing at different stages. According to the experiments on the zircon saturation in melts (Boehnke et al., 2013), the basaltic liquids require >5000 ppm Zr to directly crystallize zircon. Zircons found in mafic environments must have crystallized from late stage, evolved melts (Boehnke et al., 2013) or crustally contaminated melts (Zheng et al., 2006). Therefore, 209 ppm Zr in QL10-26 is obviously undersaturated. Probably the pyroxene and ilmenite crystallized earlier at higher temperature when the zircon failed to crystallize due to the undersaturation. In this situation, the discrepancy between WR-Hf and Zir-Hf, therefore, can be explained. When the mantle-derived magma interacts with the crustal material, the possible scenario is that Ti-rich minerals, e.g. Amp, Fe-Ti oxides, and Bt, etc., crystallize from the more mafic composition at the relatively earlier stage of mixing and preserve the isotope signature closer to the mafic endmember. Zircons do not crystallize until the later stage when the hybrid magma is saturated in Zr. This is supported by the Ti-in-zircon thermometry. For example, the Ti-in-zircon thermometry for QL10-26 is only 715 °C (Zr-in-whole rock thermometry is even lower 679 °C) (Table. 6.5). This temperature is significantly lower than the crystallization temperature for pyroxene (> 1000 °C), amphibole (>850 °C) and biotite (> 750 °C) but within the range of felsic minerals (plagioclase, k-feldspar and quartz) crystallization temperature (< 750 °C) (Bogaerts et al., 2006). This means that the mafic minerals already crystallized significantly before the crystallization of zircons. Therefore, zircons generally record isotope compositions closer to the felsic endmember. TiO_2 decreases with increasing SiO_2, implying the fewer modes of Ti-rich minerals in the more felsic rocks, hence, the smaller discrepancy between WR-Hf and Zir-Hf (Fig. 6.6F). The MME sample QL10-25 has high TiO_2 but smaller discrepancy (almost identical WR-Hf and Zir-Hf) (Fig. 6.6F). This could be explained by the alteration/metamorphic process. Almost all the amphiboles in QL10-25 that have altered into actinolite, and ilmenite is rare, indicating a fluid-

presence environment. We failed to evaluate the ability of actinolite to host Hf during metamorphism. But studies have shown that Hf can be mobile (Woodhead et al., 2001) due to the fluids while the zircon-Hf isotopes are resistant to metamorphism (Kinny and Maas, 2003). When the amphiboles which are the major Hf host apart from zircons in QL10-25 were transformed to actinolite, they probably lost their own Hf isotopes. Meanwhile, zircons are resistant and preserved their Hf isotopes. Therefore, the WR-Hf is very similar to Zir-Hf. The group 1 granitic samples have slightly higher Ti-in-zircon thermometer temperature, reflecting the higher zircon saturation thus crystallize earlier/higher temperature. But these zircons almost entirely crystallized from the felsic magma which had little contribution from the mafic magma, thus, recorded the felsic endmember and has smaller discrepancy between the WR-Hf and Zir-Hf. Note that WR-Hf isotope is decoupled from Nd isotope but Zir-Hf is not (Fig. 6.6G), which indicate that the decoupling is inherited from the mantle not the crustal melt.

As discussed above, we aim to bring cautions in interpreting the zircon *in situ* Hf isotopes, specifically when mixing two isotopically different magmas where WR-Hf analysis or Hf isotope on the Ti-rich minerals is strongly recommended.

6.7. Magma chamber evolution—mixing associated with crystal fractionation

We consider the QL10-26 as a mixture between mafic lithologies and felsic melts. The presence of pyroxene in the magmatic charnockites has been considered as the indication of 'dry' magma; Frost et al. (2000) especially pointed out that pyroxene-bearing charnockites can form in any rock type if the water activity is low enough. And the derivative product is very similar to QL10-26 in terms of mineral assemblage. It has to be pointed out that the pyroxene in QL10-26 did not crystallize from the granitic magma but from the precursor basaltic magma.

Importantly, however, the water-saturated experiments on basaltic andesites/andesites suggest that the pyroxene can be the liquidus phases in the hydrous magma at the middle-lower crust level when

the temperature is higher (>950°C) compared to the Amp (850°C) (Grove et al., 2003; Bogaerts et al., 2006; Krawczynski et al., 2012). These experiments also have shown that the crystallization of amphibole is restricted to H_2O rich system (Grove et al., 2003; Bogaerts et al., 2006; Müntener and Ulmer, 2006). The secondary Amp rims on the pyroxene and biotite reflect the decreasing of temperature, e.g., from > 950 °C to 850°C rather than the water contents in the magma, e.g., from anhydrous to hydrous compositions. The presence of pyroxene alongside abundant Fe-Ti oxides in QL10-26 simply indicates a higher crystallization temperature in a hydrous system, probably at deeper level. This interpretation is consistent with the convergent tectonic setting of Kekeli batholith where fluxes of fluids are very high.

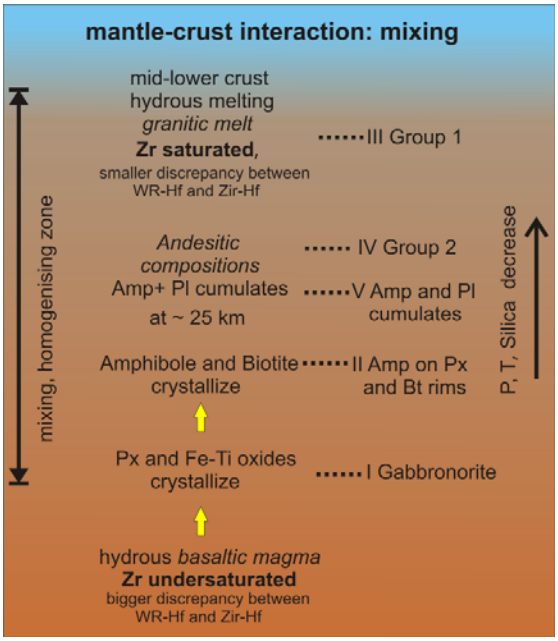

Fig. 6.9. Carton showing the mixing and crystallization process where mantle-derived lithologyinteracts with the crustal melt. See details in the text. I: Px and Ilm start to crystallize from the evolved basaltic magma at ~ 950-1100 °C (gabbronorite QL10-26). II: Amp started to crystallize by replacing Px as rims and Bt due to the lower P-T conditions and interaction with granitic melts at stage III. III: granitic melts (Group 1) by hydrous partial melting of mid-lower crust due to the basaltic magma (I) underplating. IV: hybrid andesitic magma (Group 2) of mantle lithology (part of QL10-26) and crustal melt (Group 1). V: Amp and Pl cumulated from the hybrids (Group 2).

Note that MMEs and Group 2 have overlapping Nd-Hf isotopes, indicating that MMEs were cumulates from the same magma systems as Group 2. As discussed above and based on the experiments (Grove et al., 2003; Bogaerts et al., 2006; Müntener and Ulmer, 2006), the possible crystallization order and relationship among the samples could be illustrated in Fig. 6.9. At higher temperature, the pyroxene and Fe-Ti oxides start crystallization from basalt at deeper level (QL10-26) (Fig. 6.9I). These assemblages were brought up to the shallower level, become unstable and start to crystallize amphibole and biotite due to the lower pressure and temperature (Fig. 6.9II) and also the interaction with felsic melt (Group 1). When the felsic melt homogenizing with solid mafic minerals, the hybrids reached intermediate andesitic composition at some point (Group 2). MMEs consisting of Amp and Pl (Fig. 6.9V) cumulated from this hybrid (Fig. 6.9IV). At each stage, Ti-rich minerals, e.g. Fe-Ti oxides, Px, Amp and Bt always crystallize relatively earlier at a higher temperature from a more mafic composition than Qz, Pl, Kfs and specially zircon. Therefore, their isotopes are always closer to the mafic endmember while the zircon only record hybrid isotopes with significant contributions from the felsic endmember. Different crystallization timing of different minerals results in the discrepancy between Zir-Hf and WR-Hf isotopes.

6.8. Magma generation and continental crust growth

The NQOB is an oceanic suture zone (Song et al., 2013). The oceanic basin, which was initially a back-arc basin induced by the subduction of Qilian Oceanic crust along the NQ-UHPM belt, may have started spreading since 710 Ma (Chapter 4). The tectonic evolution model is debatable in the NQOB (Yang et al., 2002; Wu et al., 2006a; Xu et al., 2006; Song et al., 2013; Chapter 4), but the Kekeli batholith along the southern margin of the NQOB is agreed to be subduction related (Song et al., 2013; Wu et al., 2010). The mafic component in QL10-26 is highly evolved basaltic melt from the partial melting of the mantle wedge due to slab dehydration. The small positive Pb and negative Ti anomalies result from the contributions of slab and crustal melts. We speculate that there is a mantle source beneath Qilian which the basalt originated from has decoupled Hf and Nd isotopes.

Based on the previous research, the decoupling maybe caused by the metasomatism (Salters and Hart, 1991; Salters and Zindler, 1995), the ancient melt depletion (Salters and Zindler, 1995), subduction zone process (Woodhead et al., 2001; Polat and Münker, 2004) and inherited garnet effect in the sources (Vervoort et al., 2000). In this study, we do not wish to discuss the detailed reasoning of Nd-Hf isotopes decoupling in the mantle wedge based on only one sample QL10-26, but suggest that radiogenic Hf isotopes must be from an ancient event.

The mantle-derived magma in the convergent zone ascends beneath the shallower crustal levels may have several effects: (1) release the fluids due to the lower water solubility with decompression (Moore et al., 1995; Papale, 1997) and the fluids lower the solidus of the crustal rocks; (2) heat the crustal rocks to solidus and mix with the derivative crustal melts. The melting of pelites and greywacks in the mid-lower crust begins at P-T of ~ 0.8GPa and ~750°C in response to influx of aqueous fluid and produce the peraluminous granitic melt (Brown, 2013), which corresponds to our Group 1 peraluminous samples with negative ε_{Nd} , ε_{Hf} and radiogenic $I_{Sr.}$ The temperature of 750 °C is also consistent with Ti-in-zircon thermometer (~780 °C) for Group 1 samples and easily achieved because the evolved basalts has high temperature 1100 °C (Dick et al., 2000; Niu et al., 2002). However, hornblende and plagioclase (MMEs) in hybrids Group 2 start cumulating at 0.8 GPa at 850 °C according to the hydrous arc magma experiments (H_2O> 4 wt%) (Grove et al., 2003; Müntener and Ulmer, 2006), which implies that the temperature before mixing was significantly higher. The whole rock suite in Kekeli batholith records the snap-shot of the magma interaction between mantle-derived melt and crustal melt in the subduction zone at ~ 500 Ma, including the ascent of mafic magma, hydrous melting of continental lower crust and mixing process as well as the mineral segregation from the andesitic hybrids in the magma chamber.

The amphibole-rich layer in the lower arc crust is considered to be the significant evidence of amphibole fractionation in the generation of the bulk andesitic continental crust in the arc magma evolution (Cawthorn and O'Hara, 1976; Moore and Carmichael, 1998; Davidson et al., 2007;

Hidalgo and Rooney, 2010). In our study, both the MMEs and Group 2 have neutral $\varepsilon_{Hf}(t)$ (>0) and $\varepsilon_{Nd}(t)$ (~ 0) (Fig. 6.6A,B). Trace element compositions of the host Group 2 are very similar to bulk continental crust (BCC) (Fig. 6.4). It is interesting to evaluate the role of the Amp+Pl bearing cumulates in the evolution of Kekeli batholith. Do they drive the magma composition from basaltic andesite to andesitic? Or do they essentially precipitate from the andesitic composition? The overlapping Nd and Hf isotopes between MMEs and host rocks indicate that the former precipitated from their hybrid andesitic host Group 2, therefore, they are essentially indirect products of the mixing process rather than the driving force to make basaltic arc magma evolve towards andesitic composition. In this case, these MMEs are not contributing to the andesitic magma generation. This concept is misleading but important in the context of the continental crust growth. For example, if we had only sampled Group 2 and MMEs, the possible interpretation would possibly be juvenile continental crust (Group 2) was produced by the amphibole fractionation (MMEs) from the basaltic arc magma based on all the geochemical data. Amp-bearing cumulates in the lower arc crust may play an important role in the arc magma evolution but not all of them have the same origin, therefore, it needs to be carefully interpreted.

6.9. Conclusions

Ti-rich minerals host abundant Hf too, especially in the more mafic lithologies. Zircon in situ Hf isotopes do not necessarily represent the whole-rock Hf isotope during magma mixing of two isotopically different sources, but only record the Hf isotopic composition closer to the felsic endmember at the time of zircon crystallization due to saturation. Ti-rich minerals, e.g. Fe-Ti oxides, Px, Amp and Bt, record the Hf isotope closer to the mafic endmember due to their early crystallization from a basaltic matrix. Generally, the early crystallization of Ti-rich minerals and later zircon crystallization causes the discrepancy between WR-Hf and Zir-Hf.

Kekeli batholith preserves the ascent of the mafic magma, interaction between mantle-derived melt and crustal melt as well as the mineral segregation from the hybrid andesitic magma in the subduction zone at ~ 500 Ma in the North Qilian Orogenic belt.

6.10. References

Amelin, Y., Lee, D.-C., Halliday, A.N., Pidgeon, R.T., 1999. Nature of the Earth's earliest crust from hafnium isotopes in single detrital zircons. Nature 399, 252-255.

Amelin, Y., Lee, D.C., Halliday, A.N., 2000. Early-middle archaean crustal evolution deduced from Lu-Hf and U-Pb isotopic studies of single zircon grains. Geochimica et Cosmochimica Acta 64, 4205-4225.

Bogaerts, M., Scaillet, B., Auwera, J.V., 2006. Phase Equilibria of the Lyngdal Granodiorite (Norway): Implications for the Origin of Metaluminous Ferroan Granitoids. Journal of Petrology 47, 2405-2431.

Brown, M., 2013. Granite: From genesis to emplacement. Geological Society of America Bulletin 125, 1079-1113.

Boehnke, P., Watson, E.B., Trail, D., Harrison, T.M., Schmitt, A.K., 2013. Zircon saturation re-revisited. Chemical Geology, 351(0): 324-334.

Cawthorn, R.G., O'Hara, M.J., 1976. Amphibole fractionation in calc-alkaline magma genesis. American Journal of Science 276, 309-329.

Claeson, D.T., Meurer, W.P., 2004. Fractional crystallization of hydrous basaltic "arc-type" magmas and the formation of amphibole-bearing gabbroic cumulates. Contributions to Mineralogy and Petrology 147, 288-304.

Clague, D.A., Frey, F.A., Thompson, G., Rindge, S., 1981. Minor and trace element geochemistry of volcanic rocks dredged from the Galapagos spreading center: Role of crystal fractionation and mantle heterogeneity. Journal of Geophysical Research: Solid Earth (1978–2012) 86, 9469-9482.

Clarke, G. L., Klepeis, K. A. and Dacko, N.R., 2000. Cretaceous high-P granulites at Milford Sound, New Zealand: metamorphic history and emplacement in a convergent margin setting. Journal of Metamorphic Geology 18, 359-374.

Collins, W.L., 2002. Hot orogens, tectonic switiching, and creation of continental crust. Geology 30, 535-538.

Collins, W.L., 2003. Hot orogens, tectonic switching, and creation of continental crust: comment and reply: reply. Geology 31, e10.

Condie, K.C., 1998. Episodic continental growth and supercontinents: a mantle avalanche connection? Earth and Planetary Science Letters 163, 97-108.

Condie, K.C., 2000. Episodic continental growth models: afterthoughts and extensions. Tectonophysics 322, 153-162.

Corfu, F., Hanchar, J.M., Hoskin, P.W., Kinny, P., 2003. Atlas of zircon textures. Reviews in mineralogy and geochemistry 53, 469-500.

Davidson, J., Turner, S., Handley, H., Macpherson, C., Dosseto, A., 2007. Amphibole "sponge" in arc crust? Geology 35, 787-790.

Dick, H.J.B., Natland, J.H., Alt, J.C., Bach, W., Bideau, D., Gee, J.S., Haggas, S., Hertogen, J.G.H., Hirth, G., Holm, P.M., Ildefonse, B., Iturrino, G.J., John, B.E., Kelley, D.S., Kikawa, E., Kingdon, A., LeRoux, P.J., Maeda, J., Meyer, P.S., Miller, D.J., Naslund, H.R., Niu, Y.-L., Robinson, P.T., Snow, J., Stephen, R.A., Trimby, P.W., Worm, H.-U., Yoshinobu, A., 2000. A long in situ section of the lower ocean crust: results of ODP Leg 176 drilling at the Southwest Indian Ridge. Earth and Planetary Science Letters 179, 31-51.

Frost, B.R., Frost, C.D., Hulsebosch, T.P., Swapp, S.M., 2000. Origin of the charnockites of the Louis lake Batholith, wind River Range, Wyoming. Journal of Petrology 41, 1759-1776.

Gehrels, G.E., Yin, A., Wang, X.F., 2003. Magmatic history of the northeastern Tibetan Plateau. Journal of Geophysical Research 108, 2423.

Griffin, W.L., Pearson, N.J., Belousova, E., Jackson, S.E., van Achterbergh, E., O'Reilly, S.Y., Shee, S.R., 2000. The Hf isotope composition of cratonic mantle: LAM-MC-ICPMS analysis of zircon megacrysts in kimberlites. Geochimica et Cosmochimica Acta 64, 133-147.

Griffin, W.L., Wang, X., Jackson, S.E., Pearson, N.J., O'Reilly, S.Y., Xu, X., Zhou, X., 2002. Zircon chemistry and magma mixing, SE China: In-situ analysis of Hf isotopes, Tonglu and Pingtan igneous complexes. Lithos 61, 237-269.

Grove, T.L., Elkins-Tanton, L.T., Parman, S.W., Chatterjee, N., Müntener, O., Gaetani, G.A., 2003. Fractional crystallization and mantle-melting controls on calc-alkaline differentiation trends. Contributions to Mineralogy and Petrology 145, 515-533.

Heinonen, A.P., Andersen, T., Ramo, O.T., 2010. Re-evaluation of Rapakivi Petrogenesis: Source Constraints from the Hf Isotope Composition of Zircon in the Rapakivi Granites and Associated Mafic Rocks of Southern Finland. Journal of Petrology 51, 1687-1709.

Hidalgo, P.J., Rooney, T.O., 2010. Crystal fractionation processes at Baru volcano from the deep to shallow crust. Geochemistry, Geophysics, Geosystems 11.

Huang, H., Niu, Y., Nowell, G., Zhao, Z., Yu, X., Zhu, D., Mo, X., Ding, S., 2014. Geochemical constraints on the petrogenesis of granitoids in the East Kunlun Orogenic blet, northern Tibetan Plateau: implications fro the continental crust growth through syncollisional felsic magmatism. Chemical Geology.

Kay, R.W., Mahlburg Kay, S., 1993. Delamination and delamination magmatism. Tectonophysics 219, 177-189.

Kemp, A., Hawkesworth, C., Foster, G., Paterson, B., Woodhead, J., Hergt, J., Gray, C., Whitehouse, M., 2007. Magmatic and crustal differentiation history of granitic rocks from Hf-O isotopes in zircon. Science 315, 980.

Kilpatrick, J.A., Ellis, D.J., 1992. C-type magmas: igneous charnockites and their extrusive equivalents. Geological Society of America Special Papers 272, 155-164.

Kinny, P.D., Compston, W., Williams, I.S., 1991. A reconnaissance ion-probe study of hafnium isotopes in zircons. Geochimica et Cosmochimica Acta 55, 849-859.

Kinny, P.D., Maas, R., 2003. Lu–Hf and Sm–Nd isotope systems in zircon. Reviews in Mineralogy and geochemistry 53, 327-341.

Krawczynski, M.J., Grove, T.L., Behrens, H., 2012. Amphibole stability in primitive arc magmas: effects of temperature, H2O content, and oxygen fugacity. Contributions to Mineralogy and Petrology 164, 317-339.

Larocque, J., Canil, D., 2010. The role of amphibole in the evolution of arc magmas and crust: the case from the Jurassic Bonanza arc section, Vancouver Island, Canada. Contributions to Mineralogy and Petrology 159, 475-492.

Mo, X.X., Niu, Y.L., Dong, G.C., Zhao, Z.D., Hou, Z.Q., Su, Z., Ke, S., 2008. Contribution of syncollisional felsic magmatism to continental crust growth: A case study of the Paleogene Linzizong volcanic Succession in southern Tibet. Chemical Geology 250, 49-67.

Moore, G., Carmichael, I.S.E., 1998. The hydrous phase equilibria (to 3 kbar) of an andesite and basaltic andesite from western Mexico: constraints on water content and conditions of phenocryst growth. Contributions to Mineralogy and Petrology 130, 304-319.

Moore, G., Vennemann, T., Carmichael, I.S.E., 1995. Solubility of water in magmas to 2 kbar. Geology 23, 1099.

Müntener, O., Ulmer, P., 2006. Experimentally derived high-pressure cumulates from hydrous arc magmas and consequences for the seismic velocity structure of lower arc crust. Geophysical Research Letters 33.

Niu, Y., Gilmore, T., Mackie, S., Greig, A., Bach, W., 2002. Mineral chemistry, whole-rock compositions, and petrogenesis of Leg 176 gabbros: data and discussion, Proceedings of the Ocean Drilling Program, Scientific Results, pp. 1-60.

Niu, Y., O'HARA, M.J., Pearce, J.A., 2003. Initiation of subduction zones as a consequence of lateral compositional buoyancy contrast within the lithosphere: a petrological perspective. Journal of Petrology 44, 851-866.

Niu, Y., Zhao, Z., Zhu, D.-C., Mo, X., 2013. Continental collision zones are primary sites for net continental crust growth — A testable hypothesis. Earth-Science Reviews 127, 96-110.

Niu, Y.L., 2005. Generation and evolution of basaltic magmas: some basic concepts and a new view on the origin of Mesozoic-Cenozoic basaltic volcanism in eastern China. Geological Journal of China Universities 1.

Niu, Y.L., Mo, X.X., Dong, G.C., Zhao, Z.D., Hou, Z.Q., Zhou, S., Ke, S., 2007. Continental Collision Zones are Primary Sites of net Continental Crustal Growth: Evidence From the Linzizong Volcanic Succession in Southern Tibet, Eos Trans. AGU, 88(52), Fall meet., Suppl., Abstract, p. 01.

Niu, Y.L., O'Hara, M.J., 2009. MORB mantle hosts the missing Eu (Sr, Nb, Ta and Ti) in the continental crust: New perspectives on crustal growth, crust–mantle differentiation and chemical structure of oceanic upper mantle. Lithos 112, 1-17.

Nowell, G.M., Pearson, D.G., Bell, D.R., Carlson, R.W., Smith, C.B., Kempton, P.D., Noble, S.R., 2004. Hf Isotope Systematics of Kimberlites and their Megacrysts: New Constraints on their Source Regions. Journal of Petrology 45, 1583-1612.

Pankhurst, M.J., Schaefer, B.F., Turner, S.P., Argles, T., Wade, C.E., 2013. The source of A-type magmas in two contrasting settings: U–Pb, Lu–Hf and Re–Os isotopic constraints. Chemical Geology 351, 175-194.

Papale, P., 1997. Modeling of the solubility of a one-component H2O or CO2 fluid in silicate liquids. Contributions to Mineralogy and Petrology 126, 237-251.

Pettingill, H.S., Patchett, P.J., 1981. Lu-Hf total-rock age for the Amîtsoq gneisses, West Greenland. Earth and Planetary Science Letters 55, 150-156.

Pietranik, A., Slodczyk, E., Hawkesworth, C.J., Breitkreuz, C., Storey, C.D., Whitehouse, M., Milke, R., 2013. Heterogeneous Zircon Cargo in Voluminous Late Paleozoic Rhyolites: Hf, O Isotope and Zr/Hf Records of Plutonic to Volcanic Magma Evolution. Journal of Petrology.

Plank, T., 2005. Constraints from thorium/lanthanum on sediment recycling at subduction zones and the evolution of the continents. Journal of Petrology 46, 921-944.

Polat, A., Münker, C., 2004. Hf–Nd isotope evidence for contemporaneous subduction processes in the source of late Archean arc lavas from the Superior Province, Canada. Chemical Geology 213, 403-429.

Rubatto, D., 2002. Zircon trace element geochemistry: Partitioning with garnet and the link between U-Pb ages and metamorphism. Chemical Geology 184, 123-138.

Rudnick, R.L., 1995. Making continental crust. Nature 378, 571-578.

Rudnick, R.L., Gao, S., 2003. Composition of the Continental Crust. Treatise on Geochemistry, 1-64.

Salters, V.J.M., Hart, S.R., 1991. The mantle sources of ocean ridges, islands and arcs: the Hf-isotope connection. Earth and Planetary Science Letters 104, 364-380.

Salters, V.J.M., Zindler, A., 1995. Extreme 176Hf/177Hf in the sub-oceanic mantle. Earth and Planetary Science Letters 129, 13-30.

Schmitz, M.D., Vervoort, J.D., Bowring, S.A., Patchett, P.J., 2004. Decoupling of the Lu-Hf and Sm-Nd isotope systems during the evolution of granulitic lower crust beneath southern Africa. Geology 32, 405.

Shi, R.D., Yang, J.S., Wu, C.L., 2004. First SHRIMP dating for teh formation of the Late Sinian Yushigou Ophiolite North Qilian Mountains. Acta Geologica Sinica 78, 649-657(in Chinese with English Abstract).

Song, S., Niu, Y., Su, L., Xia, X., 2013. Tectonics of the North Qilian orogen, NW China. Gondwana Research 23, 1378-1401.

Song, S., Niu, Y., Wei, C., Ji, J., Su, L., 2010. Metamorphism, anatexis, zircon ages and tectonic evolution of the Gongshan block in the northern Indochina continent—An eastern extension of the Lhasa Block. Lithos 120, 327-346.

Stein, M., Hofmann, A., 1994. Mantle plumes and episodic crustal growth. Nature 372, 63-68.

Sun, S.s., McDonough, W.F., 1989. Chemical and isotopic systematics of oceanic basalts: implications for mantle composition and processes. Geological Society, London, Special Publications 42, 313-345.

Taylor, S.R., 1967. The origin and growth of continents. Tectonophysics 4, 17-34.

Taylor, S.R., 1977. Island arc models and the composition of the continental crust. Island Arcs, Deep-Sea Trenches and Back-Arc Basins. Amerian Geophysical Union, Washington, DC, 325-335.

Taylor, S.R., McLennan, S.M., 1985. The continental crust: its composition and evolution.

Thirlwall, M.F., Walder, A.J., 1995. In situ hafnium isotope ratio analysis of zircon by inductively coupled plasma multiple collector mass spectrometry. Chemical Geology 122, 241-247.

Tseng, C.Y., Yang, H.J., Yang, H.Y., Liu, D., Tsai, C.L., Wu, H., Zuo, G., 2007. The Dongcaohe ophiolite from the North Qilian Mountains: A fossil oceanic crust of the Paleo-Qilian ocean. Chinese Science Bulletin.

Vervoort, J.D., Blichert-Toft, J., 1999. Evolution of the depleted mantle: Hf isotope evidence from juvenile rocks through time. Geochimica et Cosmochimica Acta 63, 533-556.

Vervoort, J.D., Patchett, P.J., Albarède, F., Blichert-Toft, J., Rudnick, R., Downes, H., 2000. Hf–Nd isotopic evolution of the lower crust. Earth and Planetary Science Letters 181, 115-129.

Walter, M.J., Nakamura, E., Trønnes, R.G., Frost, D.J., 2004. Experimental constraints on crystallization differentiation in a deep magma ocean. Geochimica et Cosmochimica Acta 68, 4267-4284.

Wooden, J.L., Frank, K., Barth, A.P., 2007. Hafnium and temperature (from titanium) variations in zircons: a potential new tool to evaluate petrologic processes in magmas, 2007 GSA Denver Annual Meeting.

Woodhead, J., Hergt, J., Davidson, J., Eggins, S., 2001. Hafnium isotope evidence for 'conservative'element mobility during subduction zone processes. Earth and Planetary Science Letters 192, 331-346.

Wu, C.L., Xu, X.Y., Gao, Q.M., Li, X.M., Lei, M., et al., 2010. Early Palaezoic granitoid magmatism and tectonic evolution in North Qilian, NW China. Acta Petrologica Sinica 26, 1027-1044 (in Chinese with English abstract). .

Wu, C.L., Yao, S.Z., Zeng, L.S., al., E., 2006a. Double subduction of the Early Paleozoic North Qilian oceanic plate: evidence from granites in the central segment of North Qilian, NW China. Geology in China 33, 1197-1208 (in Chinse with English abstract). .

Wu, F.-Y., Yang, Y.-H., Xie, L.-W., Yang, J.-H., Xu, P., 2006b. Hf isotopic compositions of the standard zircons and baddeleyites used in U–Pb geochronology. Chemical Geology 234, 105-126.

Xia, X., Song, S., 2010. Forming age and tectono-petrogenises of the Jiugequan ophiolite in the North Qilian Mountain, NW China. Chinese Science Bulletin 55, 1899-1907.

Xiang, Z., Lu, S., Li, H., Li, H., Song, B., Zheng, J., 2007. SHRIMP U-Pb zircon age of gabbro in Aoyougou in the western segment of the North Qilian Mountains, China and its geological implications. Geological Bulletin of China 26, 1686-1691 (in Chinese).

Xu, Z. et al., 2006. Timing and mechanism of formation and exhumation of the Northern Qaidam ultrahigh-pressure metamorphic belt. Journal of Asian Earth Sciences, 28(2): 160-173.

Yang, J.S., Xu, Z.Q., Zhang, J.X., Song, S.G., Wu, C.L., Shi, R.D., Li, H.B., Maurice, B., 2002. Early Palaeozoic North Qaidam UHP metamorphic belt on the north-eastern Tibetan plateau and a paired subduction model. Terra Nova 14, 397-404.

Zheng, Y.-F. et al., 2006. Zircon U–Pb age, Hf and O isotope constraints on protolith origin of ultrahigh-pressure eclogite and gneiss in the Dabie orogen. Chemical Geology, 231(1–2): 135-158.

Chapter 7: Conclusions and future work

This thesis investigated the crustal growth on the Northern Tibetan Plateau, sampled as granitoids from the East Kunlun Orogenic Belt, the Qilian Block and the North Qilian Orogenic Belt. All the tectonic histories of these orogenic belts are quite debatable largely due to that people only see part of the picture. And I am not exceptional. The following chapter is to succinctly conclude the previous four chapters in order to address the aims presented in Chapter 1 and provide suggested directions for the future work.

7.1. The East Kunlun Orogenic Belt (Chapter 3)

Early Triassic syn-collisional granitoids with mafic magmatic enclaves (MMEs) crop out along the entire East Kunlun Orogenic belt (EKOB) at the northern margin of the Tibetan Plateau. They are andesitic in composition and enriched in light rare earth elements (LREEs) with a flat heavy REE (HREE) pattern. Their average composition resembles that of the bulk continental crust. The enclosed MMEs have the same mineralogy as their host granitoids, but contain a greater mode of mafic minerals (amphibole and biotite), and thus have higher HREE abundances. Zircon U–Pb dating shows that both the granitoid hosts and MMEs have the same crystallization age of ~ 250 Ma and indistinguishable bulk rock Sr–Nd–Pb–Hf isotope compositions (I_{Sr} of 0.7080–0.7116, varying $^{206}Pb/^{204}Pb_i$ of 18.53–19.32, essentially constant $\varepsilon_{Nd(t)}$ of -5.3 to -2.1 and a small range of positive $\varepsilon_{Hf}(t)$, mostly 1.7–5.2). The complete isotopic overlapping between the granitoid hosts and the MMEs is understood to reflect that the MMEs are disintegrated cumulates formed at an early stage of the granitoid magma evolution within the same magmatic system. The isotopic data set reveals that the granitoids are variably evolved melts produced by partial melting of the subducted Paleo-Tethyan oceanic crust with terrigenous sediments under amphibolite-facies conditions in response to the continental collision.

7.2. The Qilian Orogenic Belt

The Paleozoic granitoids in the Qilian Block are important for understanding the tectonic evolution of the Northern Tibetan Plateau. We choose granitoids from the Huangyuan (HY) and Gangcha (Gcha) areas for a detailed study.

7.2.1. The Qilian Block (Chapter 4)

The granitoids are both 'S-type' and 'I-type', and record different geological events from the Neoproterozoic to the Paleozoic. Most samples studied have an emplacement age of ~ 450 Ma with three samples being significantly older (924 Ma, 797 Ma and 503 Ma vs. 450 Ma). The ~ 924 Ma and ~ 797 Ma magmatism record events of crustal growth and crustal reworking, respectively. The 503 Ma plagiogranite-like granite contains mantle isotope signatures, probably resulting from extensive fractional crystallization of mantle-derived melt in a back-arc setting. The majority of the ~ 450 Ma granitoids have varying chemical compositions, but most of them share similar trace element patterns resembling the bulk continental crust composition. Despite their large compositional and age variations, significant correlations on Harker diagrams and in isotope spaces are consistent with their being different products essentially derived from common sources. The significant mantle contributions (70% ~ 80%, apart from QL09-02) required by whole rock Sr-Nd-Pb-Hf isotope data strongly suggest the mostly likely "mantle source" being last fragments of the subducted/underthrusting oceanic crust at the onset of collision. Despite some 'S-type' composition of the 450 Ma granitoids, the isotopes indicate that they represent crust growth in a syn-collisional setting. Based on all the petrology, geochronology, geochemical data and adjacent tectonic associations, we suggest that the Qilian Ocean started opening in the Neoproterozoic between the Qaidam Block and the Qilian Block. A back-arc basin was developed between the Qilian Block and the Alashan Block shortly after. The 450 Ma granitoids are the products in response to the closure of the Qilian Ocean and the onset of the Qilian-Qaidam continental collision.

7.2.2. The Qilian Block (Chapter 5)

The Qilian Block within the Qilian Orogenic belt on the northern Tibetan Plateau contains the contemporaneous two-mica granite from Huangyuan (HY) pluton and biotite-granite from Gangcha (Gcha) pluton of ~450 Ma. These granitoids provide useful information on the tectonic evolution of the Qilian Orogenic Belt. Here we present a geochronological and multi-isotopic study on these granitoids from the Qilian Block. Together with the literature data, we found that the Gcha pluton slightly predate the HY pluton. Zircon *in situ* Hf isotopes show much smaller variations for Gcha rocks than for the HY pluton. They have continuous concordant ages spreading from 510 Ma to 440 Ma. These characters are best explained by the magmatism since the onset of the collision at ~500 Ma, following slab steepening and the ultimate slab breakoff at ~450 Ma. Zircon Hf isotopes cover the same range but have different distribution patterns for Gcha and HY plutons, reflecting of the leading edge of the Qaidam continental lithosphere beneath the overriding Qilian plate.

7.2.3. The North Qilian Orogenic belt (Chapter 6)

The Kekeli Batholith in the North Qilian Orogenic Belt contains abundant cumulate assemblages dominated by amphibole and plagioclase plus minor other felsic minerals. There is a significant discrepancy between the whole rock Hf (WR-Hf) isotopes and *in situ* zircon Hf (Zir-Hf) isotopes, which demonstrates that (1) Zir-Hf isotope composition does not necessarily represent WR-Hf composition, and (2) zircon is not the sole major host of Hf. The positive correlation between WR-Hf isotope and TiO_2 indicates that the TiO_2-rich minerals are important Hf host apart from zircons. This correlation combined with the broad negative correlations between both ε_{Nd} and ε_{Hf} and silica further constrain that Kekeli batholith suites are the hybrids of mixing. The discrepancy between WR-Hf and Zir-Hf isotope composition can be explained by different crystalline timing of different minerals during magma mixing, Ti-rich minerals such as Fe-Ti oxides, Pyroxene (Px), amphibole (Amp), biotite (Bt) etc. crystallize earlier from the more mafic composition and preserve the isotope signature closer to the mafic endmember. In our case, zircons do not crystallize until the later stage when the hybrid magma reaches Zr saturation. Therefore, zircons generally record isotope

compositions closer to the felsic endmember. The gabbronorite QL10-26 has the highest TiO_2, the most radiogenic WR-Hf ($\varepsilon_{Hf}(t) = 26$) and contains pyroxene with Amp reaction rims, therefore close to the most depleted endmember. The peraluminous Group 1 granite samples have the lowest $\varepsilon_{Hf}(t)$ and $\varepsilon_{Nd}(t)$ and thus represent the crustal endmember. Group 2 samples with intermediate andesitic compositions between these two endmembers also have the intermediate isotopic compositions in between. The cumulates enclosed in Group 2 have overlapping isotopes with Group 2 and are interpreted to precipitate from Group 2. All these observations are consistent with the scenario that the mantle-derived magma underplated the mid-lower crust and mixed with the crustal melt by hydrous partial melting of the mid-lower crust accompanying the coeval metamorphism.

7.3. Problems and Future work

The importance of more work in the Qilian Block is demonstrated by the contrasting stories proposed by Chapter 4 and Chapter 5 respectively. A detailed work (e.g. higher resolution analysis) on the continuous age spread along the Concordia is certainly required. This common age spread both in metamorphic rocks and igneous lithologies is a key element and major hindrance to understand the ~450 Ma magmatism and the tectonic evolution in the area. As for the discrepancy between whole rock Hf and zircon *in situ* Hf isotopes discussed in Chapter 6, the most straight forward way is to analysis Hf isotope for all the Ti-rich minerals, especially ilmenite.

In Chapter 3 and 4, we have demonstrated that collision zone is a reasonable site to produce the granitoids which resemble the bulk continental crust (BCC) and can explain some features of the BCC which cannot be explained by the 'Island arc' model. However, the collision model invokes partial melting of the trapped subducted oceanic crust at 40 km underneath the overlying continental crust. The crustal thickness at the initiation of collision is major concern of the collision model because it controls the partial melting depth which in turn determines the composition of derivative magma. We do not know the crust thickness in the Kunlun orogenic belt ~250 Ma ago and Qilian Orogenic belt ~450 Ma ago, but it is no doubt that the continental crust in Andes or Tibet collision

zones had been significantly thickened, e.g. >50 km (Beck et al., 1996; Holt and Wallace, 1990; Mo et al., 2007). The following concern is that if the continental crust had been significant thickened > 50 km, is it possible for the subducting slab to underthrust into the depth of 40 km which is still within the lower crust? In other words, if the overriding continental crust was thicker than 50 km, partial melting of the subducting hydrous slab accommodated underneath would be beyond the amphibolite-facies field. Would the derivative melt capture an adakitic signature and would it still resemble the BCC composition? And the concern comes from the significantly thickened crust in Andes and Tibet. The concern about crust thickness is reasonable but may not be necessary. Mo et al (2007) proposed that the dominant tectonically compression and crustal shortening in Tibet happened ~ 10 Ma after the initiation of the collision and only contribute 20 km thickness. On the contrast, the syn-collisional magmatism before the tectonically shortening and thickening contributes 30% of the total thickness of the present-day Tibetan crust. If this is the case, it means that the crust thickening results from the syn-collisional magmatism rather than the other way round. Importantly, it means that the crust thickness at the initiation of the collision remained normal, e.g. ~35 km, and it is not problematic for the subducting slab to partial melt at ~40 km. Besides, in chapter 3, an important proof of the collision at 250 Ma is the unconformity between the upper-Permian to lower-Triassic marine strata and lower Permian terrestrial strata, implying that the overlying continental plate had been above sea level at the late Permian and the crust probably had thickened, in which case, the crust thickness probably thicker than 40 km. However, there is a large uncertainty in this unconformity as the strata have not been precisely dated but only from the simple field observation. Obviously, the accurate age data for this unconformity would very much help conclude Chapter 3.

In the collision model, the subducting slab is considered as the source of the granitoids because it is basaltic and carries mantle isotopic composition. One may argue that, the subducted island arc could be the source as well. In Chapter 4, we simply mentioned that the island arc crust is

topographically high level and is too cold to melt. We would like to extend the discussion a bit more here. First of all, the Kunlun and Qilian Orogenic belts are both considered as the continental margins. It is not likely to develop island arc there. Secondly, even if there was island arc, their isotopic composition should be similar to the oceanic crust. Partial melting of the quickly recycled island arc would only enhance the 'arc' signatures in the derivative melt, which is difficult to be distinguished from the slab-derived melt in the collision zone. In this case, we take the overall products as the slab-derived melt. Additionally, reworking of the continental arcs may play a role in the syn-collision magmatism as discussed in Chapter 4. But reworking of continental arc alone cannot explain the large compositional variations in the Qilian Block granitoids and especially, cannot explain the dominant andesitic compositions in the East Kunlun Batholiths which require a more mafic source (basaltic andesite or basalt).

Arguments against collision model also arise from decompression melting of the exhumated oceanic eclogites. These eclogites carry mantle isotopes and they are basaltic too. However, partial melting of them would produce the melt with adakite signature because garnet is the residual phase preferentially hosting HREEs than LREEs. In Qilian Orogenic belt, decompression melting of the eclogites has indeed been observed and its derivative melt is adakitic (Song et al., 2014) while our granitoids do not have adakite signature. Another important thing to end this debate is to precisely constrain the exhumation of the eclogites. In the Qilian Orogenic belt, the timing of the eclogite exhumation is still controversial. Song et al., (2013) suggest that the exhumation happened at ~ 420 Ma while Xu et al. (2006) proposed that the exhumation began at 470 – 460 Ma. Maybe it is a bit too early to say that the granitoids in Chapter 4 were produced in a syn-collisional setting before we can place more constrains on the metamorphic rocks.

In the published Chapter 3, Songpai-Ganzi has been considered as a continental plate on the subducting side. However, some study suggest that Songpai-Ganzi is a huge accretionary prism (Yin and Harrison, 2000). If this is the case, the proper continental plate would be Qiangtang block

further south in the Tibetan Plateau (Yin and Harrison, 2000). But this change would not affect the theme of Chapter 3 nor collision model.

Bottom of line, the whole rock Sr-Nd-Hf-Pb isotopes were employed throughout the course of this study. Using these isotopes to trace the source of basalts is straight forward because the mineral assemblage is relatively simple in the mantle. However, as to the granitoids which are largely produced at the crustal level, more factors need to be taken into account, e.g. disequilibrium melting. The isotopic heterogeneities of the granitoids have generally been attributed to the inheritance from the source. But experiments and field observations have shown that partial melting at crust level is generally non-modal and produces melts with isotopic compositions in disequilibrium with respect to their sources (Harrison and Watson, 1984; Harris, et al., 1995; Knesel and Davidson, 2002; Zeng et al., 2005). Crust contains various mineral phases which could easily develop isotopic disequilibrium. For example, garnet has large Lu/Hf ratio and would be radiogenic in Hf isotopes with time. Biotite has high Rb/Sr ratio and would possess relatively high-time integrated $^{87}Sr/^{86}Sr$ ratio. Other accessory phases, such as zircon, apatite, ilmenite, and monazite also play an important role in controlling the distribution of trace elements and producing the isotopic disequilibrium. Whether the isotopic heterogeneities and the decoupling between Nd and Hf isotopes is related to the partial melting of crustal lithologies whose mineral phases have developed disequilibrium has not been investigated in this study. Future work on this subject is highly recommended.

Harris, NBW, Ayres M, Massey J., 1995. Geochemistry of granitic melts produced during the incongruent melting of Muscovite:implications for the extraction of Himalayan Leucogranitic Magmas. J Geophys Res 100:15767–15777.

Harrison, TM, Watson E.B.,1984. The behavior of apatite during crustal anatexis: equilibrium and kinetic onsiderations. Geochim Cosmochim Acta 48:1467–1478.

Knesel K. M., Davidson J.P., 2002. Insight into collisional magmatism from isotopic fingerprints of melting reactions. Science 296: 2206-2208.

Zeng, L.S., Saleeby, J.B., Ducea, M., 2005. Geochemical charactersitics of crustal anatexis during the formation of migmatite at the Southern Sierra Nevada, California. Contributions to Mineralogy and Petrology 150, 386-402.

Beck, S.L. et al., 1996. Crustal-thickness variations in the central Andes. Geology, 24(5): 407-410.

Holt, W.E., Wallace, T.C., 1990. Crustal thickness and upper mantle velocities in the Tibetan Plateau Region from the inversion of regional Pnl waveforms: Evidence for a thick upper mantle lid beneath southern Tibet. Journal of Geophysical Research: Solid Earth, 95(B8): 12499-12525.

Kilpatrick, J.A., Ellis, D.J., 1992. C-type magmas: igneous charnockites and their extrusive equivalents. Geological Society of America Special Papers, 272: 155-164.

Mo, X. et al., 2007. Mantle contributions to crustal thickening during continental collision: Evidence from Cenozoic igneous rocks in southern Tibet. Lithos, 96(1-2): 225-242.

Song, S., Niu, Y., Su, L., Wei, C., Zhang, L., 2014. Adakitic (tonalitic-trondhjemitic) magmas resulting from eclogite decompression and dehydration melting during exhumation in response to continental collision. Geochimica et Cosmochimica Acta, 130(0): 42-62.

Song, S., Niu, Y., Su, L., Xia, X., 2013. Tectonics of the North Qilian orogen, NW China. Gondwana Research, 23: 1378-1401.

Xu, Z. et al., 2006. Timing and mechanism of formation and exhumation of the Northern Qaidam ultrahigh-pressure metamorphic belt. Journal of Asian Earth Sciences, 28(2): 160-173.

Yin, A., Harrison, T.M., 2000. Geologic evolution of the Himalayan-Tibetan Orogen. Ann. Rev. Earth Planet. Sci, 28(2): 211-280.

Appendices: Data

Table 3.1 Sample location and brief geochemical compositions of EKOB samples

Sample	GPS position		Type	SiO_2 %	$\varepsilon_{Nd}(t)$	$\varepsilon_{Hf}(t)$
DL09-007	N35°45.201′	E98°07.565′	MME	57.9	-2.2	4
DL09-008	N35°45.201′	E98°07.565′	HR	66.8	-3.7	3.3
DL09-009	N35°45.201′	E98°07.565′	HR	68.0	-3.9	-1.3
DL09-010	N35°45.224′	E98°07.563′	HR	67.9		
DL09-011	N35°45.224′	E98°07.564′	MME	57.0		
DL09-012	N35°45.224′	E98°07.564′	HR	71.2		
DL09-013	N35°45.321′	E98°07.669′	HR	65.6	-2.1	2.5
DL09-014	N35°45.321′	E98°07.669′	MME	52.2	-4.5	4.1
DL09-015	N35°47.008′	E98°08.550′	HR	64.9	-3.1	3.5
DL09-016	N35°47.008′	E98°08.550′	MME	50.6	-4.1	5.2
DL09-017	N35°47.008′	E98°08.550′	MME	59.2	-2.2	4.4
DL09-018	N35°47.804′	E98°09.011′	HR	68.9	-2.8	3.4
DL09-019	N35°47.804′	E98°09.011′	MME	54.7		
DL09-020	N35°47.804′	E98°09.011′	MME	58.5		
DL09-021	N35°47.840′	E98°08.991′	HR	66.5	-2.6	2.8
DL09-022	N35°47.840′	E98°08.991′	MME	57.5	-2.9	4.5
DL09-023	N35°48.900′	E98°08.975′	HR	74.2		
DL09-024	N35°48.900′	E98°08.975′	MME	51.9	-4.0	1.8
DL09-025	N35°49.005′	E98°09.004′	HR	64.8		
DL09-026	N35°49.005′	E98°09.004′	MME	48.6	-3.8	4
DL09-027	N35°49.092′	E98°09.401′	HR	67.4	-2.9	2.3
DL09-028	N35°54.088′	E98°01.968′	HR	66.9		
DL09-029	N35°54.107′	E98°01.848′	HR	67.0		
DL09-030	N36°42.712′	E99°33.913'	HR	59.9	-4.9	2.3
DL09-031	N36°42.712′	E99°33.913'	MME	57.7	-5.2	-2.9
DL09-032	N36°42.712′	E99°33.913'	HR	59.3	-5.3	1.7
DL09-033	N36°42.938'	E99°47.356'	HR	65.6		
DL09-034	N36°42.938'	E99°47.356'	MME	57.6		
DL09-035	N36°42.543'	E99°48.067'	HR	66.0		
DL09-036	N36°42.543'	E99°48.067'	MME	57.5		

MME: micro magmatic enclave HR: Host rock

Table 3.2 major and trace element data for granitoid hosts and MMEs

Sample	DL09-007	DL09-008	DL09-009	DL09-010	DL09-011	DL09-012	DL09-013	DL09-014	DL09-015	DL09-016	DL09-017
pairs	1	1	1	2	2		3	3	4	4	4
	MME	HR	HR	HR	MME	HR	HR	MME	HR	MME	MME
SiO_2	57.9	66.8	68.0	67.9	57.0	71.2	65.6	52.2	64.9	50.6	59.2
TiO_2	0.66	0.54	0.36	0.46	1.08	0.22	0.54	0.81	0.58	0.78	0.97
Al_2O_3	16.5	15.3	15.9	15.3	16.6	14.8	15.7	17.3	15.8	17.3	14.1
Fe_2O_3	1.74	1.38	1.04	1.78	2.77	0.88	1.90	3.60	1.65	3.36	3.30
FeO	4.70	3.02	3.07	2.18	6.10	1.92	2.62	6.55	3.28	7.20	5.75
MnO	0.14	0.09	0.12	0.10	0.17	0.08	0.09	0.25	0.09	0.27	0.18
MgO	4.46	1.72	0.78	1.42	3.12	0.48	1.69	4.18	2.00	4.75	3.87
CaO	7.51	4.18	4.09	3.95	5.57	2.78	4.31	7.85	4.56	8.81	5.46
Na_2O	3.27	3.28	3.41	3.58	3.36	3.27	3.28	3.52	3.24	3.35	2.62
K_2O	1.27	2.49	2.10	1.82	2.27	3.26	2.65	1.53	2.46	1.42	2.33
P_2O_5	0.09	0.10	0.14	0.09	0.20	0.08	0.11	0.11	0.11	0.09	0.20
LOI	1.00	0.61	0.59	1.03	0.88	0.78	1.00	1.09	0.68	1.13	1.21
Total	99.51	99.24	99.60	99.56	99.12	99.76	99.49	98.99	99.35	99.06	99.19
A/CNK	0.81	0.97	1.04	1.02	0.92	1.06	0.97	0.80	0.97	0.75	0.84
Li	19.3	25.3	26.1	20.1	31.7	24.1	24.5	25.2	22.5	17.1	29.1
Sc	19.8	9.24	3.40	7.47	22.6	2.85	9.64	23.1	12.3	25.3	32.6
Cr	39.9	7.31	1.56	6.26	9.37	2.27	7.39	46.5	8.25	9.61	15.2
Co	19.6	8.91	3.59	7.44	18.7	2.15	8.99	19.7	10.7	21.6	19.6
Ni	5.38	2.70	0.98	2.39	4.78	0.84	2.70	8.35	2.96	6.31	5.34
Ga	15.1	16.1	19.5	16.3	19.4	17.4	16.3	19.4	16.8	19.2	18.2
Rb	50.6	81.7	81.3	63.9	88.0	106	77.0	73.7	77.4	64.1	101
Sr	232	172	367	192	177	322	186	197	204	212	169
Y	16.5	17.6	16.8	22.2	33.3	15.6	17.2	50.9	20.1	46.9	45.5
Zr	102	145	215	111	164	171	147	90	155	101	276
Nb	5.24	8.92	12.0	8.29	13.1	11.1	8.2	12.1	8.24	10.0	13.6
Ba	293	459	691	427	567	1030	587	313	523	215	555
La	17.7	12.9	35.5	9.81	32.6	33.1	29.3	15.2	23.9	13.6	27.6
Ce	33.6	23.0	66.4	16.1	64.6	61.5	45.6	45.1	40.1	43.8	62.2
Pr	3.63	3.17	7.37	2.44	8.17	6.80	5.27	7.60	4.89	7.18	8.49
Nd	13.1	12.7	25.7	9.93	31.6	24.0	18.1	34.6	18.0	32.4	35.2
Sm	2.76	2.88	4.16	2.58	6.30	4.07	3.25	8.25	3.60	7.57	7.94
Eu	1.03	0.84	1.25	0.77	1.33	1.16	0.94	1.61	0.97	1.77	1.32
Gd	2.76	2.75	3.52	2.69	5.80	3.34	3.14	7.38	3.41	6.73	7.48
Tb	0.47	0.47	0.52	0.52	1.00	0.50	0.50	1.38	0.57	1.26	1.33
Dy	2.99	3.06	2.94	3.54	6.09	2.89	3.03	8.96	3.58	8.08	8.39
Ho	0.65	0.66	0.62	0.78	1.31	0.59	0.65	1.92	0.75	1.73	1.76
Er	1.81	1.94	1.80	2.32	3.63	1.70	1.87	5.63	2.20	5.12	4.90
Tm	0.28	0.31	0.28	0.40	0.55	0.26	0.29	0.89	0.34	0.82	0.74
Yb	1.89	2.16	1.95	2.68	3.67	1.80	1.99	6.04	2.24	5.61	4.91
Lu	0.29	0.34	0.32	0.42	0.59	0.29	0.32	0.95	0.36	0.90	0.78
Hf	2.89	4.27	5.39	3.37	4.56	4.82	4.12	3.09	4.36	3.25	7.54
Ta	0.48	1.02	0.74	0.84	0.88	0.79	0.78	0.94	0.75	0.64	1.04
Pb	11.5	16.1	14.3	13.0	13.0	24.1	18.7	15.5	15.6	12.7	12.3
Th	4.07	10.2	11.7	3.6	11.1	11.9	11.6	1.73	9.11	2.11	10.6
U	0.74	1.38	1.10	0.85	0.73	1.40	1.26	0.62	1.01	0.60	1.34
Nb/Ta	11.0	8.7	16.2	9.87	14.9	14.1	10.4	12.9	11.1	15.6	13.0
Eu/Eu*	1.13	0.90	0.97	0.89	0.66	0.93	0.88	0.62	0.84	0.74	0.52
Sr/Sr*	0.96	0.78	0.76	1.12	0.32	0.72	0.54	0.35	0.62	0.40	0.28

Table 3.2 major and trace element data for granitoid hosts and MMEs (continued)

Sample	DL09-018	DL09-019	DL09-020	DL09-021	DL09-022	DL09-023	DL09-024	DL09-025	DL09-026	DL09-027
pairs				5	5	6	6	7	7	
	HR	MME	MME	HR	MME	HR	MME	HR	MME	HR
SiO_2	68.9	54.7	58.5	66.5	57.5	74.2	51.9	64.8	48.6	67.4
TiO_2	0.47	0.90	0.88	0.48	0.89	0.20	0.96	0.58	1.39	0.38
Al_2O_3	14.7	16.8	16.6	15.7	16.7	14.4	18.5	15.9	18.4	16.6
Fe_2O_3	1.33	2.68	2.68	1.55	2.84	0.50	2.48	1.63	3.33	1.36
FeO	2.57	7.10	5.00	2.60	4.92	1.06	6.05	3.30	6.65	2.02
MnO	0.08	0.25	0.18	0.09	0.18	0.02	0.17	0.09	0.17	0.10
MgO	1.39	3.89	3.01	1.46	3.40	0.60	4.57	1.97	5.48	0.98
CaO	3.55	6.07	5.50	3.79	6.70	3.36	9.45	4.72	9.10	3.74
Na_2O	3.30	3.49	3.75	3.60	3.46	4.31	2.35	3.21	2.34	4.04
K_2O	2.55	2.16	1.55	2.73	1.54	0.65	1.13	2.34	1.47	2.46
P_2O_5	0.10	0.09	0.13	0.10	0.12	0.05	0.12	0.11	0.12	0.11
LOI	0.68	0.91	1.50	0.96	1.14	0.45	1.44	0.78	2.00	0.50
Total	99.62	99.04	99.28	99.56	99.29	99.75	99.12	99.43	99.05	99.59
A/CNK	1.00	0.88	0.93	0.99	0.85	1.03	0.83	0.97	0.84	1.03
Li	28.9	45.9	38.1	29.2	30.4	0.56	19.7	23.5	17.0	22.5
Sc	7.95	28.3	22.7	10.4	26.4	1.96	32.6	11.2	32.6	5.42
Cr	5.59	15.1	11.9	5.63	24.9	1.73	23.4	8.90	49.9	3.24
Co	7.40	19.2	15.1	7.54	17.6	3.02	21.3	10.8	28.5	5.09
Ni	2.34	6.61	2.59	2.30	4.14	1.58	2.99	3.44	12.17	1.91
Ga	15.8	20.5	18.4	17.0	17.9	12.0	18.7	16.2	18.6	16.4
Rb	74.2	123	49.5	88.0	58.3	38.2	50.0	65.5	60.6	54.4
Sr	177	159	177	186	208	154	246	197	279	213
Y	18.3	57.7	33.1	23.8	29.9	14.5	26.1	17.0	30.4	12.4
Zr	157	103	106	154	77.1	123	99.4	134	84.8	153
Nb	8.47	14.6	10.5	9.02	8.25	6.91	6.29	7.61	6.74	9.19
Ba	554	395	301	607	392	168	224	564	310	698
La	31.8	10.6	9.0	29.6	17.9	10.0	13.3	20.2	16.8	18.9
Ce	53.2	31.9	23.6	51.5	46.8	21.6	34.5	32.4	34.9	32.4
Pr	6.18	5.98	4.24	6.06	6.29	2.24	4.88	4.17	4.47	3.76
Nd	21.1	29.4	19.6	21.7	24.9	8.4	20.0	15.6	18.7	13.4
Sm	3.64	8.22	4.87	4.22	4.87	1.79	4.42	3.10	4.60	2.51
Eu	0.86	1.20	1.04	0.95	1.16	0.61	1.26	0.90	1.38	0.97
Gd	3.36	7.55	4.58	3.85	4.50	1.78	4.20	2.95	4.76	2.37
Tb	0.53	1.52	0.87	0.66	0.78	0.33	0.74	0.48	0.88	0.36
Dy	3.18	9.83	5.61	4.15	5.09	2.20	4.78	3.01	5.63	2.18
Ho	0.68	2.13	1.22	0.90	1.10	0.50	1.03	0.64	1.21	0.45
Er	1.98	6.26	3.62	2.59	3.26	1.53	2.86	1.79	3.36	1.33
Tm	0.31	0.99	0.57	0.41	0.52	0.25	0.43	0.28	0.51	0.20
Yb	2.07	6.72	3.86	2.76	3.62	1.82	2.79	1.90	3.17	1.38
Lu	0.33	1.04	0.62	0.45	0.57	0.30	0.44	0.30	0.49	0.23
Hf	4.40	3.34	3.11	4.45	2.28	3.71	2.96	3.73	2.57	4.09
Ta	0.70	1.11	0.76	0.88	0.53	0.67	0.52	0.63	0.49	0.60
Pb	17.2	14.7	13.1	19.4	10.8	13.8	7.0	13.8	6.47	13.77
Th	13.8	3.33	2.47	14.1	3.39	7.40	5.29	7.72	3.84	7.10
U	1.07	0.89	0.80	1.95	0.67	1.76	1.23	1.21	1.25	0.77
Nb/Ta	12.1	13.2	13.8	10.2	15.5	10.3	12.1	12.0	13.7	15.4
Eu/Eu*	0.74	0.46	0.67	0.71	0.74	1.04	0.88	0.90	0.90	1.19
Sr/Sr*	0.44	0.35	0.56	0.46	0.48	1.01	0.71	0.70	0.88	0.86

Table 3.2 major and trace element data for granitoid hosts and MMEs (continued)

Sample	DL09-028	DL09-029	DL09-030	DL09-031	DL09-032	DL09-033	DL09-034	DL09-035	DL09-036
pairs			8	8	8	9	9	10	10
	HR	HR	HR	MME	HR	HR	MME	HR	MME
SiO_2	66.9	67.0	59.90	57.70	59.30	65.55	57.60	66.00	57.50
TiO_2	0.57	0.53	0.51	0.67	0.58	0.52	0.63	0.48	0.76
Al_2O_3	15.9	15.9	17.60	17.30	17.50	15.65	16.40	15.70	15.50
Fe_2O_3	1.34	1.50	1.72	1.89	1.39	1.17	1.64	1.32	1.42
FeO	2.27	1.70	3.33	4.33	4.03	3.06	5.15	2.57	5.40
MnO	0.06	0.05	0.09	0.12	0.11	0.08	0.15	0.07	0.15
MgO	1.58	1.30	3.50	3.59	3.99	2.02	3.80	1.82	4.29
CaO	3.64	3.70	6.15	7.06	6.78	4.47	6.74	4.53	6.95
Na_2O	3.95	3.95	2.75	2.34	2.66	3.00	3.09	3.07	2.81
K_2O	2.07	2.50	1.38	1.65	1.08	3.40	3.04	3.20	3.64
P_2O_5	0.16	0.14	0.09	0.10	0.10	0.10	0.10	0.09	0.15
LOI	1.17	1.27	2.40	2.53	1.92	0.44	0.78	0.60	0.63
Total	99.61	99.54	99.42	99.28	99.44	99.46	99.12	99.45	99.20
A/CNK	1.03	1.00	1.02	0.94	0.98	0.93	0.79	0.94	0.73
Li	29.4	26.6	22.7	22.2	22.0	51.8	44.8	38.8	44.8
Sc	5.28	4.55	13.9	21.3	16.4	11.2	24.6	9.65	18.6
Cr	8.41	7.93	47.2	19.4	55.4	25.2	14.1	21.1	95.6
Co	6.90	6.60	11.9	13.2	13.1	10.9	18.8	10.1	19.4
Ni	4.64	4.39	11.8	3.13	11.42	7.09	7.76	6.31	23.7
Ga	20.0	19.6	17.5	17.8	17.6	16.6	18.1	16.2	17.0
Rb	44.5	47.9	43.3	38.2	39.4	154	160	114	179
Sr	466	502	348	270	347	223	192	213	195
Y	10.7	9.13	15.5	20.5	18.2	21.0	34.2	18.9	17.5
Zr	181	166	111	129	116	184	74.3	177	126
Nb	9.84	9.15	7.28	7.75	7.75	10.8	14.1	9.64	11.8
Ba	688	867	288	314	238	424	408	427	508
La	28.6	31.4	17.3	21.2	20.2	27.6	24.6	22.6	28.3
Ce	52.3	56.2	34.4	42.5	42.2	52.0	58.5	42.6	50.9
Pr	6.38	6.43	4.23	5.13	4.91	6.15	7.85	5.24	5.61
Nd	23.5	22.5	16.0	19.5	18.7	22.0	30.2	19.5	19.9
Sm	3.96	3.66	3.14	3.91	3.73	4.09	6.34	3.73	3.76
Eu	1.01	0.96	0.76	0.97	0.84	0.84	0.83	0.86	0.80
Gd	3.15	2.92	2.82	3.56	3.28	3.61	5.61	3.31	3.40
Tb	0.43	0.37	0.47	0.62	0.55	0.60	0.98	0.54	0.54
Dy	2.19	1.86	2.81	3.80	3.35	3.69	6.08	3.30	3.29
Ho	0.39	0.34	0.60	0.78	0.70	0.77	1.26	0.71	0.68
Er	1.04	0.91	1.68	2.22	1.94	2.24	3.65	2.07	1.92
Tm	0.15	0.12	0.26	0.33	0.30	0.35	0.57	0.31	0.29
Yb	0.99	0.80	1.68	2.22	1.95	2.36	3.86	2.12	2.03
Lu	0.14	0.12	0.27	0.35	0.31	0.37	0.61	0.33	0.34
Hf	4.78	4.41	3.20	3.53	3.36	5.14	2.72	4.87	3.46
Ta	0.73	0.68	0.63	0.58	0.63	1.17	1.52	0.93	1.03
Pb	8.17	9.07	9.79	7.52	10.4	17.2	16.7	15.8	15.6
Th	10.8	8.96	6.94	7.39	7.25	17.5	11.6	13.4	12.9
U	1.80	1.65	0.83	1.30	0.98	0.93	0.87	0.67	1.20
Nb/Ta	13.5	13.4	11.6	13.4	12.3	9.22	9.29	10.4	11.4
Eu/Eu*	0.84	0.87	0.76	0.78	0.72	0.66	0.42	0.73	0.67
Sr/Sr*	1.09	1.19	1.21	0.77	1.04	0.55	0.36	0.60	0.53

Table 3.3 LA-ICP-MS U-Pb zircon data

Spot	U (ppm)	Pb (ppm)	Th (ppm)	Th/U	$^{207}Pb/^{206}Pb$ Ratio	1σ	$^{207}Pb/^{235}U$ Ratio	1σ	$^{206}Pb/^{238}U$ Ratio	1σ	$^{207}Pb/^{206}Pb$ Age	1σ	$^{207}Pb/^{235}U$ Age	1σ	$^{206}Pb/^{238}U$ Age	1σ
DL09-07-1	418	19.6	192	0.46	0.05480	0.00234	0.29321	0.01322	0.03859	0.0005	404	78	261	10	244	3
DL09-07-2	390	18.7	157	0.40	0.05477	0.00208	0.29942	0.01089	0.03990	0.0004	403	65	266	9	252	2
DL09-07-3	830	41.4	580	0.70	0.05436	0.00173	0.29022	0.00878	0.03873	0.0003	386	53	259	7	245	2
DL09-07-4	691	33.1	330	0.48	0.05042	0.00119	0.27510	0.00634	0.03957	0.0002	214	43	247	5	250	1
DL09-07-5	522	25.0	247	0.47	0.05110	0.00164	0.27751	0.00845	0.03956	0.0003	245	57	249	7	250	2
DL09-07-6	632	30.2	348	0.55	0.05329	0.00158	0.28455	0.00810	0.03887	0.0003	341	53	254	6	246	2
DL09-07-7	456	22.3	251	0.55	0.05230	0.00132	0.28587	0.00748	0.03959	0.0003	298	48	255	6	250	2
DL09-07-8	634	29.3	268	0.42	0.04739	0.00138	0.25147	0.00697	0.03858	0.0003	69	51	228	6	244	2
DL09-07-9	483	23.3	240	0.50	0.05331	0.00211	0.28529	0.01031	0.03909	0.0004	342	65	255	8	247	2
DL09-07-10	691	35.5	509	0.74	0.05240	0.00188	0.28208	0.01017	0.03904	0.0003	303	67	252	8	247	2
DL09-07-11	1018	52.7	762	0.75	0.05162	0.00104	0.28225	0.00570	0.03961	0.0003	269	33	252	5	250	2
DL09-07-12	378	19.1	224	0.59	0.05065	0.00199	0.27257	0.01050	0.03907	0.0004	225	72	245	8	247	2
DL09-07-13	474	22.1	248	0.52	0.05619	0.00174	0.28556	0.00895	0.03674	0.0003	460	54	255	7	233	2
DL09-07-14	396	19.4	221	0.56	0.05208	0.00236	0.27940	0.01280	0.03878	0.0004	289	86	250	10	245	2
DL09-07-15	540	27.2	294	0.54	0.05360	0.00205	0.29122	0.01085	0.03941	0.0003	354	88	260	9	249	2
DL09-07-16	808	40.4	499	0.62	0.05084	0.00134	0.27507	0.00741	0.03907	0.0003	233	49	247	6	247	2
DL09-07-17	718	35.0	351	0.49	0.05096	0.00185	0.27748	0.00985	0.03958	0.0003	239	66	249	8	250	2
DL09-07-18	708	36.1	477	0.67	0.05229	0.00144	0.28526	0.00747	0.03958	0.0003	298	46	255	6	250	2
DL09-07-19	487	24.1	255	0.52	0.05427	0.00258	0.29426	0.01323	0.03932	0.0006	382	110	262	10	249	4
DL09-07-20	1092	58.3	693	0.64	0.05273	0.00130	0.31026	0.00736	0.04283	0.0005	317	35	274	6	270	3
DL09-07-21	714	36.1	473	0.66	0.05181	0.00146	0.28088	0.00777	0.03922	0.0003	277	49	251	6	248	2
DL09-07-22	248	11.6	100	0.40	0.05129	0.00245	0.27910	0.01296	0.03960	0.0005	254	83	250	10	250	3
DL09-07-23	555	27.2	308	0.56	0.05336	0.00160	0.29259	0.00869	0.03965	0.0003	344	52	261	7	251	2
DL09-07-24	604	30.0	362	0.60	0.05112	0.00154	0.27892	0.00821	0.03954	0.0003	246	53	250	7	250	2
DL09-08-1	1547	333	1900	1.23	0.05117	0.00253	0.27425	0.01326	0.03910	0.0004	248	91	246	11	247	3
DL09-08-2	3305	870	5528	1.67	0.05091	0.00170	0.27845	0.00926	0.03959	0.0004	237	61	249	7	250	2
DL09-08-3	3343	1204	8186	2.45	0.05107	0.00207	0.27167	0.01039	0.03865	0.0004	244	69	244	8	244	3
DL09-08-4	3048	1043	7113	2.33	0.05371	0.00186	0.28977	0.00980	0.03915	0.0004	359	60	258	8	248	2

Table 3.3 LA-ICP-MS U-Pb zircon data

Spot	U (ppm)	Pb (ppm)	Th (ppm)	Th/U	$^{207}Pb/^{206}Pb$ Ratio	1σ	$^{207}Pb/^{235}U$ Ratio	1σ	$^{206}Pb/^{238}U$ Ratio	1σ	$^{207}Pb/^{206}Pb$ Age	1σ	$^{207}Pb/^{235}U$ Age	1σ	$^{206}Pb/^{238}U$ Age	1σ
DL09-08-5	1756	439	2626	1.50	0.05547	0.00235	0.29789	0.01218	0.03922	0.0004	431	72	265	10	248	3
DL09-08-6	3303	1153	7913	2.40	0.05183	0.00176	0.28458	0.00999	0.03957	0.0004	278	62	254	8	250	2
DL09-08-7	1959	447	2435	1.24	0.05152	0.00197	0.27828	0.01030	0.03928	0.0004	264	65	249	8	248	3
DL09-08-8	1766	400	2296	1.30	0.04851	0.00199	0.26285	0.01099	0.03910	0.0004	124	75	237	9	247	3
DL09-08-9	2019	360	1794	0.89	0.05283	0.00233	0.28368	0.01207	0.03907	0.0004	322	78	254	10	247	3
DL09-08-10	1708	407	2215	1.30	0.05975	0.00560	0.34011	0.03138	0.04129	0.0007	594	211	297	24	261	4
DL09-08-11	3944	956	5459	1.38	0.04981	0.00150	0.29023	0.00869	0.04220	0.0004	186	53	259	7	266	2
DL09-08-12	2512	854	6085	2.42	0.05255	0.00188	0.28563	0.01011	0.03954	0.0004	309	61	255	8	250	3
DL09-08-13	1744	470	2997	1.72	0.05115	0.00247	0.27857	0.01318	0.03954	0.0004	248	89	250	10	250	3
DL09-08-14	1269	326	1663	1.31	0.05069	0.00245	0.29432	0.01407	0.04217	0.0005	227	87	262	11	266	3
DL09-08-15	1923	414	2311	1.20	0.04960	0.00184	0.27038	0.01017	0.03963	0.0004	176	68	243	8	251	3
DL09-08-16	1424	311	797	0.56	0.07205	0.00356	0.38691	0.01934	0.03899	0.0004	987	85	332	14	247	3
DL09-08-17	1807	476	2863	1.58	0.04778	0.00257	0.25709	0.01325	0.03916	0.0004	88	94	232	11	248	3
DL09-08-18	4463	949	5001	1.12	0.05118	0.00152	0.27476	0.00832	0.03873	0.0003	249	55	246	7	245	2
DL09-08-19	2329	694	4593	1.97	0.04901	0.00171	0.26468	0.00934	0.03904	0.0004	148	64	238	8	247	2
DL09-08-20	2607	726	4491	1.72	0.05205	0.00185	0.28466	0.01037	0.03974	0.0005	288	58	254	8	251	3
DL09-08-21	1152	343	801	0.70	0.05393	0.00610	0.27596	0.03101	0.03711	0.0005	368	259	247	25	235	3
DL09-08-22	1186	235	1275	1.07	0.05160	0.00242	0.28008	0.01359	0.03963	0.0005	268	87	251	11	251	3
DL09-08-23	1434	301	1542	1.08	0.05194	0.00279	0.28451	0.01537	0.03967	0.0005	283	102	254	12	251	3
DL09-08-24	2371	761	4787	2.02	0.05228	0.00188	0.28528	0.01038	0.03961	0.0005	298	59	255	8	250	3
DL09-09-1	244	18.8	11.1	0.05	0.05782	0.00179	0.56331	0.01702	0.07083	0.0006	523	65	454	11	441	4
DL09-09-2	520	50.4	328	0.63	0.05459	0.00106	0.58086	0.01108	0.07724	0.0006	395	40	465	7	480	3
DL09-09-3	302	29.3	185	0.61	0.05634	0.00142	0.60421	0.01590	0.07763	0.0006	466	57	480	10	482	4
DL09-09-4	485	27.3	564	1.16	0.05258	0.00167	0.28557	0.00888	0.03956	0.0004	311	69	255	7	250	2
DL09-09-5	2100	105	1620	0.77	0.05590	0.00103	0.33091	0.00672	0.04285	0.0004	448	42	290	5	270	2
DL09-09-6	794	40.1	572	0.72	0.05180	0.00126	0.28291	0.00730	0.03956	0.0004	277	55	253	6	250	3
DL09-09-7	1577	77.4	612	0.39	0.05127	0.00094	0.30081	0.00561	0.04254	0.0003	253	41	267	4	269	2
DL09-09-8	349	29.1	167	0.48	0.05686	0.00139	0.55681	0.01568	0.07098	0.0011	486	54	449	10	442	6

Table 3.3 LA-ICP-MS U-Pb zircon data

Spot	U (ppm)	Pb (ppm)	Th (ppm)	Th/U	$^{207}Pb/^{206}Pb$ Ratio	1σ	$^{207}Pb/^{235}U$ Ratio	1σ	$^{206}Pb/^{238}U$ Ratio	1σ	$^{207}Pb/^{206}Pb$ Age	1σ	$^{207}Pb/^{235}U$ Age	1σ	$^{206}Pb/^{238}U$ Age	1σ
DL09-09-9	1811	87.5	1264	0.70	0.05813	0.00105	0.33576	0.00627	0.04182	0.0003	535	39	294	5	264	2
DL09-09-10	712	33.1	280	0.39	0.05099	0.00142	0.27814	0.00752	0.03962	0.0003	241	61	249	6	250	2
DL09-09-11	964	46.8	282	0.29	0.05106	0.00132	0.29881	0.00750	0.04245	0.0003	244	56	265	6	268	2
DL09-09-12	716	35.1	302	0.42	0.05449	0.00157	0.32089	0.00967	0.04261	0.0005	391	64	283	7	269	3
DL09-09-13	2372	115	1427	0.60	0.05415	0.00098	0.32146	0.00573	0.04300	0.0003	377	37	283	4	271	2
DL09-09-14	2740	163.4	3163	1.15	0.05203	0.00080	0.30859	0.00488	0.04297	0.0003	287	32	273	4	271	2
DL09-09-15	1740	86.2	667	0.38	0.05043	0.00090	0.29651	0.00534	0.04253	0.0003	215	40	264	4	269	2
DL09-09-16	1174	50.7	551	0.47	0.05076	0.00111	0.26085	0.00565	0.03722	0.0003	230	47	235	5	236	2
DL09-09-17	390	64.7	77.2	0.20	0.06814	0.00131	1.37670	0.02597	0.14634	0.0011	873	37	879	11	880	6
DL09-09-18	1978	111	1713	0.87	0.05218	0.00092	0.30658	0.00539	0.04254	0.0003	293	38	272	4	269	2
DL09-09-19	861	38.0	511	0.59	0.05344	0.00142	0.26728	0.00711	0.03621	0.0003	347	59	241	6	229	2
DL09-09-20	825	36.4	403	0.49	0.05310	0.00127	0.27146	0.00664	0.03700	0.0003	333	53	244	5	234	2
DL09-09-21	222	11.2	202	0.91	0.05035	0.00282	0.25546	0.01385	0.03720	0.0006	211	121	231	11	235	3
DL09-09-22	453	20.5	235	0.52	0.05416	0.00145	0.28185	0.00757	0.03770	0.0003	378	59	252	6	239	2
DL09-09-23	1302	70.0	940	0.72	0.05170	0.00102	0.30578	0.00621	0.04280	0.0003	272	44	271	5	270	2
DL09-09-24	739	39.9	493	0.67	0.05098	0.00118	0.30261	0.00747	0.04292	0.0004	240	54	268	6	271	3
DL09-13-1	430	20.0	177	0.41	0.05019	0.00170	0.27249	0.00870	0.03954	0.0003	204	60	245	7	250	2
DL09-13-2	332	15.8	150	0.45	0.05334	0.00175	0.29178	0.00960	0.03954	0.0003	343	60	260	8	250	2
DL09-13-3	517	24.4	229	0.44	0.05051	0.00164	0.27332	0.00843	0.03929	0.0003	218	55	245	7	248	2
DL09-13-4	456	21.9	203	0.45	0.05293	0.00213	0.28707	0.01130	0.03933	0.0003	326	93	256	9	249	2
DL09-13-5	639	30.4	319	0.50	0.05252	0.00123	0.28746	0.00668	0.03956	0.0003	308	40	257	5	250	2
DL09-13-6	474	22.7	239	0.50	0.05080	0.00195	0.27740	0.01055	0.03954	0.0004	232	70	249	8	250	2
DL09-13-7	516	24.7	259	0.50	0.05095	0.00160	0.27840	0.00859	0.03955	0.0003	238	57	249	7	250	2
DL09-13-8	507	24.0	227	0.45	0.05150	0.00151	0.28043	0.00773	0.03957	0.0003	263	49	251	6	250	2
DL09-13-9	726	35.7	410	0.57	0.05107	0.00199	0.27728	0.01063	0.03938	0.0003	244	92	248	8	249	2
DL09-13-10	448	21.7	222	0.50	0.05179	0.00208	0.28183	0.01111	0.03947	0.0003	276	94	252	9	250	2
DL09-13-11	410	19.5	182	0.44	0.05097	0.00209	0.27719	0.01117	0.03944	0.0003	239	97	248	9	249	2
DL09-13-12	603	29.0	367	0.61	0.04957	0.00184	0.26415	0.00939	0.03873	0.0003	175	67	238	8	245	2

Table 3.3 LA-ICP-MS U-Pb zircon data

Spot	U (ppm)	Pb (ppm)	Th (ppm)	Th/U	$^{207}Pb/^{206}Pb$ Ratio	1σ	$^{207}Pb/^{235}U$ Ratio	1σ	$^{206}Pb/^{238}U$ Ratio	1σ	$^{207}Pb/^{206}Pb$ Age	1σ	$^{207}Pb/^{235}U$ Age	1σ	$^{206}Pb/^{238}U$ Age	1σ
DL09-13-13	695	33.8	386	0.56	0.05229	0.00139	0.28521	0.00740	0.03956	0.0003	298	46	255	6	250	2
DL09-13-14	466	22.5	251	0.54	0.05012	0.00169	0.27328	0.00915	0.03954	0.0003	201	64	245	7	250	2
DL09-13-15	350	16.4	134	0.38	0.05400	0.00175	0.29398	0.00925	0.03968	0.0004	371	54	262	7	251	2
DL09-13-16	722	35.4	399	0.55	0.05141	0.00150	0.28045	0.00829	0.03954	0.0003	259	54	251	7	250	2
DL09-13-17	574	27.7	289	0.50	0.05048	0.00135	0.27572	0.00733	0.03966	0.0003	217	48	247	6	251	2
DL09-13-18	643	31.7	359	0.56	0.05360	0.00166	0.29208	0.00880	0.03954	0.0003	354	53	260	7	250	2
DL09-13-19	792	39.2	483	0.61	0.05094	0.00134	0.27248	0.00669	0.03889	0.0003	238	42	245	5	246	2
DL09-13-20	554	27.0	295	0.53	0.05109	0.00146	0.27770	0.00773	0.03954	0.0004	245	48	249	6	250	2
DL09-13-21	747	38.2	568	0.76	0.05402	0.00204	0.29088	0.01044	0.03908	0.0004	372	64	259	8	247	2
DL09-13-22	428	20.7	207	0.48	0.05231	0.00267	0.28309	0.01411	0.03925	0.0004	299	119	253	11	248	3
DL09-13-23	918	47.2	744	0.81	0.04920	0.00133	0.26581	0.00702	0.03911	0.0004	158	44	239	6	247	2
DL09-13-24	412	20.0	198	0.48	0.04998	0.00178	0.27387	0.00950	0.03966	0.0003	194	65	246	8	251	2
DL09-15-1	546	26.3	298	0.54	0.05381	0.00167	0.29471	0.00959	0.03963	0.0005	363	53	262	8	251	3
DL09-15-2	272	12.6	101	0.37	0.04853	0.00169	0.26400	0.00890	0.03966	0.0004	125	62	238	7	251	2
DL09-15-3	514	24.5	245	0.48	0.05428	0.00153	0.29704	0.00844	0.03967	0.0004	383	47	264	7	251	2
DL09-15-4	418	19.7	169	0.40	0.05222	0.00177	0.28418	0.00925	0.03955	0.0003	295	59	254	7	250	2
DL09-15-5	573	27.7	312	0.54	0.04799	0.00155	0.25873	0.00803	0.03915	0.0003	99	58	234	6	248	2
DL09-15-6	411	19.7	168	0.41	0.05004	0.00177	0.27232	0.00943	0.03955	0.0003	197	66	245	8	250	2
DL09-15-7	481	22.8	214	0.44	0.05464	0.00172	0.29160	0.00915	0.03868	0.0003	397	56	260	7	245	2
DL09-15-8	454	21.3	185	0.41	0.05096	0.00173	0.27806	0.00939	0.03954	0.0004	239	61	249	7	250	2
DL09-15-9	521	25.3	274	0.53	0.05336	0.00149	0.29083	0.00786	0.03958	0.0003	344	47	259	6	250	2
DL09-15-10	416	19.5	179	0.43	0.05085	0.00203	0.28060	0.01249	0.03960	0.0004	234	83	251	10	250	3
DL09-15-11	397	18.6	179	0.45	0.05083	0.00155	0.27808	0.00858	0.03964	0.0004	233	54	249	7	251	2
DL09-15-12	425	20.5	221	0.52	0.05153	0.00145	0.28135	0.00784	0.03954	0.0003	265	48	252	6	250	2
DL09-15-13	957	47.9	675	0.71	0.05115	0.00114	0.27977	0.00590	0.03966	0.0003	247	36	250	5	251	2
DL09-15-14	655	31.7	355	0.54	0.05133	0.00119	0.28165	0.00636	0.03970	0.0003	256	39	252	5	251	2
DL09-15-15	552	26.3	267	0.48	0.04909	0.00138	0.26792	0.00731	0.03961	0.0003	152	51	241	6	250	2
DL09-15-16	412	20.2	183	0.44	0.05075	0.00144	0.28597	0.00814	0.04080	0.0003	230	50	255	6	258	2

Table 3.3 LA-ICP-MS U-Pb zircon data

Spot	U (ppm)	Pb (ppm)	Th (ppm)	Th/U	$^{207}Pb/^{206}Pb$ Ratio	1σ	$^{207}Pb/^{235}U$ Ratio	1σ	$^{206}Pb/^{238}U$ Ratio	1σ	$^{207}Pb/^{206}Pb$ Age	1σ	$^{207}Pb/^{235}U$ Age	1σ	$^{206}Pb/^{238}U$ Age	1σ
DL09-15-17	377	17.6	160	0.42	0.05149	0.00180	0.28096	0.00963	0.03960	0.0004	263	62	251	8	250	2
DL09-15-18	364	17.2	156	0.43	0.05281	0.00165	0.28846	0.00894	0.03963	0.0004	321	54	257	7	251	2
DL09-15-19	492	23.8	208	0.42	0.05141	0.00309	0.28038	0.01664	0.03955	0.0004	259	140	251	13	250	2
DL09-15-20	436	20.9	216	0.50	0.04946	0.00136	0.26999	0.00742	0.03958	0.0003	170	48	243	6	250	2
DL09-15-21	434	20.9	207	0.48	0.05237	0.00155	0.28671	0.00837	0.03966	0.0003	301	52	256	7	251	2
DL09-15-22	461	22.4	236	0.51	0.05139	0.00133	0.28023	0.00684	0.03965	0.0003	258	43	251	5	251	2
DL09-15-23	484	21.7	224	0.46	0.05094	0.00149	0.26098	0.00779	0.03706	0.0003	238	53	235	6	235	2
DL09-15-24	446	21.5	214	0.48	0.05577	0.00163	0.30253	0.00876	0.03929	0.0003	443	50	268	7	248	2
DL09-17-1	396	19.1	170	0.43	0.04996	0.00203	0.27327	0.01127	0.03960	0.0004	193	77	245	9	250	3
DL09-17-2	1006	53.1	768	0.76	0.05290	0.00129	0.28915	0.00729	0.03946	0.0003	325	41	258	6	249	2
DL09-17-3	525	25.8	271	0.52	0.05195	0.00147	0.28522	0.00823	0.03970	0.0004	283	48	255	7	251	2
DL09-17-4	381	19.0	183	0.48	0.05750	0.00180	0.31493	0.01025	0.03954	0.0004	511	54	278	8	250	2
DL09-17-5	781	39.0	527	0.67	0.05567	0.00162	0.29788	0.00891	0.03871	0.0004	439	47	265	7	245	3
DL09-17-6	754	38.1	486	0.64	0.05115	0.00155	0.27803	0.00839	0.03940	0.0004	248	53	249	7	249	2
DL09-17-7	602	29.4	303	0.50	0.04943	0.00160	0.26995	0.00902	0.03945	0.0004	168	60	243	7	249	2
DL09-17-8	606	30.0	346	0.57	0.05237	0.00167	0.28129	0.00891	0.03892	0.0003	302	57	252	7	246	2
DL09-17-9	464	22.7	230	0.50	0.05128	0.00188	0.27886	0.01011	0.03939	0.0003	253	68	250	8	249	2
DL09-17-10	391	18.7	163	0.42	0.05418	0.00197	0.29690	0.01120	0.03955	0.0004	378	67	264	9	250	2
DL09-17-11	467	22.6	173	0.37	0.04605	0.00326	0.21146	0.01487	0.03331	0.0003		157	195	12	211	2
DL09-17-12	361	17.7	165	0.46	0.05307	0.00244	0.28622	0.01253	0.03936	0.0004	332	80	256	10	249	3
DL09-17-13	482	23.5	214	0.44	0.05173	0.00169	0.28216	0.00879	0.03959	0.0004	274	54	252	7	250	2
DL09-17-14	163	8.9	63.3	0.39	0.05899	0.00366	0.35200	0.01987	0.04446	0.0007	567	95	306	15	280	4
DL09-17-15	459	23.5	298	0.65	0.05150	0.00300	0.27578	0.01579	0.03884	0.0004	263	135	247	13	246	2
DL09-17-16	997	50.9	746	0.75	0.05167	0.00139	0.27684	0.00757	0.03875	0.0003	271	49	248	6	245	2
DL09-17-17	496	25.8	233	0.47	0.05458	0.00195	0.30924	0.01059	0.04125	0.0004	395	61	274	8	261	2
DL09-17-18	1135	56.9	700	0.62	0.05240	0.00130	0.28133	0.00710	0.03886	0.0003	303	44	252	6	246	2
DL09-17-19	334	16.3	151	0.45	0.05285	0.00225	0.28789	0.01257	0.03954	0.0004	322	81	257	10	250	2
DL09-17-20	417	20.4	207	0.50	0.04805	0.00175	0.26044	0.00912	0.03960	0.0004	102	62	235	7	250	2

Table 3.3 LA-ICP-MS U-Pb zircon data

Spot	U (ppm)	Pb (ppm)	Th (ppm)	Th/U	$^{207}Pb/^{206}Pb$ Ratio	1σ	$^{207}Pb/^{235}U$ Ratio	1σ	$^{206}Pb/^{238}U$ Ratio	1σ	$^{207}Pb/^{206}Pb$ Age	1σ	$^{207}Pb/^{235}U$ Age	1σ	$^{206}Pb/^{238}U$ Age	1σ
DL09-17-21	567	27.0	230	0.41	0.05223	0.00182	0.28363	0.00960	0.03947	0.0004	295	60	254	8	250	2
DL09-17-22	426	20.5	178	0.42	0.05262	0.00176	0.28583	0.00923	0.03963	0.0004	313	58	255	7	251	2
DL09-17-23	440	21.3	201	0.46	0.05252	0.00181	0.28396	0.00984	0.03908	0.0003	308	65	254	8	247	2
DL09-17-24	538	26.9	292	0.54	0.05218	0.00175	0.28473	0.00947	0.03955	0.0004	293	60	254	7	250	2
DL09-18-1	708	33.2	275	0.39	0.05131	0.00154	0.29846	0.00849	0.04238	0.0004	255	64	265	7	268	2
DL09-18-2	191	9.9	113	0.59	0.04993	0.00227	0.29201	0.01272	0.04280	0.0006	192	98	260	10	270	3
DL09-18-3	898	42.8	357	0.40	0.05000	0.00097	0.27765	0.00548	0.04023	0.0003	195	44	249	4	254	2
DL09-18-4	243	12.4	192	0.79	0.05054	0.00206	0.27341	0.01093	0.03958	0.0005	220	90	245	9	250	3
DL09-18-5	921	42.2	347	0.38	0.05056	0.00132	0.27578	0.00713	0.03958	0.0004	221	57	247	6	250	2
DL09-18-6	1117	53.1	528	0.47	0.05267	0.00125	0.28749	0.00665	0.03961	0.0003	315	51	257	5	250	2
DL09-18-7	778	38.8	422	0.54	0.05828	0.00162	0.31581	0.00781	0.03965	0.0003	540	52	279	6	251	2
DL09-18-8	203	69.4	132	0.65	0.09689	0.00175	3.53638	0.06541	0.26465	0.0022	1565	32	1535	15	1514	11
DL09-18-9	681	31.7	226	0.33	0.05286	0.00122	0.29002	0.00664	0.03976	0.0003	323	50	259	5	251	2
DL09-18-10	1141	58.7	613	0.54	0.05811	0.00120	0.33068	0.00686	0.04114	0.0003	534	44	290	5	260	2
DL09-18-11	570	27.7	273	0.48	0.05241	0.00133	0.28658	0.00718	0.03959	0.0003	303	56	256	6	250	2
DL09-18-12	689	34.3	363	0.53	0.05337	0.00143	0.29212	0.00790	0.03955	0.0003	345	60	260	6	250	2
DL09-18-13	570	26.8	219	0.38	0.05188	0.00211	0.27889	0.01073	0.03910	0.0004	280	87	250	9	247	2
DL09-18-14	800	34.2	360	0.45	0.05393	0.00133	0.25203	0.00651	0.03371	0.0003	368	56	228	5	214	2
DL09-18-15	887	42.2	341	0.38	0.05260	0.00110	0.28803	0.00603	0.03961	0.0003	312	46	257	5	250	2
DL09-18-16	715	33.3	351	0.49	0.04978	0.00116	0.25833	0.00614	0.03749	0.0002	185	54	233	5	237	2
DL09-18-17	764	36.6	288	0.38	0.04979	0.00110	0.27290	0.00582	0.03970	0.0002	185	49	245	5	251	1
DL09-18-18	529	26.2	284	0.54	0.05006	0.00128	0.27345	0.00709	0.03954	0.0003	198	59	245	6	250	2
DL09-18-19	443	34.5	180	0.41	0.05900	0.00159	0.50262	0.01365	0.06162	0.0005	567	58	413	9	385	3
DL09-18-20	315	58.1	223	0.71	0.06680	0.00119	1.28368	0.02356	0.13891	0.0010	831	36	838	10	838	5
DL09-18-21	850	57.0	72.8	0.09	0.05562	0.00114	0.46688	0.00925	0.06075	0.0004	437	42	389	6	380	3
DL09-18-22	338	36.6	323	0.96	0.06043	0.00146	0.60522	0.01921	0.07213	0.0015	619	54	481	12	449	9
DL09-18-23	626	29.6	290	0.46	0.04963	0.00131	0.27134	0.00701	0.03969	0.0003	178	58	244	6	251	2
DL09-18-24	622	76.3	116	0.19	0.06650	0.00119	1.01113	0.02078	0.10981	0.0013	822	36	709	10	672	8

Table 3.3 LA-ICP-MS U-Pb zircon data

Spot	U (ppm)	Pb (ppm)	Th (ppm)	Th/U	$^{207}Pb/^{206}Pb$ Ratio	1σ	$^{207}Pb/^{235}U$ Ratio	1σ	$^{206}Pb/^{238}U$ Ratio	1σ	$^{207}Pb/^{206}Pb$ Age	1σ	$^{207}Pb/^{235}U$ Age	1σ	$^{206}Pb/^{238}U$ Age	1σ
DL09-21-1	707	33.5	256	0.36	0.05151	0.00145	0.28379	0.00804	0.03985	0.0004	264	48	254	6	252	2
DL09-21-2	641	30.5	256	0.40	0.05208	0.00154	0.28394	0.00805	0.03958	0.0003	289	49	254	6	250	2
DL09-21-3	1317	78.5	1146	0.87	0.06471	0.00640	0.35928	0.03540	0.04026	0.0004	765	217	312	26	254	2
DL09-21-4	1208	60.4	435	0.36	0.05616	0.00331	0.32570	0.02043	0.04189	0.0005	459	118	286	16	265	3
DL09-21-5	1027	48.3	341	0.33	0.05047	0.00145	0.27693	0.00774	0.03975	0.0003	217	51	248	6	251	2
DL09-21-6	790	38.0	332	0.42	0.05014	0.00150	0.27629	0.00862	0.03972	0.0004	202	56	248	7	251	2
DL09-21-7	429	20.4	197	0.46	0.05275	0.00191	0.30599	0.01154	0.04198	0.0005	318	64	271	9	265	3
DL09-21-8	968	51.3	536	0.55	0.06088	0.00244	0.32619	0.01279	0.03886	0.0003	635	89	287	10	246	2
DL09-21-9	622	31.7	348	0.56	0.05164	0.00298	0.28179	0.01605	0.03958	0.0004	269	134	252	13	250	2
DL09-21-10	765	37.6	316	0.41	0.05190	0.00230	0.28361	0.01234	0.03964	0.0003	281	104	254	10	251	2
DL09-21-11	684	32.6	248	0.36	0.05240	0.00159	0.28875	0.00878	0.03977	0.0004	303	53	258	7	251	2
DL09-21-12	698	33.6	281	0.40	0.05209	0.00187	0.28764	0.01055	0.03983	0.0004	289	65	257	8	252	2
DL09-21-13	622	29.5	217	0.35	0.05420	0.00199	0.30645	0.01225	0.04055	0.0005	379	66	271	10	256	3
DL09-21-14	1046	49.6	378	0.36	0.05110	0.00156	0.28058	0.00841	0.03956	0.0003	245	56	251	7	250	2
DL09-21-15	1093	61.2	968	0.89	0.05369	0.00268	0.29011	0.01431	0.03919	0.0003	358	116	259	11	248	2
DL09-21-16	1053	53.0	525	0.50	0.05457	0.00135	0.30159	0.00730	0.03998	0.0003	395	42	268	6	253	2
DL09-21-17	816	38.5	285	0.35	0.04774	0.00125	0.26228	0.00691	0.03968	0.0003	86	48	237	6	251	2
DL09-21-18	856	43.6	271	0.32	0.05215	0.00240	0.30104	0.01355	0.04186	0.0004	292	108	267	11	264	2
DL09-21-19	1145	54.4	441	0.38	0.05027	0.00145	0.27341	0.00764	0.03948	0.0004	208	48	245	6	250	2
DL09-21-20	692	32.7	305	0.44	0.05299	0.00143	0.29002	0.00807	0.03954	0.0004	328	46	259	6	250	2
DL09-21-21	625	29.9	238	0.38	0.04897	0.00158	0.26711	0.00854	0.03955	0.0003	146	59	240	7	250	2
DL09-21-22	925	44.5	377	0.41	0.05042	0.00123	0.27558	0.00671	0.03959	0.0003	214	41	247	5	250	2
DL09-21-23	993	46.5	329	0.33	0.04898	0.00124	0.26899	0.00701	0.03966	0.0003	147	47	242	6	251	2
DL09-21-24	1044	51.8	434	0.42	0.05018	0.00126	0.28225	0.00705	0.04064	0.0003	203	43	252	6	257	2
DL09-22-1	235	11.4	105	0.45	0.05184	0.00270	0.28119	0.01432	0.03957	0.0005	278	96	252	11	250	3
DL09-22-2	270	12.9	113	0.42	0.05015	0.00229	0.27089	0.01221	0.03966	0.0005	202	80	243	10	251	3
DL09-22-3	1113	67.4	1631	1.47	0.05144	0.00161	0.27522	0.00864	0.03873	0.0003	261	57	247	7	245	2
DL09-22-4	501	26.3	387	0.77	0.05238	0.00341	0.28500	0.01831	0.03946	0.0004	302	151	255	14	249	3

Table 3.3 LA-ICP-MS U-Pb zircon data

Spot	U (ppm)	Pb (ppm)	Th (ppm)	Th/U	$^{207}Pb/^{206}Pb$ Ratio	1σ	$^{207}Pb/^{235}U$ Ratio	1σ	$^{206}Pb/^{238}U$ Ratio	1σ	$^{207}Pb/^{206}Pb$ Age	1σ	$^{207}Pb/^{235}U$ Age	1σ	$^{206}Pb/^{238}U$ Age	1σ
DL09-22-5	357	17.9	189	0.53	0.05332	0.00190	0.29124	0.01037	0.03967	0.0004	342	62	260	8	251	3
DL09-22-6	159	8.0	89.1	0.56	0.05582	0.00387	0.29975	0.02029	0.03912	0.0006	445	123	266	16	247	4
DL09-22-7	612	32.3	473	0.77	0.05110	0.00262	0.27369	0.01383	0.03884	0.0003	246	120	246	11	246	2
DL09-22-8	174	8.5	80.2	0.46	0.05359	0.00327	0.28961	0.01696	0.03941	0.0005	354	112	258	13	249	3
DL09-22-9	335	17.3	237	0.71	0.05184	0.00224	0.28007	0.01206	0.03922	0.0004	279	81	251	10	248	2
DL09-22-10	385	21.3	360	0.94	0.05203	0.00204	0.28448	0.01104	0.03972	0.0004	287	71	254	9	251	2
DL09-22-11	275	13.2	96.4	0.35	0.05234	0.00361	0.27767	0.01891	0.03848	0.0004	300	159	249	15	243	3
DL09-22-12	846	40.0	320	0.38	0.05484	0.00165	0.29530	0.00857	0.03913	0.0003	406	50	263	7	247	2
DL09-22-13	731	36.6	422	0.58	0.05242	0.00178	0.28454	0.00945	0.03934	0.0003	304	61	254	7	249	2
DL09-22-14	374	19.5	266	0.71	0.04965	0.00187	0.27094	0.01020	0.03972	0.0004	179	68	243	8	251	3
DL09-22-15	337	17.5	243	0.72	0.04992	0.00548	0.26273	0.02869	0.03817	0.0004	191	247	237	23	241	3
DL09-22-16	471	23.3	250	0.53	0.05103	0.00217	0.27991	0.01172	0.03985	0.0004	242	78	251	9	252	3
DL09-22-17	742	36.7	446	0.60	0.05146	0.00154	0.27970	0.00821	0.03954	0.0004	261	50	250	7	250	2
DL09-22-18	738	39.1	609	0.83	0.05132	0.00171	0.27978	0.00945	0.03941	0.0004	255	59	250	7	249	3
DL09-22-19	479	24.1	323	0.67	0.05004	0.00191	0.27438	0.01086	0.03979	0.0005	197	71	246	9	252	3
DL09-22-20	191	9.1	89.8	0.47	0.04687	0.00270	0.24782	0.01364	0.03905	0.0006	43	93	225	11	247	3
DL09-22-21	623	29.3	210	0.34	0.05271	0.00256	0.28457	0.01350	0.03915	0.0004	317	114	254	11	248	3
DL09-22-22	757	37.0	399	0.53	0.05125	0.00167	0.27977	0.00944	0.03946	0.0004	252	60	250	7	249	2
DL09-22-23	330	15.7	134	0.41	0.04982	0.00226	0.27339	0.01208	0.03991	0.0005	187	82	245	10	252	3
DL09-22-24	814	41.3	531	0.65	0.05011	0.00140	0.27357	0.00755	0.03947	0.0004	200	47	246	6	250	2
DL09-24-1	395	19.5	217	0.55	0.04964	0.00183	0.27253	0.01014	0.03958	0.0004	178	68	245	8	250	2
DL09-24-2	371	19.2	218	0.59	0.05552	0.00234	0.30250	0.01243	0.03948	0.0005	433	71	268	10	250	3
DL09-24-3	658	33.8	481	0.73	0.05651	0.00167	0.30147	0.00879	0.03857	0.0003	473	49	268	7	244	2
DL09-24-4	428	23.7	305	0.71	0.05925	0.00405	0.31671	0.02135	0.03877	0.0004	576	153	279	16	245	3
DL09-24-5	490	27.8	423	0.86	0.05012	0.00489	0.25895	0.02508	0.03747	0.0004	201	222	234	20	237	3
DL09-24-6	967	51.4	725	0.75	0.05140	0.00131	0.28266	0.00731	0.03966	0.0004	259	40	253	6	251	3
DL09-24-7	858	46.0	662	0.77	0.05664	0.00368	0.30070	0.01930	0.03851	0.0004	477	148	267	15	244	3
DL09-24-8	1730	109.0	1729	1.00	0.05895	0.00263	0.35103	0.01545	0.04319	0.0003	565	100	305	12	273	2

Table 3.3 LA-ICP-MS U-Pb zircon data

Spot	U (ppm)	Pb (ppm)	Th (ppm)	Th/U	$^{207}Pb/^{206}Pb$ Ratio	1σ	$^{207}Pb/^{235}U$ Ratio	1σ	$^{206}Pb/^{238}U$ Ratio	1σ	$^{207}Pb/^{206}Pb$ Age	1σ	$^{207}Pb/^{235}U$ Age	1σ	$^{206}Pb/^{238}U$ Age	1σ
DL09-24-9	172	8.1	71.4	0.42	0.05381	0.00291	0.28906	0.01482	0.03950	0.0006	363	90	258	12	250	4
DL09-24-10	1714	124.7	3037	1.77	0.05160	0.00095	0.31288	0.00567	0.04377	0.0003	268	30	276	4	276	2
DL09-24-11	1372	77.6	1518	1.11	0.05238	0.00141	0.28496	0.00770	0.03929	0.0003	302	48	255	6	248	2
DL09-24-12	1907	140.0	3406	1.79	0.05102	0.00111	0.31502	0.00658	0.04467	0.0003	242	36	278	5	282	2
DL09-24-13	980	56.2	1085	1.11	0.05536	0.00308	0.30024	0.01650	0.03933	0.0003	427	127	267	13	249	2
DL09-24-14	670	33.1	339	0.51	0.06516	0.00397	0.35140	0.02119	0.03911	0.0004	780	132	306	16	247	2
DL09-24-15	910	39.0	45.3	0.05	0.05147	0.00157	0.28129	0.00882	0.03942	0.0003	262	58	252	7	249	2
DL09-24-16	582	36.8	393	0.68	0.05517	0.00383	0.32599	0.02237	0.04286	0.0005	419	160	286	17	271	3
DL09-24-17	1280	220.7	101	0.08	0.06978	0.00162	1.44817	0.03259	0.15051	0.0009	922	49	909	14	904	5
DL09-24-18	983	54.8	976	0.99	0.05095	0.00145	0.28057	0.00795	0.03982	0.0003	238	50	251	6	252	2
DL09-24-19	248	11.9	128	0.51	0.05015	0.00246	0.26788	0.01268	0.03891	0.0004	202	90	241	10	246	3
DL09-24-20	661	37.6	516	0.78	0.06429	0.00201	0.36927	0.01139	0.04160	0.0004	751	51	319	8	263	2
DL09-24-21	615	39.1	454	0.74	0.04605	0.01113	0.24815	0.05988	0.03909	0.0006		394	225	49	247	4
DL09-24-22	988	52.1	743	0.75	0.04970	0.00125	0.26811	0.00658	0.03913	0.0004	181	39	241	5	247	2
DL09-24-23	134	6.0	48.8	0.37	0.04986	0.00328	0.25834	0.01699	0.03782	0.0005	189	124	233	14	239	3
DL09-24-24	583	37.2	204	0.35	0.05190	0.00756	0.28227	0.04093	0.03944	0.0006	281	312	252	32	249	3
DL09-27-1	1134	53.1	339	0.30	0.05138	0.00151	0.28037	0.00803	0.03940	0.0003	258	52	251	6	249	2
DL09-27-2	1296	63.4	538	0.41	0.05037	0.00128	0.27944	0.00680	0.04005	0.0003	212	44	250	5	253	2
DL09-27-3	1057	52.3	542	0.51	0.04984	0.00124	0.27453	0.00683	0.03973	0.0003	188	42	246	5	251	2
DL09-27-4	716	33.6	392	0.55	0.02986	0.00142	0.15632	0.00746	0.03811	0.0003	290	53	147	7	241	2
DL09-27-5	705	35.4	406	0.58	0.05208	0.00159	0.28539	0.00864	0.03956	0.0003	289	53	255	7	250	2
DL09-27-6	597	28.1	304	0.51	0.05161	0.00173	0.28300	0.01014	0.03967	0.0006	268	54	253	8	251	4
DL09-27-7	1157	55.9	480	0.41	0.05060	0.00140	0.27893	0.00739	0.03984	0.0003	223	46	250	6	252	2
DL09-27-8	682	33.4	379	0.56	0.04952	0.00153	0.26558	0.00818	0.03873	0.0003	173	58	239	7	245	2
DL09-27-9	1202	60.0	688	0.57	0.05005	0.00113	0.27528	0.00605	0.03969	0.0003	197	36	247	5	251	2
DL09-27-10	756	37.3	286	0.38	0.06206	0.00203	0.35129	0.01214	0.04065	0.0004	676	57	306	9	257	2
DL09-27-11	956	48.1	551	0.58	0.05058	0.00128	0.27682	0.00667	0.03956	0.0003	222	41	248	5	250	2

Table 3.3 LA-ICP-MS U-Pb zircon data

Spot	U (ppm)	Pb (ppm)	Th (ppm)	Th/U	$^{207}Pb/^{206}Pb$ Ratio	1σ	$^{207}Pb/^{235}U$ Ratio	1σ	$^{206}Pb/^{238}U$ Ratio	1σ	$^{207}Pb/^{206}Pb$ Age	1σ	$^{207}Pb/^{235}U$ Age	1σ	$^{206}Pb/^{238}U$ Age	1σ
DL09-27-12	968	47.2	453	0.47	0.04996	0.00163	0.27514	0.00917	0.03961	0.0004	193	60	247	7	250	2
DL09-27-13	282	13.2	119	0.42	0.05314	0.00240	0.28884	0.01337	0.03963	0.0005	335	82	258	11	251	3
DL09-27-14	1194	57.2	432	0.36	0.04946	0.00150	0.27403	0.00792	0.04012	0.0003	170	53	246	6	254	2
DL09-27-15	898	43.0	326	0.36	0.04984	0.00148	0.27690	0.00790	0.04025	0.0003	188	51	248	6	254	2
DL09-27-16	698	33.2	285	0.41	0.04951	0.00153	0.27102	0.00812	0.03982	0.0004	172	51	244	6	252	2
DL09-27-17	541	25.4	186	0.34	0.04948	0.00162	0.27064	0.00895	0.03971	0.0003	171	61	243	7	251	2
DL09-27-18	669	35.3	267	0.40	0.04960	0.00174	0.29991	0.01060	0.04388	0.0005	176	60	266	8	277	3
DL09-27-19	754	35.5	242	0.32	0.05105	0.00163	0.27955	0.00880	0.03984	0.0003	243	57	250	7	252	2
DL09-27-20	1114	52.3	362	0.33	0.04903	0.00129	0.26812	0.00709	0.03961	0.0003	149	49	241	6	250	2
DL09-27-21	519	25.4	215	0.41	0.05026	0.00145	0.27477	0.00745	0.03985	0.0003	207	47	247	6	252	2
DL09-27-22	817	41.0	454	0.56	0.05011	0.00122	0.27530	0.00679	0.03974	0.0003	200	43	247	5	251	2
DL09-27-23	1405	74.2	633	0.45	0.05277	0.00143	0.31277	0.00873	0.04277	0.0004	319	48	276	7	270	2
DL09-27-24	1062	53.2	420	0.40	0.05129	0.00148	0.28928	0.00816	0.04083	0.0004	254	49	258	6	258	2
DL09-30-1	240	12.2	152	0.63	0.05744	0.00371	0.31290	0.01982	0.03951	0.0005	508	146	276	15	250	3
DL09-30-2	148	7.3	91	0.62	0.04775	0.00318	0.25866	0.01618	0.03990	0.0007	87	107	234	13	252	4
DL09-30-3	239	11.7	136	0.57	0.04829	0.00298	0.26083	0.01619	0.03926	0.0005	113	114	235	13	248	3
DL09-30-4	307	15.7	214	0.70	0.04926	0.00257	0.26484	0.01376	0.03892	0.0004	160	99	239	11	246	3
DL09-30-5	143	7.2	82	0.57	0.05996	0.00322	0.33182	0.01866	0.03997	0.0005	602	101	291	14	253	3
DL09-30-6	169	9.2	106	0.63	0.05840	0.00537	0.31067	0.02808	0.03858	0.0006	545	208	275	22	244	4
DL09-30-7	197	9.9	160	0.81	0.05828	0.00344	0.29212	0.01556	0.03721	0.0006	540	89	260	12	236	4
DL09-30-8	161	8.1	82	0.51	0.04948	0.00291	0.27039	0.01579	0.03980	0.0006	171	105	243	13	252	4
DL09-30-9	180	9.1	116	0.64	0.05674	0.00334	0.29781	0.01575	0.03886	0.0006	481	92	265	12	246	3
DL09-30-10	229	11.0	154	0.67	0.05411	0.00245	0.27312	0.01186	0.03698	0.0005	376	75	245	9	234	3
DL09-30-11	315	16.4	238	0.76	0.04868	0.00223	0.26202	0.01160	0.03952	0.0005	133	79	236	9	250	3
DL09-30-12	247	12.5	159	0.64	0.05115	0.00222	0.27671	0.01154	0.03954	0.0004	248	76	248	9	250	3
DL09-30-13	229	11.6	150	0.66	0.05295	0.00254	0.28889	0.01472	0.03957	0.0005	327	91	258	12	250	3
DL09-30-14	317	16.2	207	0.65	0.05180	0.00229	0.28191	0.01214	0.03960	0.0004	276	80	252	10	250	3
DL09-30-15	197	10.0	128	0.65	0.04877	0.00224	0.26365	0.01175	0.03956	0.0005	137	78	238	9	250	3

Table 3.3 LA-ICP-MS U-Pb zircon data

Spot	U (ppm)	Pb (ppm)	Th (ppm)	Th/U	$^{207}Pb/^{206}Pb$ Ratio	1σ	$^{207}Pb/^{235}U$ Ratio	1σ	$^{206}Pb/^{238}U$ Ratio	1σ	$^{207}Pb/^{206}Pb$ Age	1σ	$^{207}Pb/^{235}U$ Age	1σ	$^{206}Pb/^{238}U$ Age	1σ
DL09-30-16	175	8.7	99	0.57	0.05342	0.00463	0.28001	0.02202	0.03941	0.0006	346	150	251	17	249	4
DL09-30-17	277	14.0	168	0.60	0.05098	0.00268	0.27412	0.01326	0.03947	0.0005	240	90	246	11	250	3
DL09-30-18	224	10.9	128	0.57	0.05217	0.00330	0.27118	0.01637	0.03807	0.0005	293	115	244	13	241	3
DL09-30-19	261	12.9	143	0.55	0.05178	0.00255	0.27344	0.01285	0.03857	0.0004	276	88	245	10	244	3
DL09-30-20	208	10.4	118	0.57	0.05321	0.00287	0.28978	0.01510	0.03975	0.0005	338	94	258	12	251	3
DL09-30-21	257	13.4	179	0.70	0.05199	0.00217	0.28562	0.01158	0.03988	0.0005	285	72	255	9	252	3
DL09-30-22	238	12.0	139	0.58	0.05218	0.00307	0.28160	0.01589	0.03935	0.0005	294	105	252	13	249	3
DL09-30-23	256	12.4	138	0.54	0.05270	0.00279	0.28052	0.01468	0.03880	0.0005	316	98	251	12	245	3
DL09-30-24	177	9.0	100	0.57	0.05069	0.00272	0.27808	0.01444	0.04027	0.0005	227	96	249	11	255	3
DL09-31-1	3450	226.9	4407	1.28	0.05115	0.00092	0.31196	0.00551	0.04402	0.0002	248	31	276	4	278	1
DL09-31-2	742	38.7	548	0.74	0.04953	0.00150	0.26800	0.00769	0.03933	0.0003	173	54	241	6	249	2
DL09-31-3	2372	147.1	2500	1.05	0.05098	0.00095	0.31074	0.00569	0.04410	0.0003	240	30	275	4	278	2
DL09-31-4	769	41.2	672	0.87	0.05478	0.00217	0.30124	0.01235	0.03971	0.0005	403	71	267	10	251	3
DL09-31-5	119	5.9	70	0.59	0.05007	0.00349	0.26710	0.01758	0.03928	0.0006	198	121	240	14	248	4
DL09-31-6	202	10.0	119	0.59	0.05749	0.00296	0.30316	0.01510	0.03889	0.0005	510	87	269	12	246	3
DL09-31-7	186	9.7	153	0.82	0.05116	0.00294	0.27160	0.01486	0.03951	0.0005	248	104	244	12	250	3
DL09-31-8	257	14.7	244	0.95	0.04927	0.00516	0.25674	0.02662	0.03780	0.0006	160	235	232	22	239	4
DL09-31-9	1380	82.8	1310	0.95	0.04928	0.00103	0.29930	0.00634	0.04392	0.0003	161	36	266	5	277	2
DL09-31-10	923	51.2	753	0.82	0.05218	0.00481	0.30619	0.02782	0.04256	0.0006	293	211	271	22	269	4
DL09-31-11	2009	127.2	2280	1.14	0.05113	0.00113	0.31015	0.00656	0.04389	0.0003	247	34	274	5	277	2
DL09-31-12	1062	54.4	756	0.71	0.05158	0.00230	0.27813	0.01215	0.03911	0.0004	267	105	249	10	247	2
DL09-31-13	1131	64.6	1208	1.07	0.05104	0.00155	0.28329	0.00846	0.04008	0.0003	242	54	253	7	253	2
DL09-31-14	212	10.5	121	0.57	0.06516	0.00354	0.34746	0.01797	0.03896	0.0005	780	88	303	14	246	3
DL09-31-15	992	54.6	938	0.95	0.05323	0.00142	0.29674	0.00844	0.04013	0.0003	339	49	264	7	254	2
DL09-31-16	141	8.2	99	0.70	0.05255	0.00725	0.27412	0.03742	0.03784	0.0008	309	306	246	30	239	5
DL09-31-17	4109	273.5	5600	1.36	0.05178	0.00094	0.31715	0.00568	0.04417	0.0003	276	29	280	4	279	2
DL09-31-18	2676	167.0	2925	1.09	0.05085	0.00108	0.31056	0.00654	0.04400	0.0003	234	36	275	5	278	2
DL09-31-19	1975	111.3	1382	0.70	0.05117	0.00120	0.31207	0.00757	0.04398	0.0005	249	37	276	6	277	3

Table 3.3 LA-ICP-MS U-Pb zircon data

Spot	U (ppm)	Pb (ppm)	Th (ppm)	Th/U	$^{207}Pb/^{206}Pb$ Ratio	1σ	$^{207}Pb/^{235}U$ Ratio	1σ	$^{206}Pb/^{238}U$ Ratio	1σ	$^{207}Pb/^{206}Pb$ Age	1σ	$^{207}Pb/^{235}U$ Age	1σ	$^{206}Pb/^{238}U$ Age	1σ
DL09-31-20	162	8.3	110	0.68	0.06243	0.00463	0.33361	0.02311	0.03985	0.0007	689	120	292	18	252	4
DL09-31-21	2884	179.3	3049	1.06	0.06187	0.00141	0.37625	0.00879	0.04375	0.0003	670	39	324	6	276	2
DL09-31-22	251	12.5	161	0.64	0.04800	0.00224	0.26486	0.01237	0.03993	0.0005	99	82	239	10	252	3
DL09-31-23	1431	84.1	1250	0.87	0.05025	0.00106	0.30917	0.00639	0.04434	0.0003	206	35	274	5	280	2
DL09-31-24	136	7.2	112	0.82	0.05866	0.00354	0.31362	0.01749	0.03985	0.0006	555	98	277	14	252	3

Table 3.4 Whole rock Sr isotopic data. The last column refers to the analytical session during which the sample was analysed for Sr isotope composition. The blank, the average $^{87}Sr/^{86}Sr$ and reproducibility of multiple measurements of the NBS987 Sr isotope standard during the appropriate session are given below:

1: 0.710267±01 (2SD, n=13), blank=8 pg

2: 0.710283±02(2SD, n=8), blank=23 pg

3: 0.710284±05(2SD, n=9), blank=24 pg

$^{87}Sr/^{86}Sr$ are reported relative to an accepted $^{87}Sr/^{86}Sr$ ratio for NBS987 of 0.71024 (Thirlwall, 1991)

Sample	Type	Rb(ppm)	Sr(ppm)	$^{87}Rb/^{86}Sr$	$^{87}Sr/^{86}Sr$(2SD)	I_{sr}	Analytical sessions
DL09-07	MME	50.6	232	0.62	0.711636(12)	0.70944	1
DL09-08	HR	81.7	172	1.35	0.714290(10)	0.70950	1
DL09-09	HR	81.3	367	0.63	0.713877(13)	0.71164	1
DL09-13	HR	77.0	186	1.17	0.713729(20)	0.70956	1
DL09-14	MME	74.0	197	1.06	0.713029(12)	0.70925	2
DL09-15	HR	77.4	204	1.07	0.713498(11)	0.70968	1
DL09-16	MME	64.0	212	0.86	0.712413(11)	0.70937	2
DL09-17	MME	101	169	1.69	0.715355(13)	0.70933	1
DL09-18	HR	74.2	177	1.18	0.714678(13)	0.71046	1
DL09-21	HR	88.0	186	1.34	0.714763(09)	0.70999	1
DL09-22	MME	58.3	208	0.79	0.712593(12)	0.70977	1
DL09-24	HR	50.0	246	0.58	0.712486(07)	0.71044	3
DL09-26	MME	60.6	279	0.62	0.711845(11)	0.70966	2
DL09-27	HR	54.4	213	0.72	0.712073(12)	0.70950	1
DL09-30	HR	43.3	348	0.35	0.709680(09)	0.70843	1
DL09-31	MME	38.2	270	0.40	0.709370(12)	0.70795	1
DL09-32	HR	39.4	347	0.32	0.709288(11)	0.70814	1

$I_{Sr}=(^{87}Sr/^{86}Sr)_{sample}-(^{87}Rb/^{86}Sr)_{sample}*(e^{\lambda t}-1)$, $\lambda(^{87}Rb)=1.42\times10^{-11}yr^{-1}$

Table 3.5 Whole rock Nd isotopic data. The last column refers to the analytical session during which the sample was analysed for Nd isotope composition. The blank and average $^{143}Nd/^{144}Nd$ and reproducibility of multiple measurements of the J&M isotope standard during the appropriate session are given below:

1: 0.511116±11 (2SD, n=19), blank=2 pg

2: 0.511101±09 (2SD, n=19), blank=3 pg

$^{143}Nd/^{144}Nd$ are reported relative to an accepted ratio for J&M of 0.511110 (Thirlwall, 1991)

Sample	Type	Nd(ppm)	Sm(ppm)	$^{147}Sm/^{144}Nd$	$^{143}Nd/^{144}Nd$	ε_{Nd} (t)	F_M %	Analytical sessions
DL09-07	MME	13.1	2.76	0.1282	0.512414(09)	-2.2	68	1
DL09-08	HR	12.7	2.88	0.1431	0.512362(10)	-3.7	67	1
DL09-09	HR	25.7	4.16	0.0980	0.512278(09)	-3.9	74	1
DL09-13	HR	18.1	3.25	0.1089	0.512385(08)	-2.1	70	1
DL09-14	MME	34.6	8.25	0.1448	0.512324(11)	-4.5	71	2
DL09-15	HR	18.0	3.60	0.1215	0.512354(10)	-3.1	73	1
DL09-16	MME	32.4	7.57	0.1418	0.512337(09)	-4.1	75	2
DL09-17	MME	35.2	7.94	0.1370	0.512340(09)	-3.9	74	1
DL09-18	HR	21.1	3.64	0.1046	0.512342(08)	-2.8	63	1
DL09-21	HR	21.7	4.22	0.1179	0.512377(08)	-2.6	65	1
DL09-22	MME	24.9	4.87	0.1188	0.512360(08)	-2.9	66	1
DL09-24	HR	20.0	4.42	0.1342	0.512330(14)	-4.0	71	2
DL09-26	MME	18.7	4.60	0.1491	0.512395(12)	-3.8	66	2
DL09-27	HR	13.4	2.50	0.1132	0.512366(06)	-2.9	67	1
DL09-30	HR	16.0	3.14	0.0282	0.512278(09)	-4.9	63	1
DL09-31	MME	19.5	3.91	0.0287	0.512257(09)	-5.2	60	1
DL09-32	HR	18.7	3.73	0.0286	0.512253(07)	-5.3	60	1

$\varepsilon_{Nd}(t)=[(^{143}Nd/^{144}Nd)_{sample(t)}/(^{143}Nd/^{144}Nd)_{CHUR(t)}-1]*10{,}000$, where $(^{143}Nd/^{144}Nd)_{CHUR(present)}-(^{147}Sm/^{144}Nd)_{CHUR(present)}*(e^{\lambda t}-1)$, $\lambda(^{147}Sm)=6.54\times10^{-12}yr^{-1}$. The $^{147}Sm/^{144}Nd$ and $^{143}Nd/^{144}Nd$ ratios at the present day are 0.1967 and 0.512638 for chondrite,respectively. t=crystallization age of zircon,250 Ma. ， F_M : mantle contribution. F_M calculation: $Nd_{sample}=Nd_{mantle}*F_M+Nd_{crust}*(1-F_M)$,

$^{143}Nd/^{144}Nd_{sample}=^{143}Nd/^{144}Nd_{Mantle}*F_M*Nd_{mantle}/Nd_{sample}+^{143}Nd/^{144}Nd_{crust}*(1-F_M)*Nd_{crust}/Nd_{mantle}$

Table 3.6 Whole rock Hf isotopic data.The last column refers to the analytical session during which the sample was analysed for Hf isotope composition. The blank and average $^{176}Hf/^{177}Hf$ and reproducibility of multiple measurements of the JMC475 isotope standard during the appropriate session are given below:

1: 0.282148±08 (2SD, n=7), blank=8 pg

2: 0.282143±08 (2SD, n=10), blank=4 pg

3: 0.282146±09 (2SD, n=8), blank=1 pg

$^{176}Hf/^{177}Hf$ are reported relative to an accepted ratio for JMC475 of 0.282160 (Nowell et al., 1998)

Samle	Type	Lu(ppm)	Hf(ppm)	$^{176}Lu/^{177}Hf$	$^{176}Hf/^{177}Hf$(2SD)	$\varepsilon_{Hf}(t)$	F_M %	Analytical sessions
DL09-07	MME	0.29	2.89	0.014	0.282792(14)	4.0	75	1
DL09-08	HR	0.34	4.27	0.011	0.282758(08)	3.3	73	2
DL09-09	HR	0.32	5.39	0.008	0.282615(11)	-1.3	62	1
DL09-13	HR	0.32	4.12	0.011	0.282735(12)	2.5	71	1
DL09-14	MME	0.95	3.09	0.043	0.282934(11)	4.1	75	3
DL09-15	HR	0.36	4.36	0.012	0.282766(12)	3.5	74	1
DL09-16	MME	0.90	3.25	0.038	0.282943(11)	5.2	77	3
DL09-17	MME	0.78	7.54	0.014	0.282805(08)	4.4	75	1
DL09-18	HR	0.33	4.40	0.010	0.282758(11)	3.4	73	1
DL09-21	HR	0.45	4.45	0.014	0.282759(11)	2.8	72	1
DL09-22	MME	0.57	2.28	0.035	0.282906(11)	4.5	76	1
DL09-24	HR	0.44	2.96	0.021	0.282764(09)	1.8	70	1
DL09-26	MME	0.49	2.57	0.027	0.282854(09)	4.0	75	3
DL09-27	HR	0.21	4.38	0.007	0.282709(07)	2.3	71	2
DL09-30	HR	0.27	3.20	0.012	0.282732(11)	2.3	71	1
DL09-31	MME	0.35	3.53	0.014	0.282595(08)	-2.9	58	1
DL09-32	HR	0.31	3.36	0.013	0.282721(08)	1.7	70	1

$\varepsilon_{Hf}(t)=[(^{176}Hf/^{177}Hf)_{sample(t)}/(^{176}Hf/^{177}Hf)_{sample(t)}-1]*10{,}000$, where $(^{176}Hf/^{177}Hf)_{CHUR(present)}-(^{176}Lu/^{177}Hf)_{CHUR(present)}*(e^{\lambda t}-1)$.The $^{176}Lu/^{177}Hf$ and $^{176}Hf/^{177}Hf$ ratios at the present day are 0.0332 and 0.282772 for chondrite,respectively. t=250 Ma. $\lambda(^{176}Lu)=1.93\times10^{-11}yr^{-1}$， F_M : mantle contribution.F_M calculation:$Hf_{sample}=Hf_{mantle}*F_M+Hf_{crust}*(1-F_M)$,

$^{176}Hf/^{177}Hf_{sample}=^{176}Hf/^{177}Hf_{Mantle}*F_M*Hf_{mantle}/Hf_{sample}+^{176}Hf/^{177}Hf_{crust}*(1-F_M)*Hf_{crust}/Hf_{mantle}$

Table 3.7 Whole rock Pb isotopic data.The last column refers to the analytical session during which the sample was analysed forPb isotope composition. The blank and averages and reproducibility ofr multiple measurements of the NBS981 Pb isotope standard during the appropriate session are given below:

1: $^{206}Pb/^{204}Pb$:16.94052±092; $^{207}Pb/^{204}Pb$:15.49770±119; $^{208}Pb/^{204}Pb$:36.71710±382 (2SD, n=8), blank=10 pg

2: $^{206}Pb/^{204}Pb$:16.94102±184; $^{207}Pb/^{204}Pb$:15.49811±142; $^{208}Pb/^{204}Pb$:36.71791±512 (2SD, n=11), blank=80 pg

3: $^{206}Pb/^{204}Pb$:16.94083±274; $^{207}Pb/^{204}Pb$:15.49706±115; $^{208}Pb/^{204}Pb$:36.71478±399 (2SD, n=17), blank=79 pg

Sample	Type	Pb(ppm)	Th(ppm)	U(ppm)	$^{206}Pb/^{204}Pb$(2SD)	$^{207}Pb/^{204}Pb$(2SD)	$^{208}Pb/^{204}Pb$(2SD)	$^{208}Pb/^{204}Pb_i$	$^{207}Pb/^{204}Pb_i$	$^{206}Pb/^{204}Pb_i$	Analytical sessions
DL09-07	MME	11.5	4.1	0.7	18.634(1)	15.642(1)	38.752(4)	38.475	15.634	18.480	1
DL09-08	HR	16.1	10.2	1.4	19.184(1)	15.671(1)	39.009(5)	38.513	15.661	18.978	2
DL09-09	HR	14.3	11.7	1.1	18.675(1)	15.654(1)	39.241(3)	38.601	15.644	18.489	1
DL09-13	HR	18.7	11.6	1.3	18.775(1)	15.649(1)	38.977(3)	38.491	15.640	18.612	1
DL09-14	MME	15.5	1.7	0.6	18.658(1)	15.642(1)	38.574(3)	38.487	15.637	18.561	1
DL09-15	HR	15.6	9.1	1.0	18.860(1)	15.652(1)	38.988(3)	38.532	15.644	18.704	1
DL09-16	MME	12.7	2.1	0.6	18.527(1)	15.635(1)	38.568(3)	38.439	15.629	18.414	2
DL09-17	MME	12.3	10.6	1.3	18.972(1)	15.661(1)	39.198(4)	38.525	15.648	18.709	2
DL09-18	HR	17.2	13.8	1.1	18.645(1)	15.645(1)	39.130(4)	38.502	15.638	18.496	1
DL09-21	HR	19.4	14.1	2.0	18.780(1)	15.651(1)	39.049(3)	38.479	15.639	18.538	1
DL09-22	MME	10.8	3.4	0.7	18.580(1)	15.641(1)	38.680(3)	38.435	15.633	18.431	1
DL09-24	HR	7.0	5.3	1.2	19.074(1)	15.669(1)	39.172(4)	38.579	15.647	18.650	3
DL09-26	MME	6.5	3.8	1.3	18.968(1)	15.665(1)	38.996(3)	38.533	15.641	18.503	2
DL09-27	HR	12.7	7.2	0.8	18.674(2)	15.646(1)	38.943(4)	38.498	15.638	18.517	1
DL09-30	HR	9.79	6.94	0.83	18.660(1)	15.641(1)	38.971(3)	36.021	15.548	16.876	2
DL09-31	MME	7.52	7.39	1.30	18.652(1)	15.640(1)	39.151(5)	36.175	15.545	16.818	2
DL09-32	HR	10.4	7.25	0.98	18.610(1)	15.638(1)	38.963(4)	35.990	15.543	16.786	2

$^{206}Pb/^{204}Pb_i=(^{206}Pb/^{204}Pb)_{sample}-(^{238}U/^{204}Pb)_{sample}*(e^{\lambda t}-1)$ t=250 Ma. $^{208}Pb/^{204}Pbi$ and $^{207}Pb/^{204}Pbi$ are similar.$\lambda(^{238}U)=1.55\times10^{-10}yr^{-1}$,$\lambda(^{235}U)=9.85\times10^{-10}yr^{-1}$, $\lambda(^{232}Th)=4.95\times10^{-11}yr^{-1}$

Table 4.1 Compilation of Paleozoic granitoids in Qilian Orogenic Belt (QOB).

	Location	Age	Rock-type	Refs.
	Kekeli	476-512	I	1 (Wu et al., 2010)
	Kekeli	501	I	1
	Chaidanuo	508	S	1
	Niuxinshan	477	I	1
NQOB		435	S	1
	Minle	463	I,S	1
	Jinfosi	424	S	1
	Chaidanuo	516	S	2 (Song et al., 2012a)
	Leigongshan	453	I	3 (Tseng et al., 2009)
	Aolaoshan	473	I	4 (Wu et al., 2001)
	Dachaidam	446	S	5 (Wu et al., 2002)
	Dachaidam	446	S	6 (Wu et al., 2007)
		408	S	6
NQ-UHPM		460-470	I	6
		370	S	6
	Dachaidam	442	?	7 (Gehrels et al., 2003b)
	Ulan	493	I	8 (Chen et al., 2011)
	Ulan	422	S	8
QB	Huangyuan	450~446	S	9 (Yong et al., 2008)

Nuberms refer to the numbers in Fig. 1B

Table 4.2 Sample locations and brief descriptions in the Qilian Block

	Sample	Age	GPS position		Mineral assemblage	SiO_2%	A/CNK
old rocks	QL09-15	924	N36°48.726'	E101°09.977'	Pl, Kfs, Grt, Ms, Qz, slightly deformed	70.0	1.17
	QL09-01	797	N36°27.116'	E101°05.634'	Qz, Kfs, Pl, Bt, Ms, Grt	72.7	1.31
	QL09-18	503	N37°22.712'	E101°23.887'	Qz, Pl, Chl, minor Kfs, slightly deformed	72.3	1.23
	QL09-19		N37°22.712'	E101°23.887'	Amp, Pl	51.6	0.79
S-type	QL09-02	430	N36°27.116'	E101°05.634'	Qz, Kfs, Pl, Bt, Ms	72.4	1.17
	QL09-07		N36°27.047'	E101°05.557'	Qz, Kfs, Pl, Chl, calcite vein	71.9	1.66
	QL09-09		N36°34.895'	E101°13.520'	Qz, Kfs, Pl, Bt, Ms	70.8	1.06
	QL09-10	430	N36°34.895'	E101°13.520'	Qz, Pl, Bt, Ms, Grt	75.1	1.05
	QL09-12	430	N36°46.731'	E101°07.428'	Qz, Kfs, Pl, Bt, Aln	71.3	1.10
	QL09-17		N36°48.672'	E101°09.914'	Qz, Kfs, Pl, Bt, Ms	69.6	1.17
	QL10-40F		N37°23.678′	E100°27.800′	minor Bt, Ms, Q, altered feldspar, ***F***	74.8	1.10
	QL10-41F		N37°23.678′	E100°27.800′	similar to QL10-40(F), thermol equiliabrated with QL10-41(C) in the thin section, ***F***	74.8	1.15
I-type	QL09-14	450	N36°46.903'	E101°07.562'	Qz, Pl, Amp>Bt, ***F***	56.0	0.79
	QL10-32		N37°25.962′	E100°27.615′	Bt, Pl, Qz, Amp, Chl, ***F***	62.0	0.94
	QL10-33		N37°25.962′	E100°27.615′	Bt, Amp, Pl, Qz, ***F***	62.2	0.95
	QL10-34	450	N37°25.962′	E100°27.615′	Bt, Amp, Pl, Qz, ***F***	62.1	0.92
	QL10-35		N37°25.962′	E100°27.615′	Bt, Amp, Pl, Qz, ***F***	61.7	0.90
	QL10-44		N37°23.678′	E100°27.800′	Bt, Amp, Pl, Qz, ***F***	60.2	0.96
	QL10-45		N37°23.678′	E100°27.800′	Bt, Amp, Pl, Qz, ***F***	62.4	1.00
	QL10-37	450	N37°23.678′	E100°27.800′	Bt, Qz, Pl, ***C***	74.1	1.05
	QL10-38		N37°23.678′	E100°27.800′	Bt, Qz, Pl, more Bt and Pl, ***C***	62.1	1.08
	QL10-40C		N37°23.678′	E100°27.800′	Bt, Qz, Pl, ***C***	69.3	1.11
	QL10-41C		N37°23.678′	E100°27.800′	Bt, Qz, Pl, ***C***	67.9	1.12
	QL10-42		N37°22.629′	E100°28.641′	Bt, Qz, Pl, ***C***	65.0	1.11

Pl: plagioclase; Kfs: K-feldspare; Grt: garnet; Ms: muscovite; Qz: quartz; Bt: biotite; Amp: amphibole; Chl: chlorite; Aln: allanite

F : fine-grained; ***C*** : coarse-grained

Mineral abbreviations follow Whitney and Evans, 2010.

Table 4.3 Zircon in situ LA-ICP-MS dating results

	Pb	Th	U	Th/U	CORRECTED RATIOS						CORRECTED AGES (Ma)					
	Total ppm	232 ppm	238 ppm		$^{207}Pb/^{206}Pb$		$^{207}Pb/^{235}U$		$^{206}Pb/^{238}U$		$^{207}Pb/^{206}Pb$		$^{207}Pb/^{235}U$		$^{206}Pb/^{238}U$	
Analysed in China University of Geosciences (Wuhan)																
QL09-01-1	14.3	30.9	31.7	0.97	0.11204	0.00365	4.94249	0.16114	0.32071	0.0039	1833	42	1810	28	1793	19
QL09-01-2	16.8	85.6	103	0.83	0.06829	0.00399	1.12727	0.06430	0.11971	0.0015	878	124	766	31	729	9
QL09-01-3	18.1	38.0	130	0.29	0.06578	0.00210	1.15504	0.04428	0.12589	0.0023	799	50	780	21	764	13
QL09-01-4	98.3	280	600	0.47	0.06547	0.00117	1.19706	0.02230	0.13188	0.0009	790	27	799	10	799	5
QL09-01-5	144	715	923	0.77	0.07338	0.00165	1.13298	0.02602	0.11144	0.0008	1025	35	769	12	681	5
QL09-01-6	234	143	620	0.23	0.12536	0.00214	5.34166	0.09476	0.30702	0.0021	2034	22	1876	15	1726	10
QL09-01-7	21.1	91.1	124	0.73	0.06402	0.00220	1.12407	0.03809	0.12759	0.0013	742	54	765	18	774	8
QL09-01-8	135	114	254	0.45	0.16630	0.00264	9.25834	0.15048	0.40186	0.0029	2521	18	2364	15	2178	13
QL09-01-9	34.0	71.3	203	0.35	0.06937	0.00174	1.33851	0.03285	0.13974	0.0010	910	38	863	14	843	6
QL09-01-10	83.2	88.7	131	0.67	0.17168	0.00273	10.7527	0.17666	0.4524	0.0034	2574	17	2502	15	2406	15
QL09-01-11	50.3	48.8	94.4	0.52	0.15159	0.00424	8.11327	0.21277	0.38817	0.0038	2364	49	2244	24	2114	18
QL09-01-12	19.5	108	109	1.00	0.06945	0.00228	1.21749	0.03972	0.12757	0.0014	912	50	809	18	774	8
QL09-01-13	22.7	115	122	0.94	0.06616	0.00205	1.21439	0.03751	0.13321	0.0012	811	49	807	17	806	7
QL09-01-14	48.6	121	337	0.36	0.06463	0.00154	1.07707	0.02561	0.12071	0.0010	762	37	742	13	735	6
QL09-01-15	23.7	109	147	0.74	0.06699	0.00178	1.21585	0.03045	0.13213	0.0012	838	37	808	14	800	7
QL09-01-16	103	117	236	0.50	0.15038	0.00337	6.47008	0.13659	0.31204	0.0023	2350	39	2042	19	1751	11
QL09-01-17	16.7	76.2	92.0	0.83	0.07066	0.00278	1.32590	0.05373	0.1364	0.0017	947	63	857	23	824	9
QL09-01-18	223	184	353	0.52	0.19836	0.00405	12.3579	0.23322	0.45184	0.0035	2813	34	2632	18	2403	16
QL09-01-20	54.0	312	287	1.09	0.06826	0.00146	1.25471	0.02727	0.13318	0.0011	876	31	826	12	806	6
QL09-01-21	32.0	112	189	0.59	0.06445	0.00168	1.18513	0.03033	0.13373	0.0011	756	40	794	14	809	6
QL09-01-22	96.3	66.2	158	0.42	0.17286	0.00335	10.9805	0.19401	0.46071	0.0036	2586	33	2521	16	2443	16
QL09-01-23	162	326	211	1.55	0.16689	0.00243	10.8900	0.16653	0.47168	0.0033	2527	16	2514	14	2491	14
QL09-01-24	28.8	127	163	0.78	0.06611	0.00203	1.23788	0.03869	0.13638	0.0015	810	47	818	18	824	9
QL09-02-1	258	524	556	0.94	0.06473	0.00117	1.18927	0.02171	0.13286	0.0009	765	27	796	10	804	5
QL09-02-3	62.2	104	239	0.44	0.06026	0.00145	0.93525	0.02615	0.11207	0.0016	613	36	670	14	685	9
QL09-02-4	184	349	505	0.69	0.06522	0.00122	1.14587	0.02333	0.12656	0.0010	755	29	775	11	768	6
QL09-02-5	185	428	288	1.49	0.08134	0.00257	1.21834	0.04072	0.10781	0.0012	1230	48	809	19	660	7
QL09-02-6	167	302	723	0.42	0.06135	0.00128	0.92607	0.02117	0.10887	0.0012	651	31	666	11	666	7
QL09-02-7	105	181	501	0.36	0.06501	0.00181	0.90625	0.02541	0.1006	0.0008	775	46	655	14	618	4

Table 4.3 Zircon in situ LA-ICP-MS dating results

	Pb	Th	U	Th/U	CORRECTED RATIOS						CORRECTED AGES (Ma)					
	Total	232	238		$^{207}Pb/^{206}Pb$		$^{207}Pb/^{235}U$		$^{206}Pb/^{238}U$		$^{207}Pb/^{206}Pb$		$^{207}Pb/^{235}U$		$^{206}Pb/^{238}U$	
	ppm	ppm	ppm													
QL09-02-8	128	240	355	0.68	0.06409	0.00143	1.11720	0.02463	0.12601	0.0010	745	34	762	12	765	5
QL09-02-10	163	322	378	0.85	0.06712	0.00185	1.17192	0.03221	0.12605	0.0010	841	45	788	15	765	5
QL09-02-11	48.4	75.9	136	0.56	0.06235	0.00209	1.24158	0.04114	0.14419	0.0016	686	52	820	19	868	9
QL09-02-12	319	559	1487	0.38	0.06935	0.00221	0.96116	0.02957	0.10052	0.0008	909	67	684	15	617	5
QL09-02-13	133	221	641	0.34	0.06279	0.00144	0.94257	0.02250	0.10832	0.0010	701	34	674	12	663	6
QL09-02-15	22.9	28.3	287	0.10	0.05919	0.00181	0.60293	0.01844	0.07376	0.0006	574	53	479	12	459	4
QL09-02-16	40.6	38.3	460	0.08	0.05730	0.00329	0.53889	0.02937	0.06821	0.0012	503	130	438	19	425	7
QL09-02-18	211	394	642	0.61	0.06073	0.00153	1.05130	0.02725	0.12517	0.0012	630	40	730	13	760	7
QL09-02-19	149	460	811	0.57	0.05201	0.00137	0.53595	0.01377	0.07460	0.0006	286	44	436	9	464	4
QL09-02-20	57.6	90.7	700	0.13	0.05355	0.00116	0.52144	0.01100	0.07056	0.0005	352	34	426	7	440	3
QL09-02-21	144	262	385	0.68	0.06356	0.00131	1.15777	0.02399	0.13172	0.0010	727	31	781	11	798	6
QL09-02-24	100	166	364	0.46	0.06451	0.00159	1.14056	0.02795	0.12795	0.0011	758	37	773	13	776	6
QL09-02-2	309	155	323	0.48	0.15315	0.00228	8.89974	0.13566	0.41962	0.0026	2381	18	2328	14	2259	12
QL09-02-9	373	124	482	0.26	0.17630	0.00278	10.7723	0.17193	0.44083	0.0028	2618	18	2504	15	2354	12
QL09-02-14	130	90.0	378	0.24	0.12336	0.00320	3.29337	0.07710	0.19362	0.0022	2005	47	1479	18	1141	12
QL09-02-17	299	126	767	0.16	0.13801	0.00306	4.13892	0.08512	0.21751	0.0018	2202	39	1662	17	1269	10
QL09-02-22	345	78.1	738	0.11	0.16434	0.00264	8.39809	0.13695	0.36892	0.0024	2501	19	2275	15	2024	11
QL09-02-23	557	395	965	0.41	0.14106	0.00253	5.60155	0.13279	0.28551	0.0040	2240	22	1916	20	1619	20
QL09-10-1	25	47	214	0.22	0.05860	0.00129	0.65139	0.01410	0.08013	0.0006	552	35	509	9	497	3
QL09-10-2	37	86	361	0.24	0.05691	0.00127	0.56616	0.01262	0.07171	0.0005	488	38	456	8	446	3
QL09-10-3	121	249	1271	0.20	0.05536	0.00153	0.54628	0.01536	0.07107	0.0005	427	51	443	10	443	3
QL09-10-4	1366	2511	16324	0.15	0.05224	0.00156	0.51691	0.01561	0.07143	0.0006	296	54	423	10	445	4
QL09-10-5	158	412	1280	0.32	0.05568	0.00163	0.60166	0.01724	0.07812	0.0006	439	51	478	11	485	3
QL09-10-6	12	18	112	0.16	0.07154	0.00246	0.64105	0.02211	0.06470	0.0006	973	57	503	14	404	3
QL09-10-7	1752	4183	15983	0.26	0.05304	0.00174	0.56685	0.01834	0.07729	0.0006	331	59	456	12	480	4
QL09-10-8	19	56	167	0.33	0.05895	0.00188	0.58380	0.01827	0.07169	0.0006	565	53	467	12	446	4
QL09-10-9	25	46	247	0.18	0.05587	0.00189	0.56429	0.01892	0.07298	0.0007	447	58	454	12	454	4
QL09-10-10	19	34	183	0.19	0.05585	0.00174	0.54927	0.01645	0.07133	0.0006	446	71	445	11	444	4
QL09-10-11	1	2	13	0.18	0.06002	0.00149	0.59582	0.01512	0.07158	0.0006	604	42	475	10	446	3
QL09-10-12	21	33	230	0.14	0.05761	0.00171	0.56465	0.01585	0.07109	0.0007	515	67	455	10	443	4

Table 4.3 Zircon in situ LA-ICP-MS dating results

	Pb	Th	U	Th/U	CORRECTED RATIOS						CORRECTED AGES (Ma)					
	Total ppm	232 ppm	238 ppm		$^{207}Pb/^{206}Pb$		$^{207}Pb/^{235}U$		$^{206}Pb/^{238}U$		$^{207}Pb/^{206}Pb$		$^{207}Pb/^{235}U$		$^{206}Pb/^{238}U$	
QL09-10-13	21	31	160	0.19	0.05965	0.00204	0.67182	0.02184	0.08169	0.0009	591	76	522	13	506	5
QL09-10-14	242	827	1252	0.66	0.05587	0.00161	0.56260	0.01738	0.07232	0.0007	447	52	453	11	450	4
QL09-10-15	4	6	32	0.19	0.05852	0.00221	0.55256	0.02041	0.06848	0.0005	549	84	447	13	427	3
QL09-10-16	4	9	36	0.26	0.05527	0.00184	0.53709	0.01745	0.07047	0.0005	423	76	437	12	439	3
QL09-10-17	16	23	172	0.13	0.05545	0.00167	0.49582	0.01444	0.06485	0.0005	431	69	409	10	405	3
QL09-10-18	74	121	752	0.16	0.05763	0.00112	0.61972	0.01180	0.07736	0.0005	516	30	490	7	480	3
QL09-10-19	110	181	1130	0.16	0.05570	0.00123	0.59538	0.01288	0.07700	0.0007	441	33	474	8	478	4
QL09-10-20	35	61	367	0.17	0.05528	0.00160	0.53708	0.01492	0.07047	0.0006	424	66	436	10	439	4
QL09-10-21	302	457	3282	0.14	0.05655	0.00101	0.60792	0.01047	0.07753	0.0005	474	27	482	7	481	3
QL09-10-22	437	877	4771	0.18	0.05576	0.00107	0.54860	0.01030	0.07095	0.0005	443	30	444	7	442	3
QL09-10-23	269	524	2882	0.18	0.05557	0.00110	0.55034	0.01073	0.07149	0.0005	435	32	445	7	445	3
QL09-10-24	78	157	781	0.20	0.05529	0.00113	0.54773	0.01240	0.07140	0.0008	424	30	444	8	445	5
QL09-12-1	397	1361	1010	1.35	0.06054	0.00410	0.58793	0.03911	0.07044	0.0009	623	150	470	25	439	5
QL09-12-2	528	1497	1101	1.36	0.09139	0.00860	0.93795	0.08700	0.07444	0.0012	1455	186	672	46	463	7
QL09-12-3	155	522	615	0.85	0.05640	0.00155	0.55923	0.01557	0.07144	0.0006	468	47	451	10	445	4
QL09-12-4	730	1607	1447	1.11	0.04951	0.00566	0.42918	0.04872	0.06287	0.0009	172	254	363	35	393	5
QL09-12-5	596	1802	1331	1.35	0.07511	0.00195	0.77712	0.02130	0.07447	0.0008	1071	38	584	12	463	5
QL09-12-6	196	585	679	0.86	0.05649	0.00364	0.53695	0.03416	0.06894	0.0007	472	147	436	23	430	4
QL09-12-7	191	520	726	0.72	0.05568	0.00342	0.54025	0.03252	0.07037	0.0009	440	141	439	21	438	5
QL09-12-8	337	420	783	0.54	0.04735	0.00999	0.41532	0.08744	0.06361	0.0009	67	363	353	63	398	6
QL09-12-9	195	616	749	0.82	0.05962	0.00146	0.59079	0.01486	0.07120	0.0005	590	42	471	9	443	3
QL09-12-10	252	623	716	0.87	0.06084	0.00564	0.56205	0.05163	0.06700	0.0008	634	207	453	34	418	5
QL09-12-11	437	782	789	0.99	0.06495	0.00927	0.58178	0.08250	0.06496	0.0010	773	318	466	53	406	6
QL09-12-12	348	880	1002	0.88	0.08846	0.00278	0.88699	0.02824	0.07194	0.0006	1392	48	645	15	448	4
QL09-12-13	376	1046	1549	0.68	0.05818	0.00301	0.57567	0.02905	0.07177	0.0008	536	116	462	19	447	5
QL09-12-14	398	1178	1068	1.10	0.05670	0.00373	0.56287	0.03673	0.07199	0.0006	480	150	453	24	448	4
QL09-12-15	283	616	716	0.86	0.07517	0.00572	0.72113	0.05432	0.06958	0.0008	1073	158	551	32	434	4
QL09-12-16	231	777	740	1.05	0.06005	0.00147	0.58434	0.01329	0.07031	0.0005	605	37	467	9	438	3
QL09-12-17	162	502	723	0.69	0.05760	0.00141	0.56229	0.01324	0.07063	0.0005	515	39	453	9	440	3
QL09-12-18	175	419	530	0.79	0.06854	0.00474	0.65885	0.04463	0.06972	0.0010	885	147	514	27	434	6

Table 4.3 Zircon in situ LA-ICP-MS dating results

	Pb	Th	U	Th/U	CORRECTED RATIOS						CORRECTED AGES (Ma)					
	Total	232	238		$^{207}Pb/^{206}Pb$		$^{207}Pb/^{235}U$		$^{206}Pb/^{238}U$		$^{207}Pb/^{206}Pb$		$^{207}Pb/^{235}U$		$^{206}Pb/^{238}U$	
	ppm	ppm	ppm													
QL09-12-19	440	1320	1272	1.04	0.06067	0.00147	0.65434	0.01628	0.07789	0.0007	628	39	511	10	484	4
QL09-12-20	346	1086	1216	0.89	0.05894	0.00142	0.60715	0.01403	0.07447	0.0005	565	38	482	9	463	3
QL09-12-21	263	839	905	0.93	0.06074	0.00284	0.59792	0.02747	0.07139	0.0006	630	103	476	17	445	4
QL09-12-22	410	1267	1225	1.03	0.05917	0.00268	0.57977	0.02581	0.07106	0.0006	573	101	464	17	443	3
QL09-12-23	434	1208	1064	1.13	0.06187	0.00648	0.57110	0.05924	0.06695	0.0010	669	234	459	38	418	6
QL09-12-24	490	1210	1195	1.01	0.06628	0.00672	0.71900	0.07233	0.07867	0.0010	815	221	550	43	488	6
QL09-14-1	70	99	778	0.13	0.05786	0.00147	0.56526	0.01378	0.07086	0.0005	524	57	455	9	441	3
QL09-14-2	46	156	197	0.79	0.07061	0.00205	0.65187	0.01825	0.06734	0.0006	946	43	510	11	420	4
QL09-14-3	190	240	1019	0.24	0.09277	0.00221	0.91591	0.02396	0.07132	0.0006	1483	37	660	13	444	3
QL09-14-4	410	1164	1626	0.72	0.07390	0.00251	0.72673	0.02154	0.07202	0.0006	1039	46	555	13	448	4
QL09-14-5	23	53	183	0.29	0.05779	0.00178	0.56688	0.01727	0.07151	0.0008	522	48	456	11	445	4
QL09-14-6	1290	1539	2988	0.52	0.05970	0.00802	0.54368	0.07277	0.06605	0.0008	593	304	441	48	412	5
QL09-14-7	28	90	164	0.55	0.05219	0.00213	0.51209	0.02061	0.07144	0.0009	294	70	420	14	445	5
QL09-14-8	350	395	863	0.46	0.07478	0.00260	1.66908	0.05574	0.16188	0.0016	1063	72	997	21	967	9
QL09-14-9	26	67	214	0.31	0.05745	0.00194	0.56564	0.02003	0.07139	0.0008	509	58	455	13	445	5
QL09-14-10	139	81	852	0.10	0.06645	0.00240	0.99968	0.03184	0.10911	0.0019	821	77	704	16	668	11
QL09-14-11	98	77	476	0.16	0.07092	0.00110	1.59303	0.02696	0.16220	0.0014	955	21	967	11	969	8
QL09-14-12	187	277	1116	0.25	0.05816	0.00186	0.72824	0.02169	0.09081	0.0011	536	72	556	13	560	6
QL09-14-13	1330	1114	2113	0.53	0.07003	0.01214	0.62354	0.10750	0.06458	0.0012	929	384	492	67	403	7
QL09-14-14	277	150	950	0.16	0.07062	0.00205	1.33558	0.03769	0.13717	0.0009	946	61	861	16	829	5
QL09-14-15	25	28	98	0.29	0.06118	0.00517	0.56184	0.04691	0.06661	0.0009	645	188	453	30	416	5
QL09-14-16	400	327	1517	0.22	0.07171	0.00138	1.55580	0.02791	0.15735	0.0011	978	40	953	11	942	6
QL09-14-17	65	236	298	0.79	0.05448	0.00135	0.53904	0.01378	0.07154	0.0007	391	39	438	9	445	4
QL09-14-18	70	204	507	0.40	0.05711	0.00154	0.56700	0.01590	0.07157	0.0007	496	44	456	10	446	4
QL09-14-19	332	184	321	0.57	0.14153	0.00302	7.00337	0.13986	0.35889	0.0027	2246	38	2112	18	1977	13
QL09-14-20	101	342	394	0.87	0.06122	0.00178	0.60390	0.01644	0.07153	0.0005	647	46	480	10	445	3
QL09-14-21	108	283	489	0.58	0.07595	0.00160	0.75585	0.01687	0.07179	0.0007	1094	30	572	10	447	4
QL09-14-22	23	68	145	0.47	0.05785	0.00231	0.56541	0.02081	0.07140	0.0007	524	63	455	13	445	4
QL09-14-23	44	146	213	0.68	0.05820	0.00168	0.57800	0.01683	0.07176	0.0006	537	48	463	11	447	4

Table 4.3 Zircon in situ LA-ICP-MS dating results

	Pb	Th	U	Th/U	CORRECTED RATIOS						CORRECTED AGES (Ma)					
	Total ppm	232 ppm	238 ppm		$^{207}Pb/^{206}Pb$		$^{207}Pb/^{235}U$		$^{206}Pb/^{238}U$		$^{207}Pb/^{206}Pb$		$^{207}Pb/^{235}U$		$^{206}Pb/^{238}U$	
QL09-14-24	79	257	433	0.59	0.05512	0.00127	0.54332	0.01226	0.07128	0.0005	417	37	441	8	444	3
QL09-15-1	112	128	366	0.35	0.07004	0.00125	1.48930	0.02848	0.15392	0.0015	930	23	926	12	923	8
QL09-15-2	187	93	224	0.42	0.10331	0.00365	3.56049	0.11822	0.24995	0.0031	1684	67	1541	26	1438	16
QL09-15-3	79	103	254	0.41	0.07120	0.00130	1.51978	0.02908	0.15440	0.0012	963	26	938	12	926	7
QL09-15-4	177	170	552	0.31	0.07515	0.00119	1.72028	0.02994	0.16545	0.0014	1072	21	1016	11	987	8
QL09-15-5	108	137	340	0.40	0.06911	0.00119	1.47183	0.02569	0.15426	0.0013	902	22	919	11	925	7
QL09-15-6	132	136	582	0.23	0.07166	0.00162	1.51156	0.03288	0.15268	0.0012	976	32	935	13	916	7
QL09-15-7	180	195	736	0.26	0.07118	0.00120	1.51504	0.02561	0.15400	0.0010	963	23	936	10	923	6
QL09-15-8	125	169	394	0.43	0.06946	0.00120	1.48267	0.02662	0.15446	0.0012	912	24	923	11	926	7
QL09-15-9	92	114	280	0.41	0.07144	0.00132	1.52064	0.02793	0.15415	0.0012	970	25	939	11	924	7
QL09-15-10	162	196	518	0.38	0.07055	0.00115	1.50542	0.02493	0.15430	0.0011	944	23	933	10	925	6
QL09-15-11	73	69	296	0.23	0.07159	0.00135	1.52436	0.03039	0.15410	0.0015	974	25	940	12	924	8
QL09-15-12	98	67	368	0.18	0.07153	0.00183	1.49866	0.03674	0.15196	0.0011	972	53	930	15	912	6
QL09-15-13	123	174	326	0.53	0.07128	0.00153	1.51714	0.03207	0.15414	0.0013	966	30	937	13	924	7
QL09-15-14	143	121	365	0.33	0.08493	0.00153	2.29015	0.04904	0.19379	0.0020	1314	26	1209	15	1142	11
QL09-15-15	109	145	296	0.49	0.07248	0.00132	1.54529	0.02854	0.15434	0.0012	999	25	949	11	925	7
QL09-15-16	62	68	225	0.30	0.07303	0.00151	1.55895	0.03174	0.15463	0.0011	1015	30	954	13	927	6
QL09-15-17	99	107	347	0.31	0.06964	0.00135	1.48600	0.02910	0.15432	0.0011	918	28	925	12	925	6
QL09-15-18	154	112	281	0.40	0.10652	0.00258	3.17241	0.07252	0.21601	0.0017	1741	45	1450	18	1261	9
QL09-15-19	75	89	243	0.37	0.07273	0.00143	1.55115	0.03146	0.15424	0.0014	1006	27	951	13	925	8
QL09-15-20	106	104	296	0.35	0.07302	0.00327	1.52746	0.06713	0.15172	0.0013	1014	93	941	27	911	7
QL09-15-21	70	72	283	0.25	0.07040	0.00140	1.50080	0.02885	0.15411	0.0009	940	29	931	12	924	5
QL09-15-22	87	103	312	0.33	0.07154	0.00125	1.52702	0.02734	0.15432	0.0013	973	23	941	11	925	7
QL09-15-23	82	101	226	0.44	0.07183	0.00172	1.53190	0.03541	0.15414	0.0011	981	35	943	14	924	6
QL09-15-24	47	51	129	0.39	0.07075	0.00198	1.50752	0.04108	0.15408	0.0014	950	41	933	17	924	8
QL09-18-1	95	241	500	0.48	0.05750	0.00125	0.64760	0.01360	0.08148	0.0007	511	31	507	8	505	4
QL09-18-2	60	135	309	0.44	0.05877	0.00146	0.66234	0.01791	0.08129	0.0009	558	40	516	11	504	5
QL09-18-3	62	171	296	0.58	0.05537	0.00176	0.62251	0.01933	0.08125	0.0008	427	52	491	12	504	5
QL09-18-4	130	297	675	0.44	0.05946	0.00110	0.66966	0.01209	0.08136	0.0005	584	28	521	7	504	3

Table 4.3 Zircon in situ LA-ICP-MS dating results

	Pb	Th	U	Th/U	CORRECTED RATIOS						CORRECTED AGES (Ma)					
	Total	232	238		$^{207}Pb/^{206}Pb$		$^{207}Pb/^{235}U$		$^{206}Pb/^{238}U$		$^{207}Pb/^{206}Pb$		$^{207}Pb/^{235}U$		$^{206}Pb/^{238}U$	
	ppm	ppm	ppm													
QL09-18-5	51	131	283	0.46	0.05989	0.00156	0.65350	0.01697	0.07882	0.0006	600	42	511	10	489	4
QL09-18-6	79	199	373	0.53	0.05425	0.00134	0.61123	0.01577	0.08143	0.0009	381	39	484	10	505	5
QL09-18-7	39	99	200	0.49	0.05674	0.00278	0.63674	0.03127	0.08093	0.0010	482	87	500	19	502	6
QL09-18-8	78	201	366	0.55	0.05829	0.00180	0.65054	0.01973	0.08064	0.0007	541	52	509	12	500	4
QL09-18-9	23	53	134	0.40	0.05802	0.00194	0.65108	0.02212	0.08111	0.0008	530	58	509	14	503	5
QL09-18-10	49	104	225	0.46	0.05875	0.00150	0.65636	0.01616	0.08079	0.0007	558	39	512	10	501	4
QL09-18-11	75	178	404	0.44	0.05819	0.00119	0.66032	0.01328	0.08199	0.0007	537	29	515	8	508	4
QL09-18-12	21	50	126	0.40	0.05664	0.00227	0.63370	0.02456	0.08104	0.0009	477	67	498	15	502	5
QL09-18-13	63	159	355	0.45	0.05659	0.00135	0.63649	0.01461	0.08120	0.0007	476	36	500	9	503	4
QL09-18-14	70	162	398	0.41	0.05679	0.00156	0.63384	0.01674	0.08068	0.0008	483	41	498	10	500	5
QL09-18-15	67	155	358	0.43	0.05744	0.00195	0.63916	0.02104	0.08070	0.0007	509	77	502	13	500	4
QL09-18-16	89	239	446	0.53	0.05716	0.00146	0.63862	0.01592	0.08076	0.0006	498	42	501	10	501	4
QL09-18-17	118	323	565	0.57	0.05792	0.00117	0.65056	0.01310	0.08127	0.0006	527	31	509	8	504	4
QL09-18-18	26	54	135	0.40	0.05444	0.00202	0.61292	0.02364	0.08123	0.0008	389	68	485	15	503	5
QL09-18-19	37	81	208	0.39	0.05791	0.00255	0.64465	0.02747	0.08074	0.0009	526	99	505	17	501	5
QL09-18-20	54	129	310	0.42	0.05811	0.00153	0.65257	0.01800	0.08124	0.0008	534	43	510	11	504	5
QL09-18-21	38	89	228	0.39	0.05533	0.00151	0.62238	0.01757	0.08128	0.0007	426	47	491	11	504	4
QL09-18-22	95	227	476	0.48	0.05729	0.00117	0.64046	0.01305	0.08083	0.0006	503	33	503	8	501	3
QL09-18-23	66	165	366	0.45	0.05924	0.00131	0.66163	0.01414	0.08109	0.0006	576	33	516	9	503	4
QL09-18-24	80	182	344	0.53	0.05706	0.00140	0.63729	0.01523	0.08084	0.0006	494	39	501	9	501	4
QL10-34-01	258	603	1045	0.58	0.05639	0.00094	0.63204	0.01079	0.08081	0.0006	468	25	497	7	501	3
QL10-34-02	401	870	1175	0.74	0.06053	0.00114	0.67510	0.01286	0.08035	0.0005	623	30	524	8	498	3
QL10-34-03	389	847	1199	0.71	0.06874	0.00198	0.76581	0.02436	0.08000	0.0007	891	51	577	14	496	4
QL10-34-04	103	204	595	0.34	0.05815	0.00116	0.59526	0.01172	0.07378	0.0006	535	30	474	7	459	3
QL10-34-05	639	1419	1513	0.94	0.05551	0.00101	0.64115	0.01141	0.08320	0.0007	433	25	503	7	515	4
QL10-34-06	244	499	860	0.58	0.05878	0.00111	0.67483	0.01277	0.08267	0.0007	559	27	524	8	512	4
QL10-34-07	178	374	683	0.55	0.05760	0.00124	0.60978	0.01276	0.07641	0.0006	515	31	483	8	475	4
QL10-34-08	300	666	1030	0.65	0.05813	0.00146	0.61861	0.01740	0.07668	0.0011	535	38	489	11	476	6
QL10-34-09	224	485	778	0.62	0.05862	0.00119	0.64594	0.01274	0.07973	0.0006	553	29	506	8	495	4
QL10-34-10	400	857	1138	0.75	0.05738	0.00129	0.65522	0.01669	0.08208	0.0008	506	40	512	10	509	5

Table 4.3 Zircon in situ LA-ICP-MS dating results

	Pb	Th	U	Th/U	CORRECTED RATIOS						CORRECTED AGES (Ma)					
	Total	232	238		$^{207}Pb/^{206}Pb$		$^{207}Pb/^{235}U$		$^{206}Pb/^{238}U$		$^{207}Pb/^{206}Pb$		$^{207}Pb/^{235}U$		$^{206}Pb/^{238}U$	
	ppm	ppm	ppm													
QL10-34-11	308	598	752	0.79	0.08090	0.00391	0.86980	0.04143	0.07798	0.0007	1219	98	635	22	484	4
QL10-34-12	416	1042	1182	0.88	0.05778	0.00104	0.60863	0.01116	0.07600	0.0005	521	29	483	7	472	3
QL10-34-13	309	676	946	0.71	0.06498	0.00257	0.69063	0.02651	0.07709	0.0008	774	85	533	16	479	4
QL10-34-14	100	182	590	0.31	0.05786	0.00205	0.60334	0.02089	0.07562	0.0006	525	80	479	13	470	4
QL10-34-15	288	672	899	0.75	0.05466	0.00118	0.60084	0.01252	0.07929	0.0006	398	32	478	8	492	4
QL10-34-16	111.6	115	1415	0.08	0.05791	0.00128	0.58742	0.01313	0.07307	0.0007	526	32	469	8	455	4
QL10-34-17	364	853	1183	0.72	0.05830	0.00118	0.62821	0.01304	0.07766	0.0007	541	30	495	8	482	4
QL10-34-18	228	605	715	0.85	0.07838	0.00272	0.81436	0.02950	0.07469	0.0006	1157	58	605	17	464	4
QL10-34-19	344	799	1139	0.70	0.06112	0.00129	0.66151	0.01582	0.07782	0.0007	643	36	516	10	483	4
QL10-34-20	330	841	1047	0.80	0.05858	0.00104	0.63200	0.01175	0.07785	0.0006	552	27	497	7	483	4
QL10-37-01	75.5	325	722	0.45	0.05885	0.00209	0.62329	0.02157	0.07681	0.0006	562	79	492	13	477	4
QL10-37-02	190	553	2027	0.27	0.05783	0.00089	0.64671	0.00882	0.08100	0.0006	523	18	506	5	502	3
QL10-37-03	111	340	1175	0.29	0.05953	0.00148	0.66269	0.01555	0.08074	0.0007	586	55	516	9	501	4
QL10-37-04	54.4	128	533	0.24	0.09554	0.00234	1.09069	0.02936	0.08203	0.0006	1539	39	749	14	508	4
QL10-37-05	88.7	228	964	0.24	0.05566	0.00096	0.62585	0.01061	0.08122	0.0005	439	26	494	7	503	3
QL10-37-06	109	287	1095	0.26	0.06112	0.00125	0.73183	0.01652	0.08603	0.0006	644	36	558	10	532	4
QL10-37-07	73.8	203	806	0.25	0.05468	0.00124	0.61049	0.01346	0.08068	0.0006	399	37	484	8	500	3
QL10-37-08	10.66	66.6	117	0.57	0.05684	0.00290	0.56163	0.02653	0.07239	0.0008	485	85	453	17	451	5
QL10-37-09	120	401	1405	0.29	0.06087	0.00193	0.60477	0.01839	0.07206	0.0007	635	70	480	12	449	4
QL10-37-10	39.4	66.9	102	0.66	0.10467	0.00193	4.40830	0.09139	0.30379	0.0031	1709	23	1714	17	1710	16
QL10-37-11	121	706	1199	0.59	0.05677	0.00094	0.63478	0.01054	0.08073	0.0005	482	26	499	7	500	3
QL10-37-12	42.5	233	485	0.48	0.05479	0.00125	0.54443	0.01259	0.07173	0.0005	404	39	441	8	447	3
QL10-37-13	47.5	248	543	0.46	0.05778	0.00107	0.57606	0.01073	0.07197	0.0005	521	30	462	7	448	3
QL10-37-14	203	902	353	2.55	0.10773	0.00144	4.78717	0.06708	0.32065	0.0024	1761	15	1783	12	1793	12
QL10-37-15	44.3	102	116	0.88	0.09732	0.00198	3.78404	0.07424	0.28172	0.0026	1573	23	1589	16	1600	13
QL10-37-16	79.0	273	858	0.32	0.05246	0.00177	0.58923	0.01869	0.08082	0.0007	305	57	470	12	501	4
QL10-37-17	133	301	1203	0.25	0.09905	0.00582	1.15547	0.06212	0.08380	0.0009	1606	84	780	29	519	5
QL10-37-18	54.9	168	660	0.25	0.04923	0.00441	0.49881	0.04083	0.07238	0.0006	159	170	411	28	450	3
QL10-37-19	51.4	285	564	0.51	0.05732	0.00692	0.58415	0.06413	0.07247	0.0005	504	235	467	41	451	3
QL10-37-20	27.4	160	308	0.52	0.04683	0.00734	0.47863	0.06807	0.07237	0.0006	40	257	397	47	450	4

Table 4.3 Zircon in situ LA-ICP-MS dating results

	Pb	Th	U	Th/U	CORRECTED RATIOS						CORRECTED AGES (Ma)					
	Total ppm	232 ppm	238 ppm		$^{207}Pb/^{206}Pb$		$^{207}Pb/^{235}U$		$^{206}Pb/^{238}U$		$^{207}Pb/^{206}Pb$		$^{207}Pb/^{235}U$		$^{206}Pb/^{238}U$	
QL10-37-21	133	387	1171	0.33	0.09224	0.01524	1.10335	0.16555	0.08433	0.0006	1472	289	755	80	522	4
QL10-37-22	107	240	140	1.72	0.13693	0.01884	8.92275	1.11621	0.46298	0.0031	2189	216	2330	114	2453	13
QL10-37-23	47.4	154	531	0.29	0.04703	0.00532	0.50605	0.05234	0.07673	0.0005	51	214	416	35	477	3
QL10-37-24	39.3	50.8	156	0.33	0.07775	0.00688	2.27742	0.18796	0.20856	0.0029	1141	144	1205	58	1221	15
QL10-37-25	96.1	335	1018	0.33	0.05227	0.00345	0.58837	0.03577	0.08074	0.0004	297	131	470	23	501	3
Analysed in China University of Geosciences (Beijing)																
QL09-01																
0901-01	20.2	48.5	48.8	0.99	0.11029	0.00425	4.68313	0.17796	0.30789	0.00558	1804	43	1764	32	1730	28
0901-02	45.5	268	285	0.94	0.06613	0.00243	1.11895	0.04076	0.1227	0.0021	810	48	762	20	746	12
0901-03	61.9	399	353	1.13	0.06705	0.00245	1.214	0.04405	0.13129	0.00224	839	47	807	20	795	13
0901-04	77.4	248	101	2.46	0.15272	0.01721	8.70105	0.95091	0.41321	0.01137	2377	200	2307	100	2230	52
0901-05	135	205	217	0.95	0.17229	0.00616	10.82438	0.38549	0.45561	0.00773	2580	37	2508	33	2420	34
0901-06	94.5	140	167	0.84	0.16974	0.00615	9.86511	0.35584	0.42148	0.0072	2555	38	2422	33	2267	33
0901-07	9.44	60.6	54.0	1.12	0.06813	0.00332	1.21856	0.05802	0.12972	0.00262	873	65	809	27	786	15
0901-08	116	200	246	0.81	0.13715	0.00509	6.78917	0.25059	0.35898	0.00617	2192	40	2084	33	1977	29
0901-09	77.8	70.2	131	0.54	0.17282	0.00653	11.17488	0.41975	0.46895	0.00823	2585	39	2538	35	2479	36
0901-10	79.2	128	154	0.83	0.16095	0.009	8.24874	0.43253	0.3717	0.00722	2466	97	2259	47	2037	34
0901-11	50.0	63.8	77.7	0.82	0.17447	0.00702	11.55627	0.46083	0.48041	0.00874	2601	42	2569	37	2529	38
0901-12	7.46	15.3	19.2	0.80	0.11679	0.00592	4.86635	0.24034	0.3022	0.00657	1908	58	1796	42	1702	33
0901-13	9.04	73.3	49.8	1.47	0.06554	0.00424	1.15349	0.07298	0.12766	0.00284	792	95	779	34	775	16
0901-14	33.5	84.7	234	0.36	0.06503	0.00292	1.14107	0.0507	0.12727	0.00236	775	62	773	24	772	13
0901-15	59.8	82.7	282	0.29	0.14251	0.00603	3.56173	0.14929	0.18127	0.0033	2258	47	1541	33	1074	18
0901-16	31.8	55.2	89.5	0.62	0.10764	0.00496	4.26401	0.19356	0.28731	0.00557	1760	55	1686	37	1628	28
0901-17	46.0	23.0	125	0.18	0.16695	0.00744	7.26563	0.31978	0.31566	0.00594	2527	49	2145	39	1768	29
0901-18	137	102	421	0.24	0.15577	0.00769	5.88609	0.26882	0.27406	0.00513	2410	86	1959	40	1561	26
0901-19	34.3	180	218	0.83	0.06957	0.00333	1.20314	0.05675	0.12544	0.00241	916	65	802	26	762	14
0901-20	385	58	907	0.06	0.17872	0.00821	9.11269	0.41438	0.36983	0.0069	2641	51	2349	42	2029	32
0901-21	24.3	61.3	163	0.38	0.06675	0.00352	1.21108	0.06287	0.13159	0.00266	830	74	806	29	797	15
0901-22	19.9	97.4	125	0.78	0.07186	0.00391	1.25399	0.0672	0.12656	0.0026	982	76	825	30	768	15
0901-23	14.5	49.0	95	0.51	0.07126	0.00401	1.26781	0.07003	0.12903	0.00273	965	78	831	31	782	16

Table 4.3 Zircon in situ LA-ICP-MS dating results

	Pb	Th	U	Th/U	CORRECTED RATIOS						CORRECTED AGES (Ma)					
	Total ppm	232 ppm	238 ppm		$^{207}Pb/^{206}Pb$		$^{207}Pb/^{235}U$		$^{206}Pb/^{238}U$		$^{207}Pb/^{206}Pb$		$^{207}Pb/^{235}U$		$^{206}Pb/^{238}U$	
0901-24	25.4	134	165	0.81	0.06738	0.00363	1.14738	0.0608	0.12351	0.00253	850	76	776	29	751	15
0901-25	89.6	102	179	0.57	0.17897	0.01112	9.44774	0.5522	0.38287	0.00804	2643	106	2382	54	2090	37
0901-26	74.4	49.7	130	0.38	0.17431	0.00936	11.2535	0.59684	0.46825	0.00954	2599	61	2544	49	2476	42
0901-27	150	96.4	237	0.41	0.22842	0.01241	15.54472	0.83427	0.49356	0.01004	3041	60	2849	51	2586	43
0901-28	117	86.5	215	0.40	0.18519	0.01024	11.2797	0.61602	0.44175	0.00907	2700	63	2547	51	2358	41
0901-29	128	48.4	269	0.18	0.16352	0.0092	9.30069	0.51685	0.41251	0.00856	2492	66	2368	51	2226	39
0901-30	11.6	59.5	70.7	0.84	0.06995	0.00437	1.25808	0.07727	0.13044	0.00291	927	89	827	35	790	17
0901-31	16.4	108.5	93.4	1.16	0.06806	0.00433	1.22618	0.0768	0.13065	0.00295	870	92	813	35	792	17
0901-32	20.9	117	135	0.87	0.06817	0.00438	1.1539	0.07297	0.12275	0.00274	874	94	779	34	746	16
0901-33	14.3	106	81	1.31	0.07638	0.00509	1.30764	0.08556	0.12415	0.0029	1105	93	849	38	754	17
0901-35	212	316	340	0.93	0.17357	0.01109	11.0977	0.70021	0.46364	0.0103	2592	75	2531	59	2456	45
0901-36	86.8	67.9	154	0.44	0.18048	0.01192	11.39228	0.74301	0.45769	0.01042	2657	78	2556	61	2429	46
0901-37	115	77.2	203	0.38	0.19408	0.01301	12.41457	0.82166	0.4638	0.01063	2777	78	2636	62	2456	47
0901-38	17.3	59.8	120	0.50	0.06995	0.00497	1.19109	0.08335	0.12345	0.00296	927	104	796	39	750	17
0901-39	80.2	118	176	0.67	0.15326	0.01061	7.61041	0.5202	0.36002	0.00842	2383	84	2186	61	1982	40
0901-40	139	50.8	295	0.17	0.16955	0.01189	9.52256	0.65976	0.40718	0.00958	2553	84	2390	64	2202	44
0901-41	115	86.9	202	0.43	0.19075	0.014	12.18047	0.88322	0.46289	0.01122	2749	87	2618	68	2452	49
0901-42	208	292	338	0.86	0.19312	0.01437	12.16809	0.89493	0.45674	0.01115	2769	89	2617	69	2425	49
0901-43	13.2	77.7	73	1.06	0.06694	0.00586	1.26547	0.10859	0.13703	0.00394	836	131	830	49	828	22
0901-44	8.23	49.6	50.0	0.99	0.07382	0.00637	1.29179	0.10937	0.12684	0.00357	1037	126	842	48	770	20
0901-46	49.4	64.2	86.9	0.74	0.18531	0.01488	11.12404	0.88326	0.43506	0.01128	2701	97	2534	74	2328	51
0901-45	71.3	112	123	0.92	0.1783	0.0139	10.49273	0.80873	0.42655	0.01081	2637	94	2479	71	2290	49
0901-47	63.1	341	385	0.89	0.06947	0.00568	1.24913	0.10098	0.13031	0.00339	913	124	823	46	790	19
0901-48	49.5	356	291	1.22	0.07048	0.00586	1.21034	0.09951	0.12444	0.00328	942	126	805	46	756	19
QL09-02																
0902-01	72.1	372	437	0.85	0.06658	0.00146	1.22632	0.02874	0.13356	0.00207	825	25	813	13	808	12
0902-02	31.5	160	201	0.80	0.06646	0.00164	1.17716	0.03035	0.12844	0.00205	821	29	790	14	779	12
0902-03	37.9	336	244	1.38	0.07064	0.00174	1.11274	0.02862	0.11423	0.00182	947	28	759	14	697	11
0902-04	68.1	270	602	0.45	0.0626	0.00138	0.85483	0.02006	0.09902	0.00153	695	26	627	11	609	9
0902-05	37.9	98.3	511	0.19	0.05578	0.00138	0.54729	0.01416	0.07114	0.00112	444	31	443	9	443	7
0902-06	70.1	36.4	200	0.18	0.14761	0.0041	6.32483	0.14648	0.31077	0.00478	2318	49	2022	20	1745	24

Table 4.3 Zircon in situ LA-ICP-MS dating results

	Pb	Th	U	Th/U	CORRECTED RATIOS						CORRECTED AGES (Ma)					
	Total	232	238		$^{207}Pb/^{206}Pb$		$^{207}Pb/^{235}U$		$^{206}Pb/^{238}U$		$^{207}Pb/^{206}Pb$		$^{207}Pb/^{235}U$		$^{206}Pb/^{238}U$	
	ppm	ppm	ppm													
0902-07	55.2	10.4	757	0.01	0.05601	0.00128	0.56896	0.0138	0.07366	0.00114	453	28	457	9	458	7
0902-08	39.5	56.0	486	0.12	0.057	0.00139	0.62261	0.01589	0.0792	0.00125	492	30	491	10	491	7
0902-09	9.93	56.9	57.8	0.99	0.06433	0.00257	1.20223	0.0478	0.13553	0.0025	752	53	802	22	819	14
0902-11	109	145	482	0.30	0.0888	0.00318	2.39007	0.07673	0.1952	0.00308	1400	70	1240	23	1149	17
0902-12	45.0	258	277	0.93	0.06573	0.00162	1.18052	0.03034	0.13024	0.00206	798	29	792	14	789	12
0902-13	54.3	13.9	708	0.02	0.06074	0.00178	0.63802	0.01603	0.07618	0.00115	630	65	501	10	473	7
0902-14	105	36.6	1427	0.03	0.05618	0.00127	0.57774	0.01385	0.07457	0.00115	459	28	463	9	464	7
0902-15	59.1	191	442	0.43	0.06601	0.00157	1.08526	0.027	0.11923	0.00186	807	27	746	13	726	11
0902-16	14.5	37.4	186	0.20	0.05939	0.00218	0.60242	0.02196	0.07356	0.00132	581	48	479	14	458	8
0902-17	55.7	59.0	744	0.08	0.05956	0.00191	0.59954	0.01683	0.073	0.00112	588	71	477	11	454	7
0902-18	69.6	98.1	208	0.47	0.13152	0.00527	4.64702	0.16915	0.25626	0.00431	2118	72	1758	30	1471	22
0902-19	57.7	222	428	0.52	0.06605	0.00167	1.06968	0.02806	0.11744	0.00187	808	29	739	14	716	11
0902-20	78.4	89.4	193	0.46	0.14564	0.0051	6.61978	0.2048	0.32965	0.0054	2295	62	2062	27	1837	26
0902-21	56.5	27.7	785	0.04	0.05695	0.00148	0.57045	0.01525	0.07264	0.00115	490	32	458	10	452	7
0902-22	175	181	429	0.42	0.14848	0.00498	6.98811	0.20565	0.34134	0.00549	2328	59	2110	26	1893	26
0902-23	44.8	251	278	0.90	0.06857	0.00189	1.2181	0.03421	0.12882	0.00209	886	32	809	16	781	12
0902-24	79.4	156	708	0.22	0.06029	0.00229	0.87789	0.03026	0.1056	0.00168	614	84	640	16	647	10
0902-25	39.7	35	544	0.06	0.05756	0.00166	0.57684	0.01686	0.07266	0.00119	513	36	462	11	452	7
0902-26	16.2	134	85	1.57	0.06658	0.00232	1.24239	0.04299	0.13531	0.0024	825	43	820	19	818	14
0902-27	48.6	47	105	0.45	0.14889	0.00587	7.55668	0.26757	0.3681	0.00636	2333	69	2180	32	2020	30
0902-28	14.2	43	188	0.23	0.05671	0.00198	0.56909	0.01979	0.07277	0.00126	480	47	457	13	453	8
0902-29	35.1	58	432	0.13	0.05797	0.00175	0.57071	0.0174	0.07139	0.00118	529	39	458	11	445	7
0902-30	61.1	221	425	0.52	0.06678	0.00188	1.17166	0.03345	0.12721	0.00207	831	33	787	16	772	12
0902-31	28.5	68	378	0.18	0.05556	0.00173	0.56543	0.0177	0.07379	0.00123	435	41	455	11	459	7
0902-32	52.9	410	658	0.62	0.05557	0.00165	0.53906	0.01617	0.07034	0.00116	435	38	438	11	438	7
0902-33	98.3	136	1153	0.12	0.07895	0.00226	0.90346	0.02619	0.08297	0.00135	1171	32	654	14	514	8
0902-34	24.4	164	156	1.05	0.06552	0.00221	1.10506	0.03713	0.1223	0.00212	791	42	756	18	744	12
0902-35	45.2	166	339	0.49	0.06396	0.00198	1.04186	0.03235	0.11811	0.00198	740	38	725	16	720	11
0902-36	103	104	195	0.54	0.16688	0.00649	9.95461	0.34698	0.43262	0.00745	2527	67	2431	32	2318	34
0902-37	12.3	21.6	28.3	0.76	0.10846	0.00384	5.44752	0.19172	0.3642	0.00699	1774	37	1892	30	2002	33
0902-38	408	98.4	938	0.10	0.16662	0.00493	9.07813	0.27057	0.39507	0.0065	2524	29	2346	27	2146	30

Table 4.3 Zircon in situ LA-ICP-MS dating results

	Pb	Th	U	Th/U	CORRECTED RATIOS						CORRECTED AGES (Ma)					
	Total ppm	232 ppm	238 ppm		$^{207}Pb/^{206}Pb$		$^{207}Pb/^{235}U$		$^{206}Pb/^{238}U$		$^{207}Pb/^{206}Pb$		$^{207}Pb/^{235}U$		$^{206}Pb/^{238}U$	
0902-39	43.6	140	307	0.46	0.0658	0.00211	1.16319	0.03731	0.12817	0.00217	800	39	783	18	777	12
0902-40	36.2	192	254	0.76	0.06428	0.00213	1.06679	0.03511	0.12035	0.00206	751	41	737	17	733	12
0902-41	16.4	196	168	1.16	0.07047	0.00263	0.71686	0.02633	0.07376	0.00134	942	46	549	16	459	8
QL09-10																
0910-01	99.3	193	1287	0.15	0.05706	0.00104	0.59115	0.0119	0.07512	0.00111	494	21	472	8	467	7
0910-02	86.7	203	1095	0.19	0.05587	0.00176	0.57189	0.01588	0.07424	0.0011	447	72	459	10	462	7
0910-03	41.2	125	530	0.24	0.05612	0.00111	0.5752	0.01232	0.07432	0.00111	457	23	461	8	462	7
0910-04	80.7	324	985	0.33	0.05789	0.00203	0.59423	0.01884	0.07445	0.00112	526	79	474	12	463	7
0910-05	90.3	316	1100	0.29	0.05773	0.00202	0.59229	0.01873	0.0744	0.00111	520	79	472	12	463	7
0910-06	62.2	186	796	0.23	0.05751	0.00114	0.59134	0.01262	0.07457	0.00112	511	23	472	8	464	7
0910-07	41.7	156	521	0.30	0.05637	0.00115	0.58634	0.01286	0.07542	0.00114	467	24	469	8	469	7
0910-09	35.7	137	446	0.31	0.05897	0.0013	0.60642	0.01417	0.07457	0.00114	566	26	481	9	464	7
0910-10	136	771	1607	0.48	0.06225	0.00121	0.64773	0.01362	0.07546	0.00113	683	22	507	8	469	7
0910-12	40.1	112	524	0.21	0.0563	0.0019	0.55869	0.01689	0.07197	0.00109	464	77	451	11	448	7
0910-13	61.3	134	786	0.17	0.057	0.00118	0.59518	0.01319	0.07572	0.00114	492	24	474	8	471	7
0910-14	53.7	191	682	0.28	0.05729	0.00119	0.58629	0.013	0.0742	0.00112	503	24	468	8	461	7
0910-15	68.8	193	872	0.22	0.05696	0.00115	0.59549	0.01298	0.07581	0.00114	490	24	474	8	471	7
0910-16	61.2	188	754	0.25	0.06037	0.00125	0.6321	0.01404	0.07592	0.00115	617	24	497	9	472	7
0910-17	36.3	175	461	0.38	0.05594	0.00133	0.55842	0.01389	0.07239	0.00113	450	29	450	9	451	7
0910-18	50.7	183	630	0.29	0.05884	0.00216	0.60753	0.02015	0.07488	0.00116	561	82	482	13	466	7
0910-19	92.3	655	1045	0.63	0.06044	0.00126	0.64045	0.0143	0.07684	0.00116	619	24	503	9	477	7
0910-20	50.0	183	617	0.30	0.05705	0.00212	0.58736	0.01982	0.07466	0.00115	494	84	469	13	464	7
0910-21	65.9	190	844	0.22	0.05611	0.00119	0.58173	0.01317	0.07518	0.00114	457	25	466	8	467	7
0910-22	95.1	234	1193	0.20	0.05762	0.00202	0.58773	0.01849	0.07398	0.00113	515	79	469	12	460	7
0910-23	127	436	1543	0.28	0.05736	0.00221	0.58994	0.02085	0.0746	0.00115	505	87	471	13	464	7
0910-24	22.5	122	283	0.43	0.05593	0.00141	0.55666	0.01449	0.07217	0.00114	450	31	449	9	449	7
0910-25	49.9	409	572	0.71	0.05902	0.00135	0.59745	0.01436	0.0734	0.00113	568	27	476	9	457	7
0910-26	50.0	176	632	0.28	0.05596	0.00125	0.58051	0.01369	0.07522	0.00116	451	27	465	9	468	7
0910-27	52.2	212	640	0.33	0.05744	0.00225	0.58984	0.02121	0.07447	0.00116	509	88	471	14	463	7
0910-28	28.0	219	314	0.70	0.05827	0.00339	0.59307	0.03299	0.07382	0.00124	540	131	473	21	459	7
0910-29	54.6	172	686	0.25	0.05739	0.0013	0.60103	0.01429	0.07594	0.00117	507	27	478	9	472	7

Table 4.3 Zircon in situ LA-ICP-MS dating results

	Pb	Th	U	Th/U	CORRECTED RATIOS						CORRECTED AGES (Ma)					
	Total ppm	232 ppm	238 ppm		$^{207}Pb/^{206}Pb$		$^{207}Pb/^{235}U$		$^{206}Pb/^{238}U$		$^{207}Pb/^{206}Pb$		$^{207}Pb/^{235}U$		$^{206}Pb/^{238}U$	
0910-30	34.3	142	433	0.33	0.05562	0.00131	0.57105	0.01405	0.07444	0.00116	437	29	459	9	463	7
0910-31	81.8	177	1038	0.17	0.05577	0.00185	0.58293	0.01719	0.07581	0.00117	443	76	466	11	471	7
0910-32	56.7	234	694	0.34	0.05657	0.00238	0.57925	0.02253	0.07426	0.00118	475	95	464	14	462	7
0910-33	19.8	62.1	254	0.24	0.05797	0.0015	0.59547	0.01585	0.07449	0.00119	529	32	474	10	463	7
0910-34	69.3	230	906	0.25	0.05507	0.00206	0.54864	0.01863	0.07226	0.00113	415	86	444	12	450	7
0910-35	83.9	191	1073	0.18	0.05744	0.0013	0.59998	0.01434	0.07574	0.00117	508	27	477	9	471	7
0910-36	47.4	131	613	0.21	0.05486	0.00137	0.56518	0.01466	0.0747	0.00118	407	31	455	10	464	7
QL10-37																
1037-01	51.5	96.6	138		0.11295	0.00197	4.77779	0.0933	0.30671	0.00462	1847	16	1781	16	1724	23
1037-02	19.7	121	244	0.50	0.05647	0.00136	0.56323	0.01427	0.07233	0.00112	471	30	454	9	450	7
1037-06	64.1	84.3	826	0.10	0.05753	0.00175	0.57899	0.01536	0.07299	0.00109	512	68	464	10	454	7
1037-07	28.4	221	337	0.66	0.05793	0.00161	0.57871	0.0165	0.07244	0.00119	527	35	464	11	451	7
1037-08	130.8	323	319	1.01	0.11292	0.00192	4.92152	0.09481	0.31604	0.00472	1847	16	1806	16	1770	23
1037-09	58.4	216	765	0.28	0.05633	0.00107	0.5607	0.01172	0.07217	0.00108	465	22	452	8	449	6
1037-10	171	267	273	0.98	0.1736	0.00288	11.3625	0.21501	0.4746	0.00707	2593	15	2553	18	2504	31
1037-11	63.2	141	193	0.73	0.09701	0.00174	3.6186	0.07232	0.27049	0.00408	1567	18	1554	16	1543	21
1037-12	40.0	95	101	0.94	0.1098	0.00206	4.72204	0.09729	0.31186	0.00479	1796	18	1771	17	1750	24
1037-13	34.4	240	418	0.57	0.05707	0.00117	0.56812	0.01259	0.07219	0.0011	494	24	457	8	449	7
1037-14	30.9	153	387	0.39	0.063	0.00138	0.62826	0.01468	0.07231	0.00112	708	25	495	9	450	7
1037-15	40.9	83.5	110	0.76	0.10991	0.00212	4.6213	0.09739	0.30489	0.00471	1798	18	1753	18	1716	23
1037-16	38.1	68.8	313	0.22	0.0674	0.00142	1.04396	0.02357	0.11231	0.00173	850	23	726	12	686	10
1037-17	86.4	123	224	0.55	0.11359	0.00201	5.15567	0.10197	0.32912	0.00496	1858	17	1845	17	1834	24
1037-19	51.8	200	675	0.30	0.05777	0.00111	0.57991	0.01224	0.07279	0.0011	521	22	464	8	453	7
1037-20	47.0	205	601	0.34	0.05683	0.0012	0.57031	0.01295	0.07278	0.00112	485	25	458	8	453	7
1037-21	25.4	116	325	0.36	0.05643	0.00123	0.56467	0.01314	0.07256	0.00112	469	26	455	9	452	7
1037-22	83.2	70.1	254	0.28	0.10303	0.00184	4.25657	0.08511	0.29956	0.00452	1679	17	1685	16	1689	22
1037-23	102	89.2	1367	0.07	0.05774	0.00106	0.59583	0.01216	0.07482	0.00112	520	21	475	8	465	7
1037-24	81.6	295	950	0.31	0.05751	0.00107	0.64406	0.01326	0.08121	0.00122	511	22	505	8	503	7
1037-25	13.0	42.4	29.3	1.45	0.11083	0.00294	4.89863	0.13325	0.32051	0.00549	1813	26	1802	23	1792	27
1037-27	81.1	343	932	0.37	0.06123	0.00114	0.67943	0.01404	0.08047	0.00121	647	21	526	8	499	7
1037-28	64.5	204	792	0.26	0.05728	0.00108	0.61538	0.01278	0.0779	0.00117	502	22	487	8	484	7

Table 4.3 Zircon in situ LA-ICP-MS dating results

	Pb	Th	U	Th/U	CORRECTED RATIOS						CORRECTED AGES (Ma)					
	Total ppm	232 ppm	238 ppm		$^{207}Pb/^{206}Pb$		$^{207}Pb/^{235}U$		$^{206}Pb/^{238}U$		$^{207}Pb/^{206}Pb$		$^{207}Pb/^{235}U$		$^{206}Pb/^{238}U$	
1037-29	91.4	349	1080	0.32	0.0579	0.00119	0.63589	0.01417	0.07964	0.00122	526	24	500	9	494	7
1037-30	43.1	161	549	0.29	0.06194	0.00217	0.61268	0.01924	0.07174	0.00111	672	77	485	12	447	7
QL10-43																
1043-01	41.1	499	443	1.13	0.05707	0.00118	0.57232	0.01272	0.07272	0.00111	494	24	460	8	453	7
1043-02	13.8	74.6	173	0.43	0.05671	0.00173	0.56499	0.01742	0.07225	0.00121	480	39	455	11	450	7
1043-03	46.3	248	580	0.43	0.05805	0.00101	0.57943	0.0113	0.07237	0.00107	532	20	464	7	450	6
1043-04	19.0	161	224	0.72	0.05612	0.00158	0.55915	0.01612	0.07225	0.00117	457	36	451	10	450	7
1043-05	54.7	179	730	0.25	0.05618	0.00183	0.53238	0.01536	0.06873	0.00103	459	74	433	10	428	6
1043-06	144	679	1837	0.37	0.05754	0.00084	0.57604	0.00999	0.0726	0.00105	512	17	462	6	452	6
1043-07	87.3	316	1142	0.28	0.05668	0.00124	0.56444	0.01313	0.07222	0.00111	479	26	454	9	450	7
1043-08	25.8	203	323	0.63	0.05545	0.00174	0.52881	0.01679	0.06916	0.00116	430	41	431	11	431	7
1043-09	41.9	100	557	0.18	0.05573	0.00115	0.55831	0.01243	0.07265	0.0011	442	25	450	8	452	7
1043-12	92.7	385	1183	0.33	0.05891	0.00094	0.59121	0.01083	0.07278	0.00106	564	18	472	7	453	6
1043-16	27.5	136	350	0.39	0.0562	0.00136	0.56109	0.0142	0.07239	0.00112	460	30	452	9	451	7
1043-18	100	551	1235	0.45	0.05996	0.00207	0.59131	0.01836	0.07153	0.00108	602	76	472	12	445	6
1043-19	30.9	139	394	0.35	0.05703	0.00114	0.57121	0.01239	0.07263	0.0011	493	24	459	8	452	7
1043-20	166	522	2136	0.24	0.05838	0.00178	0.56974	0.01524	0.07078	0.00104	544	68	458	10	441	6
1043-21	10.6	46.9	138	0.34	0.05587	0.00164	0.55211	0.01654	0.07166	0.00116	447	38	446	11	446	7
1043-26	60.9	250	778	0.32	0.05861	0.00187	0.58507	0.01654	0.0724	0.00108	553	71	468	11	451	6

Table 4.4 Major and trace elements of granitoids in Qilian Block

	Old rocks				450 Ma S-type							
	QL09-15	QL09-01	QL09-18	QL09-19	QL09-02	QL09-07	QL09-09	QL09-10	QL09-12	QL09-17	QL10-40F	QL10-41F
SiO_2	70.0	72.7	72.3	51.6	72.4	71.9	70.8	75.1	71.3	69.6	74.8	74.8
TiO_2	0.28	0.52	0.36	0.72	0.22	0.75	0.32	0.07	0.24	0.31	0.06	0.07
Al_2O_3	15.5	12.3	14.3	17.4	14.6	11.7	14.9	13.4	14.8	15.8	13.9	14.1
Fe_2O_3	1.19	1.14	0.96	3.61	0.46	1.40	0.69	0.35	0.87	0.98	0.32	0.41
FeO	1.32	2.40	1.97	6.05	0.75	4.00	1.76	0.60	0.90	1.87	0.50	0.45
FeO_T	2.39	3.43	2.83	9.30	1.16	5.26	2.38	0.91	1.68	2.75	0.79	0.82
MnO	0.04	0.07	0.05	0.19	0.02	0.11	0.06	0.07	0.04	0.05	0.03	0.03
MgO	0.59	1.46	1.05	4.76	0.50	2.31	0.66	0.19	0.76	0.63	0.17	0.17
CaO	1.85	1.31	1.18	8.19	0.86	1.07	2.21	1.11	1.66	2.05	0.56	0.53
Na_2O	3.23	2.48	5.11	1.27	2.40	2.03	3.44	3.14	3.44	3.30	3.70	3.66
K_2O	4.23	2.67	0.97	3.53	6.44	1.63	3.98	5.16	4.45	4.01	5.14	4.86
P_2O_5	0.09	0.06	0.08	0.15	0.11	0.09	0.13	0.02	0.10	0.09	0.09	0.10
LOI	1.41	2.43	1.35	1.73	1.05	2.50	0.73	0.50	1.14	0.96	0.55	0.53
Total	98.3	97.1	98.3	97.5	98.8	97.0	98.9	99.2	98.6	98.7	99.3	99.2
A/CNK	1.17	1.31	1.23	0.79	1.17	1.66	1.06	1.05	1.10	1.17	1.10	1.15
Li	55.8	25.8	4.39	5.61	9.94	21.9	76.0	32.0	54.7	56.9	12.9	13.9
Sc	5.36	8.60	7.76	33.7	2.80	6.61	5.22	1.81	4.51	7.59	2.79	2.29
Cr	9.18	47.3	2.90	16.3	19.9	16.0	3.89	1.16	16.2	10.9	5.02	5.55
Co	3.81	7.3	2.20	24.5	2.0	4.63	2.65	0.44	2.98	5.14	0.68	0.69
Ni	4.02	12.6	2.50	11.9	3.4	12.5	1.66	0.67	2.48	4.84	0.90	1.03
Ga	18.4	16.0	19.0	18.0	13.8	16.6	20.2	13.6	18.3	21.0	18.0	18.0
Rb	138	104	21.3	25.9	177	119	163	175	166	181	245	231
Sr	109	254	208	325	336	181	332	97.3	336	103	24.3	18.6
Y	19.8	17.4	12.5	22.8	5.97	6.86	18.9	25.8	17.2	25.8	20.0	18.9
Zr	144	263	130	26.5	107	100	181	73	137	149	43.5	50.4
Nb	9.1	12.7	8.11	6.06	5.98	10.7	19.0	8.0	13.0	10.8	21.5	25.2
Ba	824	668	366	411	1542	580	870	207	978	616	135	78.0
La	25.8	45.0	14.0	18.2	28.6	25.9	43.9	17.8	32.4	33.1	10.0	9.69
Ce	50.3	78.3	31.3	38.2	54.0	51.2	80.7	31.1	56.7	67.4	18.6	19.0
Pr	6.41	8.95	3.48	5.08	6.46	6.09	9.24	4.11	6.84	8.17	2.59	2.58
Nd	24.6	31.3	13.4	21.4	23.1	22.7	32.5	15.2	24.0	30.6	9.41	9.73
Sm	5.05	5.15	2.73	4.56	4.65	4.87	5.47	3.03	4.34	6.38	2.50	2.66
Eu	1.00	1.17	0.78	1.23	1.57	0.86	1.14	0.40	1.01	0.99	0.20	0.14
Gd	4.37	4.38	2.75	4.04	3.61	3.75	4.32	2.46	3.49	5.40	2.54	2.66
Tb	0.68	0.62	0.44	0.69	0.45	0.45	0.63	0.48	0.55	0.86	0.57	0.58
Dy	3.83	3.39	2.42	4.23	1.77	1.84	3.49	3.77	3.14	4.91	3.69	3.59
Ho	0.76	0.68	0.51	0.89	0.25	0.30	0.70	1.06	0.63	0.95	0.71	0.69
Er	2.08	1.93	1.54	2.48	0.53	0.71	1.99	3.92	1.74	2.59	2.01	1.97
Tm	0.30	0.30	0.28	0.38	0.06	0.09	0.31	0.74	0.27	0.38	0.33	0.32
Yb	1.92	1.91	1.66	2.49	0.38	0.58	2.14	5.49	1.82	2.43	2.25	2.13
Lu	0.29	0.30	0.28	0.37	0.06	0.08	0.34	0.96	0.28	0.36	0.32	0.30
Hf	4.38	6.90	4.16	1.14	3.30	2.86	5.56	2.88	4.30	4.62	2.22	2.51
Ta	0.98	0.74	0.70	0.34	0.65	0.68	1.90	1.13	1.52	1.23	4.21	6.09
Pb	26.6	28.5	3.41	6.82	52.2	22.7	40.2	54.7	42.5	30.3	33.7	27.7
Th	11.7	12.7	5.05	1.86	11.4	11.6	20.9	20.3	17.7	14.3	7.33	7.45
U	1.76	1.57	1.02	0.62	1.21	0.79	7.80	4.90	2.13	2.06	2.37	3.15

Table 4.4 Major and trace elements of granitoids in Qilian Block (continued)

	450 Ma I-type											
	QL09-14	QL10-32	QL10-33	QL10-34	QL10-35	QL10-37	QL10-38	QL10-40C	QL10-41C	QL10-42	QL10-44	QL10-45
SiO_2	56.0	62.0	62.2	62.1	61.7	74.1	62.1	69.3	67.9	65.0	60.2	62.4
TiO_2	0.90	0.76	0.76	0.74	0.76	0.27	0.78	0.55	0.66	0.74	0.89	0.81
Al_2O_3	16.4	16.3	16.5	16.2	16.2	13.1	17.4	15.1	15.6	16.2	16.3	16.2
Fe_2O_3	2.44	1.27	0.88	0.90	0.95	0.40	1.26	0.74	0.78	1.17	1.39	1.24
FeO	4.98	3.82	3.92	4.10	4.10	1.42	4.20	2.70	3.31	3.77	5.82	4.96
FeO_T	7.18	4.96	4.71	4.91	4.95	1.78	5.33	3.37	4.01	4.82	7.07	6.08
MnO	0.13	0.09	0.08	0.09	0.09	0.03	0.07	0.04	0.07	0.06	0.15	0.12
MgO	5.12	3.29	3.05	3.34	3.38	0.66	2.08	1.50	1.72	1.92	2.99	2.68
CaO	7.90	5.34	5.12	5.43	5.45	1.64	3.72	2.97	3.38	3.22	4.67	4.24
Na_2O	2.59	3.10	3.12	3.04	3.00	2.46	3.72	3.07	3.36	3.33	3.65	3.51
K_2O	1.88	2.29	2.68	2.55	2.91	5.05	2.90	2.88	2.10	3.00	2.30	2.47
P_2O_5	0.17	0.19	0.23	0.18	0.19	0.22	0.33	0.16	0.19	0.26	0.31	0.28
LOI	0.86	1.01	0.94	0.89	0.84	0.37	0.94	0.68	0.61	0.83	0.65	0.59
Total	98.5	98.5	98.5	98.7	98.7	99.3	98.6	99.0	99.1	98.7	98.7	98.9
A/CNK	0.79	0.94	0.95	0.92	0.90	1.05	1.08	1.11	1.12	1.11	0.05	0.05
Li	16.0	45.8	52.8	43.2	46.8	59.0	114	90.6	124	145	68.9	68.4
Sc	22.7	16.6	13.8	16.6	15.1	5.24	12.5	9.44	9.19	13.5	28.6	14.8
Cr	68.4	59.3	58.0	61.1	61.5	14.7	38.0	28.2	32.2	40.4	83.5	58.0
Co	22.5	15.3	14.4	14.8	15.2	3.60	10.5	7.19	8.80	9.75	13.8	13.0
Ni	12.4	10.8	14.2	10.7	11.4	3.68	9.70	6.85	8.18	8.56	22.2	17.8
Ga	17.9	18.3	19.1	17.8	18.2	15.7	26.6	20.4	21.2	25.9	22.5	21.6
Rb	83.6	124	144	130	141	172	170	153	148	193	145	152
Sr	267	219	214	211	216	214	274	280	286	254	230	264
Y	26.7	19.6	17.5	22.0	20.2	33.5	38.9	15.5	11.6	32.4	52.7	36.2
Zr	170	191	200	194	199	137	228	194	212	258	232	216
Nb	9.4	12.6	12.4	12.1	12.3	10.4	31.2	14.6	15.2	27.8	20.6	18.8
Ba	413	470	604	470	716	1120	321	821	382	566	267	429
La	24.5	43.5	48.2	34.0	40.4	57.8	18.6	43.2	60.5	62.5	39.5	47.2
Ce	50.5	82.6	87.4	63.2	75.8	113	37.2	78.2	111	121	65.3	82.4
Pr	6.34	9.35	10.2	8.00	8.80	13.6	4.94	9.08	13.0	14.9	10.0	11.4
Nd	24.5	33.4	35.3	30.3	32.1	50.6	19.8	31.5	45.9	55.8	41.2	43.4
Sm	5.10	5.76	5.74	5.70	5.67	10.2	5.3	4.91	6.88	11.0	10.6	9.10
Eu	1.12	1.19	1.28	1.19	1.26	1.38	1.36	1.31	1.32	1.40	1.17	1.28
Gd	4.73	5.09	4.88	5.12	5.1	8.94	5.87	4.06	5.52	9.52	10.6	8.24
Tb	0.82	0.74	0.68	0.79	0.75	1.39	1.22	0.6	0.70	1.41	1.96	1.38
Dy	4.98	3.95	3.57	4.42	4.12	7.53	7.62	3.26	3.09	7.28	11.6	7.77
Ho	1.04	0.74	0.65	0.84	0.77	1.25	1.42	0.58	0.50	1.23	2.11	1.41
Er	2.88	1.99	1.80	2.28	2.06	3.08	3.83	1.54	1.12	3.05	5.41	3.68
Tm	0.42	0.29	0.26	0.33	0.30	0.41	0.54	0.23	0.14	0.41	0.75	0.50
Yb	2.73	1.82	1.70	2.20	1.89	2.50	3.45	1.47	0.96	2.51	4.52	3.09
Lu	0.42	0.27	0.26	0.33	0.30	0.37	0.5	0.23	0.16	0.37	0.62	0.43
Hf	4.44	5.06	5.46	5.65	5.47	4.4	6.72	5.53	6.06	7.73	6.69	6.70
Ta	0.61	0.92	0.92	1.07	0.99	0.93	2.41	1.32	1.40	2.17	1.22	1.46
Pb	8.6	19.7	21.1	20.9	22.6	54.5	25.6	25.9	20.2	32.3	14.3	18.0
Th	7.7	15.40	17.6	13.6	14.2	35.5	7.88	10.9	17.0	33.6	12.8	17.0
U	0.80	1.64	1.82	1.70	1.69	4.15	3.18	2.21	2.21	3.73	2.02	3.19

Table 4.5 Whole rock Sr-Nd-Pb-Hf isotopic data.The subscribe refers to the analytical session during which the sample was analysed for isotopic compositions. The averages and reproducibility of multiple measurements of the isotope standards during the appropriate sessions are given below:

1: JMC475, 0.282160±08 (2SD, n=10); 2: 0.282160±06 (2SD, n=12). $^{176}Hf/^{177}Hf$ are reported relative to an accepted ratio for JMC475 of 0.282160 (Nowell et al., 1998)

3: J&M, 0.511110±11 (2SD, n=19); 4: 0.511110±07 (2SD, n=11). $^{143}Nd/^{144}Nd$ are reported relative to an accepted ratio for J&M of 0.511110 (Thirlwall, 1991)

5: NBS987, 0.710267±10 (2SD, n=13); 6: 0.710277±15(2SD, n=9). $^{87}Sr/^{86}Sr$ are reported relative to an accepted $^{87}Sr/^{86}Sr$ ratio for NBS987 of 0.71024 (Thirlwall, 1991)

7: NBS981, $^{206}Pb/^{204}Pb$:16.94102±184; $^{207}Pb/^{204}Pb$:15.49811±142; $^{208}Pb/^{204}Pb$:36.71791±512 (2SD, n=11)

8: NBS981, $^{206}Pb/^{204}Pb$:16.94083±274; $^{207}Pb/^{204}Pb$:15.49706±115; $^{208}Pb/^{204}Pb$:36.71478±399 (2SD, n=16)

	Old rocks			S-type (450 Ma)			
	QL09-15 (924 Ma)	QL09-01 (797 Ma)	QL09-18 (500 Ma)	QL09-02	QL09-10	QL09-12	QL10-40(F)
$^{176}Lu/^{177}Hf$	0.009	0.006	0.01	0.004	0.048	0.01	0.006
$^{176}Hf/^{177}Hf$	$0.282453(06)_1$	$0.282112(07)_1$	$0.283021(09)_1$	$0.282174(08)_1$	$0.282897(07)_1$	$0.282539(06)_1$	$0.282508(12)_2$
$\varepsilon_{Hf}(450)$	-4	-15	16	-12	0.1	-1	-0.9
	3.8 (924 Ma)	-8 (797 Ma)	17 (503 Ma)				
$^{147}Sm/^{144}Nd$	0.1214	0.0979	0.1236	0.1319	0.1214	0.1011	0.0946
$^{143}Nd/^{144}Nd$	$0.511989(06)_3$	$0.511621(07)_3$	$0.512556(12)_3$	$0.511821(06)_3$	$0.512192(06)_3$	$0.512183(05)_3$	$0.512056(08)_4$
$\varepsilon_{Nd}(450)$	-8.3	-14.2	2.6	-12.2	-4.4	-3.4	-5.5
	-3.8 (924 Ma)	-9.8 (797 Ma))	3.1 (503 Ma))				
$^{87}Rb/^{86}Sr$	3.61	1.16	0.29	1.49	5.1	1.4	28.56
$^{87}Sr/^{86}Sr$	$0.764464(11)_5$	$0.722690(12)_5$	$0.708230(13)_5$	$0.724259(09)_5$	$0.737846(12)_5$	$0.719163(09)_5$	$0.721548(10)_6$
$I_{Sr}(450)$	0.74134	0.7153	0.7064	0.7147	0.7051	0.7102	0.5875
	0.7169 (924 Ma))	0.7095 (797 Ma))	0.7062 (503 Ma)				
$^{206}Pb/^{204}Pb$	$18.561(1)_7$	$17.799(1)_7$	$21.940(3)_7$	$17.671(1)_7$	$19.272(1)_7$	$19.159(2)_7$	$19.054(1)_8$
$^{207}Pb/^{204}Pb$	$15.656(1)_7$	$15.589(1)_7$	$15.816(3)_7$	$15.580(1)_7$	$15.693(1)_7$	$15.689(2)_7$	$15.687(1)_8$
$^{208}Pb/^{204}Pb$	$38.721(6)_7$	$38.641(5)_7$	$41.924(10)_7$	$38.278(4)_7$	$38.602(5)_7$	$38.967(6)_7$	$39.086(03)_8$
$^{208}Pb/^{204}Pb_i(450)$	38.099	38.011	39.829	37.979	38.088	38.375	38.491
	37.431 (924 Ma)	37.512 (797 Ma)	39.594 (503 Ma)				
$^{207}Pb/^{204}Pb_i(450)$	15.64	15.576	15.741	15.576	15.670	15.678	15.665
	15.612 (924 Ma)	15.560 (797 Ma)	15.731 (503 Ma)				
$^{206}Pb/^{204}Pb_i(450)$	18.27	17.56	20.626	17.587	18.873	18.954	18.679
	17.942 (924 Ma)	17.356 (797 Ma)	20.465 (503 Ma)				

Table 4.5 Whole rock Sr-Nd-Pb-Hf isotopic data(continued).

	I-type (450 Ma)			
	QL09-14	QL10-34	QL10-37	QL10-40(C)
$^{176}Lu/^{177}Hf$	0.013	0.008	0.012	0.02
$^{176}Hf/^{177}Hf$	$0.282665(11)_1$	$0.282490(07)_2$	$0.282519(07)_2$	$0.282715(16)_2$
$\varepsilon_{Hf(t)}(450)$	2.6	-2.3	-2.3	2
$^{147}Sm/^{144}Nd$	0.1214	0.1141	0.1223	0.1612
$^{143}Nd/^{144}Nd$	$0.512210(08)_3$	$0.512059(01)_4$	$0.512093(08)_4$	$0.512302(15)_4$
$\varepsilon_{Nd}(450)$	-3.8	-6.6	-6.4	-4.5
$^{87}Rb/^{86}Sr$	0.89	1.75	2.28	1.55
$^{87}Sr/^{86}Sr$	$0.714467(11)_5$	$0.720432(09)_6$	$0.729853(09)_6$	$0.770567(15)_6$
$I_{Sr}(450)$	0.7088	0.7092	0.7153	0.7606
$^{206}Pb/^{204}Pb$	$18.685(1)_7$	$19.000(1)_8$	$19.199(1)_8$	$19.731(1)_8$
$^{207}Pb/^{204}Pb$	$15.652(1)_7$	$15.734(1)_8$	$15.698(1)_8$	$15.753(1)_8$
$^{208}Pb/^{204}Pb$	$39.300(7)_7$	$39.268(04)_8$	$40.007(04)_8$	$38.684(04)_8$
$^{208}Pb/^{204}Pb_i(450)$	38.043	38.348	39.086	38.377
$^{207}Pb/^{204}Pb_i(450)$	15.624	15.714	15.679	15.735
$^{206}Pb/^{204}Pb_i(450)$	18.197	18.642	18.864	19.422

Table 5.1 Major and trace elements of granitoids in Qilian Block

	S-type				I-type		
	QL09-04	QL09-08	QL09-11	QL09-13	QL10-36	QL10-39	QL10-43
SiO_2	70.0	67.4	70.0	72.4	72.0	68.4	68.7
TiO_2	0.46	0.50	0.23	0.26	0.49	0.61	0.51
Al_2O_3	14.7	16.2	15.8	14.1	13.9	15.1	15.3
Fe_2O_3	0.74	1.06	0.62	0.61	0.82	0.57	0.67
FeO	1.98	2.57	1.06	1.30	2.30	3.57	2.75
FeO_T	2.65	3.52	1.62	1.85	3.04	4.08	3.35
MnO	0.04	0.07	0.04	0.04	0.05	0.05	0.06
MgO	0.95	0.99	0.64	0.73	1.21	1.57	1.38
CaO	1.25	3.08	1.75	1.95	2.46	3.26	2.93
Na_2O	2.34	4.33	3.53	3.17	2.65	3.30	3.29
K_2O	5.90	2.38	5.15	4.37	3.06	2.22	3.54
P_2O_5	0.23	0.22	0.10	0.10	0.11	0.22	0.16
LOI	1.00	0.77	0.82	0.76	0.71	0.65	0.43
Total	98.6	98.8	98.9	99.0	99.1	98.9	99.3
A/CNK	1.17	1.06	1.08	1.04	1.14	1.10	1.05
Li	39.0	89.8	54.5	66.1	56.8	114	49.2
Sc	5.43	7.09	4.36	5.38	9.98	10.4	7.33
Cr	22.7	1.44	8.95	13.2	25.9	29.8	26.6
Co	6.08	3.78	2.54	3.02	6.76	7.84	6.47
Ni	10.6	1.41	2.22	2.42	7.23	7.42	7.64
Ga	21.5	23.9	19.2	18.8	18.6	23.4	19.6
Rb	332	95	179	196	146	162	134
Sr	135	281	292	284	258	249	305
Y	13.9	30.5	15.9	17.2	16.6	25.3	18.5
Zr	249	250	134	131	235	253	210
Nb	20.9	27.7	14.0	17.8	11.0	25.0	14.1
Ba	555	551	969	726	892	273	905
La	63.8	57.0	39.6	28.6	77.6	33.0	53.2
Ce	134	98.9	78.1	48.7	144	61.5	95.9
Pr	16.4	11.5	8.59	5.94	16.6	7.38	11.9
Nd	60.1	39.3	29.8	21.3	58.9	27.5	42.0
Sm	10.5	6.92	5.11	3.86	8.68	5.67	6.82
Eu	0.92	0.99	1.04	0.90	1.42	1.24	1.43
Gd	6.92	6.02	4.07	3.28	6.61	5.39	5.64
Tb	0.81	0.92	0.58	0.53	0.84	0.98	0.76
Dy	3.47	5.38	3.02	3.10	3.88	5.51	3.91
Ho	0.56	1.11	0.59	0.61	0.64	0.96	0.7
Er	1.37	3.07	1.58	1.73	1.6	2.43	1.88
Tm	0.16	0.46	0.23	0.26	0.22	0.34	0.27
Yb	0.84	3.07	1.47	1.76	1.38	2.14	1.73
Lu	0.12	0.46	0.22	0.26	0.21	0.31	0.27
Hf	7.09	6.59	4.09	4.21	6.83	7.64	6.24
Ta	1.22	3.14	1.52	1.81	1.21	1.94	1.20
Pb	42.1	29.1	46.8	42.2	31.9	24.6	27.1
Th	43.0	16.3	19.2	13.5	29.2	13.7	19.5
U	2.81	3.72	1.86	2.57	2.83	2.98	1.41

Table 5.2 Whole rock Sr-Nd-Pb-Hf isotopic data.The subscribe refers to the analytical session during which the sample was analysed for isotopic compositions. The averages and reproducibility of multiple measurements of the isotope standards during the appropriate sessions are given below:

1: JMC475, 0.282160±08 (2SD, n=10); 2: 0.282160±06 (2SD, n=12). $^{176}Hf/^{177}Hf$ are reported relative to an accepted ratio for JMC475 of 0.282160 (Nowell et al., 1998)

3: J&M, 0.511110±11 (2SD, n=19); 4: 0.511110±07 (2SD, n=11). $^{143}Nd/^{144}Nd$ are reported relative to an accepted ratio for J&M of 0.511110 (Thirlwall, 1991)

5: NBS987, 0.710267±10 (2SD, n=13); 6: 0.710277±15(2SD, n=9). $^{87}Sr/^{86}Sr$ are reported relative to an accepted $^{87}Sr/^{86}Sr$ ratio for NBS987 of 0.71024 (Thirlwall, 1991)

7: NBS981, $^{206}Pb/^{204}Pb$:16.94102±184;$^{207}Pb/^{204}Pb$:15.49811±142;$^{208}Pb/^{204}Pb$:36.71791±512 (2SD, n=11)

8: NBS981, $^{206}Pb/^{204}Pb$:16.94083±274;$^{207}Pb/^{204}Pb$:15.49706±115;$^{208}Pb/^{204}Pb$:36.71478±399 (2SD, n=16)

	S-type			I-type		
	QL09-04	QL09-08	QL09-13	QL10-36	QL10-39	QL10-43
$^{176}Lu/^{177}Hf$	0.005	0.011	0.01	0.004	0.006	0.006
$^{176}Hf/^{177}Hf$	$0.282209(09)_1$	$0.282617(05)_1$	$0.282526(05)_1$	$0.282400(19)_2$	$0.282510(07)_2$	$0.282505(08)_2$
$\varepsilon_{Hf}(450)$	-11	1.5	-1.5	-4.3	-0.8	-1.1
$^{147}Sm/^{144}Nd$	0.1112	0.1089	0.1156	0.0894	0.1251	0.0985
$^{143}Nd/^{144}Nd$	$0.511806(07)_3$	$0.512191(08)_3$	$0.512177(07)_3$	$0.511992(06)_4$	$0.512096(11)_4$	$0.512102(07)_4$
$\varepsilon_{Nd}(450)$	-11	-3.7	-4.3	-6.4	-6.5	-4.8
$^{87}Rb/^{86}Sr$	6.98	0.96	1.95	1.60	1.84	1.24
$^{87}Sr/^{86}Sr$	$0.757360(12)_5$	$0.716540(12)_5$	$0.721497(11)_5$	$0.724951(12)_6$	$0.725992(08)_6$	$0.718970(10)_6$
$I_{Sr}(450)$	0.7126	0.7104	0.709	0.7147	0.7142	0.7116
$^{206}Pb/^{204}Pb$	$18.016(1)_7$	$19.775(2)_7$	$18.997(1)_7$	$18.961(1)_8$	$19.407(1)_8$	$18.848(1)_8$
$^{207}Pb/^{204}Pb$	$15.619(1)_7$	$15.721(1)_7$	$15.678(1)_7$	$15.682(1)_8$	$15.707(1)_8$	$15.672(1)_8$
$^{208}Pb/^{204}Pb$	$39.488(5)_7$	$39.203(5)_7$	$38.659(5)_7$	$40.019(04)_8$	$39.141(04)_8$	$39.352(03)_8$
$^{208}Pb/^{204}Pb_i(450)$	38.040	38.423	38.221	38.725	38.353	38.335
$^{207}Pb/^{204}Pb_i(450)$	15.601	15.686	15.660	15.660	15.676	15.659
$^{206}Pb/^{204}Pb_i(450)$	17.702	19.169	18.683	18.572	18.875	18.620

Table 5.2 Whole rock Sr-Nd-Pb-Hf isotopic data(continued).

	I-type				S-type			
	QL09-14	QL10-34	QL10-37	QL10-40(C)	QL09-02	QL09-10	QL09-12	QL10-40(F)
$^{176}Lu/^{177}Hf$	0.013	0.008	0.012	0.02	0.004	0.048	0.01	0.006
$^{176}Hf/^{177}Hf$	$0.282665(11)_1$	$0.282490(07)_2$	$0.282519(07)_2$	$0.282715(16)_2$	$0.282174(08)_1$	$0.282897(07)_1$	$0.282539(06)_1$	$0.282508(12)_2$
$\varepsilon_{Hf(t)}(450)$	2.6	-2.3	-2.3	2	-12	0.1	-1	-0.9
$^{147}Sm/^{144}Nd$	0.1214	0.1141	0.1223	0.1612	0.1319	0.1214	0.1011	0.0946
$^{143}Nd/^{144}Nd$	$0.512210(08)_3$	$0.512059(01)_4$	$0.512093(08)_4$	$0.512302(15)_4$	$0.511821(06)_3$	$0.512192(06)_3$	$0.512183(05)_3$	$0.512056(08)_4$
$\varepsilon_{Nd}(450)$	-3.8	-6.6	-6.4	-4.5	-12.2	-4.4	-3.4	-5.5
$^{87}Rb/^{86}Sr$	0.89	1.75	2.28	1.55	1.49	5.1	1.4	28.56
$^{87}Sr/^{86}Sr$	$0.714467(11)_5$	$0.720432(09)_6$	$0.729853(09)_6$	$0.770567(15)_6$	$0.724259(09)_5$	$0.737846(12)_5$	$0.719163(09)_5$	$0.721548(10)_6$
$I_{Sr}(450)$	0.7088	0.7092	0.7153	0.7606	0.7147	0.7051	0.7102	0.5875
$^{206}Pb/^{204}Pb$	$18.685(1)_7$	$19.000(1)_8$	$19.199(1)_8$	$19.731(1)_8$	$17.671(1)_7$	$19.272(1)_7$	$19.159(2)_7$	$19.054(1)_8$
$^{207}Pb/^{204}Pb$	$15.652(1)_7$	$15.734(1)_8$	$15.698(1)_8$	$15.753(1)_8$	$15.580(1)_7$	$15.693(1)_7$	$15.689(2)_7$	$15.687(1)_8$
$^{208}Pb/^{204}Pb$	$39.300(7)_7$	$39.268(04)_8$	$40.007(04)_8$	$38.684(04)_8$	$38.278(4)_7$	$38.602(5)_7$	$38.967(6)_7$	$39.086(03)_8$
$^{208}Pb/^{204}Pb_i(450)$	38.043	38.348	39.086	38.377	37.979	38.088	38.375	38.491
$^{207}Pb/^{204}Pb_i(450)$	15.624	15.714	15.679	15.735	15.576	15.670	15.678	15.665
$^{206}Pb/^{204}Pb_i(450)$	18.197	18.642	18.864	19.422	17.587	18.873	18.954	18.679

Table 5.3 Zircon *in situ* Hf isotopes

	Age (Ma)	$^{176}Yb/^{177}Hf$	$^{176}Lu/^{177}Hf$	$^{176}Hf/^{177}Hf$	2s	$\varepsilon_{Hf}(0)$	$\varepsilon_{Hf}(t)$	$\varepsilon_{Hf}(450)$	T_{DM}^{C} (Ma)
Analysed in Chinese Academy of Sciences, beijing									
QL10-34-01	501	0.044265	0.001719	0.282337	2.1E-05	-15.4	-4.9	-6.0	1772
QL10-34-02	498	0.045397	0.001793	0.282321	2.3E-05	-15.9	-5.6	-6.6	1811
QL10-34-03	496	0.059053	0.002298	0.282313	3.0E-05	-16.2	-6.1	-7.0	1841
QL10-34-04	459	0.028810	0.001127	0.282334	2.0E-05	-15.5	-5.8	-5.9	1792
QL10-34-05	515	0.054860	0.002143	0.282372	2.3E-05	-14.1	-3.6	-4.9	1696
QL10-34-06	512	0.037937	0.001535	0.282316	2.9E-05	-16.1	-5.4	-6.7	1809
QL10-34-07	475	0.045546	0.001791	0.282373	2.3E-05	-14.1	-4.2	-4.8	1709
QL10-34-08	476	0.033586	0.001316	0.282341	2.3E-05	-15.2	-5.2	-5.7	1770
QL10-34-09	495	0.046970	0.001842	0.282372	2.5E-05	-14.2	-3.9	-4.8	1701
QL10-34-10	509	0.057154	0.002241	0.282362	2.3E-05	-14.5	-4.1	-5.3	1723
QL10-34-11	484	0.039545	0.001600	0.282375	2.3E-05	-14.0	-3.9	-4.6	1696
QL10-34-12	472	0.039228	0.001566	0.282336	2.1E-05	-15.4	-5.5	-6.0	1787
QL10-34-13	479	0.034857	0.001414	0.282340	2.3E-05	-15.3	-5.2	-5.8	1771
QL10-34-14	470	0.026468	0.001088	0.282314	2.1E-05	-16.2	-6.2	-6.6	1828
QL10-34-15	492	0.023653	0.000988	0.282454	2.7E-05	-11.2	-0.7	-1.6	1503
QL10-34-16	455	0.041750	0.001660	0.282398	2.0E-05	-13.2	-3.7	-3.8	1661
QL10-34-17	482	0.047708	0.001850	0.282365	2.4E-05	-14.4	-4.4	-5.1	1724
QL10-34-18	464	0.028659	0.001143	0.282400	2.2E-05	-13.2	-3.3	-3.6	1642
QL10-34-19	483	0.041592	0.001617	0.282403	2.1E-05	-13.1	-2.9	-3.6	1634
QL10-34-20	483	0.053098	0.002063	0.282326	2.3E-05	-15.8	-5.8	-6.5	1813
QL10-36-01	492	0.023302	0.000969	0.282370	2.2E-05	-14.2	-3.7	-4.6	1689
QL10-36-02	479	0.025261	0.001024	0.282408	2.3E-05	-12.9	-2.7	-3.3	1613
QL10-36-03	451	0.014524	0.000608	0.282394	2.1E-05	-13.4	-3.6	-3.7	1653
QL10-36-04	1508	0.028793	0.001168	0.282039	2.3E-05	-25.9	6.4	-16.4	1836
QL10-36-05	1780	0.016768	0.000677	0.281946	2.1E-05	-29.2	9.7	-19.5	1847
QL10-36-06	495	0.022213	0.000914	0.282372	2.0E-05	-14.2	-3.6	-4.5	1682
QL10-36-07	452	0.015256	0.000629	0.282379	2.2E-05	-13.9	-4.2	-4.2	1687
QL10-36-08	467	0.020370	0.000828	0.282411	2.3E-05	-12.8	-2.7	-3.1	1609
QL10-36-09	495	0.021472	0.000879	0.282438	2.2E-05	-11.8	-1.2	-2.2	1535
QL10-36-10	494	0.013659	0.000575	0.282424	2.6E-05	-12.3	-1.6	-2.6	1560
QL10-36-11	512	0.028813	0.001154	0.282404	2.1E-05	-13.0	-2.2	-3.5	1607
QL10-36-12	502	0.030388	0.001183	0.282416	2.1E-05	-12.6	-1.9	-3.0	1585
QL10-36-13	535	0.021920	0.000886	0.282390	2.0E-05	-13.5	-2.1	-3.9	1618
QL10-36-14	975	0.026025	0.001062	0.281692	2.2E-05	-38.2	-17.4	-28.6	2902
QL10-36-15	504	0.017766	0.000733	0.282412	1.9E-05	-12.7	-1.9	-3.1	1583
QL10-36-16	441	0.019288	0.000772	0.282384	2.1E-05	-13.7	-4.2	-4.0	1683
QL10-36-17	488	0.020469	0.000884	0.282384	2.6E-05	-13.7	-3.3	-4.1	1659
QL10-36-18	486	0.028027	0.001101	0.282361	2.0E-05	-14.5	-4.2	-5.0	1715
QL10-36-19	452	0.015974	0.000660	0.282389	2.1E-05	-13.5	-3.8	-3.8	1664
QL10-36-20	510	0.026279	0.001058	0.282431	2.1E-05	-12.1	-1.2	-2.5	1546
QL10-37-01	477	0.036331	0.001439	0.282427	2.7E-05	-12.2	-2.2	-2.7	1581
QL10-37-02	502	0.022891	0.000924	0.282371	2.2E-05	-14.2	-3.4	-4.6	1679
QL10-37-03	501	0.021528	0.000871	0.282424	2.3E-05	-12.3	-1.6	-2.7	1563
QL10-37-04	508	0.012017	0.000496	0.282450	3.1E-05	-11.4	-0.4	-1.6	1491
QL10-37-05	503	0.020318	0.000818	0.282366	2.2E-05	-14.4	-3.6	-4.7	1689
QL10-37-06	532	0.018348	0.000761	0.282373	2.2E-05	-14.1	-2.7	-4.4	1654
QL10-37-07	500	0.016710	0.000694	0.282402	2.3E-05	-13.1	-2.3	-3.4	1608
QL10-37-08	451	0.014209	0.000627	0.282408	2.5E-05	-12.9	-3.1	-3.2	1622
QL10-37-09	449	0.023193	0.000943	0.282392	1.9E-05	-13.4	-3.9	-3.8	1666
QL10-37-10	1710	0.015729	0.000664	0.281673	2.5E-05	-38.9	-1.6	-29.2	2486
QL10-37-11	500	0.061546	0.002435	0.282398	2.3E-05	-13.2	-3.0	-4.0	1651

	Age (Ma)	$^{176}Yb/^{177}Hf$	$^{176}Lu/^{177}Hf$	$^{176}Hf/^{177}Hf$	2s	$\varepsilon_{Hf}(0)$	$\varepsilon_{Hf}(t)$	$\varepsilon_{Hf}(450)$	T_{DM}^{C} (Ma)
QL10-37-12	447	0.026949	0.001111	0.282371	2.3E-05	-14.2	-4.7	-4.6	1715
QL10-37-13	448	0.048696	0.001932	0.282411	2.3E-05	-12.8	-3.5	-3.5	1642
QL10-37-14	1761	0.036647	0.001427	0.281644	2.1E-05	-39.9	-2.4	-30.4	2574
QL10-37-15	1573	0.009382	0.000403	0.281996	2.1E-05	-27.4	7.1	-17.7	1844
QL10-37-16	501	0.018924	0.000783	0.282410	2.2E-05	-12.8	-2.0	-3.1	1591
QL10-37-17	519	0.035608	0.001400	0.282416	1.8E-05	-12.6	-1.7	-3.1	1581
QL10-37-18	450	0.019486	0.000813	0.282451	1.8E-05	-11.4	-1.7	-1.7	1531
QL10-37-19	451	0.033229	0.001316	0.282395	2.5E-05	-13.3	-3.8	-3.8	1664
QL10-37-20	450	0.027763	0.001101	0.282443	2.5E-05	-11.6	-2.1	-2.1	1554
QL10-37-21	522	0.032026	0.001262	0.282402	2.2E-05	-13.1	-2.0	-3.6	1606
QL10-37-22	2189	0.016400	0.000659	0.281105	2.1E-05	-59.0	-11.1	-49.3	3429
QL10-37-23	477	0.018625	0.000767	0.282397	2.1E-05	-13.2	-3.0	-3.6	1633
QL10-37-24	1141	0.021296	0.000880	0.281960	1.8E-05	-28.7	-4.1	-19.1	2209
QL10-37-25	501	0.019440	0.000800	0.282381	1.9E-05	-13.8	-3.1	-4.2	1657
									0
QL10-39-1	497	0.040204	0.001602	0.282405	2.3E-05	-13.0	-2.6	-3.6	1621
QL10-39-2	406	0.053536	0.002068	0.282379	2.6E-05	-13.9	-5.5	-4.6	1737
QL10-39-3	394	0.052402	0.002008	0.282481	2.5E-05	-10.3	-2.2	-1.0	1517
QL10-39-4	477	0.020599	0.000837	0.282402	2.3E-05	-13.1	-2.9	-3.4	1624
QL10-39-5	518	0.025330	0.000891	0.282392	1.8E-05	-13.4	-2.3	-3.8	1623
QL10-39-6	518	0.020929	0.000855	0.282489	2.1E-05	-10.0	1.1	-0.4	1405
QL10-39-7	492	0.026468	0.001077	0.282405	2.2E-05	-13.0	-2.5	-3.4	1613
QL10-39-8	496	0.045501	0.001805	0.282402	2.2E-05	-13.1	-2.8	-3.7	1632
QL10-39-9	420	0.018604	0.000770	0.282391	2.0E-05	-13.5	-4.5	-3.8	1681
QL10-39-10	462	0.024017	0.000982	0.282468	3.9E-05	-10.7	-0.9	-1.1	1488
QL10-39-11	488	0.019274	0.000784	0.282368	1.9E-05	-14.3	-3.8	-4.6	1691
QL10-39-12	377	0.032388	0.001278	0.282409	1.9E-05	-12.9	-4.9	-3.3	1676
QL10-39-13	444	0.024745	0.001017	0.282356	2.2E-05	-14.7	-5.3	-5.1	1750
QL10-39-14	485	0.021250	0.000862	0.282355	2.0E-05	-14.7	-4.3	-5.1	1724
QL10-39-15	500	0.019434	0.000802	0.282392	1.9E-05	-13.4	-2.7	-3.8	1632
QL10-39-16	499	0.019500	0.000790	0.282377	2.9E-05	-14.0	-3.3	-4.3	1666
QL10-39-17	496	0.021693	0.000889	0.282395	1.9E-05	-13.3	-2.7	-3.7	1631
QL10-39-18	763	0.060651	0.002372	0.282177	2.0E-05	-21.0	-5.4	-11.9	2001
QL10-39-19	1689	0.017695	0.000709	0.281627	2.1E-05	-40.5	-3.7	-30.8	2603
QL10-39-20	554	0.014890	0.000632	0.282136	2.0E-05	-22.5	-10.6	-12.8	2164
QL10-39-21	496	0.023202	0.000932	0.282375	1.7E-05	-14.0	-3.4	-4.4	1674
QL10-43-01	455	0.027675	0.001130	0.282416	2.6E-05	-12.6	-2.9	-3.0	1612
QL10-43-02	500	0.022411	0.000922	0.282382	2.1E-05	-13.8	-3.1	-4.2	1657
QL10-43-03	501	0.021546	0.000894	0.282386	2.0E-05	-13.7	-2.9	-4.0	1648
QL10-43-04	305	0.035604	0.001394	0.282426	2.1E-05	-12.2	-5.8	-2.8	1679
QL10-43-05	461	0.024558	0.001042	0.282401	2.3E-05	-13.1	-3.3	-3.5	1639
QL10-43-06	462	0.013640	0.000582	0.282385	1.9E-05	-13.7	-3.7	-4.0	1666
QL10-43-07	459	0.015990	0.000671	0.282407	2.4E-05	-12.9	-3.0	-3.2	1620
QL10-43-08	462	0.024626	0.000997	0.282477	2.4E-05	-10.4	-0.6	-0.8	1468
QL10-43-09	502	0.019067	0.000782	0.282392	2.1E-05	-13.4	-2.7	-3.8	1631
QL10-43-10	461	0.019203	0.000788	0.282390	2.1E-05	-13.5	-3.6	-3.9	1659
QL10-43-11	460	0.021951	0.000913	0.282368	2.2E-05	-14.3	-4.4	-4.7	1711
QL10-43-12	461	0.024933	0.001011	0.282421	2.0E-05	-12.4	-2.6	-2.8	1596
QL10-43-13	501	0.022745	0.000931	0.282467	1.9E-05	-10.8	-0.1	-1.2	1468
QL10-43-14	502	0.023132	0.000950	0.282315	2.1E-05	-16.1	-5.4	-6.5	1804
QL10-43-15	460	0.015423	0.000639	0.282396	1.9E-05	-13.3	-3.4	-3.6	1644
QL10-43-16	460	0.025361	0.001034	0.282341	2.2E-05	-15.2	-5.4	-5.7	1774
QL10-43-17	460	0.014529	0.000607	0.282319	1.9E-05	-16.0	-6.1	-6.3	1814
QL10-43-18	500	0.020547	0.000864	0.282298	2.1E-05	-16.8	-6.0	-7.1	1842

	Age (Ma)	$^{176}Yb/^{177}Hf$	$^{176}Lu/^{177}Hf$	$^{176}Hf/^{177}Hf$	2s	$\varepsilon_{Hf}(0)$	$\varepsilon_{Hf}(t)$	$\varepsilon_{Hf}(450)$	T_{DM}^{C} (Ma)
QL10-43-19	501	0.016334	0.000664	0.282373	1.9E-05	-14.1	-3.3	-4.4	1670
QL10-43-20	1424	0.022224	0.001047	0.281999	2.5E-05	-27.3	3.3	-17.8	1966
Analysed in Northwest University, Xi'an									
QL09-02-01	804	0.011406	0.000468	0.282228	3.3E-05	-19.2	-1.7	-9.5	1775
QL09-02-02	2381	0.013722	0.000558	0.281572	3.0E-05	-42.4	10.0	-32.7	2295
QL09-02-03	685	0.030023	0.001218	0.281852	2.2E-05	-32.5	-18.0	-23.0	2727
QL09-02-06	666	0.017669	0.000702	0.282076	4.3E-05	-24.6	-10.3	-14.9	2211
QL09-02-07	618	0.014192	0.000667	0.282115	3.3E-05	-23.2	-9.9	-13.6	2141
QL09-02-08	765	0.020462	0.000874	0.281950	4.1E-05	-29.1	-12.7	-19.5	2434
QL09-02-09	2618	0.013058	0.000566	0.281044	3.3E-05	-61.1	-3.4	-51.4	3277
QL09-02-10	765	0.018858	0.000799	0.281929	4.2E-05	-29.8	-13.4	-20.2	2495
QL09-02-11	868	0.023098	0.000941	0.281912	3.1E-05	-30.4	-11.8	-20.8	2478
QL09-02-13	663	0.022326	0.000947	0.281907	4.3E-05	-30.6	-16.4	-21.0	2604
QL09-02-15	459	0.012241	0.000496	0.282065	4.6E-05	-25.0	-15.1	-15.3	2320
QL09-02-18	760	0.014592	0.000621	0.282005	4.8E-05	-27.1	-10.7	-17.4	2327
QL09-02-19	464	0.015613	0.000548	0.282137	3.0E-05	-22.5	-12.4	-12.7	2177
QL09-02-20	440	0.005585	0.000284	0.282102	3.9E-05	-23.7	-14.1	-13.9	2225
QL09-02-21	798	0.033493	0.001330	0.281947	3.1E-05	-29.2	-12.3	-19.7	2429
QL09-02-22	2501	0.015617	0.000633	0.280914	2.6E-05	-65.7	-10.8	-56.0	3646
QL09-02-24	776	0.014556	0.000594	0.282051	2.4E-05	-25.5	-8.7	-15.8	2183
QL09-04-01	1833	0.009829	0.000395	0.281369	3.7E-05	-49.6	-9.3	-39.9	3027
QL09-04-02	729	0.014267	0.000590	0.281755	3.6E-05	-36.0	-20.2	-26.3	2780
QL09-04-03	764	0.010845	0.000459	0.282319	4.8E-05	-16.0	0.6	-6.3	1590
QL09-04-04	799	0.020249	0.000781	0.282165	4.1E-05	-21.5	-4.3	-11.8	1901
QL09-04-05	681	0.059758	0.002218	0.281755	2.8E-05	-36.0	-22.0	-26.8	3044
QL09-04-07	774	0.016874	0.000676	0.281802	3.9E-05	-34.3	-17.6	-24.6	2626
QL09-04-09	843	0.011759	0.000460	0.282296	3.4E-05	-16.8	1.5	-7.1	1587
QL09-04-10	2574	0.012325	0.000496	0.280991	3.0E-05	-63.0	-6.2	-53.3	3384
QL09-04-11	2364	0.006080	0.000246	0.281379	4.5E-05	-49.3	3.3	-39.5	2685
QL09-04-12	774	0.016343	0.000712	0.281604	2.5E-05	-41.3	-24.6	-31.6	3155
QL09-04-13	806	0.014198	0.000615	0.281814	3.1E-05	-33.9	-16.5	-24.2	2601
QL09-04-14	735	0.007721	0.000331	0.282272	4.8E-05	-17.7	-1.6	-7.9	1682
QL09-04-15	800	0.013375	0.000598	0.281790	3.3E-05	-34.7	-17.4	-25.0	2636
QL09-04-17	824	0.018428	0.000780	0.281809	3.5E-05	-34.0	-16.3	-24.4	2590
QL09-04-18	2813	0.020438	0.000839	0.280873	3.1E-05	-67.2	-5.6	-57.6	3539
QL09-04-19	532	0.021519	0.000830	0.282033	3.4E-05	-26.1	-14.7	-16.5	2404
QL09-04-20	806	0.055174	0.002028	0.281662	2.0E-05	-39.3	-22.6	-30.0	3081
QL09-04-21	809	0.023104	0.000933	0.281813	2.6E-05	-33.9	-16.6	-24.3	2696
QL09-04-22	2586	0.015518	0.000654	0.281203	2.9E-05	-55.5	1.4	-45.8	2969
QL09-04-23	2527	0.018381	0.000717	0.281064	3.7E-05	-60.4	-5.0	-50.8	3294
QL09-04-24	824	0.023241	0.000934	0.281913	3.7E-05	-30.4	-12.7	-20.8	2465
QL09-08-01	441	0.024772	0.001008	0.282343	2.6E-05	-15.2	-5.8	-5.6	1779
QL09-08-06	472	0.078906	0.003055	0.282081	3.1E-05	-24.4	-15.0	-15.5	2471
QL09-08-10	471	0.111241	0.004103	0.282022	3.9E-05	-26.5	-17.5	-17.9	2702
QL09-08-11	446	0.053882	0.002068	0.282266	2.2E-05	-17.9	-8.7	-8.6	2029
QL09-08-12	520	0.068650	0.002515	0.282177	2.8E-05	-21.1	-10.5	-11.9	2186
QL09-08-13	443	0.032159	0.001336	0.282315	2.0E-05	-16.2	-6.8	-6.7	1864
QL09-08-17	439	0.057836	0.002185	0.282262	1.9E-05	-18.0	-9.0	-8.8	2007
QL09-08-18	490	0.079142	0.002955	0.282148	2.3E-05	-22.1	-12.3	-13.1	2327
QL09-08-18	490	0.081222	0.002759	0.282049	3.1E-05	-25.6	-15.7	-16.5	2511
QL09-08-22	492	0.084031	0.003225	0.282118	2.6E-05	-23.1	-13.4	-14.2	2421
QL09-08-23	441	0.043249	0.001676	0.282369	2.7E-05	-14.3	-5.1	-4.9	1767

	Age (Ma)	$^{176}Yb/^{177}Hf$	$^{176}Lu/^{177}Hf$	$^{176}Hf/^{177}Hf$	2s	$\varepsilon_{Hf}(0)$	$\varepsilon_{Hf}(t)$	$\varepsilon_{Hf}(450)$	T_{DM}^{C} (Ma)
QL09-08-24	501	0.022035	0.000900	0.282356	2.2E-05	-14.7	-4.0	-5.1	1706
QL09-10-01	497	0.018437	0.000757	0.282402	3.6E-05	-13.1	-2.4	-3.4	1592
QL09-10-02	446	0.023797	0.000957	0.282406	3.1E-05	-12.9	-3.4	-3.3	1607
QL09-10-03	443	0.025950	0.001068	0.282356	3.5E-05	-14.7	-5.3	-5.1	1759
QL09-10-04	445	0.025811	0.001050	0.282378	5.5E-05	-13.9	-4.5	-4.4	1684
QL09-10-05	485	0.027559	0.001098	0.282353	3.2E-05	-14.8	-4.5	-5.3	1711
QL09-10-07	404	0.024100	0.000987	0.282322	3.2E-05	-15.9	-7.3	-6.3	1821
QL09-10-08	480	0.032964	0.001240	0.282303	2.7E-05	-16.6	-6.4	-7.1	1856
QL09-10-09	446	0.022762	0.000912	0.282319	4.3E-05	-16.0	-6.5	-6.4	1816
QL09-10-12	454	0.028949	0.001187	0.282315	3.8E-05	-16.2	-6.5	-6.6	1755
QL09-10-14	450	0.039149	0.001521	0.282291	3.2E-05	-17.0	-7.6	-7.6	1813
QL09-10-16	439	0.022292	0.000857	0.282407	4.5E-05	-12.9	-3.5	-3.3	1554
QL09-10-18	480	0.044663	0.001717	0.282240	2.1E-05	-18.8	-8.8	-9.4	1934
QL09-10-19	478	0.024713	0.001003	0.282340	3.0E-05	-15.3	-5.1	-5.7	1696
QL09-10-21	481	0.022476	0.000905	0.282317	3.3E-05	-16.1	-5.8	-6.5	1740
QL09-10-22	442	0.026007	0.001057	0.282359	3.5E-05	-14.6	-5.2	-5.0	1680
QL09-10-23	445	0.021008	0.000849	0.282304	3.2E-05	-16.6	-7.0	-6.9	1769
QL09-10-24	445	0.021551	0.000878	0.282416	4.9E-05	-12.6	-3.1	-2.9	1581
QL09-12-01	441	0.008561	0.000350	0.282458	3.1E-05	-11.1	-1.5	-1.3	1464
QL09-12-05	445	0.029669	0.001250	0.282338	2.8E-05	-15.3	-5.9	-5.8	1816
QL09-12-07	445	0.015425	0.000650	0.282355	3.6E-05	-14.8	-5.2	-5.1	1741
QL09-12-09	445	0.017282	0.000713	0.282360	3.6E-05	-14.6	-5.0	-4.9	1730
QL09-12-11	969	0.024660	0.000984	0.281896	3.1E-05	-31.0	-10.2	-21.4	2466
QL09-12-12	560	0.044780	0.001628	0.282329	1.7E-05	-15.7	-4.0	-6.3	1780
QL09-12-16	942	0.057165	0.002366	0.282075	2.0E-05	-24.6	-5.3	-15.5	2181
QL09-12-17	445	0.024659	0.000922	0.282336	2.3E-05	-15.4	-5.9	-5.8	1790
QL09-12-18	446	0.025085	0.001000	0.282321	2.7E-05	-16.0	-6.4	-6.4	1838
QL09-12-20	445	0.040597	0.001648	0.282302	1.8E-05	-16.6	-7.3	-7.2	1918

$\varepsilon_{Hf}(t)$: Age corrected to zircon crystallization age.

The last two numbers in the first column refer to the same numbers in the zircon U-Pb ages analyzed in CUG in Table S1.

Table 5.4 Zircon in situ LA-ICP-MS dating results

	Pb	Th	U	Th/U	CORRECTED RATIOS						CORRECTED AGES (Ma)					
	Total ppm	232 ppm	238 ppm		$^{207}Pb/^{206}Pb$		$^{207}Pb/^{235}U$		$^{206}Pb/^{238}U$		$^{207}Pb/^{206}Pb$		$^{207}Pb/^{235}U$		$^{206}Pb/^{238}U$	
Analyzed in China University of Geosciences (Wuhan), CUG																
QL09-04-1	23.0	50	222	0.23	0.05406	0.00171	0.52638	0.016	0.07073	0.0007	373	50	429	11	441	4
QL09-04-10	11.5	33	90	0.37	0.05303	0.00251	0.51777	0.02499	0.07104	0.00078	330	90	424	17	442	5
QL09-04-11	285	822	556	1.48	0.06138	0.00145	0.83615	0.01992	0.09846	0.0007	653	39	617	11	605	4
QL09-04-12	218	667	383	1.74	0.05958	0.00195	0.80565	0.02782	0.09779	0.00139	588	50	600	16	601	8
QL09-04-13	165	477	357	1.33	0.05835	0.00171	0.76174	0.0225	0.09446	0.00086	543	49	575	13	582	5
QL09-04-14	175.4	477	428	1.11	0.0615	0.00149	0.82997	0.01982	0.09768	0.00071	657	39	614	11	601	4
QL09-04-15	19.2	50	155	0.32	0.05762	0.00249	0.56033	0.02305	0.07097	0.00072	515	73	452	15	442	4
QL09-04-16	64.5	176	209	0.84	0.05613	0.00165	0.68488	0.02125	0.08842	0.00133	458	42	530	13	546	8
QL09-04-17	98.8	275	214	1.28	0.06	0.00179	0.81023	0.02528	0.0978	0.00106	604	49	603	14	602	6
QL09-04-18	41.1	122	128	0.95	0.05796	0.00229	0.65879	0.02595	0.08266	0.00094	528	66	514	16	512	6
QL09-04-19	151	414	352	1.18	0.05937	0.00143	0.80785	0.01944	0.09834	0.00083	581	38	601	11	605	5
QL09-04-2	221	618	634	0.97	0.05706	0.00119	0.69607	0.0153	0.08808	0.00088	494	31	536	9	544	5
QL09-04-20	50.0	80	172	0.47	0.06144	0.00236	0.81467	0.03279	0.09567	0.00118	655	65	605	18	589	7
QL09-04-21	296	1081	783	1.38	0.0605	0.00136	0.6301	0.01431	0.07512	0.00054	621	37	496	9	467	3
QL09-04-22	151	455	443	1.03	0.0596	0.00144	0.67323	0.01568	0.08171	0.00058	589	38	523	10	506	3
QL09-04-23	381	1030	813	1.27	0.06079	0.00127	0.77939	0.01518	0.09267	0.00076	632	28	585	9	571	5
QL09-04-24	12.1	30	97	0.31	0.05308	0.00242	0.52165	0.02475	0.07086	0.00082	332	87	426	17	441	5
QL09-04-24	12.1	30	97	0.31	0.05308	0.00242	0.52165	0.02475	0.07086	0.00082	332	87	426	17	441	5
QL09-04-3	39.6	105	131	0.80	0.05818	0.00201	0.71195	0.02527	0.08838	0.00098	536	58	546	15	546	6
QL09-04-4	57.9	168	157	1.07	0.05609	0.00223	0.68156	0.02636	0.08854	0.00112	456	63	528	16	547	7
QL09-04-5	74.4	233	193	1.21	0.05836	0.0022	0.69811	0.02576	0.08659	0.00086	543	63	538	15	535	5
QL09-04-6	93.8	248	209	1.19	0.06134	0.00228	0.824	0.03046	0.09724	0.00103	651	61	610	17	598	6
QL09-04-7	22.5	34	261	0.13	0.05517	0.00254	0.54047	0.02416	0.07091	0.0008	419	80	439	16	442	5
QL09-04-8	121	356	345	1.03	0.05746	0.00156	0.70317	0.01906	0.08862	0.00091	509	41	541	11	547	5
QL09-04-9	141	405	327	1.24	0.05802	0.00156	0.78841	0.0227	0.09817	0.0011	531	43	590	13	604	6
QL09-08-1	99.8	211	934	0.23	0.05534	0.00107	0.54244	0.01049	0.07075	0.00048	426	31	440	7	441	3
QL09-08-3	333	894	2281	0.39	0.05814	0.00116	0.57562	0.01266	0.07141	0.0007	535	31	462	8	445	4
QL09-08-4	137	126	794	0.16	0.056	0.00484	0.51112	0.04379	0.06619	0.00073	452	198	419	29	413	4

	Pb	Th	U	Th/U	CORRECTED RATIOS						CORRECTED AGES (Ma)					
	Total ppm	232 ppm	238 ppm		$^{207}Pb/^{206}Pb$		$^{207}Pb/^{235}U$		$^{206}Pb/^{238}U$		$^{207}Pb/^{206}Pb$		$^{207}Pb/^{235}U$		$^{206}Pb/^{238}U$	
QL09-08-5	375	484	2189	0.22	0.05636	0.00327	0.55463	0.03171	0.07138	0.00068	467	132	448	21	444	4
QL09-08-6	439	1127	2640	0.43	0.05833	0.00238	0.61095	0.02422	0.07597	0.00076	542	92	484	15	472	5
QL09-08-7	441	1196	2597	0.46	0.05842	0.00117	0.619	0.01324	0.07651	0.00078	546	29	489	8	475	5
QL09-08-8	250	383	2589	0.15	0.05767	0.00109	0.64342	0.01164	0.08076	0.00077	517	23	504	7	501	5
QL09-08-9	678	1993	3453	0.58	0.05783	0.00194	0.60592	0.01956	0.076	0.00068	523	75	481	12	472	4
QL09-08-10	415	1194	1991	0.60	0.05772	0.00192	0.60355	0.0192	0.07584	0.00072	519	75	479	12	471	4
QL09-08-11	109	371	487	0.76	0.05482	0.00132	0.54272	0.01282	0.07162	0.00055	405	39	440	8	446	3
QL09-08-12	270	728	1238	0.59	0.0571	0.0012	0.66228	0.01329	0.08409	0.00088	495	26	516	8	520	5
QL09-08-13	81.0	257	486	0.53	0.05461	0.00141	0.53621	0.01343	0.07108	0.00057	396	42	436	9	443	3
QL09-08-14	544	1433	2550	0.56	0.05766	0.00371	0.55394	0.03389	0.06967	0.0014	517	146	448	22	434	8
QL09-08-15	578	1227	1998	0.61	0.06809	0.00339	0.73021	0.03589	0.07778	0.0006	871	106	557	21	483	4
QL09-08-16	353	855	1947	0.44	0.06339	0.00116	0.67191	0.01209	0.07661	0.00071	721	23	522	7	476	4
QL09-08-17	107	350	483	0.72	0.05651	0.00244	0.54891	0.02331	0.07044	0.00055	473	98	444	15	439	3
QL09-08-18	283	806	1636	0.49	0.06409	0.0013	0.7021	0.0145	0.07892	0.00054	745	32	540	9	490	3
QL09-08-19	315	765	1562	0.49	0.0622	0.00259	0.65231	0.02653	0.07606	0.00067	681	91	510	16	473	4
QL09-08-2	127	271	914	0.30	0.0587	0.00221	0.55425	0.02049	0.06848	0.0005	556	84	448	13	427	3
QL09-08-20	106	227	677	0.33	0.05937	0.00322	0.55908	0.02996	0.0683	0.00057	581	121	451	20	426	3
QL09-08-21	101	166	809	0.21	0.07097	0.00148	0.64353	0.0128	0.06563	0.00046	957	29	504	8	410	3
QL09-08-22	406	1085	2518	0.43	0.05524	0.00091	0.6069	0.01051	0.07928	0.00064	422	24	482	7	492	4
QL09-08-23	189	664	826	0.80	0.05756	0.00136	0.5642	0.01327	0.07086	0.00052	513	39	454	9	441	3
QL09-08-24	102	213	694	0.31	0.05976	0.00135	0.66795	0.01548	0.08081	0.0007	595	35	519	9	501	4
QL09-11-1	204	624	853	0.73	0.06086	0.00279	0.58445	0.02623	0.06964	0.00063	634	101	467	17	434	4
QL09-11-3	192	637	925	0.69	0.06335	0.00148	0.61687	0.01374	0.07031	0.00052	720	35	488	9	438	3
QL09-11-4	300	286	1151	0.25	0.13032	0.00315	1.25207	0.03176	0.06913	0.00055	2102	33	824	14	431	3
QL09-11-5	212	419	1064	0.39	0.06126	0.00238	0.62361	0.02376	0.07383	0.00058	649	86	492	15	459	4
QL09-11-8	219	533	857	0.62	0.06754	0.00173	0.87721	0.02181	0.09358	0.00077	854	38	639	12	577	5
QL09-11-9	1402	5569	6256	0.89	0.06502	0.00115	0.6415	0.01111	0.07099	0.0005	775	25	503	7	442	3
QL09-11-10	467	441	1253	0.35	0.05685	0.00592	0.59261	0.06138	0.0756	0.00079	486	237	473	39	470	5
QL09-11-11	339	585	1174	0.50	0.10732	0.00443	1.21826	0.04994	0.0817	0.00065	1754	64	809	23	506	4
QL09-11-12	1423	778	3121	0.25	0.06937	0.00687	0.72887	0.07159	0.0762	0.00094	910	212	556	42	473	6
QL09-11-13	283	276	1122	0.25	0.06379	0.00503	0.63019	0.04901	0.07165	0.00093	735	173	496	31	446	6

	Pb	Th	U	Th/U	CORRECTED RATIOS						CORRECTED AGES (Ma)					
	Total ppm	232 ppm	238 ppm		$^{207}Pb/^{206}Pb$		$^{207}Pb/^{235}U$		$^{206}Pb/^{238}U$		$^{207}Pb/^{206}Pb$		$^{207}Pb/^{235}U$		$^{206}Pb/^{238}U$	
QL09-11-15	327	477	2142	0.22	0.05821	0.00221	0.60606	0.02166	0.07552	0.00097	538	85	481	14	469	6
QL09-11-16	874	624	2900	0.22	0.06877	0.00747	0.73485	0.07916	0.0775	0.00104	892	234	559	46	481	6
QL09-11-17	513	241	2135	0.11	0.11765	0.00248	1.34059	0.02818	0.08247	0.00092	1921	22	863	12	511	5
QL09-11-18	213	261	1204	0.22	0.05645	0.00267	0.59889	0.02779	0.07695	0.00069	470	107	477	18	478	4
QL09-11-19	637	281	1574	0.18	0.0689	0.00743	0.72351	0.07737	0.07616	0.00104	896	232	553	46	473	6
QL09-11-20	416	953	1529	0.62	0.06555	0.00335	0.68623	0.03439	0.07593	0.00075	792	110	531	21	472	4
QL09-11-21	191	468	578	0.81	0.10671	0.00325	1.06644	0.03712	0.07164	0.00099	1744	44	737	18	446	6
QL09-11-22	223	800	729	1.10	0.05651	0.00305	0.54866	0.02918	0.07042	0.00061	472	122	444	19	439	4
QL09-11-23	111	142	863	0.16	0.06221	0.00198	0.6719	0.02371	0.0773	0.00067	681	61	522	14	480	4
QL09-11-24	716	1543	2102	0.73	0.10046	0.00297	1.12898	0.03499	0.08065	0.00052	1633	48	767	17	500	3
QL09-11-24	716	1543	2102	0.73	0.10046	0.00297	1.12898	0.03499	0.08065	0.00052	1633	48	767	17	500	3
QL09-13-3	336	335	3409	0.10	0.05775	0.00113	0.61073	0.01128	0.0767	0.0005	520	44	484	7	476	3
QL09-13-4	197	617	827	0.75	0.06196	0.00223	0.62443	0.02201	0.07309	0.00055	673	79	493	14	455	3
QL09-13-5	285	344	1844	0.19	0.06095	0.0021	0.58408	0.01958	0.0695	0.00056	637	76	467	13	433	3
QL09-13-9	336	324	631	0.51	0.12857	0.00382	3.57205	0.09723	0.2015	0.00242	2079	54	1543	22	1183	13
QL09-13-10	74.5	203	276	0.74	0.05618	0.00308	0.53235	0.02895	0.06872	0.00052	460	125	433	19	428	3
QL09-13-11	250	363	1362	0.27	0.06138	0.00201	0.69481	0.02222	0.0821	0.00061	652	72	536	13	509	4
QL09-13-14	177	172	806	0.21	0.06841	0.00152	1.35655	0.02728	0.14382	0.00134	881	47	870	12	866	8
QL09-13-16	179	378	1332	0.28	0.0583	0.00153	0.63808	0.01629	0.07937	0.00047	541	59	501	10	492	3
QL09-13-2	385	412	4686	0.09	0.05695	0.00101	0.55258	0.00916	0.07037	0.00045	490	40	447	6	438	3
QL09-13-20	52.5	169	293	0.58	0.05728	0.00144	0.56342	0.01431	0.0713	0.00072	502	38	454	9	444	4
QL09-13-21	218	255	545	0.47	0.08652	0.00397	1.86592	0.08419	0.15641	0.00126	1350	91	1069	30	937	7
QL09-13-22	471	165	1190	0.14	0.07753	0.0031	1.30374	0.05019	0.12196	0.00131	1135	81	847	22	742	8
QL09-13-23	81.0	323	253	1.28	0.0575	0.00221	0.56187	0.02202	0.07064	0.00082	511	66	453	14	440	5
QL09-13-24	88.7	306	462	0.66	0.05545	0.00134	0.53917	0.01317	0.0705	0.00059	430	39	438	9	439	4
QL10-36-01	74.7	223	802	0.28	0.05950	0.00148	0.65047	0.01558	0.07929	0.0005	585	55	509	10	492	3
QL10-36-02	158	437	1783	0.25	0.05824	0.00086	0.62217	0.00990	0.07722	0.0005	539	23	491	6	479	3
QL10-36-03	49.2	160	581	0.28	0.05566	0.00132	0.55781	0.01355	0.07252	0.0006	439	40	450	9	451	3
QL10-36-04	158	469	412	1.14	0.09293	0.00154	3.38243	0.05635	0.26351	0.0019	1487	21	1500	13	1508	10

	Pb	Th	U	Th/U	CORRECTED RATIOS						CORRECTED AGES (Ma)					
	Total ppm	232 ppm	238 ppm		$^{207}Pb/^{206}Pb$		$^{207}Pb/^{235}U$		$^{206}Pb/^{238}U$		$^{207}Pb/^{206}Pb$		$^{207}Pb/^{235}U$		$^{206}Pb/^{238}U$	
QL10-36-05	113	86	294	0.29	0.10670	0.00194	4.68401	0.08282	0.31806	0.0023	1744	22	1764	15	1780	11
QL10-36-06	69.5	249	750	0.33	0.05689	0.00123	0.62600	0.01330	0.07978	0.0007	487	32	494	8	495	4
QL10-36-07	33.7	70	413	0.17	0.05450	0.00129	0.54691	0.01307	0.07270	0.0005	392	41	443	9	452	3
QL10-36-08	51.1	157	586	0.27	0.05680	0.00093	0.58784	0.01056	0.07521	0.0006	484	25	469	7	467	4
QL10-36-09	90.3	279	972	0.29	0.05817	0.00097	0.64211	0.01107	0.07988	0.0005	536	27	504	7	495	3
QL10-36-10	53.9	133	597	0.22	0.05390	0.00107	0.59273	0.01179	0.07972	0.0006	367	31	473	8	494	4
QL10-36-11	154	650	1551	0.42	0.05869	0.00111	0.66840	0.01153	0.08266	0.0006	556	26	520	7	512	3
QL10-36-12	141	439	1461	0.30	0.05917	0.00125	0.66078	0.01344	0.08099	0.0005	573	47	515	8	502	3
QL10-36-13	123	325	1238	0.26	0.05855	0.00085	0.69965	0.00984	0.08662	0.0005	550	21	539	6	535	3
QL10-36-14	150	247	750	0.33	0.10039	0.00327	2.26133	0.06874	0.16337	0.0019	1631	62	1200	21	975	10
QL10-36-15	74.0	216	792	0.27	0.05849	0.00130	0.65345	0.01328	0.08125	0.0006	548	32	511	8	504	4
QL10-36-16	31.8	99	317	0.31	0.08781	0.00223	0.95065	0.02323	0.07859	0.0007	1378	33	678	12	488	4
QL10-36-17	116.3	560	1160	0.48	0.07185	0.00295	0.70080	0.02823	0.07074	0.0006	982	86	539	17	441	3
QL10-36-18	118.6	361	1133	0.32	0.06938	0.00211	0.74908	0.02227	0.07831	0.0005	910	64	568	13	486	3
QL10-36-19	29.5	124	349	0.36	0.05466	0.00117	0.54813	0.01244	0.07256	0.0007	398	34	444	8	452	4
QL10-36-20	139.1	440	1440	0.31	0.06353	0.00111	0.71935	0.01209	0.08228	0.0007	726	22	550	7	510	4
QL10-39-01	228	657	2372	0.28	0.05957	0.00122	0.65791	0.01293	0.08010	0.0005	588	45	513	8	497	3
QL10-39-02	216	669	2397	0.28	0.05828	0.00293	0.52204	0.02572	0.06497	0.0007	540	113	427	17	406	4
QL10-39-04	75.3	120	792	0.15	0.06013	0.00167	0.63719	0.01705	0.07685	0.0006	608	62	501	11	477	4
QL10-39-05	70.9	186	546	0.34	0.06077	0.00435	0.70103	0.04945	0.08367	0.0010	631	159	539	30	518	6
QL10-39-06	92.6	176	1016	0.17	0.05866	0.00128	0.64097	0.01332	0.07924	0.0005	555	49	503	8	492	3
QL10-39-07	120	442	1240	0.36	0.06018	0.00141	0.66397	0.01513	0.07995	0.0006	610	37	517	9	496	3
QL10-39-08	218	611	2536	0.24	0.05850	0.00161	0.54270	0.01457	0.06728	0.0004	549	62	440	10	420	2
QL10-39-09	59.6	223	675	0.33	0.05454	0.00113	0.56072	0.01220	0.07426	0.0007	394	32	452	8	462	4
QL10-39-10	82.3	213	877	0.24	0.06408	0.00129	0.69812	0.01465	0.07866	0.0007	744	30	538	9	488	4
QL10-39-12	37.8	226	421	0.54	0.05445	0.00153	0.53488	0.01425	0.07125	0.0006	390	46	435	9	444	3
QL10-39-13	109	321	1136	0.28	0.05950	0.00162	0.64137	0.01697	0.07817	0.0005	586	60	503	10	485	3
QL10-39-14	88.9	232	955	0.24	0.05593	0.00092	0.62361	0.01052	0.08069	0.0006	450	25	492	7	500	3
QL10-39-15	97.5	295	1031	0.29	0.05724	0.00098	0.63699	0.01113	0.08052	0.0005	501	27	500	7	499	3
QL10-39-16	114	350	1192	0.29	0.06027	0.00158	0.66453	0.01677	0.07997	0.0006	613	58	517	10	496	3

	Pb	Th	U	Th/U	CORRECTED RATIOS						CORRECTED AGES (Ma)					
	Total	232	238		$^{207}Pb/^{206}Pb$		$^{207}Pb/^{235}U$		$^{206}Pb/^{238}U$		$^{207}Pb/^{206}Pb$		$^{207}Pb/^{235}U$		$^{206}Pb/^{238}U$	
	ppm	ppm	ppm													
QL10-39-19	48.8	148	500	0.30	0.07340	0.00234	0.95198	0.04206	0.08971	0.0016	1025	60	679	22	554	10
QL10-39-20	105	338	1111	0.30	0.06143	0.00151	0.67814	0.01600	0.08006	0.0006	654	54	526	10	496	3
QL10-39-17	424	493	2736	0.18	0.07008	0.00182	1.21372	0.03005	0.12562	0.0010	931	55	807	14	763	6
QL10-39-18	123	206	308	0.67	0.10884	0.00165	4.50816	0.07194	0.29946	0.0024	1780	18	1732	13	1689	12
QL10-43-01	185	1303	1938	0.67	0.05723	0.00086	0.58108	0.00848	0.07315	0.0004	500	23	465	5	455	2
QL10-43-02	168	234	1854	0.13	0.05722	0.00086	0.64079	0.00944	0.08070	0.0004	500	23	503	6	500	3
QL10-43-03	87.2	236	944	0.25	0.05702	0.00094	0.63864	0.01079	0.08077	0.0006	492	24	501	7	501	4
QL10-43-05	70.3	203	822	0.25	0.05345	0.00138	0.54967	0.01381	0.07433	0.0009	348	35	445	9	462	5
QL10-43-06	16.5	78	184	0.42	0.05236	0.00184	0.53889	0.01955	0.07409	0.0007	301	65	438	13	461	4
QL10-43-07	46.9	126	542	0.23	0.05762	0.00142	0.59181	0.01411	0.07426	0.0006	515	38	472	9	462	4
QL10-43-08	224	1938	2236	0.87	0.05577	0.00174	0.56798	0.01705	0.07387	0.0006	443	71	457	11	459	4
QL10-43-09	82.0	267	872	0.31	0.05655	0.00105	0.63278	0.01123	0.08095	0.0005	474	28	498	7	502	3
QL10-43-10	61.0	210	704	0.30	0.05544	0.00124	0.57108	0.01289	0.07410	0.0005	430	37	459	8	461	3
QL10-43-11	42.8	210	476	0.44	0.05605	0.00134	0.57296	0.01336	0.07402	0.0005	454	39	460	9	460	3
QL10-43-12	154	415	1782	0.23	0.05891	0.00131	0.60179	0.01269	0.07409	0.0005	564	49	478	8	461	3
QL10-43-13	109	296	1169	0.25	0.05555	0.00093	0.62170	0.01031	0.08077	0.0005	434	27	491	6	501	3
QL10-43-14	170	572	1699	0.34	0.07243	0.00171	0.81372	0.01982	0.08096	0.0006	998	37	605	11	502	4
QL10-43-15	30.3	138	337	0.41	0.05176	0.00160	0.52952	0.01601	0.07398	0.0007	275	51	431	11	460	4
QL10-43-16	39.9	165	449	0.37	0.05314	0.00137	0.54540	0.01420	0.07403	0.0006	335	45	442	9	460	3
QL10-43-17	31.0	114	351	0.33	0.05713	0.00180	0.58565	0.01832	0.07401	0.0006	497	54	468	12	460	4
QL10-43-18	30.5	89	338	0.26	0.05493	0.00158	0.61604	0.01994	0.08065	0.0009	409	52	487	13	500	5
QL10-43-19	106	264	1149	0.23	0.05555	0.00091	0.62128	0.01003	0.08075	0.0005	434	26	491	6	501	3
QL10-43-20	37.5	134	101	1.33	0.09202	0.00203	3.14659	0.07024	0.24727	0.0020	1468	30	1444	17	1424	10
Analyzed in China University of Geosciences (Beijing), CUGB																
QL09-04-01	9.44	67.3	91.6	0.73	0.05819	0.00395	0.63909	0.04179	0.07965	0.00143	537	153	502	26	494	9
QL09-04-02	57.5	500	575	0.87	0.06174	0.00121	0.68724	0.01456	0.08072	0.00121	665	22	531	9	500	7
QL09-04-03	47.5	526	368	1.43	0.06328	0.00115	0.83286	0.01668	0.09544	0.00141	718	20	615	9	588	8
QL09-04-04	28.9	264	237	1.12	0.05927	0.00235	0.78916	0.03088	0.09656	0.00182	577	53	591	18	594	11
QL09-04-06	14.5	130	129	1.00	0.064	0.00176	0.78879	0.02228	0.08937	0.00144	742	33	590	13	552	9
QL09-04-07	68.3	790	519	1.52	0.05973	0.00105	0.79078	0.01548	0.096	0.00142	594	20	592	9	591	8

	Pb	Th	U	Th/U	CORRECTED RATIOS						CORRECTED AGES (Ma)					
	Total ppm	232 ppm	238 ppm		$^{207}Pb/^{206}Pb$		$^{207}Pb/^{235}U$		$^{206}Pb/^{238}U$		$^{207}Pb/^{206}Pb$		$^{207}Pb/^{235}U$		$^{206}Pb/^{238}U$	
QL09-04-08	69.0	821	512	1.60	0.05927	0.00104	0.78826	0.01544	0.09644	0.00142	577	20	590	9	594	8
QL09-04-09	24.4	346	201	1.72	0.06295	0.00171	0.72515	0.02013	0.08353	0.00136	707	32	554	12	517	8
QL09-04-10	7.63	45	101	0.45	0.05495	0.00198	0.53093	0.01911	0.07007	0.00121	410	50	432	13	437	7
QL09-04-11	5.97	28	70	0.40	0.0568	0.00385	0.59051	0.03839	0.07541	0.00146	484	154	471	25	469	9
QL09-04-12	34.8	361	273	1.32	0.06205	0.00132	0.82852	0.0188	0.09683	0.00148	676	24	613	10	596	9
QL09-04-13	42.2	611	287	2.13	0.0632	0.00129	0.83928	0.01834	0.0963	0.00146	715	23	619	10	593	9
QL09-04-14	22.1	247	178	1.38	0.06014	0.00159	0.7636	0.0209	0.09206	0.00144	609	33	576	12	568	9
QL09-04-15	16.5	122	148	0.83	0.05894	0.00193	0.75189	0.02518	0.0925	0.00146	565	46	569	15	570	9
QL09-04-16	28.6	291	235	1.24	0.06533	0.00136	0.83099	0.01852	0.09224	0.00141	785	23	614	10	569	8
QL09-04-17	5.58	30	74	0.41	0.0555	0.00272	0.54295	0.02643	0.07094	0.00129	432	76	440	17	442	8
QL09-04-18	7.81	54	83	0.65	0.06364	0.00226	0.69948	0.02495	0.0797	0.00136	730	47	538	15	494	8
QL09-04-19	65.7	877	490	1.79	0.06148	0.00116	0.78494	0.01616	0.09259	0.00138	656	21	588	9	571	8
QL09-04-20	58.6	581	505	1.15	0.06233	0.0012	0.79004	0.01649	0.09191	0.00138	685	22	591	9	567	8
QL09-04-21	15.6	50	203	0.24	0.05887	0.00138	0.58726	0.0144	0.07233	0.00112	562	28	469	9	450	7
QL09-04-22	5.59	28	75	0.37	0.05929	0.00234	0.56928	0.02248	0.06963	0.00121	578	56	458	15	434	7
QL09-04-23	6.99	37	94	0.39	0.05525	0.00184	0.52882	0.01769	0.06941	0.00117	422	45	431	12	433	7
QL09-04-24	56.6	656	421	1.56	0.06093	0.00114	0.81714	0.0167	0.09725	0.00145	637	21	606	9	598	9
QL09-04-25	47.2	610	331	1.84	0.0625	0.00135	0.83776	0.01923	0.09719	0.00148	691	25	618	11	598	9
QL09-04-26	57.9	766	420	1.82	0.05951	0.00124	0.78686	0.01754	0.09588	0.00146	586	24	589	10	590	9
QL09-04-27	27.7	335	203	1.65	0.06277	0.00136	0.83223	0.01913	0.09615	0.00148	700	25	615	11	592	9
QL09-04-28	28.1	344	225	1.53	0.05849	0.00124	0.7275	0.01654	0.0902	0.00136	548	25	555	10	557	8
QL09-04-29	23.5	262	185	1.42	0.06098	0.00179	0.79541	0.02362	0.09459	0.00157	639	36	594	13	583	9
QL09-04-30	26.4	225	222	1.01	0.05947	0.00138	0.77367	0.01883	0.09433	0.00147	584	27	582	11	581	9
QL09-04-31	36.3	432	284	1.52	0.05939	0.0016	0.76138	0.02111	0.09296	0.00149	581	33	575	12	573	9
QL09-04-32	25.1	240	213	1.13	0.05994	0.00144	0.74657	0.01872	0.09031	0.00141	601	29	566	11	557	8
QL09-04-33	18.3	175	181	0.97	0.05982	0.00182	0.66797	0.02068	0.08097	0.00132	597	39	519	13	502	8
QL09-08-01	329.2	3256	3375	0.96	0.05744	0.00094	0.6397	0.01188	0.08075	0.00118	508	19	502	7	501	7
QL09-08-02	47.2	190	611	0.31	0.05839	0.00222	0.58181	0.02012	0.07227	0.00113	544	85	466	13	450	7
QL09-08-03	72.9	823	824	1.00	0.05644	0.00143	0.56348	0.01472	0.07239	0.00115	470	31	454	10	451	7
QL09-08-04	110	467	1288	0.36	0.05817	0.00117	0.64861	0.01403	0.08085	0.00122	536	23	508	9	501	7
QL09-08-06	75.9	1002	818	1.23	0.05722	0.00125	0.57115	0.01325	0.07238	0.0011	500	26	459	9	450	7

	Pb	Th	U	Th/U	CORRECTED RATIOS						CORRECTED AGES (Ma)					
	Total	232	238		$^{207}Pb/^{206}Pb$		$^{207}Pb/^{235}U$		$^{206}Pb/^{238}U$		$^{207}Pb/^{206}Pb$		$^{207}Pb/^{235}U$		$^{206}Pb/^{238}U$	
	ppm	ppm	ppm													
QL09-08-07	147.1	862	1802	0.48	0.0615	0.0022	0.6199	0.02006	0.07311	0.0011	657	78	490	13	455	7
QL09-08-11	62.4	638	718	0.89	0.05744	0.00115	0.57328	0.01245	0.07237	0.00108	508	24	460	8	450	6
QL09-08-12	193	1496	2344	0.64	0.06014	0.00097	0.6005	0.01106	0.07241	0.00105	609	18	478	7	451	6
QL09-08-13	21.3	86	298	0.29	0.05526	0.00122	0.52369	0.01221	0.06872	0.00105	423	27	428	8	428	6
QL09-08-14	24.1	204	290	0.70	0.06174	0.00336	0.58224	0.03013	0.0684	0.00115	665	120	466	19	426	7
QL09-08-15	75.6	360	991	0.36	0.06061	0.0023	0.56221	0.01959	0.06728	0.00102	625	84	453	13	420	6
QL09-08-16	22.0	170	261	0.65	0.05644	0.00157	0.56576	0.01614	0.07269	0.00116	470	36	455	10	452	7
QL09-08-21	109	933	1346	0.69	0.05906	0.00312	0.53434	0.02689	0.06562	0.00106	569	118	435	18	410	6
QL09-08-22	193	957	2299	0.42	0.06119	0.00101	0.65544	0.01228	0.07767	0.00113	646	19	512	8	482	7
QL09-08-23	44.7	238	556	0.43	0.05613	0.00232	0.55845	0.02137	0.07216	0.00112	458	94	451	14	449	7
QL09-08-24	25.2	208	302	0.69	0.05603	0.00138	0.56215	0.01442	0.07275	0.00114	454	30	453	9	453	7
QL09-08-25	122	584	1555	0.38	0.05475	0.00224	0.51797	0.01966	0.06862	0.00105	402	94	424	13	428	6
QL09-08-26	128	394	1673	0.24	0.05508	0.00197	0.53605	0.01738	0.07058	0.00107	415	82	436	11	440	6
QL09-08-27	42.9	190	566	0.34	0.05771	0.00229	0.54559	0.01992	0.06857	0.00106	519	89	442	13	428	6
QL09-08-28	282	2577	3133	0.82	0.05608	0.00304	0.55201	0.02856	0.07139	0.00114	455	123	446	19	445	7
QL09-08-29	153.8	417	1941	0.21	0.05902	0.00171	0.62267	0.01555	0.07651	0.00112	568	64	492	10	475	7
QL09-08-30	48.9	156	679	0.23	0.05697	0.00202	0.52556	0.01682	0.06691	0.00102	490	80	429	11	418	6
QL09-11-01	184	1014	2177	0.47	0.06201	0.00105	0.657	0.01249	0.07683	0.00112	674	19	513	8	477	7
QL09-11-02	156	279	1873	0.15	0.05485	0.00265	0.52013	0.02386	0.06877	0.00106	406	111	425	16	429	6
QL09-11-03	31.2	158	401	0.39	0.05828	0.0013	0.58432	0.01377	0.0727	0.00111	540	27	467	9	452	7
QL09-11-06	76.4	191	852	0.22	0.0585	0.00366	0.54144	0.0327	0.06713	0.00109	548	141	439	22	419	7
QL09-11-07	85.6	196	1167	0.17	0.05787	0.00106	0.58148	0.01177	0.07287	0.00108	525	21	465	8	453	6
QL09-11-08	120	322	1513	0.21	0.05652	0.00219	0.55234	0.01966	0.07087	0.00107	473	88	447	13	441	6
QL09-11-09	8.83	43	115	0.38	0.05632	0.00214	0.56056	0.02117	0.07217	0.00128	465	52	452	14	449	8
QL09-11-10	152	191	1882	0.10	0.0556	0.00258	0.53166	0.02322	0.06936	0.00109	436	106	433	15	432	7
QL09-11-17	91.7	87	772	0.11	0.06561	0.00307	0.88578	0.03904	0.09792	0.00155	794	101	644	21	602	9
QL09-11-20	162	378	2023	0.19	0.05748	0.00189	0.59361	0.01736	0.0749	0.00112	510	74	473	11	466	7
QL09-11-24	143	846	1731	0.49	0.05652	0.0027	0.5488	0.02472	0.07042	0.00111	473	108	444	16	439	7
QL09-11-26	81.0	640	853	0.75	0.06306	0.0036	0.64118	0.035	0.07374	0.00121	710	125	503	22	459	7
QL09-11-28	196	349	2105	0.17	0.05612	0.00357	0.54589	0.03362	0.07055	0.00113	457	145	442	22	439	7
QL09-11-29	133	1293	1477	0.88	0.05682	0.00123	0.59626	0.01368	0.0761	0.00116	485	26	475	9	473	7

	Pb	Th	U	Th/U	CORRECTED RATIOS						CORRECTED AGES (Ma)					
	Total ppm	232 ppm	238 ppm		$^{207}Pb/^{206}Pb$		$^{207}Pb/^{235}U$		$^{206}Pb/^{238}U$		$^{207}Pb/^{206}Pb$		$^{207}Pb/^{235}U$		$^{206}Pb/^{238}U$	
QL09-11-32	47.9	227	609	0.37	0.05545	0.00228	0.55719	0.02115	0.07288	0.00114	430	94	450	14	453	7
QL09-13-02	121	228	936	0.24	0.05789	0.00596	0.72371	0.07327	0.09067	0.00166	526	233	553	43	559	10
QL09-13-03	18.5	107	211	0.51	0.05501	0.00267	0.54895	0.02708	0.07225	0.00133	413	77	444	18	450	8
QL09-13-08	253	371	3375	0.11	0.0557	0.00271	0.51515	0.02347	0.06707	0.00115	441	111	422	16	418	7
QL09-13-15	20.7	133	252	0.53	0.05545	0.00284	0.5209	0.02718	0.06804	0.00136	430	81	426	18	424	8
QL09-13-17	100	426	1221	0.35	0.055	0.00406	0.50724	0.03625	0.06689	0.00124	412	170	417	24	417	7
QL09-13-21	74.1	270	872	0.31	0.05483	0.00451	0.5107	0.0409	0.06756	0.00128	405	189	419	27	421	8
QL09-13-22	50.3	264	627	0.42	0.05523	0.00239	0.51752	0.02354	0.06789	0.00126	422	68	423	16	423	8
QL09-13-25	87.4	159	1067	0.15	0.05576	0.00365	0.54231	0.03395	0.07054	0.00135	443	150	440	22	439	8
QL09-13-28	114	351	1209	0.29	0.05903	0.00608	0.56343	0.05692	0.06922	0.00137	568	233	454	37	431	8
QL09-13-31	136	179	1563	0.11	0.05435	0.00489	0.51333	0.04505	0.06851	0.00134	385	206	421	30	427	8
QL09-13-33	31.7	378	312	1.21	0.05464	0.00264	0.54444	0.02742	0.07223	0.00144	398	77	441	18	450	9
QL10-36-01	142	489	1770	0.28	0.05835	0.00174	0.60504	0.01574	0.07521	0.00108	543	67	480	10	467	7
QL10-36-02	81.4	85	341	0.25	0.10134	0.00156	3.08301	0.05457	0.22059	0.00318	1649	15	1428	14	1285	17
QL10-36-03	50.5	64	686	0.09	0.05618	0.00097	0.57035	0.01097	0.07361	0.00107	459	20	458	7	458	6
QL10-36-04	106	421	1264	0.33	0.06324	0.00199	0.66223	0.01841	0.07594	0.00111	716	68	516	11	472	7
QL10-36-05	81.6	195	1051	0.19	0.05785	0.00097	0.60263	0.01133	0.07554	0.00109	524	19	479	7	469	7
QL10-36-06	67.3	199	885	0.22	0.05678	0.00099	0.57405	0.01113	0.0733	0.00107	483	20	461	7	456	6
QL10-36-07	54.0	190	704	0.27	0.05574	0.00103	0.56319	0.01137	0.07326	0.00107	442	22	454	7	456	6
QL10-36-08	75.7	298	935	0.32	0.06423	0.00204	0.6565	0.01848	0.07413	0.0011	749	69	512	11	461	7
QL10-36-09	199	267	625	0.43	0.1073	0.0016	4.14545	0.07195	0.28014	0.00402	1754	14	1663	14	1592	20
QL10-36-10	97.2	444	1201	0.37	0.05997	0.001	0.61911	0.01166	0.07486	0.00108	602	19	489	7	465	6
QL10-36-11	93.0	308	1175	0.26	0.05673	0.00098	0.59227	0.01143	0.0757	0.0011	481	20	472	7	470	7
QL10-36-12	67.7	312	878	0.35	0.0555	0.00101	0.55285	0.01104	0.07223	0.00106	432	21	447	7	450	6
QL10-36-13	69.2	257	908	0.28	0.05648	0.001	0.56417	0.01106	0.07242	0.00106	471	21	454	7	451	6
QL10-36-14	75.1	249	983	0.25	0.05945	0.00107	0.59659	0.01186	0.07277	0.00107	584	21	475	8	453	6
QL10-36-15	21.1	181	247	0.73	0.05594	0.00152	0.55958	0.01556	0.07254	0.00116	450	34	451	10	451	7
QL10-36-16	68.6	120	934	0.13	0.05743	0.00154	0.57274	0.013	0.07233	0.00104	508	61	460	8	450	6
QL10-36-17	58.2	175	783	0.22	0.05724	0.00107	0.56564	0.01155	0.07165	0.00106	501	22	455	7	446	6
QL10-36-18	60.1	180	800	0.22	0.059	0.0018	0.58423	0.01562	0.07182	0.00107	567	68	467	10	447	6

	Pb	Th	U	Th/U	CORRECTED RATIOS						CORRECTED AGES (Ma)					
	Total ppm	232 ppm	238 ppm		$^{207}Pb/^{206}Pb$		$^{207}Pb/^{235}U$		$^{206}Pb/^{238}U$		$^{207}Pb/^{206}Pb$		$^{207}Pb/^{235}U$		$^{206}Pb/^{238}U$	
QL10-36-19	54.2	194	719	0.27	0.05625	0.00106	0.55933	0.01151	0.07211	0.00106	462	22	451	7	449	6
QL10-36-20	74.4	169	1041	0.16	0.05799	0.00108	0.56001	0.01141	0.07003	0.00103	529	22	452	7	436	6
QL10-36-21	79.3	234	1044	0.22	0.0572	0.00177	0.56636	0.01538	0.07181	0.00106	499	70	456	10	447	6
QL10-36-22	112.2	105	480	0.22	0.09591	0.00245	2.87707	0.06039	0.21756	0.00316	1546	49	1376	16	1269	17
QL10-36-23	20.2	107	265	0.40	0.05512	0.00146	0.53785	0.01468	0.07075	0.00111	417	34	437	10	441	7
QL10-36-24	35.6	104	112	0.93	0.09274	0.00171	3.26995	0.06586	0.25566	0.00385	1483	18	1474	16	1468	20
QL10-36-25	86.4	502	565	0.89	0.06899	0.00116	1.14487	0.0216	0.12033	0.00176	898	18	775	10	732	10
QL10-36-26	22.5	95	270	0.35	0.05689	0.00229	0.60073	0.02225	0.07659	0.0012	487	91	478	14	476	7
QL10-36-27	97.5	469	315	1.49	0.08562	0.00139	2.62859	0.04844	0.22261	0.00324	1330	16	1309	14	1296	17
QL10-39-01	44.1	247	554	0.45	0.0564	0.00145	0.56591	0.01512	0.07276	0.00117	468	32	455	10	453	7
QL10-39-02	55.7	143	328	0.43	0.07071	0.00141	1.50107	0.03262	0.15394	0.00236	949	22	931	13	923	13
QL10-39-04	61.5	195	822	0.24	0.05653	0.0012	0.5631	0.01288	0.07223	0.00111	473	25	454	8	450	7
QL10-39-06	130	464	1667	0.28	0.05716	0.00107	0.58816	0.01223	0.07461	0.00113	498	22	470	8	464	7
QL10-39-07	16.5	98	206	0.47	0.05589	0.00192	0.55858	0.01947	0.07247	0.0012	448	48	451	13	451	7
QL10-39-08	24.0	119	259	0.46	0.06089	0.0043	0.58459	0.03988	0.06963	0.00127	635	157	467	26	434	8
QL10-39-09	27.1	178	331	0.54	0.05892	0.00151	0.58949	0.01571	0.07254	0.00116	564	31	471	10	451	7
QL10-39-10	12.4	63	158	0.40	0.0587	0.00176	0.58728	0.01788	0.07255	0.00122	556	38	469	11	452	7
QL10-39-11	20.1	156	223	0.70	0.05765	0.00186	0.61905	0.02021	0.07787	0.00133	516	42	489	13	483	8
QL10-39-12	34.6	76	286	0.27	0.06869	0.00156	1.10221	0.02646	0.11635	0.00183	889	25	754	13	710	11
QL10-39-14	72.0	245	944	0.26	0.0565	0.00133	0.568	0.01405	0.0729	0.00115	472	28	457	9	454	7
QL10-39-15	34.2	195	427	0.46	0.05534	0.00129	0.55588	0.01372	0.07284	0.00115	426	29	449	9	453	7
QL10-39-16	107	384	1238	0.31	0.06051	0.00233	0.64158	0.02264	0.0769	0.0012	622	85	503	14	478	7
QL10-39-17	117	548	1496	0.37	0.0609	0.00119	0.60851	0.01304	0.07246	0.0011	636	22	483	8	451	7
QL10-39-18	79.3	230	1056	0.22	0.05591	0.00122	0.5617	0.01315	0.07285	0.00113	449	26	453	9	453	7
QL10-39-20	106	296	1208	0.25	0.06128	0.00278	0.62332	0.02643	0.07377	0.00118	649	100	492	17	459	7
QL10-39-21	72.7	290	929	0.31	0.06185	0.00128	0.62197	0.01391	0.07292	0.00112	669	24	491	9	454	7
QL10-39-22	80.2	287	953	0.30	0.05744	0.00224	0.60172	0.02151	0.07598	0.00119	508	88	478	14	472	7
QL10-39-23	60.1	242	782	0.31	0.05745	0.00123	0.57637	0.0133	0.07275	0.00113	509	26	462	9	453	7
QL10-39-24	88.5	201	952	0.21	0.05877	0.00351	0.57961	0.03327	0.07152	0.00117	559	134	464	21	445	7
QL10-39-25	94.7	345	1159	0.30	0.06223	0.00124	0.65982	0.01439	0.07688	0.00118	682	23	515	9	477	7
QL10-39-26	42.5	212	544	0.39	0.05692	0.00141	0.56674	0.01469	0.07219	0.00116	488	30	456	10	449	7

	Pb	Th	U	Th/U	CORRECTED RATIOS						CORRECTED AGES (Ma)					
	Total ppm	232 ppm	238 ppm		$^{207}Pb/^{206}Pb$		$^{207}Pb/^{235}U$		$^{206}Pb/^{238}U$		$^{207}Pb/^{206}Pb$		$^{207}Pb/^{235}U$		$^{206}Pb/^{238}U$	
QL10-39-27	110.4	325	1298	0.25	0.05843	0.00202	0.63882	0.01974	0.0793	0.00122	546	77	502	12	492	7
QL10-39-28	75.1	212	902	0.24	0.0584	0.0019	0.64107	0.01844	0.07961	0.00122	545	73	503	11	494	7
QL10-39-29	53.2	182	682	0.27	0.06199	0.00228	0.61007	0.02027	0.07137	0.00112	674	81	484	13	444	7
QL10-39-30	148	518	1732	0.30	0.06195	0.00279	0.61375	0.0259	0.07185	0.00115	672	99	486	16	447	7
QL10-39-31	106	394	1288	0.31	0.06144	0.00124	0.66385	0.0146	0.07835	0.0012	655	23	517	9	486	7
QL10-43-01	41.1	499	443	1.13	0.05707	0.00118	0.57232	0.01272	0.07272	0.00111	494	24	460	8	453	7
QL10-43-02	13.8	75	173	0.43	0.05671	0.00173	0.56499	0.01742	0.07225	0.00121	480	39	455	11	450	7
QL10-43-03	46.3	248	580	0.43	0.05805	0.00101	0.57943	0.0113	0.07237	0.00107	532	20	464	7	450	6
QL10-43-04	19.0	161	224	0.72	0.05612	0.00158	0.55915	0.01612	0.07225	0.00117	457	36	451	10	450	7
QL10-43-05	54.7	179	730	0.25	0.05618	0.00183	0.53238	0.01536	0.06873	0.00103	459	74	433	10	428	6
QL10-43-06	144	679	1837	0.37	0.05754	0.00084	0.57604	0.00999	0.0726	0.00105	512	17	462	6	452	6
QL10-43-07	87.3	316	1142	0.28	0.05668	0.00124	0.56444	0.01313	0.07222	0.00111	479	26	454	9	450	7
QL10-43-08	25.8	203	323	0.63	0.05545	0.00174	0.52881	0.01679	0.06916	0.00116	430	41	431	11	431	7
QL10-43-09	41.9	100	557	0.18	0.05573	0.00115	0.55831	0.01243	0.07265	0.0011	442	25	450	8	452	7
QL10-43-10	28.4	76	162	0.47	0.06711	0.0028	1.36022	0.05228	0.14699	0.00236	841	89	872	22	884	13
QL10-43-11	68.7	249	861	0.29	0.05654	0.00121	0.58799	0.01345	0.07541	0.00115	474	26	470	9	469	7
QL10-43-12	92.7	385	1183	0.33	0.05891	0.00094	0.59121	0.01083	0.07278	0.00106	564	18	472	7	453	6
QL10-43-13	89.4	499	1064	0.47	0.05656	0.00101	0.59263	0.01177	0.07598	0.00113	474	21	473	8	472	7
QL10-43-15	78.5	220	979	0.22	0.05658	0.00114	0.59792	0.01304	0.07663	0.00116	475	24	476	8	476	7
QL10-43-16	27.5	136	350	0.39	0.0562	0.00136	0.56109	0.0142	0.07239	0.00112	460	30	452	9	451	7
QL10-43-18	100	551	1235	0.45	0.05996	0.00207	0.59131	0.01836	0.07153	0.00108	602	76	472	12	445	6
QL10-43-19	30.9	139	394	0.35	0.05703	0.00114	0.57121	0.01239	0.07263	0.0011	493	24	459	8	452	7
QL10-43-20	166	522	2136	0.24	0.05838	0.00178	0.56974	0.01524	0.07078	0.00104	544	68	458	10	441	6
QL10-43-21	10.6	47	138	0.34	0.05587	0.00164	0.55211	0.01654	0.07166	0.00116	447	38	446	11	446	7
QL10-43-22	76.0	272	951	0.29	0.05647	0.00088	0.58974	0.01071	0.07573	0.00111	471	18	471	7	471	7
QL10-43-23	33.1	105	370	0.28	0.06318	0.00155	0.70303	0.01791	0.08069	0.00128	714	29	541	11	500	8
QL10-43-25	41.9	112	546	0.21	0.05659	0.001	0.57801	0.01141	0.07407	0.0011	476	21	463	7	461	7
QL10-43-26	60.9	250	778	0.32	0.05861	0.00187	0.58507	0.01654	0.0724	0.00108	553	71	468	11	451	6
QL10-43-27	110	291	1317	0.22	0.05656	0.0009	0.62724	0.01151	0.08042	0.00118	474	19	494	7	499	7
QL10-43-28	93.4	120	1211	0.10	0.05636	0.00085	0.5971	0.0106	0.07683	0.00112	467	18	475	7	477	7

Table 6.1 sample location and brief description of samples Kekeli, North Qilian Orogenic Belt

Sample	Age (Ma)	GPS position		mineral assemblage	SiO_2%	A/CNK
QL10-14	498	N38°24'45.7"	E99°25'38.1″	**Group1,**Bt 13%, Pl30%, Kfs15%, Qz42%	70.0	1.1
QL10-15	502	N38°24'45.7"	E99°25'38.1″	**Group1,**Bt /Chl22%, Kfs11%, Pl 20%, Qz46%, secondary Ms	72.5	1.2
QL10-20		N38°23'49.3"	E99°20'07.7"	**MME**, Amp 50%, Pl 26%, Kfs10%, Qz10%, Ep2.5%, Ilm 1.6%	47.1	0.4
QL10-21	502	N38°23'49.3"	E99°20'07.7"	**MME**, Amp 62%, Pl 23%, Kfs, Qz13%, Ep0.75%	51.1	0.7
QL10-22		N38°23'49.3"	E99°20'07.7"	**MME**, Amp80%, interstitial Pl, Kfs, Qz, cumulate texture	45.2	0.4
QL10-23	507	N38°23'49.3"	E99°20'07.7"	**Group2,** Amp27%, Pl44%, Kfs10%, Qz16%	55.9	0.8
QL10-24	501	N38°23'49.3"	E99°20'07.7"	**Group2,** Amp24%, Pl36%, Kfs25%, Qz15%	60.1	0.9
QL10-25	500	N38°23'49.3"	E99°20'07.7"	**MME**, Tremolite (Amp) 64%, Pl34%,Kfs0.5%.Qz 1.75%	46.6	0.7
QL10-26	498	N38°23'49.3"	E99°20'07.7"	**MME,** Pyroxene28%, Bt10%, Amp12%, Qz18%,Pl18%, Kfs:9%, Fe-Ti oxides: 4.2%	48.4	0.7
QL10-27	503	N38°23'49.3"	E99°20'07.7"	**Group2,** tremolite 34%,Pl 25%, Qz30%, Kfs 10%	60.8	1.0

Bt: biotite; Pl: plagioclase; Kfs: K-feldspar; Qz: quartz; Ms: muscovite; Amp: amphibole; Chl: chlorite

Table 6.2 Major and trace elements of samples in Kekeli

	QL10-014	QL10-015	QL10-023	QL10-024	QL10-027	QL10-020	QL10-021	QL10-022	QL10-025	QL10-026
	Group 1	Group 1	Group 2	Group 2	Group 2	MME	MME	MME	MME	Gabbronorite
SiO_2	70	72.5	55.9	60.1	60.8	47.1	51.1	45.2	46.6	48.4
TiO_2	0.45	0.33	0.78	0.64	0.73	1.29	0.92	1.91	1.1	3.02
Al_2O_3	14.1	13.6	17.3	15.5	15.8	11.4	16.1	10.6	15.45	15.2
Fe_2O_3	0.66	0.59	2.55	1.49	1.31	4.22	3.65	5.48	2.54	3.97
FeO	2.32	1.64	4.87	4.57	4.65	9.8	5.72	11.3	7.48	8.76
MnO	0.053	0.044	0.13	0.11	0.093	0.29	0.19	0.31	0.16	0.21
MgO	1.52	1.2	3.07	3.27	3.1	6.44	4.22	7.25	11.4	4.38
CaO	1.74	1.67	7.12	4.21	2.95	12.1	8.93	11.9	8.88	7.54
Na_2O	2.9	2.56	3.25	2.8	3.78	1.78	2.82	1.11	2.23	3.19
K_2O	4.53	4.17	2.62	4.73	3.77	1.06	3.31	1.15	0.9	2.72
P_2O_5	0.1	0.082	0.52	0.4	0.5	2.21	1.01	0.92	0.17	1.2
LOI	1.39	1.39	1.37	1.62	1.93	1.14	1.34	1.59	2.23	0.4
Total	98.37	98.39	98.11	97.82	97.48	97.69	97.97	97.13	96.91	98.59
A/CNK	1.10	1.15	0.82	0.89	1.01	0.44	0.66	0.43	0.74	0.69
Li	34.6	44.8	6.53	15.4	18	8.1	6.22	6.37	10.6	17.5
Sc	9.47	8.47	17.5	16.3	18.1	26	22.2	42.7	25.1	28.4
Cr	27.4	15.9	16.8	36.8	37.2	22.9	17.8	48.1	50.6	13.8
Co	5.69	2.86	17.6	16.2	14	34.2	24.6	36.9	55.6	26.8
Ni	10.1	9.21	7.14	9.13	6.9	15.7	11.5	14.6	23.5	10.4
Ga	19.7	17.2	21.6	19	19.5	25	21.1	27	15.4	23.5
Rb	207	186	89.1	168	165	24.2	97.2	21.1	36.3	94.2
Sr	98.2	81.9	866	607	450	450	860	461	214	430
Y	44.3	40.8	28.8	24.8	32.6	71.7	38.1	83.6	21.4	55.5
Zr	237	159	232	276	274	834	311	512	103	209
Nb	19.7	13.1	16.2	17	19	25	14.9	53	6.92	21.9
Ba	612	470	1010	1270	1010	101	2010	91	275	2000
La	49.4	32.7	40.1	57.4	101	318	122	265	12.2	62.6
Ce	99.8	64.5	98.1	110	178	589	229	439	27	134
Pr	12.5	7.97	14	13.6	20.6	65.1	28	50.3	3.92	18.5
Nd	46.7	29.4	58.1	51.6	75.1	225	109	184	17.6	78.7
Sm	9	6.01	10.9	9.42	12.9	32.6	19.2	32.7	4.09	15.5
Eu	1.05	0.98	2.59	2.29	2.86	7.34	3.75	6.37	1.29	4.33
Gd	8.24	5.83	8.9	7.79	10.5	26.5	15.5	26.5	4.11	13.7
Tb	1.39	1.14	1.23	1.06	1.39	3.24	1.93	3.69	0.68	2.04
Dy	8.06	7.24	6.06	5.11	6.82	14.8	8.69	18	4.09	11.5
Ho	1.59	1.47	1.04	0.91	1.15	2.56	1.41	3.09	0.83	2.16
Er	4.42	4.21	2.69	2.37	3.06	6.9	3.48	8.1	2.27	5.67
Tm	0.67	0.66	0.38	0.34	0.44	1	0.47	1.15	0.34	0.79
Yb	4.28	4.29	2.45	2.19	2.77	6.72	2.99	7.49	2.19	4.98
Lu	0.63	0.64	0.38	0.34	0.41	1.07	0.47	1.09	0.33	0.75
Hf	7.84	5.26	6.24	7.24	7.29	20.7	7.92	14.5	3.13	5.88
Ta	1.72	1.27	0.85	1.12	1.2	1.56	0.67	4.69	0.43	1.22
Pb	27.1	21.4	26.4	52.2	17.8	46.1	64.2	17.2	7.06	9.77
Th	25.8	12	6.79	18.2	27.8	82.8	17.3	72.6	2.51	4.6
U	5.12	2.84	3.66	4.53	4.94	21.5	5.13	13.1	0.61	0.89

Table 6.3 Zircon in situ LA-ICP-MS dating results

	Pb	Th	U	Th/U	CORRECTED RATIOS						CORRECTED AGES (Ma)					
	Total ppm	232 ppm	238 ppm		$^{207}Pb/^{206}Pb$		$^{207}Pb/^{235}U$		$^{206}Pb/^{238}U$		$^{207}Pb/^{206}Pb$		$^{207}Pb/^{235}U$		$^{206}Pb/^{238}U$	
Analysed in Chinese Academy of Sciences, Wuhan																
QL10-14-01	33.1	183	325	0.56	0.0564	0.0015	0.6363	0.0181	0.0812	0.0007	468	47	500	11	503	4
QL10-14-03	41.0	212	375	0.57	0.0571	0.0030	0.6327	0.0320	0.0804	0.0009	495	117	498	20	498	5
QL10-14-04	51.9	348	491	0.71	0.0574	0.0024	0.6314	0.0255	0.0799	0.0007	505	93	497	16	495	4
QL10-14-05	38.6	230	340	0.68	0.0587	0.0028	0.6799	0.0316	0.0840	0.0008	557	106	527	19	520	5
QL10-14-06	56.2	266	514	0.52	0.0632	0.0035	0.7063	0.0390	0.0811	0.0007	715	122	543	23	502	4
QL10-14-07	30.5	153	307	0.50	0.0574	0.0019	0.6434	0.0220	0.0806	0.0008	508	58	504	14	500	5
QL10-14-08	82.7	50.5	930	0.05	0.0596	0.0016	0.6633	0.0150	0.0807	0.0011	589	59	517	9	501	6
QL10-14-09	6.40	39.8	63.4	0.63	0.0581	0.0027	0.6337	0.0287	0.0807	0.0011	534	75	498	18	501	7
QL10-14-10	60.3	292	576	0.51	0.0602	0.0013	0.7060	0.0151	0.0846	0.0007	612	32	542	9	524	4
QL10-14-11	71.7	381	652	0.58	0.0642	0.0030	0.7323	0.0321	0.0828	0.0013	747	101	558	19	513	8
QL10-14-12	38.2	173	387	0.45	0.0587	0.0013	0.6551	0.0145	0.0807	0.0007	555	34	512	9	500	4
QL10-14-13	57.5	338	551	0.61	0.0645	0.0014	0.7201	0.0152	0.0806	0.0006	757	32	551	9	500	3
QL10-14-15	55.0	291	507	0.57	0.0594	0.0021	0.6433	0.0227	0.0785	0.0005	582	80	504	14	487	3
QL10-14-16	219	130	2306	0.06	0.0597	0.0011	0.6827	0.0124	0.0830	0.0003	591	41	528	7	514	2
QL10-14-17	36.6	199	348	0.57	0.0575	0.0019	0.6348	0.0207	0.0801	0.0005	509	75	499	13	497	3
QL10-14-19	57.8	282	572	0.49	0.0648	0.0015	0.7241	0.0159	0.0811	0.0008	767	31	553	9	502	4
QL10-14-20	40.1	213	399	0.53	0.0584	0.0012	0.6518	0.0138	0.0809	0.0007	546	32	510	8	501	4
QL10-15-01	4.3	0.84	48.7	0.02	0.0586	0.0028	0.6553	0.0326	0.0808	0.0011	552	85	512	20	501	7
QL10-15-02	76.6	40.3	660	0.06	0.0591	0.0010	0.8490	0.0148	0.1037	0.0008	569	24	624	8	636	5
QL10-15-03	10.9	15.7	120	0.13	0.0544	0.0020	0.6051	0.0214	0.0809	0.0009	389	59	480	14	501	5
QL10-15-04	55.5	443	501	0.88	0.0549	0.0012	0.6143	0.0134	0.0807	0.0006	408	36	486	8	500	3
QL10-15-05	30.3	169	105	1.61	0.1780	0.0206	2.3575	0.2640	0.0961	0.0027	2634	200	1230	80	591	16
QL10-15-06	106	119	767	0.15	0.0614	0.0011	1.0505	0.0198	0.1230	0.0010	654	26	729	10	748	6
QL10-15-07	89.7	117	684	0.17	0.0638	0.0011	1.0168	0.0177	0.1148	0.0007	736	27	712	9	700	4
QL10-15-08	92.6	129	871	0.15	0.0550	0.0010	0.7252	0.0140	0.0949	0.0008	413	28	554	8	585	5

Table 6.3 Zircon in situ LA-ICP-MS dating results

	Pb	Th	U	Th/U	CORRECTED RATIOS						CORRECTED AGES (Ma)					
	Total ppm	232 ppm	238 ppm		$^{207}Pb/^{206}Pb$		$^{207}Pb/^{235}U$		$^{206}Pb/^{238}U$		$^{207}Pb/^{206}Pb$		$^{207}Pb/^{235}U$		$^{206}Pb/^{238}U$	
QL10-15-09	125	204	869	0.23	0.0615	0.0010	1.0499	0.0195	0.1230	0.0012	656	23	729	10	748	7
QL10-15-10	54.2	55.6	391	0.14	0.0611	0.0012	1.0399	0.0198	0.1230	0.0010	644	27	724	10	748	6
QL10-15-11	132	83.9	957	0.09	0.0631	0.0011	1.0766	0.0190	0.1231	0.0009	712	25	742	9	749	5
QL10-15-12	33.4	133	341	0.39	0.0587	0.0018	0.6521	0.0182	0.0807	0.0009	556	41	510	11	500	5
QL10-15-13	214	279	803	0.35	0.0851	0.0031	2.0444	0.0735	0.1743	0.0014	1317	73	1130	24	1036	8
QL10-15-14	68.2	221	445	0.50	0.0623	0.0015	1.0598	0.0247	0.1232	0.0009	686	38	734	12	749	5
QL10-15-15	89.2	94.3	770	0.12	0.0586	0.0010	0.8419	0.0151	0.1038	0.0008	553	27	620	8	637	4
QL10-15-16	60.9	75.4	433	0.17	0.0634	0.0012	1.0782	0.0210	0.1231	0.0009	722	28	743	10	748	5
QL10-15-17	62.9	41.6	591	0.07	0.0604	0.0013	0.7904	0.0175	0.0946	0.0007	619	35	591	10	583	4
QL10-15-18	43.5	51.3	453	0.11	0.0553	0.0013	0.6568	0.0149	0.0863	0.0007	422	37	513	9	534	4
QL10-15-19	48.8	73.3	348	0.21	0.0639	0.0014	1.0874	0.0228	0.1232	0.0010	739	31	747	11	749	6
QL10-15-20	5.73	56.0	47.2	1.19	0.0605	0.0035	0.6697	0.0386	0.0808	0.0012	622	99	521	23	501	7
QL10-21-01	26.8	93.7	277	0.34	0.0577	0.0024	0.6362	0.0256	0.0800	0.0006	518	92	500	16	496	4
QL10-21-02	30.3	168	306	0.55	0.0564	0.0013	0.6305	0.0145	0.0809	0.0007	468	36	496	9	502	4
QL10-21-03	69.0	311	712	0.44	0.0584	0.0012	0.6549	0.0137	0.0810	0.0008	546	28	511	8	502	5
QL10-21-04	112	528	1040	0.51	0.0578	0.0009	0.7105	0.0112	0.0887	0.0007	524	22	545	7	548	4
QL10-21-05	114	775	984	0.79	0.0584	0.0010	0.7182	0.0119	0.0889	0.0005	544	25	550	7	549	3
QL10-21-06	26.0	93.2	271	0.34	0.0585	0.0017	0.6528	0.0194	0.0807	0.0007	549	50	510	12	500	4
QL10-21-07	39.3	212	389	0.54	0.0582	0.0013	0.6486	0.0147	0.0807	0.0006	536	37	508	9	500	3
QL10-21-08	59.1	242	595	0.41	0.0585	0.0013	0.6615	0.0138	0.0819	0.0006	547	33	516	8	507	4
QL10-21-09	88.1	451	793	0.57	0.0588	0.0010	0.7226	0.0117	0.0888	0.0005	561	26	552	7	548	3
QL10-21-10	51.9	325	502	0.65	0.0566	0.0013	0.6243	0.0140	0.0798	0.0006	474	37	493	9	495	3
QL10-21-11	113	454	1052	0.43	0.0581	0.0010	0.7111	0.0127	0.0884	0.0005	533	29	545	8	546	3
QL10-21-12	59	207	612	0.34	0.0563	0.0010	0.6315	0.0109	0.0811	0.0005	465	28	497	7	502	3
QL10-21-13	102	393	954	0.41	0.0552	0.0008	0.6778	0.0098	0.0890	0.0007	419	18	525	6	549	4
QL10-21-14	132	786	1154	0.68	0.0572	0.0007	0.7019	0.0087	0.0887	0.0005	500	17	540	5	548	3

Table 6.3 Zircon in situ LA-ICP-MS dating results

	Pb	Th	U	Th/U	CORRECTED RATIOS						CORRECTED AGES (Ma)					
	Total ppm	232 ppm	238 ppm		$^{207}Pb/^{206}Pb$		$^{207}Pb/^{235}U$		$^{206}Pb/^{238}U$		$^{207}Pb/^{206}Pb$		$^{207}Pb/^{235}U$		$^{206}Pb/^{238}U$	
QL10-21-15	47.7	234	457	0.51	0.0707	0.0015	0.7959	0.0195	0.0811	0.0006	949	38	595	11	503	4
QL10-21-16	66.7	224	647	0.35	0.0544	0.0008	0.6501	0.0091	0.0865	0.0005	388	20	509	6	535	3
QL10-21-17	78.7	360	700	0.51	0.0647	0.0011	0.7984	0.0148	0.0891	0.0005	765	30	596	8	550	3
QL10-21-18	34.4	120	343	0.35	0.0536	0.0011	0.6190	0.0126	0.0837	0.0006	353	34	489	8	518	3
QL10-21-19	91.0	420	836	0.50	0.0559	0.0009	0.6896	0.0109	0.0890	0.0005	450	24	533	7	550	3
QL10-21-20	21.4	87.7	222	0.40	0.0545	0.0015	0.6113	0.0166	0.0811	0.0007	390	46	484	10	503	4
QL10-21-21	44.1	164	467	0.35	0.0562	0.0012	0.6253	0.0127	0.0804	0.0006	460	32	493	8	499	3
QL10-21-22	124	631	1244	0.51	0.0630	0.0010	0.7049	0.0117	0.0809	0.0008	707	20	542	7	502	4
QL10-21-23	74.6	351	713	0.49	0.0566	0.0010	0.6821	0.0131	0.0869	0.0008	476	27	528	8	537	4
QL10-21-24	106	432	865	0.50	0.0732	0.0014	0.9496	0.0181	0.0937	0.0005	1020	29	678	9	578	3
QL10-21-25	105	593	894	0.66	0.0639	0.0027	0.7503	0.0311	0.0851	0.0006	739	91	568	18	527	3
QL10-23-01	64.6	237	664	0.36	0.0571	0.0010	0.6495	0.0110	0.0823	0.0006	495	25	508	7	510	3
QL10-23-02	90.7	380	870	0.44	0.0571	0.0010	0.6952	0.0125	0.0879	0.0007	496	26	536	7	543	4
QL10-23-03	210	397	1283	0.31	0.0871	0.0067	1.3011	0.0985	0.1084	0.0014	1362	153	846	43	663	8
QL10-23-04	59.9	155	518	0.30	0.0585	0.0041	0.6798	0.0477	0.0843	0.0007	548	159	527	29	522	4
QL10-23-05	96.6	285	931	0.31	0.0607	0.0017	0.7326	0.0196	0.0875	0.0007	630	62	558	11	541	4
QL10-23-06	50.3	245	497	0.49	0.0577	0.0018	0.6488	0.0202	0.0816	0.0006	517	72	508	12	506	4
QL10-23-07	106	439	1018	0.43	0.0570	0.0010	0.6967	0.0126	0.0883	0.0008	493	25	537	8	545	4
QL10-23-08	38.1	140	380	0.37	0.0579	0.0018	0.6484	0.0189	0.0812	0.0006	526	68	507	12	503	4
QL10-23-09	171	1546	1421	1.09	0.0907	0.0013	1.0540	0.0148	0.0840	0.0005	1440	18	731	7	520	3
QL10-23-10	77.3	318	742	0.43	0.0576	0.0011	0.7048	0.0140	0.0882	0.0008	516	27	542	8	545	5
QL10-23-11	56.1	260	524	0.49	0.0623	0.0016	0.7308	0.0187	0.0847	0.0008	684	38	557	11	524	5
QL10-23-12	68.3	242	648	0.37	0.0588	0.0010	0.7174	0.0127	0.0882	0.0006	558	26	549	8	545	4
QL10-23-13	73.9	270	699	0.39	0.0616	0.0011	0.7395	0.0130	0.0869	0.0006	659	26	562	8	537	4
QL10-23-14	103	394	957	0.41	0.0600	0.0011	0.7322	0.0131	0.0882	0.0005	602	29	558	8	545	3
QL10-23-15	64.5	228	613	0.37	0.0583	0.0014	0.7031	0.0163	0.0872	0.0006	541	38	541	10	539	4

Table 6.3 Zircon in situ LA-ICP-MS dating results

	Pb	Th	U	Th/U	CORRECTED RATIOS						CORRECTED AGES (Ma)					
	Total ppm	232 ppm	238 ppm		$^{207}Pb/^{206}Pb$		$^{207}Pb/^{235}U$		$^{206}Pb/^{238}U$		$^{207}Pb/^{206}Pb$		$^{207}Pb/^{235}U$		$^{206}Pb/^{238}U$	
QL10-23-16	99.9	383	928	0.41	0.0576	0.0012	0.7009	0.0141	0.0879	0.0006	514	33	539	8	543	3
QL10-23-17	82.4	306	763	0.40	0.0607	0.0012	0.7384	0.0139	0.0879	0.0005	629	30	561	8	543	3
QL10-23-18	119	565	1082	0.52	0.0591	0.0010	0.7197	0.0118	0.0879	0.0005	572	26	551	7	543	3
QL10-23-19	72.1	264	681	0.39	0.0580	0.0010	0.7038	0.0111	0.0878	0.0006	531	23	541	7	542	3
QL10-23-20	89.5	350	839	0.42	0.0598	0.0013	0.7329	0.0173	0.0883	0.0006	595	39	558	10	545	4
QL10-24-01	30.1	163	305	0.53	0.0526	0.0017	0.5826	0.0182	0.0807	0.0007	309	54	466	12	500	4
QL10-24-02	28.9	134	298	0.45	0.0539	0.0012	0.6009	0.0140	0.0808	0.0006	368	39	478	9	501	4
QL10-24-03	45.4	282	444	0.64	0.0533	0.0014	0.5946	0.0160	0.0807	0.0006	343	47	474	10	500	4
QL10-24-04	36.1	187	357	0.52	0.0566	0.0011	0.6290	0.0123	0.0805	0.0005	475	33	495	8	499	3
QL10-24-05	40.1	189	414	0.46	0.0570	0.0021	0.6129	0.0220	0.0780	0.0006	490	83	485	14	484	3
QL10-24-06	53.9	234	543	0.43	0.0549	0.0011	0.6112	0.0120	0.0808	0.0005	409	33	484	8	501	3
QL10-24-07	45.8	194	473	0.41	0.0640	0.0009	0.7156	0.0109	0.0807	0.0005	742	23	548	6	500	3
QL10-24-08	44.5	195	454	0.43	0.0563	0.0010	0.6291	0.0117	0.0808	0.0006	465	28	496	7	501	3
QL10-24-09	33.4	162	338	0.48	0.0558	0.0013	0.6221	0.0142	0.0808	0.0006	442	39	491	9	501	3
QL10-24-10	28.2	138	282	0.49	0.0566	0.0018	0.6307	0.0192	0.0807	0.0007	475	52	497	12	500	4
QL10-24-11	68.9	276	667	0.41	0.0581	0.0016	0.6489	0.0177	0.0807	0.0006	532	46	508	11	500	4
QL10-24-12	42.2	189	431	0.44	0.0559	0.0011	0.6670	0.0135	0.0862	0.0007	446	30	519	8	533	4
QL10-24-13	46.1	252	451	0.56	0.0548	0.0012	0.6127	0.0130	0.0808	0.0006	405	34	485	8	501	4
QL10-24-14	56.1	323	528	0.61	0.0588	0.0018	0.6560	0.0197	0.0807	0.0007	559	52	512	12	501	4
QL10-24-15	31.1	153	308	0.49	0.0679	0.0015	0.7540	0.0163	0.0802	0.0006	864	33	571	9	497	4
QL10-24-16	31.1	152	312	0.49	0.0581	0.0025	0.6421	0.0265	0.0801	0.0008	535	95	504	16	497	5
QL10-24-17	52.1	226	532	0.43	0.0561	0.0015	0.6265	0.0159	0.0807	0.0006	457	43	494	10	500	4
QL10-24-18	46.3	237	464	0.51	0.0578	0.0012	0.6454	0.0130	0.0807	0.0006	520	32	506	8	500	3
QL10-24-19	34.5	169	346	0.49	0.0564	0.0013	0.6312	0.0140	0.0808	0.0006	469	35	497	9	501	4
QL10-25-01	121	1090	963	1.13	0.0549	0.0008	0.6639	0.0102	0.0872	0.0006	409	22	517	6	539	3

Table 6.3 Zircon in situ LA-ICP-MS dating results

	Pb	Th	U	Th/U	CORRECTED RATIOS						CORRECTED AGES (Ma)					
	Total ppm	232 ppm	238 ppm		$^{207}Pb/^{206}Pb$		$^{207}Pb/^{235}U$		$^{206}Pb/^{238}U$		$^{207}Pb/^{206}Pb$		$^{207}Pb/^{235}U$		$^{206}Pb/^{238}U$	
QL10-25-02	23.6	131	229	0.57	0.0554	0.0017	0.6156	0.0193	0.0803	0.0007	427	53	487	12	498	4
QL10-25-03	32.0	202	295	0.69	0.0573	0.0028	0.6308	0.0301	0.0799	0.0008	501	110	497	19	496	4
QL10-25-04	22.1	123	210	0.58	0.0575	0.0018	0.6407	0.0188	0.0807	0.0006	512	51	503	12	500	4
QL10-25-05	58.5	595	489	1.22	0.0534	0.0009	0.5978	0.0106	0.0807	0.0005	344	30	476	7	501	3
QL10-25-06	90.0	630	827	0.76	0.0540	0.0011	0.6078	0.0143	0.0811	0.0009	372	33	482	9	502	5
QL10-25-07	84.0	717	725	0.99	0.0566	0.0012	0.6341	0.0150	0.0808	0.0011	475	30	499	9	501	6
QL10-25-08	83.0	779	692	1.13	0.0567	0.0015	0.6355	0.0165	0.0810	0.0009	481	38	500	10	502	5
QL10-25-09	70.8	404	665	0.61	0.0568	0.0010	0.6417	0.0114	0.0815	0.0006	482	27	503	7	505	3
QL10-25-10	67.2	598	582	1.03	0.0569	0.0014	0.6279	0.0151	0.0797	0.0006	488	40	495	9	494	3
QL10-25-11	91.7	806	776	1.04	0.0618	0.0018	0.6940	0.0198	0.0810	0.0006	666	48	535	12	502	4
QL10-25-12	89.0	809	752	1.08	0.0566	0.0017	0.6329	0.0176	0.0809	0.0007	475	45	498	11	501	4
QL10-25-13	24.9	257	204	1.26	0.0566	0.0026	0.6298	0.0287	0.0805	0.0010	477	79	496	18	499	6
QL10-25-14	55.1	695	438	1.59	0.0574	0.0015	0.6196	0.0161	0.0779	0.0006	506	44	490	10	483	4
QL10-25-15	66.4	417	639	0.65	0.0569	0.0018	0.6386	0.0211	0.0810	0.0011	487	49	501	13	502	7
QL10-25-16	52.2	339	501	0.68	0.0593	0.0018	0.6643	0.0215	0.0808	0.0009	579	52	517	13	501	5
QL10-25-17	79.9	576	735	0.78	0.0584	0.0014	0.6568	0.0168	0.0811	0.0007	546	40	513	10	502	4
QL10-25-18	42.9	248	419	0.59	0.0587	0.0026	0.6531	0.0303	0.0801	0.0010	557	80	510	19	497	6
QL10-25-19	21.5	165	196	0.84	0.0547	0.0019	0.6077	0.0211	0.0805	0.0007	400	62	482	13	499	4
QL10-25-20	98.2	756	911	0.83	0.0551	0.0015	0.6171	0.0174	0.0809	0.0012	418	37	488	11	501	7
QL10-26-01	58.5	671	495	1.36	0.0592	0.0015	0.6342	0.0157	0.0776	0.0006	575	41	499	10	482	3
QL10-26-02	41.4	192	427	0.45	0.0577	0.0015	0.6425	0.0169	0.0807	0.0008	518	40	504	10	500	5
QL10-26-03	22.9	167	212	0.79	0.0589	0.0021	0.6525	0.0220	0.0807	0.0008	563	55	510	14	500	5
QL10-26-04	87.4	1116	626	1.78	0.0625	0.0027	0.6976	0.0297	0.0808	0.0007	690	76	537	18	501	4
QL10-26-05	19.9	126	193	0.65	0.0568	0.0021	0.6314	0.0220	0.0808	0.0009	484	58	497	14	501	5
QL10-26-06	35.9	320	313	1.02	0.0589	0.0016	0.6559	0.0175	0.0807	0.0008	564	40	512	11	500	5
QL10-26-07	24.6	172	233	0.74	0.0572	0.0020	0.6343	0.0208	0.0808	0.0009	499	53	499	13	501	5

Table 6.3 Zircon in situ LA-ICP-MS dating results

	Pb	Th	U	Th/U	CORRECTED RATIOS						CORRECTED AGES (Ma)					
	Total ppm	232 ppm	238 ppm		$^{207}Pb/^{206}Pb$		$^{207}Pb/^{235}U$		$^{206}Pb/^{238}U$		$^{207}Pb/^{206}Pb$		$^{207}Pb/^{235}U$		$^{206}Pb/^{238}U$	
QL10-26-08	28.4	252	262	0.96	0.0579	0.0019	0.6208	0.0190	0.0778	0.0007	524	52	490	12	483	4
QL10-26-09	40.4	381	364	1.05	0.0619	0.0017	0.6959	0.0211	0.0809	0.0009	670	45	536	13	502	6
QL10-26-10	88.9	1000	683	1.46	0.0572	0.0013	0.6439	0.0170	0.0810	0.0011	499	34	505	11	502	7
QL10-26-11	34.1	305	311	0.98	0.0587	0.0016	0.6304	0.0167	0.0775	0.0007	556	41	496	10	481	4
QL10-26-12	17.6	112	168	0.67	0.0550	0.0026	0.6083	0.0276	0.0804	0.0008	411	84	482	17	499	5
QL10-26-13	22.1	168	203	0.83	0.0580	0.0020	0.6457	0.0221	0.0807	0.0009	529	55	506	14	500	6
QL10-26-14	23.5	201	210	0.96	0.0568	0.0018	0.6321	0.0204	0.0807	0.0008	483	53	497	13	500	5
QL10-26-15	23.8	181	227	0.80	0.0572	0.0020	0.6189	0.0217	0.0784	0.0009	500	57	489	14	487	5
QL10-26-16	99.7	1113	746	1.49	0.0612	0.0015	0.6870	0.0160	0.0811	0.0007	645	35	531	10	503	4
QL10-26-17	20.2	147	198	0.74	0.0545	0.0023	0.5797	0.0244	0.0773	0.0009	392	73	464	16	480	6
QL10-26-18	22.1	159	207	0.77	0.0572	0.0020	0.6394	0.0233	0.0807	0.0008	499	62	502	14	500	5
QL10-26-19	19.0	121	177	0.68	0.0530	0.0021	0.5889	0.0228	0.0808	0.0008	330	70	470	15	501	5
QL10-26-20	43.7	553	365	1.51	0.0583	0.0019	0.6061	0.0188	0.0752	0.0006	542	53	481	12	467	4
Analysed in Chinese Academy of Sciences, Beijing																
QL10-14-01	68.2	81.4	698	0.12	0.0628	0.0018	0.8346	0.0208	0.0964	0.0015	701	64	616	11	593	9
QL10-14-02	82.9	97.6	931	0.10	0.0589	0.0017	0.7139	0.0177	0.0880	0.0013	562	65	547	10	543	8
QL10-14-03	32.2	46.4	299	0.15	0.0640	0.0015	0.9310	0.0222	0.1055	0.0017	742	26	668	12	646	10
QL10-14-04	82.2	635	825	0.77	0.0682	0.0037	0.7570	0.0388	0.0805	0.0014	876	115	572	22	499	8
QL10-14-05	48.6	84	583	0.14	0.0602	0.0020	0.6643	0.0200	0.0800	0.0013	612	75	517	12	496	8
QL10-14-06	41.7	294	444	0.66	0.0632	0.0015	0.7024	0.0172	0.0806	0.0013	714	27	540	10	500	8
QL10-14-07	38.4	223	433	0.51	0.0552	0.0035	0.5454	0.0332	0.0717	0.0012	419	145	442	22	446	7
QL10-14-08	36.3	236	388	0.61	0.0595	0.0014	0.6703	0.0166	0.0817	0.0013	585	28	521	10	506	8
QL10-14-09	75.6	578	728	0.79	0.0661	0.0015	0.7863	0.0186	0.0863	0.0014	808	25	589	11	534	8
QL10-14-10	79.8	347	764	0.45	0.0618	0.0033	0.7269	0.0367	0.0854	0.0014	666	117	555	22	528	8
QL10-14-11	27.9	178	306	0.58	0.0618	0.0016	0.6818	0.0186	0.0800	0.0013	667	32	528	11	496	8
QL10-14-12	52.3	245	462	0.53	0.0627	0.0041	0.7416	0.0471	0.0858	0.0015	698	144	563	27	531	9
QL10-14-13	34.2	269	356	0.76	0.0608	0.0015	0.6776	0.0177	0.0809	0.0013	630	30	525	11	501	8

Table 6.3 Zircon in situ LA-ICP-MS dating results

	Pb	Th	U	Th/U	CORRECTED RATIOS						CORRECTED AGES (Ma)					
	Total ppm	232 ppm	238 ppm		$^{207}Pb/^{206}Pb$		$^{207}Pb/^{235}U$		$^{206}Pb/^{238}U$		$^{207}Pb/^{206}Pb$		$^{207}Pb/^{235}U$		$^{206}Pb/^{238}U$	
QL10-14-14	111	615	1134	0.54	0.0613	0.0031	0.6979	0.0332	0.0826	0.0014	649	111	538	20	512	8
QL10-14-15	57.7	292	642	0.45	0.0598	0.0027	0.6640	0.0274	0.0806	0.0013	595	99	517	17	500	8
QL10-14-16	88.8	257	1134	0.23	0.0621	0.0021	0.6398	0.0193	0.0748	0.0012	677	74	502	12	465	7
QL10-14-17	57.3	274	594	0.46	0.0622	0.0034	0.6787	0.0356	0.0791	0.0013	682	121	526	22	491	8
QL10-14-18	30.0	190	324	0.59	0.0602	0.0032	0.6613	0.0338	0.0796	0.0014	612	119	515	21	494	8
QL10-14-19	35.6	245	365	0.67	0.0581	0.0035	0.6396	0.0374	0.0799	0.0014	533	137	502	23	495	8
QL10-14-20	88.1	319	920	0.35	0.0608	0.0041	0.6012	0.0396	0.0717	0.0012	633	151	478	25	446	7
QL10-14-21	30.3	151	339	0.45	0.0595	0.0015	0.6626	0.0177	0.0808	0.0013	585	31	516	11	501	8
QL10-14-22	24.3	129	265	0.49	0.0580	0.0017	0.6615	0.0192	0.0827	0.0014	529	36	516	12	512	8
QL10-14-23	82.3	172	856	0.20	0.0632	0.0021	0.8003	0.0236	0.0919	0.0014	714	73	597	13	567	8
QL10-14-24	65.0	89.0	663	0.13	0.0622	0.0020	0.8259	0.0225	0.0963	0.0015	681	69	611	13	593	9
QL10-14-25	77.1	63.4	750	0.08	0.0638	0.0019	0.8876	0.0232	0.1010	0.0016	734	66	645	12	620	9
QL10-14-26	83.1	539	800	0.67	0.0629	0.0010	0.7703	0.0139	0.0888	0.0013	706	17	580	8	548	8
QL10-15-01	29.8	54.1	263	0.21	0.0627	0.0013	0.9393	0.0211	0.1086	0.0017	699	24	673	11	664	10
QL10-15-02	17.3	52.8	202	0.26	0.0585	0.0016	0.6571	0.0185	0.0814	0.0013	550	34	513	11	505	8
QL10-15-03	27.8	38.2	310	0.12	0.0587	0.0014	0.7176	0.0176	0.0886	0.0014	556	28	549	10	547	8
QL10-15-04	47.0	95.8	409	0.23	0.0657	0.0013	0.9913	0.0210	0.1094	0.0017	797	22	699	11	669	10
QL10-15-05	83.3	61.4	692	0.09	0.0663	0.0017	1.0763	0.0234	0.1178	0.0017	815	56	742	11	718	10
QL10-15-06	47.5	62.1	131	0.47	0.1100	0.0021	4.7915	0.0990	0.3159	0.0049	1799	18	1783	17	1770	24
QL10-15-07	15.4	44.0	165	0.27	0.0580	0.0018	0.7151	0.0227	0.0894	0.0015	531	41	548	13	552	9
QL10-15-08	53.2	137	400	0.34	0.0652	0.0013	1.1130	0.0242	0.1238	0.0019	780	22	760	12	752	11
QL10-15-09	6.04	10.9	73.5	0.15	0.0628	0.0028	0.6968	0.0312	0.0805	0.0016	700	62	537	19	499	9
QL10-15-10	201	84.6	802	0.11	0.0984	0.0025	3.2375	0.0652	0.2387	0.0035	1593	48	1466	16	1380	18
QL10-15-11	5.57	44.2	58	0.76	0.0545	0.0035	0.6080	0.0391	0.0810	0.0017	390	108	482	25	502	10
QL10-15-12	20.3	178	188	0.95	0.0592	0.0015	0.7178	0.0192	0.0879	0.0014	575	32	549	11	543	8
QL10-15-13	104	248	1140	0.22	0.0588	0.0010	0.7160	0.0143	0.0883	0.0013	559	21	548	8	546	8

Table 6.3 Zircon in situ LA-ICP-MS dating results

	Pb	Th	U	Th/U	CORRECTED RATIOS						CORRECTED AGES (Ma)					
	Total ppm	232 ppm	238 ppm		$^{207}Pb/^{206}Pb$		$^{207}Pb/^{235}U$		$^{206}Pb/^{238}U$		$^{207}Pb/^{206}Pb$		$^{207}Pb/^{235}U$		$^{206}Pb/^{238}U$	
QL10-15-14	56.4	107	427	0.25	0.0661	0.0012	1.1459	0.0235	0.1258	0.0019	809	21	775	11	764	11
QL10-15-15	7.12	37.2	79.0	0.47	0.0624	0.0022	0.6984	0.0245	0.0811	0.0014	689	46	538	15	503	8
QL10-15-16	12.0	38.5	129	0.30	0.0600	0.0019	0.7277	0.0235	0.0880	0.0015	603	41	555	14	543	9
QL10-15-17	54.8	46.1	524	0.09	0.0613	0.0020	0.8708	0.0247	0.1030	0.0016	650	71	636	13	632	9
QL10-15-18	35.6	64.3	262	0.24	0.0655	0.0013	1.1685	0.0256	0.1294	0.0020	790	23	786	12	784	11
QL10-15-19	48.5	155	525	0.30	0.0619	0.0012	0.7490	0.0162	0.0878	0.0013	669	23	568	9	543	8
QL10-15-20	76.3	211	279	0.76	0.0894	0.0037	2.7296	0.1022	0.2214	0.0036	1413	80	1337	28	1289	19
QL10-15-21	105	264	612	0.43	0.1024	0.0018	2.1840	0.0434	0.1547	0.0023	1667	17	1176	14	927	13
QL10-15-22	30.8	74.0	299	0.25	0.0621	0.0013	0.8338	0.0189	0.0973	0.0015	678	24	616	10	599	9
QL10-15-23	51.2	71.6	420	0.17	0.0641	0.0013	1.0485	0.0229	0.1186	0.0018	746	23	728	11	722	10
QL10-15-24	98.2	137	187	0.73	0.1683	0.0054	9.4460	0.2588	0.4070	0.0066	2541	55	2382	25	2201	30
QL10-15-25	57.5	65.8	421	0.16	0.0649	0.0013	1.1940	0.0263	0.1333	0.0020	772	23	798	12	807	12
QL10-15-26	1.04	1.48	11.9	0.12	0.0645	0.0134	0.7454	0.1524	0.0838	0.0036	759	376	566	89	519	21
QL10-15-27	12.3	21.4	150	0.14	0.0575	0.0020	0.6386	0.0220	0.0806	0.0014	510	46	501	14	499	8
QL10-15-28	2.20	0.62	24.9	0.03	0.0564	0.0057	0.6894	0.0688	0.0886	0.0024	468	175	532	41	547	14
QL10-15-29	3.98	23.7	39.6	0.60	0.0601	0.0031	0.7304	0.0370	0.0882	0.0018	606	74	557	22	545	11
QL10-21-01	26.8	133	310	0.43	0.0595	0.0013	0.6586	0.0152	0.0802	0.0012	586	25	514	9	498	7
QL10-21-02	17.5	107	195	0.55	0.0595	0.0014	0.6633	0.0166	0.0809	0.0013	584	29	517	10	501	8
QL10-21-03	35.7	233	389	0.60	0.0579	0.0011	0.6510	0.0140	0.0815	0.0012	527	23	509	9	505	7
QL10-21-04	37.7	193	420	0.46	0.0575	0.0012	0.6565	0.0144	0.0828	0.0013	511	24	512	9	513	8
QL10-21-05	50.9	330	431	0.76	0.0944	0.0059	1.0178	0.0609	0.0782	0.0015	1516	122	713	31	485	9
QL10-21-06	49.6	281	551	0.51	0.0583	0.0011	0.6573	0.0140	0.0818	0.0012	540	23	513	9	507	7
QL10-21-07	85.0	462	925	0.50	0.0597	0.0012	0.6959	0.0151	0.0845	0.0013	593	23	536	9	523	8
QL10-21-08	35.9	172	392	0.44	0.0576	0.0012	0.6739	0.0153	0.0849	0.0013	513	25	523	9	525	8
QL10-21-09	46.9	250	528	0.47	0.0574	0.0012	0.6480	0.0145	0.0819	0.0013	506	25	507	9	507	7
QL10-21-10	122	284	659	0.43	0.0770	0.0013	1.7967	0.0348	0.1692	0.0025	1122	18	1044	13	1007	14

Table 6.3 Zircon in situ LA-ICP-MS dating results

	Pb	Th	U	Th/U	CORRECTED RATIOS						CORRECTED AGES (Ma)					
	Total ppm	232 ppm	238 ppm		$^{207}Pb/^{206}Pb$		$^{207}Pb/^{235}U$		$^{206}Pb/^{238}U$		$^{207}Pb/^{206}Pb$		$^{207}Pb/^{235}U$		$^{206}Pb/^{238}U$	
QL10-21-11	34.9	220	390	0.56	0.0569	0.0012	0.6317	0.0142	0.0805	0.0012	488	25	497	9	499	7
QL10-21-12	57.8	283	630	0.45	0.0599	0.0012	0.6950	0.0151	0.0842	0.0013	600	23	536	9	521	8
QL10-21-13	22.5	88.6	245	0.36	0.0592	0.0026	0.6849	0.0282	0.0840	0.0014	573	99	530	17	520	8
QL10-21-14	26.9	134	309	0.43	0.0590	0.0014	0.6572	0.0167	0.0807	0.0013	568	29	513	10	501	8
QL10-21-15	60.4	356	677	0.53	0.0584	0.0013	0.6501	0.0150	0.0807	0.0013	546	25	509	9	500	7
QL10-21-16	31.1	161	350	0.46	0.0579	0.0013	0.6492	0.0157	0.0813	0.0013	525	27	508	10	504	8
QL10-21-17	86.4	715	857	0.83	0.0616	0.0012	0.7109	0.0149	0.0837	0.0013	660	22	545	9	518	8
QL10-21-18	38.9	198	421	0.47	0.0579	0.0013	0.6767	0.0157	0.0848	0.0013	525	26	525	9	524	8
QL10-21-19	29.8	170	334	0.51	0.0574	0.0013	0.6425	0.0156	0.0812	0.0013	507	27	504	10	503	8
QL10-21-20	72.3	459	795	0.58	0.0633	0.0013	0.7004	0.0153	0.0802	0.0012	720	23	539	9	497	7
QL10-21-21	19.9	89.5	229	0.39	0.0582	0.0014	0.6520	0.0163	0.0812	0.0013	537	29	510	10	503	8
QL10-21-22	61.3	273	510	0.54	0.0588	0.0135	0.3411	0.0776	0.0421	0.0010	558	470	298	59	266	6
QL10-21-23	34.8	147	405	0.36	0.0580	0.0013	0.6497	0.0151	0.0812	0.0013	530	26	508	9	503	8
QL10-21-24	37.6	126	445	0.28	0.0575	0.0014	0.6435	0.0161	0.0812	0.0013	510	29	504	10	503	8
QL10-21-25	27.1	138	312	0.44	0.0588	0.0013	0.6469	0.0153	0.0799	0.0012	558	26	507	9	495	7
QL10-21-26	122	777	1267	0.61	0.0668	0.0028	0.7632	0.0301	0.0828	0.0013	832	91	576	17	513	8
QL10-21-27	96.9	515	917	0.56	0.0660	0.0032	0.7742	0.0356	0.0851	0.0014	805	105	582	20	527	8
QL10-26-01	61.0	890	542	1.64	0.0562	0.0011	0.6247	0.0136	0.0806	0.0013	461	23	493	8	499	7
QL10-26-02	27.2	285	271	1.05	0.0545	0.0017	0.6065	0.0191	0.0807	0.0014	391	41	481	12	500	8
QL10-26-03	31.9	346	314	1.10	0.0574	0.0017	0.6393	0.0194	0.0808	0.0014	507	38	502	12	501	8
QL10-26-04	8.97	59	98	0.60	0.0576	0.0026	0.6404	0.0281	0.0806	0.0016	515	62	503	17	500	9
QL10-26-05	22.8	224	224	1.00	0.0563	0.0016	0.6271	0.0178	0.0807	0.0013	465	35	494	11	500	8
QL10-26-06	32.6	384	311	1.24	0.0573	0.0018	0.6369	0.0204	0.0806	0.0014	504	41	500	13	499	8
QL10-26-07	50.3	792	430	1.84	0.0555	0.0012	0.6129	0.0139	0.0800	0.0012	434	25	485	9	496	7
QL10-26-08	23.1	204	237	0.86	0.0553	0.0016	0.6172	0.0178	0.0809	0.0013	425	36	488	11	501	8
QL10-26-09	32.1	421	307	1.37	0.0545	0.0014	0.5854	0.0160	0.0779	0.0013	391	34	468	10	484	7

Table 6.3 Zircon in situ LA-ICP-MS dating results

	Pb	Th	U	Th/U	CORRECTED RATIOS						CORRECTED AGES (Ma)					
	Total ppm	232 ppm	238 ppm		$^{207}Pb/^{206}Pb$		$^{207}Pb/^{235}U$		$^{206}Pb/^{238}U$		$^{207}Pb/^{206}Pb$		$^{207}Pb/^{235}U$		$^{206}Pb/^{238}U$	
QL10-26-10	20.4	185	222	0.83	0.0561	0.0020	0.5901	0.0210	0.0763	0.0014	455	48	471	13	474	8
QL10-26-11	12.7	95	134	0.71	0.0573	0.0023	0.6473	0.0262	0.0819	0.0015	502	57	507	16	508	9
QL10-26-12	37.2	426	381	1.12	0.0564	0.0013	0.5967	0.0144	0.0767	0.0012	469	27	475	9	476	7
QL10-26-13	15.0	121	158	0.77	0.0565	0.0023	0.6303	0.0257	0.0808	0.0015	474	58	496	16	501	9
QL10-26-14	72.5	1125	603	1.87	0.0546	0.0011	0.6112	0.0135	0.0812	0.0013	395	24	484	9	503	7
QL10-26-15	31.7	76	408	0.19	0.0568	0.0013	0.5940	0.0139	0.0758	0.0012	484	26	473	9	471	7
QL10-26-16	12.6	101	132	0.76	0.0605	0.0021	0.6692	0.0230	0.0803	0.0014	620	45	520	14	498	8
QL10-26-17	21.6	164	242	0.68	0.0565	0.0017	0.5905	0.0180	0.0758	0.0013	471	38	471	11	471	8
QL10-26-18	15.5	104	172	0.60	0.0578	0.0020	0.6433	0.0219	0.0807	0.0014	523	45	504	14	500	8
QL10-26-19	13.1	115	134	0.86	0.0573	0.0024	0.6382	0.0264	0.0807	0.0015	503	58	501	16	501	9
QL10-26-20	10.6	72.6	115	0.63	0.0594	0.0019	0.6540	0.0214	0.0798	0.0014	583	42	511	13	495	8
QL10-26-21	12.1	86.9	129	0.67	0.0565	0.0018	0.6301	0.0205	0.0808	0.0014	473	42	496	13	501	8
QL10-26-22	58.9	806	531	1.52	0.0561	0.0012	0.6233	0.0137	0.0805	0.0012	458	24	492	9	499	7
QL10-26-23	49.1	574	458	1.25	0.0574	0.0011	0.6420	0.0135	0.0811	0.0012	507	22	504	8	503	7
QL10-26-24	50.1	406	523	0.78	0.0563	0.0011	0.6301	0.0132	0.0811	0.0012	465	22	496	8	503	7
QL10-26-25	9.7	65.0	106	0.62	0.0618	0.0020	0.6868	0.0221	0.0806	0.0014	665	40	531	13	500	8
QL10-26-26	29.5	317	284	1.12	0.0565	0.0015	0.6300	0.0171	0.0808	0.0013	472	33	496	11	501	8
QL10-26-27	18.6	197	183	1.08	0.0620	0.0016	0.6889	0.0187	0.0806	0.0013	674	31	532	11	500	8
QL10-26-28	70.8	955	636	1.50	0.0544	0.0011	0.6066	0.0129	0.0808	0.0012	389	23	481	8	501	7
QL10-26-29	43.9	490	422	1.16	0.0562	0.0011	0.6232	0.0132	0.0804	0.0012	459	23	492	8	499	7
QL10-26-30	17.3	140	180	0.78	0.0570	0.0018	0.6397	0.0199	0.0813	0.0014	493	39	502	12	504	8
QL10-26-31	11.0	75.9	119	0.64	0.0532	0.0017	0.5935	0.0197	0.0809	0.0014	337	45	473	13	501	8
QL10-26-32	25.7	266	250	1.07	0.0564	0.0013	0.6299	0.0152	0.0810	0.0013	469	27	496	9	502	8
QL10-26-33	18.5	156	193	0.81	0.0579	0.0014	0.6413	0.0165	0.0803	0.0013	525	30	503	10	498	8
QL10-26-34	23.3	214	238	0.90	0.0556	0.0012	0.6195	0.0145	0.0808	0.0013	435	26	490	9	501	8
QL10-26-35	40.4	462	404	1.14	0.0566	0.0016	0.5995	0.0170	0.0768	0.0013	476	34	477	11	477	8
QL10-26-36	10.4	72.3	113	0.64	0.0564	0.0019	0.6296	0.0215	0.0809	0.0014	469	46	496	13	502	8

Table 6.3 Zircon in situ LA-ICP-MS dating results

	Pb	Th	U	Th/U	CORRECTED RATIOS						CORRECTED AGES (Ma)					
	Total ppm	232 ppm	238 ppm		$^{207}Pb/^{206}Pb$		$^{207}Pb/^{235}U$		$^{206}Pb/^{238}U$		$^{207}Pb/^{206}Pb$		$^{207}Pb/^{235}U$		$^{206}Pb/^{238}U$	
QL10-27-01	21.8	113	248	0.45	0.0571	0.0012	0.6289	0.0144	0.0799	0.0012	495	26	495	9	495	7
QL10-27-02	91.2	429	666	0.64	0.0770	0.0061	0.8150	0.0629	0.0767	0.0014	1122	163	605	35	477	8
QL10-27-03	33.5	206	375	0.55	0.0571	0.0012	0.6253	0.0139	0.0794	0.0012	495	25	493	9	493	7
QL10-27-04	72.8	363	767	0.47	0.0651	0.0011	0.7611	0.0139	0.0848	0.0012	778	18	575	8	525	7
QL10-27-05	28.5	229	296	0.77	0.0603	0.0012	0.6722	0.0141	0.0809	0.0012	613	22	522	9	501	7
QL10-27-06	72.8	391	744	0.52	0.0638	0.0024	0.7429	0.0250	0.0845	0.0013	734	80	564	15	523	8
QL10-27-07	31.8	170	356	0.48	0.0590	0.0011	0.6494	0.0135	0.0799	0.0012	566	22	508	8	495	7
QL10-27-08	16.8	97.0	186	0.52	0.0590	0.0014	0.6545	0.0158	0.0804	0.0012	567	28	511	10	499	7
QL10-27-09	68.6	351	748	0.47	0.0590	0.0010	0.6747	0.0126	0.0829	0.0012	568	19	524	8	513	7
QL10-27-10	40.1	241	446	0.54	0.0561	0.0010	0.6184	0.0124	0.0800	0.0012	454	21	489	8	496	7
QL10-27-11	105	498	927	0.54	0.0663	0.0041	0.7023	0.0415	0.0769	0.0013	815	132	540	25	477	7
QL10-27-12	85.3	365	749	0.49	0.0608	0.0036	0.6793	0.0383	0.0810	0.0013	634	129	526	23	502	8
QL10-27-13	72.0	343	788	0.43	0.0573	0.0009	0.6597	0.0122	0.0835	0.0012	503	19	514	7	517	7
QL10-27-14	27.0	144	308	0.47	0.0567	0.0012	0.6222	0.0141	0.0796	0.0012	478	25	491	9	494	7
QL10-27-15	66.0	431	726	0.59	0.0573	0.0010	0.6287	0.0119	0.0796	0.0012	502	19	495	7	494	7
QL10-27-16	39.9	218	445	0.49	0.0576	0.0011	0.6400	0.0135	0.0805	0.0012	515	23	502	8	499	7
QL10-27-17	17.9	93.3	210	0.44	0.0577	0.0017	0.6156	0.0179	0.0774	0.0013	517	36	487	11	481	7
QL10-27-18	60.7	326	677	0.48	0.0570	0.0010	0.6354	0.0125	0.0808	0.0012	492	21	499	8	501	7
QL10-27-19	69.9	337	704	0.48	0.0647	0.0014	0.7848	0.0174	0.0880	0.0013	763	23	588	10	544	8
QL10-27-20	34.4	207	373	0.56	0.0558	0.0012	0.6289	0.0140	0.0817	0.0012	446	25	495	9	506	7
QL10-27-21	59.9	339	670	0.51	0.0631	0.0011	0.6876	0.0132	0.0790	0.0012	711	19	531	8	490	7
QL10-27-22	21.9	115	246	0.47	0.0581	0.0013	0.6418	0.0151	0.0801	0.0012	535	27	503	9	496	7
QL10-27-23	44.3	299	483	0.62	0.0574	0.0011	0.6301	0.0132	0.0797	0.0012	505	23	496	8	494	7
QL10-27-24	34.5	211	387	0.54	0.0576	0.0012	0.6257	0.0142	0.0787	0.0012	515	25	493	9	489	7
QL10-27-25	50.2	307	540	0.57	0.0575	0.0011	0.6499	0.0130	0.0820	0.0012	509	21	508	8	508	7
QL10-27-26	44.3	216	494	0.44	0.0580	0.0010	0.6530	0.0129	0.0817	0.0012	529	21	510	8	506	7

Table 6.3 Zircon in situ LA-ICP-MS dating results

	Pb	Th	U	Th/U	CORRECTED RATIOS					CORRECTED AGES (Ma)					
	Total ppm	232 ppm	238 ppm		$^{207}Pb/^{206}Pb$		$^{207}Pb/^{235}U$		$^{206}Pb/^{238}U$	$^{207}Pb/^{206}Pb$		$^{207}Pb/^{235}U$		$^{206}Pb/^{238}U$	
QL10-27-27	24.9	119	280	0.42	0.0583	0.0012	0.6509	0.0144	0.0810	0.0012	541	24	509	9	502	7
QL10-27-28	19.3	91.8	217	0.42	0.0584	0.0013	0.6541	0.0154	0.0812	0.0012	546	27	511	9	503	7
QL10-27-29	61.0	283	687	0.41	0.0588	0.0010	0.6583	0.0125	0.0811	0.0012	561	19	514	8	503	7
QL10-27-30	60.4	345	659	0.52	0.0569	0.0010	0.6426	0.0122	0.0819	0.0012	488	20	504	8	507	7

Table 6.4 Zircon in situ Hf isotope results

	$^{176}Yb/^{177}Hf$		$^{176}Lu/^{177}Hf$		$^{176}Hf/^{177}Hf$	2s	$^{176}Hf/^{177}Hf_i$	$\varepsilon_{Hf}(0)$	$\varepsilon_{Hf}(t)$
QL10-14-01	0.02353	0.00021	0.0009	8E-06	0.28231593	2E-05	0.282307	-16.1	-5.4
QL10-14-02	0.03533	0.00103	0.00139	4E-05	0.28232675	2E-05	0.282314	-15.7	-5.2
QL10-14-03	0.02919	0.00036	0.00111	1E-05	0.28230333	2E-05	0.282293	-16.6	-5.9
QL10-14-04	0.02923	0.00032	0.0011	1E-05	0.28230079	2E-05	0.282290	-16.7	-6.0
QL10-14-05	0.03163	0.00033	0.00121	1E-05	0.28234326	2E-05	0.282332	-15.2	-4.6
QL10-14-06	0.02928	0.00062	0.00112	2E-05	0.28231191	2E-05	0.282301	-16.3	-5.6
QL10-14-07	0.01991	6.5E-05	0.00077	2E-06	0.28227355	2E-05	0.282266	-17.6	-6.9
QL10-14-08	0.03833	0.0023	0.00156	9E-05	0.28229556	2E-05	0.282281	-16.8	-6.4
QL10-14-09	0.00233	0.00022	8.3E-05	9E-06	0.28227362	2E-05	0.282273	-17.6	-6.7
QL10-14-10	0.0223	0.00015	0.00087	7E-06	0.28231794	2E-05	0.282310	-16.1	-5.4
QL10-14-11	0.04027	0.00018	0.00154	8E-06	0.28228022	3E-05	0.282266	-17.4	-6.9
QL10-14-12	0.03023	0.00062	0.00114	2E-05	0.28229815	2E-05	0.282287	-16.8	-6.1
QL10-14-13	0.02517	0.0004	0.00092	1E-05	0.28228738	2E-05	0.282279	-17.1	-6.5
QL10-14-14	0.03387	0.00069	0.00129	2E-05	0.28233223	2E-05	0.282320	-15.6	-5.0
QL10-14-15	0.02393	0.00024	0.00092	1E-05	0.28235444	2E-05	0.282346	-14.8	-4.1
QL10-14-16	0.03662	0.0005	0.00145	2E-05	0.28236101	2E-05	0.282347	-14.5	-4.0
QL10-14-17	0.03097	0.00059	0.00118	2E-05	0.28231486	2E-05	0.282304	-16.2	-5.6
QL10-14-18	0.03683	0.00075	0.00142	3E-05	0.28231556	2E-05	0.282302	-16.1	-5.6
QL10-14-19	0.02507	0.00015	0.00096	5E-06	0.28231725	1E-05	0.282308	-16.1	-5.4
QL10-14-20	0.02723	0.00017	0.00104	6E-06	0.28222884	2E-05	0.282219	-19.2	-8.6
								Ave.	**-5.6**
QL10-15-01	0.00674	0.0005	0.00023	2E-05	0.28233266	1E-05	0.282331	-15.5	-4.6
QL10-15-02	0.02649	0.00046	0.00106	2E-05	0.28225199	1E-05	0.282242	-18.4	-7.7
QL10-15-03	0.00782	0.00064	0.00028	3E-05	0.28232346	2E-05	0.282321	-15.9	-5.0
QL10-15-04	0.03029	8.1E-05	0.00114	3E-06	0.28241212	1E-05	0.282401	-12.7	-2.1
QL10-15-05	0.10933	0.00155	0.00411	6E-05	0.2823061	2E-05	0.282268	-16.5	-6.8
QL10-15-06	0.05672	0.00045	0.00221	2E-05	0.28228953	1E-05	0.282269	-17.1	-6.8
QL10-15-07	0.06244	0.00152	0.00242	5E-05	0.2823711	2E-05	0.282348	-14.2	-4.0
QL10-15-08	0.05776	0.00176	0.00223	7E-05	0.28231427	1E-05	0.282293	-16.2	-5.9
QL10-15-10	0.04432	0.00073	0.00174	3E-05	0.28222786	1E-05	0.282212	-19.2	-8.8
QL10-15-11	0.0573	0.00029	0.00223	1E-05	0.28227366	2E-05	0.282253	-17.6	-7.4
QL10-15-12	0.02684	0.00051	0.001	2E-05	0.2823624	1E-05	0.282353	-14.5	-3.8
QL10-15-13	0.06737	0.00117	0.00268	4E-05	0.28187617	2E-05	0.281851	-31.7	-21.6
QL10-15-14	0.00246	8E-05	7.1E-05	3E-06	0.28233162	1E-05	0.282331	-15.6	-4.6
QL10-15-15	0.07295	0.00026	0.00277	8E-06	0.28227518	2E-05	0.282249	-17.6	-7.5
QL10-15-16	0.04069	0.00104	0.00161	4E-05	0.2822676	2E-05	0.282253	-17.8	-7.4
QL10-15-17	0.01702	0.00177	0.00065	7E-05	0.28230278	1E-05	0.282297	-16.6	-5.8
QL10-15-18	0.08523	0.0065	0.00336	0.0003	0.28224186	1E-05	0.282210	-18.7	-8.9
QL10-15-19	0.04946	0.00037	0.00197	1E-05	0.28223515	1E-05	0.282217	-19.0	-8.6
QL10-15-20	0.05675	0.0011	0.00209	4E-05	0.2823509	2E-05	0.282331	-14.9	-4.6
								Ave.	**-7.0**
QL10-21-01	0.01487	0.00031	0.00063	1E-05	0.28229691	3E-05	0.282291	-16.8	-6.0
QL10-21-02	0.01728	0.00051	0.0007	2E-05	0.28237383	3E-05	0.282367	-14.1	-3.3
QL10-21-03	0.01864	0.00046	0.00076	2E-05	0.28242297	3E-05	0.282416	-12.3	-1.6
QL10-21-04	0.02512	0.00034	0.00107	2E-05	0.28241464	3E-05	0.282405	-12.6	-2.0
QL10-21-05	0.02441	0.00166	0.00098	6E-05	0.2824728	3E-05	0.282464	-10.6	0.1
QL10-21-06	0.01223	0.00011	0.00051	5E-06	0.28237089	2E-05	0.282366	-14.2	-3.4
QL10-21-07	0.0255	0.00019	0.00102	7E-06	0.28231206	3E-05	0.282303	-16.3	-5.6
QL10-21-08	0.01684	5.5E-05	0.00072	2E-06	0.28243372	2E-05	0.282427	-12.0	-1.2
QL10-21-09	0.01455	0.00015	0.00062	6E-06	0.28240307	2E-05	0.282397	-13.0	-2.3
QL10-21-10	0.01626	0.00015	0.00068	7E-06	0.28244063	2E-05	0.282434	-11.7	-0.9
QL10-21-11	0.01912	0.00049	0.00079	2E-05	0.28243354	3E-05	0.282426	-12.0	-1.2
QL10-21-12	0.01523	0.00025	0.00065	1E-05	0.28240651	2E-05	0.282400	-12.9	-2.1
QL10-21-13	0.02465	0.00052	0.00101	2E-05	0.28240895	3E-05	0.282399	-12.8	-2.2
QL10-21-14	0.01442	0.00013	0.00061	5E-06	0.28236217	2E-05	0.282356	-14.5	-3.7
QL10-21-15	0.02155	0.00055	0.00088	2E-05	0.28236059	2E-05	0.282352	-14.5	-3.8
QL10-21-16	0.01241	7.6E-05	0.00053	3E-06	0.28251198	2E-05	0.282507	-9.2	1.6
QL10-21-17	0.01353	0.00013	0.00057	5E-06	0.28247839	2E-05	0.282473	-10.4	0.4
QL10-21-18	0.00992	8.7E-05	0.00042	4E-06	0.28240861	2E-05	0.282405	-12.9	-2.0
QL10-21-19	0.0134	0.00027	0.00058	1E-05	0.28245034	2E-05	0.282445	-11.4	-0.6
QL10-21-20	0.01244	8.2E-05	0.00052	3E-06	0.28230622	2E-05	0.282301	-16.5	-5.6
QL10-21-21	0.0111	6.2E-05	0.00046	2E-06	0.28234683	3E-05	0.282342	-15.0	-4.2

Table 6.4 Zircon in situ Hf isotope results

	$^{176}Yb/^{177}Hf$		$^{176}Lu/^{177}Hf$		$^{176}Hf/^{177}Hf$	2s	$^{176}Hf/^{177}Hf_i$	$\varepsilon_{Hf}(0)$	$\varepsilon_{Hf}(t)$
QL10-21-22	0.02384	0.00055	0.00097	2E-05	0.28253456	4E-05	0.282525	-8.4	2.3
QL10-21-23	0.01301	8.2E-05	0.00055	4E-06	0.28239721	2E-05	0.282392	-13.3	-2.4
QL10-21-24	0.02035	0.00016	0.00085	6E-06	0.2824319	3E-05	0.282424	-12.0	-1.3
QL10-21-25	0.02893	0.00117	0.00115	4E-05	0.28236999	2E-05	0.282359	-14.2	-3.6
								Ave.	**-2.2**
QL10-23-01	0.02202	0.00019	0.0009	7E-06	0.28244458	3E-05	0.282436	-11.6	-0.9
QL10-23-02	0.01356	0.00029	0.00057	1E-05	0.28251221	2E-05	0.282507	-9.2	1.6
QL10-23-03	0.019	0.00018	0.00076	8E-06	0.28225003	2E-05	0.282243	-18.5	-7.7
QL10-23-04	0.01318	9.5E-05	0.00059	3E-06	0.28238447	2E-05	0.282379	-13.7	-2.9
QL10-23-05	0.01508	0.00017	0.00065	7E-06	0.28230763	2E-05	0.282302	-16.4	-5.6
QL10-23-06	0.01583	0.00024	0.00066	1E-05	0.28243467	3E-05	0.282428	-11.9	-1.2
QL10-23-07	0.01244	8.5E-05	0.00053	3E-06	0.2824941	3E-05	0.282489	-9.8	1.0
QL10-23-08	0.01222	0.00012	0.00051	5E-06	0.28243365	2E-05	0.282429	-12.0	-1.1
QL10-23-09	0.03559	0.00157	0.00137	5E-05	0.28257925	3E-05	0.282566	-6.8	3.7
QL10-23-10	0.01507	6.7E-05	0.00065	2E-06	0.28246937	2E-05	0.282463	-10.7	0.1
QL10-23-11	0.01501	0.00099	0.00062	4E-05	0.28239465	2E-05	0.282389	-13.3	-2.6
QL10-23-12	0.01085	0.00015	0.00047	6E-06	0.28244142	2E-05	0.282437	-11.7	-0.8
QL10-23-13	0.01376	9.1E-05	0.00058	4E-06	0.28243625	2E-05	0.282431	-11.9	-1.1
QL10-23-14	0.01245	6.1E-05	0.00053	2E-06	0.28242168	2E-05	0.282417	-12.4	-1.6
QL10-23-15	0.0123	2.1E-05	0.00052	1E-06	0.28235349	2E-05	0.282349	-14.8	-4.0
QL10-23-16	0.01881	0.00054	0.00079	2E-05	0.28248981	2E-05	0.282482	-10.0	0.8
QL10-23-17	0.01365	0.00013	0.00059	5E-06	0.28245063	2E-05	0.282445	-11.4	-0.6
QL10-23-18	0.01984	0.00024	0.00079	8E-06	0.28249822	2E-05	0.282491	-9.7	1.1
QL10-23-19	0.01222	0.00016	0.00052	7E-06	0.28240602	2E-05	0.282401	-12.9	-2.1
QL10-23-20	0.01311	4.3E-05	0.00056	2E-06	0.28246426	2E-05	0.282459	-10.9	-0.1
								Ave.	**-1.2**
QL10-24-01	0.01052	0.00021	0.00036	8E-06	0.28245932	2E-05	0.282456	-11.1	-0.2
QL10-24-02	0.01037	8.1E-05	0.00035	9E-07	0.28247896	2E-05	0.282476	-10.4	0.5
QL10-24-03	0.01322	0.00015	0.00045	3E-06	0.282458	2E-05	0.282454	-11.1	-0.3
QL10-24-04	0.02058	0.00033	0.00068	8E-06	0.28242501	2E-05	0.282419	-12.3	-1.5
QL10-24-05	0.01866	0.00023	0.00063	6E-06	0.2824628	2E-05	0.282457	-10.9	-0.1
QL10-24-06	0.01189	0.00015	0.00041	3E-06	0.2824482	2E-05	0.282444	-11.5	-0.6
QL10-24-07	0.01202	2.2E-05	0.00041	1E-06	0.28245597	2E-05	0.282452	-11.2	-0.3
QL10-24-08	0.01924	0.00039	0.00064	1E-05	0.28244129	2E-05	0.282435	-11.7	-0.9
QL10-24-09	0.01236	0.00016	0.00042	3E-06	0.28247456	2E-05	0.282471	-10.5	0.3
QL10-24-10	0.01986	0.00039	0.00066	1E-05	0.28250641	2E-05	0.282500	-9.4	1.4
QL10-24-11	0.01981	0.00085	0.00072	3E-05	0.28246788	3E-05	0.282461	-10.8	0.0
QL10-24-12	0.01324	4.3E-05	0.00045	9E-07	0.28248594	2E-05	0.282482	-10.1	0.7
QL10-24-13	0.01265	3.2E-05	0.00043	2E-06	0.28245755	2E-05	0.282454	-11.1	-0.3
QL10-24-14	0.02133	0.00048	0.00072	1E-05	0.28245234	2E-05	0.282446	-11.3	-0.5
QL10-24-15	0.02115	0.00048	0.00069	1E-05	0.28244039	2E-05	0.282434	-11.7	-1.0
QL10-24-16	0.01623	0.00022	0.00057	1E-05	0.28252163	2E-05	0.282516	-8.9	2.0
QL10-24-17	0.01931	0.00016	0.00065	8E-06	0.2824662	2E-05	0.282460	-10.8	0.0
QL10-24-18	0.01178	6.5E-05	0.0004	9E-07	0.2824747	2E-05	0.282471	-10.5	0.4
QL10-24-19	0.01444	0.00013	0.00048	3E-06	0.28247871	2E-05	0.282474	-10.4	0.5
QL10-24-20	0.01377	0.00013	0.00046	2E-06	0.28248123	2E-05	0.282477	-10.3	0.6
								Ave.	**0.0**
QL10-25-01	0.04278	0.00022	0.00172	1E-05	0.28263861	2E-05	0.282622	-4.7	5.7
QL10-25-02	0.022	0.00012	0.00099	4E-06	0.28262855	2E-05	0.282619	-5.1	5.6
QL10-25-03	0.02651	0.00049	0.00115	2E-05	0.28265019	2E-05	0.282639	-4.3	6.3
QL10-25-04	0.02721	0.0008	0.00119	3E-05	0.28261633	2E-05	0.282605	-5.5	5.1
QL10-25-05	0.03071	0.00083	0.0013	3E-05	0.28264448	3E-05	0.282632	-4.5	6.1
QL10-25-06	0.03111	0.00031	0.00124	1E-05	0.28262095	2E-05	0.282609	-5.3	5.3
QL10-25-07	0.04868	0.00044	0.002	2E-05	0.28260067	2E-05	0.282582	-6.1	4.3
QL10-25-08	0.02815	0.0004	0.00118	2E-05	0.2826315	2E-05	0.282620	-5.0	5.6
QL10-25-09	0.02835	0.00054	0.00139	2E-05	0.28263883	3E-05	0.282626	-4.7	5.8
QL10-25-10	0.04914	9.4E-05	0.00207	4E-06	0.28264746	2E-05	0.282628	-4.4	5.9
QL10-25-11	0.0587	0.00058	0.00235	2E-05	0.28261409	2E-05	0.282592	-5.6	4.6
QL10-25-12	0.07148	0.00031	0.00283	9E-06	0.28264475	3E-05	0.282618	-4.5	5.6
QL10-25-13	0.03694	0.00083	0.00151	3E-05	0.2826664	2E-05	0.282652	-3.7	6.8
QL10-25-14	0.0349	0.00134	0.00141	5E-05	0.28262798	2E-05	0.282615	-5.1	5.4
QL10-25-15	0.02883	7.3E-05	0.00116	4E-06	0.28266036	2E-05	0.282649	-3.9	6.7
QL10-25-16	0.03209	0.00011	0.00125	5E-06	0.28265858	2E-05	0.282647	-4.0	6.6

Table 6.4 Zircon in situ Hf isotope results

	$^{176}Yb/^{177}Hf$		$^{176}Lu/^{177}Hf$		$^{176}Hf/^{177}Hf$	2s	$^{176}Hf/^{177}Hf_i$	$\varepsilon_{Hf}(0)$	$\varepsilon_{Hf}(t)$
QL10-25-17	0.02469	5.7E-05	0.00101	2E-06	0.28262343	2E-05	0.282614	-5.3	5.4
QL10-25-18	0.01723	0.00018	0.00073	7E-06	0.28262177	1E-05	0.282615	-5.3	5.5
QL10-25-19	0.03076	0.00015	0.00133	6E-06	0.28260441	2E-05	0.282592	-5.9	4.6
QL10-25-20	0.02655	0.00043	0.00108	2E-05	0.28262675	1E-05	0.282617	-5.1	5.5
								Ave.	**5.6**
QL10-26-01	0.02601	0.00198	0.00105	8E-05	0.28251245	3E-05	0.282503	-9.2	1.5
QL10-26-02	0.01775	0.00165	0.00073	6E-05	0.28255956	2E-05	0.282553	-7.5	3.2
QL10-26-03	0.01863	0.00161	0.00076	6E-05	0.28256355	2E-05	0.282556	-7.4	3.4
QL10-26-04	0.10134	0.00579	0.00382	0.0002	0.2825177	2E-05	0.282482	-9.0	0.7
QL10-26-05	0.01779	0.00109	0.00073	4E-05	0.28253067	3E-05	0.282524	-8.5	2.2
QL10-26-06	0.06058	0.00237	0.00229	9E-05	0.28264451	3E-05	0.282623	-4.5	5.7
QL10-26-07	0.04381	0.00295	0.00167	0.0001	0.28256611	4E-05	0.282550	-7.3	3.2
QL10-26-08	0.01504	0.00054	0.00064	2E-05	0.28246004	2E-05	0.282454	-11.0	-0.2
QL10-26-09	0.02348	0.00167	0.00094	6E-05	0.28244672	2E-05	0.282438	-11.5	-0.8
QL10-26-10	0.0401	0.00327	0.00153	0.0001	0.28258267	3E-05	0.282568	-6.7	3.8
QL10-26-11	0.02347	0.00267	0.00092	0.0001	0.28264906	3E-05	0.282640	-4.3	6.4
QL10-26-12	0.04442	0.00372	0.00174	0.0001	0.28252604	2E-05	0.282510	-8.7	1.7
QL10-26-13	0.01749	0.00153	0.00071	6E-05	0.28248104	2E-05	0.282474	-10.3	0.5
QL10-26-14	0.02187	0.00159	0.00087	6E-05	0.28253973	3E-05	0.282532	-8.2	2.5
QL10-26-15	0.0347	0.00127	0.00135	4E-05	0.28248903	2E-05	0.282476	-10.0	0.5
QL10-26-16	0.01241	0.00047	0.00052	2E-05	0.28250621	2E-05	0.282501	-9.4	1.4
QL10-26-17	0.01976	0.00184	0.0008	7E-05	0.28248637	3E-05	0.282479	-10.1	0.6
QL10-26-18	0.01645	0.00153	0.00066	6E-05	0.28255463	3E-05	0.282548	-7.7	3.1
QL10-26-19	0.01636	0.00117	0.00068	5E-05	0.28245993	2E-05	0.282454	-11.0	-0.3
								Ave.	**2.1**
QL10-27-01	0.01388	0.00021	0.00059	9E-06	0.2824995	2E-05	0.282494	-9.6	1.2
QL10-27-02	0.01327	0.0002	0.00056	8E-06	0.28248021	2E-05	0.282475	-10.3	0.5
QL10-27-03	0.01087	1.9E-05	0.00047	8E-07	0.28246203	2E-05	0.282458	-11.0	-0.1
QL10-27-04	0.00986	0.00011	0.00041	4E-06	0.28234064	2E-05	0.282337	-15.3	-4.4
QL10-27-05	0.013	0.00011	0.00055	4E-06	0.28246234	2E-05	0.282457	-11.0	-0.1
QL10-27-06	0.01972	0.00015	0.00082	6E-06	0.28250613	2E-05	0.282498	-9.4	1.3
QL10-27-07	0.01659	0.00024	0.0007	9E-06	0.28245848	2E-05	0.282452	-11.1	-0.3
QL10-27-08	0.01223	7.7E-05	0.00052	3E-06	0.2824541	2E-05	0.282449	-11.2	-0.4
QL10-27-09	0.01468	0.00021	0.00062	8E-06	0.28248705	2E-05	0.282481	-10.1	0.7
QL10-27-10	0.01449	6.6E-05	0.00062	2E-06	0.28246251	2E-05	0.282457	-10.9	-0.2
QL10-27-11	0.0129	0.00021	0.00054	9E-06	0.28249689	2E-05	0.282492	-9.7	1.1
QL10-27-12	0.00993	0.00035	0.00043	1E-05	0.28248474	3E-05	0.282481	-10.2	0.7
QL10-27-13	0.02094	0.00015	0.00089	6E-06	0.28252702	2E-05	0.282519	-8.7	2.0
QL10-27-14	0.01734	0.00053	0.00071	2E-05	0.28252168	2E-05	0.282515	-8.9	1.9
QL10-27-15	0.01357	0.00012	0.00057	4E-06	0.28239068	2E-05	0.282385	-13.5	-2.7
QL10-27-16	0.0136	0.00011	0.00058	4E-06	0.28228712	2E-05	0.282282	-17.1	-6.3
QL10-27-17	0.02731	0.00041	0.00113	2E-05	0.28246439	2E-05	0.282454	-10.9	-0.3
QL10-27-18	0.01156	0.00017	0.00049	7E-06	0.28234976	2E-05	0.282345	-14.9	-4.1
QL10-27-19	0.01593	0.00031	0.00067	1E-05	0.28247095	2E-05	0.282465	-10.6	0.1
QL10-27-20	0.01823	0.00051	0.00074	2E-05	0.28243178	2E-05	0.282425	-12.0	-1.3
QL10-27-21	0.01964	0.00039	0.0008	2E-05	0.28238238	2E-05	0.282375	-13.8	-3.0
								Ave.	**-0.7**

Table 6.5 Whole-rock Sr-Nd-Hf-Pb isotopic data of samples in Kekeli. Age corrected to 500 Ma. Zircon in situ Hf average for each sample is listed for comparison.

	QL10-14 Group 1	QL10-15 Group 1	QL10-23 Group 2	QL10-24 Group 2	QL10-27 Group 2	QL10-20 MME	QL10-21 MME	QL10-25 MME	QL10-26 MME
$^{176}Lu/^{177}Hf$	0.011	0.017	0.008	0.007	0.008	0.007	0.008	0.015	0.018
$^{176}Hf/^{177}Hf$	0.282520	0.282489	0.282675	0.282689	0.282646	0.282763	0.282695	0.282796	0.283364
2σ	5	7	9	8	7	6	9	7	9
$\varepsilon_{Hf}(t)$	-1.38	-4.45	5.04	6.20	4.23	8.59	5.82	7.19	26.24
$\varepsilon_{Hf}(t)$-Zircon	-5.6	-7.0	-1.2	0.0	-0.7		-2.2	5.6	2.1
Ti-thermal meter (ºC)	782	783	693	744	751		733	736	715
Zr-WR temperature (ºC)	822	795	747	787	805	656	712	636	679
$^{147}Sm/^{144}Nd$	0.116938	0.124039	0.113837	0.110773	0.104227	0.087916	0.106882	0.141007	0.119506
$^{143}Nd/^{144}Nd$	0.512067	0.512057	0.512371	0.512359	0.512365	0.512286	0.512369	0.512483	0.512289
2σ	11	14	7	7	7	11	9	9	5
$\varepsilon_{Nd}(t)$	-6.0	-6.7	0.1	0.0	0.6	0.1	0.5	0.5	-1.9
$^{87}Rb/^{86}Sr$	5.97	6.43	0.29	0.78	1.04	0.15	0.32	0.48	0.62
$^{87}Sr/^{86}Sr$	0.77537	0.78554	0.70999	0.71295	0.71428	0.70929	0.71036	0.71171	0.71441
2σ	7	10	9	9	9	10	6	8	8
I_{Sr}	0.7328	0.7397	0.7079	0.7074	0.7069	0.7082	0.7081	0.7083	0.7100
$^{206}Pb/^{204}Pb$	19.960	19.608	19.362	19.142	20.837	21.051	18.888	19.195	19.106
2σ	1	1	1	2	1	2	1	1	2
$^{207}Pb/^{204}Pb$	15.712	15.688	15.688	15.673	15.773	15.783	15.661	15.672	15.668
2σ	1	1	1	1	1	2	1	1	1
$^{208}Pb/^{204}Pb$	39.795	38.678	38.503	38.730	40.418	41.175	38.534	39.101	39.229
2σ	4	4	4	4	4	5	3	4	3
$^{208}Pb/^{204}Pbi$	38.30	37.80	38.10	38.18	37.96	38.35	38.11	38.54	38.49
$^{207}Pb/^{204}Pbi$	15.66	15.65	15.65	15.65	15.69	15.65	15.64	15.65	15.64
$^{206}Pb/^{204}Pbi$	19.03	18.96	18.68	18.72	19.48	18.77	18.50	18.77	18.66

Table 6.6 Calculation of Hf isotopic composition in non-zircon phases

		compent A	Mixture	component B			compent A	Mixture	component B
QL10-14		*zircon phase*	*WR*	*no zircon-phase*	**QL10-15**		*zircon phase*	*WR*	*no zircon-phase*
R	$^{176}Hf/^{177}Hf$	0.2823076	0.28252	0.283064	**R**	$^{176}Hf/^{177}Hf$	0.282282	0.282489	0.283137
C	Hf ppm	11895	7.84	2.2028	**C**	Hf ppm	12534	5.26	1.2746
X		0.000474		0.9995	**X**		0.000318		0.9997
	Zr ppm		237			Zr ppm		159	
ε_{Hf}		-16.4	-8.9	10.3	ε_{Hf}		-17.3	-10.0	12.9

		compent A	Mixture	component B			compent A	Mixture	component B
QL10-23		*zircon phase*	*WR*	*no zircon-phase*	**QL10-24**		*zircon phase*	*WR*	*no zircon-phase*
R	$^{176}Hf/^{177}Hf$	0.2824333	0.282675	0.283509	**R**	$^{176}Hf/^{177}Hf$	0.282467	0.282689	0.283227
C	Hf ppm	10427	6.24	1.4025	**C**	Hf ppm	9286	7.24	2.1153
X		0.000464		0.9995	**X**		0.000552		0.9994
	Zr ppm		232			Zr ppm		276	
ε_{Hf}		-12.0	-3.4	26.1	ε_{Hf}		-10.8	-2.9	16.1

		compent A	Mixture	component B			compent A	Mixture	component B
QL10-27		*zircon phase*	*WR*	*no zircon-phase*	**QL10-21**		*zircon phase*	*WR*	*no zircon-phase*
R	$^{176}Hf/^{177}Hf$	0.2824486	0.282646	0.283208	**R**	$^{176}Hf/^{177}Hf$	0.282406	0.282695	0.283786
C	Hf ppm	9843	7.29	1.8971	**C**	Hf ppm	10067	7.92	1.6594
X		0.000548		0.9995	**X**		0.000622		0.9994
	Zr ppm		274			Zr ppm		311	
ε_{Hf}		-11.4	-4.5	15.4	ε_{Hf}		-12.9	-2.7	35.9

		compent A	Mixture	component B			compent A	Mixture	component B
QL10-25		*zircon phase*	*WR*	*no zircon-phase*	**QL10-26**		*zircon phase*	*WR*	*no zircon-phase*
R	$^{176}Hf/^{177}Hf$	0.2826333	0.282796	0.282995	**R**	$^{176}Hf/^{177}Hf$	0.2825303	0.283364	0.285398
C	Hf ppm	8368	3.13	1.4065	**C**	Hf ppm	9978	5.88	1.7099
X		0.000206		0.9998	**X**		0.000418		0.9996
	Zr ppm		103			Zr ppm		209	
ε_{Hf}		-4.9	0.8	7.9	ε_{Hf}		-8.5	20.9	92.9

$C_M=X_A*C_A+X_B*C_B$	C: element concentration	Zircon:component A	Assuming all the Zr in the zircon, then X for zircon in the WR can be calculated (maxium estimate). R,C,X for zircon are known. R,C,X for WR are given. Then, R,C,X for B can be calculated.
$R_M=R_A*(X_A*C_A/C_M)+R_B*(X_B*C_B/C_M)$	R: isotope ratio	Mixture:whole rock (WR)	
X_A=(Zirconium in WR)/(Zr% in zircon) *maxium estimate*	X: fraction	Non-zircon:component B	

Appendix A. Reference standards GSR-1, GSR-3, GSR-8 and GSR-9 analyzed by ICP-MS at Tianjin Institute of Geology and Mineral Resources, China

	GSR-1	RSD	GSR-3	RSD	GSR-8	RSD	GSR-9	RSD
	ppm	%	ppm	%	ppm	%	ppm	%
Li	128	0.7	9.25	1.2	18.2	0.8	17.9	1.5
Sc	5.12	0.4	14.6	0.5	7.87	1.3	11.0	0.6
Cr	2.39	1.4	140	0.3	7.25	1.1	41.4	0.5
Co	2.68	1.4	48.2	0.1	7.30	0.5	15.1	1.0
Ni	1.58	4.2	144	0.6	12.0	2.5	29.5	0.4
Ga	19.6	1.5	25.4	0.4	21.1	0.7	21.8	1.2
Rb	460	0.5	42.8	4.5	188	0.9	66.7	1.3
Sr	94.2	0.2	1130	0.1	309	0.5	1319	11
Y	62.9	0.7	22.4	0.7	30.8	0.5	16.9	0.9
Zr	168	0.7	290	0.5	320	0.4	199	0.4
Nb	41.1	0.6	74.7	0.3	21.8	0.5	10.4	0.5
Ba	315	0.5	561	0.6	1073	0.1	1976	0.6
La	56.2	0.7	60.0	0.7	64.7	0.5	62.8	0.6
Ce	108	0.3	111	0.6	119	0.3	113	0.5
Pr	13.0	0.6	13.6	0.9	14.2	0.6	14.0	0.6
Nd	46.5	0.6	55.0	0.7	51.4	0.1	51.4	1.0
Sm	9.77	0.1	10.7	1.2	8.78	2.1	7.82	1.4
Eu	0.80	0.8	3.28	0.6	2.08	1.1	2.16	1.6
Gd	8.43	0.3	8.73	0.0	7.16	0.4	5.99	2.0
Tb	1.57	0.4	1.21	0.1	1.04	0.9	0.71	2.2
Dy	10.1	0.7	5.80	2.1	5.91	0.5	3.50	1.6
Ho	2.13	0.3	0.95	1.0	1.19	1.6	0.64	2.6
Er	6.53	0.4	2.07	1.7	3.34	0.7	1.78	1.4
Tm	1.06	1.1	0.23	2.2	0.50	2.4	0.25	3.3
Yb	7.47	0.4	1.33	4.6	3.38	1.4	1.64	2.8
Lu	1.16	1.1	0.18	4.7	0.53	0.7	0.25	1.4
Hf	6.19	0.9	6.65	0.8	8.09	0.7	5.13	1.0
Ta	7.17	0.9	4.53	0.4	1.41	2.3	0.63	2.0
Pb	32.0	0.2	6.68	0.3	100	0.5	18.1	0.5
Th	55.8	0.4	6.29	1.1	16.9	0.9	10.9	0.5
U	18.2	0.7	1.49	1.1	3.33	1.1	1.46	0.7

Appendix B. Standard NBS987, J&M and JMC run on Neptune PIMMS instrument throughout the course of this study.

J&M		Sm doped J&M		NBS987		JMC475		
$^{143}Nd/^{144}Nd$	1SE	$^{143}Nd/^{144}Nd$	1SE	$^{87}Sr/^{86}Sr$	1SE	$^{176}Hf/^{177}Hf$	1SE	
0.511106	0.000004	0.511106	0.000003	0.710285	0.000004	0.282152	0.000003	
0.511114	0.000004	0.511109	0.000004	0.710287	0.000004	0.282153	0.000004	
0.511110	0.000004	0.511094	0.000004	0.710281	0.000004	0.282149	0.000004	
0.511106	0.000004	0.511111	0.000003	0.710282	0.000004	0.282143	0.000004	
0.511107	0.000003	0.511111	0.000003	0.710281	0.000003	0.282150	0.000005	
0.511114	0.000004	0.511109	0.000004	0.710284	0.000004	0.282144	0.000004	
0.511107	0.000003	0.511111	0.000003	0.710286	0.000004	0.282144	0.000005	
0.511108	0.000004	0.511115	0.000005	0.710284	0.000003	0.282151	0.000003	
0.511110	0.000003	0.511114	0.000004	0.710287	0.000004	0.282149	0.000004	
0.511104	0.000003	0.511106	0.000003	0.710272	0.000004	0.282144	0.000005	
0.511101	0.000003	0.511106	0.000004	0.710284	0.000004	0.282144	0.000005	
0.511103	0.000003	0.511106	0.000004	0.710263	0.000003	0.282152	0.000004	
0.511111	0.000004	0.511109	0.000003	0.710273	0.000005	0.282143	0.000005	
0.511111	0.000004	0.511106	0.000004	0.710272	0.000004	0.282142	0.000004	
0.511101	0.000003	0.511104	0.000003	0.710275	0.000004	0.282139	0.000004	
0.511107	0.000004	0.511102	0.000003	0.710284	0.000005	0.282150	0.000005	
0.511113	0.000005	0.511098	0.000003	0.710284	0.000005	0.282145	0.000004	
0.511101	0.000003	0.511108	0.000003	0.710283	0.000004	0.282143	0.000005	
0.511099	0.000004	0.511094	0.000004	0.710272	0.000005	0.282149	0.000003	
0.511103	0.000004	0.511098	0.000004	0.710280	0.000005	0.282143	0.000005	
0.511105	0.000003	0.511092	0.000004	0.710284	0.000005	0.282140	0.000003	
0.511103	0.000003	0.511106	0.000003	0.710264	0.000005	0.282140	0.000004	
0.511099	0.000004	0.511096	0.000003	0.710294	0.000004	0.282141	0.000003	
0.511097	0.000005	0.511104	0.000003	0.710280	0.000005	0.282138	0.000004	
0.511100	0.000004	0.511102	0.000003	0.710302	0.000006	0.282139	0.000004	
0.511108	0.000003	0.511098	0.000003	0.710288	0.000005	0.282145	0.000003	
0.511104	0.000004	0.511108	0.000003	0.710262	0.000006	0.282146	0.000003	
0.511101	0.000003	0.511094	0.000004	0.710269	0.000005	0.282149	0.000003	
0.511099	0.000004	0.511098	0.000004	0.710263	0.000005	0.282137	0.000004	
0.511103	0.000004	0.511092	0.000004	0.710268	0.000004	0.282148	0.000004	
0.511105	0.000003	0.511106	0.000003	0.710267	0.000004	0.282143	0.000005	
0.511103	0.000003	0.511096	0.000003	0.710266	0.000004	0.282144	0.000004	
0.511099	0.000004	0.511121	0.000004	0.710275	0.000004	0.282146	0.000005	
0.511097	0.000005	0.511108	0.000003	0.710274	0.000005	0.282147	0.000004	
0.511100	0.000004	0.511119	0.000003	0.710275	0.000006	0.282148	0.000004	
0.511108	0.000003	0.511109	0.000003	0.710263	0.000005	0.282147	0.000004	
0.511104	0.000004	0.511118	0.000003	0.710259	0.000005	0.282146	0.000005	
0.511113	0.000004	0.511129	0.000004	0.710266	0.000005			
0.511119	0.000003	0.511118	0.000003	0.710269	0.000005			
0.511110	0.000003	0.511113	0.000004					
0.511110	0.000004	0.511115	0.000004					
0.511109	0.000003							
0.511118	0.000003							
0.511119	0.000002							
0.511112	0.000003							
0.511118	0.000003							
0.511114	0.000003							
0.511107		0.511106		0.710277		0.282145		**Ave.**
0.000012		0.000017		0.000020		0.000008		**2SD.**

Appendix C. Standard NBS981 run on Neptune PIMMS instrument throughout the course of this study.

Ratio $^{206}Pb/^{204}Pb$	2SE	Ratio $^{207}Pb/^{204}Pb$	2SE	Ratio $^{208}Pb/^{204}Pb$	2SE	
16.94068	0.00081	15.49848	0.00087	36.71968	0.00302	
16.94114	0.00077	15.49861	0.00084	36.71920	0.00304	
16.94060	0.00080	15.49776	0.00109	36.71603	0.00396	
16.94088	0.00067	15.49808	0.00067	36.71764	0.00243	
16.94036	0.00080	15.49732	0.00095	36.71672	0.00292	
16.94220	0.00080	15.49852	0.00113	36.72004	0.00503	
16.94252	0.00109	15.49909	0.00126	36.72087	0.00449	
16.93978	0.00059	15.49699	0.00071	36.71314	0.00287	
16.94002	0.00070	15.49719	0.00074	36.71594	0.00290	
16.93994	0.00089	15.49701	0.00093	36.71601	0.00292	
16.94025	0.00066	15.49778	0.00078	36.71735	0.00241	
16.94114	0.00058	15.49839	0.00064	36.71754	0.00225	
16.94001	0.00051	15.49675	0.00060	36.71397	0.00233	
16.94041	0.00061	15.49737	0.00060	36.71569	0.00237	
16.94022	0.00061	15.49728	0.00072	36.71584	0.00236	
16.94016	0.00056	15.49732	0.00055	36.71630	0.00208	
16.94072	0.00053	15.49753	0.00063	36.71627	0.00227	
16.94085	0.00064	15.49767	0.00061	36.71587	0.00230	
16.94051	0.00059	15.49776	0.00079	36.71598	0.00318	
16.93939	0.00083	15.49624	0.00097	36.71084	0.00335	
16.93986	0.00064	15.49691	0.00087	36.71362	0.00325	
16.93967	0.00079	15.49657	0.00078	36.71541	0.00367	
16.93951	0.00088	15.49643	0.00075	36.71252	0.00254	
16.93980	0.00085	15.49637	0.00093	36.71312	0.00379	
16.94045	0.00066	15.49681	0.00075	36.71419	0.00372	
16.94177	0.00075	15.49675	0.00080	36.71339	0.00340	
16.94276	0.00065	15.49712	0.00067	36.71544	0.00328	
16.94221	0.00080	15.49664	0.00080	36.71323	0.00238	
16.94421	0.00075	15.49782	0.00079	36.71742	0.00315	
16.93984	0.00065	15.49705	0.00068	36.71424	0.00270	
16.93981	0.00082	15.49705	0.00096	36.71569	0.00323	
16.94078	0.00079	15.49781	0.00081	36.71648	0.00259	
16.94171	0.00067	15.49796	0.00073	36.71861	0.00320	
16.94092	0.00055	15.49762	0.00070	36.71631	0.00258	
16.94020	0.00085	15.49611	0.00092	36.71153	0.00338	
16.93976	0.00070	15.49569	0.00063	36.71079	0.00259	
16.94112	0.00069	15.49718	0.00074	36.71508	0.00317	
16.94043	0.00075	15.49661	0.00091	36.71250	0.00332	
16.94029	0.00079	15.49674	0.00100	36.71401	0.00390	
16.94101	0.00082	15.49748	0.00101	36.71457	0.00379	
16.94016	0.00057	15.49615	0.00078	36.71062	0.00314	
16.94098	0.00077	15.49628	0.00090	36.71337	0.00363	
16.94004	0.00053	15.49702	0.00062	36.71558	0.00243	
16.94055	0.00073	15.49797	0.00075	36.71920	0.00240	
16.94097	0.00087	15.49817	0.00092	36.71894	0.00283	
16.94069	0.00074	15.49793	0.00079	36.71786	0.00276	
16.94028	0.00089	15.49769	0.00100	36.71769	0.00313	
16.93976	0.00065	15.49666	0.00069	36.71341	0.00224	
16.94110	0.00054	15.49846	0.00063	36.71779	0.00232	
16.94076	0.00070	15.49773	0.00087	36.71636	0.00295	
16.94066		15.49732		36.71560		**Ave.**
0.00184		0.00150		0.00492		**2SD.**

Appendix D. Repeated analyses of Nd isotopes

Sample ID	Old value	error	Repeated value	error	Differences(in ppm)
DL09-07	0.512412	0.000005	0.512395	0.000004	-33
DL09-08	0.512362	0.000005	0.512356	0.000005	-12
DL09-14	0.512324	0.000006	0.512327	0.000004	6
DL09-21	0.512377	0.000004	0.512343	0.000004	-66
DL09-24	0.512330	0.000007	0.512298	0.000004	-62
QL09-04	0.511806	0.000004	0.511799	0.000002	-14
QL09-18	0.512556	0.000006	0.512556	0.000004	0
QL09-21	0.512016	0.000003	0.512026	0.000004	20
QL09-27	0.511900	0.000004	0.511899	0.000004	-2
QL09-40	0.512067	0.000005	0.512068	0.000003	2

Appendix E. Isotope blanks for each batch of chemistry run for Sr-Nd-Hf-Pb isotope analysis.

Blank ID	Sr(pg)	Nd(pg)	Hf(pg)	Pb(pg)
134.10	8	1	29	30
134.20	53	2	8	55
136.9	23	21	20	274
136.19	81	3	4	80
137.10	24	15	55	79
137.20	362	2	1	124
139.10	66	4	4	186
139.20	32	3	3	21
143.14	91	37	17	123
145.20	66	6	15	20
Ave.	81	10	16	99
Sample Ave.	283ppm	42ppm	6ppm	23ppm

Appendix F. Zircon trace elements for Chapter 4, analysed in Beijing

Element	SiO_2	Ti	Y	Nb	La	Ce	Pr	Nd	Sm	Eu	Gd	Tb	Dy	Ho	Er	Tm	Yb	Lu	Hf	Ta	Pb	Pb	Pb	Th	U	Pb
	29	49	89	93	139	140	141	143	147	151	155	159	163	165	166	169	173	175	179	181	206	207	208	232	238	204
QL09-01																										
0901-01	32.2	17.8	689	4.0	0.1	25.7	0.2	2.2	5.1	0.6	19.5	6	72	25	106	24	253	49	8677	1.3	60	7.4	7.6	49	49	20
0901-02	32.2	3.1	2053	2.5	51	92.2	11	52	19.7	1.2	61.4	19	219	77	320	70	718	135	8604	1.1	141	10.2	17.8	268	285	45
0901-03	32.2	13.2	1223	2.6	0.0	11.5	0.4	5.1	8.4	4.7	41	13	132	44	174	39	413	83	6409	1.0	186	13.7	26.6	399	353	62
0901-04	32.2	3.1	961	0.6	0.1	16.3	0.6	9.5	9.5	3.1	31.0	8	94	35	150	34	375	78	6652	0.3	173	33.6	53.8	248	101	77
0901-05	32.2	4.6	1176	1.8	0.1	23.3	0.1	2.7	6.7	0.9	29	10	115	41	176	39	415	79	9459	0.9	397	74.9	44.4	205	217	135
0901-06	32.2	6.5	677	3.0	0.1	20.0	0.1	0.8	2.2	0.2	13.6	5	62	23	102	24	263	51	9604	1.2	282	52.4	28.6	140	167	95
0901-07	32.2	17.0	281	1.8	0.0	19.0	0.1	1.7	2.8	1.8	10.2	3	30	9	39	8	93	16	6467	0.8	28	2.1	4.2	61	54	9
0901-08	32.2	6.5	734	0.9	0.1	12.4	0.2	3.1	5.2	1.1	19.6	6	71	25	113	27	302	58	8485	0.5	354	53.1	36.3	200	246	116
0901-09	32.2	7.3	451	1.7	0.1	14.7	0.1	1.1	2.1	0.4	10.9	4	42	16	68	16	177	36	9236	0.8	246	46.4	15.8	70	131	78
0901-10	32.2	23.2	907	2.3	0.0	10.7	0.3	4.5	6.9	1.1	27	8	97	33	137	30	312	60	8745	0.9	233	43.6	25.7	128	154	79
0901-11	32.2	11.8	570	0.9	0.1	10.9	0.1	1.1	2.7	0.9	13.5	5	57	20	90	20	221	44	8489	0.5	149	28.3	14.8	64	78	50
0901-12	32.2	21.9	538	1.0	0.1	4.6	0.1	3.0	5.3	1.0	19.7	6	62	20	81	17	183	34	7390	0.4	23	2.9	2.3	15	19	7
0901-13	32.2	11.3	847	0.7	0.1	14.6	0.1	3.5	5.8	1.5	26	8	89	31	127	29	293	57	8583	0.4	25	1.8	4.8	73	50	9
0901-14	32.2	26.8	454	4.0	0.2	2.6	0.1	0.9	1.8	0.3	10.3	4	43	15	69	16	177	35	9302	1.7	119	8.4	5.6	85	234	33
0901-15	32.2	4.3	724	2.4	0.0	10.9	0.1	1.6	3.7	0.6	16.8	6	68	25	112	26	292	55	9612	1.2	205	31.5	6.6	83	282	60
0901-16	32.2	6.2	538	3.9	0.1	18.9	0.1	2.0	3.5	0.2	14.4	5	54	19	84	20	216	41	9294	1.2	103	11.9	8.5	55	89	32
0901-17	32.2	5.0	259	0.3	0.1	1.6	0.1	0.4	1.6	0.2	8.0	3	30	8	31	6	58	10	9963	0.2	157	28.3	3.6	23	125	46
0901-18	32.2	5.4	611	4.3	0.1	3.9	0.0	0.9	2.0	0.2	11.0	5	59	21	86	20	208	38	12425	2.0	464	79.5	15.4	102	421	137
0901-19	32.2	4.3	788	3.6	0.1	16.8	0.1	1.9	3.5	0.4	16.7	6	76	28	127	30	324	63	9626	1.4	109	8.1	12.0	180	218	34
0901-20	32.2	6.5	467	2.3	0.2	3.8	0.1	0.9	1.0	0.2	6.1	3	36	15	77	20	240	52	15017	2.2	1339	256	10.7	58	907	385
0901-21	32.2	6.8	164	0.6	0.1	3.6	0.0	0.6	0.7	0.2	3.6	1	14	5	25	7	86	19	9065	0.5	86	6.1	4.4	61	163	24
0901-22	32.2	17.2	440	1.9	0.2	9.4	0.1	1.0	2.2	0.5	9.0	3	40	14	66	16	182	36	8611	1.0	63	4.8	6.9	97	125	20
0901-23	32.2	15.6	531	1.3	0.0	1.4	0.1	1.5	3.0	0.4	13.4	5	54	19	84	20	224	45	7351	0.6	49	3.7	3.5	49	95	14
0901-24	32.2	2.6	1011	2.9	0.0	14.1	0.1	2.1	5.1	0.5	24	8	100	36	157	37	397	75	8627	1.3	81	5.8	8.8	134	165	25
0901-25	32.2	4.3	495	1.7	0.1	13.1	0.0	0.8	1.7	0.5	9.1	3	41	16	78	21	255	55	9998	0.7	276	54.7	20.9	102	179	90
0901-26	32.2	2.2	554	1.0	0.0	12.1	0.1	0.8	2.0	1.2	9.9	4	50	19	89	23	281	60	8916	0.4	242	44.7	11.5	50	130	74
0901-27	32.2	8.2	286	1.1	0.0	11.3	0.0	0.7	1.4	0.5	5.8	2	24	9	44	12	148	32	8855	0.7	466	112.5	24.1	96	237	150
0901-28	32.2	6.4	1049	1.9	0.1	7.9	0.1	1.5	3.5	1.0	21.0	8	99	37	164	39	441	87	7766	0.9	377	73.8	18.9	87	215	117
0901-29	32.2	3.0	273	3.2	0.1	2.7	0.0	0.3	0.3	0.1	1.3	1	16	9	55	18	263	64	10338	1.2	441	76.0	9.4	48	269	128
0901-30	32.2	3.8	756	2.4	0.0	15.1	0.1	1.4	3.5	1.0	17.3	6	71	26	115	27	301	59	9040	0.7	37	2.7	4.1	59	71	12
0901-31	32.2	7.6	1436	1.2	0.1	10.7	0.6	8.0	12.3	1.6	47	15	158	54	217	47	486	88	7296	0.5	48	3.5	7.5	109	93	16
0901-32	32.2	47.4	537	1.8	0.9	16.7	0.4	3.5	3.4	1.0	10.8	4	45	18	86	24	302	67	8263	0.7	66	4.7	7.7	117	135	21

Appendix F. Zircon trace elements for Chapter 4, analysed in Beijing

Element	SiO_2	Ti	Y	Nb	La	Ce	Pr	Nd	Sm	Eu	Gd	Tb	Dy	Ho	Er	Tm	Yb	Lu	Hf	Ta	Pb	Pb	Pb	Th	U	Pb
	29	49	89	93	139	140	141	143	147	151	155	159	163	165	166	169	173	175	179	181	206	207	208	232	238	204
0901-33	32.2	6.6	516	0.9	0.6	16.6	0.4	3.7	3.0	1.2	10.6	4	44	16	79	22	281	61	8461	0.4	40	3.2	7.7	106	81	14
0901-34	32.2	33.3	3008	21.1	0.2	151	1.3	21	29	4.0	99	30	316	107	452	103	1012	164	6478	5.2	540	37.5	91.7	1505	1239	187
0901-35	32.2	4.2	760	3.0	0.1	61.9	0.1	1.6	3.5	1.2	16.6	6	65	24	117	31	365	74	9686	1.1	625	113.2	70.2	316	340	212
0901-36	32.2	5.1	273	1.3	0.1	10.5	0.0	0.5	1.0	0.3	4.6	2	23	9	42	11	137	28	9292	0.6	279	52.5	15.0	68	154	87
0901-37	32.2	4.8	482	0.8	0.0	5.2	0.0	1.0	1.8	0.7	9.8	4	42	17	81	21	239	52	7753	0.4	373	75.1	17.3	77	203	115
0901-38	32.2	3.5	314	1.9	0.0	10.0	0.1	0.6	1.0	0.1	4.8	2	27	10	50	14	165	32	9467	0.8	59	4.3	4.2	60	120	17
0901-39	32.2	6.9	414	1.4	0.0	10.1	0.1	0.5	1.4	0.3	7.8	3	38	14	66	16	180	36	9481	0.9	250	39.8	21.1	118	176	80
0901-40	32.2	3.0	131	0.5	0.1	7.8	0.1	0.3	0.5	0.2	2.2	1	11	4	20	6	84	19	8651	0.4	475	83.3	10.8	51	295	139
0901-41	32.2	5.8	850	1.7	0.1	5.0	0.1	1.1	2.6	1.0	16.0	6	76	29	124	30	335	65	7129	0.7	369	72.6	19.9	87	202	115
0901-42	32.2	5.8	582	1.2	0.1	14.5	0.1	1.0	2.3	0.2	13.1	5	55	20	87	20	223	45	10457	1.0	610	121.3	64.4	292	338	208
0901-43	32.2	6.3	832	1.4	0.1	9.7	0.2	2.5	4.8	0.9	20	7	85	30	128	30	304	62	7189	0.5	40	2.7	5.8	78	73	13
0901-44	32.2	8.7	476	0.9	0.0	10.8	0.0	1.2	2.3	0.6	10.8	4	44	16	73	18	209	43	8203	0.5	25	1.9	3.3	50	50	8
0901-45	32.2	4.4	535	1.5	0.0	19.5	0.1	1.7	3.3	0.7	13.0	5	52	19	79	19	214	40	8453	0.5	206	37.7	25.3	112	123	71
0901-46	32.2	3.8	298	0.8	0.1	28.3	0.1	2.3	3.1	1.4	10.3	3	30	10	44	10	125	25	7835	0.3	149	28.3	13.7	64	87	49
0901-47	32.2	5.3	2301	4.3	0.2	17.5	0.4	7.4	14.3	1.1	61.6	21	252	89	363	83	873	158	9059	1.5	198	14.0	23.5	341	385	63
0901-48	32.2	38.1	2078	3.6	0.0	21.9	0.5	9.6	15.7	1.6	64	21	230	79	320	73	755	138	7856	1.1	143	10.3	24.5	356	291	50
0901-49	32.2	6.5	625	8.5	0.7	14.1	0.5	3.0	2.6	0.8	9.7	4	50	20	96	27	327	70	10629	3.1	310	27.7	20.6	252	728	92
QL09-02																										
0902-01	32.2	5.3	795	6.6	0.1	43.1	0.1	2.3	5.1	2.0	22	7	78	28	118	29	338	67	9890	2.8	227	16.3	26.6	372	437	72
0902-02	32.2	5.3	1037	2.0	0.1	12.1	0.1	3.4	6.4	0.8	25	9	105	38	160	39	436	83	8834	1.1	100	7.2	11.0	160	201	31
0902-03	32.2	7.4	760	5.0	2.3	52.3	2.6	18.3	12.3	3.2	23	7	70	26	113	31	408	89	9351	1.1	108	8.3	19.1	336	244	38
0902-04	32.2	7.9	1220	4.1	0.7	12.2	1.1	10.1	9.1	1.2	29	10	125	43	182	44	517	99	11352	1.7	231	15.7	16.9	270	602	68
0902-05	32.2	8.8	957	2.0	0.0	1.7	0.2	4.5	12.9	0.5	55	17	140	35	106	20	176	28	10517	1.3	141	8.5	3.8	98	511	38
0902-06	32.2	5.2	391	0.7	0.1	1.4	0.0	0.3	0.6	0.3	6	3	35	14	64	17	215	44	7657	0.7	242	39.0	6.1	36	200	70
0902-07	32.2	2.6	1025	1.0	0.0	0.2	0.0	0.3	1.2	0.1	15	8	110	36	143	33	349	62	13319	1.4	216	13.1	0.4	10	757	55
0902-08	32.2	3.3	710	1.6	0.0	1.7	0.0	0.6	2.8	0.2	18	8	84	24	87	20	216	44	11864	0.9	149	9.2	2.9	56	486	40
0902-09	32.2	13.4	752	1.2	0.0	12.2	0.1	2.4	5.1	1.1	21	7	77	27	115	28	321	64	7934	0.4	30	2.1	4.1	57	58	10
0902-11	32.2	5.9	699	2.3	0.0	8.6	0.0	0.8	2.4	0.2	14	6	72	25	104	25	274	53	10815	1.6	370	40.6	20.3	145	482	109
0902-12	32.2	3.7	970	3.8	0.0	31.2	0.2	4.0	7.1	2.8	25	9	93	32	141	36	436	88	9757	1.2	139	10.0	17.7	258	277	45
0902-13	32.2	2.7	1284	1.5	0.1	0.8	0.0	0.3	1.9	0.1	17	10	129	44	189	46	496	92	12985	1.7	209	14.5	1.3	14	708	54
0902-14	32.2	3.9	2067	2.4	0.1	0.7	0.1	1.4	6.6	0.4	56	26	279	73	223	40	355	54	12235	2.3	411	25.1	1.5	37	1427	105
0902-15	32.2	4.0	952	2.2	0.5	11.4	0.2	2.2	4.0	0.4	20	7	90	34	153	39	446	85	10003	1.8	203	14.6	13.1	191	442	59
0902-16	32.2	14.5	1063	2.9	0.3	7.0	0.5	6.4	6.5	1.3	25	8	101	36	162	40	481	97	8458	1.1	53	3.4	1.8	37	186	14

Appendix F. Zircon trace elements for Chapter 4, analysed in Beijing

Element	SiO_2	Ti	Y	Nb	La	Ce	Pr	Nd	Sm	Eu	Gd	Tb	Dy	Ho	Er	Tm	Yb	Lu	Hf	Ta	Pb	Pb	Pb	Th	U	Pb
	29	49	89	93	139	140	141	143	147	151	155	159	163	165	166	169	173	175	179	181	206	207	208	232	238	204
0902-17	32.2	83.7	1699	2.2	1.9	2.8	1.4	8.0	6.3	0.8	30	14	176	59	235	52	474	108	16654	2.0	211	14.6	3.3	59	744	56
0902-18	32.2	3.7	375	1.5	0.0	10.4	0.0	0.4	1.1	0.2	6	2	29	12	60	16	209	44	10631	0.7	213	36.5	19.5	98	208	70
0902-19	32.2	4.7	829	3.9	0.5	23.3	0.5	5.0	6.3	1.9	22	8	84	31	130	32	379	72	9544	1.7	194	14.0	15.1	222	428	58
0902-20	32.2	4.5	272	1.2	0.0	23.6	0.1	1.0	2.0	0.4	9	3	28	9	39	10	118	23	10910	0.6	248	42.1	17.5	89	193	78
0902-21	32.2	4.6	1179	2.0	0.5	3.3	0.9	6.6	7.0	0.6	35	16	155	41	131	25	252	42	12336	1.8	219	13.7	1.3	28	785	56
0902-22	32.2	14.7	709	1.7	0.1	10.8	0.1	1.5	2.6	0.4	13	5	63	24	112	29	352	71	9744	1.2	567	94.7	33.0	181	429	175
0902-23	32.2	5.8	1048	5.6	0.6	34.3	0.6	6.3	6.5	2.1	26	8	96	35	154	40	465	96	8545	1.6	138	10.4	17.7	251	278	45
0902-24	32.2	8.9	976	3.2	0.4	7.3	0.4	3.9	4.3	0.7	21	8	99	32	132	31	357	68	11853	1.5	289	20.5	10.2	156	708	79
0902-25	32.2	2.6	607	0.8	0.1	1.5	0.1	1.4	2.2	0.2	15	7	71	20	70	14	133	23	12289	0.9	152	9.6	2.0	35	544	40
0902-26	32.2	7.4	705	0.8	0.0	15.1	0.2	3.4	5.0	2.3	18	6	66	24	107	28	342	72	7857	0.3	44	3.2	9.2	134	85	16
0902-27	32.2	4.4	544	0.9	0.1	9.4	0.1	1.6	3.0	0.9	13	5	54	19	82	19	217	43	8570	0.4	152	27.4	11.5	47	105	49
0902-28	32.2	2.3	398	2.5	0.0	1.8	0.0	0.2	0.8	0.1	5	2	34	14	66	17	207	41	10759	2.2	52	3.3	1.6	43	188	14
0902-29	32.2	5.9	422	1.4	0.1	1.0	0.1	1.2	5.3	0.1	26	8	65	15	40	7	58	9	10273	1.0	118	7.5	9.5	58	432	35
0902-30	32.2	3.3	829	3.5	23	50.8	5.1	25	8.5	0.9	19	6	72	28	132	35	430	90	8945	1.8	207	15.2	15.0	221	425	61
0902-31	32.2	7.4	691	1.6	0.1	1.8	0.2	2.4	7.2	0.4	30	10	87	24	83	17	173	30	10366	0.9	107	6.5	2.6	68	378	29
0902-32	32.2	6.6	1195	4.4	0.0	8.6	0.4	6.8	14.3	0.8	49	15	143	43	158	34	331	59	9756	2.3	177	10.8	15.0	410	658	53
0902-33	32.2	9.0	1161	3.2	2.9	12.7	3.5	27	18.7	2.7	53	17	156	41	130	25	233	38	12010	1.8	366	31.9	5.8	136	1153	98
0902-34	32.2	4.5	570	0.5	0.0	17.9	0.2	2.8	3.9	2.1	14	4	45	18	84	23	308	68	7223	0.2	73	5.3	10.8	164	156	24
0902-35	32.2	4.7	1085	2.4	0.1	18.4	0.4	5.3	8.7	3.0	34	11	114	37	155	36	414	82	9570	1.1	153	10.8	11.4	166	339	45
0902-36	32.2	5.4	574	1.4	1.6	16.0	0.9	4.0	3.6	0.5	13	4	51	19	87	22	258	54	9015	0.7	323	61.2	23.0	104	195	103
0902-37	32.2	12.5	447	1.4	0.1	13.0	0.1	2.1	3.8	0.9	13	4	46	16	66	15	170	32	8085	0.6	39	4.7	3.4	22	28	12
0902-38	32.2	8.1	802	4.9	0.0	7.5	0.1	0.7	2.3	0.1	13	6	76	29	122	29	306	58	10233	1.4	1414	261	18.1	98	938	408
0902-39	32.2	6.6	596	2.2	37	83	10	47.1	12.2	0.6	20	6	60	20	90	22	252	50	9444	1.4	150	10.9	9.7	140	307	44
0902-40	32.2	4.6	1257	1.4	0.0	12.7	0.3	5.1	9.6	1.8	35	11	126	44	184	43	458	85	8137	0.8	116	8.3	12.0	192	254	36
0902-41	32.2	14.7	933	1.7	38	114	17	104	45	2.2	69	16	128	36	135	30	310	57	9298	0.9	47	3.7	7.9	196	168	16
QL09-12																										
0912-01	32.2	5.6	1247	1.3	0.0	8.6	0.3	4.0	5.7	2.1	25	9	109	41	192	50	617	129	7939	0.6	50	2.9	7.5	364	332	17
0912-02	32.2	5.5	950	0.9	0.1	6.7	0.2	3.6	5.6	1.5	20	7	90	34	154	41	493	100	7836	0.5	36	2.1	5.0	238	242	12
0912-03	32.2	8.9	955	1.1	0.7	9.5	0.5	5.4	6.3	1.8	20	7	83	32	146	39	458	98	7232	0.6	33	2.2	5.6	257	206	11
0912-04	32.2	14.3	2877	18.8	33	303	29	190	106	16	145	33	309	101	429	106	1214	248	9168	7.5	652	48.8	64.2	1738	2588	202
0912-05	32.2	46.5	2013	17.5	991	1316	175	865	209	43	186	30	219	63	261	64	716	154	9144	10.2	715	57.2	53.8	1678	3254	213
0912-06	32.2	8.9	2905	2.6	0.4	15.1	0.8	9.9	13.2	2.4	65	23	266	101	444	106	1152	222	7274	1.6	1124	88.1	95.7	1260	1795	340
0912-07	32.2	5.6	636	0.9	0.3	6.2	0.1	1.0	1.9	0.6	9	3	48	20	102	29	390	89	7807	0.5	33	2.3	3.3	151	224	10

Appendix F. Zircon trace elements for Chapter 4, analysed in Beijing

Element	SiO_2	Ti	Y	Nb	La	Ce	Pr	Nd	Sm	Eu	Gd	Tb	Dy	Ho	Er	Tm	Yb	Lu	Hf	Ta	Pb	Pb	Pb	Th	U	Pb
	29	49	89	93	139	140	141	143	147	151	155	159	163	165	166	169	173	175	179	181	206	207	208	232	238	204
0912-08	32.2	6.3	956	0.8	1.8	9.1	0.6	5.4	4.7	1.6	19	7	86	32	150	40	489	102	8074	0.5	38	2.5	5.5	255	252	13
0912-09	32.2	7.1	4222	4.6	0.4	23.8	1.0	12.9	20	3.5	95	35	407	153	658	162	1721	325	6910	2.2	1907	146	192.1	2429	3046	593
0912-10	32.2	10.3	1545	2.0	0.1	12.4	0.2	3.1	4.9	1.7	25	10	130	51	241	64	763	158	6810	0.8	55	3.1	9.3	471	367	19
0912-11	32.2	8.5	2073	2.0	0.1	13.6	0.5	7.3	11.6	3.4	45	16	192	71	316	82	979	206	7125	0.8	69	3.9	12.3	619	469	24
0912-12	32.2	5.3	1457	1.1	0.1	9.6	0.3	4.9	6.6	2.0	30	11	130	49	226	60	714	153	7555	0.8	60	3.4	9.0	448	406	20
0912-13	32.2	11.3	2540	3.1	0.5	24.6	0.7	10.0	14.9	4.6	59	20	238	91	400	105	1221	251	7358	1.1	94	5.6	18.6	919	633	34
0912-14	32.2	6.1	794	1.0	0.1	6.7	0.1	1.7	3.7	1.1	14	5	66	26	125	35	456	97	7982	0.6	34	2.1	4.1	195	230	11
0912-15	32.2	11.0	1112	1.7	0.2	8.9	0.1	1.1	2.9	1.0	16	7	86	36	178	49	598	132	6854	0.7	40	2.5	5.1	249	270	13
0912-16	32.2	6.3	1109	1.0	0.0	7.2	0.2	3.2	4.9	1.7	22	8	96	37	172	45	544	118	7215	0.5	40	2.2	5.7	274	268	13
0912-17	32.2	8.4	1539	1.8	0.1	12.0	0.2	3.8	5.3	1.8	26	10	129	51	238	63	764	159	7697	0.8	63	3.6	10.2	482	418	21
0912-18	32.2	7.8	1848	1.7	0.5	13.2	0.6	6.7	9.7	2.7	38	14	168	65	290	75	921	189	7753	0.8	74	4.4	12.7	617	497	25
0912-19	32.2	3.1	788	0.7	0.0	6.9	0.1	1.9	3.3	1.1	15	6	68	27	124	32	394	86	9421	0.5	53	3.0	6.6	311	355	17
0912-20	32.2	10.9	1766	3.1	0.1	15.0	0.2	3.0	4.9	1.8	25	10	139	58	275	74	905	192	7285	1.1	76	4.2	11.4	546	500	25
0912-21	32.2	6.2	1184	1.0	0.0	7.3	0.3	3.8	5.6	1.8	24	8	105	40	184	49	589	122	6978	0.5	39	2.2	5.7	269	257	13
0912-22	32.2	5.3	1251	1.2	0.4	10.1	0.4	4.6	6.0	1.8	24	9	106	42	194	51	612	132	8197	0.7	65	3.7	9.5	450	434	21
0912-23	32.2	7.2	2156	1.9	0.0	13.1	0.4	6.8	12.0	3.8	48	17	195	73	330	86	1002	208	7184	0.8	74	4.3	13.4	650	494	26
0912-24	32.2	14.5	2696	4.4	0.1	28.6	0.3	4.6	9.6	3.2	51	20	252	97	436	110	1261	254	6889	1.3	111	6.2	25.6	1261	741	41
0912-25	32.2	4.3	510	0.5	0.0	4.2	0.1	1.2	2.1	0.7	9	3	44	17	79	21	266	57	8364	0.3	20	1.2	2.2	111	140	6
0912-26	32.2	4.7	846	0.8	0.0	7.3	0.2	3.4	4.2	1.3	15	6	74	28	132	35	442	94	8518	0.5	49	2.7	5.7	279	318	15
0912-27	32.2	6.0	1045	1.8	0.0	9.7	0.1	2.1	3.4	1.0	16	6	81	34	170	46	579	123	7833	0.9	60	3.4	6.9	319	398	19
0912-28	32.2	4.6	801	0.8	0.0	6.2	0.1	2.4	3.6	1.2	15	6	69	27	124	33	415	89	8006	0.5	42	2.3	5.0	243	276	13
0912-29	32.2	8.0	1117	1.8	0.1	9.0	0.1	2.5	3.8	1.1	17	7	89	37	178	48	594	123	7379	0.7	49	2.8	6.9	327	326	16
0912-30	32.2	10.2	822	0.7	0.4	6.2	0.3	2.6	4.1	1.3	17	6	73	28	131	34	423	90	7040	0.4	33	2.3	4.9	210	217	11
QL09-10																										
0910-01	32.2	1.6	1103	6.7	0.4	5.1	0.4	2.6	4.2	0.3	17	7	102	40	189	50	567	162	11725	3.5	374	23.3	7.6	193	1287	99
0910-02	32.2	18.1	1375	33	4.6	22	3.0	18	16	1.6	35	13	145	52	235	61	699	196	10578	4.6	317	21.8	10.4	203	1095	87
0910-03	32.2	3.1	838	4.5	0.1	4.5	0.1	1.2	3.5	0.3	17	6	77	30	143	36	422	122	10060	2.0	152	9.4	4.7	125	530	41
0910-04	32.2	4.6	1768	14	4.8	21	3.1	19	18	2.0	52	18	210	71	307	75	825	219	9668	2.1	285	19.7	14.3	324	985	81
0910-05	32.2	4.9	1772	12	10	33	5.7	33	24	3.0	52	19	215	72	313	78	877	237	10395	3.0	320	23.1	15.3	316	1100	90
0910-06	32.2	2.2	876	6.1	0.7	5.0	0.3	2.4	3.2	0.4	16	6	80	31	145	37	425	121	10283	2.3	229	14.4	7.0	186	796	62
0910-07	32.2	5.1	800	4.6	0.9	7.0	0.4	3.5	4.2	0.5	17	6	76	29	128	32	363	107	9828	1.7	152	9.4	5.8	156	521	42
0910-09	32.2	5.6	886	5.3	0.7	7.1	0.5	4.1	5.5	0.7	21	7	88	32	145	37	407	119	9102	1.6	129	8.3	5.5	137	446	36
0910-10	32.2	4.4	2629	17	5	26	3	21	20	2.4	64	24	284	101	432	107	1180	316	9873	3.0	469	31.9	31.3	771	1607	136

Appendix F. Zircon trace elements for Chapter 4, analysed in Beijing

Element	SiO_2	Ti	Y	Nb	La	Ce	Pr	Nd	Sm	Eu	Gd	Tb	Dy	Ho	Er	Tm	Yb	Lu	Hf	Ta	Pb	Pb	Pb	Th	U	Pb
	29	49	89	93	139	140	141	143	147	151	155	159	163	165	166	169	173	175	179	181	206	207	208	232	238	204
0910-11	32.2	35	1771	97	30	65	15	84	54	6.1	89	26	250	72	285	67	735	191	9984	6.6	205	23.6	18.2	171	857	64
0910-12	32.2	3.2	857	6.1	2.2	9.0	1.3	8.3	7.3	0.7	21	7	82	30	135	35	395	113	10257	1.7	146	9.7	5.0	112	524	40
0910-13	32.2	1.8	963	5.5	0.7	4.4	0.3	2.2	3.1	0.3	15	6	86	34	167	43	509	148	10328	2.8	230	14.4	5.3	134	786	61
0910-14	32.2	3.6	913	5.1	0.9	6.7	0.5	3.5	4.6	0.5	19	7	90	33	149	38	439	128	9691	2.0	195	12.3	7.3	191	682	54
0910-15	32.2	2.5	1165	6.8	0.3	5.8	0.2	2.5	3.9	0.6	20	8	105	42	200	52	598	171	10183	2.7	255	15.9	7.3	193	872	69
0910-16	32.2	2.4	1091	5.2	92	119	13	55	12	1.0	25	9	106	39	178	45	517	144	10734	2.0	221	14.6	9.0	188	754	61
0910-17	32.2	5.3	994	2.7	0.3	6.1	0.3	3.6	6.7	0.7	27	9	100	35	152	37	413	118	9062	1.0	129	7.9	6.7	175	461	36
0910-18	32.2	3.5	1289	7.7	16	29	3.5	17	11	1.1	33	12	140	49	211	53	560	159	10306	1.6	182	12.2	7.7	183	630	51
0910-19	32.2	4.6	1668	22	3.7	21	2.1	17	19	2.0	57	18	195	66	273	66	711	194	10507	4.2	310	20.5	25.1	655	1045	92
0910-20	32.2	2.9	993	4.3	1.9	8.9	0.8	5.1	5.4	0.5	23	8	96	36	162	40	461	128	10249	1.7	179	12.1	8.1	183	617	50
0910-21	32.2	1.6	1097	3.5	0.0	3.9	0.1	1.4	4.6	0.4	26	9	110	39	164	40	445	123	11029	1.6	245	15.1	6.9	190	844	66
0910-22	32.2	7.8	1575	39	7.0	23	3.7	22	15	1.6	40	14	164	60	271	70	804	223	10767	7.6	344	25.1	12.6	234	1193	95
0910-23	32.2	4.6	1994	18	6.5	33	4.8	27	23	2.5	54	20	236	80	352	88	1009	267	10647	4.3	449	32.9	22.0	436	1543	127
0910-24	32.2	4.2	811	1.8	0.0	5.0	0.2	2.9	5.9	0.8	23	8	86	30	124	30	317	89	8600	0.7	79	4.8	4.6	122	283	22
0910-25	32.2	6.8	1665	6.1	2.8	16	1.7	16	19	2.1	56	17	182	61	255	61	661	175	7955	1.7	162	10.5	16.3	409	572	50
0910-26	32.2	2.7	821	5.3	0.0	5.4	0.1	1.3	3.7	0.3	17	6	75	29	132	34	392	109	9923	1.9	183	11.3	6.5	176	632	50
0910-27	32.2	9.1	1076	16	3.1	10	1.7	11	10	1.2	28	10	109	38	161	42	466	128	9257	1.9	185	12.6	9.3	212	640	52
0910-28	32.2	26	1014	2.1	2.1	9.2	0.9	9.7	13	2.0	37	11	111	36	146	34	375	105	7723	0.7	90	6.5	9.2	219	314	28
0910-29	32.2	3.0	977	6.3	0.6	6.0	0.3	2.4	4.1	0.3	19	7	90	35	159	40	472	135	9740	2.5	201	12.6	6.6	172	686	55
0910-30	32.2	4.4	874	3.4	0.0	5.0	0.1	2.5	4.8	0.6	21	7	86	31	138	34	379	109	8908	1.2	124	7.6	5.3	142	433	34
0910-31	32.2	3.5	1285	12	2.2	11	1.4	8.0	7.2	0.7	24	10	129	49	229	61	723	195	10403	3.8	304	19.5	8.1	177	1038	82
0910-32	32.2	6.8	1345	27	9.2	21	3.8	24	19	2.1	46	15	157	52	223	54	592	160	9507	4.9	200	13.7	10.5	234	694	57
0910-33	32.2	3.9	447	2.0	0.0	3.0	0.1	0.8	1.9	0.2	10	3	42	16	72	18	210	61	10011	0.9	73	4.6	2.3	62	254	20
0910-34	32.2	3.1	1358	11	2.1	9.6	1.1	6.6	7.6	0.8	31	12	144	53	234	57	664	175	10256	1.8	252	15.9	9.4	230	906	69
0910-35	32.2	2.7	1273	10	1.1	8.2	0.8	5.6	6.0	0.6	23	9	125	48	224	59	683	187	10237	3.7	312	19.7	8.1	191	1073	84
0910-36	32.2	2.2	852	3.5	0.2	3.9	0.2	1.6	3.8	0.4	17	6	83	31	143	38	451	126	9605	1.4	176	10.6	5.1	131	613	47
0910-37	32.2	4.2	991	6.3	2.1	11	1.2	8.2	8.3	1.0	26	9	112	39	171	44	505	136	9441	1.7	163	11.2	7.7	161	565	46
QL09-14																										
0914-01	32.2	33	945	6	13	359	21	145	107	13	121	24	162	38	126	27	273	48	8438	0.7	48	10.3	10.8	83	285	20
0914-02	32.2	29	2153	24	95	917	76	432	193	26	189	38	295	83	333	80	896	164	13684	10.7	717	90.8	63.4	310	2714	227
0914-03	32.2	18	914	3	2	21	3	16	13	1	27	8	95	34	145	35	391	71	10105	1.8	163	12.0	7.3	138	575	46
0914-04	32.2	27	1198	11	2	32	3	22	20	2	47	13	137	45	186	43	465	84	8949	1.5	129	23.9	25.6	206	407	50
0914-05	32.2	29	2173	16	20	878	32	240	169	19	224	48	350	87	306	68	708	129	10372	5.9	247	53.2	54.8	447	877	101

Appendix F. Zircon trace elements for Chapter 4, analysed in Beijing

Element	SiO_2	Ti	Y	Nb	La	Ce	Pr	Nd	Sm	Eu	Gd	Tb	Dy	Ho	Er	Tm	Yb	Lu	Hf	Ta	Pb	Pb	Pb	Th	U	Pb
	29	49	89	93	139	140	141	143	147	151	155	159	163	165	166	169	173	175	179	181	206	207	208	232	238	204
0914-06	32.2	72	1456	15	15	237	21	138	99	9	122	28	211	56	216	50	543	100	9581	3.6	286	48.1	42.7	244	964	102
0914-07	32.2	11	2101	18	37	756	46	282	178	26	209	41	302	81	300	65	686	118	11154	5.4	497	133	141.3	1114	1568	225
0914-08	32.2	8	362	1	0.0	4.4	0.0	0.8	1.8	0.4	8.3	2.9	35	12	56	14	165	32	8089	0.5	37	2.2	2.5	65	135	11
0914-09	32.2	34	2766	44	53	692	63	395	240	24	261	55	405	108	426	107	1186	217	12068	14.3	653	189	184	240	2631	297
0914-10	32.2	6.0	1504	2.5	0.1	12.6	0.4	7.3	12.3	2.2	45.1	14	159	56	236	56	624	117	8912	1.1	123	7.5	11.9	314	432	38
0914-11	32.2	7.7	3010	7.1	3	29	2.9	34	43	8	134	39	388	114	411	84	816	133	7693	2.1	191	11.9	22.9	591	678	61
0914-12	32.2	17.9	960	5.5	2	411	2.1	12	10	1.4	25	8	96	35	153	38	436	84	9375	2.3	173	19.8	18.9	216	606	56
0914-13	32.2	5.8	1177	1.1	0.0	0.9	0.0	0.8	3.5	0.1	25	12	128	40	141	29	279	45	11089	0.8	229	17.6	4.8	59	383	62
0914-15	32.2	3.7	1722	13	21	368	32	204	123	16	130	25	203	61	256	61	703	126	11305	6.6	520	63	44	224	1857	163
0914-16	32.2	49.1	2822	43	76	1447	102	620	361	46	361	69	452	111	395	88	929	162	11802	12.9	554	145	136	445	2092	239
0914-17	32.2	10.5	1490	14	11	207	13	87	64	6.7	92	22	187	54	215	50	551	100	9734	4.2	318	34.6	27.5	295	1094	99
0914-18	32.2	3.8	1834	8.8	7.4	85	9	60	34	4.6	53	15	177	64	291	73	830	154	11166	4.4	634	51.3	26.1	312	2189	178
0914-19	32.2	27	3266	34	49	870	60	387	252	26	297	62	480	127	489	110	1157	208	11183	8.5	832	212	197	547	2722	353
0914-20	32.2	8.2	1017	6.9	2.5	41	6	39	34	3.5	55	14	123	37	150	35	402	75	10108	1.6	113	12.0	9.8	122	447	35
0914-21	32.2	51	3448	21	63	1024	82	513	360	48	417	84	566	133	457	102	1067	200	9993	6.3	404	60.4	79.3	1507	1475	153
0914-22	32.2	12.2	1334	3	4	100	7	50	40	5	64	16	150	47	196	47	536	105	9838	1.0	203	14.7	19.6	491	783	62
0914-23	32.2	15.7	1671	11	18	233	27	158	105	9	110	26	207	60	249	60	684	127	12346	5.9	471	42.7	23.0	232	1687	135
0914-24	32.2	23	1078	2.6	0.8	20	1.3	12	14	2	38	12	121	39	157	36	392	71	7477	0.7	89	10.5	11.4	158	306	30
0914-25	32.2	51.1	2227	12	14	126	18	111	85	13	129	33	284	83	328	72	771	135	9645	3.6	246	22.5	25.9	759	958	78
0914-26	32.2	7.6	1299	1.9	0.0	7.0	0.3	6.1	11.1	1.5	41.5	13	147	49	196	43	470	82	7983	0.8	84	5.2	8.2	217	311	26
0914-27	32.2	30	5771	39	48	1047	75	471	312	35	398	97	821	232	897	202	2126	377	7271	6.0	681	168	242	2622	2092	330
0914-29	32.2	4.1	2680	23	19	149	15	89	47	8	78	23	265	97	441	110	1264	238	13960	12.5	1171	207	171.7	492	4033	420
0914-30	32.2	4.7	2445	16	4.4	192	7.0	47	39	5.9	85	26	279	94	395	89	954	172	10462	4.5	447	35.4	44.5	909	1512	139
0914-31	32.2	15.1	1907	20	26	306	34	226	138	19	154	31	232	67	273	66	736	136	12903	10.5	579	66.6	44.2	301	2046	178
0914-32	32.2	30	2707	28	80	794	92	552	251	44	255	45	338	97	392	92	1012	193	11464	10.6	671	146	135	437	2690	266
0914-33	32.2	27	2801	23	32	422	41	248	167	17	206	48	394	111	432	102	1117	204	12021	7.5	763	138	122	683	2740	280
0914-34	32.2	5.4	1245	7.2	5.1	58.7	5.3	35	21.6	2.5	40	12	131	45	189	45	494	93	10125	3.1	266	31.2	26.0	264	901	85
0914-35	32.2	35	5901	46	117	1181	142	889	470	64.5	513	99	782	218	836	196	2061	363	9835	8.9	1244	434	443	1402	3776	633
0914-36	32.2	54	1109	13.0	7.7	113.6	11.0	76	64	8	80	19	151	42	163	38	412	77	10376	3.1	186	18.6	15.0	202	690	57
0914-37	32.2	47	1305	7.6	5.1	117.1	8.7	55.1	45	5	67	18	157	50	205	48	537	97	10545	2.2	183	18.8	15.7	173	658	57
0914-38	32.2	35	2529	26	85	854	91.1	550	307	34	311	57	381	93	339	75	775	139	11387	9.6	493	81.4	73.9	704	1959	176
0914-39	32.2	38	3505	39	118	1081	96	530	232	31	246	56	458	135	514	117	1270	223	10157	6.5	647	113.6	125	1565	2470	248
0914-40	32.2	50	2691	22	62	844	82	512	348	44	371	75	487	110	373	80	838	146	9825	3.6	262	59.5	62.1	619	1092	109

Appendix F. Zircon trace elements for Chapter 4, analysed in Beijing

Element	SiO_2	Ti	Y	Nb	La	Ce	Pr	Nd	Sm	Eu	Gd	Tb	Dy	Ho	Er	Tm	Yb	Lu	Hf	Ta	Pb	Pb	Pb	Th	U	Pb
	29	49	89	93	139	140	141	143	147	151	155	159	163	165	166	169	173	175	179	181	206	207	208	232	238	204
0914-42	32.2	13.0	1913	3.8	2.3	64.9	4.6	36	32	4	71	20	202	68	291	70	778	150	8373	1.2	273	17.6	26.7	691	946	84
0914-43	32.2	32.1	2750	21	34	837	52	329	245	25	279	61	424	106	385	89	935	172	12763	8.0	659	97.0	77.8	415	2181	222
QL09-15																										
0915-01	32.2	11.3	2459	2.6	0.1	2.5	0.2	4.2	9.6	0.8	54	22	274	102	442	105	1139	205	8498	1.2	191	15.1	12.0	147	312	56
0915-02	32.2	12.9	2742	2.8	0.1	4.3	0.4	7.4	17.1	1.1	79	28	325	117	489	112	1170	214	10364	1.3	283	22.0	23.2	322	486	85
0915-03	32.2	11.3	2791	2.0	0.0	2.5	0.3	5.4	13.1	0.9	65	26	325	118	505	117	1258	224	8053	0.8	146	11.2	14.0	176	251	45
0915-04	32.2	8.7	1743	1.7	0.0	3.1	0.3	5.3	10.5	0.8	49	16	194	73	320	77	843	159	8706	0.8	220	16.9	16.5	213	373	65
0915-05	32.2	8.6	1385	2.5	1.3	6.2	0.6	7.5	16.6	0.9	74	21	188	51	180	39	410	72	10780	1.2	388	30.2	19.6	239	653	111
0915-06	32.2	5.4	1302	2.7	0.0	2.2	0.1	1.4	4.3	0.2	26	10	128	48	218	52	589	111	10266	1.3	197	15.1	9.0	109	325	55
0915-07	32.2	2.4	956	1.6	0.0	1.9	0.0	0.8	3.3	0.1	19	7	97	37	160	40	453	84	11296	1.1	168	12.8	6.8	86	283	47
0915-08	32.2	8.3	2851	2.1	0.0	3.4	0.3	7.2	15.9	1.0	78	29	346	122	501	113	1192	211	9159	0.9	215	16.6	18.7	234	361	65
0915-09	32.2	7.3	4223	9.6	2.3	15.6	2.3	18.3	21.0	2.0	96	39	483	168	680	150	1539	265	11770	5.3	1315	105	59.1	781	2417	371
0915-10	32.2	23	3665	8.1	0.4	12.8	0.7	11.5	23	1.5	105	38	434	152	623	142	1516	267	8780	2.2	617	48.3	59.7	792	1019	191
0915-11	32.2	133	2120	6.0	0.2	3.9	0.1	2.0	5.8	0.3	40	17	224	86	376	90	983	188	12061	3.2	655	51.0	27.4	347	986	183
0915-12	32.2	7.7	1288	2.0	0.0	1.9	0.1	2.2	6.5	0.4	35	12	139	48	198	45	491	89	9706	0.9	197	15.1	9.5	113	324	56
0915-13	32.2	5.4	1921	1.8	0.1	3.4	0.4	5.9	14.5	0.8	70	23	240	79	309	71	744	130	10196	0.9	297	23.5	19.5	230	500	87
0915-14	32.2	5.1	715	0.8	11	10.6	1.3	5.6	4.4	0.3	23	8	84	26	99	22	228	40	10860	0.5	124	9.4	4.2	51	207	34
0915-15	32.2	6.6	584	3.2	0.1	4.7	0.1	1.0	1.7	0.5	8	4	50	19	95	26	332	67	11215	3.5	1425	301	30.7	123	772	426
0915-16	32.2	9.6	1369	1.9	0.0	10.7	0.1	1.2	3.4	0.8	21	8	113	48	229	60	719	143	8447	0.9	220	23.7	17.7	127	207	68
0915-17	32.2	7.2	1779	2.3	0.1	1.9	0.1	2.1	7.3	0.3	41	15	189	67	282	64	689	127	9881	1.1	200	15.3	9.1	115	340	56
0915-18	32.2	3.9	862	1.8	0.0	1.6	0.1	1.7	5.4	0.3	31	10	103	31	112	24	252	44	10651	1.1	246	18.8	8.2	101	424	68
0915-19	32.2	4.0	2066	2.8	0.9	8.2	1.1	10.5	15.6	1.1	62	22	243	85	345	76	794	146	10515	1.5	314	25.9	19.6	376	539	92
0915-20	32.2	9.9	786	1.3	1.1	3.2	0.3	3.4	7.6	0.5	37	11	101	28	98	21	209	35	11289	0.7	230	17.8	7.6	96	382	63
0915-21	32.2	4.9	1389	1.7	0.0	2.2	0.1	2.0	5.5	0.3	31	12	149	54	231	56	630	113	10617	1.0	194	14.8	9.7	118	335	55
0915-22	32.2	5.7	1419	2.7	0.1	2.3	0.1	2.6	6.8	0.4	37	15	164	52	189	39	398	66	9949	1.3	265	20.3	10.0	127	450	74
0915-23	32.2	4.4	1396	1.2	0.0	1.5	0.1	2.1	6.3	0.4	34	13	153	52	212	50	522	95	10165	0.7	173	13.0	7.5	95	294	48
0915-24	32.2	6.7	2192	3.9	0.7	9.1	0.8	7.8	13.2	1.1	58	21	242	89	373	87	927	172	9636	1.4	435	35.3	37.4	487	662	132
0915-25	32.2	1.4	2196	2.4	0.1	3.1	0.2	3.0	8.3	0.4	52	21	252	88	365	84	892	157	11768	1.6	530	41.0	17.0	208	849	146
0915-26	32.2	622	3076	6.1	1.3	10.7	0.8	7.9	13.9	1.7	70	28	336	125	536	122	1322	242	10547	2.3	568	50.3	34.2	347	941	166
0915-27	32.2	6.7	2187	2.4	0.1	2.2	0.2	2.5	5.9	0.5	40	17	228	84	368	86	968	176	10689	1.4	282	22.1	9.0	106	475	78
0915-28	32.2	14.3	1410	2.5	0.1	2.4	0.1	1.5	4.1	0.3	26	11	138	53	237	57	632	118	9832	1.1	176	13.6	9.6	115	297	50
0915-29	32.2	3.4	1447	1.6	0.0	1.7	0.2	3.3	9.0	0.5	44	16	174	55	209	46	478	82	11224	0.9	296	22.9	10.5	129	500	82
0915-30	32.2	28	1515	3.7	21	40.7	4.6	25	14.0	3.3	43	17	179	56	219	51	555	98	10468	2.0	406	47.4	27.6	201	467	123

Appendix F. Zircon trace elements for Chapter 4, analysed in Beijing

Element	SiO_2	Ti	Y	Nb	La	Ce	Pr	Nd	Sm	Eu	Gd	Tb	Dy	Ho	Er	Tm	Yb	Lu	Hf	Ta	Pb	Pb	Pb	Th	U	Pb
	29	49	89	93	139	140	141	143	147	151	155	159	163	165	166	169	173	175	179	181	206	207	208	232	238	204
QL09-18																										
0918-01	32.2	4.8	1973	8.9	1.6	27.3	0.6	5.8	6.4	0.8	35	14	182	75	360	93	1116	229	10732	3.0	207	13.0	15.6	390	660	61
0918-02	32.2	5.2	1318	3.1	0.1	10.9	0.1	2.2	5.2	1.1	26	9	121	47	225	59	714	146	8261	1.2	103	6.7	8.0	184	324	31
0918-03	32.2	6.8	1010	2.4	7.7	23.4	2.1	12.3	5.9	0.9	20	7	95	38	176	44	521	104	8345	0.9	63	4.0	4.2	101	198	18
0918-04	32.2	5.6	3638	7.1	0.1	33.1	0.6	10.4	20.1	3.0	93	33	392	144	624	153	1720	324	8010	2.1	215	13.7	23.2	569	696	67
0918-05	32.2	2.7	1360	2.9	0.0	11.3	0.1	1.6	4.0	0.6	24	9	123	50	235	59	705	143	9953	1.3	102	6.4	7.0	161	325	30
0918-06	32.2	5.9	607	1.7	19	43.6	5.6	29	7.5	0.6	15	5	56	22	101	26	320	66	8448	0.8	43	2.7	2.5	58	136	12
0918-07	32.2	3.1	1710	7.7	5.9	29.8	1.8	9.3	6.2	0.6	27	11	147	61	290	78	945	195	9564	2.4	174	11.0	11.6	276	558	50
0918-08	32.2	5.7	953	2.4	0.1	8.2	0.1	1.2	3.3	0.7	17	6	83	34	157	41	505	103	8327	1.0	50	3.3	3.3	76	161	14
0918-09	32.2	3.4	1685	2.3	0.0	13.1	0.1	3.2	7.9	1.2	38	14	169	65	288	72	836	161	9310	1.0	87	5.4	7.0	169	281	26
0918-10	32.2	3.0	1268	6.4	0.1	14.8	0.1	0.9	2.9	0.3	18	7	104	45	220	59	740	153	9867	2.4	131	8.3	8.0	181	425	37
0918-11	32.2	4.1	1738	3.3	0.4	16.6	0.3	3.5	7.2	1.0	36	13	169	66	292	74	867	170	9978	1.3	115	7.1	9.1	215	376	34
0918-12	32.2	4.6	1689	8.3	0.0	24.3	0.1	2.1	4.7	0.6	28	11	151	61	286	74	879	175	9635	2.7	169	10.6	12.6	293	553	50
0918-13	32.2	3.2	1528	4.3	0.5	15.1	0.2	2.5	4.8	0.7	27	10	137	55	264	69	832	167	9320	1.6	144	9.0	10.1	235	469	42
0918-14	32.2	2.6	1667	2.9	0.1	14.8	0.1	2.3	6.0	0.7	32	12	155	61	285	71	846	167	10136	1.4	123	7.8	9.3	217	400	36
0918-15	32.2	3.7	1779	4.7	0.2	17.8	0.3	3.8	7.0	1.0	36	13	168	66	305	78	932	181	9679	1.7	121	7.8	9.4	224	403	36
0918-16	32.2	5.1	1110	4.7	0.0	10.7	0.0	1.0	2.7	0.5	16	7	87	37	184	50	631	127	8318	1.6	72	4.5	3.8	86	234	20
0918-17	32.2	4.9	1173	1.8	0.0	8.6	0.1	2.1	5.1	0.9	24	9	109	43	195	51	587	117	8647	0.9	64	4.1	4.8	110	200	19
0918-18	32.2	3.6	1469	3.3	0.2	14.3	0.3	3.6	5.7	0.7	25	10	127	51	242	63	764	150	9582	1.4	103	6.4	7.2	166	340	30
0918-19	32.2	10.5	1813	8.6	1.6	26.4	0.5	4.1	5.3	0.7	29	12	159	67	315	82	984	196	9832	2.6	164	10.3	12.1	288	535	48
0918-20	32.2	4.9	1329	2.4	0.4	10.6	0.2	2.5	4.8	0.9	26	10	124	48	222	59	683	135	9335	1.0	73	4.5	4.8	115	236	21
0918-21	32.2	4.4	975	4.4	0.1	12.4	0.1	1.9	2.9	0.4	16	6	83	34	163	44	526	107	9742	1.7	81	5.1	4.7	113	264	23
0918-22	32.2	3.2	958	4.4	0.0	12.5	0.0	0.8	2.3	0.4	14	6	82	34	165	43	533	109	9445	1.8	98	6.2	6.4	147	320	28
0918-23	32.2	3.1	1056	3.4	0.1	11.8	0.1	1.4	2.5	0.3	14	6	80	35	183	50	574	149	14711	2.7	183	12.0	6.5	187	583	50
0918-24	32.2	6.4	1189	4.5	0.2	11.7	0.1	1.4	3.0	0.6	18	7	101	42	207	54	673	135	8188	1.4	93	5.8	6.2	139	296	27
0918-25	32.2	6.0	876	2.8	4.3	14.7	1.1	5.8	3.7	0.5	16	6	79	32	148	39	458	92	9152	1.3	80	21.5	23.5	85	192	37
0918-26	32.2	5.4	968	2.9	0.0	8.5	0.1	0.9	3.1	0.7	16	6	85	35	167	44	550	113	8817	1.1	52	3.3	2.9	69	172	15
0918-27	32.2	4.1	1550	8.7	0.1	21.4	0.1	1.4	4.3	0.5	24	10	134	56	268	71	857	173	9798	3.1	168	10.8	11.8	272	545	49
0918-28	32.2	5.4	1307	4.4	0.0	12.5	0.1	1.8	3.9	0.7	21	9	116	47	220	57	702	138	8791	1.5	88	5.5	6.0	136	287	26
0918-29	32.2	5.9	718	2.0	0.0	6.6	0.0	0.8	2.1	0.5	13	5	61	26	123	32	385	80	7968	0.8	36	2.2	2.4	53	119	10
0918-30	32.2	4.6	590	1.8	0.0	6.5	0.0	0.7	1.8	0.4	10	4	55	21	104	27	336	65	8404	0.8	46	2.7	2.8	66	150	13
0918-31	32.2	6.3	1037	3.8	0.2	10.3	0.1	1.6	3.0	0.6	17	7	91	37	182	49	585	119	8361	1.4	61	3.8	3.3	82	201	17
0918-32	32.2	6.5	884	2.1	0.1	7.7	0.1	1.2	3.0	0.8	17	6	81	33	153	38	447	86	8146	0.8	46	2.8	3.4	82	147	13

Appendix F. Zircon trace elements for Chapter 4, analysed in Beijing

Element	SiO_2	Ti	Y	Nb	La	Ce	Pr	Nd	Sm	Eu	Gd	Tb	Dy	Ho	Er	Tm	Yb	Lu	Hf	Ta	Pb	Pb	Pb	Th	U	Pb
	29	49	89	93	139	140	141	143	147	151	155	159	163	165	166	169	173	175	179	181	206	207	208	232	238	204
0918-33	32.2	5.1	964	1.5	0.0	7.0	0.1	1.8	3.7	0.9	19	7	89	35	160	40	468	93	7810	0.6	38	2.4	2.8	66	126	11
0918-34	32.2	4.5	1832	5.6	0.1	18.3	0.1	2.6	7.1	0.9	35	14	172	70	327	82	991	194	9899	2.0	135	8.5	9.9	236	436	39
0918-35	32.2	3.8	1384	7.0	2.3	21.1	0.7	4.2	3.9	0.6	20	8	118	50	245	64	777	160	9702	2.2	112	7.3	7.0	161	363	32
0918-36	32.2	15.1	1701	9.0	5.8	31.6	1.7	9.4	6.0	0.7	28	11	147	63	306	81	990	203	9401	2.7	157	9.7	10.2	241	505	45
0918-37	32.2	3.2	1435	6.7	0.8	23.1	0.3	2.4	4.6	0.6	25	10	133	54	254	65	788	159	9375	2.6	209	13.4	15.3	374	673	61
0918-38	32.2	5.6	1107	2.1	0.1	8.4	0.1	2.1	4.3	1.1	23	8	106	41	183	46	539	108	8275	0.8	46	2.9	4.0	95	149	14
0918-39	32.2	4.3	1262	4.5	0.2	17.0	0.2	1.7	4.0	0.6	21	9	116	45	212	55	634	126	9816	1.7	116	7.3	8.4	200	375	34
0918-40	32.2	5.4	1153	2.9	1.9	14.0	0.6	4.5	4.3	0.8	22	8	101	41	193	50	590	120	7868	1.0	58	3.6	3.9	90	190	17
QL10-34																										
1034-01	32.2	8.33	3457	6.22	2.11	22.1	1.88	18.4	26.7	1.6	106	35	395	137	568	126	1335	238	8019.73	2.59	388.9	25.63	43.05	1094	1334	121.9
1034-02	32.2	13.1	2816	8.52	5.78	28.8	3.39	23.5	24.4	1.4	83.8	28	316	108	454	103	1135	216	10399.9	5.81	550.8	36.33	48.19	1236	1872	166.1
1034-03	32.2	10.8	1540	4.33	3.25	12.91	1.76	13.5	10.7	0.9	32.3	11	135	52.8	241	57.6	647.2	127	8852.38	2.66	287.5	18.95	15.78	374.7	958.1	81.78
1034-04	32.2	8.76	2228	9.97	35.3	94.73	14.5	72.1	32.2	2.2	65.9	21	231	81.2	353	82.4	900.6	175	11587.7	7.14	613.4	42.03	53.37	1451	2014	185.2
1034-05	32.2	9.7	1809	6.26	0.97	12.85	0.75	7.13	9.44	0.8	38.9	15	179	64.9	279	65.6	696.2	131	8394.55	2.62	373.3	24.19	44.91	1113	1220	118.8
1034-06	32.2	15.9	1780	6.81	13.6	58.05	9.09	65.3	39.2	3.8	71	17	187	64.8	271	64.3	706.1	129	8663.14	3	294	20.7	27.77	714	1048	90.02
1034-07	32.2	12.5	1271	3.49	15.4	34.06	8.02	44	18.5	1.2	38	11	125	43.9	197	45.4	470.7	90	7779.21	1.44	218.8	14.87	23.66	531.2	716.9	68.4
1034-08	32.2	11.3	1696	6.67	9.75	31.83	5.32	33.9	20.8	1.8	51.4	15	175	62.9	258	58.1	618.2	115	8126.25	2.56	353.9	23.47	43.48	1099	1148	113.3
1034-09	32.2	9.45	1572	5.51	0.19	9.11	0.21	2.58	6.29	0.5	31.4	13	156	56.6	250	58.7	664	116	8562.03	2.23	247.5	16.02	23.41	585.7	878	75.45
1034-10	32.2	11.5	1994	7.91	0.33	13.89	0.32	5.2	9.46	0.7	47.2	18	207	76.2	316	69.7	754.5	139	7907.72	2.81	370.4	23.31	48.62	1243	1271	119.9
1034-11	32.2	19	1982	4.86	4.98	18.88	2.95	23.2	22.5	1.8	53	17	192	70.5	305	68.9	748.2	144	8034.62	1.88	237.5	16.02	24.31	571	816.1	73.52
1034-12	32.2	10.9	2221	7.08	6.05	23.15	2.67	20.7	18.7	2.1	58.5	19	226	82.6	352	78.7	859.5	160	7839.09	2.53	324.2	23.97	38.59	923.7	1101	103.7
1034-13	32.2	13.8	2327	9.09	8.99	37.86	4.71	31.7	20.3	1.8	63.7	20	235	84.1	347	79.4	850.5	163	8431.58	3.65	420.2	27.93	53.98	1360	1370	135.7
1034-14	32.2	4.53	742.4	2.3	4.85	23.7	2.91	15.6	9.29	0.7	18	5.8	68.1	25.3	115	29.8	366.3	74	12271.3	3.09	312.7	20.65	7.2	200.7	1052	83.69
1034-15	32.2	20.1	1910	3.37	3.67	14.61	2.36	19.8	18.9	1.5	57.3	18	198	70.6	297	68.2	751.2	134	7842.6	1.44	198.2	13.63	19.99	526.1	763.8	61.25
1034-16	32.2	15.6	1945	4.54	3.36	13.65	1.74	15.1	16.9	1.4	55.2	18	209	71.2	300	69.5	727.2	133	7584.87	1.87	268.4	17.4	32.49	898.3	967.8	85.56
1034-17	32.2	16.4	2327	5.72	4	18.44	2.34	20.7	19	2.4	62.9	20	240	86.1	367	84	892.6	168	7546.24	2.03	263	17.78	26.58	597.9	859.5	81.24
1034-18	32.2	11.9	1054	3.27	0.63	6.44	0.42	3.68	5.4	0.5	23	8.2	102	37.8	166	39.5	435.2	82	8103.6	1.48	174.1	11.8	16.94	427.4	642.8	53.44
1034-19	32.2	13.8	2092	5.18	3.17	13.26	1.41	10.9	12.7	1.5	53.3	19	219	76.3	320	73.2	774.3	143	7810.84	2.13	291.6	18.53	35.23	879	1039	92.83
1034-20	32.2	8.65	1917	7.9	1.9	16.5	1.04	8.4	10.9	0.6	47.1	16	199	69.8	298	68.7	747.8	135	8206.3	3.54	436.5	28.14	52.56	1412	1568	138.9
1034-21	32.2	10.4	1966	6.76	0.08	10.55	0.2	3.75	8.96	0.7	42.8	16	196	71.4	302	70.6	748.1	140	7921.18	2.52	311.8	21.17	34.8	886.1	1091	98.06
1034-22	32.2	13.7	2486	11.4	12.5	61.91	8.39	53.5	36.8	2.9	80.2	22	250	87.4	376	85	924.5	170	10232.2	5.71	589.2	40.6	66.49	1827	2122	185.9
1034-23	32.2	165	1868	9.23	179	232.8	51.6	210	71.6	6.8	98	22	213	67.1	262	57.8	602.4	114	8568.19	4.03	453.6	127.4	147.9	1273	1268	216.4
1034-24	32.2	22.9	3064	4.4	9.21	26.91	4.58	36.4	33.1	2.5	103	32	351	117	484	109	1117	203	8217.58	1.87	284.8	23.87	36.15	836.4	1044	92.94

Appendix F. Zircon trace elements for Chapter 4, analysed in Beijing

Element	SiO_2	Ti	Y	Nb	La	Ce	Pr	Nd	Sm	Eu	Gd	Tb	Dy	Ho	Er	Tm	Yb	Lu	Hf	Ta	Pb	Pb	Pb	Th	U	Pb
	29	49	89	93	139	140	141	143	147	151	155	159	163	165	166	169	173	175	179	181	206	207	208	232	238	204
1034-25	32.2	16.8	1996	3.78	8.8	29.68	4.88	33.5	21	2.1	56.7	17	198	68.3	290	67.1	719.4	####	7957.78	1.82	209.8	15.02	20.89	516.7	741.5	64.91
1034-26	32.2	9.96	1963	2.8	0.33	5.48	0.47	6.58	12.1	1.1	52.3	18	207	72.2	292	68.2	717.2	####	7656.77	1.23	173.1	11.19	16.09	410.6	599.4	52.61
1034-27	32.2	11.5	2241	2.77	30.6	96.84	17.1	118	62.1	6.1	107	26	259	84.1	337	76	802.5	####	8394.96	1.96	236	18.31	20.43	477.8	902.1	71.7
1034-28	32.2	11.6	1316	4.27	9.17	26.59	4.29	27.3	18.8	1.6	45	12	133	46.3	201	48.7	537	####	11144.7	3.85	337.1	21.76	17.17	856.3	1169	95.04
1034-29	32.2	4.12	2872	5.12	0.21	14.81	0.6	10.2	18.4	1.1	81	28	326	111	471	106	1101	####	9917.54	2.36	359.8	22.22	36.52	962.5	1241	110.8
1034-30	32.2	13.3	2543	3.27	15.8	51.6	9.09	53.2	36.4	2.6	89.5	27	289	96.9	402	91	942.8	####	8257.58	1.75	256.8	19.54	28.4	742	887.3	81.14
QL10-27																										
1037-01	32.2	11.6	784	1.39	0.03	10.22	0.06	1.21	2.71	0.3	16	6	75	28.4	125	29.7	321.9	62	9975.88	0.81	163.9	20.09	14.54	96.6	138.4	51.55
1037-02	32.2	12.3	1052	1.3	0.05	6.39	0.17	3.4	6.7	0.9	29.7	9.9	112	39.2	163	37.7	396.4	77	9284.51	0.69	67.99	4.17	4.55	120.9	243.7	19.69
1037-03	32.2	44.2	1385	7.04	10.2	122.5	5.95	38.8	27.4	5	65.2	19	177	50	192	45.6	513.8	103	10616.1	1.69	486.2	77.95	43.55	152.8	724.2	157.7
1037-04	32.2	29.3	1398	4.74	17.7	37.65	4.26	22.2	13.4	2.7	42.8	16	160	51.6	213	54.5	648.2	130	11347.7	3.43	530.5	63.78	17.54	111.3	798.7	151.3
1037-05	32.2	15.3	421	1.1	0.06	1.104	0.09	1.78	3.69	0.1	13.6	5	49.9	14.8	52.5	10.9	99.82	16	11938.6	0.51	305.8	33.19	6.81	51.74	327.8	84.61
1037-06	32.2	4.79	738.6	2.39	0.86	15.62	0.66	4.09	2.94	0.9	11.2	4.7	64.9	26.1	129	36	445.7	89	14067.9	2.54	235.7	17.51	6.51	84.26	826.1	64.14
1037-07	32.2	10.3	1514	2.43	0.13	12.29	0.25	4.46	9.55	1.6	42.2	14	165	57.1	235	53.7	576.9	106	8804.55	1.12	94	5.91	8.5	221.5	336.8	28.41
1037-08	32.2	13.6	2279	2.3	0.09	19.04	0.37	5.95	11.2	2.8	56.1	19	232	85.9	368	82.8	888	168	8036.75	0.95	388.6	47.63	50.91	322.7	319.1	130.8
1037-09	32.2	3.63	974.1	4.3	0.1	5.58	0.06	1.2	3.15	0.2	18.2	7	92.6	35.6	157	39.1	451.6	85	10071.1	2.7	212.7	13.01	8.16	215.8	765.1	58.41
1037-10	32.2	13.2	552.9	1.61	0.06	10.11	0.07	1.94	3.92	0.3	15.8	5.4	60.5	20.4	84.5	19.6	209.5	39	9680.12	0.59	498.7	93.99	57.95	266.5	272.9	171.3
1037-11	32.2	10.1	927	3.45	0.06	20.67	0.05	0.75	2.79	0.3	14.3	6.2	82.9	33.4	154	39.2	454.3	87	10128.2	1.83	201.1	21.18	19.13	140.6	193.1	63.17
1037-12	32.2	19.2	965.8	2	0.08	4.86	0.11	1.85	4.65	0.3	22.3	8.1	98.6	35.6	151	34.8	370.9	70	9827.33	0.89	121.1	14.43	14.59	95.18	100.9	40.01
1037-13	32.2	10.8	1662	2.57	0.03	4.34	0.43	7.34	12.3	1	53.8	18	195	67.1	268	60.1	632.6	112	7845.98	0.95	116.1	7.2	9.18	239.6	418	34.39
1037-14	32.2	5.92	902.6	3.38	1.24	12.83	0.64	5.15	5.76	0.9	21.7	7.6	92.9	32.8	138	33.3	368.2	69	9362.16	1.68	107.8	7.37	6.22	152.7	387.3	30.9
1037-15	32.2	3.87	869.7	4.19	0.12	13.81	0.07	1.29	3.23	0.7	18.2	6.7	84.2	31.5	143	34.6	393.3	73	9223.15	1.95	128.4	15.33	12.47	83.47	109.5	40.88
1037-16	32.2	19.8	701.2	2.7	0.06	9.03	0.09	1.61	3.23	0.9	15.5	5.7	68.6	25.2	118	32	386.1	77	10144.3	1.66	135.1	9.89	6.33	68.79	313	38.07
1037-17	32.2	15.7	611.2	3.02	0.03	12.93	0.04	1.08	2.22	0.2	11.8	4.6	57	21.4	94.9	23.1	257.2	48	9282.41	1.52	282.7	34.89	20.16	123.5	223.5	86.41
1037-18	32.2	12.7	1196	2.71	6.38	42.47	3.81	21.9	14	2.2	34	11	121	42.2	182	44.5	494.6	92	10440	1.46	302.3	45.92	26.82	114.6	335.4	97.18
1037-19	32.2	3.37	900.5	3.69	0.11	7.66	0.09	1.01	2.9	0.3	16.4	6.4	82.9	32.5	145	35.6	406.8	76	10678.6	2.61	188.7	11.84	7.11	199.9	675	51.84
1037-20	32.2	5.39	1333	2.45	0.02	6.45	0.08	2.14	6.41	0.5	32.5	12	145	52.1	222	53	581	104	10485.2	1.55	167.9	10.37	8.14	205.3	600.7	47.02
1037-21	32.2	6.25	869.5	2.72	0.02	9.35	0.05	1.34	3.52	0.6	17.5	6.9	83.7	31.3	140	34.1	384.4	72	9310.24	1.77	90.63	5.56	4.47	115.7	325.3	25.41
1037-22	32.2	12.4	1749	0.84	0.05	0.888	0.07	1.62	5.46	0.1	32	13	172	65.5	285	69.1	748.4	138	10195.6	0.62	292.6	32.76	10.42	70.12	254.5	83.23
1037-23	32.2	2	913.1	2.6	0.05	1.45	0.02	0.54	1.57	0.1	12.1	5.7	80.6	33.4	165	48	622	125	12832.7	2.61	392.7	24.64	3.69	89.18	1367	102
1037-24	32.2	2.43	1044	4.46	0.48	8.9	0.36	2.53	4.05	0.4	19.2	7.8	97.5	36.4	168	42.9	478.9	92	10388.3	3.16	296	18.5	11.69	294.9	950	81.56
1037-25	32.2	23.5	442.1	1.9	0.05	5.27	0.06	1.08	1.78	0.1	9.65	3.4	43.5	15.5	69.4	16.6	185.1	35	9205.7	0.67	36.04	4.34	6.48	42.41	29.32	13.04
1037-26	32.2	15.1	1062	4.62	2.75	34.28	1.73	13	11.7	1.5	34.4	11	116	38.8	154	36	369.7	68	9902.99	1.95	472.4	71.48	33.61	191.4	374.3	147.4

Appendix F. Zircon trace elements for Chapter 4, analysed in Beijing

Element	SiO_2	Ti	Y	Nb	La	Ce	Pr	Nd	Sm	Eu	Gd	Tb	Dy	Ho	Er	Tm	Yb	Lu	Hf	Ta	Pb	Pb	Pb	Th	U	Pb
	29	49	89	93	139	140	141	143	147	151	155	159	163	165	166	169	173	175	179	181	206	207	208	232	238	204
1037-27	32.2	2.48	1266	4.93	4.29	22.4	2.49	15.8	10.3	0.6	32	11	128	45.9	198	47.4	520.4	98	10222.4	3.16	287.6	19.14	14.43	343	932.2	81.1
1037-28	32.2	4.13	1182	4.77	0.29	6.5	0.19	2.03	3.97	0.4	21.6	8.5	110	42	191	47.3	536.9	101	10277.8	3.14	236.5	14.73	8.08	203.5	792.1	64.49
1037-29	32.2	3.38	1660	7.82	0.38	15.23	0.34	3.17	5.34	0.5	30.7	13	165	61.5	280	68	733.3	140	10724.1	4.68	329.6	20.74	14.11	348.5	1080	91.45
1037-30	32.2	4.00	839.2	4.99	1.17	20.85	0.83	5.53	5.69	1	18.7	7	81.1	30	132	32.7	364.2	71	10075.9	3.05	152.2	11.23	7.4	160.9	549.4	43.06

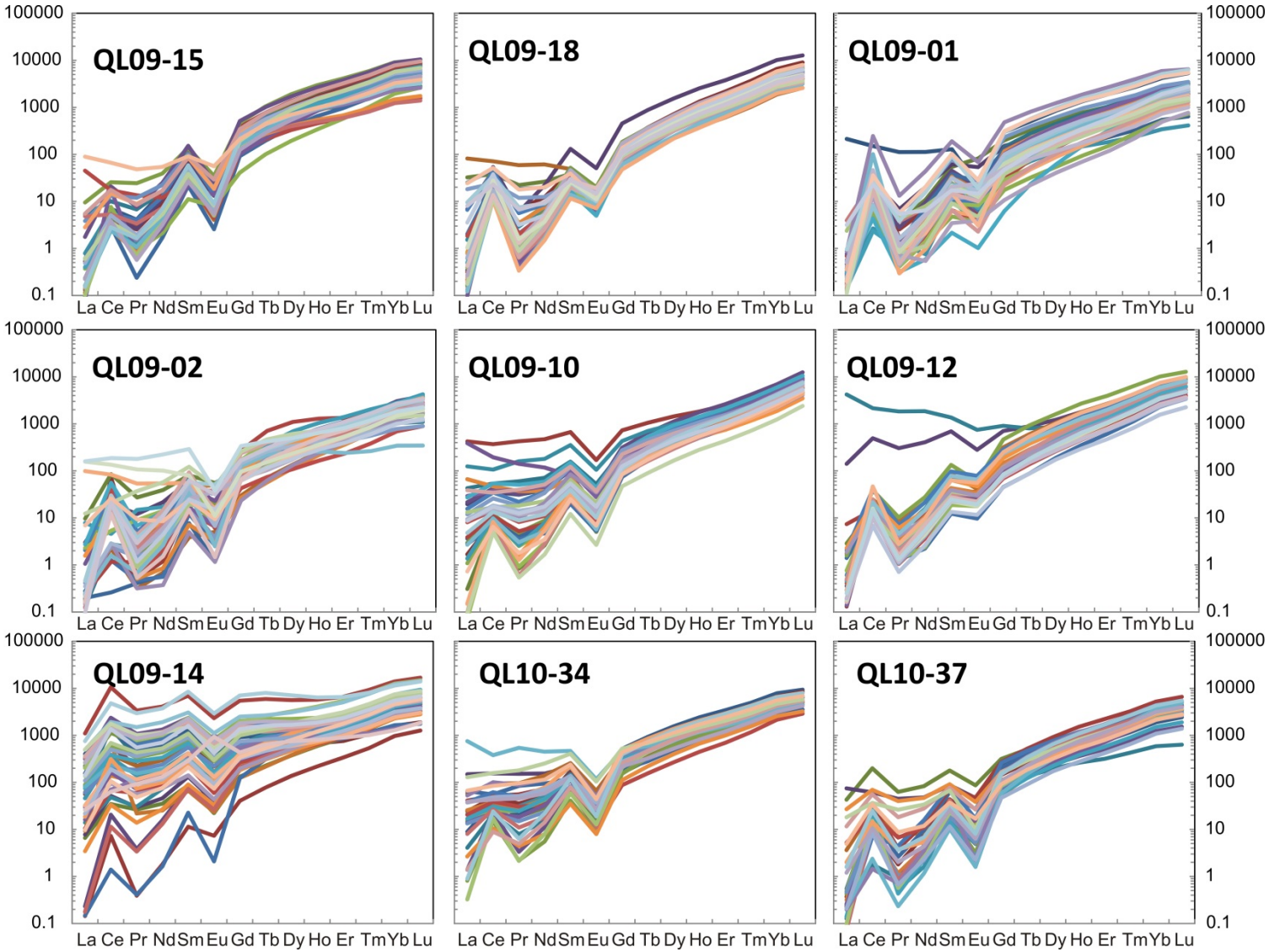
QL09-15
QL09-18
QL09-01
QL09-02
QL09-10
QL09-12
QL09-14
QL10-34
QL10-37
100000
10000
1000
100
10
1
0.1
La Ce Pr Nd Sm Eu Gd Tb Dy Ho Er Tm Yb Lu

Appendix G. Zircon trace elements for Chapter 5, analysed in Beijing

Element	SiO_2	Ti	Y	Nb	La	Ce	Pr	Nd	Sm	Eu	Gd	Tb	Dy	Ho	Er	Tm	Yb	Lu	Hf	Ta	Pb	Pb	Pb	Th	U	Pb
	29	49	89	93	139	140	141	143	147	151	155	159	163	165	166	169	173	175	179	181	206	207	208	232	238	204
QL09-04																										
0904-01	32.2	10.4	663	0.9	0.1	5.7	0.2	4.0	6.3	1.4	22	7	72	24	94	21	219	41	8384	0.5	28	2.6	3.8	67	92	9
0904-02	32.2	63	2808	11	1.9	44.9	1.2	17.8	24	2.8	98	32	337	110	443	101	1012	174	7197	3.7	175	11.8	24.1	500	575	57
0904-03	32.2	34.1	5343	11	0.8	80.5	3.9	61	80	13	277	81	799	217	723	138	1224	175	6123	2.9	133	9.1	25.8	526	368	47
0904-04	32.2	8.8	1745	4.3	0.5	30.2	0.7	12.6	17.8	1.9	71	21	218	65	242	48	447	69	8147	1.4	86	5.6	13.0	264	237	29
0904-05	32.2	14.6	2677	4.7	0.2	31.5	0.9	15.8	25	4.9	96	31	328	107	404	89	836	149	9662	1.9	76	5.6	13.8	326	231	27
0904-06	32.2	3.2	1700	2.2	0.1	13.1	0.5	9.7	14.6	3.6	60	18	202	65	249	55	546	93	7642	0.8	44	3.1	6.4	130	129	15
0904-07	32.2	37	5004	12	1.2	100	4.5	63	78	15	261	76	725	202	660	129	1107	160	6372	3.2	188	12.3	38.7	790	519	68
0904-08	32.2	50	6369	14	1.0	109	5.4	79	106	20	348	98	937	258	861	168	1484	213	6781	3.2	186	12.1	40.8	821	512	69
0904-09	32.2	15.5	2556	3.8	0.6	25.5	0.9	19.5	30.4	6.6	110	33	337	104	381	80	814	142	8002	1.1	63	4.4	15.6	346	201	24
0904-10	32.2	7.3	713	0.7	0.1	8.0	0.1	1.7	3.0	1.7	14	5	63	24	112	30	360	76	7204	0.3	27	1.6	1.6	45	101	8
0904-11	32.2	3.6	237	0.5	0.0	2.0	0.0	0.5	0.9	0.3	4.8	1.8	22.3	8.2	37	9.1	104	22	8258	0.3	20	1.5	1.5	28	70	6
0904-12	32.2	10.6	4154	5.4	0.3	41.1	1.6	30	45	8.4	172	53	542	165	600	124	1154	178	6694	2.1	100	6.7	17.7	361	273	35
0904-13	32.2	22	5435	8.1	0.3	62.4	3.0	51	71.2	16	247	72	718	217	796	163	1547	256	7324	2.1	104	7.2	29.5	611	287	42
0904-14	32.2	13.9	2521	3.9	0.2	25.7	0.9	16.1	24	4.6	94	29	303	96	364	79	802	137	8181	1.4	62	4.1	12.0	247	178	22
0904-15	32.2	3.1	1165	2.6	0.0	16.2	0.3	4.3	7.8	1.0	32	11	125	42	174	40	412	71	8185	1.3	52	3.3	6.3	122	148	16
0904-16	32.2	12.6	2756	5.2	0.2	29.3	0.9	15.7	26	4.5	98	31	337	108	423	92	921	161	8193	3.7	82	5.8	14.5	291	235	29
0904-17	32.2	3.8	148	0.3	0.0	0.7	0.1	0.3	0.5	0.2	2.6	1.0	11.8	5.1	24	6.5	85	19	8003	0.3	20	1.2	1.0	30	74	6
0904-18	32.2	2.9	561	1.0	0.1	5.1	0.1	2.5	3.8	0.8	15	5	59	20	80	18	204	37	7747	0.5	25	1.7	2.7	54	83	8
0904-19	32.2	31	5350	8.4	0.6	75.7	2.4	38	57	9.2	218	67	687	214	775	164	1563	250	7326	2.8	171	11.5	41.8	877	490	66
0904-20	32.2	50	3183	14	0.7	57.8	1.1	17.1	27	1.9	117	37	397	122	440	89	809	142	8197	4.8	175	11.9	26.2	581	505	59
0904-21	32.2	4.3	406	1.0	0.0	3.7	0.1	2.0	3.2	0.8	12.4	4.0	44.8	14.9	60	13.8	151	29	8613	0.5	55	3.6	2.7	50	203	16
0904-22	32.2	3.0	122	0.3	0.0	0.7	0.0	0.2	0.3	0.1	2.2	0.7	9.8	4.0	19.9	5.3	68	15	7894	0.2	20	1.3	1.1	28	75	6
0904-23	32.2	3.5	135	0.5	0.0	0.8	0.0	0.2	0.2	0.1	2.1	0.8	10.9	4.5	21.8	5.8	73	16	8355	0.3	25	1.5	1.4	37	94	7
0904-24	32.2	29	4917	9.9	0.7	76.9	2.8	45	61.8	9.9	222	68	675	201	707	141	1270	190	7157	3.2	155	10.3	32.4	656	421	57
0904-25	32.2	30	4711	8.5	0.4	53.1	1.7	31.1	51	10	197	60	621	192	721	149	1434	234	7822	2.4	121	8.3	30.8	610	331	47
0904-26	32.2	33	5357	12	0.5	71.5	2.0	37	61	10	217	68	684	211	764	156	1501	242	7538	3.8	152	9.9	36.5	766	420	58
0904-27	32.2	15.3	2758	4.6	0.3	28.1	0.9	16.8	28	5.5	106	33	342	110	410	89	854	152	7703	1.5	74	5.0	16.8	335	203	28
0904-28	32.2	11.8	2987	4.8	0.3	33.1	1.4	24	35	7.5	124	38	389	121	455	95	942	152	7482	1.5	77	4.9	16.3	344	225	28
0904-29	32.2	11.1	2851	4.1	0.2	29.6	1.2	18.9	29	5.8	106	34	360	114	446	95	934	160	7423	1.7	66	4.4	12.7	262	185	24
0904-30	32.2	6.4	1989	3.5	0.1	27.0	1.0	15.6	23	4.2	81	25	254	77	272	57	540	83	7822	1.5	79	5.1	11.8	225	222	26
0904-31	32.2	11.1	2930	4.2	0.3	33.9	1.3	21	29	6.4	110	34	363	115	434	95	909	150	8119	1.8	100	6.5	20.6	432	284	36
0904-32	32.2	14.7	1809	4.7	0.2	21.1	0.7	11.8	17.2	1.9	66	21	217	70	272	58	570	95	7719	1.3	73	4.7	12.5	240	213	25

Appendix G. Zircon trace elements for Chapter 5, analysed in Beijing

Element	SiO_2	Ti	Y	Nb	La	Ce	Pr	Nd	Sm	Eu	Gd	Tb	Dy	Ho	Er	Tm	Yb	Lu	Hf	Ta	Pb	Pb	Pb	Th	U	Pb
	29	49	89	93	139	140	141	143	147	151	155	159	163	165	166	169	173	175	179	181	206	207	208	232	238	204
0904-33	32.2	5.3	904	4.1	0.1	14.6	0.2	2.7	5.4	0.9	23	8	96	33	130	30	314	55	7787	1.8	55	3.6	8.0	175	181	18
QL09-08																										
0908-01	32.2	7.0	4240	46	0.9	42.3	1.3	18.4	34	4.6	129	42	491	164	704	167	1797	343	7770	8.2	1029	64.4	127.6	3256	3375	329
0908-02	32.2	9.7	906	34	3.2	18.6	1.7	9.6	9.6	1.0	25	9	103	34	151	38	414	78	9910	3.9	168	11.3	8.2	190	611	47
0908-03	32.2	14.5	3541	7.0	0.6	13.4	1.3	21.7	41	5.9	144	43	438	143	564	126	1295	241	7408	1.8	225	13.9	29.6	823	824	73
0908-04	32.2	5.6	2001	17	0.8	10.3	0.7	5.2	9.4	1.3	41	16	188	74	331	82	951	189	9452	3.4	393	24.9	18.8	467	1288	110
0908-05	32.2	78	4961	126	37	88.8	16	96	74	9.4	173	57	609	201	833	202	2164	414	7928	16.4	982	226.2	264.0	1673	3463	427
0908-06	32.2	5.5	3549	8.7	1.3	26.5	2.7	40	56	8.0	170	47	464	144	545	119	1203	222	7319	1.5	224	14.0	36.1	1002	818	76
0908-07	32.2	21	2809	82	7.3	44.7	4.6	29	28	3.6	81	29	325	112	491	123	1368	262	8888	17.8	500	35.3	35.8	862	1802	147
0908-08	32.2	55	5686	161	17	107	11.5	81	81.2	9.7	212	68	708	229	963	224	2386	442	7560	25.0	756	53.5	100.2	2566	2759	247
0908-09	32.2	57	1934	216	13.1	58.3	7.6	43	36	4.1	73	26	266	81	332	81	890	156	10267	22.8	339	30.2	26.6	505	1368	103
0908-10	32.2	17	1908	11	116	161.3	18	80	31	5.6	70	21	221	70	284	67	714	129	7352	1.3	105	9.1	15.3	345	382	35
0908-11	32.2	7.1	2789	5.2	1.2	15.0	1.8	26	38	5.9	117	34	336	109	422	96	989	183	7732	1.4	196	12.3	23.7	638	718	62
0908-12	32.2	24.7	4643	62	15	85.2	10	64	61.8	7.6	159	54	593	187	774	185	2012	352	8144	6.6	641	42.0	56.2	1496	2344	193
0908-13	32.2	11.9	676	2.2	0.0	3.1	0.1	2.0	4.1	0.6	14	5	56	23	110	29	347	73	7334	1.0	77	4.7	3.2	86	298	21
0908-14	32.2	10.1	1552	11.2	3.6	12.2	2.0	17.2	19.4	3.2	58	17	179	58	233	53	574	106	6681	1.9	76	6.0	8.5	204	290	24
0908-15	32.2	19.5	1635	71.5	14	30.9	5.8	31	21.4	2.7	49	17	193	64	278	71	801	149	8934	12.3	257	20.9	17.4	360	991	76
0908-16	32.2	5.6	1097	2.2	0.1	8.6	0.3	5.9	9.2	2.0	32	10	115	39	162	39	446	85	7248	0.9	72	4.4	6.6	170	261	22
0908-17	32.2	171	3300	260	44	159	26	138	96	12	164	57	559	151	603	150	1650	289	6952	39.4	397	62.5	69.6	775	1517	146
0908-18	32.2	23	1585	41	15	42.7	7.4	44	34	3.7	66	21	209	63	248	61	666	118	9581	2.5	193	16.6	13.1	193	820	57
0908-19	32.2	17.9	1778	61	12	51.8	7.6	45	36	4.2	70	25	254	75	310	74	834	144	9522	8.5	222	18.6	13.8	249	937	65
0908-20	32.2	14.8	2397	55	14.1	50.0	8.4	47	35	4.7	78	28	302	98	417	104	1150	202	8874	7.6	356	27.3	23.6	416	1338	104
0908-21	32.2	47	3612	91	33	109	18	117	91.1	12	179	58	552	155	602	141	1498	259	8101	13.4	341	27.9	39.5	933	1346	109
0908-22	32.2	26	3021	77	5.2	41.4	4.2	26	24	3.4	71	27	325	115	512	134	1529	284	7599	9.2	675	45.0	39.9	957	2299	193
0908-23	32.2	16.5	1315	6.6	0.4	8.2	0.4	5.5	9.8	1.1	35	12	133	48	203	48	532	100	7783	1.4	153	10.5	10.5	238	556	45
0908-24	32.2	7.4	1245	1.6	0.1	7.2	0.4	8.0	11.1	2.3	39	12	132	44	183	43	481	89	7900	0.7	83	5.1	7.9	208	302	25
0908-25	32.2	21.7	2638	73	16	49.9	7.9	49	40	5.3	92	32	334	110	443	113	1289	233	8286	17.5	412	31.9	29.8	584	1555	122
0908-26	32.2	42	2441	133	24	69.5	11.0	63	42	4.3	84	29	309	100	422	105	1183	210	9986	29.8	453	32.9	21.4	394	1673	128
0908-27	32.2	5.7	1042	9.2	1.9	12.0	0.8	6.0	6.8	0.9	24	9	101	37	162	40	463	85	8959	1.6	149	11.0	8.9	190	566	43
0908-28	32.2	53	5352	221	10	105	10.1	70	73	7.6	188	62	668	216	917	219	2411	433	6536	27.4	861	66.2	114.3	2577	3133	282
0908-29	32.2	4.7	2362	14	5.6	15.8	2.3	13.5	13.8	1.4	52	20	235	84	360	90	1004	184	9930	3.4	563	37.6	18.7	417	1941	154
0908-30	32.2	6.8	1052	25	6.2	20.7	2.9	16.8	11.9	1.4	29	11	122	41	184	47	542	100	8966	4.6	174	12.8	7.9	156	679	49
QL09-11																										

Appendix G. Zircon trace elements for Chapter 5, analysed in Beijing

Element	SiO_2	Ti	Y	Nb	La	Ce	Pr	Nd	Sm	Eu	Gd	Tb	Dy	Ho	Er	Tm	Yb	Lu	Hf	Ta	Pb	Pb	Pb	Th	U	Pb
	29	49	89	93	139	140	141	143	147	151	155	159	163	165	166	169	173	175	179	181	206	207	208	232	238	204
0911-01	32.2	4.5	3063	21	2.0	57.5	2.5	17.4	17.0	3.3	61	24	303	117	522	130	1484	284	7995	6.4	632	42.7	41.4	1014	2177	184
0911-02	32.2	13.0	1534	16.7	12	96.3	10	63	39	4.5	59	16	155	53	230	58	647	131	11492	8.9	515	54.7	36.9	279	1873	156
0911-03	32.2	3.9	854	3.9	0.1	7.3	0.1	1.5	3.0	0.5	17	7	77	30	134	33	374	73	10069	1.9	110	7.0	5.9	158	401	31
0911-04	32.2	37.2	2811	38	43	284	41	262	152	13	178	40	341	106	426	103	1099	211	13079	11.8	795	99.6	71.4	470	2982	252
0911-05	32.2	13.1	5259	64	23	317.1	21.1	134	103	13	212	62	624	200	810	187	1955	354	8278	10.5	1004	104	176	4568	4075	358
0911-06	32.2	14.9	1531	13.8	12	70.6	7.8	48	28	3.0	53	15	161	55	229	54	590	112	10918	2.2	235	30.7	24.4	191	852	76
0911-07	32.2	1.1	1514	9.8	0.0	4.9	0.0	0.9	3.9	0.2	27	11	138	53	244	61	695	138	11646	5.2	321	20.2	7.1	196	1167	86
0911-08	32.2	6.0	1485	12.1	6.7	101	7.8	49.1	28	2.0	44	13	150	54	233	59	653	126	11178	5.6	417	35.3	22.9	322	1513	120
0911-09	32.2	9.7	408	1.0	0.0	3.7	0.1	0.9	2.0	0.4	10	3	39	15	65	15	172	34	8391	0.5	31	1.9	1.7	43	115	9
0911-10	32.2	3.0	1644	17	22	318	22	130	73	7.2	89	20	183	59	240	61	679	127	12982	7.5	517	51.7	29.7	191	1882	152
0911-11	32.2	27.4	3262	58	81	413	80	491	268	24	289	60	471	121	491	122	1373	254	14102	19.0	1069	179	137	365	4373	371
0911-12	32.2	105	4685	96	98	914	107	669	434	48	524	101	769	177	644	158	1874	359	19106	13.6	1038	204	167	381	4515	385
0911-13	32.2	11.2	3631	28	15	479	14	97	67	15	147	41	421	138	551	132	1407	257	8725	6.0	429	41.2	77.5	1656	1465	153
0911-14	32.2	44.1	3105	54	66	302	62	405	237	24	265	57	439	119	436	99	1030	183	12030	10.4	792	131.5	119.9	1109	3110	284
0911-15	32.2	23.2	3163	52	28	984	35	248	169	21	249	60	455	125	468	108	1143	207	10936	13.1	604	50.6	35.5	561	2391	176
0911-17	32.2	10.2	1096	11	11	149	14	85	55	4.9	69	16	140	40	148	33	360	65	11263	2.5	303	35.8	20.4	87	772	92
0911-18	32.2	7.2	1744	14	30	185	25	143	78	7.3	96	23	205	63	259	62	706	133	10476	3.4	383	52.9	44.4	398	1586	128
0911-20	32.2	2.2	2005	17.0	6.3	53.4	6.8	42.1	27	2.4	50	16	193	71	315	80	879	167	11667	7.6	581	43.2	22.7	378	2023	162
0911-22	32.2	138	3366	119	114	485	121	732	410	35	434	87	586	135	465	102	1041	183	11500	13.1	849	219	205	464	3142	363
0911-23	32.2	5.5	4132	27	7.7	70.6	7.0	46	33	4.4	97	36	437	156	636	152	1549	271	10205	7.2	975	91	103	1941	3309	310
0911-24	32.2	4.6	2057	10.9	7.8	123.1	8.9	60	41.5	4.4	76	21	214	75	327	83	995	191	7595	3.1	471	37.3	40.9	846	1731	143
0911-25	32.2	189	2787	35	115	659	120	711	359	26	339	62	431	107	386	89	922	173	11906	7.6	619	184	176	988	1932	284
0911-26	32.2	9.1	1606	6.2	7.7	136	8.4	63.1	49	5.5	80	21	191	59	236	58	640	124	9059	1.5	245	23.1	31.8	640	853	81
0911-27	32.2	21.5	2939	64	40	207	31	189	108	6.8	158	40	385	119	460	99	1029	180	12450	23.9	479	56.4	45.6	343	1427	152
0911-28	32.2	11.7	1938	22.1	28	307	33	207	121	11	142	31	253	72	275	66	728	131	12350	9.4	610	78.5	58.6	349	2105	196
0911-29	32.2	8.6	3995	10.3	0.9	32.0	1.7	24.1	43	5.4	157	48	507	164	630	142	1437	254	8774	3.1	425	26.3	47.2	1293	1477	133
0911-30	32.2	12.7	2401	21.6	39	428	37	223	114	8.7	125	29	261	86	376	98	1093	202	14103	11.7	877	98.6	61.3	320	3486	266
0911-31	32.2	20.3	1448	10.1	16	156	14	94	68	10	99	23	189	53	206	48	515	95	7887	1.8	103	17.6	21.1	225	382	40
0911-32	32.2	4.9	1307	6.5	0.9	19.9	0.9	7.8	8.2	1.2	30	10	124	47	207	52	593	116	9319	2.3	169	10.7	9.5	227	609	48
0911-33	32.2	398	2391	43	72	506	76	439	287	24	291	57	393	91	313	72	731	130	11352	7.2	566	167	158	368	1875	258
QL09-13																										
0913-01	32.2	19.8	1881	25	35	201	26	152	80.1	9.6	98	25	229	70	287	69	762	142	12489	9.9	608	58.2	32.5	258	2022	177
0913-02	32.2	152	1577	47	33	1502	33	236	130	8.4	135	27	214	61	238	55	610	112	10094	4.8	385	47.2	34.2	228	936	121

Appendix G. Zircon trace elements for Chapter 5, analysed in Beijing

Element	SiO_2	Ti	Y	Nb	La	Ce	Pr	Nd	Sm	Eu	Gd	Tb	Dy	Ho	Er	Tm	Yb	Lu	Hf	Ta	Pb	Pb	Pb	Th	U	Pb
	29	49	89	93	139	140	141	143	147	151	155	159	163	165	166	169	173	175	179	181	206	207	208	232	238	204
0913-03	32.2	6.1	700	1.4	0.1	4.6	0.1	2.3	4.9	0.8	19	6	73	25	107	24	264	51	8970	0.6	64	3.9	4.2	107	211	19
0913-04	32.2	13.9	3501	61	100	921	86	497	272	23	313	71	551	142	525	116	1205	214	12594	12.1	861	120	104	1018	2881	290
0913-05	32.2	8.0	3728	25	23	305	28	186	119	12	201	54	492	147	581	129	1356	239	8887	4.1	481	65.1	83.6	1187	1576	175
0913-06	32.2	8.5	1896	23	15	118.9	12	77	43	3.9	72	19	197	67	288	71	792	150	9722	4.1	362	33.1	25.2	384	1328	108
0913-07	32.2	2.2	1432	6.6	0.1	6.5	0.1	1.4	4.7	0.6	28	11	136	51	234	58	666	128	10863	3.0	217	13.8	7.5	192	797	59
0913-08	32.2	2.2	2231	23	2.9	27.1	1.5	8.2	5.5	1.1	25	13	182	74	362	94	1067	199	11260	12.7	955	62.3	17.7	371	3375	253
0913-09	32.2	14.5	2573	63	41	814	33	195	102	7	132	33	301	92	391	94	1025	191	11525	23.8	862	132	108	447	3045	295
0913-10	32.2	11.1	4176	63	65	661	66	415	248	19	310	78	618	164	612	138	1443	259	11603	17.9	763	113.7	98.9	677	2620	262
0913-11	32.2	14.7	2041	50	47	352	33	190	84	8	111	25	232	70	294	72	802	151	10086	6.4	596	62.5	66.1	1122	2098	192
0913-12	32.2	7.8	4822	28	36	232	19	125	89	12	193	56	586	188	755	174	1876	346	9288	4.2	635	81.0	111.8	1751	2063	230
0913-13	32.2	9.4	1172	10	2.0	31.0	2.1	15.1	14	2	35	11	115	41	179	45	516	101	7928	1.9	198	15.3	18.7	390	686	61
0913-14	32.2	28	4343	46	168	1522	125	763	359	32	416	88	678	172	603	129	1331	229	8419	3.6	404	109	125	1171	1432	188
0913-15	32.2	11.5	1050	1.6	0.1	6.8	0.3	4.9	8.1	1.6	31	10	109	38	164	38	412	81	7609	0.8	72	4.4	4.9	133	252	21
0913-17	32.2	7.1	1997	8.5	5.9	85	6.6	45	31	6.2	70	21	225	75	301	70	738	132	9615	2.5	347	26.1	20.8	426	1221	100
0913-18	32.2	7.2	3214	35	24	98	13	78	39	4	70	24	297	115	556	147	1707	329	15345	22.8	1312	105	40.2	354	5314	361
0913-19	32.2	13.7	3147	50	104	1362	83	520	283	25	311	62	460	117	429	94	1009	182	12351	15.4	932	154	128	460	3627	327
0913-20	32.2	7.8	2130	10	4.0	66	4.4	34	31	5.3	81	24	238	78	315	74	809	148	9008	2.1	284	21.8	41.8	946	948	95
0913-21	32.2	7.7	1364	19	6.8	56.9	5.9	40	24	2.0	44	13	137	48	206	50	572	106	10556	3.2	252	21.4	16.3	270	872	74
0913-22	32.2	3.0	1615	3.4	0.1	7.5	0.2	4.3	8.8	1.1	39	14	162	58	254	61	675	129	9738	1.5	177	10.8	10.1	264	627	50
0913-24	32.2	56	1385	52	20	79	6.6	45	30	4.5	60	16	160	51	197	44	472	83	10419	2.5	149	31.3	34.4	270	451	61
0913-25	32.2	5.5	1234	14	4.5	42	5	35	21	1.7	35	10	109	41	182	47	526	103	11123	5.4	317	24.0	10.7	159	1067	87
0913-27	32.2	58	5451	95	341	1334	124	628	294	31	364	88	752	209	820	187	2019	379	7373	13.0	933	174	195	2378	3273	367
0913-28	32.2	41	1250	43	12	82	11	75	51	3.8	74	18	157	46	182	43	472	86	10994	7.6	367	41.5	31.4	351	1209	114
0913-29	32.2	65	2595	71	57	369	52	329	194	17	239	52	400	102	373	82	850	150	10952	7.0	475	75.1	77.4	1179	1596	172
0913-30	32.2	131	3150	101	122	321	49	273	142	11	201	49	425	123	469	106	1081	197	8042	21.2	756	103	129	2190	2559	274
0913-31	32.2	15.6	1337	37	20	174	16	99.1	58	7.1	71	18	154	46	193	47	538	98	13037	7.9	464	46.9	26.2	179	1563	136
0913-32	32.2	54.1	2269	57	33	1343	32	214	125	8.1	148	33	283	84	343	83	910	171	11194	17.5	866	78.1	40.0	339	2990	247
0913-33	32.2	12.6	1986	3	0	34	1	13	18	4	62	20	221	75	298	65	686	124	7820	1.0	93	5.7	15.3	378	312	32
0913-34	32.2	8.4	6152	75	181	972	141	844	357	41	410	99	848	237	935	210	2215	396	14420	35.3	1399	131.4	74.7	982	9436	406
QL10-36																										
1036-01	32.2	9.24	1860	10.7	4.84	27.89	3.38	19.5	12	3.8	38.4	15	186	72.7	321	80.4	922.4	166	10114.1	6.43	511.4	34.48	21.76	489.2	1770	142.3
1036-02	32.2	4.15	611	1.58	0.03	10.7	0.02	0.49	1.32	0.2	9.18	3.9	52.9	21.5	97.5	24.2	280.8	53	12511.6	0.97	288.2	32.15	9.3	85.33	341.3	81.44
1036-03	32.2	1.66	995	2.01	0.04	1.45	0.02	0.27	1.21	0.1	10.9	5.7	85.9	36.2	177	46.5	545.1	106	11752.9	2.01	193.3	11.95	2.51	63.73	685.9	50.53

Appendix G. Zircon trace elements for Chapter 5, analysed in Beijing

Element	SiO_2	Ti	Y	Nb	La	Ce	Pr	Nd	Sm	Eu	Gd	Tb	Dy	Ho	Er	Tm	Yb	Lu	Hf	Ta	Pb	Pb	Pb	Th	U	Pb
	29	49	89	93	139	140	141	143	147	151	155	159	163	165	166	169	173	175	179	181	206	207	208	232	238	204
1036-04	32.2	21	1414	6.55	13.6	61.42	7.92	42.7	18.8	9.7	38.4	13	148	52.1	223	53.5	584.4	109	10241	4.52	370	27.99	19.65	420.7	1264	105.7
1036-05	32.2	4.25	1031	3.48	0.67	6.48	0.51	4.23	4.03	0.8	17.7	7.4	96.1	36.8	167	41.6	476.6	92	10765.7	2.84	303.9	19.35	7.76	195	1051	81.58
1036-06	32.2	1.52	867	3.59	0.05	4.88	0.07	0.74	2.58	0.2	14.4	5.8	80.6	31.8	142	36	411	79	10612.9	2.98	248.2	15.51	7.71	199	884.9	67.28
1036-07	32.2	2.58	724.1	5.11	0.02	8.21	0.03	0.49	1.75	0.3	11.8	4.7	66.8	25.8	117	28.8	323.5	63	10313.5	3.14	197.3	12.1	7.28	189.9	703.9	54.04
1036-08	32.2	9.02	1133	4.75	5.48	34.22	3.47	19.9	10.9	4.1	27.2	9.7	114	40.4	179	43.8	498.8	96	10856.5	3.43	266.6	20.09	13.24	298.3	935	75.69
1036-09	32.2	4.01	825	4.12	0.46	8.67	0.39	2.83	2.75	0.6	11.1	4.6	65.1	27.4	138	39.2	493.5	102	13240.5	2.83	669.4	79.05	38.71	267.1	624.8	199.1
1036-10	32.2	4.26	2029	3.16	1.71	16.96	1.28	9.19	9.96	2.1	44.4	17	204	74.1	312	74.6	785.4	145	10176.4	2.46	343.9	22.69	17.7	443.7	1201	97.16
1036-11	32.2	2.24	1314	6.75	0.05	7.31	0.08	1.01	3.64	0.3	20.5	9.1	122	47.8	217	54.5	618.5	117	10572.4	4.62	340.1	21.23	12.14	307.7	1175	93.01
1036-12	32.2	2.61	1623	2.4	0.03	8.25	0.11	1.71	5.83	0.4	32.3	13	162	59.7	257	60	630.2	117	10431.6	1.87	242.5	14.81	11.37	311.7	878.3	67.68
1036-13	32.2	1.32	1346	4.42	0.53	8.25	0.3	2.29	4.26	0.5	22.5	9.6	124	48.6	215	51.8	589.5	110	10158.6	2.94	251.4	15.62	9.87	256.9	908	69.2
1036-14	32.2	1.97	1031	4.4	2.44	12.86	1.23	8.4	5.3	0.8	19.1	7.7	98.8	37.1	164	40.1	447.4	87	10570.9	3.3	273.3	17.88	10.02	249.4	982.8	75.07
1036-15	32.2	10.5	1384	1.36	0.04	12.29	0.25	5.7	10.5	2.2	43.7	14	155	52.1	207	46	469.6	86	8687.03	0.63	68.57	4.22	6.95	180.7	247.4	21.1
1036-16	32.2	2.15	893	2.8	0.06	3.37	0.05	0.92	2.02	0.2	13.9	5.8	81.5	32.5	155	40.7	492.5	99	10380.9	2.77	258.6	16.63	5.04	120.3	934.3	68.63
1036-17	32.2	1.19	1054	3.7	0.03	5.23	0.03	0.77	2.44	0.2	17.1	7.4	97.4	38.4	171	42.5	481.3	91	10197	2.46	214.4	13.51	6.76	175.1	783.3	58.21
1036-18	32.2	3.01	807	3.52	0.13	5.4	0.13	1.05	2.24	0.3	13.2	5.7	75.6	28.8	137	33.7	380	75	10708.9	2.89	220	14.61	7.36	180.1	800.4	60.11
1036-19	32.2	2.41	944	4.26	0.79	7.85	0.24	1.79	3.15	0.3	15.9	6.7	85.6	33.7	151	37	406.3	82	10106.9	2.96	197.9	12.25	7.25	193.7	718.7	54.21
1036-20	32.2	1.66	963	2.96	0.08	3.38	0.04	0.58	2.32	0.1	13.2	6.4	86.1	33.9	160	40.9	477.7	97	11481.9	2.8	278.3	17.76	6.46	168.7	1041	74.39
1036-21	32.2	3.89	1121	4.05	46.8	116	18.6	100	32.1	4	43.9	11	117	40	173	42.2	472.6	90	11228.2	3.29	287.9	19.5	10.63	233.7	1044	79.27
1036-22	32.2	3.02	1025	2.56	0.06	5.32	0.05	0.71	2.59	0.6	15.4	6.3	89.1	36.5	176	48.5	588.1	123	11660.7	2.53	399.3	42.8	12.47	105	479.8	112.2
1036-23	32.2	5.03	746	1.96	0.06	7.62	0.04	1.28	2.96	0.4	15.8	5.8	74.3	27	115	27.2	291.1	56	9234.72	1.03	71.48	4.33	3.91	106.7	264.7	20.23
1036-24	32.2	14.4	1799	1.38	0.02	14.06	0.12	3.51	8.89	1.6	44.3	16	187	68.9	283	65.9	703.4	133	8876.4	0.73	108.9	11.11	13.12	103.5	111.6	35.58
1036-25	32.2	3.74	993	3.19	10.2	48.97	2.38	8.99	5.6	1	19.8	6.7	84.9	32.9	156	41.8	523	117	10625.8	1.8	259.3	19.68	37.26	502	564.6	86.36
1036-26	32.2	6.04	885	1.87	0.04	6.69	0.05	1.01	3.06	0.4	17.3	6.9	88.6	32.2	146	34.6	394.2	76	10106.5	1.12	79.23	5.21	4.2	94.5	270.1	22.49
1036-27	32.2	10.4	4648	4.03	0.18	69.96	2.38	44.9	90.8	4.7	305	92	817	198	606	119	1085	150	8180.11	2.23	267.9	25.24	52.16	469.1	315.5	97.48
QL10-39																										
1039-01	32.2	5.06	1378	3.7	2.61	16.66	1.12	8.91	7.55	0.6	31.5	11	141	51	220	50.4	543.6	108	9677.16	1.75	154.5	9.47	9.1	247.4	554.4	44.08
1039-02	32.2	13.7	2170	0.85	0.03	1.88	0.12	3.08	8.92	0.1	54.3	20	234	81.3	315	67.3	664.2	117	10894	0.56	193.2	14.85	11.09	142.6	327.9	55.66
1039-03	32.2	4.2	906	3.27	0.04	3.09	0.04	0.94	2.52	0.3	15.5	7	86.7	32	137	33.8	384.8	74	11460.7	2.53	381.7	34.66	6.16	150.4	847.9	102.9
1039-04	32.2	7.25	993	3.77	0.29	7.3	0.5	4.08	5.66	0.6	22.9	8.7	99.1	35.5	156	38.9	423.2	80	10969.9	2.82	227.1	13.96	6.96	194.5	821.7	61.46
1039-05	32.2	15.2	1149	3.7	2.42	22.97	2.03	15.3	13.2	3.5	38.2	13	133	43.4	175	39.2	401.2	77	9133.31	1.27	76.44	6.33	6.93	163.1	275.7	23.45
1039-06	32.2	3.3	1578	8.37	0.34	10.34	0.32	3.3	5.26	0.6	27.8	12	152	57.3	253	61.9	689.4	129	10680.8	5.93	475.7	29.56	17.05	463.6	1667	130.1
1039-07	32.2	7.43	757	1.57	0.09	8.97	0.08	1.54	3.47	0.6	18.6	6.6	78	28.1	120	27.9	303.9	56	9662.08	0.93	57.2	3.48	3.71	98.01	206.4	16.5
1039-08	32.2	14.2	979	1.9	0.24	4.79	0.4	4.92	7.82	0.8	28.6	9.3	106	37.4	155	36.4	384.9	71	8505.82	0.9	73.21	8.45	8.58	118.7	259	24.01

Appendix G. Zircon trace elements for Chapter 5, analysed in Beijing

Element	SiO_2	Ti	Y	Nb	La	Ce	Pr	Nd	Sm	Eu	Gd	Tb	Dy	Ho	Er	Tm	Yb	Lu	Hf	Ta	Pb	Pb	Pb	Th	U	Pb
	29	49	89	93	139	140	141	143	147	151	155	159	163	165	166	169	173	175	179	181	206	207	208	232	238	204
1039-09	32.2	12.4	1197	3.1	0.05	11.64	0.16	3.49	6.86	1.1	30.4	11	125	45.6	192	44.7	471.4	90	8342.55	1.35	91.72	5.88	6.99	178.3	330.8	27.07
1039-10	32.2	9.48	543	1.19	0.03	3.27	0.05	1.17	2.96	0.4	12.1	4.4	50.5	18.6	83.9	20.6	239.8	49	8024.61	0.65	43.71	2.79	2.34	63.14	157.7	12.38
1039-11	32.2	5.1	809	1.43	0.09	15.79	0.16	3.08	5.29	1.4	19.6	7	79.7	27.9	124	31	357.2	71	8755.87	0.71	66.29	4.16	6.03	155.8	222.8	20.05
1039-12	32.2	12.7	950	1.64	0.1	7.03	0.1	1.66	3.43	0.8	23	8.4	99.1	34	133	31.2	344.4	64	9066.54	0.74	127.3	9.51	3.55	76.1	286.5	34.64
1039-13	32.2	47	3129	12.3	60.9	275.5	32.5	170	68.8	23	110	34	344	114	474	116	1282	239	11657.2	4.72	561.1	73.61	48.76	286.8	2033	177.7
1039-14	32.2	3.2	1179	5.83	0.06	7.33	0.11	1.08	3.69	0.3	19.1	8.3	114	43.1	196	48.5	557.2	101	10204.5	3.81	262.8	16.15	9.67	245.4	944.2	71.96
1039-15	32.2	4.95	1078	2.38	0.03	11.12	0.1	1.89	5	0.6	25.7	9.4	114	40.2	168	41	440.6	80	9711.83	1.31	118.8	7.15	7.71	195.1	427.3	34.25
1039-16	32.2	6.42	1487	7.08	46.8	120.9	17.6	94.7	31	4.2	50.4	15	157	52.7	228	54.2	597.7	109	10521.8	3.61	369.1	29.31	21.74	383.6	1238	106.8
1039-17	32.2	4.48	1590	8.22	2.18	20.59	1.24	8.45	7.77	1.4	33	13	160	58.4	252	61.6	689.6	124	10189.5	5.07	413.4	27.39	22.17	547.9	1496	117.3
1039-18	32.2	1.75	1207	5.17	0.03	5.84	0.04	0.77	2.82	0.3	18	8.2	114	41.6	200	50.4	567.2	109	10798.9	3.61	293.4	17.85	8.89	229.8	1056	79.3
1039-19	32.2	90.7	2813	20.9	35.8	172.7	23.7	145	82.7	27	141	40	364	106	401	89.1	961.4	172	11661.9	3.95	411.2	76.23	71.65	1476	1472	154.2
1039-20	32.2	14.7	1644	16	11.6	47.13	6.16	34.2	18.3	5.8	43.2	15	168	58.9	254	62.3	703.3	127	10495.4	6.23	353	34.91	24.77	296.4	1208	105.9
1039-21	32.2	8.41	1247	6.59	1.35	17.84	1.06	6.85	7.27	1.6	25.9	10	125	46.5	202	48.9	546.5	103	10012.5	3.58	258.1	17.37	12.54	289.6	929	72.66
1039-22	32.2	19.6	969	4.68	5.77	13.78	1.08	5.34	4.35	0.7	19.2	7.8	94.4	34.4	158	38.5	437.2	80	10138.3	2.94	279.7	20.72	15.58	286.9	953.1	80.21
1039-23	32.2	2.67	974	4.66	0.99	11.82	0.32	2.76	3.71	0.4	18.7	7.5	95.5	35.1	156	38.3	432.3	79	9947.94	2.97	216.6	13.55	9.36	241.8	781.9	60.11
1039-24	32.2	28.5	1548	9.26	4.54	25.65	3.06	20.6	14.9	4.2	41.8	14	157	54.5	234	56	618.6	113	9882.83	3.65	278.3	33.91	26.07	201	952.1	88.5
1039-25	32.2	7.4	1401	7.45	1.9	16.59	1.46	9.68	8.99	1.9	30.5	11	138	49.5	211	52	569.3	105	10307.3	4.1	339.2	22.97	15.04	345	1159	94.7
1039-26	32.2	3.87	932	4.44	0.07	14.31	0.14	1.51	3.85	0.4	20.3	7.6	90.3	34.5	145	35.9	413.8	71	9566.18	2.26	149.6	9.27	8.43	212.5	544.4	42.51
1039-27	32.2	31.1	2268	10	36.2	140.6	27	147	69	23	109	30	291	87.2	341	77.6	787.7	134	10660.8	3.8	387.4	52.63	40.82	340	1410	126.8
1039-28	32.2	5.48	1382	7.03	0.76	11.48	0.55	4.3	5.39	0.8	24.8	11	136	51.3	233	57.9	651.4	121	10478.4	4.5	394.9	27.84	17.17	325.3	1298	110.4
1039-29	32.2	3.94	1140	5.68	0.78	10.15	0.71	5.17	5.54	0.9	21.4	8.4	107	40.3	180	45.8	515.2	97	10484.9	3.79	273.8	17.92	9.81	212.3	902.5	75.1
1039-30	32.2	14.8	1220	6.25	1.95	16.08	1.72	12.2	10.6	2.3	31	11	126	43.8	191	45.7	514.9	99	10112.4	2.79	187.3	14.5	9.16	182.2	682.2	53.22
1039-31	32.2	39.9	2226	13.4	13	65.82	8.77	59.2	37.2	9	85.9	27	273	85.2	333	76.9	792.8	147	10677.5	5.84	490.4	47.64	36.71	517.6	1732	148.2
1039-32	32.2	21.6	1300	6.65	1.5	14.1	1.14	8.13	7.75	1.6	27.8	10	128	45.8	202	49.2	532.6	102	11020.9	4.23	383.4	25.65	15.82	394.1	1288	106.4
QL10-43																										
1043-01	32.2	8.07	1990	3.32	0.07	31.5	0.52	9.68	16.7	3.7	61.8	20	227	78.8	326	76.4	828.7	109	8487	1.19	124.4	7.75	18.02	499.4	443	41.13
1043-02	32.2	10.8	652	1.48	0.02	5.93	0.03	1.07	2.95	0.5	16.2	5.7	66.8	24.4	105	25.4	280.2	37.8	9607	0.77	48.3	2.99	2.83	74.58	173.2	13.78
1043-03	32.2	4.22	965	4.07	0.05	15.32	0.07	1.5	4.71	0.5	22.1	8	98	35.8	156	36.9	408	52.5	10094	2.27	162	10.26	9.44	247.7	579.9	46.25
1043-04	32.2	11.4	1236	1.31	0.04	8.19	0.24	5.24	7.54	1.9	34.9	11	128	46.2	193	44	477.6	63.7	8045	0.62	62.32	3.82	6.04	160.6	223.5	19.03
1043-05	32.2	5.94	992	3.44	2.56	13.56	1.47	10.4	8.66	0.7	23.7	8.1	96	36.5	161	39.8	441	60.5	9928	2.25	195.5	13.63	8.66	178.9	729.9	54.71
1043-06	32.2	5.17	2375	11.3	6.68	50.99	5.05	28.9	22.2	2	60.4	21	242	88.2	382	93	993.8	129	10545	6.33	514.3	32.29	24.49	678.8	1837	143.9
1043-07	32.2	1.52	1102	5.55	0.26	7.77	0.18	1.51	3.04	0.2	18.8	8.2	101	38.1	180	44.3	513.8	66.8	10940	3.67	318.1	19.67	12.09	315.8	1142	87.34
1043-08	32.2	7.31	1482	2.15	0.41	8.64	0.53	7.37	12.4	2	51.6	16	180	58.1	236	54.7	581.3	70.9	8839	1	86.15	5.21	7.51	202.5	323.1	25.85

Appendix G. Zircon trace elements for Chapter 5, analysed in Beijing

Element	SiO_2	Ti	Y	Nb	La	Ce	Pr	Nd	Sm	Eu	Gd	Tb	Dy	Ho	Er	Tm	Yb	Lu	Hf	Ta	Pb	Pb	Pb	Th	U	Pb
	29	49	89	93	139	140	141	143	147	151	155	159	163	165	166	169	173	175	179	181	206	207	208	232	238	204
1043-09	32.2	2.06	604	2.63	0.09	4.54	0.05	0.8	1.78	0.2	12.6	4.8	57.9	22	100	24.8	284.6	38.1	11871	2.91	156	9.48	4.22	99.69	557	41.9
1043-10	32.2	5.58	533	2.77	0.14	17.73	0.11	1.15	1.8	0.3	9.26	3.5	46.2	18.9	91.9	25.7	327.5	49.1	12259	1.23	93.48	8.23	7.67	76.42	162.1	28.37
1043-11	32.2	1.41	991	4.59	0.1	6.69	0.05	0.93	2.95	0.1	17.8	6.9	91.2	34.5	161	38.7	429.5	56.7	9998	3.13	250.1	15.42	9.59	249.3	860.6	68.7
1043-12	32.2	6.46	1702	4.01	2.63	27.57	1.84	14.6	15.6	1.3	45.6	16	179	64.9	273	66.3	724.9	91.4	10111	2.55	331.7	21.31	15.38	385	1183	92.72
1043-13	32.2	8.89	1632	5.24	58.6	137.1	18.7	97.1	28.1	1.6	48.6	15	167	58.6	268	62.8	661.7	91.2	9545	2.6	311.5	19.22	19.23	499.2	1064	89.4
1043-14	32.2	35	2944	20.3	34.3	225.7	23.9	161	113	7.2	175	40	375	118	492	119	1264	158	10794	6.54	341.5	33.15	25.69	293.3	1684	103.3
1043-15	32.2	8.52	1039	5.23	1.43	15.8	0.81	5.74	4.99	0.4	20.8	7.9	96.6	38	172	43	483.8	66.1	11228	3.67	288.7	17.81	9.57	219.9	978.7	78.52
1043-16	32.2	5.45	1092	2.17	0.53	7.71	0.27	2.39	4.68	0.4	24.3	9.4	110	40.4	174	42.2	477.8	60.1	9802	1.19	97.45	5.97	5.22	135.6	349.8	27.54
1043-18	32.2	88.6	1708	7.88	42.3	174	18.7	126	53.9	4.6	79.5	20	202	65	269	62.5	678.7	84.7	8830	3.68	342	24.05	23.54	551.2	1235	100.1
1043-19	32.2	7.96	936	3.24	0.67	17.05	0.5	3.92	5.22	0.5	22	7.9	94.5	35	148	35.6	402.2	49.3	9543	1.42	110.2	6.85	5.41	138.7	394.3	30.89
1043-20	32.2	18.1	2305	10.4	54.4	280.5	39.6	218	128	6.2	168	42	337	90.6	351	80.6	862.8	108	11393	6.22	588.8	43.77	27.44	522.3	2136	166
1043-21	32.2	13.6	476	0.78	0.03	2.98	0.04	0.76	2.35	0.4	11.1	4	47.7	17.1	74.1	18.2	200.2	26	8330	0.41	37.96	2.31	1.85	46.87	137.8	10.63
1043-22	32.2	2.21	1216	4.34	6.3	23.52	2.53	13.3	7.39	0.4	25.8	9.7	124	45.4	198	49.4	543.9	68.8	10369	3.1	276.7	17.03	10.59	271.6	950.6	76
1043-23	32.2	2.49	491	2.54	0.76	9.37	0.35	2.97	2.78	0.3	9.8	3.7	47.5	18.2	81.4	20.4	246.2	31.5	10146	1.65	114.7	7.9	7.03	105.2	369.9	33.07
1043-24	32.2	7.26	1432	9.37	8.83	166.7	5.52	33.4	27.1	2.2	54	14	148	52.1	224	55	617	79.6	11072	5.86	499	37.8	29.76	676	2019	144.3
1043-25	32.2	7.97	709	3.13	0.75	15.6	0.5	3.86	4.08	0.3	14.3	5.4	68.6	26	121	31	362.7	48.4	10505	2.71	155.3	9.57	4.51	112.3	545.7	41.9
1043-26	32.2	9.56	1146	8.21	8.39	63.15	4.05	22.7	16	1.4	32.9	11	118	41.5	176	43.5	491.7	61.7	9568	3.5	216.9	14.32	10.47	249.7	778.1	60.93
1043-27	32.2	2.81	1165	6.99	1.77	16.12	1.12	7.3	6.14	0.5	22.7	8.5	111	42.5	193	49.3	554.5	72.2	10709	4.73	406.8	25.07	11.81	291.3	1317	109.8
1043-28	32.2	1.94	664	6.67	0.53	6.01	0.38	2.27	2.18	0.2	8.37	4	54.7	23.1	114	31.1	366.1	49.6	12399	6.97	357.3	21.93	4.72	119.9	1211	93.42

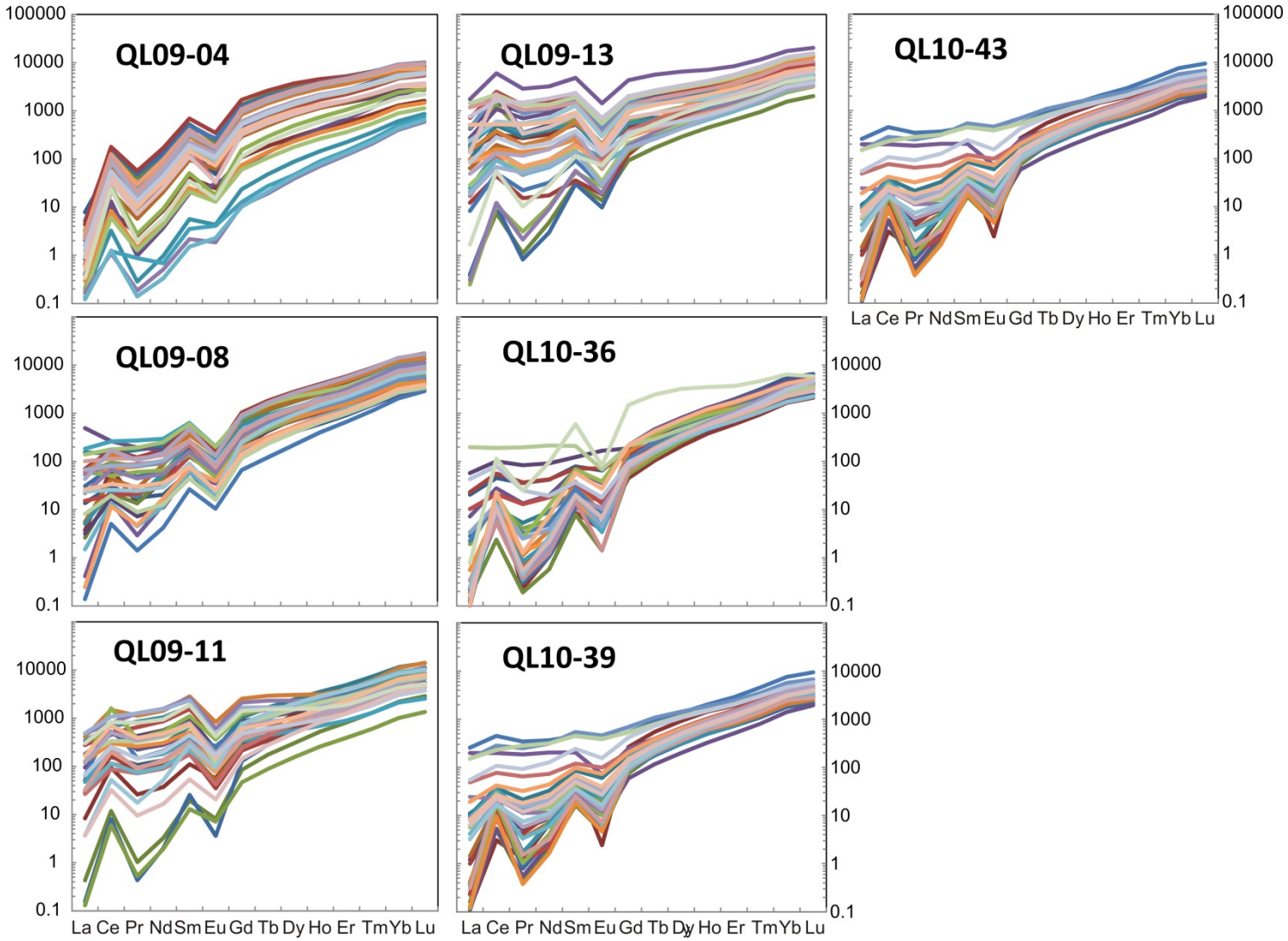
QL09-04
QL09-13
QL10-43
QL09-08
QL10-36
QL09-11
QL10-39
100000
10000
1000
100
10
1
0.1
La Ce Pr Nd Sm Eu Gd Tb Dy Ho Er Tm Yb Lu

Appendix H. Zircon trace elements for Chapter 6, analysed in Wuhan

	SiO_2	Ti	Sr	Y	Nb	La	Ce	Pr	Nd	Sm	Eu	Gd	Tb	Dy	Ho	Er	Tm	Yb	Lu	Hf	Ta	Pb	Pb	Pb	Th	U	Pb
	29	49	88	89	93	139	140	141	143	147	151	155	159	163	165	166	169	173	175	179	181	206	207	208	232	238	204
QL10-14-01	31.6	9.9	1.5	1328	3.2	9.6	41.2	6.0	38.3	21.3	0.3	49.3	12.8	138	46	208	39.8	395	66.3	11249	1.6	67	14.7	113	167	308	51
QL10-14-02	32.3	15.0	0.8	2208	6.6	1.7	32.9	1.5	14.5	18.7	1.1	76.5	22.3	247	79	336	61.4	584	92.5	11233	3.1	185	132.3	867	427	703	578
QL10-14-03	32.1	26.7	5.3	1296	3.0	75	210	29	144	38	0.6	57	13.4	136	45	202	38.5	381	63.8	10793	1.5	73	18.8	141	181	336	89
QL10-14-04	33.2	12.0	1.8	2095	2.7	14.6	54.0	6.1	33.5	18.3	0.6	63.7	18.2	214	74	325	60.0	585	95.2	10918	1.3	115	29.3	261	370	530	43
QL10-14-05	31.5	2099	3.0	2015	7.7	22.5	83.7	12.7	77.3	34.5	0.6	74.7	19.7	216	70	308	57.7	554	88.7	11143	1.3	77	22.1	197	243	349	78
QL10-14-06	32.2	8.3	1.3	1299	4.5	8.7	44.0	5.0	26.8	12.2	0.3	32.7	10.3	125	45	210	41.1	412	67.9	11753	2.3	108	31.1	198	243	495	71
QL10-14-07	32.9	52.8	0.3	910	2.5	0.5	8.8	0.2	1.8	3.2	0.1	18.6	6.2	80	28	138	27.0	279	46.8	11613	1.3	61	12.7	87	133	283	16
QL10-14-08	30.8	14.3	0.2	181	2.6	0.3	5.0	0.3	2.3	3.1	0.7	13.3	3.1	22	5	15	2.2	19	2.9	13607	2.6	191	42.2	37	45	881	38
QL10-14-09	32.8	69.9	0.1	323	1.0	0.1	9.1	0.9	13.2	16.7	0.3	36.6	6.5	46	10	29	4.0	32	4.0	12596	0.4	12	2.5	21	34	58	18
QL10-14-10	33.0	7.4	2.0	1238	5.0	38.6	124	15.9	82.5	21.7	0.3	41.2	10.9	122	42	192	38.4	385	64.2	11899	2.3	119	25.2	169	256	534	10
QL10-14-11	30.8	15.6	2.9	2570	5.1	9.5	45.7	5.1	29.6	19.4	0.6	64.1	20.4	252	88	409	79.6	784	129.4	11162	1.9	132	35.6	254	344	610	73
QL10-14-12	32.7	3043	3.3	1294	15	36.3	113	14.3	74.6	20.0	0.3	38.8	10.5	122	44	204	40.6	418	70.5	11204	2.9	97	20.1	130	202	450	46
QL10-14-13	31.7	12.4	3.4	1279	4.3	34	107	13	61	19	0.4	41	10.9	127	44	195	38.2	373	61.5	10965	1.9	113	26.7	201	302	518	51
QL10-14-14	30.2	14.8	12.0	3002	4.7	201	555	79	400	107	1.7	150	33.2	329	104	456	84.0	806	132.0	10843	1.6	154	96.5	634	379	654	401
QL10-14-15	32.7	19.2	4.8	1295	4.3	80	241	33	159	43	0.6	62	13.5	138	44	198	37.9	374	61.8	11042	1.9	104	30.2	221	264	471	73
QL10-14-16	30.9	2.5	2.8	1697	14	1.4	12.0	1.6	8.4	5.1	0.3	17.4	7.5	121	54	316	76.9	889	162.6	19253	20	484	105.8	101	112	2177	45
QL10-14-17	32.5	10.9	1.9	1799	2.2	22.8	77.4	9.9	50.7	19.0	0.3	49.9	14.6	174	60	279	53.6	529	88.8	11280	1.1	75	17.6	135	191	340	3
QL10-14-18	31.3	10.4	0.9	1905	9.0	1.8	24.5	1.2	7.8	9.2	0.3	41.3	14.0	178	64	302	59.6	591	99.1	12129	4.1	191	48.4	302	437	828	47
QL10-14-19	31.4	8.8	0.6	1492	5.6	0.4	12.5	0.3	3.3	6.2	0.1	31.6	11.1	139	50	234	45.1	456	76.2	11902	2.3	115	27.1	162	251	530	22
QL10-14-20	32.1	14.1	0.6	1102	3.7	5.0	23.7	2.0	11.1	6.1	0.1	25.4	8.3	103	37	172	33.4	334	56.7	11321	1.6	80	16.8	121	190	371	24
QL10-15-01	32.2	104	0.2	586	2.8	0.0	0.5	0.2	2.6	5.1	0.0	31.1	8.3	73	17	52	7.5	56	6.9	14263	1.2	10	2.2	1	1	47	0
QL10-15-02	31.8	17.4	0.4	1883	1.4	0.2	0.9	0.1	0.6	1.9	0.1	16.8	8.6	140	60	331	74.3	826	140.4	13462	1.4	177	39.6	34	39	618	8
QL10-15-03	31.8	47.5	0.1	636	0.7	0.0	2.5	0.2	3.4	7.0	0.2	25.2	6.9	65	18	75	15.0	165	26.9	14061	0.3	25	4.9	10	14	113	11
QL10-15-04	32.5	12.0	0.4	1971	6.5	0.0	9.8	0.1	1.7	4.9	0.1	32.0	12.0	169	66	334	68.0	703	113.4	12274	2.4	103	21.1	273	408	480	14
QL10-15-05	32.6	11.8	1.9	1799	3.6	10.6	27.1	3.4	19.7	7.9	1.9	28.4	10.1	147	60	310	66.4	740	129.7	9455	1.2	54	57.1	341	191	180	308
QL10-15-06	32.4	46.3	2.0	3527	3.4	0.2	2.3	0.2	2.1	4.8	0.2	39.7	18.2	280	116	600	124.6	1316	222.5	12596	2.1	232	53.2	107	107	738	12
QL10-15-07	32.6	7.5	0.7	3094	2.7	0.3	2.3	0.2	2.3	4.1	0.1	33.4	15.7	243	102	538	114.1	1242	210.6	12561	1.5	179	42.5	96	104	591	14
QL10-15-08	33.3	9.8	0.7	3307	8.0	0.1	2.2	0.1	1.0	4.8	0.1	40.0	17.5	281	110	583	127.5	1427	239.3	13874	3.6	167	34.6	75	105	739	13
QL10-15-09	32.2	11.1	0.7	3891	2.1	1.8	6.8	0.7	4.7	6.9	0.1	49.4	22.2	325	128	654	135.4	1424	234.2	12784	1.4	256	58.2	142	150	805	3
QL10-15-10	32.2	7.7	0.5	2548	1.2	0.0	0.7	0.0	1.0	3.1	0.1	30.2	13.5	206	84	433	90.9	962	161.9	12377	0.8	121	27.4	53	51	373	0
QL10-15-11	31.9	6.8	0.9	3354	1.9	0.2	1.4	0.1	1.5	3.9	0.0	31.3	16.3	264	111	599	134.7	1512	257.5	13483	1.6	291	68.3	81	77	901	63
QL10-15-12	32.0	13.8	0.4	1146	3.7	0.1	11.7	0.1	1.8	4.5	0.2	24.1	8.2	105	38	180	35.3	360	58.8	10823	1.7	67	14.7	85	118	314	32

Appendix H. Zircon trace elements for Chapter 6, analysed in Wuhan

	SiO_2	Ti	Sr	Y	Nb	La	Ce	Pr	Nd	Sm	Eu	Gd	Tb	Dy	Ho	Er	Tm	Yb	Lu	Hf	Ta	Pb	Pb	Pb	Th	U	Pb
	29	49	88	89	93	139	140	141	143	147	151	155	159	163	165	166	169	173	175	179	181	206	207	208	232	238	204
QL10-15-13	32.6	5.7	0.6	1067	3.9	0.3	28.2	0.7	9.8	9.3	3.6	30.7	8.4	94	33	156	34.3	389	70.9	11070	3.1	339	153.5	742	222	804	48
QL10-15-14	32.1	10.6	0.4	2546	1.4	0.6	3.5	0.4	3.9	7.5	0.2	49.6	17.4	233	87	408	80.1	819	134.7	11712	0.7	117	27.4	154	150	368	17
QL10-15-15	32.2	20.8	0.6	2849	2.7	0.1	1.6	0.0	1.1	3.3	0.1	29.0	14.6	227	92	483	103.5	1114	187.0	13057	1.5	204	44.3	71	86	736	0
QL10-15-16	32.1	8.4	0.5	2839	1.2	0.0	1.0	0.1	1.3	4.2	0.1	35.3	15.4	235	95	479	98.9	1040	176.1	12197	0.8	135	31.3	72	69	414	19
QL10-15-17	30.7	3.3	2.9	608	4.0	0.2	3.0	0.2	1.6	2.0	0.2	10.5	4.1	54	19	86	16.9	170	26.6	14088	2.4	221	44.9	48	67	1023	0
QL10-15-18	32.7	3.6	0.9	5810	12	0.0	1.9	0.0	0.7	3.7	0.5	44.8	25.8	447	194	1058	236.2	2622	436.0	11973	3.8	92	18.7	31	46	410	8
QL10-15-19	32.1	12.3	0.4	2251	1.0	0.0	1.1	0.1	1.7	4.1	0.1	33.0	13.3	190	75	375	77.4	829	140.6	11857	0.7	107	24.8	64	68	335	21
QL10-15-20	32.5	20.0	0.1	180	0.8	0.2	38.2	1.1	11.9	7.3	0.4	13.2	2.7	22	5	17	2.5	23	3.3	12715	0.1	10	2.2	40	57	46	28
QL10-21-01	33.7	21.2	0.8	592	1.4	0.1	6.4	0.1	1.1	1.6	0.4	10.5	3.6	45	17	84	18.0	195	35.3	9447	0.8	55	12.9	57	85	261	12
QL10-21-02	32.8	28.5	0.2	619	0.8	0.0	9.7	0.1	2.7	4.7	1.2	19.4	5.6	59	20	87	17.8	182	32.5	8895	0.5	59	12.6	92	152	283	14
QL10-21-03	31.8	9.3	1.3	591	2.2	1.3	22.4	0.9	6.4	4.5	1.5	13.6	4.3	49	18	82	18.1	196	36.0	9754	1.1	146	35.1	189	326	672	21
QL10-21-04	30.4	5.4	1.8	870	3.7	3.6	34.7	0.8	4.3	4.3	1.4	20.3	6.4	77	29	137	29.0	320	57.9	9758	1.7	215	47.2	287	478	1012	24
QL10-21-05	30.5	4.5	0.6	2825	4.5	0.2	137	1.4	18.2	30.1	11.8	116	32.0	319	97	394	74.5	696	111.3	7534	1.4	264	56.9	825	1346	1240	16
QL10-21-06	33.3	6.4	0.1	552	1.3	0.0	7.8	0.0	0.4	1.1	0.2	8.1	2.9	40	16	79	17.0	182	33.5	10134	0.7	53	11.6	51	84	248	20
QL10-21-07	33.6	8.5	0.3	1136	0.8	0.0	9.7	0.1	2.4	5.3	0.7	28.8	9.2	109	39	174	34.7	342	59.2	9267	0.5	75	16.4	114	186	349	9
QL10-21-08	33.6	3.1	0.3	650	1.8	0.0	17.6	0.1	1.1	2.2	0.7	13.5	4.4	51	18	88	19.9	216	40.5	9563	1.2	119	26.1	134	217	547	15
QL10-21-09	30.5	2.4	0.2	678	2.5	0.0	21.9	0.1	1.4	2.7	0.9	16.6	5.0	60	21	103	22.5	249	46.7	10156	1.4	137	29.0	161	294	637	10
QL10-21-10	33.7	4.9	0.3	942	0.9	0.0	18.9	0.2	3.2	6.9	2.2	30.5	8.9	94	31	136	27.5	287	51.4	9572	0.6	105	22.4	194	318	497	12
QL10-21-11	30.8	3.6	0.6	655	2.6	0.1	20.0	0.1	1.1	2.1	0.7	15.1	4.9	59	22	103	22.8	253	45.4	10679	1.6	159	34.5	169	305	743	11
QL10-21-12	33.3	3.3	0.2	679	2.3	0.0	13.2	0.0	0.7	1.8	0.3	11.3	4.0	51	20	98	21.4	231	42.4	11303	1.5	129	28.5	116	192	605	30
QL10-21-13	30.2	2.6	0.4	668	2.9	1.1	21.8	0.4	2.3	2.6	0.6	13.7	4.4	57	22	107	24.1	264	50.2	10710	1.6	179	39.4	173	327	842	13
QL10-21-14	30.7	11.8	3.2	710	2.9	5.6	36.6	2.0	12.1	7.0	2.0	19.2	5.9	65	23	107	23.5	259	47.1	10358	1.6	210	47.6	276	458	992	24
QL10-21-15	32.5	233	0.5	1097	1.9	0.2	10.8	0.2	3.1	5.5	0.8	25.5	8.4	102	38	174	35.4	358	62.3	9732	0.7	87	26.8	168	195	397	55
QL10-21-16	29.8	1.9	0.3	578	2.2	0.1	13.8	0.1	0.4	2.0	0.5	11.1	3.9	51	19	93	20.8	231	42.6	10862	1.4	119	25.7	114	208	558	3
QL10-21-17	30.2	2.3	0.1	618	1.9	0.0	21.8	0.1	1.3	2.5	0.7	14.6	4.8	57	20	96	21.2	233	43.2	10465	1.1	118	25.7	137	260	558	10
QL10-21-18	31.5	14.6	5.8	426	1.3	29.2	74.8	7.4	32.1	6.7	0.5	11.6	3.1	35	13	61	13.2	140	25.5	10271	0.7	67	14.4	71	110	317	54
QL10-21-19	30.3	1.7	1.2	746	1.5	4.2	24.4	0.8	4.4	3.9	1.3	19.9	6.1	69	24	115	25.4	284	52.4	10457	0.8	156	34.9	191	342	725	16
QL10-21-20	32.3	9.3	0.2	636	1.0	0.0	7.0	0.0	0.8	1.9	0.2	11.0	4.0	51	20	94	19.7	205	36.3	9625	0.6	44	9.3	48	81	207	4
QL10-21-21	33.4	6.6	0.1	611	1.3	0.0	9.6	0.0	0.4	1.8	0.2	11.4	3.8	47	18	87	18.3	192	34.7	10068	0.8	79	17.1	83	136	367	7
QL10-21-22	31.6	28.2	45.3	1014	4.8	102	221	19.9	81.8	18.3	4.2	34.6	8.8	95	33	157	34.3	372	67.3	9597	2.1	241	59.2	351	568	1138	36
QL10-21-23	33.6	4.1	0.2	584	1.7	0.0	18.3	0.1	1.2	2.0	0.5	11.8	3.6	45	17	81	17.6	189	34.9	9933	1.0	127	28.9	156	256	588	12
QL10-21-24	34.3	9.8	13.4	701	2.9	62.0	141	12.1	43.3	9.2	1.4	18.1	5.0	56	21	96	20.5	224	41.8	10210	1.4	204	53.5	340	408	824	55

Appendix H. Zircon trace elements for Chapter 6, analysed in Wuhan

	SiO_2	Ti	Sr	Y	Nb	La	Ce	Pr	Nd	Sm	Eu	Gd	Tb	Dy	Ho	Er	Tm	Yb	Lu	Hf	Ta	Pb	Pb	Pb	Th	U	Pb
	29	49	88	89	93	139	140	141	143	147	151	155	159	163	165	166	169	173	175	179	181	206	207	208	232	238	204
QL10-21-25	32.7	43.6	3.8	1698	4.3	5.1	86.2	5.0	35.8	28.0	9.1	69.2	17.8	178	58	248	49.4	490	83.0	8390	1.5	203	58.5	482	683	903	64
QL10-23-01	32.2	2.7	0.2	500	1.7	0.0	15.2	0.0	0.7	1.6	0.4	9.4	3.3	39	14	68	15.2	168	31.1	10256	1.1	132	27.4	128	212	602	27
QL10-23-02	30.5	3.0	0.2	661	3.0	0.0	19.7	0.1	1.1	2.4	0.6	14.4	4.7	58	21	102	22.0	252	43.7	10511	1.6	174	35.0	185	330	789	0
QL10-23-03	31.1	15.9	4.4	916	3.6	3.0	25.7	2.4	16.0	10.3	4.3	26.1	7.1	81	29	137	29.1	309	54.2	11317	3.2	246	75.5	276	281	959	262
QL10-23-04	32.6	281	0.9	637	3.0	0.1	12.3	0.1	1.4	2.1	0.4	11.3	4.0	50	19	93	20.5	227	40.7	10619	1.1	121	37.2	181	176	515	166
QL10-23-05	33.6	47.7	4.4	953	1.3	12.6	39.5	3.6	15.9	5.5	0.6	17.7	6.1	76	29	144	30.9	330	62.0	11415	0.7	142	33.1	145	204	604	115
QL10-23-06	33.0	3.4	1.3	612	1.1	0.0	11.9	0.1	2.1	3.5	0.8	15.9	4.5	52	18	83	17.3	188	34.3	9715	0.7	96	20.5	128	199	435	69
QL10-23-07	32.8	2.9	3.7	675	2.7	9.8	41.3	2.1	8.9	3.9	1.0	14.8	4.7	56	20	95	21.1	233	42.8	10564	1.5	224	46.6	242	392	925	66
QL10-23-08	33.5	8.4	0.6	588	1.3	0.1	9.0	0.0	0.8	1.5	0.3	9.6	3.4	45	17	83	17.5	190	33.8	10282	0.8	70	17.0	83	109	312	44
QL10-23-09	32.4	106	10.8	1681	2.3	10.7	112	12.0	80.2	60.2	22.9	105	25.9	223	54	206	39.2	394	61.7	8185	0.4	291	94.9	818	1371	1311	402
QL10-23-10	31.9	1.9	16.4	719	2.1	36.4	107	11.2	47.2	12.0	2.0	23.2	5.8	64	22	104	22.9	257	46.6	10390	1.3	160	33.4	176	282	676	24
QL10-23-11	33.2	4.1	0.3	798	1.3	0.1	16.9	0.2	3.6	5.9	2.4	24.4	7.1	75	25	111	22.1	225	38.5	9143	0.6	97	20.7	143	219	442	12
QL10-23-12	31.7	3.1	8.6	409	2.0	27.3	72.4	6.6	26.7	5.0	1.3	10.0	2.7	31	11	56	12.6	146	28.0	10830	1.1	140	29.5	131	217	599	21
QL10-23-13	31.2	2.2	0.1	479	1.9	0.0	14.7	0.0	0.8	1.4	0.4	8.7	2.8	36	14	65	14.5	168	30.3	10787	1.1	136	28.6	127	223	614	8
QL10-23-14	30.9	3.2	0.5	590	2.8	0.0	19.6	0.1	1.2	2.4	0.5	12.3	4.0	51	18	90	20.6	223	40.9	10908	1.6	188	39.2	194	335	845	50
QL10-23-15	33.1	4.6	0.4	646	2.0	0.7	15.2	0.2	1.1	1.8	0.2	9.6	3.6	48	18	92	20.2	221	39.8	11715	1.3	138	28.1	123	203	614	13
QL10-23-16	30.9	3.4	0.4	491	2.0	0.0	13.0	0.0	0.7	1.5	0.5	8.3	3.0	36	14	68	15.6	180	33.2	10633	1.2	142	29.0	123	215	637	17
QL10-23-17	32.4	8.1	1.3	702	3.0	2.7	25.1	0.7	3.9	3.0	0.8	14.3	4.7	56	21	103	23.3	265	48.4	10220	1.7	170	37.1	184	278	713	67
QL10-23-18	30.6	3.3	0.3	740	3.4	0.1	23.2	0.1	1.3	2.8	1.0	14.9	5.4	65	25	117	26.0	291	53.2	10711	1.9	211	44.0	230	403	941	26
QL10-23-19	30.6	1.3	0.2	420	1.4	0.0	11.2	0.0	0.6	1.1	0.3	7.3	2.5	31	12	59	13.3	152	29.1	10093	1.0	123	26.2	102	191	549	17
QL10-23-20	30.7	3.4	12.7	804	3.8	28.7	82.7	7.1	28.6	8.8	1.3	19.2	5.8	69	25	125	28.2	306	57.4	10238	2.0	198	42.3	198	361	889	43
QL10-24-01	32.9	8.2	0.2	273	0.8	0.0	6.9	0.0	0.4	0.9	0.3	5.6	1.7	21	8	37	7.7	89	16.2	9303	0.4	43	8.5	45	74	203	7
QL10-24-02	32.4	9.5	0.2	638	1.0	0.0	10.2	0.1	2.3	3.8	1.0	17.6	5.1	54	18	83	16.5	175	31.0	8751	0.5	64	13.1	100	160	310	64
QL10-24-03	32.9	10.1	0.1	413	1.3	0.0	10.1	0.0	0.6	1.6	0.6	9.3	2.9	34	11	53	11.1	123	22.4	9000	0.6	62	12.8	82	131	301	61
QL10-24-04	33.2	8.3	0.2	961	0.9	0.0	12.7	0.3	5.3	7.9	1.9	31.9	8.9	94	31	133	25.9	271	46.5	8829	0.5	87	18.8	163	254	419	40
QL10-24-05	33.4	12.6	0.5	770	1.6	0.3	12.7	0.4	4.5	5.1	1.5	22.6	6.2	66	22	96	19.8	211	36.8	8604	0.6	76	19.5	139	188	366	73
QL10-24-06	32.1	6.3	0.1	609	2.0	0.0	13.2	0.1	1.2	2.6	0.6	13.7	4.4	49	17	81	17.1	186	32.9	9695	1.0	86	18.4	112	183	418	7
QL10-24-07	32.3	7.2	0.4	539	2.3	0.2	18.0	0.2	1.7	2.9	0.7	12.8	3.6	44	15	71	15.1	167	30.1	10352	1.0	113	28.0	159	219	536	65
QL10-24-08	32.4	6.3	0.6	573	1.3	0.1	10.9	0.1	1.8	3.1	0.8	13.5	4.3	47	16	74	15.3	170	31.3	10603	0.9	95	20.2	116	185	456	41
QL10-24-09	32.6	6.3	0.1	545	1.9	0.0	14.2	0.1	1.3	2.4	0.5	12.0	3.8	43	15	71	14.9	163	29.4	9709	0.8	92	19.3	119	187	446	21
QL10-24-10	33.1	9.0	0.2	612	1.1	0.0	9.6	0.1	2.1	3.5	0.8	16.3	5.0	53	18	83	16.6	179	32.0	8615	0.5	71	15.0	105	168	342	13

Appendix H. Zircon trace elements for Chapter 6, analysed in Wuhan

	SiO_2	Ti	Sr	Y	Nb	La	Ce	Pr	Nd	Sm	Eu	Gd	Tb	Dy	Ho	Er	Tm	Yb	Lu	Hf	Ta	Pb	Pb	Pb	Th	U	Pb
	29	49	88	89	93	139	140	141	143	147	151	155	159	163	165	166	169	173	175	179	181	206	207	208	232	238	204
QL10-24-11	32.4	10.1	0.1	461	1.2	0.1	10.2	0.1	1.1	2.3	0.6	11.3	3.4	38	13	59	12.2	131	23.1	8663	0.6	58	12.5	81	132	280	42
QL10-24-12	33.0	2.7	0.2	520	2.6	0.0	18.4	0.0	0.6	1.7	0.4	10.8	3.3	40	14	69	15.4	164	30.5	11081	1.2	145	30.0	161	249	630	25
QL10-24-13	33.0	8.2	0.2	490	1.7	0.0	13.2	0.0	1.1	2.1	0.5	11.2	3.6	39	14	63	13.0	143	25.9	9387	0.8	86	17.3	112	176	418	14
QL10-24-14	32.4	8.4	0.3	745	1.5	0.1	12.7	0.3	3.2	5.1	1.2	19.7	5.7	62	21	94	19.2	206	36.3	8835	0.7	78	18.3	129	196	387	37
QL10-24-15	32.5	9.1	0.6	1081	1.4	0.2	18.0	0.5	6.0	9.1	2.2	35.4	10.4	108	35	152	30.2	311	53.4	9293	0.6	112	27.2	225	320	533	66
QL10-24-16	34.0	8.7	0.3	568	1.4	0.1	10.5	0.1	1.8	3.6	0.8	14.8	4.3	47	15	73	14.7	158	28.3	8499	0.7	62	14.0	94	140	296	34
QL10-24-17	33.2	7.2	0.2	540	1.5	0.0	11.0	0.1	1.3	2.5	0.6	12.1	3.8	43	15	69	14.6	156	27.8	8880	0.7	62	12.8	87	137	295	61
QL10-24-18	33.4	7.6	0.1	530	2.2	0.0	15.4	0.1	0.8	2.5	0.5	12.0	3.8	42	14	68	14.4	157	28.4	9718	1.0	106	22.8	129	205	503	11
QL10-24-19	32.8	6.9	0.2	721	1.6	0.0	13.7	0.1	2.0	4.4	0.8	18.5	5.4	60	20	92	18.8	202	35.8	9236	0.9	91	19.1	132	211	432	22
QL10-24-20	33.0	9.0	0.2	512	1.3	0.0	10.7	0.1	1.3	2.9	0.7	12.2	3.8	41	14	65	13.3	143	25.6	8666	0.6	68	14.3	97	148	319	36
QL10-25-01	30.7	8.5	0.3	1517	1.6	0.0	18.9	0.1	1.8	3.6	1.6	22.5	9.0	127	51	254	53.6	592	101.0	9155	1.0	215	43.1	705	1126	979	12
QL10-25-02	33.6	5.8	0.3	574	0.5	0.0	4.8	0.0	0.2	1.0	0.4	6.4	2.7	37	16	88	20.8	253	50.0	7753	0.4	50	9.9	84	125	227	5
QL10-25-03	33.2	14.6	0.3	680	0.6	0.1	6.0	0.1	1.1	1.7	0.7	9.5	3.4	48	19	102	23.3	271	51.6	7410	0.4	61	14.3	133	185	278	29
QL10-25-04	34.1	78.5	7.8	433	0.5	0.1	4.5	0.0	0.6	0.7	0.4	5.2	2.1	30	12	66	15.5	182	36.6	7161	0.4	43	9.2	73	106	195	39
QL10-25-05	33.3	7.4	0.1	872	0.2	0.1	4.5	0.2	2.6	3.5	1.9	17.9	5.8	70	26	123	26.5	302	56.6	6670	0.2	101	19.9	349	545	461	36
QL10-25-06	30.6	5.7	0.3	1207	1.1	0.0	13.6	0.1	1.3	2.3	0.8	15.7	6.6	95	39	205	45.7	507	87.3	11992	0.7	172	34.5	372	571	773	7
QL10-25-07	30.7	4.5	4.2	1739	0.9	0.2	11.0	0.2	3.6	6.6	3.1	29.6	11.0	145	57	291	62.4	688	120.8	9512	0.5	149	31.4	437	647	675	20
QL10-25-08	33.3	6.8	0.1	938	0.3	0.0	6.0	0.2	3.7	5.4	2.0	21.8	7.1	83	30	141	29.0	315	56.8	6889	0.3	146	30.3	479	722	657	1
QL10-25-09	32.8	6.1	0.2	665	0.2	0.0	2.1	0.1	1.5	1.9	1.1	9.4	3.4	47	19	105	24.4	303	63.8	6226	0.1	144	29.5	257	403	647	0
QL10-25-10	33.6	8.5	0.4	1309	0.6	0.1	9.6	0.2	3.2	4.9	2.7	27.1	8.9	113	43	209	45.5	521	93.4	7036	0.5	115	23.1	340	521	525	11
QL10-25-11	31.0	6.8	0.5	1811	0.8	0.1	12.5	0.2	3.1	6.1	2.6	31.8	12.0	156	60	297	62.7	685	119.8	8449	0.6	153	31.8	473	705	684	0
QL10-25-12	30.7	7.2	0.3	2245	1.1	0.0	14.0	0.3	4.4	7.6	3.6	41.7	14.7	195	74	365	76.7	838	145.4	7015	0.7	191	39.7	618	957	860	7
QL10-25-13	33.8	9.1	0.1	947	0.3	0.1	5.7	0.3	3.1	4.8	2.2	22.8	7.1	81	28	136	27.5	308	54.5	6641	0.2	49	9.9	190	304	227	0
QL10-25-14	33.6	9.7	0.2	1398	0.5	0.0	5.7	0.2	3.3	6.3	3.1	34.6	10.9	130	45	209	42.4	459	81.2	6445	0.3	86	17.5	385	618	404	28
QL10-25-15	30.9	12.4	0.1	790	0.5	0.0	7.7	0.1	0.9	1.2	0.8	9.7	4.3	63	25	131	27.5	293	51.0	7153	0.9	133	26.9	222	377	601	32
QL10-25-16	33.2	5.3	0.3	1028	0.7	0.0	9.8	0.1	0.8	1.8	0.7	13.4	5.3	78	32	167	36.1	399	70.5	10908	0.5	101	21.0	197	309	472	16
QL10-25-17	32.3	7.4	0.3	1193	1.1	0.0	13.7	0.0	0.9	2.5	0.9	16.6	6.5	95	39	201	44.2	494	86.1	10913	0.8	157	32.1	351	550	709	15
QL10-25-18	33.6	5.2	0.2	730	0.8	0.0	7.5	0.0	0.5	0.9	0.5	7.5	3.1	48	21	113	25.8	298	54.7	12378	0.6	86	17.8	143	224	397	2
QL10-25-19	33.4	8.5	0.1	526	0.2	0.0	3.3	0.1	1.1	1.8	0.8	9.6	3.0	37	15	74	16.1	186	36.2	6708	0.2	40	7.8	94	138	181	4
QL10-25-20	30.7	4.2	0.3	1022	0.8	0.0	12.6	0.1	0.9	2.2	0.7	16.1	6.0	85	34	175	38.2	431	75.1	10943	0.5	184	35.8	436	670	836	22
QL10-26-01	34.0	96.4	0.9	2595	3.4	1.0	35.9	0.9	8.2	14.2	2.4	66.2	21.3	265	93	430	83.3	864	143.0	9054	1.2	83	18.2	311	484	394	39

Appendix H. Zircon trace elements for Chapter 6, analysed in Wuhan

	SiO_2	Ti	Sr	Y	Nb	La	Ce	Pr	Nd	Sm	Eu	Gd	Tb	Dy	Ho	Er	Tm	Yb	Lu	Hf	Ta	Pb	Pb	Pb	Th	U	Pb
	29	49	88	89	93	139	140	141	143	147	151	155	159	163	165	166	169	173	175	179	181	206	207	208	232	238	204
QL10-26-02	32.5	4.0	0.2	934	1.9	0.1	17.5	0.2	2.0	3.8	0.7	20.6	6.2	85	31	154	31.9	356	62.3	10960	1.1	83	17.0	121	177	394	36
QL10-26-03	33.3	5.0	0.2	1074	1.9	0.0	16.6	0.1	1.6	3.0	0.5	19.7	6.7	88	34	171	36.3	394	68.3	9295	1.0	40	8.4	87	132	186	51
QL10-26-04	32.6	34.7	0.8	5107	6.8	0.3	77.8	1.4	24.6	37.3	5.0	160	47.9	556	187	822	154.8	1536	246.3	8503	1.7	138	29.4	736	1069	623	17
QL10-26-05	33.1	4.4	0.2	577	1.2	0.1	9.4	0.0	0.8	1.4	0.2	7.8	3.2	44	18	92	20.2	234	42.5	10699	0.8	36	7.3	59	88	167	12
QL10-26-06	31.9	4.9	0.3	1157	2.0	0.0	18.2	0.1	2.3	4.5	0.7	23.8	8.3	107	40	194	40.4	440	75.8	10104	1.0	51	10.8	131	193	234	19
QL10-26-07	33.4	5.1	0.2	1103	2.0	0.1	15.9	0.1	1.7	3.4	0.5	20.3	6.8	96	37	183	39.1	431	75.0	9391	1.0	46	9.2	94	144	216	8
QL10-26-08	33.6	4.8	0.3	1200	2.1	0.0	18.4	0.1	2.1	4.2	0.7	21.8	8.4	107	40	203	41.7	459	77.3	10003	0.9	54	11.4	141	233	258	29
QL10-26-09	32.8	6.3	1.0	1860	2.2	0.4	27.8	0.4	4.9	8.2	1.4	43.2	14.0	180	64	305	61.3	642	106.9	10158	1.1	73	16.1	227	357	351	28
QL10-26-10	32.2	5.7	0.7	4695	5.1	0.3	65.6	1.3	21.0	32.1	5.1	137	42.1	496	169	748	143.0	1430	230.7	8607	1.6	148	31.3	699	978	674	15
QL10-26-11	32.3	4.8	0.3	1636	1.8	0.0	23.0	0.2	3.6	7.1	1.1	34.9	11.7	154	56	269	54.8	581	97.1	10773	1.0	61	13.0	179	278	295	20
QL10-26-12	33.6	3.4	0.1	364	0.6	0.0	7.3	0.0	0.3	0.8	0.3	4.2	1.8	25	10	55	12.1	146	27.2	11813	0.6	23	4.4	37	58	104	37
QL10-26-13	33.2	4.9	0.2	790	1.8	0.0	12.4	0.0	0.9	2.0	0.3	12.3	4.3	61	24	124	26.3	292	51.1	9808	0.9	31	6.7	60	88	144	31
QL10-26-14	33.4	5.5	0.2	1268	2.5	0.0	19.4	0.2	3.3	5.8	0.7	26.6	9.1	117	43	205	42.1	452	76.6	9864	1.0	45	9.9	136	211	212	22
QL10-26-15	33.6	5.8	0.2	856	1.5	0.0	12.9	0.1	0.8	2.0	0.5	14.1	5.2	70	28	140	29.7	327	56.5	10346	0.9	38	8.0	78	118	176	30
QL10-26-16	33.5	11.3	0.7	1457	1.7	1.6	26.6	0.3	3.3	5.3	1.5	28.7	9.3	128	49	237	50.3	530	91.7	9643	0.8	152	33.9	741	989	702	46
QL10-26-17	33.4	2.6	0.2	802	1.4	0.0	11.1	0.0	0.3	2.3	0.4	11.1	4.4	60	23	120	25.8	297	53.6	9924	0.8	31	5.5	61	90	145	22
QL10-26-18	33.2	4.7	0.2	861	1.5	0.0	14.8	0.1	0.9	2.3	0.4	15.2	5.3	72	28	139	29.0	325	55.9	10698	0.9	41	8.3	90	139	190	11
QL10-26-19	33.7	4.4	0.3	679	1.9	0.2	11.1	0.1	0.7	1.3	0.2	9.5	3.5	51	20	103	22.1	250	44.0	10784	1.2	31	6.0	52	77	139	14
QL10-26-20	33.5	7.1	0.3	2154	5.2	0.0	41.1	0.4	6.0	11.4	1.6	56.8	17.6	221	75	344	69.4	702	121.1	9130	1.8	100	21.2	521	861	485	24
QL10-27-1	33.4	24.0	10.3	706	2.5	28.1	90.0	8.9	41.2	14.3	3.6	26.3	6.8	65	20	90	19.4	218	38.4	9887	1.1	181	50.2	276	347	766	100
QL10-27-2	33.2	2.0	6.3	754	2.2	17.8	61.5	4.5	20.4	6.5	1.3	19.2	5.6	63	22	102	22.3	243	44.2	10113	1.2	182	38.6	210	363	779	35
QL10-27-3	34.1	3.8	0.4	523	1.6	0.4	20.6	0.2	1.4	2.3	0.6	11.5	3.5	43	15	70	15.1	171	30.6	9987	1.0	136	29.0	144	245	626	35
QL10-27-4	33.8	8.5	0.1	520	0.9	0.0	7.3	0.0	0.4	1.8	0.3	8.8	3.3	40	15	72	15.6	164	29.4	9543	0.5	53	11.1	52	91	247	2
QL10-27-5	34.0	24.8	1.8	750	3.0	4.5	37.5	2.5	14.9	8.6	2.9	22.4	5.9	63	21	96	21.1	234	42.4	10048	1.4	190	57.7	308	347	766	143
QL10-27-6	33.1	5.8	12.6	658	2.2	35.7	95.0	8.9	38.0	9.9	1.9	19.5	5.3	56	19	90	20.0	222	40.7	10116	1.4	145	35.1	175	244	617	84
QL10-27-7	32.8	3.1	0.2	656	2.6	0.2	21.5	0.1	1.0	2.4	0.8	13.1	4.3	51	19	92	20.0	226	41.5	10546	1.4	216	46.7	221	376	904	26
QL10-27-8	33.4	2.8	17.7	597	1.9	38.4	104	9.8	40.7	9.4	1.4	17.5	4.3	49	17	79	17.2	195	36.1	9958	1.3	140	28.9	146	248	639	34
QL10-27-9	34.0	3.6	0.4	640	2.0	0.3	22.2	0.2	1.6	2.9	0.7	13.7	4.4	50	18	86	18.7	207	38.1	10183	1.2	155	32.7	175	290	653	26
QL10-27-10	33.6	20.1	7.0	771	3.0	28.5	93.2	9.4	43.9	17.6	4.5	30.5	7.5	74	23	103	22.1	242	43.0	10143	1.4	212	64.4	342	388	840	141
QL10-27-11	33.4	4.7	0.2	621	0.9	0.2	11.7	0.3	3.4	4.8	1.0	17.1	5.0	57	19	83	17.0	181	32.1	9365	0.5	77	16.5	102	181	357	1
QL10-27-12	32.6	10.3	0.8	591	2.1	2.4	27.0	1.4	7.3	5.7	1.7	15.3	4.5	48	17	78	17.1	195	35.5	9981	1.2	136	32.7	169	251	561	47
QL10-27-13	33.7	189	17.5	1624	7.3	51.8	230	32.4	169	89.1	26.5	125	27.5	212	54	212	43.9	487	87.4	9779	2.0	267	212.9	1209	650	1012	1125

Appendix H. Zircon trace elements for Chapter 6, analysed in Wuhan

	SiO_2	Ti	Sr	Y	Nb	La	Ce	Pr	Nd	Sm	Eu	Gd	Tb	Dy	Ho	Er	Tm	Yb	Lu	Hf	Ta	Pb	Pb	Pb	Th	U	Pb
	29	49	88	89	93	139	140	141	143	147	151	155	159	163	165	166	169	173	175	179	181	206	207	208	232	238	204
QL10-27-14	33.3	3.9	0.2	610	1.9	0.1	22.9	0.1	1.1	2.3	0.8	13.2	4.1	48	17	80	17.6	194	35.5	9914	1.1	163	34.0	187	327	678	25
QL10-27-15	33.7	10.4	0.1	688	1.1	0.0	8.6	0.1	1.1	2.5	0.3	13.2	4.3	54	20	94	19.3	205	35.6	9144	0.5	65	13.3	74	128	292	0
QL10-27-16	34.8	19.0	1.1	629	2.3	1.1	15.0	0.8	5.3	4.8	1.3	13.5	4.4	51	18	84	18.6	202	37.6	10787	1.1	92	20.1	89	132	424	50
QL10-27-17	33.2	7.1	0.7	552	1.2	1.5	10.3	0.4	2.8	2.2	0.3	9.2	3.2	41	16	76	16.2	177	31.8	9020	0.6	53	10.8	50	86	241	22
QL10-27-18	31.9	10.4	36.3	520	1.3	54.7	132	15.5	70.2	15.2	1.3	20.2	4.5	44	15	70	14.9	162	30.2	9161	0.5	46	13.3	61	69	221	61
QL10-27-19	32.2	37.9	7.8	1227	2.4	26.5	104	10.3	49.5	22.3	6.1	47.1	12.4	122	39	172	35.0	376	66.1	9666	1.1	190	89.2	536	433	769	324
QL10-27-20	33.6	9.9	0.9	689	2.4	1.4	30.0	0.8	5.2	4.8	1.4	17.1	4.9	55	19	88	19.2	210	37.8	9881	1.2	182	43.7	257	385	747	27
QL10-27-21	33.2	7.8	0.3	1032	0.8	0.0	9.0	0.2	2.9	5.5	0.7	25.3	8.1	94	34	153	30.9	312	54.1	9471	0.6	75	16.0	92	162	351	23